PRECISIONARY

Compresstome® Reference Library

Peer-reviewed publications, independently verified for genuine Precisionary® instrument use.

August 2026 edition

How to use this library

Every publication here was checked against its full-text Methods to confirm a Precisionary instrument was used — not merely cited. All but one used the Compresstome®; the exception used the CF-6100 cryostat. The collection is indexed three ways — by organ system, by animal model, and by experiment — so you can enter from whichever axis fits your work. A marks a highest-impact exemplar in each section. Every entry links to its PubMed / PMC record.

Table of Contents

How to use this library 2

Part I — By Organ System 4

- Brain — live . . . 4
- Brain — fixed . . . 27
- Brainstem . . . 37
- Spinal cord . . . 38
- Eye & retina . . . 38
- Ear & cochlea . . . 39
- Heart . . . 39
- Lung . . . 40
- Liver . . . 50
- Kidney . . . 52
- Intestine & gut . . . 54
- Pancreas . . . 54
- Lymph node & spleen . . . 55
- Muscle & nerve . . . 56
- Cartilage & connective . . . 56
- Skin . . . 57
- Breast & adipose . . . 57
- Reproductive . . . 57
- Bladder . . . 58
- Adrenal & endocrine . . . 59
- Tumor . . . 59
- Plants & other . . . 62
- Materials & bioengineering . . . 62

Part II — By Animal Model 63

Human . . . 63
Non-human primate . . . 67
Mouse . . . 68
Rat . . . 88
Pig . . . 93
Chick . . . 93
Fish . . . 94
Frog . . . 94
Guinea pig . . . 94
Plants . . . 94
Part III — By Experiment **96**
Electrophysiology . . . 96
Imaging . . . 107
Immunohistochemistry . . . 110
In-situ hybridization . . . 117
Precision-cut lung slices (PCLS) . . . 121
Slice culture . . . 127
Part IV — Protocols **130**

Part I — By Organ System

Brain — live

The largest body of Compresstome work: acute live brain slices for electrophysiology, imaging, and circuit interrogation.

AN Webster, JJ Becker, C Li, DC Schwalbe… (2024). Molecular connectomics reveals a glucagon-like peptide 1-sensitive neural circuit for satiety. *bioRxiv*.
United States · Mouse · live · 500 µm PubMed

HA Emmons (2024). Moderate-intensity aerobic exercise enhanced dopamine signaling in diet-induced obese female mice without preventing body weight gain. *Neuropsychopharmacology*.
Mouse · live · 300 µm · Electrophysiology PubMed

L Dong, T Zhao, Z Jin, Y Zheng (2024). Effect of music rhythm magnetic field on long-term potentiation of hippocampal Schaffer-CA1 synapse plasticity. *Neuroscience Letters*.
China · Rat · live · 400 µm · Electrophysiology PubMed

NA Olszewski, S Tetteh-Quarshie, BJ Henderson (2024). Neuronal excitability in the medial habenula and ventral tegmental area is differentially modulated by nicotine dosage and menthol in a sex-specific manner. *eneuro*.
United States · Mouse · live · 300 µm · Electrophysiology PubMed

U Sengupta, R Kayed (2024). Tau Oligomers as Pathogenic Seeds: Preparation, Characterization, and Propagation In Vitro and In Vivo. *Tau Protein: Methods and Protocols*.
United States · Mouse · live · 375 µm · Imaging PubMed

A Asgarihafshejani, VA Raveendran, JC Pressey… (2024). LTP is Absent in the CA1 Region of the Hippocampus of Male and Female Rett Syndrome Mouse Models. *Neuroscience*.
Canada · Mouse · live · 300 µm · Electrophysiology PubMed

A Charli, J Luo, B Palanisamy, E Malovic, Z Riyaz… (2024). Mitochondrial Stress Disassembles Nuclear Architecture through Proteolytic Activation of PKCδ and Lamin B1 Phosphorylation in Neuronal Cells: Implications for …. *bioRxiv*.
Mouse · live · 300 µm · Slice culture PubMed

A Torres-Berrío, M Estill, V Patel, A Ramakrishnan… (2024). Mono-methylation of lysine 27 at histone 3 confers lifelong susceptibility to stress. *Neuron*.
United States · Mouse · live · 300 µm · Electrophysiology PubMed

A Zheng, RS Mann, D Solaja, BL Allman… (2024). Properties of the Caudal Pontine Reticular Nucleus Neurons Determine the Acoustic Startle Response in Cntnap2 KO Rats. *Journal of Integrative Neuroscience*.
Rat · live · 300 µm · Electrophysiology PubMed

AC Hunker, ME Wirthlin, G Gill, NJ Johansen… (2024). Enhancer AAV toolbox for accessing and perturbing striatal cell types and circuits. *bioRxiv*.
United States · Mouse · live · 300 µm · Electrophysiology PubMed

B Riley, E Gould, J Lloyd, LE Hallum… (2024). Dopamine transmission in the tail striatum: Regional variation and contribution of dopamine clearance mechanisms. *Journal of Neurochemistry*.
New Zealand · Rat · live · 300 µm · Imaging PubMed

BJ Henderson, LE Young, NA Olszewski… (2024). Age-dependent effects of vaping on the prefrontal cortex, ventral tegmental area, and nucleus accumbens. *Communications Biology*.
United States · Mouse · live · 300 µm · Electrophysiology PubMed

C Tian, Y Qi, Y Zheng, P Xia, Q Liu, M Luan… (2024). Exploring the Effect of Arsenic-Containing Hydrocarbon on the Bidirectional Synaptic Plasticity of the Dorsal Hippocampus. *International Journal of Molecular Sciences*.
China · Rat · live · 400 µm · Electrophysiology PubMed

CM McCarthy, KL McKevitt, SA Connolly, I Andersson… (2024). Microindentation of fresh soft biological tissue: A rapid tissue sectioning and mounting protocol. *Plos one*.
Ireland · Mouse, human · live · 150-1000 µm PubMed

CTJ van Velthoven, Y Gao, M Kunst, C Lee… (2024). The transcriptomic and spatial organization of telencephalic GABAergic neuronal types. *bioRxiv*.
United States · Mouse · live · 350 µm · Slice culture PubMed

DL Bernstein, SI Lewandowski, C Besada… (2024). Inactivation of ERK1/2 signaling in dopaminergic neurons by map kinase phosphatase MKP3 regulates dopamine signaling and motivation for cocaine. *Journal of Neuroscience*.
United States · Rat · live · 300 µm · Electrophysiology PubMed

DL Wise, SB Greene, Y Escobedo-Lozoya… (2024). Progressive circuit hyperexcitability in mouse neocortical slice cultures with increasing duration of activity silencing. *Eneuro*.
United States · Mouse · live · 300 µm · Slice culture PubMed

DL Wise, Y Escobedo-Lozoya, V Valakh, B Isaac… (2024). Prolonged Activity Deprivation Causes Pre-and Postsynaptic Compensatory Plasticity at Neocortical Excitatory Synapses. *eneuro*.
United States · Mouse · live · 300 µm · Slice culture PubMed

DVF de Siqueira, N Boaretto, RM Leão (2024). Decreases in metabolic ATP open KATP channels and reduce firing in an auditory brainstem neuron: A dynamic mechanism of firing control during intense activity. *Neuroscience*.
Rat · live · 200 µm · Electrophysiology PubMed

EM York, A Miller, SA Stopka… (2024). The dentate gyrus differentially metabolizes glucose and alternative fuels during rest and stimulation. *Journal of Neurochemistry*.
United States · Mouse · live · 450 µm PubMed

EP Hurley, B Mukherjee, LZ Fang, JR Barnes… (2024). GluN3A and excitatory glycine receptors in the adult hippocampus. *Journal of Neuroscience*.
Canada · Mouse · 350 µm · Imaging PubMed

ER Niessen (2024). Potential Treatments for Epileptiform Activity in Microgyral Cortex. *Frontiers in Immunology*.
Mouse · live · 3mm µm PubMed

F Cathomas, HY Lin, KL Chan, L Li, LF Parise… (2024). Circulating myeloid-derived MMP8 in stress susceptibility and depression. *Nature Portfolio*.
United States · Mouse · live · 250 µm · Electrophysiology PubMed

F Kadakia, A Khadka, J Yazell, S Davidson (2024). Chemogenetic modulation of posterior insula CaMKIIa neurons alters pain and thermoregulation. *The Journal of Pain*.
United States · Mouse · live · 300 µm · Electrophysiology PubMed

F Marti, P Faure, T Le Borgne, C Nguyen, E Vicq, J Jehl… (2024). Nicotine engages a VTA-NAc feedback loop to inhibit amygdala-projecting dopamine neurons and induce anxiety. *bioRxiv*.
France · Mouse · live · 250 µm · Electrophysiology PubMed

F Mei, C Zhao, S Li, Z Xue, Y Zhao, Y Xu, R Ye… (2024). Ngfr+ cholinergic projection from SI/nBM to mPFC selectively regulates temporal order recognition memory. *Nature Communications*.
China · Mouse · live · 300 µm · Electrophysiology PubMed

F Zeldenrust, N Calcini, X Yan, A Bijlsma… (2024). The tuning of tuning: How adaptation influences single cell information transfer. *PLOS Computational Biology*.
Netherlands · Mouse · live · 300 µm · Electrophysiology PubMed

GC Smith, KR Griffith, AR Sicher, DF Brockway… (2024). MODERATE ALCOHOL CONSUMPTION INDUCES LASTING IMPACTS ON PREFRONTAL CORTICAL SIGNALING IN MICE. *bioRxiv*.
United States · Mouse · live · 300 µm · Electrophysiology PubMed

H Park, J Kim, H Lee, WS Chung (2024). Selective regulation of corticostriatal synapses by astrocytic phagocytosis. *Nature Portfolio*.
South Korea · Mouse · live · 350 µm · Electrophysiology PubMed

HA Emmons, SC Fordahl (2024). Attenuating Saturated-Fat Induced Changes in Dopamine Neurotransmission. *UNCG Library*.
Mouse · live · 300 µm · Imaging PubMed

J Bär, T Fanutza, CC Reimann, L Seipold… (2024). Non-canonical function of ADAM10 in presynaptic plasticity. *Cellular and Molecular Life of Sciences*.
Germany · Mouse · live · 400 µm · Electrophysiology PubMed

JC Moffa, IN Bland, JR Tooley, V Kalyanaraman… (2024). Cell specific single viral vector CRISPR/Cas9 editing and genetically encoded tool delivery in the central and peripheral nervous systems. *eNeuro*.
United States · Mouse · live · 300 µm · Electrophysiology PubMed

JT Ting, NJ Johansen, BE Kalmbach, N Taskin, B Lee… (2024). Distinctive physiology of molecularly identified medium spiny neurons in the macaque putamen. *Cell Reports*.
United States · Monkey · live · 300 or 350 µm · Electrophysiology PubMed

KA Hagarty-Waite, HA Emmons, SC Fordahl… (2024). The Influence of Strain and Sex on High Fat Diet-Associated Alterations of Dopamine Neurochemistry in Mice. *Nutrients*.
United States · Mouse · live · 300 µm PubMed

KM Ibrahim, N Massaly, HJ Yoon, R Sandoval… (2024). Dorsal hippocampus to nucleus accumbens projections drive reinforcement via activation of accumbal dynorphin neurons. *Nature Communications*.
United States · Mouse · live · 250 µm · Electrophysiology PubMed

L Castell, A Rogliardo, T Le Borgne, C Naon, A Cathala… (2024). Midbrain dopamine D2R regulates the salience of threat-related events. *bioRxiv*.
Mouse · live · 250 µm · Electrophysiology PubMed

L Yang, LZ Fang, MR Lynch, CS Xu, H Hahm, Y Zhang… (2024). Transcriptomic landscape of mammalian ventral pallidum at single-cell resolution. *bioRxiv*.
United States · Mouse · live · 400 µm · Slice culture PubMed

M Abatis, R Perin, R Niu, E van den Burg… (2024). Fear learning induces synaptic potentiation between engram neurons in the rat lateral amygdala. *Nature Portfolio*.
Switzerland · Rat · live · 400 µm · Electrophysiology PubMed

M Marcatti, B Tumurbaatar, M Borghi… (2024). Inhibition of Calcineurin with FK506 Reduces Tau Levels and Attenuates Synaptic Impairment Driven by Tau Oligomers in the Hippocampus of Male Mouse …. *International Journal of Molecular Sciences*.
United States · Mouse · live · 350 µm · Electrophysiology PubMed

M Serranilla, JC Pressey, MA Woodin (2024). Restoring Compromised CI-in D2 Neurons of a HD Mouse Model Rescues Motor Disability. *Journal of Neuroscience*.
Canada · Mouse · live · 300 µm · Imaging PubMed

N Mojahed, M Adjei, E Qasem, S Aaflaq… (2024). Acute social defeat during adolescence promotes long-lasting aggression through activation of the medial amygdala. *Frontiers in Neuroscience*.
United States · Mouse · live · 300 µm · Electrophysiology PubMed

NC Dembrow, S Sawchuk, R Dalley, X Opitz-Araya… (2024). Areal specializations in the morpho-electric and transcriptomic properties of primate layer 5 extratelencephalic projection neurons. *Cell reports*.
United States · Macaque monkey · live · 300-350 µm · Electrophysiology PubMed

P Scaduto, M Marcatti, N Bhatt, R Kayed… (2024). Calcineurin inhibition prevents synaptic plasticity deficit induced by brain-derived tau oligomers. *Brain Communications*.
United States · Mouse · live · 350 µm · Electrophysiology PubMed

PS Zarpellon, C Murat, RM Leão (2024). Reduction in mitochondrial ATP synthesis mimics the effect of low glucose in depolarizing neurons from the subpostremal nucleus of the solitary tract of rats. *Journal of Bioenergetics and Biomembranes*.
Brazil · Rats · live · 200 µm · Electrophysiology PubMed

QA Nguyen, PM Klein, C Xie, KN Benthall… (2024). Acetylcholine receptor based chemogenetics engineered for neuronal inhibition and seizure control assessed in mice. *Nature Communications*.
United States · Mouse · live · 275 µm · Electrophysiology PubMed

R Kshetri, JO Beavers, R Hyde, R Ewa… (2024). Behavioral decline in Shank3Δex4–22 mice during early adulthood parallels cerebellar granule cell glutamatergic synaptic changes. *Molecular Autism*.
United States · Mouse · live · 250 µm · Electrophysiology PubMed

RA Serafini, Z Farzinpour, V Patel, AM Kelley, M Estill… (2024). Nucleus accumbens myocyte enhancer factor 2C mediates the maintenance of peripheral nerve injury–induced physiological and behavioral maladaptations. *Pain*.
United States · Mouse · live · 300 µm · Electrophysiology PubMed

S Basu, EJ Ro, Z Liu, H Kim, A Bennett… (2024). The Mef2c gene dose-dependently controls hippocampal neurogenesis and the expression of autism-like behaviors. *Journal of Neuroscience*.
United States · Mouse · live · 350 µm · Electrophysiology PubMed

S Brannan, L Garbe, BD Richardson (2024). Early life stress induced sex-specific changes in behavior is paralleled by altered locus coeruleus physiology in BALB/cJ mice. *Neurobiology of Stress*.
United States · Mouse · live · 250 µm · Electrophysiology PubMed

S Brennan, L Garbe, BD Richardson (2024). Early life stress induces sex-specific changes in behavior and parallel locus coeruleus neuron excitability. *bioRxiv*.
Mouse · live · 250 µm · Electrophysiology PubMed

S Logan, R Ranjit, H Rose, A Bredegaard… (2024). Simultaneous quantitative respirometry and fluorometric assays in dissected hippocampal tissue from mice. *STAR protocols*.
United States · Mouse · live · 400 µm · Electrophysiology PubMed

S Ma, S Watanabe, DC Gillespie (2024). Ultrastructure of immature synaptic inputs in the lateral superior olive of the rodent brainstem. *bioRxiv*.
Rat · live · 250 µm · Electrophysiology PubMed

S Zheng, R Banerji, R LeBourdais, S Zhang… (2024). Alteration of mechanical stresses in the murine brain by age and hemorrhagic stroke. *Journal of Translational Medicine*.
United States · Mouse · 250 µm · Imaging PubMed

SS Adel, ZJ Pranske, TF Kowalski, N Kanzler… (2024). Plexin-B1 and Plexin-B2 play non-redundant roles in GABAergic synapse formation. *bioRxiv*.
United States · Mouse · live · 300 µm · Slice culture PubMed

T Markovic, J Higginbotham, B Ruyle… (2024). A locus coeruleus to dorsal hippocampus pathway mediates cue-induced reinstatement of opioid self-administration in male and female rats. *American College of Neuropsychopharmacology*.
United States · Rat · live · 350 µm · Electrophysiology PubMed

VA Raveendran, M Serranilla, A Asgarihafshejani… (2024). SNARE protein SNAP25 regulates the chloride-transporter KCC2 in neurons. *iScience*.
Canada · Mouse · live · 300 µm · Electrophysiology PubMed

A Godino, M Salery, AM Minier-Toribio, V Patel… (2023). Dopaminoceptive D1 and D2 neurons in ventral hippocampus arbitrate approach and avoidance in anxiety. *bioRxiv*.
United States · Mouse · live · 250 µm · Electrophysiology PubMed

A Miller, EM York, SA Stopka, JR Martínez-François… (2023). Spatially resolved metabolomics and isotope tracing reveal dynamic metabolic responses of dentate granule neurons with acute stimulation. *Nature*.
United States · Mouse · live · 450 µm · Electrophysiology PubMed

A de Lange, H Tomes, J Selfe, UF Prodjinotho… (2023). Cestode larvae excite host neuronal circuits via glutamatergic signaling. *eLife*.
Human · live · 350 µm PubMed

AAA Reyes (2023). Role of Chronic Stress-Induced Neuroinflammation in Rodent Locus Coeruleus Physiology and Anxiety-Like Behaviors. *Rowan Digital Works*.
Rat · live · 300 µm · Electrophysiology PubMed

AK Muthusamy (2023). Neuropsychiatric Drug Biosensors in Organelles, Cells, Biofluids, &Behaving Animals. *Caltech*.
Mouse · live · 200 µm · Electrophysiology PubMed

AML Osse, RS Pandey, RA Wirt, AA Ortiz… (2023). Reduction in GABAB on glia induce Alzheimer's disease related changes. *Brain Behavior and Immunity*.
United States · Mouse · frozen · 30 µm · IHC / ISH PubMed

AR Sicher, WD Starnes, KR Griffith, NC Dao… (2023). Adolescent binge drinking leads to long-lasting changes in cortical microcircuits in mice. *Neuropharmacology*.
United States · Mouse · live · 300 µm · Electrophysiology PubMed

AS Abdelfattah, J Zheng, A Singh, YC Huang, D Reep… (2023). Sensitivity optimization of a rhodopsin-based fluorescent voltage indicator. *Neuron (CellPress)*.
United States · Mouse · live · 350 µm · Electrophysiology PubMed

BR Christie, A Gross, A Willoughby, E Grafe… (2023). Assessing changes in synaptic plasticity using an awake closed-head injury model of mild traumatic brain injury. *JoVE*.
Rat · live · 400 µm · Electrophysiology PubMed

C Natarajan, C Cook, K Ramaswamy… (2023). Phospholipase D1 Attenuation Therapeutics Promotes Resilience against Synaptotoxicity in 12-Month-Old 3xTg-AD Mouse Model of Progressive Neurodegeneratoin. *International Journal of Molecular Science*.
United States · Mouse · live · 350 µm · Electrophysiology PubMed

D Stajano (2023). Role of tetraspanin 15 in metabotropic glutamate receptor 5 signaling and extracellular vesicles docking at neurons from mus musculus domesticus. *University of Hamburg Library*.
Mouse · live · 350 µm · Electrophysiology PubMed

D Zhao, C Tian, M Cheng, F Yang, C Tian, Y Liu… (2023). Carrier-free quercetin nanomedicine blocks NLRP3 deubiquitination and TXNIP recruitment for Parkinson's disease therapy. *Chemical Engineering Journal*.
Mouse · live · 400 µm · Electrophysiology

DF Brockway, KR Griffith, CM Aloimonos, TT Clarity… (2023). Somatostatin peptide signaling dampens cortical circuits and promotes exploratory behavior. *Cell reports*.
United States · Mouse · live · 300 µm · Electrophysiology PubMed

DL Wise (2023). Maladaptive Homeostatic Plasticity: Impact of Prolonged Silencing on Cellular Hyperexcitability. *The Faculty of the Graduate School of Arts and Sciences Brandeis University*.
Mouse · live · 300 µm · Organoids PubMed

F Cathomas, HY Lin, KL Chan, L Li… (2023). Peripheral immune-derived matrix metalloproteinase promotes stress susceptibility. *Research Square*.
United States · Mouse · live · 250 µm · Electrophysiology PubMed

H Liu, RN Caballero-Florán, T Hergenreder, T Yang… (2023). DSCAM gene triplication causes excessive GABAergic synapses in the neocortex in Down syndrome mouse models. *PLoS Biology*.
United States · Mouse · live · 300-350 µm · Electrophysiology PubMed

H Ruiz-Garcia, N Zarco, F Watanabe… (2023). Development of Experimental Three-Dimensional Tumor Models to Study Glioblastoma Cancer Stem Cells and Tumor Microenvironment. *Tumor Angiogenesis Assay*.
United States · Mouse · live · 250-350 µm · Slice culture PubMed

HA Emmons, CW Wallace, SC Fordahl (2023). Interleukin-6 and tumor necrosis factor-α attenuate dopamine release in mice fed a high-fat diet, but not medium or low-fat diets. *Nutritional Neuroscience*.
United States · Mouse · live · 300 µm PubMed

HM Rose, B Ferrán, R Ranjit… (2023). Mitochondrial calcium uniporter deficiency in dentate granule cells remodels neuronal metabolism and impairs reversal learning. *Journal of Neurochemistry*.
United States · Mouse · live · 400 µm · Electrophysiology PubMed

HY Lin, F Cathomas, L Li, RD Cuttoli, C Guevara… (2023). Chemokine receptor 5 signaling in PFC mediates stress susceptibility in female mice. *bioRxiv*.
Mouse · live · 250 µm · Electrophysiology PubMed

J Jehl, M Ciscato, E Vicq, G Dejean de la Batie… (2023). The interpeduncular nucleus blunts the rewarding effect of nicotine. *bioRxiv*.
France · Mouse · live · 250 µm · Electrophysiology PubMed

JK Mich, S Sunil, N Johansen, RA Martinez, M Leytze… (2023). Enhancer-AAVs allow genetic access to oligodendrocytes and diverse populations of astrocytes across species. *bioRxiv*.
Mouse · live · 350 µm · Slice culture PubMed

K Egawa, M Watanabe, H Shiraishi, D Sato… (2023). Imbalanced expression of cation-chloride cotransporters as a potential therapeutic target in an Angelman syndrome mouse model. *Scientific Reports*.
Japan · Mouse · live · 350 µm · Electrophysiology PubMed

K Grycel, NY Larsen, Y Feng, K Qvortrup… (2023). CRMP2 conditional knockout changes axonal function and ultrastructure of axons in mice corpus callosum. *Molecular and Cellular Neuroscience*.
Denmark · Mouse · live · 400 µm · Electrophysiology PubMed

K Jin, Z Yao, CTJ van Velthoven, ES Kaplan… (2023). Cell-type specific molecular signatures of aging revealed in a brain-wide transcriptomic cell-type atlas. *bioRxiv*.
United States · Mouse · live · 350 µm · Imaging PubMed

KJ Brymer, EP Hurley… (2023). Asymmetric dysregulation of glutamate dynamics across the synaptic cleft in a mouse model of Alzheimer's disease. *Acta Neuropathol Commun*.

Canada · Mouse · live · 350 µm · Electrophysiology PubMed

L Dong, L Zhao, L Tian, W Zhao, C Xiong… (2023). AsHC 360 Exposure Influence on Epileptiform Discharges in Hippocampus of Infantile Male Rats In Vitro. *International Journal of Molecular Sciences*.
China · Rat · live · 400 µm · Electrophysiology PubMed

L Li, R Durand-de Cuttoli, AV Aubry, CJ Burnett… (2023). Social trauma engages lateral septum circuitry to occlude social reward. *Nature*.
United States · Mouse · live · 250 µm · Electrophysiology PubMed

L Munari, V Patel, N Johnson, C Mariottini… (2023). Memory discrimination is promoted by the expression of the transcription repressor WT1 in the dentate gyrus. *Frontiers in Behavioral Neuroscience*.
United States · Mouse · live · 200 µm · Electrophysiology PubMed

L Tian, T Zhao, L Dong, Q Liu… (2023). Passive array micro-magnetic stimulation device based on multi-carrier wireless flexible control for magnetic neuromodulation. *Journal of Neural Engineering*.
Rat · live · 400 µm · Electrophysiology PubMed

LR Shao, R Janicot… (2023). Anti-seizure effect of 2-deoxyglucose (2-DG) is not dependent on the presynaptic vacuole ATP pump (V-ATPase) or the somatic ATP-sensitive K+ channel (KATP). *Journal of Neurophysiology*.
United States · Rat · live · 350 µm · Electrophysiology PubMed

M Abdelmageed, P Palanisamy, V Vernail, Y Silberman… (2023). An altered cell-specific subcellular distribution of translesion synthesis DNA polymerase kappa (POLK) in aging neurons. *bioRxiv*.
Mouse · live · 100 µm · Electrophysiology PubMed

M Cheng, C Ye, C Tian, D Zhao, H Li, Z Sun, Y Miao… (2023). Engineered macrophage-biomimetic versatile nanoantidotes for inflammation-targeted therapy against Alzheimer's disease by neurotoxin neutralization and …. *Bioactive Materials*.
China · Mouse · live · 400 µm · Electrophysiology PubMed

M Salery, A Godino, YQ Xu, JF Fullard… (2023). Transcriptional correlates of cocaine-associated learning in striatal ARC ensembles. *bioRxiv*.
Mouse · live · 250 µm · Electrophysiology PubMed

M Singh, K Sapkota, K Sakimura, M Kano, RM Cowell… (2023). Maturation of GABAergic Synaptic Transmission from Neocortical Parvalbumin Interneurons Involves NMDA receptor Recruitment of Cav2. 1 Channels. *Neuroscience*.
Mouse · live · 300 µm · Electrophysiology PubMed

MH Kim, C Radaelli, ER Thomsen, D Monet… (2023). Target cell-specific synaptic dynamics of excitatory to inhibitory neuron connections in supragranular layers of human neocortex. *Elife*.
United States · Human · live · 350 µm · Tumor PubMed

ML Ratz-Mitchem, G Leary, A Grindeland, D Silvius… (2023). Generation and characterization of a knock-in mouse model for spastic tetraplegia, thin corpus callosum, and progressive microcephaly (SPATCCM). *Mammalian Genome*.
United States · Mouse · live · 300 µm · Imaging PubMed

MM Novakovic, KS Korshunov, RA Grant… (2023). Astrocyte reactivity and inflammation-induced depression-like behaviors are regulated by Orai1 calcium channels. *Nature Portfolio*.
United States · Mouse · live · 250 µm · Electrophysiology PubMed

MR Norris, CC Kuo, SS Dunn, JR Kim, LJ Becker… (2023). Mu opioid receptors gate the locus coeruleus pain generator. *BioRxiv*.
United States · Mouse · live · 350 µm · Electrophysiology PubMed

NM Benites, B Rodrigues… (2023). Development of electrophysiological properties of fusiform neurons from the dorsal cochlear nucleus of mice before and after hearing onset. *J Neurophysiol*.
Brazil · Mouse · live · 200 µm · Electrophysiology PubMed

Q Tang, E Godschall, CD Brennan, Q Zhang… (2023). A leptin-responsive hypothalamic circuit inputs to the circadian feeding network. *bioRxiv*.
United States · Mouse · live · 400 µm · Imaging PubMed

Q Tang, E Godschall, CD Brennan, Q Zhang… (2023). Leptin receptor neurons in the dorsomedial hypothalamus input to the circadian feeding network. *Science Advances*.
United States · Mouse · live · 400 µm · Imaging PubMed

RN Caballero-Florán, AD Nelson, L Min, PM Jenkins (2023). Effects of chronic lithium treatment on neuronal excitability and GABAergic transmission in an Ank3 mutant mouse model. *bioRxiv*.
United States · Mouse · live · 300 µm · Electrophysiology PubMed

RS Mann, BL Allman, S Schmid (2023). Developmental changes in electrophysiological properties of auditory cortical neurons in the Cntnap2 knockout rat. *J Neurophysiol*.
Canada · Rat · live · 300 µm · Electrophysiology PubMed

S Driessens, D Heyer, I Pieterse, R Wilbers, E Mertens… (2023). Genes associated with cognitive ability and HAR show overlapping expression patterns in human cortical neuron types. *Nature Communications*.
Netherlands · Human · live · 350 µm · Electrophysiology PubMed

S Mondoloni, C Nguyen, E Vicq, M Ciscato, J Jehl… (2023). Prolonged nicotine exposure reduces aversion to the drug in mice by altering nicotinic transmission in the interpeduncular nucleus. *Elife*.
France · Mouse · live · 250 µm · Electrophysiology PubMed

S Nakakubo, Y Hiramatsu, T Goto, S Kimura… (2023). Therapeutic effects of KRM-II-81, positive allosteric modulator for α2/3 subunit containing GABAA receptors, in a mouse model of Dravet syndrome. *Frontiers in Oncology*.
Japan · Mouse · live · 350 µm · Electrophysiology PubMed

SA Sorensen, NW Gouwens, Y Wang, M Mallory… (2023). Connecting single-cell transcriptomes to projectomes in mouse visual cortex. *bioRxiv*.
United States · Mouse · live · 350 µm · Electrophysiology PubMed

SJF Cronin, W Yu, A Hale, S Licht-Mayer, MJ Crabtree… (2023). Crucial neuroprotective roles of the metabolite BH4 in dopaminergic neurons. *bioRxiv*.
Austria · Mouse · live · 320 µm · Electrophysiology PubMed

SM Conway, CC Kuo, W Gardiner, RN Wu, LV Thang… (2023). An electrochemical approach for rapid, sensitive, and selective detection of dynorphin. *bioRxiv*.
Mouse · live · 300 µm PubMed

SM Ramos Rodriguez (2023). An Investigation into Cell-Type Vulnerability for Formation of Alpha-Synuclein Aggregates. *UCLA Open Access Publications*.
Mouse · live · 50 µm · IHC / ISH PubMed

SP Brown, RJ Lawson, JD Moreno… (2023). A reinterpretation of the relationship between persistent and resurgent sodium currents. *Journal of Neuroscience*.
United States · Mouse · live · 350 µm · Electrophysiology PubMed

SS Adel, VRJ Clarke, A Evans-Strong, J Maguire… (2023). Semaphorin 4D induced inhibitory synaptogenesis decreases epileptiform activity and alters progression to Status Epilepticus in mice. *Epilepsy research (ELSEVIER)*.
United States · Mouse · live · 300 µm · Slice culture PubMed

SS Salile, HJ Lee, PSF Alberts, T Abula… (2023). In vitro and in vivo anti-seizure activity of hydromethanolic extract and fractions of Pterolobium stellatum. *Journal of Ethnopharmacology*.
Mouse · live · 400 µm · Electrophysiology PubMed

SY Cooper, CV Willis, MR Richardson… (2023). Chemical flavorants in vaping products alter neurobiology in a sex-dependent manner to promote vaping-related behaviors. *J Neurosci*.
United States · Mouse · live · 250 µm · Electrophysiology PubMed

T Fanutza (2023). Deciphering the structure and plasticity of glutamatergic synapses in the hippocampus. *University of Hamburg Library*.
Mouse · live · 400 µm · Electrophysiology PubMed

TD Weber, MV Moya, K Kılıç, J Mertz… (2023). High-speed multiplane confocal microscopy for voltage imaging in densely labeled neuronal populations. *Nat Neurosci*.
United States · Mouse · live · 300 µm · Electrophysiology PubMed

V Valakh, D Wise, XA Zhu, M Sha, J Fok… (2023). A transcriptional constraint mechanism limits the homeostatic response to activity deprivation in mammalian neocortex. *Elife*.
United States · Mouse · live · 300 µm · Slice culture PubMed

W Yu (2023). Translational Rapid Ultraviolet-Excited Sectioning Tomography for Whole-Organ Imaging with Subcellular Resolution. *Scientific Reports*.
China · Mouse · live · 40 µm · IHC / ISH PubMed

X Chen, DA Wolfe, DS Bindu, M Zhang… (2023). Functional gene delivery to and across brain vasculature of systemic AAVs with endothelial-specific tropism in rodents and broad tropism in primates. *Nature Communications*.
United States · Human, Non-Human Primate · live · 300 µm · IHC / ISH PubMed

Y Jin, E Mikhailova, M Lei, SA Cowley, T Sun… (2023). Integration of 3D-printed cerebral cortical tissue into an ex vivo lesioned brain slice. *Nature Communications*.
United Kingdom · Mouse · live · 300 µm · Imaging PubMed

Y Lu, F Sciaccotta, L Kiely, B Bellanger… (2023). Rapid, activity-dependent intrinsic plasticity in the developing zebra finch auditory cortex. *The Journal of Neuroscience*.
United States · Birds (Zebra Finch) · live · 300 µm · Electrophysiology PubMed

Y Shima, H Skibbe, Y Sasagawa, N Fujimori… (2023). Distinctiveness and continuity in transcriptome and connectivity in the anterior-posterior axis of the paraventricular nucleus of the thalamus. *Cell Reports*.
Mouse · live · 300 µm · Electrophysiology PubMed

Y Zhang, J Riexinger, X Yang, E Mikhailova, Y Jin… (2023). A microscale soft ionic power source modulates neuronal network activity. *Nature Portfolio*.
United Kingdom · Mouse · live · 300 µm · Imaging PubMed

Z Yao, CTJ van Velthoven, M Kunst, M Zhang… (2023). A high-resolution transcriptomic and spatial atlas of cell types in the whole mouse brain. *Nature*.
United States · Mouse · live · 350 µm · IHC / ISH PubMed

A Bittar, R Al-Lahham, N Bhatt, K Moore… (2022). Passive Immunotherapy Targeting Tau Oligomeric Strains Reverses Tauopathy Phenotypes in Aged Human-Tau Mice in a Mouse Model-Specific Manner. *Journal of Alzheimer's disease*.
Mouse · live · 375 µm · Electrophysiology PubMed

AC Leach, EG Pitts, CA Siciliano… (2022). α7 nicotinic acetylcholine receptor modulation of accumbal dopamine release covaries with novelty seeking. *Eur J Neurosci*.
United States · Rat · live · 400 µm PubMed

CN Barnes, CW Wallace, BS Jacobowitz… (2022). Reduced phasic dopamine release and slowed dopamine uptake occur in the nucleus accumbens after a diet high in saturated but not unsaturated fat. *Nutr Neurosci*.
United States · Mouse · live · 300 µm PubMed

CW Wallace, MC Loudermilt… (2022). Effect of fasting on dopamine neurotransmission in subregions of the nucleus accumbens in male and female mice. *Nutritional neuroscience*.
United States · Mouse · live · 300 µm PubMed

D Bojovic, TL Stackhouse, A Mishra (2022). Assaying activity-dependent arteriole and capillary responses in brain slices. *Neurophotonics*.
United States · Rat · live · 300 µm · Imaging PubMed

D Koveal, PC Rosen, DJ Meyer… (2022). A high-throughput multiparameter screen for accelerated development and optimization of soluble genetically encoded fluorescent biosensors. *Nature Communications*.
United States · Mouse · live · 275 µm · Imaging PubMed

DJ Meyer, CM Díaz-García, N Nathwani, M Rahman… (2022). The Na+/K+ pump dominates control of glycolysis in hippocampal dentate granule cells. *Elife*.
United States · Mouse · live · 275 µm · Imaging PubMed

DVF de Siqueira, PS Strazza Jr, NM Benites… (2022). Salicylate activates KATP channels and reduces spontaneous firing in glycinergic cartwheel neurons in the dorsal cochlear nucleus of rats. *European Journal of Pharmacology*.
Rat · live · 200 µm · Electrophysiology PubMed

JT Lloyd, AG Yee, PK Kalligappa, A Jabed, PY Cheung… (2022). Dopamine Dysregulation and Altered Responses to Drugs Affecting Dopaminergic Transmission in a New Dopamine Transporter Knockout (DAT-KO) Rat Model. *Neuroscience*.
New Zealand · Rat · live · 300 µm · Electrophysiology PubMed

K Egawa, M Watanabe, H Shiraishi, D Sato… (2022). Therapeutic effects of bumetanide on neurological dysfunction in a mouse model of Angelman syndrome. *Sci Rep*.
Japan · Mouse · live · 350 µm · Electrophysiology PubMed

KN Nwachukwu, DM King, KL Healey… (2022). Sex-specific effects of adolescent intermittent ethanol exposure-induced dysregulation of hippocampal glial cells in adulthood. *Alcohol*.
United States · Rat · live · 40 µm · IHC / ISH PubMed

LK Cuddy, AO Alia, MA Salvo… (2022). Farnesyltransferase inhibitor LNK-754 attenuates axonal dystrophy and reduces amyloid pathology in mice. *Mol Neurodegener*.
United States · Mouse · live · 300 µm · Imaging PubMed

M Marcatti, A Fracassi, M Montalbano… (2022). Aβ/tau oligomer interplay at human synapses supports shifting therapeutic targets for Alzheimer's disease. *Cell Mol Life Sci*.
United States · Mouse · live · 350 µm PubMed

M Patiño, WN Lagos, NS Patne… (2022). Single-cell transcriptomic classification of rabies-infected cortical neurons. *Proc Natl Acad Sci USA*.
United States · Mouse · live · 400 µm PubMed

MS Nair, NC Dao, DL Melean, KR Griffith… (2022). Somatostatin Neurons in the Bed Nucleus of the Stria Terminalis Play a Sex-Dependent Role in Binge Drinking. *Brain Research Bulletin*.
Mouse · live · 300 µm · Electrophysiology PubMed

N Saviuk, Y Chong, P Wang, S Bermudez, Z Zhao… (2022). Loss of 4E-BP converts cerebellar long-term depression to long-term potentiation. *Cell Reports*.
Canada · Mouse · live · 250 µm · Electrophysiology PubMed

NM George, AG Polese, L Merle… (2022). Excitable axonal domains adapt to sensory deprivation in the olfactory system. *J Neurosci*.
United States · Mouse · live · 400 µm · Electrophysiology PubMed

P Rukundo, T Feng, V Pham, S Pieraut (2022). Moderate effect of early-life experience on dentate gyrus function. *Molecular Brain*.
United States · Mouse · live · 300 µm · Electrophysiology PubMed

S Gaige, R Barbouche… (2022). Constitutively active microglial populations limit anorexia induced by the food contaminant deoxynivalenol. *Journal of Neuroinflammation*.
France · Mouse · live · 250 µm · Imaging PubMed

SR Chadwick, AD Güler (2022). Local Drd1-neurons input to subgroups of arcuate AgRP/NPY-neurons. *iScience*.
United States · Mouse · live · 300 µm · Electrophysiology PubMed

TA Hage, A Bosma-Moody, CA Baker, MB Kratz… (2022). Synaptic connectivity to L2/3 of primary visual cortex measured by two-photon optogenetic stimulation. *Elife*.
United States · Mouse · live · 350 µm · Electrophysiology PubMed

TA Stowe, EG Pitts, AC Leach, MC Iacino, F Niere… (2022). Diurnal rhythms in cholinergic modulation of rapid dopamine signals and associative learning in the striatum. *Cell Reports*.
United States · Rat · live · 400 µm · Electrophysiology PubMed

TIH Park, LCD Smyth, M Aalderink, ZR Woolf… (2022). Routine culture and study of adult human brain cells from neurosurgical specimens. *Nature Protocols*.
New Zealand · Human · live · 250-300 µm · Slice culture PubMed

V Nickl, E Schulz, E Salvador, L Trautmann, L Diener… (2022). Glioblastoma-Derived Three-Dimensional Ex Vivo Models to Evaluate Effects and Efficacy of Tumor Treating Fields (TTFields). *Cancers*.
Germany · Mouse · live · 350 µm · Slice culture PubMed

X Lin, NM Fisher, S Dogra, RK Senter, CW Reed… (2022). Differential activity of mGlu7 allosteric modulators provides evidence for mGlu7/8 heterodimers at hippocampal Schaffer collateral-CA1 synapses. *J Biol Chem*.
United States · Mouse · live · 400 µm · Electrophysiology PubMed

Y Ma, GH Qin, X Guo, N Hao, Y Shi, HF Li, X Zhao… (2022). Activation of δ-opioid receptors in anterior cingulate cortex alleviates affective pain in rats. *Neuroscience*.
China · Rat · live · 250 µm · Electrophysiology PubMed

YS Chun, MY Kim, SY Lee, MJ Kim, TJ Hong… (2022). MEK1/2 inhibition rescues neurodegeneration by TFEB-mediated activation of autophagic lysosomal function in a model of Alzheimer's Disease. *Mol Psychiatry*.
South Korea · Mouse · live · 300 µm · Electrophysiology PubMed

A Booeshaghi, Z Yao, C van Velthoven, K Smith… (2021). Isoform cell-type specificity in the mouse primary motor cortex. *Nature*.
United States · Mouse · live · 250 µm PubMed

B Krishnan, C Natarajan, KZ Bourne, L Alikhani… (2021). Chronic low dose neutron exposure results in altered neurotransmission properties of the hippocampus-prefrontal cortex axis in both mice and rats. *Int J Mol Sci*.
United States · Mouse · live · 350 µm · Electrophysiology PubMed

BA Copits, R Gowrishankar, PR O'Neill, JN Li… (2021). A photoswitchable GPCR-based opsin for presynaptic inhibition. *Neuron*.
United States · Mouse · live · 200-350 µm · Electrophysiology PubMed

BE Kalmbach, RD Hodge, NL Jorstad, S Owen… (2021). Signature morpho-electric, transcriptomic, and dendritic properties of human layer 5 neocortical pyramidal neurons. *Neuron*.
United States · Human, Non-Human Primate, Mouse · live · 300-350 µm · Electrophysiology PubMed

BJ Sullivan, PA Kipnis, BM Carter, LR Shao… (2021). Targeting ischemia-induced KCC2 hypofunction rescues refractory neonatal seizures and mitigates epileptogenesis in a mouse model. *Sci Signal*.
United States · Mouse · live · 350 µm · Electrophysiology PubMed

C Nguyen, S Mondoloni, T Le Borgne, I Centeno… (2021). Nicotine inhibits the VTA-to-amygdala dopamine pathway to promote anxiety. *Neuron*.
France · Mouse · live · 250 µm · Electrophysiology PubMed

CM Díaz-García, DJ Meyer, N Nathwani, M Rahman… (2021). The distinct roles of calcium in rapid control of neuronal glycolysis and the tricarboxylic acid cycle. *Elife*.
United States · Mouse · live · 275 µm · Electrophysiology PubMed

CW Wallace, NS Beatty, SA Hutcherson, HA Emmons… (2021). Replacing a Palatable High-Fat Diet with a Low-Fat Alternative Heightens κ-Opioid Receptor Control over Nucleus Accumbens Dopamine. *Nutrients*.
United States · Mouse · live · 300 µm PubMed

D Thevalingam, AA Naik, J Hrabe, DP McCloskey… (2021). Brain extracellular space of the naked mole-rat expands and maintains normal diffusion under ischemic conditions. *Brain Research*.
United States · Naked mole rat · live · 400-1000 µm · Electrophysiology PubMed

J Berg, SA Sorensen, JT Ting, JA Miller, T Chartrand… (2021). Human neocortical expansion involves glutamatergic neuron diversification. *Nature*.
United States · Mouse · live · 350 µm · Electrophysiology PubMed

JH Lee, J Kim, S Noh, H Lee, SY Lee, JY Mun, H Park… (2021). Astrocytes phagocytose adult hippocampal synapses for circuit homeostasis. *Nature*.
South Korea · Mouse · live · 400 µm · Electrophysiology PubMed

JK Mich, LT Graybuck, EE Hess, JT Mahoney, Y Kojima… (2021). Functional enhancer elements drive subclass-selective expression from mouse to primate neocortex. *Cell reports*.
United States · Human, Mouse · live · 350 µm · Slice culture PubMed

JS Thacker, D Andersen, S Liang, N Zieniewicz… (2021). Unlocking the brain: A new method for Western blot protein detection from fixed brain tissue. *Journal of Neuroscience Methods*.
Canada · Rat · live · 250 µm PubMed

KD Micheva, M Kiraly, MM Perez, DV Madison (2021). Conduction velocity along the local axons of parvalbumin interneurons correlates with the degree of axonal myelination. *Cerebral Cortex*.
United States · Mouse · live · 300 µm · Electrophysiology PubMed

KD Micheva, M Kiraly, MM Perez, DV Madison (2021). Extensive structural remodeling of the axonal arbors of parvalbumin basket cells during development in mouse neocortex. *J Neurosci*.
United States · Mouse · live · 300 µm · Electrophysiology PubMed

L Kettler, H Sid, C Schaub, K Lischka… (2021). AP-2δ Expression Kinetics in Multimodal Networks in the Developing Chicken Midbrain. *Frontiers in Neural Circuits*.
Germany · Chick · live · 500-1000 µm · IHC / ISH PubMed

L Xiao, DP Merullo, TMI Koch, M Cao, M Co… (2021). Expression of FoxP2 in the basal ganglia regulates vocal motor sequences in the adult songbird. *Nature Communications*.
United States · Bird · live · 500 µm PubMed

LR Shao, R Janicot… (2021). Na+-K+-ATPase functions in the developing hippocampus: regional differences in CA1 and CA3 neuronal excitability and role in epileptiform network bursting. *Journal of Neruophysiology*.
United States · Rat · live · 350 µm · Electrophysiology PubMed

M Dongelmans, R Durand-de Cuttoli, C Nguyen… (2021). Chronic nicotine increases midbrain dopamine neuron activity and biases individual strategies towards reduced exploration in mice. *Nature Communications*.
France · Mouse · live · 250 µm · Electrophysiology PubMed

MM Maneshi, AB Toth, T Ishii, K Hori, S Tsujikawa… (2021). Orai1 channels are essential for amplification of glutamate-evoked Ca2+ signals in dendritic spines to regulate working and associative memory. *Cell Reports*.
United States · Mouse · live · 350 µm · Electrophysiology PubMed

N Massey, D Shrestha, SM Bhat, N Kondru… (2021). Organic dust-induced mitochondrial dysfunction could be targeted via cGAS-STING or cytoplasmic NOX-2 inhibition using microglial cells and brain slice culture …. *Cell and Tissue Research*.
United States · Mouse · live · 350 µm · Slice culture PubMed

QW Wang, YH Wang, B Wang, Y Chen, SY Lu… (2021). Synaptotagmin-7–mediated activation of spontaneous NMDAR currents is disrupted in bipolar disorder susceptibility variants. *PLoS biology*.
China · Mouse · live · 300 µm · Electrophysiology PubMed

SM Chou, KX Li, MY Huang, C Chen, YHL King, GG Li… (2021). Kv1. 1 channels regulate early postnatal neurogenesis in mouse hippocampus via the TrkB signaling pathway. *Elife*.
Taiwan · Mouse · live · 250 µm · Electrophysiology PubMed

SS Salile, T Abula (2021). In vitro and In vivo Anticonvulsant Effect of Hydroalcoholic Extract of Moringa stenopetala in Mice Models. *Journal of Complementary and Alternative Medicine*.
Mouse · live · 400 µm · Electrophysiology

T Feng, C Alicea, V Pham, A Kirk… (2021). Experience-dependent inhibitory plasticity is mediated by CCK+ basket cells in the developing dentate gyrus. *J Neurosci*.
United States · Mouse · live · 300 µm · Electrophysiology PubMed

VP Mathis, M Williams, C Fillinger, PJ Kenny (2021). Networks of habenula-projecting cortical neurons regulate cocaine seeking. *Science advances*.
United States · Mouse · live · 300 µm · Electrophysiology PubMed

W Huang, W Zuo, L Chen, L Wang… (2021). Acetaldehyde excitation of lateral habenular neurons via multiple cellular mechanisms. *J Neurosci*.
United States · Rat · live · 250 µm · Electrophysiology PubMed

W Zuo, Q Zuo, L Wu, Q Mei, M Shah, J Zheng, D Li… (2021). Roles of corticotropin-releasing factor signaling in the lateral habenula in anxiety-like and alcohol drinking behaviors in male rats. *Neurobiology of Stress*.
United States · Rat · live · 250 µm · Electrophysiology PubMed

Y Shi, J Lv, L Chen, G Luo, M Tao, J Pan… (2021). Phosphodiesterase-4D Knockdown in the Prefrontal Cortex Alleviates Memory Deficits and Synaptic Failure in Mouse Model of Alzheimer's Disease. *Front Aging Neurosci*.
China · Mouse · live · 350 µm · Electrophysiology PubMed

Y Xiao, L Xie, QY Xu, L Chen, H Chen… (2021). Neuroscience of Disease: Transcranial direct current stimulation relieves visceral hypersensitivity via normalizing GluN2B expression and neural activity in …. *J Neurophysiol*.
China · Rat · live · 350 µm · Electrophysiology PubMed

Y Xiao, L Xie, QY Xu, L Chen, H Chen… (2021). Transcranial direct current stimulation relieves visceral hypersensitivity via normalizing GluN2B expression and neural activity in anterior cingulate cortex. *Journal of Neurophysiology*.
China · Rat · live · 350 µm · Electrophysiology PubMed

Y Zheng, L Zhao, L Dong, C Tian, P Xia… (2021). The Time-Dependence of Three Different Modes of ELF-EMF Stimulation on LTP at Schaffer Collateral-CA1 Synapses. *Bioelectromagnetics*.
China · Rat · live · 400 µm PubMed

Y Zheng, P Xia, L Dong, L Tian… (2021). Effects of modulation on sodium and potassium channel currents by extremely low frequency electromagnetic fields stimulation on hippocampal CA1 pyramidal cells. *Bioelectromagnetics*.
China · Rat · live · 400 µm · Electrophysiology PubMed

Z Yao, CTJ van Velthoven, TN Nguyen, J Goldy… (2021). A taxonomy of transcriptomic cell types across the isocortex and hippocampal formation. *Cell*.
United States · Mouse · live · 250-350 µm PubMed

Z Yao, H Liu, F Xie, S Fischer, RS Adkins, AI Aldridge… (2021). A transcriptomic and epigenomic cell atlas of the mouse primary motor cortex. *Nature*.
United States · Mouse · live · 250-350 µm PubMed

Anderson AG, Kulkarni A, Harper M, Konopka G. (2020). Single-Cell Analysis of Foxp1-Driven Mechanisms Essential for Striatal Development. *Cell Rep*.
United States · Mouse · live · 500 µm · Single-cell RNA-sequencing PubMed

Bunner W, Landry T, Laing BT, Li P, Rao Z, Yuan Y, Huang H. (2020). ARC(AgRP/NPY) Neuron Activity Is Required for Acute Exercise-Induced Food Intake in Un-Trained Mice. *Front Physiol*.
United States · Mouse · live · 300 µm · Electrophysiology PubMed

C Linghu, SL Johnson, PA Valdes, OA Shemesh… (2020). Spatial multiplexing of fluorescent reporters for imaging signaling network dynamics. *Cell*.
United States · Mouse · live · 300 µm · Electrophysiology PubMed

CT Werner, S Mitra, BD Auerbach… (2020). Neuroadaptations in the dorsal hippocampus underlie cocaine seeking during prolonged abstinence. *PNAS*.
United States · Rat · live · 350 µm · Electrophysiology PubMed

Chen AN, Meliza CD. (2020). Experience- and Sex-Dependent Intrinsic Plasticity in the Zebra Finch Auditory Cortex during Song Memorization. *J Neurosci*.
United States · Bird · live · 300 µm · Electrophysiology PubMed

Chen S, Kadakia F, Davidson S. (2020). Group II metabotropic glutamate receptor expressing neurons in anterior cingulate cortex become sensitized after inflammatory and neuropathic pain. *Mol Pain*.
United States · Mouse · live · 300 µm · Electrophysiology PubMed

Co M, Hickey SL, Kulkarni A, Harper M, Konopka G. (2020). Cortical Foxp2 Supports Behavioral Flexibility and Developmental Dopamine D1 Receptor Expression. *Cereb Cortex*.
United States · Mouse · live · 400 µm · Single-cell RNA sequencing PubMed

Ding SL, Yao Z, Hirokawa KE, Nguyen TN, Graybuck LT, Fong O, Bohn P, Ngo K, Smith KA, Koch C, Phillips JW, Lein ES, Harris JA, Tasic B, Zeng H. (2020). Distinct Transcriptomic Cell Types and Neural Circuits of the Subiculum and Prosubiculum along the Dorsal-Ventral Axis. *Cell Rep*.
United States · Mouse · live · 250 µm · Single cell isolatio for SMART-sequencing PubMed

Fennell AM, Pitts EG, Sexton LL, Ferris MJ. (2020). Phasic Dopamine Release Magnitude Tracks Individual Differences in Sensitization of Locomotor Response following a History of Nicotine Exposure. *Sci Rep*.
United States · Rat · live · 400 µm · Ex vivo fast scan cyclic voltammetry PubMed

Fisher NM, Gould RW, Gogliotti RG, McDonald AJ, Badivuku H, Chennareddy S, Buch AB, Moore AM, Jenkins MT, Robb WH, Lindsley CW, Jones CK, Conn PJ, Niswender CM. (2020). Phenotypic profiling of mGlu(7) knockout mice reveals new implications for neurodevelopmental disorders. *Genes Brain Behav*.
United States · Mouse · live · 400 µm · Electrophysiology PubMed

Grippo RM, Tang Q, Zhang Q, Chadwick SR, Gao Y, Altherr EB, Sipe L, Purohit AM, Purohit NM, Sunkara MD, Cios KJ, Sidikpramana M, Spano AJ, Campbell JN, Steele AD, Hirsh J, Deppmann CD, Wu M, Scott MM, Gí_ler AD. (2020). Dopamine Signaling in the Suprachiasmatic Nucleus Enables Weight Gain Associated with Hedonic Feeding. *Curr Biol*.
United States · Mouse · live · Unknown µm · Electrophysiology PubMed

Hodge RD, Miller JA, Novotny M, Kalmbach BE, Ting JT, Bakken TE, Aevermann BD, Barkan ER, Berkowitz-Cerasano ML, Cobbs C, Diez-Fuertes F, Ding SL, McCorrison J, Schork NJ, Shehata SI, Smith KA, Sunkin SM, Tran DN, Venepally P, Yanny AM, Steemers FJ, Phillips JW, Bernard A, Koch C, Lasken RS, Scheuermann RH, Lein ES. (2020). Transcriptomic evidence that von Economo neurons are regionally specialized extratelencephalic-projecting excitatory neurons. *Nat Commun*.
United States · Mouse, Human · live · 300 µm · Electrophysiology PubMed

Howell, Rebecca D; Dominguez-Lopez, Sergio; Ocañas, Sarah; Freeman, Willard M; Beckstead, Michael J; (2020). Female mice are resilient to age-related decline of substantia nigra dopamine neuron firing parameters. *Neurobiology*

of ….
United States · Mouse · live · 200 µm · Electrophysiology PubMed

J Wang, T Li, JL Wang, Z Xu, W Meng, QF Wu (2020). Talpid3-Mediated Centrosome Integrity Restrains Neural Progenitor Delamination to Sustain Neurogenesis by Stabilizing Adherens Junctions. *Cell Reports*.
Mouse · live · 250 µm · Imaging PubMed

JW Cao, W Guan, YC Yu, Y Fu (2020). Synaptic Transmission from Somatostatin-expressing Interneurons to Excitatory Neurons Mediated by α5-subunit-containing GABAA Receptors in the Developing …. *Neuroscience*.
China · Mouse · live · 300 µm · Electrophysiology PubMed

K Hori, S Tsujikawa, MM Novakovic… (2020). Regulation of chemoconvulsant-induced seizures by store-operated Orai1 channels. *Journal of Physiology*.
United States · Mouse · live · 300 µm · Electrophysiology PubMed

Kim EJ, Zhang Z, Huang L, Ito-Cole T, Jacobs MW, Juavinett AL, Senturk G, Hu M, Ku M, Ecker JR, Callaway EM. (2020). Extraction of Distinct Neuronal Cell Types from within a Genetically Continuous Population. *Neuron*.
United States · Mouse · live · 350 µm · Immunohistochemistry PubMed

Kim Y, Jang YN, Kim JY, Kim N, Noh S, Kim H, Queenan BN, Bellmore R, Mun JY, Park H, Rah JC, Pak DTS, Lee KJ. (2020). Microtubule-associated protein 2 mediates induction of long-term potentiation in hippocampal neurons. *FASEB J*.
South Korea · Mouse · live · 400 µm · Electrophysiology PubMed

Kondru N, Manne S, Kokemuller R, Greenlee J, Greenlee MHW, Nichols T, Kong Q, Anantharam V, Kanthasamy A, Halbur P, Kanthasamy AG. (2020). An Ex Vivo Brain Slice Culture Model of Chronic Wasting Disease: Implications for Disease Pathogenesis and Therapeutic Development. *Sci Rep*.
United States · Mouse · live · 350 µm · Slice culture PubMed

Krishnan B, Sallam HS, Tumurbataar B, Saieva S, Baymon D, Tuvdendorj D, Micci MA, Abate N, Taglialatela G. (2020). Amelioration of hippocampal dysfunction by adipose tissue-targeted stem cell transplantation in a mouse model of type 2 diabetes. *J Neurochem*.
United States · Mouse · live · 350 µm · Electrophysiology PubMed

Mancia Leon WR, Spatazza J, Rakela B, Chatterjee A, Pande V, Maniatis T, Hasenstaub AR, Stryker MP, Alvarez-Buylla A. (2020). Clustered gamma-protocadherins regulate cortical interneuron programmed cell death. *Elife*.
United States · Mouse · live · 200 µm · Electrophysiology PubMed

NW Gouwens, SA Sorensen, F Baftizadeh, A Budzillo… (2020). Integrated morphoelectric and transcriptomic classification of cortical GABAergic cells. *Cell*.
United States · Mouse · live · 350 µm · Electrophysiology PubMed

Pitts EG, Stowe TA, Christensen BA, Ferris MJ. (2020). Comparing dopamine release, uptake, and D2 autoreceptor function across the ventromedial to dorsolateral striatum in adolescent and adult male and female rats. *Neuropharmacology*.
United States · Rat · live · 400 µm · Ex vivo voltammetry PubMed

Q Wu, MA Shaikh, ES Meymand, B Zhang, KC Luk… (2020). Neuronal activity modulates alpha-synuclein aggregation and spreading in organotypic brain slice cultures and in vivo. *Acta neuropathologica*.
United States · Mouse · live · 350 µm · Slice culture PubMed

Qian, Yong; Cosio, Danielle M Orozco; Piatkevich, Kiryl D; Aufmkolk, Sarah; Su, Wan-Chi; Celike, Orhan T; Schohl, Anne; Murdock, Mitchell H; Aggarwal, Abhi; Chang, Yu-Fen; (2020). Improved genetically encoded near-infrared fluorescent calcium ion indicators for in vivo imaging. *PLoS Biology*.
Canada · Mouse · live · 300 µm · Imaging PubMed

S Calovi, P Mut-Arbona, P Tod, A Iring… (2020). P2X7 receptor-dependent layer-specific changes in neuron-microglia reactivity in the prefrontal cortex of a phencyclidine induced mouse model of …. *Frontiers in Molecular Neuroscience*.
Hungary · Mouse · live · 300 µm · Electrophysiology PubMed

SY Cooper, AT Akers, BJ Henderson (2020). Green apple e-cigarette flavorant farnesene triggers reward-related behavior by promoting high-sensitivity nAChRs in the ventral tegmental area. *eNeuro*.
United States · Mouse · live · 250 µm · Electrophysiology PubMed

Shemesh OA, Linghu C, Piatkevich KD, Goodwin D, Celiker OT, Gritton HJ, Romano MF, Gao R, Yu CJ, Tseng HA, Bensussen S, Narayan S, Yang CT, Freifeld L, Siciliano CA, Gupta I, Wang J, Pak N, Yoon YG, Ullmann JFP, Guner-Ataman B, Noamany H, Sheinkopf ZR, Park WM, Asano S, Keating AE, Trimmer JS, Reimer J, Tolias AS, Bear MF, Tye KM, Han X, Ahrens MB, Boyden ES. (2020). Precision Calcium Imaging of Dense Neural Populations via a Cell-Body-Targeted Calcium Indicator. *Neuron.*
United States · Mouse · live · 300 µm · Electrophysiology PubMed

Srivastava AK , Roy Choudhury S , Karmakar S . (2020). Melatonin/polydopamine nanostructures for collective neuroprotection-based Parkinson's disease therapy. *Biomater Sci.*
India · Mouse · live · 400-500 µm · Culture PubMed

Srivastava AK, Roy Choudhury S, Karmakar S. (2020). Near-Infrared Responsive Dopamine/Melatonin-Derived Nanocomposites Abrogating in Situ Amyloid '_ Nucleation, Propagation, and Ameliorate Neuronal Functions. *ACS Appl Mater Interfaces.*
Mouse · live · 400 µm · Culture PubMed

Xin H, Liu Z, Buller B, Li Y, Golembieski W, Gan X, Wang F, Lu M, Ali MM, Zhang ZG, Chopp M. (2020). MiR-17-92 enriched exosomes derived from multipotent mesenchymal stromal cells enhance axon-myelin remodeling and motor electrophysiological recovery after stroke. *J Cereb Blood Flow Metab.*
United States · Rat · live · 250 µm · Culture PubMed

Zions M, Meehan EF, Kress ME, Thevalingam D, Jenkins EC, Kaila K, Puskarjov M, McCloskey DP. (2020). Nest Carbon Dioxide Masks GABA-Dependent Seizure Susceptibility in the Naked Mole-Rat. *Curr Biol.*
United States · Naked mole rat · live · 400 µm · Electrophysiology PubMed

Askoxylakis V, Ferraro GB, Badeaux M, Kodack DP, Kirst I, Shankaraiah RC, Wong CSF, Duda DG, Fukumura D, Jain RK. (2019). Dual endothelin receptor inhibition enhances T-DM1 efficacy in brain metastases from HER2-positive breast cancer. *NPJ Breast Cancer.*
United States · Mouse · live · 300 µm · Culture PubMed

Avelar AJ, Akers AT, Baumgard ZJ, Cooper SY, Casinelli GP, Henderson BJ. (2019). Why flavored vape products may be attractive: Green apple tobacco flavor elicits reward-related behavior, upregulates nAChRs on VTA dopamine neurons, and alters midbrain dopamine and GABA neuron function. *Neuropharmacology.*
United States · Mouse · live · 250 µm · Electrophysiology PubMed

Bittar A, Bhatt N, Hasan TF, Montalbano M, Puangmalai N, McAllen S, Ellsworth A, Carretero Murillo M, Taglialatela G, Lucke-Wold B, Logsdon A, Rosen C, Turner RC, Kayed R. (2019). Neurotoxic tau oligomers after single versus repetitive mild traumatic brain injury. *Brain Commun.*
United States · Mouse · live · 350 µm · Electrophysiology PubMed

Bourne KZ, Natarajan C, Perez CXM, Tumurbaatar B, Taglialatela G, Krishnan B. (2019). Suppressing aberrant phospholipase D1 signaling in 3xTg Alzheimer's disease mouse model promotes synaptic resilience. *Sci Rep.*
United States · Mouse · live · 350 µm · Electrophysiology PubMed

Burman RJ, Selfe JS, Lee JH, van den Berg M, Calin A, Codadu NK, Wright R, Newey SE, Parrish RR, Katz AA, Wilmshurst JM, Akerman CJ, Trevelyan AJ, Raimondo JV. (2019). Excitatory GABAergic signalling is associated with benzodiazepine resistance in status epilepticus. *Brain.*
South Africa · Mouse · live · 400 µm · Electrophysiology PubMed

Comerota MM, Tumurbaatar B, Krishnan B, Kayed R, Taglialatela G. (2019). Near Infrared Light Treatment Reduces Synaptic Levels of Toxic Tau Oligomers in Two Transgenic Mouse Models of Human Tauopathies. *Mol Neurobiol.*
United States · Mouse · live · 350 µm · Electrophysiology PubMed

Dao NC, Brockway DF, Crowley NA. (2019). In Vitro Optogenetic Characterization of Neuropeptide Release from Prefrontal Cortical Somatostatin Neurons. *Neuroscience.*
United States · Mouse · live · 150-300 µm · Electrophysiology PubMed

Franklin W, Krishnan B, Taglialatela G. (2019). Chronic synaptic insulin resistance after traumatic brain injury abolishes insulin protection from amyloid beta and tau oligomer-induced synaptic dysfunction. *Scientific reports.*
United States · Rat · live · 450 µm · Electrophysiology PubMed

Goussakov I, Synowiec S, Yarnykh V, Drobyshevsky A. (2019). Immediate and delayed decrease of long term potentiation and memory deficits after neonatal intermittent hypoxia. *Int J Dev Neurosci.*
United States · Mouse · live · 300 µm · Electrophysiology PubMed

Gouwens NW, Sorensen SA, Berg J, Lee C, Jarsky T, Ting J, et al. (2019). Classification of electrophysiological and morphological neuron types in the mouse visual cortex. *Nat Neurosci.*
United States · Mouse · live · 350 µm · Electrophysiology PubMed

Hodge RD, Bakken TE, Miller JA, Smith KA, Barkan ER, Graybuck LT, et al. (2019). Conserved cell types with divergent features in human versus mouse cortex. *Nature.*
United States · Human · live · NS µm · Single nucleus RNA-sequencing PubMed

Joseph DJ, Liu C, Peng J, Liang G, Wei H. (2019). Isoflurane mediated neuropathological and cognitive impairments in the triple transgenic Alzheimer's mouse model are associated with hippocampal synaptic deficits in an age-dependent manner. *PLoS One.*
United States · Mouse · live · 400 µm · Electrophysiology PubMed

Kloos M, Weigel S, Luksch H. (2019). Anatomy and Physiology of Neurons in Layer 9 of the Chicken Optic Tectum. *Front Neural Circuits.*
Germany · Chick · live · 500-2000 µm · Electrophysiology PubMed

Kolb I, Landry CR, Yip MC, Lewallen CF, Stoy WA, Lee J, Felouzis A, Yang B, Boyden ES, Rozell CJ, Forest CR. (2019). PatcherBot: a single-cell electrophysiology robot for adherent cells and brain slices. *J Neural Eng.*
United States · Mouse · live · 300 µm · Electrophysiology PubMed

Kole K, Celikel T. (2019). Neocortical Microdissection at Columnar and Laminar Resolution for Molecular Interrogation. *Curr Protoc Neurosci.*
Netherlands · Mouse · live · 300-400 µm · Microdissection, RNA sequencing PubMed

Kole K, Zhang Y, Jansen EJR, Brouns T, Bijlsma A, Calcini N, Yan X, Lantyer ADS, Celikel T. (2019). Assessing the utility of Magneto to control neuronal excitability in the somatosensory cortex. *Nat Neurosci.*
Netherlands · Mouse · live · 300 µm · Electrophysiology PubMed

Kurz A, Xu W, Wiegel P, Leukel C, N Baker S. (2019). Non-invasive assessment of superficial and deep layer circuits in human motor cortex. *J Physiol.*
Germany · Non-Human Primate · live · 450 µm · Electrophysiology PubMed

Li W, Zuo W, Wu W, Zuo QK, Fu R, Wu L, Zhang H, Ndukwe M, Ye JH. (2019). Activation of glycine receptors in the lateral habenula rescues anxiety- and depression-like behaviors associated with alcohol withdrawal and reduces alcohol intake in rats. *Neuropharmacology.*
United States · Rat · live · 250 µm · Electrophysiology PubMed

Lloyd JT, Martini A, McDouall A, Sood R, Freestone PS, Mercuri NB, Lipski J. (2019). Electrophysiological Characterization of Novel Effects of the Uptake-2 Blocker Decynium-22 (D-22) on Dopaminergic Neurons in the Substantia Nigra Pars Compacta. *Neuroscience.*
Mouse · live · 230 µm · Electrophysiology PubMed

Lv L, Liu Y, Xie J, Wu Y, Zhao J, Li Q, Zhong Y. (2019). Interplay between ‘±2-chimaerin and Rac1 activity determines dynamic maintenance of long-term memory. *Nat Commun.*
China · Mouse · live · 300 µm · Electrophysiology PubMed

Micci MA, Krishnan B, Bishop E, Zhang WR, Guptarak J, Grant A, Zolochevska O, Tumurbaatar B, Franklin W, Marino C, Widen SG, Luthra A, Kernie SG, Taglialatela G. (2019). Hippocampal stem cells promotes synaptic resistance to the dysfunctional impact of amyloid beta oligomers via secreted exosomes. *Mol Neurodegener.*
United States · Mouse · live · 350 µm · Electrophysiology PubMed

Piatkevich KD, Bensussen S, Tseng HA, Shroff SN, Lopez-Huerta VG, Park D, Jung EE, Shemesh OA, Straub C, Gritton HJ, Romano MF, Costa E, Sabatini BL, Fu Z, Boyden ES, Han X. (2019). Population imaging of neural activity in awake behaving mice. *Nature.*
United States · Mouse · live · 300 µm · Electrophysiology PubMed

Priya R, Rakela B, Kaneko M, Spatazza J, Larimer P, Hoseini MS, Hasenstaub AR, Alvarez-Buylla A, Stryker MP. (2019). Vesicular GABA Transporter Is Necessary for Transplant-Induced Critical Period Plasticity in Mouse Visual Cortex. *J Neurosci.*
United States · Mouse · live · 300 µm · Electrophysiology PubMed

Qian Y, Piatkevich KD, Mc Larney B, Abdelfattah AS, Mehta S, Murdock MH, Gottschalk S, Molina RS, Zhang W, Chen Y, Wu J, Drobizhev M, Hughes TE, Zhang J, Schreiter ER, Shoham S, Razansky D, Boyden ES, Campbell RE. (2019). A genetically encoded near-infrared fluorescent calcium ion indicator. *Nat Methods.*

Canada · Mouse · live · 300 µm · Electrophysiology PubMed

Toth AB, Hori K, Novakovic MM, Bernstein NG, Lambot L, Prakriya M. (2019). CRAC channels regulate astrocyte Ca(2+) signaling and gliotransmitter release to modulate hippocampal GABAergic transmission. *Sci Signal.*
United States · Mouse · live · 250-300 µm · Electrophysiology PubMed

Xiang Z, Lv X, Maksymetz J, Stansley BJ, Ghoshal A, Gogliotti RG, Niswender CM, Lindsley CW, Conn PJ. (2019). mGlu(5) Positive Allosteric Modulators Facilitate Long-Term Potentiation via Disinhibition Mediated by mGlu(5)-Endocannabinoid Signaling. *ACS Pharmacol Transl Sci.*
United States · Mouse · live · 400 µm · Electrophysiology PubMed

Yu Q, Shao D, Zhang R, Ouyang W, Zhang Z. (2019). Effects of drinking water fluorosis on L-type calcium channel of hippocampal neurons in mice. *Chemosphere.*
China · Mouse · live · 250 µm · Electrophysiology PubMed

Yu W, Yen YC, Lee YH, Tan S, Xiao Y, Lokman H, Ting AKT, Ganegala H, Kwon T, Ho WK, Je HS. (2019). Prenatal selective serotonin reuptake inhibitor (SSRI) exposure induces working memory and social recognition deficits by disrupting inhibitory synaptic networks in male mice. *Mol Brain.*
Singapore · Mouse · live · 300 µm · Electrophysiology PubMed

Zheng Y, Cheng J, Dong L, Ma X, Kong Q. (2019). Effects of exposure to extremely low frequency electromagnetic fields on hippocampal long-term potentiation in hippocampal CA1 region. *Biochem Biophys Res Commun.*
Rat · live · 400 µm · Electrophysiology PubMed

Zheng Y, Ma XX, Dong L, Gao Y, Tian L. (2019). Effects of single- and hybrid-frequency extremely low-frequency electromagnetic field stimulations on long-term potentiation in the hippocampal Schaffer collateral pathway. *Int J Radiat Biol.*
Rat · live · 350-400 µm · Electrophysiology PubMed

Zuo W, Wu L, Mei Q, Zuo Q, Zhou Z, Fu R, Li W, Wu W, Matthew L, Ye JH. (2019). Adaptation in 5-HT(2) receptors-CaMKII signaling in lateral habenula underlies increased nociceptive-sensitivity in ethanol-withdrawn rats. *Neuropharmacology.*
Rat · live · 250 µm · Electrophysiology PubMed

Bakken TE, Hodge RD, Miller JA, Yao Z, Nguyen TN, Aevermann B, Barkan E, Bertagnolli D, Casper T, Dee N, Garren E, Goldy J, Graybuck LT, Kroll M, Lasken RS, Lathia K, Parry S, Rimorin C, Scheuermann RH, Schork NJ, Shehata SI, Tieu M, Phillips JW, Bernard A, Smith KA, Zeng H, Lein ES, Tasic B. (2018). Single-nucleus and single-cell transcriptomes compared in matched cortical cell types. *PLoS One.*
United States · Mouse · live · 250 µm · Whole cell dissociation/dissection; RNA sequencing PubMed

Boldog E, Bakken TE, Hodge RD, Novotny M, Aevermann BD, Baka J, Bordí© S, Close JL, Diez-Fuertes F, Ding SL, Faragí_ N, Kocsis íK, Kovíçcs B, Maltzer Z, McCorrison JM, Miller JA, Molníçr G, Olíçh G, Ozsvíçr A, Rí_zsa M, Shehata SI, Smith KA, Sunkin SM, Tran DN, Venepally P, Wall A, Puskíçs LG, Barzí_ P, Steemers FJ, Schork NJ, Scheuermann RH, Lasken RS, Lein ES, Tamíçs G. (2018). Transcriptomic and morphophysiological evidence for a specialized human cortical GABAergic cell type. *Nat Neurosci.*
Hungary · Human · live · 350 µm · In-situ hybridization PubMed

Borodovitsyna O, Flamini MD, Chandler DJ. (2018). Acute Stress Persistently Alters Locus Coeruleus Function and Anxiety-like Behavior in Adolescent Rats. *Neuroscience.*
United States · Rat · live · 200 µm · Electrophysiology PubMed

Chen AN, Meliza CD. (2018). Phasic and tonic cell types in the zebra finch auditory caudal mesopallium. *J Neurophysiol.*
United States · Bird · live · 300 µm · Electrophysiology PubMed

Durand-de Cuttoli R, Mondoloni S, Marti F, Lemoine D, Nguyen C, Naudí© J, d'Izarny-Gargas T, Pons S, Maskos U, Trauner D, Kramer RH, Faure P, Mourot A. (2018). Manipulating midbrain dopamine neurons and reward-related behaviors with light-controllable nicotinic acetylcholine receptors. *Elife.*
France · Mouse · live · 250 µm · Electrophysiology PubMed

Fisher, Nicole M; Gogliotti, Rocco G; Vermudez, Sheryl Anne D; Stansley, Branden J; Conn, P Jeffrey; Niswender, Colleen M; (2018). Genetic Reduction or Negative Modulation of mGlu7 Does Not Impact Anxiety and Fear Learning Phenotypes in a Mouse Model of MECP2 Duplication Syndrome. *ACS Chem Neurosci.*
United States · Mouse · live · 400 µm · Electrophysiology PubMed

Forget B, Scholze P, Langa F, Morel C, Pons S, Mondoloni S, Besson M, Durand-de Cuttoli R, Hay A, Tricoire L, Lambolez B, Mourot A, Faure P, Maskos U. (2018). A Human Polymorphism in CHRNA5 Is Linked to Relapse to Nicotine Seeking in Transgenic Rats. *Curr Biol.*
France · Rat · live · 250 µm · Electrophysiology PubMed

Garrido-Charad F, Vega-Zuniga T, Gutií©rrez-Ibíçí±ez C, Fernandez P, Lí_pez-Jury L, Gonzíçlez-Cabrera C, Karten HJ, Luksch H, Marí_n GJ. (2018). "Shepherd's crook" neurons drive and synchronize the enhancing and suppressive mechanisms of the midbrain stimulus selection network. *Proc Natl Acad Sci U S A.*
Chile · Chick · live · 1000 µm · Electrophysiology PubMed

Jhang J, Lee H, Kang MS, Lee HS, Park H, Han JH. (2018). Anterior cingulate cortex and its input to the basolateral amygdala control innate fear response. *Nat Commun.*
South Korea · Mouse · live · 400 µm · Electrophysiology PubMed

Krishnan B, Kayed R, Taglialatela G. (2018). Elevated phospholipase D isoform 1 in Alzheimer's disease patients' hippocampus: Relevance to synaptic dysfunction and memory deficits. *Alzheimers Dement (N Y).*
United States · Mouse · live · 350 µm · Electrophysiology PubMed

LR Shao, CE Stafstrom (2018). Glycolytic inhibition by 2-deoxy-D-glucose abolishes both neuronal and network bursts in an in vitro seizure model. *Journal of Neurophysiology.*
United States · Rat · live · 350 µm · Electrophysiology PubMed

Laing BT, Li P, Schmidt CA, Bunner W, Yuan Y, Landry T, Prete A, McClung JM, Huang H. (2018). AgRP/NPY Neuron Excitability Is Modulated by Metabotropic Glutamate Receptor 1 During Fasting. *Front Cell Neurosci.*
United States · Mouse · live · 200-300 µm · Electrophysiology PubMed

Lischka K, Yan J, Weigel S, Luksch H. (2018). Effects of early eye removal on the morphology of a multisensory neuron in the chicken optic tectum. *Brain Res.*
Germany · Chick · live · 1000 µm · Immunohistochemistry PubMed

Liu Y, Lv L, Wang L, Zhong Y. (2018). Social Isolation Induces Rac1-Dependent Forgetting of Social Memory. *Cell Rep.*
China · Mouse · live · 250 µm · Precision-cut tissue slices PubMed

Liu Y, Wang HY, Zhou L, Su Y, Shen WC. (2018). Biodistribution, activation, and retention of proinsulin-transferrin fusion protein in the liver: Mechanism of liver-targeting as an insulin prodrug. *J Control Release.*
Mouse · live · 300 µm · Electrophysiology PubMed

Nelson AD, Caballero-Floríçn RN, Rodrí_guez Dí_az JC, Hull JM, Yuan Y, Li J, Chen K, Walder KK, Lopez-Santiago LF, Bennett V, McInnis MG, Isom LL, Wang C, Zhang M, Jones KS, Jenkins PM. (2018). Ankyrin-G regulates forebrain connectivity and network synchronization via interaction with GABARAP. *Mol Psychiatry.*
United States · Mouse · live · 300-350 µm · Electrophysiology PubMed

Seeman SC, Campagnola L, Davoudian PA, Hoggarth A, Hage TA, Bosma-Moody A, Baker CA, Lee JH, Mihalas S, Teeter C, Ko AL, Ojemann JG, Gwinn RP, Silbergeld DL, Cobbs C, Phillips J, Lein E, Murphy G, Koch C, Zeng H, Jarsky T. (2018). Sparse recurrent excitatory connectivity in the microcircuit of the adult mouse and human cortex. *Elife.*
United States · Mouse, Human · live · 350 µm · Electrophysiology PubMed

Shao LR, Wang G, Stafstrom CE. (2018). The Glycolytic Metabolite, Fructose-1,6-bisphosphate, Blocks Epileptiform Bursts by Attenuating Voltage-Activated Calcium Currents in Hippocampal Slices. *Frontiers in Cellular Neuroscience.*
United States · Rat · live · 350 µm · Electrophysiology PubMed

Stansley BJ, Fisher NM, Gogliotti RG, Lindsley CW, Conn PJ, Niswender CM. (2018). Contextual Fear Extinction Induces Hippocampal Metaplasticity Mediated by Metabotropic Glutamate Receptor 5. *Cereb Cortex.*
United States · Mouse · live · 400 µm · Electrophysiology PubMed

Subramanian D, Pralong E, Daniel RT, Chacko AG, Stoop R, Babu KS. (2018). Gamma oscillatory activity in vitro: a model system to assess pathophysiological mechanisms of comorbidity between autism and epilepsy. *Transl Psychiatry.*
India · Rat · live · 450 µm · Electrophysiology PubMed

Tasic B, Yao Z, Graybuck LT, Smith KA, Nguyen TN, Bertagnolli D, et al. (2018). Shared and distinct transcriptomic cell types across neocortical areas. *Nature.*
United States · Mouse · live · 250 µm · Single-cell isolation; DNA sequencing PubMed

Terburg D, Scheggia D, Triana Del Rio R, Klumpers F, Ciobanu AC, Morgan B, Montoya ER, Bos PA, Giobellina G, van den Burg EH, de Gelder B, Stein DJ, Stoop R, van Honk J. (2018). The Basolateral Amygdala Is Essential for Rapid Escape: A Human and Rodent Study. *Cell*.
Netherlands · Rat · live · 350 µm · Electrophysiology PubMed

Ting JT, Kalmbach B, Chong P, de Frates R, Keene CD, Gwinn RP, Cobbs C, Ko AL, Ojemann JG, Ellenbogen RG, Koch C, Lein E. (2018). A robust ex vivo experimental platform for molecular-genetic dissection of adult human neocortical cell types and circuits. *Sci Rep*.
United States · Human · live · 350 µm · Electrophysiology PubMed

Ting JT, Lee BR, Chong P, Soler-Llavina G, Cobbs C, Koch C, Zeng H, Lein E. (2018). Preparation of Acute Brain Slices Using an Optimized N-Methyl-D-glucamine Protective Recovery Method. *J Vis Exp*.
United States · Mouse · live · 300 µm · Electrophysiology PubMed

Vega-Zuniga T, Trost D, Schicker K, Bogner EM, Luksch H. (2018). The Medial Ventrothalamic Circuitry: Cells Implicated in a Bimodal Network. *Front Neural Circuits*.
Germany · Chick · live · 1000 µm · Immunohistochemistry PubMed

Xu W, Baker SN. (2018). In vitro characterization of intrinsic properties and local synaptic inputs to pyramidal neurons in macaque primary motor cortex. *Eur J Neurosci*.
United Kingdom · Non-Human Primate · live · 450 µm · Electrophysiology PubMed

Zhang C, Xu Y, Chowdhary A, Fox D 3rd, Gurney ME, Zhang HT, Auerbach BD, Salvi RJ, Yang M, Li G, O'Donnell JM. (2018). Memory enhancing effects of BPN14770, an allosteric inhibitor of phosphodiesterase-4D, in wild-type and humanized mice. *Neuropsychopharmacology*.
United States · Mouse · live · 350 µm · Electrophysiology PubMed

Guan W, Cao JW, Liu LY, Zhao ZH, Fu Y, Yu YC. (2017). Eye opening differentially modulates inhibitory synaptic transmission in the developing visual cortex. *Elife*.
China · Mouse · live · 300 µm · Electrophysiology PubMed

Gusachenko I, Nylk J, Tello JA, Dholakia K. (2017). Multimode fibre based imaging for optically cleared samples. *Biomed Opt Express*.
United Kingdom · Mouse · live · 300 µm · Optically cleared tissue sections PubMed

Li J, Kang S, Fu R, Wu L, Wu W, Liu H, Gregor D, Zuo W, Bekker A, Ye JH. (2017). Inhibition of AMPA receptor and CaMKII activity in the lateral habenula reduces depressive-like behavior and alcohol intake in rats. *Neuropharmacology*.
United States · Rat · live · 300 µm · Electrophysiology PubMed

Long B, Zhou Z, Cetin A, Ting J, Gwinn R, Tasic B, Daigle T, Lein E, Zeng H, Saggau P, Hawrylycz M, Peng H. (2017). SmartScope2: Simultaneous Imaging and Reconstruction of Neuronal Morphology. *Sci Rep*.
United States · Human · live · 350 µm · Electrophysiology PubMed

Moehle MS, Pancani T, Byun N, Yohn SE, Wilson GH 3rd, Dickerson JW, Remke DH, Xiang Z, Niswender CM, Wess J, Jones CK, Lindsley CW, Rook JM, Conn PJ. (2017). Cholinergic Projections to the Substantia Nigra Pars Reticulata Inhibit Dopamine Modulation of Basal Ganglia through the M(4) Muscarinic Receptor. *Neuron*.
United States · Mouse · live · 300 µm · Electrophysiology PubMed

Niederleitner B, Gutierrez-Ibanez C, Krabichler Q, Weigel S, Luksch H. (2017). A Novel Relay Nucleus Between the InferiorColliculus and the Optic Tectum inthe Chicken (Gallus gallus). *J Comp Neurol*.
Chick · live · 500 µm · Electrophysiology PubMed

Zheng Y, Dou JR, Gao Y, Dong L, Li G. (2017). Effects of 15 Hz square wave magnetic fields on the voltage-gated sodium and potassium channels in prefrontal cortex pyramidal neurons. *Int J Radiat Biol*.
Mouse · live · 400-500 µm · Electrophysiology PubMed

Zuo W, Wang L, Chen L, KrnjeviÛˆ K, Fu R, Feng X, He W, Kang S, Shah A, Bekker A, Ye JH. (2017). Ethanol potentiates both GABAergic and glutamatergic signaling in the lateral habenula. *Neuropharmacology*.
United States · Rat · live · 250 µm · Electrophysiology PubMed

Buffington SA, Di Prisco GV, Auchtung TA, Ajami NJ, Petrosino JF, Costa-Mattioli M. (2016). Microbial Reconstitution Reverses Maternal Diet-Induced Social and Synaptic Deficits in Offspring. *Cell*.
United States · Mouse · live · 225-300 µm · Electrophysiology PubMed

Carr GV, Chen J, Yang F, Ren M, Yuan P, Tian Q, Bebensee A, Zhang GY, Du J, Glineburg P, Xun R, Akhile O, Akuma D, Pickel J, Barrow JC, Papaleo F, Weinberger DR. (2016). KCNH2-3.1 expression impairs cognition and alters neuronal function in a model of molecular pathology associated with schizophrenia. *Mol Psychiatry.*
United States · Mouse · live · 300 µm · Electrophysiology PubMed

Fox ME, Bucher ES, Johnson JA, Wightman RM. (2016). Medullary Norepinephrine Projections Release Norepinephrine into the Contralateral Bed Nucleus of the Stria Terminalis. *ACS Chem Neurosci.*
United States · Rat · live · 300 µm · Imaging PubMed

Grannan MD, Mielnik CA, Moran SP, Gould RW, Ball J, Lu Z, Bubser M, Ramsey AJ, Abe M, Cho HP, Nance KD, Blobaum AL, Niswender CM, Conn PJ, Lindsley CW, Jones CK. (2016). Prefrontal Cortex-Mediated Impairments in a Genetic Model of NMDA Receptor Hypofunction Are Reversed by the Novel M(1) PAM VU6004256. *ACS Chem Neurosci.*
United States · Mouse · live · 400 µm · Electrophysiology PubMed

Guan YZ, Ye JH. (2016). Glycine blocks long-term potentiation of GABAergic synapses in the ventral tegmental area. *Neuroscience.*
United States · Rat · live · 200-250 µm · Electrophysiology PubMed

Huang W, Placzek AN, Viana Di Prisco G, Khatiwada S, Sidrauski C, KrnjeviÛˆ K, Walter P, Dani JA, Costa-Mattioli M. (2016). Translational control by eIF2α phosphorylation regulates vulnerability to the synaptic and behavioral effects of cocaine. *Elife.*
United States · Mouse · live · 225-300 µm · Electrophysiology PubMed

Kirkpatrick DC, McKinney CJ, Manis PB, Wightman RM. (2016). Expanding neurochemical investigations with multi-modal recording: simultaneous fast-scan cyclic voltammetry, iontophoresis, and patch clamp measurements. *Analyst.*
United States · Rat · live · 300 µm · Electrophysiology PubMed

Kirkpatrick DC, Walton LR, Edwards MA, Wightman RM. (2016). Quantitative analysis of iontophoretic drug delivery from micropipettes. *Analyst.*
United States · Rat · live · 300 µm · Electrophysiology PubMed

Kirkpatrick DC, Wightman RM. (2016). Evaluation of Drug Concentrations Delivered by Microiontophoresis. *Anal Chem.*
United States · Rat · live · 300 µm PubMed

Klipec WD, Burrow KR, O'Neill C, Cao JL, Lawyer CR, Ostertag E, Fowler M, Bachtell RK, Illig KR, Cooper DC. (2016). Loss of the trpc4 gene is associated with a reduction in cocaine self-administration and reduced spontaneous ventral tegmental area dopamine neuronal activity, without deficits in learning for natural rewards. *Behav Brain Res.*
Rat · live · 250 µm · Electrophysiology PubMed

Kolson DR, Wan J, Wu J, Dehoff M, Brandebura AN, Qian J, Mathers PH, Spirou GA. (2016). Temporal patterns of gene expression during calyx of held development. *Dev Neurobiol.*
United States · Mouse · live · 200 µm · Electrophysiology PubMed

Li J, Zuo W, Fu R, Xie G, Kaur A, Bekker A, Ye JH. (2016). High Frequency Electrical Stimulation of Lateral Habenula Reduces Voluntary Ethanol Consumption in Rats. *Int J Neuropsychopharmacol.*
United States · Rat · live · 230-350 µm · Electrophysiology PubMed

Liu Y, Du S, Lv L, Lei B, Shi W, Tang Y, Wang L, Zhong Y. (2016). Hippocampal Activation of Rac1 Regulates the Forgetting of Object Recognition Memory. *Curr Biol.*
China · Mouse · live · 300 µm · Electrophysiology PubMed

Nylk J, McCluskey K, Aggarwal S, Tello JA, Dholakia K. (2016). Enhancement of image quality and imaging depth with Airy light-sheet microscopy in cleared and non-cleared neural tissue. *Biomed Opt Express.*
United Kingdom · Mouse · live · 400 µm · Imaging PubMed

Papaleo F, Yang F, Paterson C, Palumbo S, Carr GV, Wang Y, Floyd K, Huang W, Thomas CJ, Chen J, Weinberger DR, Law AJ. (2016). Behavioral, Neurophysiological, and Synaptic Impairment in a Transgenic Neuregulin1 (NRG1-IV) Murine Schizophrenia Model. *J Neurosci.*
Italy · Mouse · live · 300 µm · Electrophysiology PubMed

Pekala D, Szkudlarek H, Raastad M. (2016). Typical gray matter axons in mammalian brain fail to conduct action potentials faithfully at fever-like temperatures. *Physiol Rep.*

United States · Rat · live · 300 µm · Electrophysiology PubMed

Placzek AN, Molfese DL, Khatiwada S, Viana Di Prisco G, Huang W, Sidrauski C, KrnjeviÛˆ K, Amos CL, Ray R, Dani JA, Walter P, Salas R, Costa-Mattioli M. (2016). Translational control of nicotine-evoked synaptic potentiation in mice and neuronal responses in human smokers by eIF2α. *Elife*.
United States · Mouse · live · 225-300 µm · Electrophysiology PubMed

Placzek AN, Prisco GV, Khatiwada S, Sgritta M, Huang W, KrnjeviÛˆ K, Kaufman RJ, Dani JA, Walter P, Costa-Mattioli M. (2016). eIF2α-mediated translational control regulates the persistence of cocaine-induced LTP in midbrain dopamine neurons. *Elife*.
United States · Mouse · live · 225-300 µm · Electrophysiology PubMed

V Askoxylakis, GB Ferraro, DP Kodack… (2016). Preclinical efficacy of ado-trastuzumab emtansine in the brain microenvironment. *Journal of the National Cancer Institute*.
United States · Mouse · live · 200 µm · Slice culture PubMed

Xiao Y, Chen X, Zhang PA, Xu Q, Zheng H, Xu GY. (2016). TRPV1-mediated presynaptic transmission in basolateral amygdala contributes to visceral hypersensitivity in adult rats with neonatal maternal deprivation. *Sci Rep*.
China · Rat · live · 400 µm · Electrophysiology PubMed

Yang WZ, Liu TT, Cao JW, Chen XF, Liu X, Wang M, Su X, Zhang SQ, Qiu BL, Hu WX, Liu LY, Ma L, Yu YC. (2016). Fear Erasure Facilitated by Immature Inhibitory Neuron Transplantation. *Neuron*.
China · Mouse · live · 300-350 µm · Electrophysiology PubMed

Yao XH, Wang M, He XN, He F, Zhang SQ, Lu W, Qiu ZL, Yu YC. (2016). Electrical coupling regulates layer 1 interneuron microcircuit formation in the neocortex. *Nat Commun*.
China · Mouse · live · 200 µm · Electrophysiology PubMed

Yen CF, Harischandra DS, Kanthasamy A, Sivasankar S. (2016). Copper-induced structural conversion templates prion protein oligomerization and neurotoxicity. *Sci Adv*.
United States · Mouse · live · 350 µm · Slice culture PubMed

Zuo W, Zhang Y, Xie G, Gregor D, Bekker A, Ye JH. (2016). Serotonin stimulates lateral habenula via activation of the post- synaptic serotonin 2/3 receptors and transient receptor potential channels. *Neuropharmacology*.
United States · Rat · live · 250-300 µm · Electrophysiology PubMed

Chang AJ, Ortega FE, Riegler J, Madison DV, Krasnow MA. (2015). Oxygen regulation of breathing through an olfactory receptor activated by lactate. *Nature*.
United States · Mouse · live · 100 µm · Imaging PubMed

Jaafari N, Marret E, Canepari M. (2015). Using simultaneous voltage and calcium imaging to study fast Ca2+ channels. *Neurophotonics*.
France · Mouse · live · 250 µm · Electrophysiology PubMed

Kim S, Ma L, Unruh J, McKinney S, Yu CR. (2015). Intracellular chloride concentration of the mouse vomeronasal neuron. *BMC Neurosci*.
United States · Mouse · live · 100 µm · Electrophysiology PubMed

Klar R, Walker AG, Ghose D, Grueter BA, Engers DW, Hopkins CR, Lindsley CW, Xiang Z, Conn PJ, Niswender CM. (2015). Activation of Metabotropic Glutamate Receptor 7 Is Required for Induction of Long-Term Potentiation at SC-CA1 Synapses in the Hippocampus. *J Neurosci*.
United States · Mouse · live · 300-400 µm · Electrophysiology PubMed

Liu Y, Huang D, Wen R, Chen X, Yi H. (2015). Glycine receptor-mediated inhibition of medial prefrontal cortical pyramidal cells. *Biochem Biophys Res Commun*.
China · Rat · live · 250 µm · Electrophysiology PubMed

Lovelace JW, Corches A, Vieira PA, Hiroto AS, Mackie K, Korzus E. (2015). An animal model of female adolescent cannabinoid exposure elicits a long-lasting deficit in presynaptic long-term plasticity. *Neuropharmacology*.
United States · Mouse · live · 300 µm · Electrophysiology PubMed

Jaafari N, De Waard M, Canepari M. (2014). Imaging fast calcium currents beyond the limitations of electrode techniques. *Biophys J*.
France · Mouse · live · 250 µm · Electrophysiology PubMed

Jalan-Sakrikar N, Field JR, Klar R, Mattmann ME, Gregory KJ, Zamorano R, Engers DW, Bollinger SR, Weaver CD, Days EL, Lewis LM, Utley TJ, Hurtado M, Rigault D, Acher F, Walker AG, Melancon BJ, Wood MR, Lindsley CW, Conn

PJ, Xiang Z, Hopkins CR, Niswender CM. (2014). Identification of positive allosteric modulators VU0155094 (ML397) and VU0422288 (ML396) reveals new insights into the biology of metabotropic glutamate receptor 7. *ACS Chem Neurosci.*
United States · Mouse · live · 400 µm · Electrophysiology PubMed

Jin H, Kanthasamy A, Harischandra DS, Kondru N, Ghosh A, Panicker N, Anantharam V, Rana A, Kanthasamy AG. (2014). Histone hyperacetylation up-regulates protein kinase C‘Ç in dopaminergic neurons to induce cell death: relevance to epigenetic mechanisms of neurodegeneration in Parkinson disease. *J Biol Chem.*
United States · Mouse · live · 250 µm · Slice culture PubMed

Kirkpatrick DC, Edwards MA, Flowers PA, Wightman RM. (2014). Characterization of solute distribution following iontophoresis from a micropipet. *Anal Chem.*
United States · Rat · live · 300 µm PubMed

Kohashi T, Carlson BA. (2014). A fast BK-type KCa current acts as a postsynaptic modulator of temporal selectivity for communication signals. *Front Cell Neurosci.*
United States · Fish · live · 300 µm · Electrophysiology PubMed

Pekala D, Baginskas A, Szkudlarek HJ, Raastad M. (2014). Components of action potential repolarization in cerebellar parallel fibres. *J Physiol.*
United States · Rat · live · 300 µm · Electrophysiology PubMed

Pií±ol RA, Jameson H, Popratiloff A, Lee NH, Mendelowitz D. (2014). Visualization of oxytocin release that mediates paired pulse facilitation in hypothalamic pathways to brainstem autonomic neurons. *PLoS One.*
United States · Rat · live · 300 µm · Electrophysiology PubMed

Shi L, Rodrí_guez-Contreras A, Budansky Y, Pu Y, Nguyen TA, Alfano RR. (2014). Deep two-photon microscopic imaging through brain tissue using the second singlet state from fluorescent agent chlorophyll α in spinach leaf. *J Biomed Opt.*
United States · Rat · live · 200, 400, 450, 500 µm · Imaging PubMed

Ting JT, Daigle TL, Chen Q, Feng G. (2014). Acute brain slice methods for adult and aging animals: application of targeted patch clamp analysis and optogenetics. *Methods Mol Biol.*
United States · Mouse · live · 100-150; 300 µm · Electrophysiology PubMed

Yin S, Noetzel MJ, Johnson KA, Zamorano R, Jalan-Sakrikar N, Gregory KJ, Conn PJ, Niswender CM. (2014). Selective actions of novel allosteric modulators reveal functional heteromers of metabotropic glutamate receptors in the CNS. *J Neurosci.*
Australia · Rat · live · 300 µm · Electrophysiology PubMed

Chen-Roetling J, Lu X, Regan KA, Regan RF. (2013). A rapid fluorescent method to quantify neuronal loss after experimental intracerebral hemorrhage. *J Neurosci Methods.*
United States · Mouse · live · 300 µm · Imaging PubMed

Dergacheva O, Boychuk CR, Mendelowitz D. (2013). Developmental changes in GABAergic neurotransmission to presympathetic and cardiac parasympathetic neurons in the brainstem. *J Neurophysiol.*
United States · Rat · live · 300 µm · Electrophysiology PubMed

Fleming RL, Li Q, Risher ML, Sexton HG, Moore SD, Wilson WA, Acheson SK, Swartzwelder HS. (2013). Binge-Pattern Ethanol Exposure During Adolescence, butNot Adulthood, Causes Persistent Changes in GABAAReceptor-Mediated Tonic Inhibition in Dentate GranuleCells. *Alcohol Clin Exp Res.*
United States · Rat · live · 350 µm · Electrophysiology PubMed

Haddad-Tí_volli R, Szabí_ NE, Zhou X, Alvarez-Bolado G. (2013). Genetic manipulation of the mouse developing hypothalamus through in utero electroporation. *J Vis Exp.*
Mouse · live · Unknown µm · IHC / ISH PubMed

Holcomb PS, Hoffpauir BK, Hoyson MC, Jackson DR, Deerinck TJ, Marrs GS, Dehoff M, Wu J, Ellisman MH, Spirou GA. (2013). Synaptic inputs compete during rapid formation of the calyx of Held: a new model system for neural development. *J Neurosci.*
United States · Mouse · live · 250-350 µm · Electrophysiology PubMed

Jaafari N, Henson M, Graham J, Canepari M. (2013). Economic and simple system to combine single-spot photolysis and whole-field fluorescence imaging. *J Biomed Opt.*
France · Mouse · live · 250 µm · Electrophysiology PubMed

Liu CH, Yang J, Ren JQ, Liu CM, You Z, Liu PK. (2013). MRI reveals differential effects of amphetamine exposure on neuroglia in vivo. *FASEB J.*
United States · Mouse · live · 60 µm · Imaging PubMed

Liu YW, Zuo W, Ye JH. (2013). Propofol stimulates noradrenalin-inhibited neurons in the ventrolateral preoptic nucleus by reducing GABAergic inhibition. *Anesth Analg.*
United States · Rat · live · 230-250 µm · Electrophysiology PubMed

Xie Z, Li G, Ye JH. (2013). Acute effects of ethanol on GABAA and glycine currents in the lateral habenula neurons of young rats. *Open J Neurosci.*
United States · Rat · live · 300 µm · Electrophysiology PubMed

Zuo W, Chen L, Wang L, Ye JH. (2013). Cocaine facilitates glutamatergic transmission and activates lateral habenular neurons. *Neuropharmacology.*
China · Rat · live · 200-250 µm · Electrophysiology PubMed

Garcia I, Huang L, Ung K, Arenkiel BR. (2012). Tracing synaptic connectivity onto embryonic stem cell-derived neurons. *Stem Cells.*
United States · Mouse · live · 300 µm · Electrophysiology PubMed

Kim S, Ma L, Jensen KL, Kim MM, Bond CT, Adelman JP, Yu CR. (2012). Paradoxical contribution of SK3 and GIRK channels to the activation of mouse vomeronasal organ. *Nat Neurosci.*
United States · Mouse · live · 200 µm · Electrophysiology PubMed

Marrs GS, Spirou GA. (2012). Embryonic assembly of auditory circuits: spiral ganglion and brainstem. *J Physiol.*
United States · Mouse · live · 200-350 µm · Electrophysiology PubMed

Niederleitner B, Luksch H. (2012). Neuronal morphology in subdivisions of the inferior colliculus of chicken (Gallus gallus). *J Chem Neuroanat.*
Germany · Chick · live · 500 µm · Electrophysiology PubMed

Tarr JC, Turlington ML, Reid PR, Utley TJ, Sheffler DJ, Cho HP, Klar R, Pancani T, Klein MT, Bridges TM, Morrison RD, Blobaum AL, Xiang Z, Daniels JS, Niswender CM, Conn PJ, Wood MR, Lindsley CW. (2012). Targeting selective activation of M(1) for the treatment of Alzheimer's disease: further chemical optimization and pharmacological characterization of the M(1) positive allosteric modulator ML169. *ACS Chem Neurosci.*
United States · Mouse · live · 300 µm · Electrophysiology PubMed

Weigel S, Luksch H. (2012). Spatiotemporal analysis of electrically evoked activity in the chicken optic tectum: a VSDI study. *J Neurophysiol.*
Germany · Chick · live · 500 µm · Electrophysiology PubMed

Xie G, Hipí_lito L, Zuo W, Polache A, Granero L, Krnjevic K, Ye JH. (2012). Salsolinol Stimulates Dopamine Neurons in Slices of Posterior Ventral Tegmental Area Indirectly by Activating µ-Opioid Receptors. *J Pharmacol Exp Ther.*
United States · Rat · live · 250-300 µm · Electrophysiology PubMed

Xie G, Ye JH. (2012). Salsolinol facilitates glutamatergic transmission to dopamine neurons in the posterior ventral tegmental area of rats. *PLoS One.*
United States · Rat · live · 200-250 µm · Electrophysiology PubMed

George AA, Lyons-Warren AM, Ma X, Carlson BA. (2011). A diversity of synaptic filters are created by temporal summation of excitation and inhibition. *J Neurosci.*
United States · Fish · live · 300 µm · Electrophysiology PubMed

Kim S, Ma L, Yu CR. (2011). Requirement of calcium-activated chloride channels in the activation of mouse vomeronasal neurons. *Nat Commun.*
United States · Mouse · live · 200 µm · Electrophysiology PubMed

Li G, Yang K, Zheng C, Liu Q, Chang Y, Kerrigan JF, Wu J. (2011). Functional rundown of gamma-aminobutyric acid(A) receptors in human hypothalamic hamartomas. *Ann Neurol.*
United States · Human · live · 350-400 µm · Electrophysiology PubMed

Lu Y, Ye JH. (2011). Glycine-activated chloride currents of neurons freshly isolated from the prefrontal cortex of young rats. *Brain Res.*
United States · Rat · live · 250 µm · Electrophysiology PubMed

Ma L, Haga-Yamanaka S, Yu QE, Qiu Q, Kim S, Yu CR. (2011). Imaging neuronal responses in slice preparations of vomeronasal organ expressing a genetically encoded calcium sensor. *J Vis Exp.*

United States · Mouse · live · 180-200 µm · Imaging PubMed

Peí_a J, Feliciano C, Ting JT, Wang W, Wells MF, Venkatraman TN, Lascola CD, Fu Z, Feng G. (2011). Shank3 mutant mice display autistic-like behaviours and striatal dysfunction. *Nature.*
United States · Mouse · live · 300 µm · Electrophysiology PubMed

Zhao S, Ting JT, Atallah HE, Qiu L, Tan J, Gloss B, Augustine GJ, Deisseroth K, Luo M, Graybiel AM, Feng G. (2011). Cell type-specific channelrhodopsin-2 transgenic mice for optogenetic dissection of neural circuitry function. *Nat Methods.*
United States · Mouse · live · 300 µm · Electrophysiology PubMed

Caudill MS, Eggebrecht AT, Gruberg ER, Wessel R. (2010). Electrophysiological properties of isthmic neurons in frogs revealed by in vitro and in vivo studies. *J Comp Physiol A Neuroethol Sens Neural Behav Physiol.*
United States · Frog · live · 300 µm · Electrophysiology PubMed

Guan YZ, Ye JH. (2010). Ethanol Blocks Long-Term Potentiation of GABAergic Synapses in the Ventral Tegmental Area Involving µ-Opioid Receptors. *Neuropsychopharmacology.*
United States · Rat · live · 200-250 µm · Electrophysiology PubMed

Hoffpauir BK, Kolson DR, Mathers PH, Spirou GA. (2010). Maturation of synaptic partners: functional phenotype and synaptic organization tuned in synchrony. *J Physiol.*
United States · Mouse · live · 200-300 µm · Electrophysiology PubMed

Liu YW, Li J, Ye JH. (2010). Histamine regulates activities of neurons in the ventrolateral preoptic nucleus. *J Physiol.*
United States · Rat · live · 250 µm · Electrophysiology PubMed

Viviani D, Terrettaz T, Magara F, Stoop R. (2010). Oxytocin enhances the inhibitory effects of diazepam in the rat central medial amygdala. *Neuropharmacology.*
Switzerland · Rat · live · 350 µm · Electrophysiology PubMed

Deng C, Li KY, Zhou C, Ye JH. (2009). Ethanol enhances glutamate transmission by retrograde dopamine signaling in a postsynaptic neuron/synaptic bouton preparation from the ventral tegmental area. *Neuropsychopharmacology.*
Rat · live · 300 µm · Electrophysiology PubMed

Li KY, Guan YZ, KrnjeviÛˆ K, Ye JH. (2009). Propofol facilitates glutamatergic transmission to neurons of the ventrolateral preoptic nucleus. *Anesthesiology.*
United States · Rat · live · 300 µm · Electrophysiology PubMed

Nguyen HT, Li KY, daGraca RL, Delphin E, Xiong M, Ye JH. (2009). Behavior and cellular evidence for propofol-induced hypnosis involving brain glycine receptors. *Anesthesiology.*
United States · Rat · live · 300 µm · Electrophysiology PubMed

Pan BX, Dong Y, Ito W, Yanagawa Y, Shigemoto R, Morozov A. (2009). Selective gating of glutamatergic inputs to excitatory neurons of amygdala by presynaptic GABAb receptor. *Neuron.*
United States · Rat · live · 400 µm · Electrophysiology PubMed

Xiao C, Yang KC, Zhou CY, Jin GZ, Wu J, Ye JH. (2009). Nicotine modulates GABAergic transmission to dopaminergic neurons in substantia nigra pars compacta. *Acta Pharmacol Sin.*
United States · Rat · live · 300 µm · Electrophysiology PubMed

Li KY, Xiao C, Xiong M, Delphin E, Ye JH. (2008). Nanomolar propofol stimulates glutamate transmission to dopamine neurons: a possible mechanism of abuse potential?. *J Pharmacol Exp Ther.*
United States · Rat · live · 300 µm · Electrophysiology PubMed

Meyer U, Shao J, Chakrabarty S, Brandt SF, Luksch H, Wessel R. (2008). Distributed delays stabilize neural feedback systems. *Biol Cybern.*
Germany · Chick · live · 500 µm · Electrophysiology PubMed

Xiao C, Ye JH. (2008). Ethanol dually modulates GABAergic synaptic transmission onto dopaminergic neurons in ventral tegmental area: role of µ-opioid receptors. *Neuroscience.*
United States · Rat · live · 250-300 µm · Electrophysiology PubMed

Xiao C, Zhou C, Atlas G, Delphin E, Ye JH. (2008). Labetalol facilitates GABAergic transmission to rat periaqueductal gray neurons via antagonizing β1- adrenergic receptors - a possible mechanism underlying labetalol- induced analgesia. *Brain Res.*
United States · Rat · live · 300 µm · Electrophysiology PubMed

Xiao C, Zhou C, Li K, Davies DL, Ye JH. (2008). Purinergic type 2 receptors at GABAergic synapses on ventral tegmental area dopamine neurons are targets for ethanol action. *J Pharmacol Exp Ther.*
United States · Rat · live · 400 µm · Electrophysiology PubMed

Xiao C, Zhang J, KrnjeviÛˆ K, Ye JH. (2007). Effects of Ethanol on Midbrain Neurons: Role of OpioidReceptors. *Alcohol Clin Exp Res.*
Rat · live · 230-300 µm · Electrophysiology PubMed

Xiao C, Zhou C, Li K, Ye JH. (2007). Presynaptic GABAA receptors facilitate GABAergic transmission to dopaminergic neurons in the ventral tegmental area of young rats. *The Journal of physiology.*
United States · Rat · live · 250-300 µm · Electrophysiology PubMed

Zhou C, Xiao C, Deng C, Hong Ye J. (2007). Extracellular proton modulates GABAergic synaptic transmission in rat hippocampal CA3 neurons. *Brain Research.*
United States · Rat · live · 300 µm · Electrophysiology PubMed

Hejazi N, Zhou C, Oz M, Sun H, Ye JH, Zhang L. (2006). Delta9-tetrahydrocannabinol and endogenous cannabinoid anandamide directly potentiate the function of glycine receptors. *Mol Pharmacol.*
United States · Rat · live · 400 µm · Electrophysiology PubMed

N Hejazi, C Zhou, M Oz, H Sun, JH Ye, L Zhang (2006). Δ9-Tetrahydrocannabinol and endogenous cannabinoid anandamide directly potentiate the function of glycine receptors. *Molecular pharmacology.*
Rat · live · 400 µm · Electrophysiology PubMed

Ye JH, Zhang J, Xiao C, Kong JQ. (2006). Patch-clamp studies in the CNS illustrate a simple new method for obtaining viable neurons in rat brain slices: glycerol replacement of NaCl protects CNS neurons. *Journal of Neuroscience Methods.*
United States · Rat · live · 250-400 µm · Electrophysiology PubMed

Zhou C, Xiao C, McArdle JJ, Ye JH. (2006). Mefloquine Enhances Nigral γ-Aminobutyric Acid Release via Inhibition of Cholinesterase. *J Pharmacol Exp Ther.*
Rat · live · 300 µm · Electrophysiology PubMed

Wang F, Xiao C, Ye JH. (2005). Taurine activates excitatory non-synaptic glycine receptors on dopamine neurones in ventral tegmental area of young rats. *J Physiol.*
United States · Rat · live · 300-400 µm · Electrophysiology PubMed

Ye JH, Wang F, Krnjevic K, Wang W, Xiong ZG, Zhang J. (2004). Presynaptic glycine receptors on GABAergic terminals facilitate discharge of dopaminergic neurons in ventral tegmental area. *J Neurosci.*
United States · Rat · live · 250-300 µm · Electrophysiology PubMed

Brain — fixed

Fixed and post-mortem brain sectioning for histology, connectomics, and imaging.

500 (2024). Optical Clearing and Labeling for Light-Ssheet Flourescence Microscopy in Large-Scale human Brain Imaging. *JoVE (Journal of Visualized Experiments.*
Human · fixed · 400 or 500 µm · IHC / ISH PubMed

CF Suarez, OA Harb, A Robledo, G Largoza, JJ Ahn… (2024). MEK signaling represents a viable therapeutic vulnerability of KRAS-driven somatic brain arteriovenous malformations. *bioRxiv.*
Mouse · fixed · 35 µm PubMed

CS Park, M Yan, M Zhu, MA Akram, NN Foster… (2024). Dendritome Mapping Unveils Spatial Organization of Striatal D1/D2-Neuron Morphology. *bioRxiv.*
Mouse · fixed · 500 µm · IHC / ISH PubMed

D Ackerman, E Avetissian, CKE Bleck, JA Bogovic… (2024). Data Release: High-Resolution Imaging and Segmentation of P7 Mouse Tissue Microarchitecture Using FIB-SEM and Machine Learning. *bioRxiv.*
Mouse · fixed · 300 µm · Imaging PubMed

D Markman, AZ Wasilczuk… (2024). General Anesthesia Occludes Ketamine's Antidepressant Response in a Rodent Model of Chronic Stress. *Psychedelic Medicine.*
United States · Mouse · fixed · 40 µm · IHC / ISH PubMed

Di Meo D,1, Ramazzoti J,1,Scardigli M, Cheli F, Pesce L, Brady N, Mazzamuto G, Costantini I, Pavone SF (2024). Calcium-Sensing Receptor Negative Allosteric Modulators Oppose Contraction of Mouse Airways. *Jove*.
Human · fixed · 400 or 500 µm · IHC / ISH

G Chen, S Lai, S Jiang, F Li, K Sun, X Wu, K Zhou… (2024). Cellular and circuit architecture of the lateral septum for reward processing. *Neuron*.
China · Mouse · fixed · 300 µm · IHC / ISH PubMed

HE Mohammed, JC Nelson, SA Marshall (2024). Ethanol Exacerbates the Alzheimer's Disease Pathology in the 5xFAD Mouse Model. *Neuroglia*.
United States · Mouse · fixed · 40 µm · IHC / ISH PubMed

HR Li, M Harb, JE Heath, JS Trippett… (2024). Engineering viral vectors for acoustically targeted gene delivery. *Nature Communications*.
United States · Mouse · fixed · 50 µm · IHC / ISH PubMed

J Hu, K He, Y Yang, C Huang, Y Dou, H Wang… (2024). Amino acid formula induces microbiota dysbiosis and depressive-like behavior in mice. *Cell Reports*.
China · Mouse · fixed · 300 µm · IHC / ISH PubMed

L Yang, F Liu, H Hahm, T Okuda, X Li, Y Zhang… (2024). Projection-TAGs enable multiplex projection tracing and multi-modal profiling of projection neurons. *bioRxiv*.
United States · Mouse · fixed · 30 and 400 µm PubMed

M Lindman (2024). RIPK3 Regulates Neuroinflammation During Flavivirus Infection of the Central Nervous System. *Rutgers Unversity*.
Mouse · fixed · 50 µm · IHC / ISH PubMed

M Lindman, I Estevez, E Marmut, EM DaPrano… (2024). Astrocytic RIPK3 exerts protective anti-inflammatory activity during viral encephalitis via induction of serpin protease inhibitors. *bioRxiv*.
United States · Mouse · fixed · Unknown µm · IHC / ISH PubMed

M Xue, QY Chen, W Shi, Z Zhou, X Li, F Xu… (2024). Whole-brain mapping of afferents to the anterior cingulate cortex in adult mice. *Molecular Pain*.
China · Mouse · fixed · 300 µm · IHC / ISH PubMed

S McCracken, L McCoy, Z Hu, J Hodges, K Valkova… (2024). Mistargeted retinal axons form synaptically segregated subcircuits in the visual thalamus of albino mice. *bioRxiv*.
United States · Mouse · fixed · 50-200 µm · Imaging PubMed

SB Park, G Lur (2024). Repeated exposure to multiple concurrent stressors alters visual processing in the adult posterior parietal cortex. *Neurobiology of Stress*.
United States · Mouse · fixed · 50 µm · IHC / ISH PubMed

T Qin, Y Xia, N Nazari, T Sepahvand… (2024). Correlational patterns of neuronal activation and epigenetic marks in the basolateral amygdala and piriform cortex following olfactory threat conditioning and …. *Frontiers in Molecular …*.
Canada · Rat · fixed · 50 µm · IHC / ISH PubMed

T Sepahvand, SJ Carew, Q Yuan (2024). The ventral hippocampus is activated in olfactory but not auditory threat memory. *Frontiers in Neural Circuits*.
Canada · Rat · fixed · 50 µm · IHC / ISH PubMed

TL Dunham, JR Wilkerson, RC Johnson, RL Huganir… (2024). WWC2 modulates GABAA-receptor-mediated synaptic transmission, revealing class-specific mechanisms of synapse regulation by WWC family proteins. *Cell Reports*.
United States · Mouse · fixed · 200 µm · IHC / ISH PubMed

V Nikitin, G Wildenberg, A Mittone… (2024). Laminography as a tool for imaging large-size samples with high resolution. *Journal of Synchrotron Radiation*.
United States · Mouse · fixed · Unknown µm · IHC / ISH PubMed

W Zhang, Y Li, AA Fung, Z Li, H Jang, H Zha… (2024). Multi-molecular hyperspectral PRM-SRS imaging. *Nature Communications*.
Human, mouse · fixed · 30, 120 µm PubMed

WR Evans, SS Baskar, ARCE Costa, S Ravoori… (2024). Functional activation of dorsal striatum astrocytes improves movement deficits in hemi-parkinsonian mice. *bioRxiv*.
United States · Mouse · fixed · 60 µm · IHC / ISH PubMed

XH Li, W Shi, ZX Zhao, T Matsuura, JS Lu… (2024). Increased GluK1 Subunit Receptors in Corticostriatal Projection from the Anterior Cingulate Cortex Contributed to Seizure-Like Activities. *Advanced Science*.
China · Mouse · fixed · 300 µm · Imaging PubMed

Y Ge, C Yang, M Zadeh, SM Sprague, YD Lin, HS Jain… (2024). Functional regulation of microglia by vitamin B12 alleviates ischemic stroke-induced neuroinflammation in mice. *Iscience*.
United States · Mouse · fixed · 30 µm · IHC / ISH PubMed

Z Zhou, X Yang, A Mao, H Xu, C Lin, M Yang, W Hu… (2024). Deficiency of CAMSAP2 impairs olfaction and the morphogenesis of mitral cells. *EMBO reports*.
China · Mouse · fixed · 300-400 µm · IHC / ISH PubMed

A Godino, M Salery, R Durand-de Cuttoli, MS Estill… (2023). Transcriptional control of nucleus accumbens neuronal excitability by retinoid X receptor alpha tunes sensitivity to drug rewards. *Neuron*.
United States · Mouse · fixed · 250 µm · Electrophysiology PubMed

A Hall (2023). Analysis of cFos Expression and Microglial Branch Density in a Mouse Model of Trauma-Induced Hyperarousal. *ProQuest*.
Mouse · fixed · 50 µm · IHC / ISH PubMed

A Maziar, TN Critch, S Ghosh, V Rajani… (2023). Aging differentially affects LTCC function in hippocampal CA1 and piriform cortex pyramidal neurons. *Cereb Cortex*.
Canada · Rat · fixed · 50 µm · IHC / ISH PubMed

A Ozgur, SB Park, AY Flores, M Oijala, G Lur (2023). A comprehensive, affordable, open-source hardware-software solution for flexible implementation of complex behaviors in head-fixed mice. *Eneuro*.
United States · Mouse · fixed · 50 µm · Imaging PubMed

AA Fung (2023). Development of a Label-free Optical Analysis Platform for Cells and Tissues. *Public Access from UC San Diego*.
Mouse, Human · fixed · 120, 30 µm PubMed

AG Salinas, JO Lee, SM Augustin, S Zhang… (2023). Distinct sub-second dopamine signaling in dorsolateral striatum measured by a genetically-encoded fluorescent sensor. *Nature Communications*.
United States · Mouse · fixed · 100 µm · IHC / ISH PubMed

C Yang, Z Gong, X Zhang, S Miao, B Li, W Xie… (2023). Neuropeptide Y in the medial habenula alleviates migraine-like behaviors through the Y1 receptor. *The Journal of Headache and Pain*.
China · Mouse · fixed · 300 µm · IHC / ISH PubMed

CD Walker (2023). Adolescence, Alcohol, and Astrocytes: The Impact of Adolescent Alcohol Use on Astrocyte-Synaptic Interactions, Structure, Function, and Behavior. *Marshall University Digital Scholar*.
Rat · fixed · 250 µm · IHC / ISH PubMed

D Na, J Zhang, HJ Beaulac… (2023). Increased central auditory gain in 5xFAD Alzheimer's disease mice as an early biomarker candidate for Alzheimer's disease diagnosis. *Frontiers in Neuroscience*.
United States · Mouse · fixed · 80 µm · IHC / ISH PubMed

DJ Lievano Parra (2023). Effects of the unilateral lesion of the substantia nigra compacta with 6-OHDA on reversal learning and prepulse inhibition in male and female Wistar rats. *Universidad de Los Andes Colombia Library*.
Rat and Mouse · fixed · 20 µm · IHC / ISH PubMed

DK Kasaragod, H Aizawa (2023). Deep ultraviolet fluorescence microscopy of three-dimensional structures in the mouse brain. *Scientific Reports*.
Japan · Mouse · fixed · 50 µm · Imaging PubMed

G Chen, S Lai, G Bao, J Ke, X Meng, S Lu, X Wu, H Xu… (2023). Distinct reward processing by subregions of the nucleus accumbens. *Cell Reports*.
China · Mouse · fixed · 300 µm · Imaging PubMed

G Rosen, D Kirsch, S Horowitz, JD Cherry… (2023). Three dimensional evaluation of cerebrovascular density and branching in chronic traumatic encephalopathy. *Acta Neuropathologica Communications*.
United States · Human · fixed · 200 µm · Imaging PubMed

G Wildenberg, K Boergens, V Nikitin, A Deriy… (2023). A Pipeline for a Primate Projectome: mapping every individual myelinated axon across the whole brain. *bioRxiv*.
Various · fixed · 200 µm · Imaging PubMed

H Mason, G Rai, A Kozyr, N De Jonge, E Gliniewicz… (2023). Development of an improved and specific inhibitor of NADPH oxidase 2 to treat traumatic brain injury. *Redox Biology*.
United States · Mouse · fixed · 100 µm · Imaging PubMed

J Larochelle, RJ Tishko, C Yang, Y Ge, LT Phan… (2023). Receptor-interacting protein kinase 2 (RIPK2) profoundly contributes to post-stroke neuroinflammation and behavioral deficits with microglia as unique …. *Journal of Neuroinflammation*.
United States · Mouse · fixed · 30 µm · IHC / ISH PubMed

JA Hatter, MM Scott (2023). Selective ablation of VIP interneurons in the rodent prefrontal cortex results in increased impulsivity. *PloS One*.
United States · Mouse · fixed · 40 µm · IHC / ISH PubMed

JJ Privitt, BN Van Nest, SE Fahrbach (2023). Altered synaptic organization in the mushroom bodies of honey bees exposed as foragers to the pesticide fipronil. *Frontiers in Bee Science*.
Bees · fixed · 100 µm · Imaging PubMed

JT Ahrendsen, Y Nong, Y Huo, J Steele… (2023). CD8 cytotoxic T-cell infiltrates and cellular damage in the hypothalamus in human obesity. *Acta Neuropathologica Communications*.
United States · Mouse · fixed · 100 µm · IHC / ISH PubMed

JY Min, S Park, J Cho, Y Huh (2023). The anterior insular cortex processes social recognition memory. *Scientific Reports*.
South Korea · Mouse · fixed · 40 µm · IHC / ISH PubMed

L Kang, W Yu, Y Zhang, TTW Wong (2023). Automated whole-organ histological imaging assisted with ultraviolet-excited sectioning tomography and deep learning. *bioRxiv*.
Mouse · fixed · 50 µm · IHC / ISH PubMed

L Kang, W Yu, Y Zhang, Z Chen, TTW Wong (2023). Deep Learning Enables Rapid Whole-Organ Histological Imaging with Ultraviolet-Excited Sectioning Tomography. *ACS Photonics*.
Mouse · fixed · 200 µm · IHC / ISH PubMed

L Smith-Osborne, A Duong, A Resendez, R Palme… (2023). Female dominance hierarchies influence responses to psychosocial stressors. *Current Biology*.
United States · Mouse · fixed · 60 µm · IHC / ISH PubMed

LD Quigley, R Pendry, ML Mendoza, BE Pfeiffer… (2023). Experience alters hippocampal and cortical network communication via a KIBRA-dependent mechanism. *Cell Reports*.
United States · Mouse · fixed · 75 µm · IHC / ISH PubMed

M Dorofeikova, CD Borkar, K Weissmuller… (2023). Effects of footshock stress on social behavior and neuronal activation in the medial prefrontal cortex and amygdala of male and female mice. *Plos one*.
United States · Mouse · fixed · 80 µm · IHC / ISH PubMed

M Dorofeikova, CE Stelly, A Duong, S Basavanhalli… (2023). The role of genetically distinct central amygdala neurons in appetitive and aversive responding assayed with a novel dual valence operant conditioning paradigm. *Eneuro*.
United States · Mouse · fixed · 100 µm · IHC / ISH PubMed

M Lindman, JP Angel, I Estevez, NP Chang… (2023). RIPK3 promotes brain region-specific interferon signaling and restriction of tick-borne flavivirus infection. *PLOS Pathogens*.
United States · Mouse · fixed · 50 µm · IHC / ISH PubMed

M Serranilla (2023). Chloride Dysregulation and Impaired Gamma-Amino Butyric Acid Signaling in the Basal Ganglia in Huntington's Disease. *Frontiers in Cellular Neuroscience*.
Canada · Mouse · fixed · 300 µm · IHC / ISH PubMed

MM Naffaa, RR Khan, CT Kuo, HH Yin (2023). Cortical regulation of neurogenesis and cell proliferation in the ventral subventricular zone. *Cell Reports*.
United States · Mouse · fixed · 50 µm · IHC / ISH PubMed

MÁ García-Cabezas, JL Hacker… (2023). Homology of neocortical areas in rats and primates based on cortical type analysis: an update of the hypothesis on the dual origin of the neocortex. *Brain Structure and Function*.
Spain · Rat, Human · fixed · 50 or 75 µm · Imaging PubMed

P Hoffman, MN Svalina, C Flores, C Brzezinski… (2023). Developmental Characterization of Neuronal Migration Anomalies and Axon Proliferation in mTOR pathway-associated Malformations of Cortical Development. *bioRxiv*.
Mouse · fixed · 30-50 µm · IHC / ISH PubMed

R Sim, J Lee, J Chieng, KH Tan, G Lim, A Foo… (2023). Fluorescent Peptide-based Probe for the Detection of Alpha-synuclein Aggregates in the Gut. *bioRxiv*.
Mouse · fixed · 50 µm · IHC / ISH PubMed

S Mamani, S Shintre, Z Li, A Rodríguez-Contreras… (2023). OAM transmission of polarized multipole laser beams in rat cerebellum tissue. *Optics Communications (ELSEVIER)*.
Rat · fixed · 600 µm PubMed

S Venkadesh, A Santarelli, T Boesen… (2023). Combinatorial quantification of distinct neural projections from retrograde tracing. *Nature Communications*.
United States · Mouse · fixed · 50 µm · IHC / ISH PubMed

SJ Carew (2023). The smell of fear: comparing the neural ensembles underlying odor fear memory conditioned by innate, inherent, and learned sources of danger. *Memorial university of Newfoundland and Labrador*.
Rat · fixed · 50 µm · IHC / ISH PubMed

SN Jiang, JW Cao, LY Liu, Y Zhou, GY Shan… (2023). Sncg, Mybpc1, and Parm1 Classify subpopulations of VIP-expressing interneurons in layers 2/3 of the somatosensory cortex. *Cerebral Cortex (Oxford University Press)*.
China · Mouse · fixed · 300 µm · Electrophysiology PubMed

TR Sides, JC Nelson, KN Nwachukwu, J Boston… (2023). The Influence of Arsenic Co-Exposure in a Model of Alcohol-Induced Neurodegeneration in C57BL/6J Mice. *Brain Sciences*.
United States · Mouse · fixed · 40 µm · IHC / ISH PubMed

X Fang, JJ Border, PL Rivers, H Zhang, JM Williams… (2023). Amyloid beta accumulation in TgF344-AD rats is associated with reduced cerebral capillary endothelial Kir2. 1 expression and neurovascular uncoupling. *GeroScience*.
United States · Rat · fixed · 35 µm · IHC / ISH PubMed

XH Li, W Shi, QY Chen, S Hao, HH Miao… (2023). Activation of the glutamatergic cingulate cortical-cortical connection facilitates pain in adult mice. *Nature Portfolio*.
China · Mouse · fixed · 300 µm PubMed

Y Liu, MR Fontenot, A Kulkarni, N Khandelwal… (2023). An extra-circadian function for human CLOCK in the neocortex. *bioRxiv*.
Mouse · fixed · 40 µm · IHC / ISH PubMed

Y Wu, P Li, N Bhat, H Fan, M Liu (2023). Effects of repeated sleep deprivation on brain pericytes in mice. *Scientific Reports*.
United States · Mouse · fixed · 40 µm · IHC / ISH PubMed

A Brodovskaya, S Shiono, T Batabyal… (2022). Construction of Local Field Potential Microelectrodes for in vivo Recordings from Multiple Brain Structures Simultaneously. *JoVE (Journal of Visualized Experiments)*.
Mouse · fixed · 40 µm · IHC / ISH PubMed

DJ Rindner, A Proddutur, G Lur (2022). Cell-type-specific integration of feedforward and feedback synaptic inputs in the posterior parietal cortex. *Neuron*.
United States · Mouse · fixed · 50 µm · IHC / ISH PubMed

EA Kiffmeyer, JA Cosgrove, JK Siganos, HE Bien… (2022). Deficits in cerebellum-dependent learning and cerebellar morphology in male and female BTBR autism model mice. *NeuroSci*.
United States · Mouse · fixed · 50-120 µm · IHC / ISH PubMed

ES Norton, LA Whaley, MJ Ulloa-Navas… (2022). Glioblastoma disrupts the ependymal wall and extracellular matrix structures of the subventricular zone. *Fluids Barriers CNS*.
United States · Mouse · fixed · 50 µm · IHC / ISH PubMed

JD Hahn, L Gao, T Boesen, L Gou… (2022). Macroscale connections of the mouse lateral preoptic area and anterior lateral hypothalamic area. *J Comp Neurol*.
United States · Mouse · fixed · 50 µm · IHC / ISH PubMed

KN Nwachukwu, KL Healey, HS Swartzwelder… (2022). The influence of sex on hippocampal neurogenesis and neurotrophic responses on the persistent effects of adolescent intermittent ethanol exposure into adulthood. *Neuroscience*.

United States · Rat · fixed · 40 µm · IHC / ISH PubMed

L Liu, C Yang, BP Lavayen, RJ Tishko… (2022). Targeted BRD4 protein degradation by dBET1 ameliorates acute ischemic brain injury and improves functional outcomes associated with reduced …. *J Neuroinflammation*.
United States · Mouse · fixed · 30 µm · IHC / ISH PubMed

M Scheibinger, A Janesick, GH Diaz… (2022). Immunohistochemistry and In Situ mRNA detection using inner ear vibratome sections. *Developmental, Physiological, and Functional Neurobiology of the Inner Ear*.
Mouse · fixed · 50-200 µm · IHC / ISH PubMed

S Milde, GC Brown (2022). Knockout of the P2Y6 Receptor Prevents Peri-Infarct Neuronal Loss after Transient, Focal Ischemia in Mouse Brain. *International Journal of Molecular Sciences*.
United Kingdom · Mouse · fixed · 20 µm · IHC / ISH PubMed

W Shi, M Xue, F Wu, K Fan, QY Chen, F Xu… (2022). Whole-brain mapping of efferent projections of the anterior cingulate cortex in adult male mice. *Mol Pain*.
China · Mouse · fixed · 300 µm · Imaging PubMed

Y Zhang, L Kang, IHM Wong, W Dai, X Li… (2022). High-Throughput, Label-Free and Slide-Free Histological Imaging by Computational Microscopy and Unsupervised Learning. *Advanced Science*.
China · Mouse · fixed · 200 µm · IHC / ISH PubMed

C Yang, BP Lavayen, L Liu, BD Sanz, KM DeMars… (2021). Neurovascular protection by adropin in experimental ischemic stroke through an endothelial nitric oxide synthase-dependent mechanism. *Redox biology*.
United States · Mouse · fixed · 30 µm · IHC / ISH PubMed

CE Jones, AQ Chau, RJ Olson, C Moore… (2021). Early life sleep disruption alters glutamate and dendritic spines in prefrontal cortex and impairs cognitive flexibility in prairie voles. *Curr Res Neurobiol*.
United States · Prairie Vole · fixed · 200 µm · IHC / ISH PubMed

F Xu, Y Shen, L Ding, CY Yang, H Tan, H Wang… (2021). High-throughput mapping of a whole rhesus monkey brain at micrometer resolution. *Nature Biotechnology*.
China · Non-Human Primate · fixed · 300 µm · IHC / ISH PubMed

FP Mayer, H Iwamoto, MK Hahn, GJ Grumbar… (2021). There's no place like home? Return to the home cage triggers dopamine release in the mouse nucleus accumbens. *Neurochem Int*.
United States · Mouse · fixed · 40 µm · IHC / ISH PubMed

H Hintiryan, I Bowman, DL Johnson… (2021). Connectivity characterization of the mouse basolateral amygdalar complex. *Nat Commun*.
United States · Mouse · fixed · 50 µm · IHC / ISH PubMed

HD Mason, AM Johnson, NA Mihelson, P Mastorakos… (2021). Glia limitans superficialis oxidation and breakdown promote cortical cell death after repetitive head injury. *JCI insight*.
United States · Mouse · fixed · 100 µm · IHC / ISH PubMed

J Vogler, R Böttger, NAL Fayez, W Zhang, Z Qin… (2021). Altering the intra-liver distribution of phospholipid-free small unilamellar vesicles using temperature-dependent size-tunability. *Journal of Controlled Release*.
Mouse · fixed · 40 µm · IHC / ISH PubMed

J Wie, Z Liu, H Song, TF Tropea, L Yang, H Wang… (2021). A growth-factor-activated lysosomal K+ channel regulates Parkinson's pathology. *Nature*.
United States · Mouse · fixed · 40 µm · IHC / ISH PubMed

KL Elliott, J Kersigo, JH Lee, EN Yamoah… (2021). Sustained Loss of bdnf affects peripheral but not central vestibular targets. *Frontiers in Neurology*.
United States · Mouse · fixed · 50 µm · IHC / ISH PubMed

KN Nwachukwu, WA Evans, TR Sides… (2021). Chemogenetic manipulation of astrocytic signaling in the basolateral amygdala reduces binge-like alcohol consumption in male mice. *J Neurosci Res*.
United States · Mouse · fixed · 40 µm · IHC / ISH PubMed

M Puigdellívol, S Milde, M Spillantini… (2021). The microglial P2Y6 receptor mediates neuronal loss and memory deficits in neurodegeneration. *Cell reports*.
United Kingdom · Mouse · fixed · 20 µm · IHC / ISH PubMed

NL Benavidez, MS Bienkowski, M Zhu… (2021). Organization of the inputs and outputs of the mouse superior colliculus. *Nature Communications*.

United States · Mouse · fixed · 50 µm · IHC / ISH PubMed

P Mastorakos, MV Russo, T Zhou, K Johnson… (2021). Antimicrobial immunity impedes CNS vascular repair following brain injury. *Nature Immunology*.
United States · Mouse · fixed · Unknown µm · IHC / ISH PubMed

P Mastorakos, N Mihelson, M Luby, SR Burks… (2021). Temporally distinct myeloid cell responses mediate damage and repair after cerebrovascular injury. *Nature Neuroscience*.
United States · Mouse · fixed · 50-100 µm · IHC / ISH PubMed

S Milde, FW van Tartwijk, A Vilalta, TC Hornik… (2021). Inflammatory neuronal loss in the substantia nigra induced by systemic lipopolysaccharide is prevented by knockout of the P2Y6 receptor in mice. *J Neuroinflammation*.
United Kingdom · Mouse · fixed · 20 µm · IHC / ISH PubMed

SK Bose, BM White, MV Kashyap, A Dave… (2021). In utero adenine base editing corrects multi-organ pathology in a lethal lysosomal storage disease. *Nat Commun*.
United States · Mouse · fixed · 150 µm · IHC / ISH PubMed

SL Reitz, AZ Wasilczuk, GH Beh, A Proekt, MB Kelz (2021). Activation of preoptic tachykinin 1 neurons promotes wakefulness over sleep and volatile anesthetic-induced unconsciousness. *Current Biology*.
United States · Mouse · fixed · 40 µm · IHC / ISH PubMed

SR Gray, L Ye, JY Ye, M Paukert (2021). Noradrenergic terminal short-term potentiation enables modality-selective integration of sensory input and vigilance state. *Science Advances*.
United States · Mouse · fixed · 35 µm · IHC / ISH PubMed

A Caputo, Y Liang, TD Raabe, A Lo, M Horvath… (2020). Snca-GFP knock-in mice reflect patterns of endogenous expression and pathological seeding. *ENeuro*.
United States · Mouse · fixed · Unknown µm · IHC / ISH PubMed

Bariselli S, Miyazaki NL, Creed MC, Kravitz AV. (2020). Orbitofrontal-striatal potentiation underlies cocaine-induced hyperactivity. *Nat Commun*.
United States · Mouse · fixed · 40 µm · Immunohistochemistry PubMed

CE Jones, PT Wickham, MM Lim (2020). Early life sleep disruption is a risk factor for increased ethanol drinking after acute footshock stress in prairie voles. *Behavioral Neuroscience*.
United States · Prairie Vole · fixed · 40 µm · IHC / ISH PubMed

Colon LM, Poulos AM. (2020). Contextual processing elicits sex differences in dorsal hippocampus activation following footshock and context fear retrieval. *Behav Brain Res*.
United States · Mouse · fixed · 50 µm · Immunohistochemistry PubMed

Dao NC, Suresh Nair M, Magee SN, Moyer JB, Sendao V, Brockway DF, Crowley NA. (2020). Forced Abstinence From Alcohol Induces Sex-Specific Depression-Like Behavioral and Neural Adaptations in Somatostatin Neurons in Cortical and Amygdalar Regions. *Front Behav Neurosci*.
United States · Mouse · fixed · 50-300 µm · Electrophysiology PubMed

E Gonzalez-Fernandez, D Staursky, K Lucas… (2020). 20-HETE enzymes and receptors in the neurovascular unit: implications in cerebrovascular disease. *Front Neurol*.
United States · Rat · fixed · 60 µm · IHC / ISH PubMed

Griffiths KK, Wang A, Wang L, Tracey M, Kleiner G, Quinzii CM, Sun L, Yang G, Perez-Zoghbi JF, Licznerski P, Yang M, Jonas EA, Levy RJ. (2020). Inefficient thermogenic mitochondrial respiration due to futile proton leak in a mouse model of fragile X syndrome. *FASEB J*.
United States · Mouse · fixed · 150 µm · Immunohistochemistry PubMed

Li, Xiufeng; Kang, Lei; Zhang, Yan; Wong, Terence TW; (2020). High-speed Label-free Ultraviolet Photoacoustic Microscopy for Histology-like imaging of unprocessed biological tissues. *Opt Lett*.
Mouse · fixed · 200 µm · IHC / ISH PubMed

Majewski L, MaciÛfg F, Boguszewski PM, Kuznicki J. (2020). Transgenic Mice Overexpressing Human STIM2 and ORAI1 in Neurons Exhibit Changes in Behavior and Calcium Homeostasis but Show No Signs of Neurodegeneration. *Int J Mol Sci*.
Poland · Mouse · fixed · 20 µm · Immunohistochemistry PubMed

MÁ García-Cabezas, JL Hacker… (2020). A protocol for cortical type analysis of the human neocortex applied on histological samples, the atlas of Von Economo and Koskinas, and magnetic …. *Frontiers in Neuroanatomy*.

Spain · Human · fixed · 50-75 µm · IHC / ISH PubMed

Pozhidayeva DY, Farris SP, Goeke CM, Firsick EJ, Townsley KG, Guizzetti M, Ozburn AR. (2020). Chronic Chemogenetic Stimulation of the Nucleus Accumbens Produces Lasting Reductions in Binge Drinking and Ameliorates Alcohol-Related Morphological and Transcriptional Changes. *Brain Sci.*
United States · Mouse · fixed · 200 µm · Immunohistochemistry PubMed

Q Shu, X Zhao, X Geng, X Wang (2020). CD82 aggravates sevoflurane-induced neurotoxicity by regulating TRPM7 in developing neurons. *Signa Vitae.*
Rat · fixed · 200 µm · Slice culture PubMed

Sun Y, Liu M. (2020). Hypothalamic MCH Neuron Activity Dynamics during Cataplexy of Narcolepsy. *eNeuro.*
United States · Mouse · fixed · 40 µm · Histology PubMed

Veldman MB, Park CS, Eyermann CM, Zhang JY, Zuniga-Sanchez E, Hirano AA, Daigle TL, Foster NN, Zhu M, Langfelder P, Lopez IA, Brecha NC, Zipursky SL, Zeng H, Dong HW, Yang XW. (2020). Brainwide Genetic Sparse Cell Labeling to Illuminate the Morphology of Neurons and Glia with Cre-Dependent MORF Mice. *Neuron.*
United States · Mouse · fixed · 300-600 µm · Immunohistochemistry PubMed

Wang S, Lv W, Zhang H, Liu Y, Li L, Jefferson JR, Guo Y, Li M, Gao W, Fang X, Paul IA, Rajkowska G, Shaffery JP, Mosley TH, Hu X, Liu R, Wang Y, Yu H, Roman RJ, Fan F. (2020). Aging exacerbates impairments of cerebral blood flow autoregulation and cognition in diabetic rats. *Geroscience.*
United States · Rat · fixed · 50 µm · IHC / ISH PubMed

Zhang Y, Lu P, Liang F, Liufu N, Dong Y, Zheng JC, Xie Z. (2020). Cyclophilin D Contributes to Anesthesia Neurotoxicity in the Developing Brain. *Front Cell Dev Biol.*
China · Mouse · fixed · 15 µm · Immunohistochemistry PubMed

Bienkowski MS, Benavidez NL, Wu K, Gou L, Becerra M, Dong HW. (2019). Extrastriate connectivity of the mouse dorsal lateral geniculate thalamic nucleus. *J Comp Neurol.*
United States · Mouse · fixed · 50 µm · Immunohistochemistry PubMed

Feng M, Crowley NA, Patel A, Guo Y, Bugni SE, Luscher B. (2019). Reversal of a Treatment-Resistant, Depression-Related Brain State with the Kv7 Channel Opener Retigabine. *Neuroscience.*
United States · Mouse · fixed · 40 µm · Immunohistochemistry PubMed

Grifasi IR, Evans WA, Rexha AD, Sako LW, Marshall SA. (2019). A comparison of hippocampal microglial responses in aged and young rodents following dependent and non-dependent binge drinking. *Int Rev Neurobiol.*
United States · Mouse, Rat · fixed · 40 µm · Immunohistochemistry PubMed

H Reid (2019). Prenatal THC exposure has lasting detrimental effects on the rat hippocampus. *University of Victoria.*
Rat · fixed · 400 and 200 µm PubMed

MaciÛfg F, Majewski , Boguszewski PM, Gupta RK, Wasilewska I, Wojta_ B, Kuznicki J. (2019). Behavioral and electrophysiological changes in female mice overexpressing ORAI1 in neurons. *Biochim Biophys Acta Mol Cell Res.*
Poland · Mouse · fixed · 40 µm · Immunohistochemistry PubMed

Paletzki RF, Gerfen CR. (2019). Basic Neuroanatomical Methods. *Curr Protoc Neurosci.*
United States · Mouse · fixed · NS µm · Immunohistochemistry PubMed

Russell TL, Zhang J, Okoniewski M, Franke F, Bichet S, Hierlemann A. (2019). Medullary Respiratory Circuit Is Reorganized by a Seasonally-Induced Program in Preparation for Hibernation. *Front Neurosci.*
Switzerland · Hamster · fixed · 100-300 µm · Electrophysiology PubMed

Shandra O, Winemiller AR, Heithoff BP, Munoz-Ballester C, George KK, Benko MJ, Zuidhoek IA, Besser MN, Curley DE, Edwards GF 3rd, Mey A, Harrington AN, Kitchen JP, Robel S. (2019). Repetitive Diffuse Mild Traumatic Brain Injury Causes an Atypical Astrocyte Response and Spontaneous Recurrent Seizures. *J Neurosci.*
United States · Mouse · fixed · 300 µm · Immunohistochemistry PubMed

Sun Y, Blanco-Centurion C, Bendell E, Vidal-Ortiz A, Luo S, Liu M. (2019). Activity dynamics of amygdala GABAergic neurons during cataplexy of narcolepsy. *Elife.*
United States · Mouse · fixed · 40 µm · Immunohistochemistry PubMed

Sun Y, Blanco-Centurion C, Zou B, Bendell E, Shiromani PJ, Liu M. (2019). Amygdala GABA Neurons Project To vlPAG And mPFC. *IBRO Rep.*
United States · Mouse · fixed · 40 µm · Immunohistochemistry PubMed

Trutzer IM, Garcí_a-Cabezas Mí, Zikopoulos B. (2019). Postnatal development and maturation of layer 1 in the lateral prefrontal cortex and its disruption in autism. *Acta Neuropathol Commun.*
United States · Human · fixed · 50 µm · Immunohistochemistry PubMed

Wang, Hao; Zhu, Qingyuan; Ding, Lufeng; Shen, Yan; Yang, Chao-Yu; Xu, Fang; Shu, Chang; Guo, Yujie; Xiong, Zhiwei; Shan, Qinghong; (2019). Scalable volumetric imaging for ultrahigh-speed brain mapping at synaptic resolution. *Natl Sci Rev.*
China · Mouse · fixed · 300 µm · Imaging PubMed

Bienkowski MS, Bowman I, Song MY, Gou L, Ard T, Cotter K, Zhu M, Benavidez NL, Yamashita S, Abu-Jaber J, Azam S, Lo D, Foster NN, Hintiryan H, Dong HW. (2018). Integration of gene expression and brain-wide connectivity reveals the multiscale organization of mouse hippocampal networks. *Nat Neurosci.*
United States · Mouse · fixed · 50 µm · IHC / ISH PubMed

Blanco-Centurion C, Bendell E, Zou B, Sun Y, Shiromani PJ, Liu M. (2018). VGAT and VGLUT2 expression in MCH and orexin neurons in double transgenic reporter mice. *IBRO Rep.*
United States · Mouse · fixed · 40 µm · Immunohistochemistry PubMed

Doyle S, Hansen DB, Vella J, Bond P, Harper G, Zammit C, Valentino M, Fern R. (2018). Vesicular glutamate release from central axons contributes to myelin damage. *Nat Commun.*
United Kingdom · Mouse · fixed · 20 µm · Histology PubMed

Mamani S, Shi L, Ahmed T, Karnik R, Rodrí_guez-Contreras A, Nolan D, Alfano R. (2018). Transmission of classically entangled beams through mouse brain tissue. *J Biophotonics.*
United States · Mouse · fixed · 120; 600 µm · Imaging PubMed

Nylk J, McCluskey K, Preciado MA, Mazilu M, Yang Z, Gunn-Moore FJ, Aggarwal S, Tello JA, Ferrier DEK, Dholakia K. (2018). Light-sheet microscopy with attenuation-compensated propagation-invariant beams. *Sci Adv.*
United Kingdom · Mouse · fixed · 300 µm · Imaging PubMed

Szablowski JO, Lee-Gosselin A, Lue B, Malounda D, Shapiro MG. (2018). Acoustically targeted chemogenetics for the non-invasive control of neural circuits. *Nat Biomed Eng.*
United States · Mouse · fixed · 50 µm · Immunohistochemistry PubMed

Kondru N, Manne S, Greenlee J, West Greenlee H, Anantharam V, Halbur P, Kanthasamy A, Kanthasamy A. (2017). Integrated Organotypic Slice Cultures and RT-QuIC (OSCAR) Assay: Implications for Translational Discovery in Protein Misfolding Diseases. *Sci Rep.*
United States · Mouse · fixed · 350 µm · Slice culture PubMed

Miller OH, Bruns A, Ben Ammar I, Mueggler T, Hall BJ. (2017). Synaptic Regulation of a Thalamocortical Circuit Controls Depression-Related Behavior. *Cell Rep.*
Switzerland · Mouse · fixed · 100 µm · Immunohistochemistry PubMed

Pathania M, De Jay N, Maestro N, Harutyunyan AS, Nitarska J, Pahlavan P, Henderson S, Mikael LG, Richard-Londt A, Zhang Y, Costa JR, Hí©bert S, Khazaei S, Ibrahim NS, Herrero J, Riccio A, Albrecht S, Ketteler R, Brandner S, Kleinman CL, Jabado N, Salomoni P. (2017). H3.3(K27M) Cooperates with Trp53 Loss and PDGFRA Gain in Mouse Embryonic Neural Progenitor Cells to Induce Invasive High-Grade Gliomas. *Cancer Cell.*
United Kingdom · Mouse · fixed · 50-100 µm · Immunohistochemistry PubMed

Wong TTW, Zhang R, Zhang C, Hsu HC, Maslov KI, Wang L, Shi J, Chen R, Shung KK, Zhou Q, Wang LV. (2017). Label-free automated three-dimensional imaging of whole organs by microtomy-assisted photoacoustic microscopy. *Nat Commun.*
United States · Mouse · fixed · 20-500 µm · IHC / ISH PubMed

Fritzsch B, Duncan JS, Kersigo J, Gray B, Elliott KL. (2016). Neuroanatomical Tracing Techniques in the Ear: History, State of the Art, and Future Developments. *Methods Mol Biol.*
United States · Mouse · fixed · 100-200 µm · Immunohistochemistry PubMed

Garcia I, Bhullar PK, Tepe B, Ortiz-Guzman J, Huang L, Herman AM, Chaboub L, Deneen B, Justice NJ, Arenkiel BR. (2016). Local corticotropin releasing hormone (CRH) signals to its receptor CRHR1 during postnatal development of the mouse olfactory bulb. *Brain Struct Funct.*
United States · Mouse · fixed · 50 (fixed); 300 (live) µm · Electrophysiology PubMed

Garcí_a-Cabezas Mí, John YJ, Barbas H, Zikopoulos B. (2016). Distinction of Neurons, Glia and Endothelial Cells in the Cerebral Cortex: An Algorithm Based on Cytological Features. *Front Neuroanat.*

United States · Human · fixed · 50-75 µm · Immunohistochemistry PubMed

Hintiryan H, Foster NN, Bowman I, Bay M, Song MY, Gou L, Yamashita S, Bienkowski MS, Zingg B, Zhu M, Yang XW, Shih JC, Toga AW, Dong HW. (2016). The mouse cortico-striatal projectome. *Nat Neurosci.*
United States · Mouse · fixed · 50 µm · Immunohistochemistry PubMed

Huang L, Ung K, Garcia I, Quast KB, Cordiner K, Saggau P, Arenkiel BR. (2016). Task Learning Promotes Plasticity of Interneuron Connectivity Maps in the Olfactory Bulb. *J Neurosci.*
United States · Mouse · fixed · 50 (fixed); 300 (live) µm · Electrophysiology PubMed

Jameson H, Bateman R, Byrne P, Dyavanapalli J, Wang X, Jain V, Mendelowitz D. (2016). Oxytocin neuron activation prevents hypertension that occurs with chronic intermittent hypoxia/hypercapnia in rats. *Am J Physiol Heart Circ Physiol.*
United States · Mouse · fixed · 200 (fixed); 400 (live) µm · Electrophysiology PubMed

Kubota J, Mikami Y, Kanemaru K, Sekiya H, Okubo Y, Iino M. (2016). Whisker experience-dependent mGluR signalingmaintains synaptic strength in the mouse adolescentcortex. *Eur J Neurosci.*
Mouse · fixed · 300 µm · Electrophysiology PubMed

Vega-Zuniga T, Marí_n G, Gonzíçlez-Cabrera C, Planitscher E, Hartmann A, Marks V, Mpodozis J, Luksch H. (2016). Microconnectomics of the Pretectum and VentralThalamus in the Chicken (Gallus gallus). *J Comp Neurol.*
Chick · fixed · 500-900 µm · Immunohistochemistry PubMed

Wu ÎÇ_†__Â Q, Kolb I, Callahan BM, Su Z, Stoy W, Kodandaramaiah SB, Neve R, Zeng H, Boyden ES, Forest CR, Chubykin AA. (2016). Integration of autopatching with automated pipette and cell detection in vitro. *J Neurophysiol.*
United States · Mouse · fixed · 300 µm · Electrophysiology PubMed

Vieira PA, Korzus E. (2015). CBP-Dependent memory consolidation in the prefrontal cortex supports object-location learning. *Hippocampus.*
United States · Mouse · fixed · 50 µm · Immunohistochemistry PubMed

Xiao C, Miwa JM, Henderson BJ, Wang Y, Deshpande P, McKinney SL, Lester HA. (2015). Nicotinic receptor subtype-selective circuit patterns in the subthalamic nucleus. *J Neurosci.*
United States · Mouse · fixed · 350 (live); 40 (fixed) µm · Electrophysiology PubMed

Cetin A, Callaway EM. (2014). Optical control of retrogradely infected neurons using drug-regulated “TLoop” lentiviral vectors. *J Neurophysiol.*
United States · Mouse · fixed · 300 µm · Electrophysiology PubMed

Harischandra DS, Kondru N, Martin DP, Kanthasamy A, Jin H, Anantharam V, Kanthasamy AG. (2014). Role of proteolytic activation of protein kinase Cδ in the pathogenesis of prion disease. *Prion.*
United States · Mouse · fixed · 350 µm · Slice culture PubMed

Herman AM, Huang L, Murphey DK, Garcia I, Arenkiel BR. (2014). Cell type-specific and time-dependent light exposure contribute to silencing in neurons expressing Channelrhodopsin-2. *Elife.*
United States · Mouse · fixed · 50-100 (fixed); 300 (live) µm · Electrophysiology PubMed

Vega-Zuniga T, Mpodozis J, Karten HJ, Marí_n G, Hain S, Luksch H. (2014). Morphology, Projection Pattern and Neurochemical Identity of Cajal’s “Centrifugal Neurons”: The Cells of Origin of the Tectoventrogeniculate Pathway in Pigeon (Columba livia) and Chicken (Gallus gallus). *J Comp Neurol.*
Germany · Chick · fixed · 500-900 µm · Immunohistochemistry PubMed

Vieira PA, Lovelace JW, Corches A, Rashid AJ, Josselyn SA, Korzus E. (2014). Prefrontal consolidation supports the attainment of fear memory accuracy. *Learn Mem.*
United States · Mouse · fixed · 100 µm · Immunohistochemistry PubMed

Zingg B, Hintiryan H, Gou L, Song MY, Bay M, Bienkowski MS, Foster NN, Yamashita S, Bowman I, Toga AW, Dong HW. (2014). Neural networks of the mouse neocortex. *Cell.*
United States · Mouse · fixed · 50 µm · Immunohistochemistry PubMed

Huang L, Garcia I, Jen HI, Arenkiel BR. (2013). Reciprocal connectivity between mitral cells and external plexiform layer interneurons in the mouse olfactory bulb. *Front Neural Circuits.*
United States · Mouse · fixed · 50 (fixed); 300 (live) µm · Electrophysiology PubMed

Wickersham IR, Sullivan HA, Seung HS. (2013). Axonal and subcellular labelling using modified rabies viral vectors. *Nat Commun.*
United States · Mouse · fixed · 50 µm · Immunohistochemistry PubMed

Yu CR. (2013). Calcium imaging of vomeronasal organ response using slice preparations from transgenic mice expressing G-CaMP2. *Methods Mol Biol.*
United States · Mouse · fixed · 150-200 µm · Imaging PubMed

DR Kolson (2012). Temporal Patterns of Gene Expression in the MNTB During Calyx of Held Development. *Dev Neurobiol.*
United States · Mouse · fixed · 200 µm PubMed

Guan Y, Xiao C, Krnjevic K, Xie G, Zuo W, Ye JH. (2012). GABAergic actions mediate opposite ethanol effects on dopaminergic neurons in the anterior and posterior ventral tegmental area. *J Pharmacol Exp Ther.*
United States · Rat · fixed · 250-300 µm · Electrophysiology PubMed

Haddad-Tí_volli R, Heide M, Zhou X, Blaess S, Alvarez-Bolado G. (2012). Mouse thalamic differentiation: gli-dependent pattern and gli-independent prepattern. *Front Neurosci.*
Germany · Mouse · fixed · 75 µm · Immunohistochemistry PubMed

Duncan J, Kersigo J, Gray B, Fritzsch B. (2011). Combining lipophilic dye, in situ hybridization, immunohistochemistry, and histology. *J Vis Exp.*
United States · Mouse · fixed · Unknown µm · Immunohistochemistry PubMed

Selever J, Kong JQ, Arenkiel BR. (2011). A rapid approach to high-resolution fluorescence imaging in semi-thick brain slices. *J Vis Exp.*
United States · Mouse · fixed · 200 µm · Immunohistochemistry PubMed

Shao J, Lai D, Meyer U, Luksch H, Wessel R. (2009). Generating oscillatory bursts from a network of regular spiking neurons without inhibition. *J Comput Neurosci.*
United States · Chick · fixed · 500 µm · Electrophysiology PubMed

Xiao C, Shao XM, Olive MF, Griffin WC 3rd, Li KY, KrnjeviÛˆ K, Zhou C, Ye JH. (2009). Ethanol facilitates glutamatergic transmission to dopamine neurons in the ventral tegmental area. *Neuropsychopharmacology.*
United States · Rat · fixed · 250 µm · Electrophysiology PubMed

Hsieh CY, Hong CT, Cramer KS. (2007). Deletion of EphA4 enhances deafferentation-induced ipsilateral sprouting in auditory brainstem projections. *J Comp Neurol.*
United States · Mouse · fixed · 50 µm · Immunohistochemistry PubMed

Brainstem

DVF de Siqueira, N Boaretto, RM Leão (2024). Decreases in metabolic ATP open KATP channels and reduce firing in an auditory brainstem neuron: A dynamic mechanism of firing control during intense activity. *Neuroscience.*
Rat · live · 200 µm · Electrophysiology PubMed

PS Zarpellon, C Murat, RM Leão (2024). Reduction in mitochondrial ATP synthesis mimics the effect of low glucose in depolarizing neurons from the subpostremal nucleus of the solitary tract of rats. *Journal of Bioenergetics and Biomembranes.*
Brazil · Rats · live · 200 µm · Electrophysiology PubMed

S Ma, S Watanabe, DC Gillespie (2024). Ultrastructure of immature synaptic inputs in the lateral superior olive of the rodent brainstem. *bioRxiv.*
Rat · live · 250 µm · Electrophysiology PubMed

NM Benites, B Rodrigues… (2023). Development of electrophysiological properties of fusiform neurons from the dorsal cochlear nucleus of mice before and after hearing onset. *J Neurophysiol.*
Brazil · Mouse · live · 200 µm · Electrophysiology PubMed

DVF de Siqueira, PS Strazza Jr, NM Benites… (2022). Salicylate activates KATP channels and reduces spontaneous firing in glycinergic cartwheel neurons in the dorsal cochlear nucleus of rats. *European Journal of Pharmacology.*
Rat · live · 200 µm · Electrophysiology PubMed

S Gaige, R Barbouche… (2022). Constitutively active microglial populations limit anorexia induced by the food contaminant deoxynivalenol. *Journal of Neuroinflammation.*
France · Mouse · live · 250 µm · Imaging PubMed

C Nguyen, S Mondoloni, T Le Borgne, I Centeno… (2021). Nicotine inhibits the VTA-to-amygdala dopamine pathway to promote anxiety. *Neuron.*
France · Mouse · live · 250 µm · Electrophysiology PubMed

Q Wu, MA Shaikh, ES Meymand, B Zhang, KC Luk… (2020). Neuronal activity modulates alpha-synuclein aggregation and spreading in organotypic brain slice cultures and in vivo. *Acta neuropathologica*.
United States · Mouse · live · 350 µm · Slice culture PubMed

Spinal cord

M Zhang, Y Liang, Q Dai, H Gao, H Wang… (2024). A spinal neural circuit for electroacupuncture that regulates gastric functional disorders. *Journal of Integrative Medicine*.
China · Mouse · fixed · 300 µm PubMed

L Yang, F Liu, H Hahm, T Okuda, X Li, Y Zhang… (2024). Projection-TAGs enable multiplex projection tracing and multi-modal profiling of projection neurons. *bioRxiv*.
United States · Mouse · fixed · 30 and 400 µm PubMed

S Tsujikawa, KE DeMeulenaere, MV Centeno… (2023). Regulation of neuropathic pain by microglial Orai1 channels. *Science Advances*.
United States · Mouse · live · 400 µm · Electrophysiology PubMed

I Navickaite, N Pauziene, DH Pauza (2021). Anatomical evidence of non-parasympathetic cardiac nitrergic nerve fibres in rat. *Journal of Anatomy*.
Lithuania · Rat · fixed · 150 µm · IHC / ISH PubMed

Cooper JG, Sicard D, Sharma S, Van Gulden S, McGuire TL, Cajiao MP, Tschumperlin DJ, Kessler JA. (2020). Spinal Cord Injury Results in Chronic Mechanical Stiffening. *J Neurotrauma*.
United States · Mouse · live · 500 µm · Atomic force microscopy PubMed

NF Nolta, A Liberti, R Makol, M Han (2020). Gelatin embedding and LED autofluorescence reduction for rodent spinal cord histology. *Journal of Neuroscience Methods*.
United States · Rat · fixed · 40 µm · IHC / ISH PubMed

Nakano Y, Wiechert S, Bíçnfi B. (2019). Overlapping Activities of Two Neuronal Splicing Factors Switch the GABA Effect from Excitatory to Inhibitory by Regulating REST. *Cell Rep*.
United States · Mouse · live · 250 µm · Slice culture PubMed

Kalmbach BE, Buchin A, Long B, Close J, Nandi A, Miller JA, Bakken TE, Hodge RD, Chong P, de Frates R, Dai K, Maltzer Z, Nicovich PR, Keene CD, Silbergeld DL, Gwinn RP, Cobbs C, Ko AL, Ojemann JG, Koch C, Anastassiou CA, Lein ES, Ting JT. (2018). h-Channels Contribute to Divergent Intrinsic Membrane Properties of Supragranular Pyramidal Neurons in Human versus Mouse Cerebral Cortex. *Neuron*.
United States · Human · live · 350 µm · Electrophysiology PubMed

Premkumar LS. (2011). Methods Used for Studying TRP Channel Functions in Sensory Neurons. *TRP Channels*.
Mouse, Rat · live · 250 µm · Electrophysiology PubMed

Jeffry JA, Yu SQ, Sikand P, Parihar A, Evans MS, Premkumar LS. (2009). Selective targeting of TRPV1 expressing sensory nerve terminals in the spinal cord for long lasting analgesia. *PLoS One*.
United States · Rat · live · 300 µm · Electrophysiology PubMed

Eye & retina

M Chakraborty, AG Lara, A Dang… (2023). Sex-linked gene traffic underlies the acquisition of sexually dimorphic UV color vision in Heliconius butterflies. *PNAS*.
United States · Butterfly · fixed · 50 µm · Peer-reviewed publication PubMed

K Friedrichsen, P Ramakrishna, J Hsiang… (2022). Reconstructing neural circuits using multiresolution correlated light and electron microscopy. *Frontiers in Neural Circuits*.
United States · Mouse · fixed · 150 µm · Imaging PubMed

PL Rochon, C Theriault, AGR Olguin, A Krishnaswamy (2021). The cell adhesion molecule Sdk1 shapes assembly of a retinal circuit that detects localized edges. *Elife*.
Canada · Mouse · fixed · 100 µm · IHC / ISH PubMed

SK Bose, BM White, MV Kashyap, A Dave… (2021). In utero adenine base editing corrects multi-organ pathology in a lethal lysosomal storage disease. *Nat Commun*.
United States · Mouse · fixed · 150 µm · IHC / ISH PubMed

Lewis TR, Shores CR, Cady MA, Hao Y, Arshavsky VY, Burns ME. (2020). The F220C and F45L rhodopsin mutations identified in retinitis pigmentosa patients do not cause pathology in mice. *Sci Rep.*
United States · Mouse · fixed · 100 µm · IHC / ISH PubMed

Ear & cochlea

KE Murtha, WD Sese, K Sleiman, J Halpage… (2024). Absence of oncomodulin increases susceptibility to noise-induced outer hair cell death and alters mitochondrial morphology. *Frontiers in Neurology.*
United States · Mouse · fixed · 50 µm · IHC / ISH PubMed

M Scheibinger, A Janesick, GH Diaz… (2022). Immunohistochemistry and In Situ mRNA detection using inner ear vibratome sections. *Developmental, Physiological, and Functional Neurobiology of the Inner Ear.*
Mouse · fixed · 50-200 µm · IHC / ISH PubMed

Fritzsch B, Duncan JS, Kersigo J, Gray B, Elliott KL. (2016). Neuroanatomical Tracing Techniques in the Ear: History, State of the Art, and Future Developments. *Methods Mol Biol.*
United States · Mouse · fixed · 100-200 µm · Immunohistochemistry PubMed

Heart

CM McCarthy, KL McKevitt, SA Connolly, I Andersson… (2024). Microindentation of fresh soft biological tissue: A rapid tissue sectioning and mounting protocol. *Plos one.*
Ireland · Mouse, human · live · 150-1000 µm PubMed

D Ackerman, E Avetissian, CKE Bleck, JA Bogovic… (2024). Data Release: High-Resolution Imaging and Segmentation of P7 Mouse Tissue Microarchitecture Using FIB-SEM and Machine Learning. *bioRxiv.*
Mouse · fixed · 300 µm · Imaging PubMed

M Shammas (2024). Mitochondrial Dysfunction and Stress Responses in CHCHD10 Myopathy and Neurodegeneration. *University of Cambridge.*
Mouse · fixed · 35 µm · IHC / ISH PubMed

D Dileep, TA Syed, TFW Sloan, PS Dhandapany… (2023). Cardiomyocyte orientation recovery at micrometer scale reveals long-axis fiber continuum in heart walls. *The EMBO Journal.*
India · Mouse · fixed · 300 µm · Imaging PubMed

Z Li, EG Solomonidis, B Berkeley… (2023). Multi-species meta-analysis identifies transcriptional signatures associated with cardiac endothelial responses in the ischaemic heart. *Cardiovascular Research (European Society of Cardiology).*
United Kingdom · Mouse · fixed · 100 µm · IHC / ISH PubMed

DJ Chung, GP Madison, AM Aponte… (2022). Metabolic design in a mammalian model of extreme metabolism, the North American least shrew (Cryptotis parva). *J Physiol.*
United States · Shrew · fixed · 700 µm · Imaging PubMed

SK Bose, BM White, MV Kashyap, A Dave… (2021). In utero adenine base editing corrects multi-organ pathology in a lethal lysosomal storage disease. *Nat Commun.*
United States · Mouse · fixed · 150 µm · IHC / ISH PubMed

YT Liu, DA Sliter, MK Shammas, X Huang, C Wang… (2021). Mt-Keima detects PINK1-PRKN mitophagy in vivo with greater sensitivity than mito-QC. *Autophagy.*
United States · Mouse · fixed · 40-70 µm · IHC / ISH PubMed

Wen Q, Gandhi K, Capel RA, Hao G, O'Shea C, Neagu G, Pearcey S, Pavlovic D, Terrar DA, Wu J, Faggian G, Camelliti P, Lei M. (2018). Transverse cardiac slicing and optical imaging for analysis of transmural gradients in membrane potential and Ca(2+) transients in murine heart. *J Physiol.*
China · Mouse · live · 100, 300, 500 µm · Imaging PubMed

Hoffman JJ, Johnson BL, Holland MR, Fedewa RJ, Nair A, Miller JG. (2011). Layer-dependent variation in the anisotropy of apparent integrated backscatter from human coronary arteries. *Ultrasound Med Biol.*
United States · Human · live · 750 µm · Imaging PubMed

Kamari Y, Cohen H, Shaish A, Bitzur R, Afek A, Shen S, Vainshtein A, Harats D. (2008). Characterisation of atherosclerotic lesions with scanning electron microscopy (SEM) of wet tissue. *Diab Vasc Dis Res.*

Israel · Mouse · fixed · 200 µm · Immunohistochemistry PubMed

Lung

Precision-cut lung slices (PCLS) for airway pharmacology, fibrosis, and infection biology.

K Jankowski, SE Lemay, D Lozano-Ojalvo… (2024). Pharmacological Inhibition of Epac1 Protects against Pulmonary Fibrosis by Blocking FoxO3a Neddylation. *bioRxiv*.
United States · Human · live · 400 µm · PCLS PubMed

B Villa, B Erranz, P Cruces, J Retamal, DE Hurtado (2024). Mechanical and morphological characterization of the emphysematous lung tissue. *Acta Biomaterialia*.
Chile · Rat · live · Unknown µm · Electrophysiology PubMed

C Diaz-Nicieza, L Sahyoun, C Michalaki… (2024). Ageing results in an exacerbated inflammatory response to LPS by resident lung cells. *Immunity & Ageing*.
United Kingdom · Mouse · live · 300 µm · PCLS PubMed

C Zeng, H Yue, C Wang, X Ju, T Wang, X Fu… (2024). Albendazole ameliorates aerobic glycolysis in myofibroblasts to reverse pulmonary fibrosis. *Journal of Translational Medicine*.
China · Human · live · 400 µm · PCLS PubMed

C Zeng, Q Wang, X Liu, K Wang, C Wang… (2024). Localized administration of Bcar3 siRNA via nano-self-assembly to treat idiopathic pulmonary fibrosis by disrupting macrophage-fibroblast crosstalk. *International Journal of Nanomedicine*.
China · Human · live · 400 µm · PCLS PubMed

CL Wilkinson, K Nakano, SA Grimm… (2024). GM-CSF-dependent CD301b+ lung dendritic cells confer tolerance to inhaled allergens. *Research Square*.
United States · Mouse · live · 110 µm · PCLS PubMed

D Yang, N Almanzar, J Xia, S Udit, ST Yeung… (2024). Vagal TRPV1+ sensory neurons regulate myeloid cell dynamics and protect against influenza virus infection. *bioRxiv*.
Mouse · live · 200 µm · PCLS PubMed

DJM Kollareth, AK Sharma (2024). Precision cut lung slices: an innovative tool for lung transplant research. *Frontiers in Immunology*.
United States · Human, mouse · live · 150-500 µm · PCLS PubMed

DW Ahmed, ML Tan, J Gabbard, Y Liu, MM Hu… (2024). Local photo-crosslinking of native tissue matrix regulates cell function. *bioRxiv*.
United States · Mouse · live · 300 µm · PCLS PubMed

H Osman-Ponchet, L Perdigon, M Barthe… (2024). Advances in In Vitro Modeling of Pulmonary Fibrosis: Focus on Precision-Cut Lung Slices (PCLS) Model. *LIVe 2024-Lung In Vitro Event*.
Human · live · 200-300 µm · PCLS PubMed

HA Flaxman, MA Chrysovergi, H Han, F Kabir… (2024). Sanglifehrin A mitigates multi-organ fibrosis by targeting the collagen chaperone cyclophilin B. *JCI Insight*.
Mouse · live · 200-300 µm · PCLS PubMed

HM Gomez, TJ Haw, D Ilic, P Robinson… (2024). Landscape fire smoke airway exposure impairs respiratory and cardiac function and worsens experimental asthma. *Journal of Allergy and Clinical Immunology*.
Australia · Mouse · live · 150 µm · PCLS PubMed

JD Cala Garcia, CF Arce Deza, AR Waich… (2024). Testing the Viability and Efficacy of Small Molecule Inhibitors in T-cells in Cryopreserved Precision Cut Lung Slices: New Insights for Long Term-storage Lung …. *A71 CUTTINGEDGE TECHNOLOGIES FOR LUNGDISCOVERY*.
Mouse · live · 500 µm · PCLS PubMed

L Perdigon, M Barthe, H Osman-Ponchet… (2024). Successful Development of Human Precision-Cut Lung Slice (hPCLS) Model for Studying Lung Disease. *HAL Open Science*.
Human · live · 300 µm · PCLS PubMed

M Boucher, C Henry, L Gélinas, R Packwood… (2024). High throughput screening of airway constriction in mouse lung slices. *Scientific Reports*.

Canada · Mouse · live · 200 µm · PCLS PubMed

M Bruegger, C Machahua, B Zumkehr, C Cismaru… (2024). Aging shapes infection profiles of influenza A virus and SARS-CoV-2 in human lung slices. *bioRxiv*.
Human · live · 400 µm · PCLS PubMed

M Chioccioli, S Liu, S Magruder, A Tata, L Borriello… (2024). Stem cell migration drives lung repair in living mice. *Developmental cell*.
Mouse · live · 300 µm · PCLS PubMed

M Lehmann, R Krishnan, J Sucre… (2024). Precision Cut Lung Slices: Emerging Tools for Preclinical and Translational Lung Research. An Official American Thoracic Society Workshop Report. *American Thoracic Society Documents*.
Mouse · live · Unknown µm · PCLS PubMed

M Vierhout, A Ayoub, P Ali, V Kumaran, S Naiel… (2024). A Novel Ex Vivo Approach for Investigating Profibrotic Macrophage Polarization Using Murine Precision-Cut Lung Slices. *Biochemical and Biophysical Research Communications*.
Canada · Mouse · live · 500 µm · PCLS PubMed

ML Cohen, AN Brumwell, TC Ho, K Garakani… (2024). A fibroblast-dependent TGF-β1/sFRP2 noncanonical Wnt signaling axis promotes epithelial metaplasia in idiopathic pulmonary fibrosis. *The Journal of Clinical Investigation*.
United States · Human · live · 400 µm · PCLS PubMed

N Schaunaman, D Cervantes, T Nichols, M Numata… (2024). Cooperation of immune regulators Tollip and surfactant protein A inhibits influenza a virus infection in mice. *Respiratory Research*.
United States · Mouse · live · 250 µm · Electrophysiology PubMed

R Joulia, F Puttur, H Stölting, WJ Traves… (2024). Mast cell activation disrupts interactions between endothelial cells and pericytes during early life allergic asthma. *The Journal of Clinical Investigation*.
United Kingdom · Mouse · fixed · 100-200 µm · Imaging PubMed

RE Lee-Ferris, K Okuda, JR Galiger, SA Schworer… (2024). Prolonged airway explant culture enables study of health, disease, and viral pathogenesis. *bioRxiv*.
Human · live · 300 µm · PCLS PubMed

S Bozzini, E Bozza, C Bagnera… (2024). Assessment of Imatinib Anti-Remodeling Activity on a Human Precision Cut Lung Slices Model. *International Journal of Molecular Sciences*.
Italy · human · live · 300-350 µm · PCLS PubMed

S Hall, S Liu, I Liang, S Schulz, C Ezran, M Tan… (2024). Cellular and molecular characterization of peripheral glia in the lung and other organs. *PloS one*.
United States · Mice · fixed · 300 µm · IHC / ISH PubMed

SE Lemay, MS Montesinos, Y Grobs, T Yokokawa… (2024). Exploring Integrin α5β1 as a Potential Therapeutic Target for Pulmonary Arterial Hypertension: Insights from Comprehensive Multicenter Preclinical Studies. *bioRxiv*.
Human · live · 400 µm · PCLS PubMed

SM Lingamallu, A Deshpande, N Joy, K Ganeshan… (2024). Neuroepithelial bodies and terminal bronchioles are niches for distinctive club cells that repair the airways following acute notch inhibition. *Cell Reports*.
India · Mouse · live · 200 µm · PCLS PubMed

SS Cheong, TC Luis, M Hind, CH Dean (2024). A Novel Method for Floxed Gene Manipulation Using TAT-Cre Recombinase in Ex Vivo Precision-Cut Lung Slices (PCLS). *Bio-protocol*.
United Kingdom · Mouse · live · 250 µm · PCLS PubMed

SY Kim, D McTeague, SS Cheong, M Hind… (2024). Deciphering the impacts of modulating the Wnt-planar cell polarity (PCP) pathway on alveolar repair. *Frontiers in Cell and Developmental Biology*.
United Kingdom · Mouse · live · 300 µm · Electrophysiology PubMed

W Yu, Y Zhang, CTK Lo, L Kang, TTW Wong (2024). Rapid full-color serial sectioning tomography with speckle illumination and ultraviolet excitation. *npj Imaging*.
China · Mouse · fixed · 50 µm PubMed

A Lazrak, W Song, Z Yu, S Zhang, A Nellore… (2023). Low molecular weight hyaluronan inhibits lung epithelial ion channels by activating the calcium-sensing receptor. *Matrix Biology*.
United States · Mouse · live · 250 µm · PCLS PubMed

A Urso (2023). Pathophysiology of bile acid aspiration in lung transplant recipients. *Università di Bologna*.
Mouse · live · 130 µm · PCLS PubMed

AJ Heires, D Samuelson, D Villageliu, TM Nordgren… (2023). Agricultural dust derived bacterial extracellular vesicle mediated inflammation is attenuated by DHA. *Scientific reports*.
United States · Human · live · 300 µm · PCLS PubMed

C Wang, B Hyams, NC Allen, K Cautivo, K Monahan… (2023). Dysregulated lung stroma drives emphysema exacerbation by potentiating resident lymphocytes to suppress an epithelial stem cell reservoir. *Immunity*.
United States · Mouse · fixed · 200 µm · Imaging PubMed

C Zeng, Q Wang, C Wang, Q Zhou, X Fu, J Yu, W Xiong… (2023). Local Delivery of Bcar3 siRNA by Nano-Self-Assembly for Treating Pulmonary Fibrosis via Blocking the Interaction of Macrophages and Fibroblasts. *Research Square*.
Mouse, Human · live · 400 µm · PCLS PubMed

D Cervantes, N Schaunaman, GP Downey… (2023). Desert particulate matter from Afghanistan increases airway obstruction in human distal lungs exposed to type 2 cytokine IL-13. *Frontiers in Medicine*.
United States · Human · live · 300 µm · PCLS PubMed

EB Gebski, V Parikh, H Lam, N Kim… (2023). Rhinovirus C15 attenuates relaxation and cAMP production in Human Airways and smooth muscle. *American Thoracic Society*.
United States · Human · live · 350 µm · PCLS PubMed

F Ahangari, NL Price, S Malik, M Chioccioli… (2023). microRNA-33 deficiency in macrophages enhances autophagy, improves mitochondrial homeostasis, and protects against lung fibrosis. *JCI Insight*.
United States · Mouse · live · 150 µm · PCLS PubMed

H Agraval, T Crue, N Schaunaman, M Numata… (2023). Electronic Cigarette Exposure Increases the Severity of Influenza a Virus Infection via TRAIL Dysregulation in Human Precision-Cut Lung Slices. *International Journal of Molecular Sciences*.
United States · Human · live · 450 µm · PCLS PubMed

J Sbierski-Kind, KM Cautivo, JC Wagner, MW Dahlgren… (2023). Group 2 innate lymphoid cells constrain type 3/17 lymphocytes in shared stromal niches to restrict liver fibrosis. *bioRxiv*.
Mouse · fixed · 200 µm · IHC / ISH PubMed

JC Nawroth, D Roth, A van Schadewijk, A Ravi… (2023). Breathing on chip: Dynamic flow and stretch accelerate mucociliary maturation of airway epithelium in vitro. *Materials Today Bio*.
United States · Human · fixed · 130 µm · IHC / ISH PubMed

KL Leiby, Y Yuan, R Ng, MSB Raredon… (2023). Rational engineering of lung alveolar epithelium. *NPJ Regenerative Medicine*.
United States · Rat · live · 450 µm · PCLS PubMed

KZ Wu, C Adine, A Mitriashkin, BJJ Aw… (2023). Making In Vitro Tumor Models Whole Again. *Advanced Healthcare Materials*.
Singapore · Human · live · 30-1000 µm PubMed

M Lam, E Lamanna, L Organ, C Donovan… (2023). Perspectives on precision cut lung slices—powerful tools for investigation of mechanisms and therapeutic targets in lung diseases. *Frontiers in Pharmacology*.
Australia · Mouse · live · 150-300 µm · PCLS PubMed

MCF Llerena (2023). Participación del canal de cloruro activado por calcio (tmem16a) en la contracción inducida por atp en células musculares lisas de venas intrapulmonares de rata. *Universidad de Chile Facultad de medicina Escuela de Postgrado*.
Rat · live · 150 µm · PCLS PubMed

P Yadav, JG Ortega, W Tamaki, C Chien, K Chang… (2023). Macrophage-fibroblast crosstalk drives Arg1-dependent lung fibrosis via ornithine loading. *bioRxiv*.
Human, Mouse · live · 400 µm · PCLS PubMed

R Joulia, F Puttur, H Stölting, LJ Entwistle, A Voitovich… (2023). Adventitial Mast Cell Activation Disrupts Endothelial Cell/Pericyte Interactions During Early Life Allergic Asthma. *The Journal of Clinical Investigation*.
Mouse · fixed · 100-200 µm · PCLS PubMed

S Ahn, H Maarsingh, JKL Walker… (2023). Allosteric modulator potentiates β2AR agonist-promoted bronchoprotection in asthma models. *The Journal of Clinical Investigation*.
United States · Guinea pig · live · 500 µm · PCLS PubMed

S Naiel, N Dowdall, SD Revill, V Kumaran… (2023). Reprogramming Rogue Macrophages: Yeast Beta-glucan Microparticles as a Macrophage Modulator for Lung Fibrosis. *B65. Immune and Endothelial Cells Hit Back at Lung Repair*.
Mouse · live · Unknown µm · PCLS PubMed

S Uribe, PD Yim, JF Perez-Zoghbi (2023). Airway Smooth Muscle Relaxation Via Opsin 3 Activation With Beta-carotene Metabolites. *A70 RELAX ALREADY! MECHANISTIC INSIGHTS INTO AIRWAY SMOOTH MUSCLE BIOLOGY*.
Mouse · live · 130 µm · PCLS PubMed

SN Sveiven, SY Kim, V Barrientos, J Li… (2023). Myeloid-and epithelial-derived RELMα contribute to tissue repair following lung helminth infection. *Frontiers in Oncology*.
United States · Mouse · live · 300 µm · PCLS PubMed

SS Cheong, TC Luis, M Stewart… (2023). A method for TAT-Cre recombinase-mediated floxed allele modification in ex vivo tissue slices. *Disease Models & Mechanisms*.
United Kingdom · Mouse · live · 250 µm · PCLS PubMed

T Crue, GY Lee, JY Peng, N Schaunaman… (2023). Single cell RNA-sequencing of human precision-cut lung slices: A novel approach to study the effect of vaping and viral infection on lung health. *Innate Immunity (Sage Publication)*.
United States · Human · live · 450 µm · PCLS PubMed

Y Bai, G Li, L Yung, PB Yu, X Ai (2023). Intrapulmonary arterial contraction assay reveals region-specific deregulation of vasoreactivity to lung injuries. *American Journal of Physiology*.
United States · Mouse · live · 150 µm · Imaging PubMed

Y Cui, Z Yang, Z Lv, J Lei (2023). Disruption of extracellular redox balance drives persistent lung fibrosis and impairs fibrosis resolution. *Biochimica et Biophysica Acta (BBA) - Molecular Basis of Disease*.
China · Mouse · live · 250 µm · PCLS PubMed

Z Zeng, M Cheng, M Li, T Wang, F Wen… (2023). Inherent differences of small airway contraction and Ca2+ oscillations in airway smooth muscle cells between BALB/c and C57BL/6 mouse strains. *Frontiers in Cell and Developmental Biology*.
China · Mouse · live · 180 µm · PCLS PubMed

C Michalaki, C Dean, C Johansson (2022). The Use of Precision-Cut Lung Slices for Studying Innate Immunity to Viral Infections. *Current Protocols*.
United Kingdom · Mouse · live · Unknown µm · PCLS PubMed

D Shrestha, N Massey, SM Bhat… (2022). Nrf2 Activation Protects Against Organic Dust and Hydrogen Sulfide Exposure Induced Epithelial Barrier Loss and K. pneumoniae Invasion. *Front Cell Infect Microbiol*.
United States · Mouse · live · 300 µm · PCLS PubMed

JF Perez-Zoghbi, DR Sajorda, DA Webb… (2022). Imidazobenzodiazepine PI320 Relaxes Mouse Peripheral Airways by Inhibiting Calcium Mobilization. *American Journal of Respiratory Cell and Molecular Biology*.
United States · Mouse · live · 130 µm · PCLS PubMed

KM Cautivo, PR Matatia, CO Lizama, NM Mroz… (2022). Interferon gamma constrains type 2 lymphocyte niche boundaries during mixed inflammation. *Immunity*.
United States · Mouse · fixed · 200-500 µm · IHC / ISH PubMed

M Chioccioli, S Roy, R Newell, L Pestano, B Dickinson… (2022). A lung targeted miR-29 Mimic as a Therapy for Pulmonary Fibrosis. *EBioMedicine*.
United States · Human · live · 300 µm · PCLS PubMed

M Looney, M Magnen, R You, A Rao, R Davis… (2022). Immediate myeloid depot for SARS-CoV-2 in the human lung. *Neurobio of Inner Ear*.
United States · Book/book chapter PubMed

R Guidi, D Xu, DF Choy, TR Ramalingam… (2022). Steroid-induced fibroblast growth factors drive an epithelial-mesenchymal inflammatory axis in severe asthma. *Science translational medicine*.
United States · Human, Mouse · live · 350 µm · PCLS PubMed

SA Guler, C Machahua, TK Geiser, G Kocher… (2022). Dehydroepiandrosterone in fibrotic interstitial lung disease: a translational study. *Respir Res.*
Switzerland · Human · live · 400 µm · PCLS PubMed

E Luković, JF Perez-Zoghbi, Y Zhang… (2021). Ginger metabolites and metabolite-inspired synthetic products modulate intracellular calcium and relax airway smooth muscle. *Am J Physiol Lung Cell Mol Physiol.*
United States · Mouse · live · 130 µm · PCLS PubMed

H Maarsingh, A Oldenburger, B Han, AB Zuidhof… (2021). Effects of (a Combination of) the Beta2-Adrenoceptor Agonist Indacaterol and the Muscarinic Receptor Antagonist Glycopyrrolate on Intrapulmonary Airway …. *Cells.*
United States · Guinea pig · live · 500 µm · PCLS PubMed

M Sponchiado, YS Liao, KR Atanasova… (2021). Overexpression of substance P in pig airways increases MUC5AC through an NF-kβ pathway. *Physiological Reports.*
United States · Pig · live · 300 µm · PCLS PubMed

P Lu, MK ElMallah, Z Liu, C Wu, J Chen… (2021). Genetic deletion of the Tas2r143/Tas2r135/Tas2r126 cluster reveals that TAS2Rs may not mediate bitter tastant-induced bronchodilation. *J Cell Physiol.*
United States · Mouse · live · 180 µm · PCLS PubMed

R Basoalto, LF Damiani, MC Bachmann… (2021). Acute lung injury secondary to hydrochloric acid instillation induces small airway hyperresponsiveness. *American Journal of Translational Research.*
Chile · Rat · live · 150 µm · PCLS PubMed

SK Bose, BM White, MV Kashyap, A Dave… (2021). In utero adenine base editing corrects multi-organ pathology in a lethal lysosomal storage disease. *Nat Commun.*
United States · Mouse · fixed · 150 µm · IHC / ISH PubMed

SY Kim, R Mongey, P Wang, S Rothery, DCA Gaboriau… (2021). The acid injury and repair (AIR) model: A novel ex-vivo tool to understand lung repair. *Biomaterials.*
United Kingdom · Mouse · live · 300 µm · PCLS PubMed

YN Dong, FC Hsu, CJ Koziol-White, V Stepanova… (2021). Functional NMDA receptors are expressed by human pulmonary artery smooth muscle cells. *Scientific reports.*
United States · Human · live · 350 µm · PCLS PubMed

Alsafadi HN, Uhl FE, Pineda RH, Bailey KE, Rojas M, Wagner DE, Kí_nigshoff M. (2020). Applications and Approaches for Three-Dimensional Precision-Cut Lung Slices. Disease Modeling and Drug Discovery. *Am J Respir Cell Mol Biol.*
Sweden · Mouse, Rat, Human · live · 150-500 µm · PCLS PubMed

Branchett WJ, Stí_lting H, Oliver RA, Walker SA, Puttur F, Gregory LG, Gabryçovíç L, Wilson MS, O'Garra A, Lloyd CM. (2020). A T cell-myeloid IL-10 axis regulates pathogenic IFN-'_-dependent immunity in a mouse model of type 2-low asthma. *J Allergy Clin Immunol.*
United Kingdom · Mouse · live · 200 µm · PCLS PubMed

Bryson KJ, Garrido D, Esposito M, McLachlan G, Digard P, Schouler C, Guabiraba R, Trapp S, Vervelde L. (2020). Precision cut lung slices: a novel versatile tool to examine host-pathogen interaction in the chicken lung. *Vet Res.*
United Kingdom · Chick · live · 500 µm · PCLS PubMed

Dragunas G, Woest ME, Nijboer S, Bos ST, van Asselt J, de Groot AP, Vohlí_dalovíç E, Vermeulen CJ, Ditz B, Vonk JM, Koppelman GH, van den Berge M, Ten Hacken NHT, Timens W, Munhoz CD, Prakash YS, Gosens R, Kistemaker LEM. (2020). Cholinergic neuroplasticity in asthma driven by TrkB signaling. *FASEB J.*
Netherlands · Mouse · live · 250 µm · PCLS PubMed

Entwistle LJ, Puttur F, Gregory LG, Lloyd CM. (2020). Group 2 ILC Functional Assays in Allergic Airway Inflammation. *Innate Lymphoid Cells.*
United States · Mouse · live · 200 µm · PCLS PubMed

Heras AF, Veerappan A, Silver RB, Emala CW, Worgall TS, Perez-Zoghbi J, Worgall S. (2020). Increasing Sphingolipid Synthesis Alleviates Airway Hyperreactivity. *Am J Respir Cell Mol Biol.*
Mouse · live · 130 µm · PCLS PubMed

J Huang, H Lam, C Koziol-White… (2020). The odorant receptor OR2W3 on airway smooth muscle evokes bronchodilation via a cooperative chemosensory tradeoff between TMEM16A and CFTR. *PNAS.*
United States · Human · live · 350 µm · PCLS PubMed

Koziol-White C, Johnstone TB, Corpuz ML, Cao G, Orfanos S, Parikh V, Deeney B, Tliba O, Ostrom RS, Dainty I, Panettieri RA Jr. (2020). Budesonide enhances agonist-induced bronchodilation in human small airways by increasing cAMP production in airway smooth muscle. *Am J Physiol Lung Cell Mol Physiol*.
United States · Human · live · 350 µm · PCLS PubMed

Koziol-White CJ, Ghosh A, Sandner P, Erzurum SE, Stuehr DJ, Panettieri RA Jr. (2020). Soluble Guanylate Cyclase Agonists Induce Bronchodilation in Human Small Airways. *Am J Respir Cell Mol Biol*.
United States · Human · live · 350 µm · PCLS PubMed

Li G, Cohen JA, Martines C, Ram-Mohan S, Brain JD, Krishnan R, Ai X, Bai Y. (2020). Preserving Airway Smooth Muscle Contraction in Precision-Cut Lung Slices. *Sci Rep*.
China · Mouse · live · 150 µm · PCLS PubMed

Lu RA, Zeki AA, Ram-Mohan S, Nguyen N, Bai Y, Chmiel K, Pecic S, Ai X, Krishnan R, Ghosh CC. (2020). Inhibiting Airway Smooth Muscle Contraction Using Pitavastatin: A Role for the Mevalonate Pathway in Regulating Cytoskeletal Proteins. *Front Pharmacol*.
United States · Mouse · live · 250 µm · PCLS PubMed

Parikh V, Scala J, Patel R, Corbi C, Lo D, Bochkov YA, Kennedy JL, Kurten RC, Liggett SB, Gern JE, Koziol-White CJ. (2020). Rhinovirus C15 Induces Airway Hyperresponsiveness via Calcium Mobilization in Airway Smooth Muscle. *Am J Respir Cell Mol Biol*.
United States · Human · live · 350 µm · PCLS PubMed

Poole JA, Nordgren TM, Heires AJ, Nelson AJ, Katafiasz D, Bailey KL, Romberger DJ. (2020). Amphiregulin modulates murine lung recovery and fibroblast function following exposure to agriculture organic dust. *Am J Physiol Lung Cell Mol Physiol*.
United States · Human · live · 300 µm · PCLS PubMed

Ram-Mohan S, Bai Y, Schaible N, Ehrlicher AJ, Cook DP, Suki B, Stoltz DA, Solway J, Ai X, Krishnan R. (2020). Tissue traction microscopy to quantify muscle contraction within precision-cut lung slices. *Am J Physiol Lung Cell Mol Physiol*.
Israel · Pig, Human · live · 250-300 µm · PCLS PubMed

S Xu-Vanpala, ME Deerhake, JD Wheaton… (2020). Functional heterogeneity of alveolar macrophage population based on expression of CXCL2. *Science Immunology*.
United States · Mouse · live · 150 µm · PCLS PubMed

SS Cheong, KM Akram, C Matellan, SY Kim… (2020). The planar polarity component VANGL2 is a key regulator of mechanosignaling. *Frontiers in Cell and Developmental Biology*.
United Kingdom · Mouse · live · 300 µm · PCLS PubMed

SU Hettiarachchi, YH Li, J Roy, F Zhang… (2020). Targeted inhibition of PI3 kinase/mTOR specifically in fibrotic lung fibroblasts suppresses pulmonary fibrosis in experimental models. *Science Translational Medicine*.
United States · Human, Mouse · live · 350 µm · PCLS PubMed

SY Kim, R Mongey, M Griffiths, M Hind… (2020). An Ex Vivo Acid Injury and Repair (AIR) Model Using Precision-Cut Lung Slices to Understand Lung Injury and Repair. *Current Protocols in Mouse Biology*.
United Kingdom · Mouse · live · 300 µm · PCLS PubMed

Shrestha S, Cho W, Stump B, Imani J, Lamattina AM, Louis PH, Pazzanese J, Rosas IO, Visner G, Perrella MA, El-Chemaly S. (2020). FK506 induces lung lymphatic endothelial cell senescence and downregulates LYVE-1 expression, with associated decreased hyaluronan uptake. *Mol Med*.
United States · Mouse · live · 200 µm · PCLS PubMed

Urso A, D'Ovidio F, Xu D, Emala CW Sr, Bunnett NW, Perez-Zoghbi JF. (2020). Bile acids inhibit cholinergic constriction in proximal and peripheral airways from humans and rodents. *Am J Physiol Lung Cell Mol Physiol*.
United States · Mouse, Human · live · 130 µm · PCLS PubMed

van den Berg M, Nijboer-Brinksma S, Bos S, van den Berge M, Lamb D, van Faassen M, Kema I, Gosens R, Kistemaker L. (2020). The novel TRPA1 antagonist BI01305834 inhibits ovalbumin-induced bronchoconstriction in guinea pigs. *Br J Pharmacol*.
Netherlands · Guinea pig · live · 500 µm · PCLS PubMed

van den Berg MPM, Kurhade SH, Maarsingh H, Erceg S, Hulsbeek IR, Boekema PH, Kistemaker LEM, van Faassen M, Kema IP, Elsinga PH, Dí_mling A, Meurs H, Gosens R. (2020). Pharmacological Screening Identifies SHK242 and

SHK277 as Novel Arginase Inhibitors with Efficacy against Allergen-Induced Airway Narrowing In Vitro and In Vivo. *J Pharmacol Exp Ther.*
Guinea pig · live · 500 µm · PCLS

Akram KM, Yates LL, Mongey R, Rothery S, Gaboriau DCA, Sanderson J, Hind M, Griffiths M, Dean CH. (2019). Live imaging of alveologenesis in precision-cut lung slices reveals dynamic epithelial cell behaviour. *Nat Commun.*
United Kingdom · Mouse · live · 300 µm · PCLS PubMed

Amarelle L, Katzen J, Shigemura M, Welch LC, Cajigas H, Peteranderl C, Celli D, Herold S, Lecuona E, Sznajder JI. (2019). Cardiac glycosides decrease influenza virus replication by inhibiting cell protein translational machinery. *Am J Physiol Lung Cell Mol Physiol.*
United States · Mouse · live · 100 µm · PCLS PubMed

Brann KR, Fullerton MS, Onyilagha FI, Prince AA, Kurten RC, Rom JS, Blevins JS, Smeltzer MS, Voth DE. (2019). Infection of Primary Human Alveolar Macrophages Alters Staphylococcus aureus Toxin Production and Activity. *Infect Immun.*
United States · Human · live · 750 µm · PCLS PubMed

Bui CB, Kolodziej M, Lamanna E, Elgass K, Sehgal A, Rudloff I, Schwenke DO, Tsuchimochi H, Kroon MAGM, Cho SX, Maksimenko A, Cholewa M, Berger PJ, Young MJ, Bourke JE, Pearson JT, Nold MF, Nold-Petry CA. (2019). Interleukin-1 Receptor Antagonist Protects Newborn Mice Against Pulmonary Hypertension. *Front Immunol.*
Australia · Mouse · live · 150 µm · PCLS PubMed

Dahlgren MW, Jones SW, Cautivo KM, Dubinin A, Ortiz-Carpena JF, Farhat S, Yu KS, Lee K, Wang C, Molofsky AV, Tward AD, Krummel MF, Peng T, Molofsky AB. (2019). Adventitial Stromal Cells Define Group 2 Innate Lymphoid Cell Tissue Niches. *Immunity.*
United States · Mouse · fixed · 300 µm · Imaging PubMed

Dragan AL, Kurten RC, Voth DE. (2019). Characterization of Early Stages of Human Alveolar Infection by the Q Fever Agent Coxiella burnetii. *Infection and immunity.*
United States · Human · live · 750 µm · PCLS PubMed

KM Akram, LL Yates, R Mongey, S Rothery… (2019). Time-lapse imaging of alveologenesis in mouse precision-cut lung slices. *Bio Protoc.*
United Kingdom · Mouse · live · 300 µm · PCLS PubMed

Kennedy JL, Kurten RC, McCullough S, Panettieri RA, Koziol-White C, Jones SM, Caid K, Gill PS, Roberts D, Jaeschke H, McGill MR, James L. (2019). Acetaminophen is both bronchodilatory and bronchoprotective in human precision cut lung slice airways. *Xenobiotica.*
United States · Human · live · 750 µm · PCLS PubMed

Maarsingh H, Bidan CM, Brook BS, Zuidhof AB, Elzinga CRS, Smit M, Oldenburger A, Gosens R, Timens W, Meurs H. (2019). Small airway hyperresponsiveness in COPD: relationship between structure and function in lung slices. *Am J Physiol Lung Cell Mol Physiol.*
Netherlands · Guinea pig; Human · live · 500 µm · PCLS PubMed

Mikami M, Perez-Zoghbi JF, Zhang Y, Emala CW Sr. (2019). Attenuation of murine and human airway contraction by a peptide fragment of the cytoskeleton regulatory protein gelsolin. *Am J Physiol Lung Cell Mol Physiol.*
United States · Mouse · live · 130 µm · PCLS PubMed

Puttur F, Denney L, Gregory LG, Vuononvirta J, Oliver R, Entwistle LJ, Walker SA, Headley MB, McGhee EJ, Pease JE, Krummel MF, Carlin LM, Lloyd CM. (2019). Pulmonary environmental cues drive group 2 innate lymphoid cell dynamics in mice and humans. *Sci Immunol.*
United Kingdom · Mouse · live · 200 µm · PCLS PubMed

Singh BK, Lu W, Schmidt Paustian AM, Ge MQ, Koziol-White CJ, Flayer CH, Killingbeck SS, Wang N, Dong X, Riese MJ, Deshpande DA, Panettieri RA Jr, Haczku A, Kambayashi T. (2019). Diacylglycerol kinase Zeta promotes allergic airway inflammation and airway hyperresponsiveness through distinct mechanisms. *Sci Signal.*
United States · Human · live · 350 µm · PCLS PubMed

Wang W, Cohen JA, Wallrapp A, Trieu KG, Barrios J, Shao F, Krishnamoorthy N, Kuchroo VK, Jones MR, Fine A, Bai Y, Ai X. (2019). Age-Related Dopaminergic Innervation Augments T Helper 2-Type Allergic Inflammation in the Postnatal Lung. *Immunity.*
United States · Mouse · live · 150 µm · PCLS PubMed

Yim PD, Gallos G, Perez-Zoghbi JF, Zhang Y, Xu D, Wu A, Berkowitz DE, Emala CW. (2019). Airway smooth muscle photorelaxation via opsin receptor activation. *Am J Physiol Lung Cell Mol Physiol.*
United States · Mouse · live · 130 µm · PCLS PubMed

Yocum GT, Perez-Zoghbi JF, Danielsson J, Kuforiji AS, Zhang Y, Li G, Rashid Roni MS, Kodali R, Stafford DC, Arnold LA, Cook JM, Emala CW Sr. (2019). A novel GABA(A) receptor ligand MIDD0301 with limited blood-brain barrier penetration relaxes airway smooth muscle ex vivo and in vivo. *Am J Physiol Lung Cell Mol Physiol.*
United States · Mouse · live · 130 µm · PCLS PubMed

Buttrick TS, Wang W, Yung C, Trieu KG, Patel K, Khoury SJ, Ai X, Elyaman W. (2018). Foxo1 Promotes Th9 Cell Differentiation and Airway Allergy. *Sci Rep.*
United States · Mouse · live · 200 µm · PCLS PubMed

Chen J, Miller M, Unno H, Rosenthal P, Sanderson MJ, Broide DH. (2018). Orosomucoid-like 3 (ORMDL3) upregulates airway smooth muscle proliferation, contraction, and Ca(2+) oscillations in asthma. *J Allergy Clin Immunol.*
China · Mouse · live · 180 µm · PCLS PubMed

Henriquez M, Fonseca M, Perez-Zoghbi JF. (2018). Purinergic receptor stimulation induces calcium oscillations and smooth muscle contraction in small pulmonary veins. *J Physiol.*
Chile · Rat · live · 150 µm · PCLS PubMed

Kennedy JL, Koziol-White CJ, Jeffus S, Rettiganti MR, Fisher P, Kurten M, Eze A, House S, Sikes JD, Askew E, Putt C, Panettieri RA, Jones SM, Kurten RC. (2018). Effects of rhinovirus 39 infection on airway hyperresponsiveness to carbachol in human airways precision cut lung slices. *J Allergy Clin Immunol.*
United States · Human · live · 150 µm · PCLS PubMed

Liu Y, Lv L, Wang L, Zhong Y. (2018). Social Isolation Induces Rac1-Dependent Forgetting of Social Memory. *Cell Rep.*
China · Mouse · live · 250 µm · Precision-cut tissue slices PubMed

Lyons-Cohen MR, Nakano H, Thomas SY, Cook DN. (2018). Imaging Precision-Cut Lung Slices to Visualize Leukocyte Localization and Trafficking. *Methods Mol Biol.*
United States · Mouse · live · 150 µm · PCLS PubMed

Nordgren TM, Heires AJ, Bailey KL, Katafiasz DM, Toews ML, Wichman CS, Romberger DJ. (2018). Docosahexaenoic acid enhances amphiregulin-mediated bronchial epithelial cell repair processes following organic dust exposure. *Am J Physiol Lung Cell Mol Physiol.*
United States · Human · live · 300 µm · PCLS PubMed

Shalaby KH, Lyons-Cohen MR, Whitehead GS, Thomas SY, Prinz I, Nakano H, Cook DN. (2018). Pathogenic T(H)17 inflammation is sustained in the lungs by conventional dendritic cells and Toll-like receptor 4 signaling. *J Allergy Clin Immunol.*
United States · Mouse · live · NS µm · PCLS PubMed

Shigemura M, Lecuona E, Angulo M, Homma T, Rodrí_guez DA, Gonzalez-Gonzalez FJ, Welch LC, Amarelle L, Kim SJ, Kaminski N, Budinger GRS, Solway J, Sznajder JI. (2018). Hypercapnia increases airway smooth muscle contractility via caspase-7-mediated miR-133a-RhoA signaling. *Sci Transl Med.*
United States · Mouse · live · 100 µm · PCLS PubMed

Thomas SY, Whitehead GS, Takaku M, Ward JM, Xu X, Nakano K, Lyons-Cohen MR, Nakano H, Gowdy KM, Wade PA, Cook DN. (2018). MyD88-dependent dendritic and epithelial cell crosstalk orchestrates immune responses to allergens. *Mucosal Immunol.*
United States · Mouse · live · 150 µm · PCLS PubMed

Barrios J, Patel KR, Aven L, Achey R, Minns MS, Lee Y, Trinkaus-Randall VE, Ai X. (2017). Early life allergen-induced mucus overproduction requires augmented neural stimulation of pulmonary neuroendocrine cell secretion. *FASEB J.*
United States · Mouse · live · 150 µm · PCLS PubMed

Chen J, Sanderson MJ. (2017). Store-operated calcium entry is required for sustained contraction and Ca2+ oscillations of airway smooth muscle. *J Physiol.*
United States · Mouse · live · 180 µm · PCLS PubMed

EJ Yoo, G Cao, CJ Koziol-White… (2017). Gα12 facilitates shortening in human airway smooth muscle by modulating phosphoinositide 3-kinase-mediated activation in a RhoA-dependent manner. *Br J Pharmacol.*
United States · Human · live · 350 µm · PCLS PubMed

Kistemaker LEM, Oenema TA, Baarsma HA, Bos IST, Schmidt M, Facchinetti F, Civelli M, Villetti G, Gosens R. (2017). The PDE4 inhibitor CHF-6001 and LAMAs inhibit bronchoconstriction-induced remodeling in lung slices. *Am J Physiol Lung Cell Mol Physiol.*
Netherlands · Guinea pig · live · 500 µm · PCLS PubMed

Lyons-Cohen MR, Thomas SY, Cook DN, Nakano H. (2017). Precision Cut Mouse Lung Slices to Visualize Live Pulmonary Dendritic Cells. *J Vis Exp.*
Mouse · live · 150 µm · PCLS PubMed

Nakano H, Lyons-Cohen MR, Whitehead GS, Nakano K, Cook DN. (2017). Distinct functions of CXCR4, CCR2, and CX3CR1 direct dendritic cell precursors from the bone marrow to the lung. *J Leukoc Biol.*
United States · Mouse · live · 150 µm · Imaging PubMed

Ng-Blichfeldt JP, Alí_ada J, Montero MA, Dean CH, Griesenbach U, Griffiths MJ, Hind M. (2017). Deficient retinoid-driven angiogenesis may contribute to failure of adult human lung regeneration in emphysema. *Thorax.*
United Kingdom · Human · fixed · 400 µm · Immunohistochemistry PubMed

Poobalasingam T, Salman D, Li H, Alí_ada J, Dean CH. (2017). Imaging the lung: the old ways and the new. *Histol Histopathol.*
United Kingdom · Human · fixed · 400 µm · Immunohistochemistry PubMed

Poobalasingam T, Yates LL, Walker SA, Pereira M, Gross NY, Ali A, Kolatsi-Joannou M, Jarvelin MR, Pekkanen J, Papakrivopoulou E, Long DA, Griffiths M, Wagner D, Kí_nigshoff M, Hind M, Minelli C, Lloyd CM, Dean CH. (2017). Heterozygous Vangl2(Looptail) mice reveal novel roles for the planar cell polarity pathway in adult lung homeostasis and repair. *Dis Model Mech.*
United Kingdom · Mouse · live · 300 µm · PCLS PubMed

Rosner SR, Pascoe CD, Blankman E, Jensen CC, Krishnan R, James AL, Elliot JG, Green FH, Liu JC, Seow CY, Park JA, Beckerle MC, Parí© PD, Fredberg JJ, Smith MA. (2017). The actin regulator zyxin reinforces airway smooth muscle and accumulates in airways of fatal asthmatics. *PLoS One.*
United States · Mouse · live · 250 µm · PCLS PubMed

Van Dijk EM, Culha S, Menzen MH, Bidan CM, Gosens R. (2017). Elastase-Induced Parenchymal Disruption and Airway Hyper Responsiveness in Mouse Precision Cut Lung Slices: Toward an Ex vivo COPD Model. *Front Physiol.*
Netherlands · Mouse · live · 250 µm · PCLS PubMed

Velalopoulou A, Chatterjee S, Pietrofesa RA, Koziol-White C, Panettieri RA, Lin L, Tuttle S, Berman A, Koumenis C, Christofidou-Solomidou M. (2017). Synthetic Secoisolariciresinol Diglucoside (LGM2605) Protects Human Lung in an Ex Vivo Model of Proton Radiation Damage. *Int J Mol Sci.*
United States · Human · live · 350 µm · PCLS PubMed

Wong TTW, Zhang R, Zhang C, Hsu HC, Maslov KI, Wang L, Shi J, Chen R, Shung KK, Zhou Q, Wang LV. (2017). Label-free automated three-dimensional imaging of whole organs by microtomy-assisted photoacoustic microscopy. *Nat Commun.*
United States · Mouse · fixed · 20-500 µm · IHC / ISH PubMed

Yocum GT, Chen J, Choi CH, Townsend EA, Zhang Y, Xu D, Fu XW, Sanderson MJ, Emala CW. (2017). Role of transient receptor potential vanilloid 1 in the modulation of airway smooth muscle tone and calcium handling. *Am J Physiol Lung Cell Mol Physiol.*
United States · Mouse · live · 180 µm · PCLS PubMed

Yoo EJ, Cao G, Koziol-White CJ, Ojiaku CA, Sunder K, Jude JA, Michael JV, Lam H, Pushkarsky I, Damoiseaux R, Di Carlo D, Ahn K, An SS, Penn RB, Panettieri RA Jr. (2017). G-alpha(12) facilitates shortening in human airway smooth muscle by modulating phosphoinositide 3-kinase-mediated activation in a RhoA-dependent manner. *Br J Pharmacol.*
United States · Human · live · 350 µm · PCLS PubMed

Abdulnour RE, Sham HP, Douda DN, Colas RA, Dalli J, Bai Y, Ai X, Serhan CN, Levy BD. (2016). Aspirin-triggered resolvin D1 is produced during self-resolving gram-negative bacterial pneumonia and regulates host immune responses for the resolution of lung inflammation. *Mucosal Immunol.*
United States · Mouse · live · 150 µm · PCLS PubMed

Bai Y, Krishnamoorthy N, Patel KR, Rosas I, Sanderson MJ, Ai X. (2016). Cryopreserved Human Precision-Cut Lung Slices as a Bioassay for Live Tissue Banking. A Viability Study of Bronchodilation with Bitter-Taste Receptor Agonists. *Am J Respir Cell Mol Biol.*

United States · Human · live · 250 µm · PCLS PubMed

Carr R 3rd, Koziol-White C, Zhang J, Lam H, An SS, Tall GG, Panettieri RA Jr, Benovic JL. (2016). Interdicting Gq Activation in Airway Disease by Receptor-Dependent and Receptor-Independent Mechanisms. *Mol Pharmacol.*
United States · Human · live · 350 µm · PCLS PubMed

Cook DP, Rector MV, Bouzek DC, Michalski AS, Gansemer ND, Reznikov LR, Li X, Stroik MR, Ostedgaard LS, Abou Alaiwa MH, Thompson MA, Prakash YS, Krishnan R, Meyerholz DK, Seow CY, Stoltz DA. (2016). Cystic Fibrosis Transmembrane Conductance Regulator in Sarcoplasmic Reticulum of Airway Smooth Muscle. Implications for Airway Contractility. *Am J Respir Crit Care Med.*
United States · Pig · live · 150-250 µm · PCLS PubMed

Eleftheriadis N, Poelman H, Leus NGJ, Honrath B, Neochoritis CG, Dolga A, Dí_mling A, Dekker FJ. (2016). Design of a novel thiophene inhibitor of 15-lipoxygenase-1 with both anti-inflammatory and neuroprotective properties. *Eur J Med Chem.*
Netherlands · Mouse · live · 250 µm · PCLS PubMed

Ghosh A, Koziol-White CJ, Asosingh K, Cheng G, Ruple L, Groneberg D, Friebe A, Comhair SA, Stasch JP, Panettieri RA Jr, Aronica MA, Erzurum SC, Stuehr DJ. (2016). Soluble guanylate cyclase as an alternative target for bronchodilator therapy in asthma. *Proc Natl Acad Sci U S A.*
United States · Human · live · 350 microns µm · PCLS PubMed

Graham JG, Winchell CG, Kurten RC, Voth DE. (2016). Development of an Ex Vivo Tissue Platform To Study the Human Lung Response to Coxiella burnetii. *Infect Immun.*
United States · Human · live · 750 µm · PCLS PubMed

Hiorns JE, Bidan CM, Jensen OE, Gosens R, Kistemaker LE, Fredberg JJ, Butler JP, Krishnan R, Brook BS. (2016). Airway and Parenchymal Strains during Bronchoconstriction in the Precision Cut Lung Slice. *Front Physiol.*
United Kingdom · Mouse · live · 250 µm · PCLS PubMed

Koziol-White CJ, Jia Y, Baltus GA, Cooper PR, Zaller DM, Crackower MA, Sirkowski EE, Smock S, Northrup AB, Himes BE, Alves SE, Panettieri RA Jr. (2016). Inhibition of spleen tyrosine kinase attenuates IgE-mediated airway contraction and mediator release in human precision cut lung slices. *Br J Pharmacol.*
Canada · Human · live · 250 µm · PCLS PubMed

Koziol-White CJ, Yoo EJ, Cao G, Zhang J, Papanikolaou E, Pushkarsky I, Andrews A, Himes BE, Damoiseaux RD, Liggett SB, Di Carlo D, Kurten RC, Panettieri RA Jr. (2016). Inhibition of PI3K promotes dilation of human small airways in a rho kinase-dependent manner. *Br J Pharmacol.*
United States · Human · fixed · 350 µm · PCLS PubMed

Lam M, Royce SG, Donovan C, Jelinic M, Parry LJ, Samuel CS, Bourke JE. (2016). Serelaxin Elicits Bronchodilation and Enhances β-Adrenoceptor-Mediated Airway Relaxation. *Front Pharmacol.*
Australia · Rat · live · 200 µm · PCLS PubMed

Royce SG, Nold MF, Bui C, Donovan C, Lam M, Lamanna E, Rudloff I, Bourke JE, Nold-Petry CA. (2016). Airway Remodeling and Hyperreactivity in a Model of Bronchopulmonary Dysplasia and Their Modulation by IL-1 Receptor Antagonist. *Am J Respir Cell Mol Biol.*
Mouse · live · 150 µm · PCLS PubMed

Schepelmann M, Yarova PL, Lopez-Fernandez I, Davies TS, Brennan SC, Edwards PJ, Aggarwal A, Graí_a J, Rietdorf K, Matchkov V, Fenton RA, Chang W, Krssak M, Stewart A, Broadley KJ, Ward DT, Price SA, Edwards DH, Kemp PJ, Riccardi D. (2016). The vascular Ca2+-sensing receptor regulates blood vessel tone and blood pressure. *Am J Physiol Cell Physiol.*
United Kingdom · Mouse · live · 180 µm · PCLS PubMed

Watson CY, Damiani F, Ram-Mohan S, Rodrigues S, de Moura Queiroz P, Donaghey TC, Rosenblum Lichtenstein JH, Brain JD, Krishnan R, Molina RM. (2016). Screening for Chemical Toxicity Using Cryopreserved Precision Cut Lung Slices. *Toxicol Sci.*
United States · Mouse, Rat · live · 250 µm · PCLS PubMed

Danielsson J, Perez-Zoghbi J, Bernstein K, Barajas MB, Zhang Y, Kumar S, Sharma PK, Gallos G, Emala CW. (2015). Antagonists of the TMEM16A calcium-activated chloride channel modulate airway smooth muscle tone and intracellular calcium. *Anesthesiology.*
India · Mouse · live · 140 µm · PCLS PubMed

Eleftheriadis N, Neochoritis CG, Leus NG, van der Wouden PE, Dí_mling A, Dekker FJ. (2015). Rational Development of a Potent 15-Lipoxygenase-1 Inhibitor with in Vitro and ex Vivo Anti-inflammatory Properties. *J Med Chem.*
Netherlands · Mouse · live · 250 µm · PCLS PubMed

Gallos G, Yocum GT, Siviski ME, Yim PD, Fu XW, Poe MM, Cook JM, Harrison N, Perez-Zoghbi J, Emala CW Sr. (2015). Selective targeting of the α5-subunit of GABAA receptors relaxes airway smooth muscle and inhibits cellular calcium handling. *Am J Physiol Lung Cell Mol Physiol.*
United States · Mouse · live · 140 µm · PCLS PubMed

Kuo CS, Krasnow MA. (2015). Formation of a Neurosensory Organ by Epithelial Cell Slithering. *Cell.*
United States · Mouse · live · 175 µm · Slice culture PubMed

Aven L, Paez-Cortez J, Achey R, Krishnan R, Ram-Mohan S, Cruikshank WW, Fine A, Ai X. (2014). An NT4/TrkB-dependent increase in innervation links early-life allergen exposure to persistent airway hyperreactivity. *FASEB J.*
United States · Mouse · live · 200 µm · PCLS PubMed

Cao P, Tan X, Donovan G, Sanderson MJ, Sneyd J. (2014). A deterministic model predicts the properties of stochastic calcium oscillations in airway smooth muscle cells. *PLoS Comput Biol.*
New Zealand · Mouse · live · 180 µm · PCLS PubMed

Rietdorf K, Bootman MD, Sanderson MJ. (2014). Spontaneous, pro-arrhythmic calcium signals disrupt electrical pacing in mouse pulmonary vein sleeve cells. *PLoS One.*
United States · Mouse · live · 180 µm · PCLS PubMed

Rosner SR, Ram-Mohan S, Paez-Cortez JR, Lavoie TL, Dowell ML, Yuan L, Ai X, Fine A, Aird WC, Solway J, Fredberg JJ, Krishnan R. (2014). Airway contractility in the precision-cut lung slice after cryopreservation. *Am J Respir Cell Mol Biol.*
United States · Mouse · live · 250 µm · PCLS PubMed

Tan X, Sanderson MJ. (2014). Bitter tasting compounds dilate airways by inhibiting airway smooth muscle calcium oscillations and calcium sensitivity. *Br J Pharmacol.*
United States · Mouse · fixed · 180 µm · PCLS PubMed

Castro-Piedras I, Perez-Zoghbi JF. (2013). Hydrogen sulphide inhibits Ca2+ release through InsP3 receptors and relaxes airway smooth muscle. *J Physiol.*
United States · Mouse · live · 140 µm · PCLS PubMed

Goldklang MP, Perez-Zoghbi JF, Trischler J, Nkyimbeng T, Zakharov SI, Shiomi T, Zelonina T, Marks AR, D'Armiento JM, Marx SO. (2013). Treatment of experimental asthma using a single small molecule with anti-inflammatory and BK channel-activating properties. *FASEB J.*
United States · Mouse · live · 140 µm · PCLS PubMed

Mukherjee S, Trice J, Shinde P, Willis RE, Pressley TA, Perez-Zoghbi JF. (2013). Ca2+ oscillations, Ca2+ sensitization, and contraction activated by protein kinase C in small airway smooth muscle. *J Gen Physiol.*
United States · Mouse · fixed · 140-220 µm · PCLS PubMed

Oenema TA, Maarsingh H, Smit M, Groothuis GM, Meurs H, Gosens R. (2013). Bronchoconstriction Induces TGF-β Release and Airway Remodelling in Guinea Pig Lung Slices. *PLoS One.*
Netherlands · Guinea pig · fixed · 500 µm · PCLS PubMed

Yim PD, Gallos G, Perez-Zoghbi JF, Trice J, Zhang Y, Siviski M, Sonett J, Emala CW Sr. (2013). Chloride channel blockers promote relaxation of TEA-induced contraction in airway smooth muscle. *J Smooth Muscle Res.*
United States · Rat · live · 150 µm · PCLS PubMed

Sanderson MJ. (2011). Exploring lung physiology in health and disease with lung slices. *Pulm Pharmacol Ther.*
United States · Rat · live · 150-250 µm · PCLS PubMed

Ressmeyer AR, Bai Y, Delmotte P, Uy KF, Thistlethwaite P, Fraire A, Sato O, Ikebe M, Sanderson MJ. (2010). Human airway contraction and formoterol-induced relaxation is determined by Ca2+ oscillations and Ca2+ sensitivity. *Am J Respir Cell Mol Biol.*
United States · Human · live · 250 µm · PCLS PubMed

Liver

Precision-cut liver slices for metabolism, DILI, and extended ex-vivo culture.

AJ Mathiowetz, ES Meymand, KK Deol, G Parlakgül… (2024). CLCC1 promotes hepatic neutral lipid flux and nuclear pore complex assembly. *BioRxiv*.
United States · Mouse · fixed · 300 µm PubMed

CJ Liu, JT Smith, Y Wang, JN Ouellette… (2024). Assessing cell viability with dynamic optical coherence microscopy. *Biomedical Optics Express*.
United States · Mouse · live · 300 µm · Tumor PubMed

CM McCarthy, KL McKevitt, SA Connolly, I Andersson… (2024). Microindentation of fresh soft biological tissue: A rapid tissue sectioning and mounting protocol. *Plos one*.
Ireland · Mouse, human · live · 150-1000 µm PubMed

D Ackerman, E Avetissian, CKE Bleck, JA Bogovic… (2024). Data Release: High-Resolution Imaging and Segmentation of P7 Mouse Tissue Microarchitecture Using FIB-SEM and Machine Learning. *bioRxiv*.
Mouse · fixed · 300 µm · Imaging PubMed

G Parlakgül, S Pang, LL Artico, N Min… (2024). Spatial mapping of hepatic ER and mitochondria architecture reveals zonated remodeling in fasting and obesity. *Nature Communications*.
United States · Mouse · live · 300 µm · PCLS PubMed

J Lee (2024). Ultrasound Control and Imaging of Cellular Immunotherapy.
Mouse · fixed · 75 µm · IHC / ISH PubMed

S Trivedi, C Tilsed, M Liousia, RM Brody… (2024). Transcriptomic analysis-guided assessment of precision-cut tumor slices (PCTS) as an ex-vivo tool in cancer research. *Scientific Reports*.
United States · Human, mouse · fixed · 300 µm · Tumor PubMed

T Duparc, E Gore, G Combes, D Beuzelin, JP Da Silva… (2024). P2Y13 receptor deficiency favors adipose tissue lipolysis and worsens insulin resistance and fatty liver disease. *JCI insight*.
France · Mouse · live · 170 µm · PCLS PubMed

W Yu, Y Zhang, CTK Lo, L Kang, TTW Wong (2024). Rapid full-color serial sectioning tomography with speckle illumination and ultraviolet excitation. *npj Imaging*.
China · Mouse · fixed · 50 µm PubMed

A Sarkar, Y Jin, BC DeFelice, CY Logan, Y Yang… (2023). Intermittent fasting induces rapid hepatocyte proliferation to restore the hepatostat in the mouse liver. *Elife*.
United States · Mouse · fixed · 50-200 µm · IHC / ISH PubMed

DB Azizoglu, K Perez, SL Zheng, S Rahman, EY Rim… (2023). Liver size is predetermined in the neonate by adding lobules at the periphery. *bioRxiv*.
Mouse · fixed · 50 µm · IHC / ISH PubMed

J Sbierski-Kind, KM Cautivo, JC Wagner, MW Dahlgren… (2023). Group 2 innate lymphoid cells constrain type 3/17 lymphocytes in shared stromal niches to restrict liver fibrosis. *bioRxiv*.
Mouse · fixed · 200 µm · IHC / ISH PubMed

P Liu, A Anandhan, J Chen, A Shakya, M Dodson… (2023). Decreased autophagosome biogenesis, reduced NRF2, and enhanced ferroptotic cell death are underlying molecular mechanisms of non-alcoholic fatty liver …. *Redox Biology*.
United States · Mouse, Human · fixed · 20 µm · IHC / ISH PubMed

DJ Chung, GP Madison, AM Aponte… (2022). Metabolic design in a mammalian model of extreme metabolism, the North American least shrew (Cryptotis parva). *J Physiol*.
United States · Shrew · fixed · 700 µm · Imaging PubMed

G Parlakgül, AP Arruda, S Pang, E Cagampan, N Min… (2022). Regulation of liver subcellular architecture controls metabolic homeostasis. *Nature*.
United States · Mouse · fixed · 300 µm · Imaging PubMed

J Ko, M Wilkovitsch, J Oh, RH Kohler, E Bolli… (2022). Spatiotemporal multiplexed immunofluorescence imaging of living cells and tissues with bioorthogonal cycling of fluorescent probes. *Nature Biotechnology*.
United States · Mouse · live · 500 µm · PCLS PubMed

KM Cautivo, PR Matatia, CO Lizama, NM Mroz… (2022). Interferon gamma constrains type 2 lymphocyte niche boundaries during mixed inflammation. *Immunity*.
United States · Mouse · fixed · 200-500 µm · IHC / ISH PubMed

NAL Fayez, E Rouhollahi, CY Ong, J Wu… (2022). Hepatocyte-targeted delivery of imiquimod reduces hepatitis B virus surface antigen. *Journal of Controlled Release*.
Canada · Mouse · fixed · 40 µm · IHC / ISH PubMed

NAL Fayez, R Böttger, J Brown, E Rouhollahi… (2022). The mechanism of Hepatocyte-Targeting and safety profile of Phospholipid-Free small unilamellar vesicles. *International Journal of Pharmaceutics*.
Canada · Mouse · fixed · 40 µm · IHC / ISH PubMed

J Vogler, R Böttger, NAL Fayez, W Zhang, Z Qin… (2021). Altering the intra-liver distribution of phospholipid-free small unilamellar vesicles using temperature-dependent size-tunability. *Journal of Controlled Release*.
Mouse · fixed · 40 µm · IHC / ISH PubMed

N Al Fayez, R Bottger, E Rouhollahi… (2021). Improved Liver Delivery of Primaquine by Phospholipid-Free Small Unilamellar Vesicles with Reduced Hemolytic Toxicity. *Molecular Pharmaceutics*.
Canada · Mouse · fixed · 40 µm · IHC / ISH PubMed

P Liu, M Dodson, H Li, CJ Schmidlin, A Shakya… (2021). Non-canonical NRF2 activation promotes a pro-diabetic shift in hepatic glucose metabolism. *Molecular Metabolism*.
United States · Mouse · live · 150 µm PubMed

PH Tseng, SJ Chiang, SJ Chen, CY Dong (2021). Improvement in Labeling Efficiency of Hydrophilic and Hydrophobic Fluorescent Molecules in Thick Tissue Sections. *Microscopy Today*.
Pig · fixed · 250 µm · Imaging PubMed

SK Bose, BM White, MV Kashyap, A Dave… (2021). In utero adenine base editing corrects multi-organ pathology in a lethal lysosomal storage disease. *Nat Commun*.
United States · Mouse · fixed · 150 µm · IHC / ISH PubMed

B Ling, J Lee, D Maresca, A Lee-Gosselin… (2020). Biomolecular ultrasound imaging of phagolysosomal function. *ACS Nano*.
United States · Mouse · fixed · 75 µm · IHC / ISH PubMed

Harvey TN, Sandve SR, Jin Y, Vik JO, Torgersen JS. (2019). Liver slice culture as a model for lipid metabolism in fish. *PeerJ*.
Norway · Fish · live · 300 µm · Culture PubMed

Zhang W, Bí_ttger R, Qin Z, Kulkarni JA, Vogler J, Cullis PR, Li SD. (2019). Phospholipid-Free Small Unilamellar Vesicles for Drug Targeting to Cells in the Liver. *Small*.
Canada · Mouse · fixed · 40 µm · Immunohistochemistry PubMed

Liu Y, Lv L, Wang L, Zhong Y. (2018). Social Isolation Induces Rac1-Dependent Forgetting of Social Memory. *Cell Rep*.
China · Mouse · live · 250 µm · Precision-cut tissue slices PubMed

Moen T, Torgersen J, Santi N, Davidson WS, Baranski M, íÖdegí«rd J, KjíŸglum S, Velle B, Kent M, Lubieniecki KP, Isdal E, Lien S. (2015). Epithelial Cadherin Determines Resistance to Infectious Pancreatic Necrosis Virus in Atlantic Salmon. *Genetics*.
Norway · Fish · fixed · 300 µm · Immunohistochemistry PubMed

Weidinger A, Dungel P, Perlinger M, Singer K, Ghebes C, Duvigneau JC, Mí_llebner A, Schí_fer U, Redl H, Kozlov AV. (2013). Experimental data suggesting that inflammation mediated rat liver mitochondrial dysfunction results from secondary hypoxia rather than from direct effects of inflammatory mediators. *Front Physiol*.
Austria · Rat · live · 250 µm · PCLS PubMed

Kidney

Renal slices for nephrotoxicity, transport, and disease modeling.

V Veloso-Giménez, C Cárdenas-Calderón… (2024). Oxygenation by Intravascular Photosynthesis Reduces Kidney Damage During ex Vivo Preservation. *ACS Applied Bio ….*
Chile · Rat · live · 500 µm · PCLS PubMed

CM McCarthy, KL McKevitt, SA Connolly, I Andersson… (2024). Microindentation of fresh soft biological tissue: A rapid tissue sectioning and mounting protocol. *Plos one*.
Ireland · Mouse, human · live · 150-1000 µm PubMed

D Ackerman, E Avetissian, CKE Bleck, JA Bogovic… (2024). Data Release: High-Resolution Imaging and Segmentation of P7 Mouse Tissue Microarchitecture Using FIB-SEM and Machine Learning. *bioRxiv*.
Mouse · fixed · 300 µm · Imaging PubMed

D Bezwada, L Perelli, NP Lesner, L Cai, B Brooks… (2024). Mitochondrial complex I promotes kidney cancer metastasis. *Nature Portfolio*.
United States · Mouse · live · 300 µm · IHC / ISH PubMed

MB Moor, J Nordström, M Burmakin, M Raki, S Al-Saad… (2024). Comparative analysis of kidney transplantation modeled using precision-cut kidney slices and kidney transplantation in pigs. *bioRxiv*.
Human, pig · live · 300 µm · PCLS PubMed

S Zheng, R Banerji, R LeBourdais, S Zhang… (2024). Alteration of mechanical stresses in the murine brain by age and hemorrhagic stroke. *Journal of Translational Medicine*.
United States · Mouse · 250 µm · Imaging PubMed

W Yu, Y Zhang, CTK Lo, L Kang, TTW Wong (2024). Rapid full-color serial sectioning tomography with speckle illumination and ultraviolet excitation. *npj Imaging*.
China · Mouse · fixed · 50 µm PubMed

W Zhang, Y Li, AA Fung, Z Li, H Jang, H Zha… (2024). Multi-molecular hyperspectral PRM-SRS imaging. *Nature Communications*.
Human, mouse · fixed · 30, 120 µm PubMed

AA Fung (2023). Development of a Label-free Optical Analysis Platform for Cells and Tissues. *Public Access from UC San Diego*.
Mouse, Human · fixed · 120, 30 µm PubMed

D Bezwada, NP Lesner, B Brooks, HS Vu, Z Wu, L Cai… (2023). Mitochondrial metabolism in primary and metastatic human kidney cancers. *BioRxiv*.
United States · Human, Mouse · live · 300 µm · Slice culture PubMed

E Charrin, D Dabaghie, I Sen, D Unnersjö-Jess… (2023). Soluble Klotho protects against glomerular injury through regulation of ER stress response. *Communications Biology*.
Sweden · Human · fixed · 300 µm · PCLS PubMed

M Elshani, IH Um, S Leung, PA Reynolds, A Chapman… (2023). Transcription factor NFE2L1 decreases in glomerulonephropathies after podocyte damage. *Cells*.
United Kingdom · Human · live · 250 µm · PCLS PubMed

P Ferreira, R Vaja, M Lopes-Pires, M Crescente… (2023). Renal Function Underpins the Cyclooxygenase-2: Asymmetric Dimethylarginine Axis in Mouse and Man. *Kidney International Reports*.
United Kingdom · Mouse · live · 150 µm PubMed

RN Caballero-Florán, M Bendahmane, JP Gupta… (2023). Synaptotagmin-7 facilitates acetylcholine release in splanchnic nerve-chromaffin cell synapses during nerve activity. *Neuroscience Letters (ELSEVIER)*.
United States · Mouse · live · 300 µm · Electrophysiology PubMed

Z Han, JS Rao, S Ramesh, J Hergesell… (2023). Model-Guided Design and Optimization of CPA Perfusion Protocols for Whole Organ Cryopreservation. *Annals of Biomedical Engineering*.
United States · Rat · live · 300 µm · PCLS PubMed

DJ Chung, GP Madison, AM Aponte… (2022). Metabolic design in a mammalian model of extreme metabolism, the North American least shrew (Cryptotis parva). *J Physiol*.
United States · Shrew · fixed · 700 µm · Imaging PubMed

Y Zhang, L Kang, IHM Wong, W Dai, X Li… (2022). High-Throughput, Label-Free and Slide-Free Histological Imaging by Computational Microscopy and Unsupervised Learning. *Advanced Science*.
China · Mouse · fixed · 200 µm · IHC / ISH PubMed

J Vogler, R Böttger, NAL Fayez, W Zhang, Z Qin… (2021). Altering the intra-liver distribution of phospholipid-free small unilamellar vesicles using temperature-dependent size-tunability. *Journal of Controlled Release*.
Mouse · fixed · 40 µm · IHC / ISH PubMed

SK Bose, BM White, MV Kashyap, A Dave… (2021). In utero adenine base editing corrects multi-organ pathology in a lethal lysosomal storage disease. *Nat Commun.*
United States · Mouse · fixed · 150 µm · IHC / ISH PubMed

Liu Y, Lv L, Wang L, Zhong Y. (2018). Social Isolation Induces Rac1-Dependent Forgetting of Social Memory. *Cell Rep.*
China · Mouse · live · 250 µm · Precision-cut tissue slices PubMed

Wong TTW, Zhang R, Zhang C, Hsu HC, Maslov KI, Wang L, Shi J, Chen R, Shung KK, Zhou Q, Wang LV. (2017). Label-free automated three-dimensional imaging of whole organs by microtomy-assisted photoacoustic microscopy. *Nat Commun.*
United States · Mouse · fixed · 20-500 µm · IHC / ISH PubMed

Intestine & gut

CM McCarthy, KL McKevitt, SA Connolly, I Andersson… (2024). Microindentation of fresh soft biological tissue: A rapid tissue sectioning and mounting protocol. *Plos one.*
Ireland · Mouse, human · live · 150-1000 µm PubMed

P Lu, LM Lifshitz, K Bellve, R ZhuGe (2024). TMEM16A in smooth muscle cells acts as a pacemaker channel in the internal anal sphincter. *Communications Biology.*
United States · Mouse · live · 250 µm PubMed

CM McCarthy, JM Allardyce, SE Hickey… (2023). Comparison of macroscale and microscale mechanical properties of fresh and fixed-frozen porcine colonic tissue. *Journal of the Mechanical Behavior of Biomedical Materials.*
Ireland · Pig · live · 400 µm · IHC / ISH PubMed

R Sim, J Lee, J Chieng, KH Tan, G Lim, A Foo… (2023). Fluorescent Peptide-based Probe for the Detection of Alpha-synuclein Aggregates in the Gut. *bioRxiv.*
Mouse · fixed · 50 µm · IHC / ISH PubMed

A Hausmann, B Felmy, L Kunz, S Kroon… (2021). Intercrypt sentinel macrophages tune antibacterial NF-κB responses in gut epithelial cells via TNF. *Journal of Experimental Medicine.*
Switzerland · Mouse · fixed · 200 µm · IHC / ISH PubMed

N Aggarwal, ME Deerhake, D DiPalma, SK Shahi… (2021). Secreted osteopontin from CD4+ T cells limits acute graft-versus-host disease. *Cell reports.*
United States · Mouse · live · 400 µm · PCLS PubMed

P Lu, J Chen, C Zhang, D Saur, CE Baer… (2021). Oscillating calcium signals in smooth muscle cells underlie the persistent basal tone of internal anal sphincter. *Journal of Cellular Physiology.*
United States · Mouse · live · 250 µm · PCLS PubMed

SK Bose, BM White, MV Kashyap, A Dave… (2021). In utero adenine base editing corrects multi-organ pathology in a lethal lysosomal storage disease. *Nat Commun.*
United States · Mouse · fixed · 150 µm · IHC / ISH PubMed

A Caputo, Y Liang, TD Raabe, A Lo, M Horvath… (2020). Snca-GFP knock-in mice reflect patterns of endogenous expression and pathological seeding. *ENeuro.*
United States · Mouse · fixed · Unknown µm · IHC / ISH PubMed

Boone PG, Rochelle LK, Ginzel JD, Lubkov V, Roberts WL, Nicholls PJ, Bock C, Flowers ML, von Furstenberg RJ, Stripp BR, Agarwal P, Borowsky AD, Cardiff RD, Barak LS, Caron MG, Lyerly HK, Snyder JC. (2019). A cancer rainbow mouse for visualizing the functional genomics of oncogenic clonal expansion. *Nat Commun.*
United States · Mouse · fixed · 70-100 µm · Immunohistochemistry PubMed

Liu Y, Lv L, Wang L, Zhong Y. (2018). Social Isolation Induces Rac1-Dependent Forgetting of Social Memory. *Cell Rep.*
China · Mouse · live · 250 µm · Precision-cut tissue slices PubMed

Pancreas

D Ackerman, E Avetissian, CKE Bleck, JA Bogovic… (2024). Data Release: High-Resolution Imaging and Segmentation of P7 Mouse Tissue Microarchitecture Using FIB-SEM and Machine Learning. *bioRxiv.*
Mouse · fixed · 300 µm · Imaging PubMed

UN Wasko, J Jiang, TC Dalton, A Curiel-Garcia… (2024). Tumor-selective activity of RAS-GTP inhibition in pancreatic cancer. *Nature*.
United States · Human · live · 300 µm · PCLS PubMed

AR Decker (2023). Using toxin-producing bacteria to treat explants and autochthonous mouse models of pancreatic cancer.
Human · live · 300 µm · PCLS PubMed

UN Wasko, J Jiang, A Curiel-Garcia, Y Wang, B Lee… (2023). Tumor-selective effects of active RAS inhibition in pancreatic ductal adenocarcinoma. *bioRxiv*.
United States · Human · live · 300 µm · PCLS PubMed

Lymph node & spleen

D Ackerman, E Avetissian, CKE Bleck, JA Bogovic… (2024). Data Release: High-Resolution Imaging and Segmentation of P7 Mouse Tissue Microarchitecture Using FIB-SEM and Machine Learning. *bioRxiv*.
Mouse · fixed · 300 µm · Imaging PubMed

J Fergusson, J Siu, N Gupta, E Nee, S Reinke… (2024). Ex vivo Model of Functioning Human Lymph Node Reveals Pivotal Role for Innate Lymphoid Cells and Stromal Populations in Response to Vaccine Adjuvant. *bioRxiv*.
Human, mouse · live · 300 µm PubMed

J Lee (2024). Ultrasound Control and Imaging of Cellular Immunotherapy.
Mouse · fixed · 75 µm · IHC / ISH PubMed

YF Yazicioglu, E Marin, HF Andrew, K Bentkowska… (2023). Asparagine availability controls B cell homeostasis. *science Immunology*.
Mouse · live · 300 µm · Slice culture PubMed

WE Barclay, N Aggarwal, ME Deerhake, M Inoue… (2022). The AIM2 inflammasome is activated in astrocytes during the late phase of EAE. *JCI insight*.
United States · Mouse · live · 25 µm · IHC / ISH PubMed

J Vogler, R Böttger, NAL Fayez, W Zhang, Z Qin… (2021). Altering the intra-liver distribution of phospholipid-free small unilamellar vesicles using temperature-dependent size-tunability. *Journal of Controlled Release*.
Mouse · fixed · 40 µm · IHC / ISH PubMed

SK Bose, BM White, MV Kashyap, A Dave… (2021). In utero adenine base editing corrects multi-organ pathology in a lethal lysosomal storage disease. *Nat Commun*.
United States · Mouse · fixed · 150 µm · IHC / ISH PubMed

B Ling, J Lee, D Maresca, A Lee-Gosselin… (2020). Biomolecular ultrasound imaging of phagolysosomal function. *ACS Nano*.
United States · Mouse · fixed · 75 µm · IHC / ISH PubMed

Finetti F, Capitani N, Manganaro N, Tatangelo V, Libonati F, Panattoni G, Calaresu I, Ballerini L, Baldari CT, Patrussi L. (2020). Optimization of Organotypic Cultures of Mouse Spleen for Staining and Functional Assays. *Front Immunol*.
Italy · Mouse · live · 230 µm · Precision-cut spleen slices for culture PubMed

KH Hu, JP Eichorst, CS McGinnis, DM Patterson… (2020). ZipSeq: barcoding for real-time mapping of single cell transcriptomes. *Nature Methods*.
United States · Mouse · live · 150 µm · Imaging PubMed

Webb GM, Molden J, Busman-Sahay K, Abdulhaqq S, Wu HL, Weber WC, Bateman KB, Reed JS, Northrup M, Maier N, Tanaka S, Gao L, Davey B, Carpenter BL, Axthelm MK, Stanton JJ, Smedley J, Greene JM, Safrit JT, Estes JD, Skinner PJ, Sacha JB. (2020). The human IL-15 superagonist N-803 promotes migration of virus-specific CD8+ T and NK cells to B cell follicles but does not reverse latency in ART-suppressed, SHIV-infected macaques. *PLoS Pathog*.
United States · Non-Human Primate · live · NS µm · Immunohistochemistry PubMed

Li S, Folkvord JM, Kovacs KJ, Wagstaff RK, Mwakalundwa G, Rendahl AK, Rakasz EG, Connick E, Skinner PJ. (2019). Low levels of SIV-specific CD8+ T cells in germinal centers characterizes acute SIV infection. *PLoS Pathog*.
United States · Non-Human Primate · live · NS µm · Immunohistochemistry PubMed

Haran KP, Hajduczki A, Pampusch MS, Mwakalundwa G, Vargas-Inchaustegui DA, Rakasz EG, Connick E, Berger EA, Skinner PJ. (2018). Simian Immunodeficiency Virus (SIV)-Specific Chimeric Antigen Receptor-T Cells Engineered to

Target B Cell Follicles and Suppress SIV Replication. *Front Immunol*.
United States · Non-Human Primate · live · 300 µm · B cell follicle migration assay PubMed

Webb GM, Li S, Mwakalundwa G, Folkvord JM, Greene JM, Reed JS, Stanton JJ, Legasse AW, Hobbs T, Martin LD, Park BS, Whitney JB, Jeng EK, Wong HC, Nixon DF, Jones RB, Connick E, Skinner PJ, Sacha JB. (2018). The human IL-15 superagonist ALT-803 directs SIV-specific CD8(+) T cells into B-cell follicles. *Blood Adv*.
United States · Non-Human Primate · live · NS µm · Immunohistochemistry PubMed

Li S, Mwakalundwa G, Skinner PJ. (2017). In Situ MHC-tetramer Staining and Quantitative Analysis to Determine the Location, Abundance, and Phenotype of Antigen-specific CD8 T Cells in Tissues. *J Vis Exp*.
United States · Mouse · live · 200 µm · Staining antigen-specific CD8 T cells PubMed

Li S, Folkvord JM, Rakasz EG, Abdelaal HM, Wagstaff RK, Kovacs KJ, Kim HO, Sawahata R, MaWhinney S, Masopust D, Connick E, Skinner PJ. (2016). Simian Immunodeficiency Virus-Producing Cells in Follicles Are Partially Suppressed by CD8+ Cells In Vivo. *J Virol*.
United States · Non-Human Primate · fixed · 200 microns µm · Immunohistochemistry PubMed

Abdelaal HM, Kim HO, Wagstaff R, Sawahata R, Southern PJ, Skinner PJ. (2015). Comparison of Vibratome and Compresstome sectioning of fresh primate lymphoid and genital tissues for in situ MHC-tetramer and immunofluorescence staining. *Biol Proced Online*.
United States · Non-Human Primate · fixed · 200 µm · Imaging PubMed

Muscle & nerve

C Kolluru, A Todd, AR Upadhye, Y Liu, MY Berezin… (2022). Imaging peripheral nerve micro-anatomy with MUSE, 2D and 3D approaches. *Scientific reports*.
United States · Rat · fixed · NA µm · Imaging PubMed

DJ Chung, GP Madison, AM Aponte… (2022). Metabolic design in a mammalian model of extreme metabolism, the North American least shrew (Cryptotis parva). *J Physiol*.
United States · Shrew · fixed · 700 µm · Imaging PubMed

SK Bose, BM White, MV Kashyap, A Dave… (2021). In utero adenine base editing corrects multi-organ pathology in a lethal lysosomal storage disease. *Nat Commun*.
United States · Mouse · fixed · 150 µm · IHC / ISH PubMed

Liu Y, Lv L, Wang L, Zhong Y. (2018). Social Isolation Induces Rac1-Dependent Forgetting of Social Memory. *Cell Rep*.
China · Mouse · live · 250 µm · Precision-cut tissue slices PubMed

Oliver SR, Wright VP, Parinandi N, Clanton TL. (2008). Thermal tolerance of contractile function in oxidative skeletal muscle: no protection by antioxidants and reduced tolerance with eicosanoid enzyme inhibition. *Am J Physiol Regul Integr Comp Physiol*.
United States · Rat · fixed · 20-60 µm · Immunohistochemistry PubMed

Cartilage & connective

I Martinier, F Fage, A Kakar, A Castagnino… (2024). Tunable biomimetic materials elaborated by ice templating and self-assembly of collagen for tubular tissue engineering. *Biomaterials Science*.
France · Human · live · 200 µm PubMed

I Martinier, S Deville, G Mosser, L Trichet, P Davidson… (2024). State diagrams of type I collagen for the rational design of biomimetic materials. *bioRxiv*.
Unknown · live · 200 µm PubMed

A Morejon (2023). Biomechanical Analysis of Knee Meniscus Fibrocartilage. *University of Miami Library*.
Human · frozen · 1500 µm PubMed

K Orton, W Batchelor, NM Ziebarth, TM Best… (2023). Biomechanical properties of porcine meniscus as determined via AFM: Effect of region, compartment and anisotropy. *PloS one*.
United States · Pig · frozen · 1500 µm PubMed

A Morejon, AMA Mantero, TM Best, AR Jackson… (2022). Mechanisms of energy dissipation and relationship with tissue composition in human meniscus. *Osteoarthritis Cartilage*.
United States · Human · frozen · 1500 µm PubMed

M De Rosa, G Filippone, TM Best, AR Jackson… (2022). Mechanical properties of meniscal circumferential fibers using an inverse finite element analysis approach. *J Mech Behav Biomed Mater*.
United States · Pig · live · 1500 µm PubMed

A Morejon, CD Norberg, M De Rosa… (2021). Compressive properties and hydraulic permeability of human meniscus: relationships with tissue structure and composition. *Front Bioeng Biotechnol*.
United States · Human · fixed · 1500 µm PubMed

C Norberg, G Filippone, F Andreopoulos, TM Best… (2021). Viscoelastic and equilibrium shear properties of human meniscus: Relationships with tissue structure and composition. *J Biomech*.
United States · Human · live · 1000 µm PubMed

F Travascio, S Valladares-Prieto, AR Jackson (2020). Effects of solute size and tissue composition on molecular and macromolecular diffusivity in human knee cartilage. *Osteoarthr Cartil Open*.
United States · Human · live · 500 µm PubMed

Travascio F, Devaux F, Volz M, Jackson AR. (2020). Molecular and macromolecular diffusion in human meniscus: relationships with tissue structure and composition. *Osteoarthritis Cartilage*.
United States · Human · frozen · 500 µm · FRAP technique, anisotropy PubMed

Skin

L H Ziolkowski, Y A Nikolaev, A Chikamoto, M Oda, V V Feketa, D Monedero-Alonso, S A Ardasheva , S S Bae , C S Xu , S Pang , E O Gracheva, S N Bagriantsev (2025). The inner core enables transient touch detection in the Pacinian corpuscle. *Science Advances*.
United States · Duck · live · 300 µm · Imaging PubMed

D Ackerman, E Avetissian, CKE Bleck, JA Bogovic… (2024). Data Release: High-Resolution Imaging and Segmentation of P7 Mouse Tissue Microarchitecture Using FIB-SEM and Machine Learning. *bioRxiv*.
Mouse · fixed · 300 µm · Imaging PubMed

LH Ziolkowski, YA Nikolaev, A Chikamoto, M Oda… (2024). Structural and functional dissection of the Pacinian corpuscle reveals an active role of the inner core in touch detection. *bioRxiv*.
United States · Bill · fixed · 300 µm PubMed

YA Nikolaev, LH Ziolkowski, S Pang, WP Li… (2023). 3D architecture and a bicellular mechanism of touch detection in mechanosensory corpuscle. *Science Advances*.
United States · Duck · fixed · 300 µm · Imaging PubMed

JR Campbell, BR McDonald, PB Mesko, NO Siemers… (2021). Fc-Optimized Anti-CCR8 Antibody Depletes Regulatory T Cells in Human Tumor ModelsAnti-CCR8 Antibody Depletes Tregs in Human Tumor Models. *Cancer Research*.
Human · live · 300 µm · Slice culture PubMed

Breast & adipose

HJ Meyer, S Mamani, Z Li, L Shi… (2024). Femtosecond optical Kerr effect in normal and grades of cancerous breast tissues as a new optical biopsy method. *Journal of Biophotonics*.
United States · Mouse · fixed · 1000 µm · Tumor PubMed

J Sbierski-Kind, KM Cautivo, JC Wagner, MW Dahlgren… (2023). Group 2 innate lymphoid cells constrain type 3/17 lymphocytes in shared stromal niches to restrict liver fibrosis. *bioRxiv*.
Mouse · fixed · 200 µm · IHC / ISH PubMed

KM Cautivo, PR Matatia, CO Lizama, NM Mroz… (2022). Interferon gamma constrains type 2 lymphocyte niche boundaries during mixed inflammation. *Immunity*.
United States · Mouse · fixed · 200-500 µm · IHC / ISH PubMed

Morgan MM, Arendt LM, Alarid ET, Beebe DJ, Johnson BP. (2019). Mammary adipose stromal cells derived from obese women reduce sensitivity to the aromatase inhibitor anastrazole in an organotypic breast model. *FASEB J*.
United States · Human · fixed · NS µm · Tumor culture PubMed

Reproductive

AHC Anthis, S Kilchenmann, M Murdeu… (2024). Reversible Mechanical Contraception and Endometriosis Treatment Using Stimuli-Responsive Hydrogels. *Advanced Materials*.
Switzerland · Pig · live · 300 µm PubMed

CM McCarthy, KL McKevitt, SA Connolly, I Andersson… (2024). Microindentation of fresh soft biological tissue: A rapid tissue sectioning and mounting protocol. *Plos one*.
Ireland · Mouse, human · live · 150-1000 µm PubMed

J Siewiera, TI McIntyre, KM Cautivo, K Mahiddine… (2023). Circumvention of luteolysis reveals parturition pathways in mice dependent upon innate type 2 immunity. *Immunity*.
United States · Mouse · fixed · 300 µm · IHC / ISH PubMed

KM Cautivo, PR Matatia, CO Lizama, NM Mroz… (2022). Interferon gamma constrains type 2 lymphocyte niche boundaries during mixed inflammation. *Immunity*.
United States · Mouse · fixed · 200-500 µm · IHC / ISH PubMed

N Deshet-Unger, G Horn, M Rawet-Slobodkin, T Waks… (2022). Comparing Intraperitoneal and Intravenous Personalized ErbB2CAR-T for the Treatment of Epithelial Ovarian Cancer. *Biomedicines*.
Israel · Mouse · live · 250 µm · Slice culture PubMed

RA Vitek, W Huang, PG Geiger, E Heninger… (2022). Fresh tissue procurement and preparation for multicompartment and multimodal analysis of the prostate tumor microenvironment. *Prostate*.
United States · Human · live · 100 µm · Imaging PubMed

M Qu, P Lu, K Bellve, LM Lifshitz, R ZhuGe (2021). Mode switch of Ca2+ oscillation-mediated uterine peristalsis and associated embryo implantation impairments in mouse adenomyosis. *Frontiers in Physiology*.
United States · Mouse · live · 250 µm · Imaging PubMed

SK Bose, BM White, MV Kashyap, A Dave… (2021). In utero adenine base editing corrects multi-organ pathology in a lethal lysosomal storage disease. *Nat Commun*.
United States · Mouse · fixed · 150 µm · IHC / ISH PubMed

A Riad, SB Gitto, H Lee, HD Winters, PM Martorano… (2020). Parp theranostic auger emitters are cytotoxic in brca mutant ovarian cancer and viable tumors from ovarian cancer patients enable ex-vivo screening of tumor …. *Molecules*.
United States · Human · live · 300 µm · Tumor PubMed

J Wang, T Li, JL Wang, Z Xu, W Meng, QF Wu (2020). Talpid3-Mediated Centrosome Integrity Restrains Neural Progenitor Delamination to Sustain Neurogenesis by Stabilizing Adherens Junctions. *Cell Reports*.
Mouse · live · 250 µm · Imaging PubMed

SC Kerr, MM Morgan, AA Gillette… (2020). A bioengineered organotypic prostate model for the study of tumor microenvironment-induced immune cell activation. *Integrative Biology*.
United States · Cell Cultures · fixed · 100 µm · Slice culture PubMed

Johnson BP, Vitek RA, Geiger PG, Huang W, Jarrard DF, Lang JM, Beebe DJ. (2018). Vital ex vivo tissue labeling and pathology-guided micropunching to characterize cellular heterogeneity in the tissue microenvironment. *Biotechniques*.
United States · Human · live · 30-300 µm · Imaging PubMed

Abdelaal HM, Kim HO, Wagstaff R, Sawahata R, Southern PJ, Skinner PJ. (2015). Comparison of Vibratome and Compresstome sectioning of fresh primate lymphoid and genital tissues for in situ MHC-tetramer and immunofluorescence staining. *Biol Proced Online*.
United States · Non-Human Primate · fixed · 200 µm · Imaging PubMed

Bladder

J Sbierski-Kind, KM Cautivo, JC Wagner, MW Dahlgren… (2023). Group 2 innate lymphoid cells constrain type 3/17 lymphocytes in shared stromal niches to restrict liver fibrosis. *bioRxiv*.
Mouse · fixed · 200 µm · IHC / ISH PubMed

S Golan, V Bar, SJ Salpeter, G Neev… (2023). A clinical evaluation of an ex vivo organ culture system to predict patient response to cancer therapy. *Frontiers in Medicine*.
Israel · Human · live · 250 µm · Tumor PubMed

Adrenal & endocrine

RN Caballero-Florán, M Bendahmane, JP Gupta… (2023). Synaptotagmin-7 facilitates acetylcholine release in splanchnic nerve-chromaffin cell synapses during nerve activity. *Neuroscience Letters (ELSEVIER)*.
United States · Mouse · live · 300 µm · Electrophysiology PubMed

Tumor

Patient- and model-derived tumor slices for drug response and tumor-microenvironment studies.

SJ Chiang, PH Tseng, MC Lin, CY Leu… (2024). A rapid spectroscopic platform in identifying cisplatin resistance in head and neck squamous cell carcinoma. *National Taiwan University College of Medicine*.
Human · live · 150 µm · Tumor PubMed

CJ Liu, JT Smith, Y Wang, JN Ouellette… (2024). Assessing cell viability with dynamic optical coherence microscopy. *Biomedical Optics Express*.
United States · Mouse · live · 300 µm · Tumor PubMed

CM McCarthy, KL McKevitt, SA Connolly, I Andersson… (2024). Microindentation of fresh soft biological tissue: A rapid tissue sectioning and mounting protocol. *Plos one*.
Ireland · Mouse, human · live · 150-1000 µm PubMed

D Bezwada, L Perelli, NP Lesner, L Cai, B Brooks… (2024). Mitochondrial complex I promotes kidney cancer metastasis. *Nature Portfolio*.
United States · Mouse · live · 300 µm · IHC / ISH PubMed

MC Greier, A Runge, J Dudas, R Hartl, M Santer… (2024). Cytotoxic response of tumor-infiltrating lymphocytes of head and neck cancer slice cultures under mitochondrial dysfunction. *Frontiers in Oncology*.
Austria · Human · live · 250 µm · Tumor PubMed

MC Hasselluhn, AR Decker-Farrell, L Vlahos… (2024). Tumor explants elucidate a Cascade of Paracrine SHH, WNT, and VEGF signals driving pancreatic Cancer Angiosuppression. *Cancer discovery*.
United States · Mouse · fixed · 300 µm · Tumor PubMed

S Trivedi, C Tilsed, M Liousia, RM Brody… (2024). Transcriptomic analysis-guided assessment of precision-cut tumor slices (PCTS) as an ex-vivo tool in cancer research. *Scientific Reports*.
United States · Human, mouse · fixed · 300 µm · Tumor PubMed

SC Cordts, K Yuki, MF Henao Echeverri… (2024). Microdissection tools to generate organoids for modeling the tumor immune microenvironment. *Microsystems & Nanoengineering*.
United States · Mouse · live · 200, 800, 400 µm · Tumor PubMed

A Ray, KH Hu, K Kersten, NF Kuhn, B Samad… (2023). Critical role of CD206+ macrophages in organizing anti-tumor immunity. *bioRxiv*.
United States · Mouse, Human · fixed · 160 µm · Tumor PubMed

A Sathe, C Ayala, X Bai, SM Grimes, B Lee, C Kin… (2023). GITR and TIGIT immunotherapy provokes divergent multicellular responses in the tumor microenvironment of gastrointestinal cancers. *Genome Medicine*.
United States · Mouse and Primate · fixed · Unknown µm · Tumor PubMed

C Stossel, M Raitses-Gurevich, D Atias, T Beller… (2023). Spectrum of Response to Platinum and PARP Inhibitors in Germline BRCA–Associated Pancreatic Cancer in the Clinical and Preclinical Setting. *American Association for Cancer Research*.
Israel · Human · live · 250 µm · IHC / ISH PubMed

D Bezwada, NP Lesner, B Brooks, HS Vu, Z Wu, L Cai… (2023). Mitochondrial metabolism in primary and metastatic human kidney cancers. *BioRxiv*.
United States · Human, Mouse · live · 300 µm · Slice culture PubMed

E Schulz (2023). Lokale Ultraschall-vermittelte Zytostatika-Applikation zur Behandlung von Hirntumoren. *Julius-Maximilians-Universityät Würzburg*.
Mouse · fixed · 250 µm · Tumor PubMed

F Mechta-grigoriou, Y Kieffer… (2023). Antxr1 as a biomarker of immunosuppressive fibroblast populations and its use for predicting response to immunotherapy. *US Patent*.

Human · fixed · 3-50 µm · Tumor PubMed

G Pataccini, CLM Lanari (2023). Inhibidores de ciclo celular y terapia endócrina en carcinomas mamarios con distinta proporción de isoformas de receptores de progesterona. *Universidad de Buenos Aires*.
Human · fixed · 50-100 µm · Tumor PubMed

KZ Wu, C Adine, A Mitriashkin, BJJ Aw… (2023). Making In Vitro Tumor Models Whole Again. *Advanced Healthcare Materials*.
Singapore · Human · live · 30-1000 µm PubMed

M do Carmo Greier, A Runge, J Dudas… (2023). Optimizing culturing conditions in patient derived 3D primary slice cultures of head and neck cancer. *Frontiers in Oncology*.
Austria · Human · live · 300 µm · Slice culture PubMed

MH Kim, C Radaelli, ER Thomsen, D Monet… (2023). Target cell-specific synaptic dynamics of excitatory to inhibitory neuron connections in supragranular layers of human neocortex. *Elife*.
United States · Human · live · 350 µm · Tumor PubMed

S Golan, V Bar, SJ Salpeter, G Neev… (2023). A clinical evaluation of an ex vivo organ culture system to predict patient response to cancer therapy. *Frontiers in Medicine*.
Israel · Human · live · 250 µm · Tumor PubMed

V Nickl, J Eck, N Goedert, J Hübner, T Nerreter… (2023). Characterization and Optimization of the Tumor Microenvironment in Patient-Derived Organotypic Slices and Organoid Models of Glioblastoma. *Cancers*.
Germany · Human · live · 350 µm · Slice culture PubMed

W Donelan, PL Crispen, S Kusmartsev (2023). Tissue Slice Culture and Analysis of Tumor-Associated Hyaluronan in Urothelial Carcinoma. *Urothelial Carcinoma: Methods and Protocols . Second Edition*.
United States · Human · live · Unknown µm · IHC / ISH PubMed

AJ Seibel, OM Kelly, YW Dance, CM Nelson… (2022). Role of Lymphatic Endothelium in Vascular Escape of Engineered Human Breast Microtumors. *Cellular and Molecular Bioengineering*.
United States · Engineered microtumors and lymphatic vessels · live · 200 µm · Imaging PubMed

K Kersten, KH Hu, AJ Combes, B Samad, T Harwin… (2022). Spatiotemporal co-dependency between macrophages and exhausted CD8+ T cells in cancer. *Cancer Cell*.
United States · Mouse · live · 160 µm · Slice culture PubMed

N Deshet-Unger, G Horn, M Rawet-Slobodkin, T Waks… (2022). Comparing Intraperitoneal and Intravenous Personalized ErbB2CAR-T for the Treatment of Epithelial Ovarian Cancer. *Biomedicines*.
Israel · Mouse · live · 250 µm · Slice culture PubMed

N Gavert, Y Zwang, R Weiser, O Greenberg, S Halperin… (2022). Ex vivo organotypic cultures for synergistic therapy prioritization identify patient-specific responses to combined MEK and Src inhibition in colorectal cancer. *Nature cancer*.
Israel · Mouse · live · 250 µm · Slice culture PubMed

P Baldominos, A Barbera-Mourelle, O Barreiro… (2022). Quiescent cancer cells resist T cell attack by forming an immunosuppressive niche. *Cell*.
United States · Mouse · live · 300 µm · Tumor PubMed

P Baldominos, O Barreiro, U von Andrian, R Sirera… (2022). Protocol to isolate live single cells while retaining spatial information by combining cell photolabeling and FACS. *STAR protocols*.
United States · Mouse · live · 300 µm · Tumor PubMed

TIH Park, LCD Smyth, M Aalderink, ZR Woolf… (2022). Routine culture and study of adult human brain cells from neurosurgical specimens. *Nature Protocols*.
New Zealand · Human · live · 250-300 µm · Slice culture PubMed

A Farias, A Soto, F Puttur, CJ Goldin, S Sosa, C Gil… (2021). A TLR4 agonist improves immune checkpoint blockade treatment by increasing the ratio of effector to regulatory cells within the tumor microenvironment. *Scientific reports*.
Argentina · Mouse · fixed · 200 µm · IHC / ISH PubMed

A Jacob Berger, E Gigi, L Kupershmidt, Z Meir… (2021). IRS1 phosphorylation underlies the non-stochastic probability of cancer cells to persist during EGFR inhibition therapy. *Nature cancer*.
Israel · Mouse · live · 250 µm · Slice culture PubMed

GB Ferraro, A Ali, A Luengo, DP Kodack, A Deik… (2021). Fatty acid synthesis is required for breast cancer brain metastasis. *Nature cancer*.
United States · Mouse · live · 300 µm · Slice culture PubMed

JR Campbell, BR McDonald, PB Mesko, NO Siemers… (2021). Fc-Optimized Anti-CCR8 Antibody Depletes Regulatory T Cells in Human Tumor ModelsAnti-CCR8 Antibody Depletes Tregs in Human Tumor Models. *Cancer Research*.
Human · live · 300 µm · Slice culture PubMed

JW DiGiacomo, I Godet, M Trautmann-Rodriguez… (2021). Extracellular Matrix–Bound FGF2 Mediates Estrogen Receptor Signaling and Therapeutic Response in Breast CancerThe ECM Mediates FGF-Induced ER Activity. *Molecular Cancer Research*.
United States · Mouse · live · 100 µm · Slice culture PubMed

RA O'Connor, V Chauhan, L Mathieson… (2021). T cells drive negative feedback mechanisms in cancer associated fibroblasts, promoting expression of co-inhibitory ligands, CD73 and IL-27 in non-small cell lung …. *Oncoimmunology*.
United Kingdom · Human · live · 400 µm · Tumor PubMed

A Riad, SB Gitto, H Lee, HD Winters, PM Martorano… (2020). Parp theranostic auger emitters are cytotoxic in brca mutant ovarian cancer and viable tumors from ovarian cancer patients enable ex-vivo screening of tumor …. *Molecules*.
United States · Human · live · 300 µm · Tumor PubMed

Ben-Hamo R, Jacob Berger A, Gavert N, Miller M, Pines G, Oren R, Pikarsky E, Benes CH, Neuman T, Zwang Y, Efroni S, Getz G, Straussman R. (2020). Predicting and affecting response to cancer therapy based on pathway-level biomarkers. *Nat Commun*.
Israel · Mouse · live · 250 µm · Ex-vivo culture PubMed

KH Hu, JP Eichorst, CS McGinnis, DM Patterson… (2020). ZipSeq: barcoding for real-time mapping of single cell transcriptomes. *Nature Methods*.
United States · Mouse · live · 150 µm · Imaging PubMed

Kaneko K, Osada T, Morse MA, Gwin WR, Ginzel JD, Snyder JC, Yang XY, Liu CX, Diniz MA, Bodoor K, Hughes PF, Haystead TA, Lyerly HK. (2020). Heat shock protein 90-targeted photodynamic therapy enables treatment of subcutaneous and visceral tumors. *Commun Biol*.
United States · Mouse · fixed · 50 µm · Immunohistochemistry PubMed

SC Kerr, MM Morgan, AA Gillette… (2020). A bioengineered organotypic prostate model for the study of tumor microenvironment-induced immune cell activation. *Integrative Biology*.
United States · Cell Cultures · fixed · 100 µm · Slice culture PubMed

Barry KC, Hsu J, Broz ML, Cueto FJ, Binnewies M, Combes AJ, Nelson AE, Loo K, Kumar R, Rosenblum MD, Alvarado MD, Wolf DM, Bogunovic D, Bhardwaj N, Daud AI, Ha PK, Ryan WR, Pollack JL, Samad B, Asthana S, Chan V, Krummel MF. (2018). A natural killer-dendritic cell axis defines checkpoint therapy-responsive tumor microenvironments. *Nat Med*.
United States · Mouse · live · 300 µm · Imaging PubMed

Morgan MM, Livingston MK, Warrick JW, Stanek EM, Alarid ET, Beebe DJ, Johnson BP. (2018). Mammary fibroblasts reduce apoptosis and speed estrogen-induced hyperplasia in an organotypic MCF7-derived duct model. *Sci Rep*.
United States · Human · live · 100 µm · Culture PubMed

Nia HT, Datta M, Seano G, Huang P, Munn LL, Jain RK. (2018). Quantifying solid stress and elastic energy from excised or in situ tumors. *Nat Protoc*.
United States · Mouse, Human · live · 100-500 µm · Solid stress quantification PubMed

Boldajipour B, Nelson A, Krummel MF. (2016). Tumor-infiltrating lymphocytes are dynamically desensitized to antigen but are maintained by homeostatic cytokine. *JCI Insight*.
United States · Mouse · live · 300 µm · Slice culture PubMed

Nia HT, Liu H, Seano G, Datta M, Jones D, Rahbari N, Incio J, Chauhan VP, Jung K, Martin JD, Askoxylakis V, Padera TP, Fukumura D, Boucher Y, Hornicek FJ, Grodzinsky AJ, Baish JW, Munn LL, Jain RK. (2016). Solid stress and elastic energy as measures of tumour mechanopathology. *Nat Biomed Eng*.
United States · Tumor · live · 100-500 µm · Solide stress quantification PubMed

Plants & other

ECT Yeung, JB Nichol (2024). Histological Methods Used in the Study of Protocorm. I. Background Information and References. *Orchid Propagation. The Biology and Biotechnology of the Protocorm.*
Plants · live · 10 µm · Plants PubMed

MM Mira, EC Yeung, C Stasolla (2022). A Simple Guide to the Use of Compresstome in Plant Research. *Plant Tissue Culture: New Techniques and Application in Horticultural Species of Tropical Region.*
Plants · fixed · Various µm · Plants

Bracken-Grissom HD, DeLeo DM, Porter ML, Iwanicki T, Sickles J, Frank TM. (2020). Light organ photosensitivity in deep-sea shrimp may suggest a novel role in counterillumination. *Sci Rep.*
United States · Shrimp · fixed · 250 µm · Immunohistochemistry PubMed

Mira MM, El-Khateeb EA, Gaafar RM, Igamberdiev AU, Hill RD, Stasolla C. (2020). Stem cell fate in hypoxic root apical meristems is influenced by phytoglobin expression. *J Exp Bot.*
Canada · Plants · fixed · NS µm · Immunohistochemistry PubMed

Mira MM, Hill RD, Stasolla C. (2016). Phytoglobins Improve Hypoxic Root Growth by Alleviating Apical Meristem Cell Death. *Plant Physiol.*
Canada · Plants · fixed · 10 µm · Immunohistochemistry PubMed

Materials & bioengineering

L Wang, D Hu, J Xu, J Hu… (2024). Complex in vitro model: A transformative model in drug development and precision medicine. *Clinical and Translational Science.*
China · Animal and human · live · 100-300 µm · Slice culture PubMed

Y Zhou, G Pereira, Y Tang, M James, M Zhang (2023). 3D Porous Scaffold-Based High-Throughput Platform for Cancer Drug Screening. *Pharmaceutics.*
United States · Polymer · fixed · 400 µm · Imaging PubMed

WY Wang, RN Kent III, SA Huang, EH Jarman… (2021). Direct comparison of angiogenesis in natural and synthetic biomaterials reveals that matrix porosity regulates endothelial cell invasion speed and sprout diameter. *Acta Biomaterialia.*
United States · Mouse · fixed · 200 µm · Imaging PubMed

Part II — By Animal Model

Human

I Martinier, F Fage, A Kakar, A Castagnino… (2024). Tunable biomimetic materials elaborated by ice templating and self-assembly of collagen for tubular tissue engineering.

K Jankowski, SE Lemay, D Lozano-Ojalvo… (2024). Pharmacological Inhibition of Epac1 Protects against Pulmonary Fibrosis by Blocking FoxO3a Neddylation.

SJ Chiang, PH Tseng, MC Lin, CY Leu… (2024). A rapid spectroscopic platform in identifying cisplatin resistance in head and neck squamous cell carcinoma.

500 (2024). Optical Clearing and Labeling for Light-Ssheet Flourescence Microscopy in Large-Scale human Brain Imaging.

C Zeng, H Yue, C Wang, X Ju, T Wang, X Fu… (2024). Albendazole ameliorates aerobic glycolysis in myofibroblasts to reverse pulmonary fibrosis.

C Zeng, Q Wang, X Liu, K Wang, C Wang… (2024). Localized administration of Bcar3 siRNA via nano-self-assembly to treat idiopathic pulmonary fibrosis by disrupting macrophage-fibroblast crosstalk.

CM McCarthy, KL McKevitt, SA Connolly, I Andersson… (2024). Microindentation of fresh soft biological tissue: A rapid tissue sectioning and mounting protocol.

DJM Kollareth, AK Sharma (2024). Precision cut lung slices: an innovative tool for lung transplant research.

Di Meo D,1, Ramazzoti J,1,Scardigli M, Cheli F, Pesce L, Brady N, Mazzamuto G, Costantini I, Pavone SF (2024). Calcium-Sensing Receptor Negative Allosteric Modulators Oppose Contraction of Mouse Airways.

H Osman-Ponchet, L Perdigon, M Barthe… (2024). Advances in In Vitro Modeling of Pulmonary Fibrosis: Focus on Precision-Cut Lung Slices (PCLS) Model.

J Fergusson, J Siu, N Gupta, E Nee, S Reinke… (2024). Ex vivo Model of Functioning Human Lymph Node Reveals Pivotal Role for Innate Lymphoid Cells and Stromal Populations in Response to Vaccine Adjuvant.

L Perdigon, M Barthe, H Osman-Ponchet… (2024). Successful Development of Human Precision-Cut Lung Slice (hPCLS) Model for Studying Lung Disease.

L Wang, D Hu, J Xu, J Hu… (2024). Complex in vitro model: A transformative model in drug development and precision medicine.

M Bruegger, C Machahua, B Zumkehr, C Cismaru… (2024). Aging shapes infection profiles of influenza A virus and SARS-CoV-2 in human lung slices.

MB Moor, J Nordström, M Burmakin, M Raki, S Al-Saad… (2024). Comparative analysis of kidney transplantation modeled using precision-cut kidney slices and kidney transplantation in pigs.

MC Greier, A Runge, J Dudas, R Hartl, M Santer… (2024). Cytotoxic response of tumor-infiltrating lymphocytes of head and neck cancer slice cultures under mitochondrial dysfunction.

ML Cohen, AN Brumwell, TC Ho, K Garakani… (2024). A fibroblast-dependent TGF-β1/sFRP2 noncanonical Wnt signaling axis promotes epithelial metaplasia in idiopathic pulmonary fibrosis.

RE Lee-Ferris, K Okuda, JR Galiger, SA Schworer… (2024). Prolonged airway explant culture enables study of health, disease, and viral pathogenesis.

S Bozzini, E Bozza, C Bagnera… (2024). Assessment of Imatinib Anti-Remodeling Activity on a Human Precision Cut Lung Slices Model.

S Trivedi, C Tilsed, M Liousia, RM Brody… (2024). Transcriptomic analysis-guided assessment of precision-cut tumor slices (PCTS) as an ex-vivo tool in cancer research.

SE Lemay, MS Montesinos, Y Grobs, T Yokokawa… (2024). Exploring Integrin α5β1 as a Potential Therapeutic Target for Pulmonary Arterial Hypertension: Insights from Comprehensive Multicenter Preclinical Studies.

UN Wasko, J Jiang, TC Dalton, A Curiel-Garcia… (2024). Tumor-selective activity of RAS-GTP inhibition in pancreatic cancer.

W Zhang, Y Li, AA Fung, Z Li, H Jang, H Zha… (2024). Multi-molecular hyperspectral PRM-SRS imaging.

A Morejon (2023). Biomechanical Analysis of Knee Meniscus Fibrocartilage.

A Ray, KH Hu, K Kersten, NF Kuhn, B Samad… (2023). Critical role of CD206+ macrophages in organizing anti-tumor immunity.

A de Lange, H Tomes, J Selfe, UF Prodjinotho… (2023). Cestode larvae excite host neuronal circuits via glutamatergic signaling.

AA Fung (2023). Development of a Label-free Optical Analysis Platform for Cells and Tissues.

AJ Heires, D Samuelson, D Villageliu, TM Nordgren… (2023). Agricultural dust derived bacterial extracellular vesicle mediated inflammation is attenuated by DHA.

AR Decker (2023). Using toxin-producing bacteria to treat explants and autochthonous mouse models of pancreatic cancer.

C Stossel, M Raitses-Gurevich, D Atias, T Beller… (2023). Spectrum of Response to Platinum and PARP Inhibitors in Germline BRCA–Associated Pancreatic Cancer in the Clinical and Preclinical Setting.
C Zeng, Q Wang, C Wang, Q Zhou, X Fu, J Yu, W Xiong… (2023). Local Delivery of Bcar3 siRNA by Nano-Self-Assembly for Treating Pulmonary Fibrosis via Blocking the Interaction of Macrophages and Fibroblasts.
D Bezwada, NP Lesner, B Brooks, HS Vu, Z Wu, L Cai… (2023). Mitochondrial metabolism in primary and metastatic human kidney cancers.
D Cervantes, N Schaunaman, GP Downey… (2023). Desert particulate matter from Afghanistan increases airway obstruction in human distal lungs exposed to type 2 cytokine IL-13.
E Charrin, D Dabaghie, I Sen, D Unnersjö-Jess… (2023). Soluble Klotho protects against glomerular injury through regulation of ER stress response.
EB Gebski, V Parikh, H Lam, N Kim… (2023). Rhinovirus C15 attenuates relaxation and cAMP production in Human Airways and smooth muscle.
F Mechta-grigoriou, Y Kieffer… (2023). Antxr1 as a biomarker of immunosuppressive fibroblast populations and its use for predicting response to immunotherapy.
G Pataccini, CLM Lanari (2023). Inhibidores de ciclo celular y terapia endócrina en carcinomas mamarios con distinta proporción de isoformas de receptores de progesterona.
G Rosen, D Kirsch, S Horowitz, JD Cherry… (2023). Three dimensional evaluation of cerebrovascular density and branching in chronic traumatic encephalopathy.
H Agraval, T Crue, N Schaunaman, M Numata… (2023). Electronic Cigarette Exposure Increases the Severity of Influenza a Virus Infection via TRAIL Dysregulation in Human Precision-Cut Lung Slices.
JC Nawroth, D Roth, A van Schadewijk, A Ravi… (2023). Breathing on chip: Dynamic flow and stretch accelerate mucociliary maturation of airway epithelium in vitro.
KZ Wu, C Adine, A Mitriashkin, BJJ Aw… (2023). Making In Vitro Tumor Models Whole Again.
M Elshani, IH Um, S Leung, PA Reynolds, A Chapman… (2023). Transcription factor NFE2L1 decreases in glomerulonephropathies after podocyte damage.
M do Carmo Greier, A Runge, J Dudas… (2023). Optimizing culturing conditions in patient derived 3D primary slice cultures of head and neck cancer.
MH Kim, C Radaelli, ER Thomsen, D Monet… (2023). Target cell-specific synaptic dynamics of excitatory to inhibitory neuron connections in supragranular layers of human neocortex.
MÁ García-Cabezas, JL Hacker… (2023). Homology of neocortical areas in rats and primates based on cortical type analysis: an update of the hypothesis on the dual origin of the neocortex.
P Liu, A Anandhan, J Chen, A Shakya, M Dodson… (2023). Decreased autophagosome biogenesis, reduced NRF2, and enhanced ferroptotic cell death are underlying molecular mechanisms of non-alcoholic fatty liver ….
P Yadav, JG Ortega, W Tamaki, C Chien, K Chang… (2023). Macrophage-fibroblast crosstalk drives Arg1-dependent lung fibrosis via ornithine loading.
S Driessens, D Heyer, I Pieterse, R Wilbers, E Mertens… (2023). Genes associated with cognitive ability and HAR show overlapping expression patterns in human cortical neuron types.
S Golan, V Bar, SJ Salpeter, G Neev… (2023). A clinical evaluation of an ex vivo organ culture system to predict patient response to cancer therapy.
T Crue, GY Lee, JY Peng, N Schaunaman… (2023). Single cell RNA-sequencing of human precision-cut lung slices: A novel approach to study the effect of vaping and viral infection on lung health.
UN Wasko, J Jiang, A Curiel-Garcia, Y Wang, B Lee… (2023). Tumor-selective effects of active RAS inhibition in pancreatic ductal adenocarcinoma.
V Nickl, J Eck, N Goedert, J Hübner, T Nerreter… (2023). Characterization and Optimization of the Tumor Microenvironment in Patient-Derived Organotypic Slices and Organoid Models of Glioblastoma.
W Donelan, PL Crispen, S Kusmartsev (2023). Tissue Slice Culture and Analysis of Tumor-Associated Hyaluronan in Urothelial Carcinoma.
X Chen, DA Wolfe, DS Bindu, M Zhang… (2023). Functional gene delivery to and across brain vasculature of systemic AAVs with endothelial-specific tropism in rodents and broad tropism in primates.
A Morejon, AMA Mantero, TM Best, AR Jackson… (2022). Mechanisms of energy dissipation and relationship with tissue composition in human meniscus.
M Chioccioli, S Roy, R Newell, L Pestano, B Dickinson… (2022). A lung targeted miR-29 Mimic as a Therapy for Pulmonary Fibrosis.
R Guidi, D Xu, DF Choy, TR Ramalingam… (2022). Steroid-induced fibroblast growth factors drive an epithelial-mesenchymal inflammatory axis in severe asthma.

RA Vitek, W Huang, PG Geiger, E Heninger… (2022). Fresh tissue procurement and preparation for multicompartment and multimodal analysis of the prostate tumor microenvironment.
SA Guler, C Machahua, TK Geiser, G Kocher… (2022). Dehydroepiandrosterone in fibrotic interstitial lung disease: a translational study.
TIH Park, LCD Smyth, M Aalderink, ZR Woolf… (2022). Routine culture and study of adult human brain cells from neurosurgical specimens.
A Morejon, CD Norberg, M De Rosa… (2021). Compressive properties and hydraulic permeability of human meniscus: relationships with tissue structure and composition.
BE Kalmbach, RD Hodge, NL Jorstad, S Owen… (2021). Signature morpho-electric, transcriptomic, and dendritic properties of human layer 5 neocortical pyramidal neurons.
C Norberg, G Filippone, F Andreopoulos, TM Best… (2021). Viscoelastic and equilibrium shear properties of human meniscus: Relationships with tissue structure and composition.
F Xu, Y Shen, L Ding, CY Yang, H Tan, H Wang… (2021). High-throughput mapping of a whole rhesus monkey brain at micrometer resolution.
JK Mich, LT Graybuck, EE Hess, JT Mahoney, Y Kojima… (2021). Functional enhancer elements drive subclass-selective expression from mouse to primate neocortex.
JR Campbell, BR McDonald, PB Mesko, NO Siemers… (2021). Fc-Optimized Anti-CCR8 Antibody Depletes Regulatory T Cells in Human Tumor ModelsAnti-CCR8 Antibody Depletes Tregs in Human Tumor Models.
RA O'Connor, V Chauhan, L Mathieson… (2021). T cells drive negative feedback mechanisms in cancer associated fibroblasts, promoting expression of co-inhibitory ligands, CD73 and IL-27 in non-small cell lung ….
YN Dong, FC Hsu, CJ Koziol-White, V Stepanova… (2021). Functional NMDA receptors are expressed by human pulmonary artery smooth muscle cells.
A Riad, SB Gitto, H Lee, HD Winters, PM Martorano… (2020). Parp theranostic auger emitters are cytotoxic in brca mutant ovarian cancer and viable tumors from ovarian cancer patients enable ex-vivo screening of tumor ….
Alsafadi HN, Uhl FE, Pineda RH, Bailey KE, Rojas M, Wagner DE, Kí_nigshoff M. (2020). Applications and Approaches for Three-Dimensional Precision-Cut Lung Slices. Disease Modeling and Drug Discovery.
F Travascio, S Valladares-Prieto, AR Jackson (2020). Effects of solute size and tissue composition on molecular and macromolecular diffusivity in human knee cartilage.
Hodge RD, Miller JA, Novotny M, Kalmbach BE, Ting JT, Bakken TE, Aevermann BD, Barkan ER, Berkowitz-Cerasano ML, Cobbs C, Diez-Fuertes F, Ding SL, McCorrison J, Schork NJ, Shehata SI, Smith KA, Sunkin SM, Tran DN, Venepally P, Yanny AM, Steemers FJ, Phillips JW, Bernard A, Koch C, Lasken RS, Scheuermann RH, Lein ES. (2020). Transcriptomic evidence that von Economo neurons are regionally specialized extratelencephalic-projecting excitatory neurons.
J Huang, H Lam, C Koziol-White… (2020). The odorant receptor OR2W3 on airway smooth muscle evokes bronchodilation via a cooperative chemosensory tradeoff between TMEM16A and CFTR.
Koziol-White C, Johnstone TB, Corpuz ML, Cao G, Orfanos S, Parikh V, Deeney B, Tliba O, Ostrom RS, Dainty I, Panettieri RA Jr. (2020). Budesonide enhances agonist-induced bronchodilation in human small airways by increasing cAMP production in airway smooth muscle.
Koziol-White CJ, Ghosh A, Sandner P, Erzurum SE, Stuehr DJ, Panettieri RA Jr. (2020). Soluble Guanylate Cyclase Agonists Induce Bronchodilation in Human Small Airways.
MÁ García-Cabezas, JL Hacker… (2020). A protocol for cortical type analysis of the human neocortex applied on histological samples, the atlas of Von Economo and Koskinas, and magnetic ….
Parikh V, Scala J, Patel R, Corbi C, Lo D, Bochkov YA, Kennedy JL, Kurten RC, Liggett SB, Gern JE, Koziol-White CJ. (2020). Rhinovirus C15 Induces Airway Hyperresponsiveness via Calcium Mobilization in Airway Smooth Muscle.
Poole JA, Nordgren TM, Heires AJ, Nelson AJ, Katafiasz D, Bailey KL, Romberger DJ. (2020). Amphiregulin modulates murine lung recovery and fibroblast function following exposure to agriculture organic dust.
Ram-Mohan S, Bai Y, Schaible N, Ehrlicher AJ, Cook DP, Suki B, Stoltz DA, Solway J, Ai X, Krishnan R. (2020). Tissue traction microscopy to quantify muscle contraction within precision-cut lung slices.
SU Hettiarachchi, YH Li, J Roy, F Zhang… (2020). Targeted inhibition of PI3 kinase/mTOR specifically in fibrotic lung fibroblasts suppresses pulmonary fibrosis in experimental models.
Travascio F, Devaux F, Volz M, Jackson AR. (2020). Molecular and macromolecular diffusion in human meniscus: relationships with tissue structure and composition.
Urso A, D'Ovidio F, Xu D, Emala CW Sr, Bunnett NW, Perez-Zoghbi JF. (2020). Bile acids inhibit cholinergic constriction in proximal and peripheral airways from humans and rodents.
Webb GM, Molden J, Busman-Sahay K, Abdulhaqq S, Wu HL, Weber WC, Bateman KB, Reed JS, Northrup M, Maier N, Tanaka S, Gao L, Davey B, Carpenter BL, Axthelm MK, Stanton JJ, Smedley J, Greene JM, Safrit JT, Estes JD, Skinner PJ, Sacha JB.

(2020). The human IL-15 superagonist N-803 promotes migration of virus-specific CD8+ T and NK cells to B cell follicles but does not reverse latency in ART-suppressed, SHIV-infected macaques.
Brann KR, Fullerton MS, Onyilagha FI, Prince AA, Kurten RC, Rom JS, Blevins JS, Smeltzer MS, Voth DE. (2019). Infection of Primary Human Alveolar Macrophages Alters Staphylococcus aureus Toxin Production and Activity.
Dragan AL, Kurten RC, Voth DE. (2019). Characterization of Early Stages of Human Alveolar Infection by the Q Fever Agent Coxiella burnetii.
Hodge RD, Bakken TE, Miller JA, Smith KA, Barkan ER, Graybuck LT, et al. (2019). Conserved cell types with divergent features in human versus mouse cortex.
Kennedy JL, Kurten RC, McCullough S, Panettieri RA, Koziol-White C, Jones SM, Caid K, Gill PS, Roberts D, Jaeschke H, McGill MR, James L. (2019). Acetaminophen is both bronchodilatory and bronchoprotective in human precision cut lung slice airways.
Kurz A, Xu W, Wiegel P, Leukel C, N Baker S. (2019). Non-invasive assessment of superficial and deep layer circuits in human motor cortex.
Li S, Folkvord JM, Kovacs KJ, Wagstaff RK, Mwakalundwa G, Rendahl AK, Rakasz EG, Connick E, Skinner PJ. (2019). Low levels of SIV-specific CD8+ T cells in germinal centers characterizes acute SIV infection.
Maarsingh H, Bidan CM, Brook BS, Zuidhof AB, Elzinga CRS, Smit M, Oldenburger A, Gosens R, Timens W, Meurs H. (2019). Small airway hyperresponsiveness in COPD: relationship between structure and function in lung slices.
Morgan MM, Arendt LM, Alarid ET, Beebe DJ, Johnson BP. (2019). Mammary adipose stromal cells derived from obese women reduce sensitivity to the aromatase inhibitor anastrazole in an organotypic breast model.
Singh BK, Lu W, Schmidt Paustian AM, Ge MQ, Koziol-White CJ, Flayer CH, Killingbeck SS, Wang N, Dong X, Riese MJ, Deshpande DA, Panettieri RA Jr, Haczku A, Kambayashi T. (2019). Diacylglycerol kinase Zeta promotes allergic airway inflammation and airway hyperresponsiveness through distinct mechanisms.
Trutzer IM, Garcí_a-Cabezas Mí, Zikopoulos B. (2019). Postnatal development and maturation of layer 1 in the lateral prefrontal cortex and its disruption in autism.
Boldog E, Bakken TE, Hodge RD, Novotny M, Aevermann BD, Baka J, Bordí© S, Close JL, Diez-Fuertes F, Ding SL, Faragí_ N, Kocsis íK, Kovíçcs B, Maltzer Z, McCorrison JM, Miller JA, Molníçr G, Olíçh G, Ozsvíçr A, Rí_zsa M, Shehata SI, Smith KA, Sunkin SM, Tran DN, Venepally P, Wall A, Puskíçs LG, Barzí_ P, Steemers FJ, Schork NJ, Scheuermann RH, Lasken RS, Lein ES, Tamíçs G. (2018). Transcriptomic and morphophysiological evidence for a specialized human cortical GABAergic cell type.
Haran KP, Hajduczki A, Pampusch MS, Mwakalundwa G, Vargas-Inchaustegui DA, Rakasz EG, Connick E, Berger EA, Skinner PJ. (2018). Simian Immunodeficiency Virus (SIV)-Specific Chimeric Antigen Receptor-T Cells Engineered to Target B Cell Follicles and Suppress SIV Replication.
Johnson BP, Vitek RA, Geiger PG, Huang W, Jarrard DF, Lang JM, Beebe DJ. (2018). Vital ex vivo tissue labeling and pathology-guided micropunching to characterize cellular heterogeneity in the tissue microenvironment.
Kalmbach BE, Buchin A, Long B, Close J, Nandi A, Miller JA, Bakken TE, Hodge RD, Chong P, de Frates R, Dai K, Maltzer Z, Nicovich PR, Keene CD, Silbergeld DL, Gwinn RP, Cobbs C, Ko AL, Ojemann JG, Koch C, Anastassiou CA, Lein ES, Ting JT. (2018). h-Channels Contribute to Divergent Intrinsic Membrane Properties of Supragranular Pyramidal Neurons in Human versus Mouse Cerebral Cortex.
Kennedy JL, Koziol-White CJ, Jeffus S, Rettiganti MR, Fisher P, Kurten M, Eze A, House S, Sikes JD, Askew E, Putt C, Panettieri RA, Jones SM, Kurten RC. (2018). Effects of rhinovirus 39 infection on airway hyperresponsiveness to carbachol in human airways precision cut lung slices.
Morgan MM, Livingston MK, Warrick JW, Stanek EM, Alarid ET, Beebe DJ, Johnson BP. (2018). Mammary fibroblasts reduce apoptosis and speed estrogen-induced hyperplasia in an organotypic MCF7-derived duct model.
Nia HT, Datta M, Seano G, Huang P, Munn LL, Jain RK. (2018). Quantifying solid stress and elastic energy from excised or in situ tumors.
Nordgren TM, Heires AJ, Bailey KL, Katafiasz DM, Toews ML, Wichman CS, Romberger DJ. (2018). Docosahexaenoic acid enhances amphiregulin-mediated bronchial epithelial cell repair processes following organic dust exposure.
Seeman SC, Campagnola L, Davoudian PA, Hoggarth A, Hage TA, Bosma-Moody A, Baker CA, Lee JH, Mihalas S, Teeter C, Ko AL, Ojemann JG, Gwinn RP, Silbergeld DL, Cobbs C, Phillips J, Lein E, Murphy G, Koch C, Zeng H, Jarsky T. (2018). Sparse recurrent excitatory connectivity in the microcircuit of the adult mouse and human cortex.
Ting JT, Kalmbach B, Chong P, de Frates R, Keene CD, Gwinn RP, Cobbs C, Ko AL, Ojemann JG, Ellenbogen RG, Koch C, Lein E. (2018). A robust ex vivo experimental platform for molecular-genetic dissection of adult human neocortical cell types and circuits.
Webb GM, Li S, Mwakalundwa G, Folkvord JM, Greene JM, Reed JS, Stanton JJ, Legasse AW, Hobbs T, Martin LD, Park BS, Whitney JB, Jeng EK, Wong HC, Nixon DF, Jones RB, Connick E, Skinner PJ, Sacha JB. (2018). The human IL-15 superagonist ALT-803 directs SIV-specific CD8(+) T cells into B-cell follicles.

Xu W, Baker SN. (2018). In vitro characterization of intrinsic properties and local synaptic inputs to pyramidal neurons in macaque primary motor cortex.
EJ Yoo, G Cao, CJ Koziol-White… (2017). Gα12 facilitates shortening in human airway smooth muscle by modulating phosphoinositide 3-kinase-mediated activation in a RhoA-dependent manner.
Long B, Zhou Z, Cetin A, Ting J, Gwinn R, Tasic B, Daigle T, Lein E, Zeng H, Saggau P, Hawrylycz M, Peng H. (2017). SmartScope2: Simultaneous Imaging and Reconstruction of Neuronal Morphology.
Ng-Blichfeldt JP, Alí_ada J, Montero MA, Dean CH, Griesenbach U, Griffiths MJ, Hind M. (2017). Deficient retinoid-driven angiogenesis may contribute to failure of adult human lung regeneration in emphysema.
Poobalasingam T, Salman D, Li H, Alí_ada J, Dean CH. (2017). Imaging the lung: the old ways and the new.
Velalopoulou A, Chatterjee S, Pietrofesa RA, Koziol-White C, Panettieri RA, Lin L, Tuttle S, Berman A, Koumenis C, Christofidou-Solomidou M. (2017). Synthetic Secoisolariciresinol Diglucoside (LGM2605) Protects Human Lung in an Ex Vivo Model of Proton Radiation Damage.
Yoo EJ, Cao G, Koziol-White CJ, Ojiaku CA, Sunder K, Jude JA, Michael JV, Lam H, Pushkarsky I, Damoiseaux R, Di Carlo D, Ahn K, An SS, Penn RB, Panettieri RA Jr. (2017). G-alpha(12) facilitates shortening in human airway smooth muscle by modulating phosphoinositide 3-kinase-mediated activation in a RhoA-dependent manner.
Bai Y, Krishnamoorthy N, Patel KR, Rosas I, Sanderson MJ, Ai X. (2016). Cryopreserved Human Precision-Cut Lung Slices as a Bioassay for Live Tissue Banking. A Viability Study of Bronchodilation with Bitter-Taste Receptor Agonists.
Carr R 3rd, Koziol-White C, Zhang J, Lam H, An SS, Tall GG, Panettieri RA Jr, Benovic JL. (2016). Interdicting Gq Activation in Airway Disease by Receptor-Dependent and Receptor-Independent Mechanisms.
Garcí_a-Cabezas Mí, John YJ, Barbas H, Zikopoulos B. (2016). Distinction of Neurons, Glia and Endothelial Cells in the Cerebral Cortex: An Algorithm Based on Cytological Features.
Ghosh A, Koziol-White CJ, Asosingh K, Cheng G, Ruple L, Groneberg D, Friebe A, Comhair SA, Stasch JP, Panettieri RA Jr, Aronica MA, Erzurum SC, Stuehr DJ. (2016). Soluble guanylate cyclase as an alternative target for bronchodilator therapy in asthma.
Graham JG, Winchell CG, Kurten RC, Voth DE. (2016). Development of an Ex Vivo Tissue Platform To Study the Human Lung Response to Coxiella burnetii.
Koziol-White CJ, Jia Y, Baltus GA, Cooper PR, Zaller DM, Crackower MA, Sirkowski EE, Smock S, Northrup AB, Himes BE, Alves SE, Panettieri RA Jr. (2016). Inhibition of spleen tyrosine kinase attenuates IgE-mediated airway contraction and mediator release in human precision cut lung slices.
Koziol-White CJ, Yoo EJ, Cao G, Zhang J, Papanikolaou E, Pushkarsky I, Andrews A, Himes BE, Damoiseaux RD, Liggett SB, Di Carlo D, Kurten RC, Panettieri RA Jr. (2016). Inhibition of PI3K promotes dilation of human small airways in a rho kinase-dependent manner.
Li S, Folkvord JM, Rakasz EG, Abdelaal HM, Wagstaff RK, Kovacs KJ, Kim HO, Sawahata R, MaWhinney S, Masopust D, Connick E, Skinner PJ. (2016). Simian Immunodeficiency Virus-Producing Cells in Follicles Are Partially Suppressed by CD8+ Cells In Vivo.
Abdelaal HM, Kim HO, Wagstaff R, Sawahata R, Southern PJ, Skinner PJ. (2015). Comparison of Vibratome and Compresstome sectioning of fresh primate lymphoid and genital tissues for in situ MHC-tetramer and immunofluorescence staining.
Hoffman JJ, Johnson BL, Holland MR, Fedewa RJ, Nair A, Miller JG. (2011). Layer-dependent variation in the anisotropy of apparent integrated backscatter from human coronary arteries.
Li G, Yang K, Zheng C, Liu Q, Chang Y, Kerrigan JF, Wu J. (2011). Functional rundown of gamma-aminobutyric acid(A) receptors in human hypothalamic hamartomas.
Ressmeyer AR, Bai Y, Delmotte P, Uy KF, Thistlethwaite P, Fraire A, Sato O, Ikebe M, Sanderson MJ. (2010). Human airway contraction and formoterol-induced relaxation is determined by Ca2+ oscillations and Ca2+ sensitivity.

Non-human primate

JT Ting, NJ Johansen, BE Kalmbach, N Taskin, B Lee… (2024). Distinctive physiology of molecularly identified medium spiny neurons in the macaque putamen.
NC Dembrow, S Sawchuk, R Dalley, X Opitz-Araya… (2024). Areal specializations in the morpho-electric and transcriptomic properties of primate layer 5 extratelencephalic projection neurons.
A Sathe, C Ayala, X Bai, SM Grimes, B Lee, C Kin… (2023). GITR and TIGIT immunotherapy provokes divergent multicellular responses in the tumor microenvironment of gastrointestinal cancers.
X Chen, DA Wolfe, DS Bindu, M Zhang… (2023). Functional gene delivery to and across brain vasculature of systemic AAVs with endothelial-specific tropism in rodents and broad tropism in primates.

BE Kalmbach, RD Hodge, NL Jorstad, S Owen… (2021). Signature morpho-electric, transcriptomic, and dendritic properties of human layer 5 neocortical pyramidal neurons.
F Xu, Y Shen, L Ding, CY Yang, H Tan, H Wang… (2021). High-throughput mapping of a whole rhesus monkey brain at micrometer resolution.
Webb GM, Molden J, Busman-Sahay K, Abdulhaqq S, Wu HL, Weber WC, Bateman KB, Reed JS, Northrup M, Maier N, Tanaka S, Gao L, Davey B, Carpenter BL, Axthelm MK, Stanton JJ, Smedley J, Greene JM, Safrit JT, Estes JD, Skinner PJ, Sacha JB. (2020). The human IL-15 superagonist N-803 promotes migration of virus-specific CD8+ T and NK cells to B cell follicles but does not reverse latency in ART-suppressed, SHIV-infected macaques.
Kurz A, Xu W, Wiegel P, Leukel C, N Baker S. (2019). Non-invasive assessment of superficial and deep layer circuits in human motor cortex.
Li S, Folkvord JM, Kovacs KJ, Wagstaff RK, Mwakalundwa G, Rendahl AK, Rakasz EG, Connick E, Skinner PJ. (2019). Low levels of SIV-specific CD8+ T cells in germinal centers characterizes acute SIV infection.
Haran KP, Hajduczki A, Pampusch MS, Mwakalundwa G, Vargas-Inchaustegui DA, Rakasz EG, Connick E, Berger EA, Skinner PJ. (2018). Simian Immunodeficiency Virus (SIV)-Specific Chimeric Antigen Receptor-T Cells Engineered to Target B Cell Follicles and Suppress SIV Replication.
Webb GM, Li S, Mwakalundwa G, Folkvord JM, Greene JM, Reed JS, Stanton JJ, Legasse AW, Hobbs T, Martin LD, Park BS, Whitney JB, Jeng EK, Wong HC, Nixon DF, Jones RB, Connick E, Skinner PJ, Sacha JB. (2018). The human IL-15 superagonist ALT-803 directs SIV-specific CD8(+) T cells into B-cell follicles.
Xu W, Baker SN. (2018). In vitro characterization of intrinsic properties and local synaptic inputs to pyramidal neurons in macaque primary motor cortex.
Li S, Folkvord JM, Rakasz EG, Abdelaal HM, Wagstaff RK, Kovacs KJ, Kim HO, Sawahata R, MaWhinney S, Masopust D, Connick E, Skinner PJ. (2016). Simian Immunodeficiency Virus-Producing Cells in Follicles Are Partially Suppressed by CD8+ Cells In Vivo.
Abdelaal HM, Kim HO, Wagstaff R, Sawahata R, Southern PJ, Skinner PJ. (2015). Comparison of Vibratome and Compresstome sectioning of fresh primate lymphoid and genital tissues for in situ MHC-tetramer and immunofluorescence staining.

Mouse

AN Webster, JJ Becker, C Li, DC Schwalbe… (2024). Molecular connectomics reveals a glucagon-like peptide 1-sensitive neural circuit for satiety.
HA Emmons (2024). Moderate-intensity aerobic exercise enhanced dopamine signaling in diet-induced obese female mice without preventing body weight gain.
M Zhang, Y Liang, Q Dai, H Gao, H Wang… (2024). A spinal neural circuit for electroacupuncture that regulates gastric functional disorders.
NA Olszewski, S Tetteh-Quarshie, BJ Henderson (2024). Neuronal excitability in the medial habenula and ventral tegmental area is differentially modulated by nicotine dosage and menthol in a sex-specific manner.
U Sengupta, R Kayed (2024). Tau Oligomers as Pathogenic Seeds: Preparation, Characterization, and Propagation In Vitro and In Vivo.
A Asgarihafshejani, VA Raveendran, JC Pressey… (2024). LTP is Absent in the CA1 Region of the Hippocampus of Male and Female Rett Syndrome Mouse Models.
A Charli, J Luo, B Palanisamy, E Malovic, Z Riyaz… (2024). Mitochondrial Stress Disassembles Nuclear Architecture through Proteolytic Activation of PKCδ and Lamin B1 Phosphorylation in Neuronal Cells: Implications for ….
A Torres-Berrío, M Estill, V Patel, A Ramakrishnan… (2024). Mono-methylation of lysine 27 at histone 3 confers lifelong susceptibility to stress.
AC Hunker, ME Wirthlin, G Gill, NJ Johansen… (2024). Enhancer AAV toolbox for accessing and perturbing striatal cell types and circuits.
AJ Mathiowetz, ES Meymand, KK Deol, G Parlakgül… (2024). CLCC1 promotes hepatic neutral lipid flux and nuclear pore complex assembly.
BJ Henderson, LE Young, NA Olszewski… (2024). Age-dependent effects of vaping on the prefrontal cortex, ventral tegmental area, and nucleus accumbens.
C Diaz-Nicieza, L Sahyoun, C Michalaki… (2024). Ageing results in an exacerbated inflammatory response to LPS by resident lung cells.
CF Suarez, OA Harb, A Robledo, G Largoza, JJ Ahn… (2024). MEK signaling represents a viable therapeutic vulnerability of KRAS-driven somatic brain arteriovenous malformations.

CJ Liu, JT Smith, Y Wang, JN Ouellette… (2024). Assessing cell viability with dynamic optical coherence microscopy.
CL Wilkinson, K Nakano, SA Grimm… (2024). GM-CSF-dependent CD301b+ lung dendritic cells confer tolerance to inhaled allergens.
CM McCarthy, KL McKevitt, SA Connolly, I Andersson… (2024). Microindentation of fresh soft biological tissue: A rapid tissue sectioning and mounting protocol.
CS Park, M Yan, M Zhu, MA Akram, NN Foster… (2024). Dendritome Mapping Unveils Spatial Organization of Striatal D1/D2-Neuron Morphology.
CTJ van Velthoven, Y Gao, M Kunst, C Lee… (2024). The transcriptomic and spatial organization of telencephalic GABAergic neuronal types.
D Ackerman, E Avetissian, CKE Bleck, JA Bogovic… (2024). Data Release: High-Resolution Imaging and Segmentation of P7 Mouse Tissue Microarchitecture Using FIB-SEM and Machine Learning.
D Bezwada, L Perelli, NP Lesner, L Cai, B Brooks… (2024). Mitochondrial complex I promotes kidney cancer metastasis.
D Markman, AZ Wasilczuk… (2024). General Anesthesia Occludes Ketamine's Antidepressant Response in a Rodent Model of Chronic Stress.
D Yang, N Almanzar, J Xia, S Udit, ST Yeung… (2024). Vagal TRPV1+ sensory neurons regulate myeloid cell dynamics and protect against influenza virus infection.
DJM Kollareth, AK Sharma (2024). Precision cut lung slices: an innovative tool for lung transplant research.
DL Wise, SB Greene, Y Escobedo-Lozoya… (2024). Progressive circuit hyperexcitability in mouse neocortical slice cultures with increasing duration of activity silencing.
DL Wise, Y Escobedo-Lozoya, V Valakh, B Isaac… (2024). Prolonged Activity Deprivation Causes Pre-and Postsynaptic Compensatory Plasticity at Neocortical Excitatory Synapses.
DW Ahmed, ML Tan, J Gabbard, Y Liu, MM Hu… (2024). Local photo-crosslinking of native tissue matrix regulates cell function.
EM York, A Miller, SA Stopka… (2024). The dentate gyrus differentially metabolizes glucose and alternative fuels during rest and stimulation.
EP Hurley, B Mukherjee, LZ Fang, JR Barnes… (2024). GluN3A and excitatory glycine receptors in the adult hippocampus.
ER Niessen (2024). Potential Treatments for Epileptiform Activity in Microgyral Cortex.
F Cathomas, HY Lin, KL Chan, L Li, LF Parise… (2024). Circulating myeloid-derived MMP8 in stress susceptibility and depression.
F Kadakia, A Khadka, J Yazell, S Davidson (2024). Chemogenetic modulation of posterior insula CaMKIIa neurons alters pain and thermoregulation.
F Marti, P Faure, T Le Borgne, C Nguyen, E Vicq, J Jehl… (2024). Nicotine engages a VTA-NAc feedback loop to inhibit amygdala-projecting dopamine neurons and induce anxiety.
F Mei, C Zhao, S Li, Z Xue, Y Zhao, Y Xu, R Ye… (2024). Ngfr+ cholinergic projection from SI/nBM to mPFC selectively regulates temporal order recognition memory.
F Zeldenrust, N Calcini, X Yan, A Bijlsma… (2024). The tuning of tuning: How adaptation influences single cell information transfer.
G Chen, S Lai, S Jiang, F Li, K Sun, X Wu, K Zhou… (2024). Cellular and circuit architecture of the lateral septum for reward processing.
G Parlakgül, S Pang, LL Artico, N Min… (2024). Spatial mapping of hepatic ER and mitochondria architecture reveals zonated remodeling in fasting and obesity.
GC Smith, KR Griffith, AR Sicher, DF Brockway… (2024). MODERATE ALCOHOL CONSUMPTION INDUCES LASTING IMPACTS ON PREFRONTAL CORTICAL SIGNALING IN MICE.
H Park, J Kim, H Lee, WS Chung (2024). Selective regulation of corticostriatal synapses by astrocytic phagocytosis.
HA Emmons, SC Fordahl (2024). Attenuating Saturated-Fat Induced Changes in Dopamine Neurotransmission.
HA Flaxman, MA Chrysovergi, H Han, F Kabir… (2024). Sanglifehrin A mitigates multi-organ fibrosis by targeting the collagen chaperone cyclophilin B.
HE Mohammed, JC Nelson, SA Marshall (2024). Ethanol Exacerbates the Alzheimer's Disease Pathology in the 5xFAD Mouse Model.
HJ Meyer, S Mamani, Z Li, L Shi… (2024). Femtosecond optical Kerr effect in normal and grades of cancerous breast tissues as a new optical biopsy method.
HM Gomez, TJ Haw, D Ilic, P Robinson… (2024). Landscape fire smoke airway exposure impairs respiratory and cardiac function and worsens experimental asthma.
HR Li, M Harb, JE Heath, JS Trippett… (2024). Engineering viral vectors for acoustically targeted gene delivery.
J Bär, T Fanutza, CC Reimann, L Seipold… (2024). Non-canonical function of ADAM10 in presynaptic plasticity.

J Fergusson, J Siu, N Gupta, E Nee, S Reinke… (2024). Ex vivo Model of Functioning Human Lymph Node Reveals Pivotal Role for Innate Lymphoid Cells and Stromal Populations in Response to Vaccine Adjuvant.
J Hu, K He, Y Yang, C Huang, Y Dou, H Wang… (2024). Amino acid formula induces microbiota dysbiosis and depressive-like behavior in mice.
J Lee (2024). Ultrasound Control and Imaging of Cellular Immunotherapy.
JC Moffa, IN Bland, JR Tooley, V Kalyanaraman… (2024). Cell specific single viral vector CRISPR/Cas9 editing and genetically encoded tool delivery in the central and peripheral nervous systems.
JD Cala Garcia, CF Arce Deza, AR Waich… (2024). Testing the Viability and Efficacy of Small Molecule Inhibitors in T-cells in Cryopreserved Precision Cut Lung Slices: New Insights for Long Term-storage Lung ….
KA Hagarty-Waite, HA Emmons, SC Fordahl… (2024). The Influence of Strain and Sex on High Fat Diet-Associated Alterations of Dopamine Neurochemistry in Mice.
KE Murtha, WD Sese, K Sleiman, J Halpage… (2024). Absence of oncomodulin increases susceptibility to noise-induced outer hair cell death and alters mitochondrial morphology.
KM Ibrahim, N Massaly, HJ Yoon, R Sandoval… (2024). Dorsal hippocampus to nucleus accumbens projections drive reinforcement via activation of accumbal dynorphin neurons.
L Castell, A Rogliardo, T Le Borgne, C Naon, A Cathala… (2024). Midbrain dopamine D2R regulates the salience of threat-related events.
L Yang, F Liu, H Hahm, T Okuda, X Li, Y Zhang… (2024). Projection-TAGs enable multiplex projection tracing and multi-modal profiling of projection neurons.
L Yang, LZ Fang, MR Lynch, CS Xu, H Hahm, Y Zhang… (2024). Transcriptomic landscape of mammalian ventral pallidum at single-cell resolution.
M Boucher, C Henry, L Gélinas, R Packwood… (2024). High throughput screening of airway constriction in mouse lung slices.
M Chioccioli, S Liu, S Magruder, A Tata, L Borriello… (2024). Stem cell migration drives lung repair in living mice.
M Lehmann, R Krishnan, J Sucre… (2024). Precision Cut Lung Slices: Emerging Tools for Preclinical and Translational Lung Research. An Official American Thoracic Society Workshop Report.
M Lindman (2024). RIPK3 Regulates Neuroinflammation During Flavivirus Infection of the Central Nervous System.
M Lindman, I Estevez, E Marmut, EM DaPrano… (2024). Astrocytic RIPK3 exerts protective anti-inflammatory activity during viral encephalitis via induction of serpin protease inhibitors.
M Marcatti, B Tumurbaatar, M Borghi… (2024). Inhibition of Calcineurin with FK506 Reduces Tau Levels and Attenuates Synaptic Impairment Driven by Tau Oligomers in the Hippocampus of Male Mouse ….
M Serranilla, JC Pressey, MA Woodin (2024). Restoring Compromised Cl-in D2 Neurons of a HD Mouse Model Rescues Motor Disability.
M Shammas (2024). Mitochondrial Dysfunction and Stress Responses in CHCHD10 Myopathy and Neurodegeneration.
M Vierhout, A Ayoub, P Ali, V Kumaran, S Naiel… (2024). A Novel Ex Vivo Approach for Investigating Profibrotic Macrophage Polarization Using Murine Precision-Cut Lung Slices.
M Xue, QY Chen, W Shi, Z Zhou, X Li, F Xu… (2024). Whole-brain mapping of afferents to the anterior cingulate cortex in adult mice.
MC Hasselluhn, AR Decker-Farrell, L Vlahos… (2024). Tumor explants elucidate a Cascade of Paracrine SHH, WNT, and VEGF signals driving pancreatic Cancer Angiosuppression.
N Mojahed, M Adjei, E Qasem, S Aaflaq… (2024). Acute social defeat during adolescence promotes long-lasting aggression through activation of the medial amygdala.
N Schaunaman, D Cervantes, T Nichols, M Numata… (2024). Cooperation of immune regulators Tollip and surfactant protein A inhibits influenza a virus infection in mice.
P Lu, LM Lifshitz, K Bellve, R ZhuGe (2024). TMEM16A in smooth muscle cells acts as a pacemaker channel in the internal anal sphincter.
P Scaduto, M Marcatti, N Bhatt, R Kayed… (2024). Calcineurin inhibition prevents synaptic plasticity deficit induced by brain-derived tau oligomers.
QA Nguyen, PM Klein, C Xie, KN Benthall… (2024). Acetylcholine receptor based chemogenetics engineered for neuronal inhibition and seizure control assessed in mice.
R Joulia, F Puttur, H Stölting, WJ Traves… (2024). Mast cell activation disrupts interactions between endothelial cells and pericytes during early life allergic asthma.
R Kshetri, JO Beavers, R Hyde, R Ewa… (2024). Behavioral decline in Shank3Δex4–22 mice during early adulthood parallels cerebellar granule cell glutamatergic synaptic changes.
RA Serafini, Z Farzinpour, V Patel, AM Kelley, M Estill… (2024). Nucleus accumbens myocyte enhancer factor 2C mediates the maintenance of peripheral nerve injury–induced physiological and behavioral maladaptations.

S Basu, EJ Ro, Z Liu, H Kim, A Bennett… (2024). The Mef2c gene dose-dependently controls hippocampal neurogenesis and the expression of autism-like behaviors.
S Brannan, L Garbe, BD Richardson (2024). Early life stress induced sex-specific changes in behavior is paralleled by altered locus coeruleus physiology in BALB/cJ mice.
S Brennan, L Garbe, BD Richardson (2024). Early life stress induces sex-specific changes in behavior and parallel locus coeruleus neuron excitability.
S Hall, S Liu, I Liang, S Schulz, C Ezran, M Tan… (2024). Cellular and molecular characterization of peripheral glia in the lung and other organs.
S Logan, R Ranjit, H Rose, A Bredegaard… (2024). Simultaneous quantitative respirometry and fluorometric assays in dissected hippocampal tissue from mice.
S McCracken, L McCoy, Z Hu, J Hodges, K Valkova… (2024). Mistargeted retinal axons form synaptically segregated subcircuits in the visual thalamus of albino mice.
S Trivedi, C Tilsed, M Liousia, RM Brody… (2024). Transcriptomic analysis-guided assessment of precision-cut tumor slices (PCTS) as an ex-vivo tool in cancer research.
S Zheng, R Banerji, R LeBourdais, S Zhang… (2024). Alteration of mechanical stresses in the murine brain by age and hemorrhagic stroke.
SB Park, G Lur (2024). Repeated exposure to multiple concurrent stressors alters visual processing in the adult posterior parietal cortex.
SC Cordts, K Yuki, MF Henao Echeverri… (2024). Microdissection tools to generate organoids for modeling the tumor immune microenvironment.
SM Lingamallu, A Deshpande, N Joy, K Ganeshan… (2024). Neuroepithelial bodies and terminal bronchioles are niches for distinctive club cells that repair the airways following acute notch inhibition.
SS Adel, ZJ Pranske, TF Kowalski, N Kanzler… (2024). Plexin-B1 and Plexin-B2 play non-redundant roles in GABAergic synapse formation.
SS Cheong, TC Luis, M Hind, CH Dean (2024). A Novel Method for Floxed Gene Manipulation Using TAT-Cre Recombinase in Ex Vivo Precision-Cut Lung Slices (PCLS).
SY Kim, D McTeague, SS Cheong, M Hind… (2024). Deciphering the impacts of modulating the Wnt-planar cell polarity (PCP) pathway on alveolar repair.
T Duparc, E Gore, G Combes, D Beuzelin, JP Da Silva… (2024). P2Y13 receptor deficiency favors adipose tissue lipolysis and worsens insulin resistance and fatty liver disease.
TL Dunham, JR Wilkerson, RC Johnson, RL Huganir… (2024). WWC2 modulates GABAA-receptor-mediated synaptic transmission, revealing class-specific mechanisms of synapse regulation by WWC family proteins.
V Nikitin, G Wildenberg, A Mittone… (2024). Laminography as a tool for imaging large-size samples with high resolution.
VA Raveendran, M Serranilla, A Asgarihafshejani… (2024). SNARE protein SNAP25 regulates the chloride-transporter KCC2 in neurons.
W Yu, Y Zhang, CTK Lo, L Kang, TTW Wong (2024). Rapid full-color serial sectioning tomography with speckle illumination and ultraviolet excitation.
W Zhang, Y Li, AA Fung, Z Li, H Jang, H Zha… (2024). Multi-molecular hyperspectral PRM-SRS imaging.
WR Evans, SS Baskar, ARCE Costa, S Ravoori… (2024). Functional activation of dorsal striatum astrocytes improves movement deficits in hemi-parkinsonian mice.
XH Li, W Shi, ZX Zhao, T Matsuura, JS Lu… (2024). Increased GluK1 Subunit Receptors in Corticostriatal Projection from the Anterior Cingulate Cortex Contributed to Seizure-Like Activities.
Y Ge, C Yang, M Zadeh, SM Sprague, YD Lin, HS Jain… (2024). Functional regulation of microglia by vitamin B12 alleviates ischemic stroke-induced neuroinflammation in mice.
Z Zhou, X Yang, A Mao, H Xu, C Lin, M Yang, W Hu… (2024). Deficiency of CAMSAP2 impairs olfaction and the morphogenesis of mitral cells.
A Godino, M Salery, AM Minier-Toribio, V Patel… (2023). Dopaminoceptive D1 and D2 neurons in ventral hippocampus arbitrate approach and avoidance in anxiety.
A Godino, M Salery, R Durand-de Cuttoli, MS Estill… (2023). Transcriptional control of nucleus accumbens neuronal excitability by retinoid X receptor alpha tunes sensitivity to drug rewards.
A Hall (2023). Analysis of cFos Expression and Microglial Branch Density in a Mouse Model of Trauma-Induced Hyperarousal.
A Lazrak, W Song, Z Yu, S Zhang, A Nellore… (2023). Low molecular weight hyaluronan inhibits lung epithelial ion channels by activating the calcium-sensing receptor.
A Miller, EM York, SA Stopka, JR Martínez-François… (2023). Spatially resolved metabolomics and isotope tracing reveal dynamic metabolic responses of dentate granule neurons with acute stimulation.

A Ozgur, SB Park, AY Flores, M Oijala, G Lur (2023). A comprehensive, affordable, open-source hardware-software solution for flexible implementation of complex behaviors in head-fixed mice.
A Ray, KH Hu, K Kersten, NF Kuhn, B Samad… (2023). Critical role of CD206+ macrophages in organizing anti-tumor immunity.
A Sarkar, Y Jin, BC DeFelice, CY Logan, Y Yang… (2023). Intermittent fasting induces rapid hepatocyte proliferation to restore the hepatostat in the mouse liver.
A Sathe, C Ayala, X Bai, SM Grimes, B Lee, C Kin… (2023). GITR and TIGIT immunotherapy provokes divergent multicellular responses in the tumor microenvironment of gastrointestinal cancers.
A Urso (2023). Pathophysiology of bile acid aspiration in lung transplant recipients.
AA Fung (2023). Development of a Label-free Optical Analysis Platform for Cells and Tissues.
AG Salinas, JO Lee, SM Augustin, S Zhang… (2023). Distinct sub-second dopamine signaling in dorsolateral striatum measured by a genetically-encoded fluorescent sensor.
AK Muthusamy (2023). Neuropsychiatric Drug Biosensors in Organelles, Cells, Biofluids, &Behaving Animals.
AML Osse, RS Pandey, RA Wirt, AA Ortiz… (2023). Reduction in GABAB on glia induce Alzheimer's disease related changes.
AR Sicher, WD Starnes, KR Griffith, NC Dao… (2023). Adolescent binge drinking leads to long-lasting changes in cortical microcircuits in mice.
AS Abdelfattah, J Zheng, A Singh, YC Huang, D Reep… (2023). Sensitivity optimization of a rhodopsin-based fluorescent voltage indicator.
C Natarajan, C Cook, K Ramaswamy… (2023). Phospholipase D1 Attenuation Therapeutics Promotes Resilience against Synaptotoxicity in 12-Month-Old 3xTg-AD Mouse Model of Progressive Neurodegeneratoin.
C Wang, B Hyams, NC Allen, K Cautivo, K Monahan… (2023). Dysregulated lung stroma drives emphysema exacerbation by potentiating resident lymphocytes to suppress an epithelial stem cell reservoir.
C Yang, Z Gong, X Zhang, S Miao, B Li, W Xie… (2023). Neuropeptide Y in the medial habenula alleviates migraine-like behaviors through the Y1 receptor.
C Zeng, Q Wang, C Wang, Q Zhou, X Fu, J Yu, W Xiong… (2023). Local Delivery of Bcar3 siRNA by Nano-Self-Assembly for Treating Pulmonary Fibrosis via Blocking the Interaction of Macrophages and Fibroblasts.
D Bezwada, NP Lesner, B Brooks, HS Vu, Z Wu, L Cai… (2023). Mitochondrial metabolism in primary and metastatic human kidney cancers.
D Dileep, TA Syed, TFW Sloan, PS Dhandapany… (2023). Cardiomyocyte orientation recovery at micrometer scale reveals long-axis fiber continuum in heart walls.
D Na, J Zhang, HJ Beaulac… (2023). Increased central auditory gain in 5xFAD Alzheimer's disease mice as an early biomarker candidate for Alzheimer's disease diagnosis.
D Stajano (2023). Role of tetraspanin 15 in metabotropic glutamate receptor 5 signaling and extracellular vesicles docking at neurons from mus musculus domesticus.
D Zhao, C Tian, M Cheng, F Yang, C Tian, Y Liu… (2023). Carrier-free quercetin nanomedicine blocks NLRP3 deubiquitination and TXNIP recruitment for Parkinson's disease therapy.
DB Azizoglu, K Perez, SL Zheng, S Rahman, EY Rim… (2023). Liver size is predetermined in the neonate by adding lobules at the periphery.
DF Brockway, KR Griffith, CM Aloimonos, TT Clarity… (2023). Somatostatin peptide signaling dampens cortical circuits and promotes exploratory behavior.
DJ Lievano Parra (2023). Effects of the unilateral lesion of the substantia nigra compacta with 6-OHDA on reversal learning and prepulse inhibition in male and female Wistar rats.
DK Kasaragod, H Aizawa (2023). Deep ultraviolet fluorescence microscopy of three-dimensional structures in the mouse brain.
DL Wise (2023). Maladaptive Homeostatic Plasticity: Impact of Prolonged Silencing on Cellular Hyperexcitability.
E Schulz (2023). Lokale Ultraschall-vermittelte Zytostatika-Applikation zur Behandlung von Hirntumoren.
F Ahangari, NL Price, S Malik, M Chioccioli… (2023). microRNA-33 deficiency in macrophages enhances autophagy, improves mitochondrial homeostasis, and protects against lung fibrosis.
F Cathomas, HY Lin, KL Chan, L Li… (2023). Peripheral immune-derived matrix metalloproteinase promotes stress susceptibility.
G Chen, S Lai, G Bao, J Ke, X Meng, S Lu, X Wu, H Xu… (2023). Distinct reward processing by subregions of the nucleus accumbens.
H Liu, RN Caballero-Florán, T Hergenreder, T Yang… (2023). DSCAM gene triplication causes excessive GABAergic synapses in the neocortex in Down syndrome mouse models.
H Mason, G Rai, A Kozyr, N De Jonge, E Gliniewicz… (2023). Development of an improved and specific inhibitor of NADPH oxidase 2 to treat traumatic brain injury.

H Ruiz-Garcia, N Zarco, F Watanabe… (2023). Development of Experimental Three-Dimensional Tumor Models to Study Glioblastoma Cancer Stem Cells and Tumor Microenvironment.
HA Emmons, CW Wallace, SC Fordahl (2023). Interleukin-6 and tumor necrosis factor-α attenuate dopamine release in mice fed a high-fat diet, but not medium or low-fat diets.
HM Rose, B Ferrán, R Ranjit… (2023). Mitochondrial calcium uniporter deficiency in dentate granule cells remodels neuronal metabolism and impairs reversal learning.
HY Lin, F Cathomas, L Li, RD Cuttoli, C Guevara… (2023). Chemokine receptor 5 signaling in PFC mediates stress susceptibility in female mice.
J Jehl, M Ciscato, E Vicq, G Dejean de la Batie… (2023). The interpeduncular nucleus blunts the rewarding effect of nicotine.
J Larochelle, RJ Tishko, C Yang, Y Ge, LT Phan… (2023). Receptor-interacting protein kinase 2 (RIPK2) profoundly contributes to post-stroke neuroinflammation and behavioral deficits with microglia as unique ….
J Sbierski-Kind, KM Cautivo, JC Wagner, MW Dahlgren… (2023). Group 2 innate lymphoid cells constrain type 3/17 lymphocytes in shared stromal niches to restrict liver fibrosis.
J Siewiera, TI McIntyre, KM Cautivo, K Mahiddine… (2023). Circumvention of luteolysis reveals parturition pathways in mice dependent upon innate type 2 immunity.
JA Hatter, MM Scott (2023). Selective ablation of VIP interneurons in the rodent prefrontal cortex results in increased impulsivity.
JK Mich, S Sunil, N Johansen, RA Martinez, M Leytze… (2023). Enhancer-AAVs allow genetic access to oligodendrocytes and diverse populations of astrocytes across species.
JT Ahrendsen, Y Nong, Y Huo, J Steele… (2023). CD8 cytotoxic T-cell infiltrates and cellular damage in the hypothalamus in human obesity.
JY Min, S Park, J Cho, Y Huh (2023). The anterior insular cortex processes social recognition memory.
K Egawa, M Watanabe, H Shiraishi, D Sato… (2023). Imbalanced expression of cation-chloride cotransporters as a potential therapeutic target in an Angelman syndrome mouse model.
K Grycel, NY Larsen, Y Feng, K Qvortrup… (2023). CRMP2 conditional knockout changes axonal function and ultrastructure of axons in mice corpus callosum.
K Jin, Z Yao, CTJ van Velthoven, ES Kaplan… (2023). Cell-type specific molecular signatures of aging revealed in a brain-wide transcriptomic cell-type atlas.
KJ Brymer, EP Hurley… (2023). Asymmetric dysregulation of glutamate dynamics across the synaptic cleft in a mouse model of Alzheimer's disease.
L Kang, W Yu, Y Zhang, TTW Wong (2023). Automated whole-organ histological imaging assisted with ultraviolet-excited sectioning tomography and deep learning.
L Kang, W Yu, Y Zhang, Z Chen, TTW Wong (2023). Deep Learning Enables Rapid Whole-Organ Histological Imaging with Ultraviolet-Excited Sectioning Tomography.
L Li, R Durand-de Cuttoli, AV Aubry, CJ Burnett… (2023). Social trauma engages lateral septum circuitry to occlude social reward.
L Munari, V Patel, N Johnson, C Mariottini… (2023). Memory discrimination is promoted by the expression of the transcription repressor WT1 in the dentate gyrus.
L Smith-Osborne, A Duong, A Resendez, R Palme… (2023). Female dominance hierarchies influence responses to psychosocial stressors.
LD Quigley, R Pendry, ML Mendoza, BE Pfeiffer… (2023). Experience alters hippocampal and cortical network communication via a KIBRA-dependent mechanism.
M Abdelmageed, P Palanisamy, V Vernail, Y Silberman… (2023). An altered cell-specific subcellular distribution of translesion synthesis DNA polymerase kappa (POLK) in aging neurons.
M Cheng, C Ye, C Tian, D Zhao, H Li, Z Sun, Y Miao… (2023). Engineered macrophage-biomimetic versatile nanoantidotes for inflammation-targeted therapy against Alzheimer's disease by neurotoxin neutralization and ….
M Dorofeikova, CD Borkar, K Weissmuller… (2023). Effects of footshock stress on social behavior and neuronal activation in the medial prefrontal cortex and amygdala of male and female mice.
M Dorofeikova, CE Stelly, A Duong, S Basavanhalli… (2023). The role of genetically distinct central amygdala neurons in appetitive and aversive responding assayed with a novel dual valence operant conditioning paradigm.
M Lam, E Lamanna, L Organ, C Donovan… (2023). Perspectives on precision cut lung slices—powerful tools for investigation of mechanisms and therapeutic targets in lung diseases.
M Lindman, JP Angel, I Estevez, NP Chang… (2023). RIPK3 promotes brain region-specific interferon signaling and restriction of tick-borne flavivirus infection.

M Salery, A Godino, YQ Xu, JF Fullard… (2023). Transcriptional correlates of cocaine-associated learning in striatal ARC ensembles.
M Serranilla (2023). Chloride Dysregulation and Impaired Gamma-Amino Butyric Acid Signaling in the Basal Ganglia in Huntington's Disease.
M Singh, K Sapkota, K Sakimura, M Kano, RM Cowell… (2023). Maturation of GABAergic Synaptic Transmission from Neocortical Parvalbumin Interneurons Involves NMDA receptor Recruitment of Cav2. 1 Channels.
ML Ratz-Mitchem, G Leary, A Grindeland, D Silvius… (2023). Generation and characterization of a knock-in mouse model for spastic tetraplegia, thin corpus callosum, and progressive microcephaly (SPATCCM).
MM Naffaa, RR Khan, CT Kuo, HH Yin (2023). Cortical regulation of neurogenesis and cell proliferation in the ventral subventricular zone.
MM Novakovic, KS Korshunov, RA Grant… (2023). Astrocyte reactivity and inflammation-induced depression-like behaviors are regulated by Orai1 calcium channels.
MR Norris, CC Kuo, SS Dunn, JR Kim, LJ Becker… (2023). Mu opioid receptors gate the locus coeruleus pain generator.
NM Benites, B Rodrigues… (2023). Development of electrophysiological properties of fusiform neurons from the dorsal cochlear nucleus of mice before and after hearing onset.
P Ferreira, R Vaja, M Lopes-Pires, M Crescente… (2023). Renal Function Underpins the Cyclooxygenase-2: Asymmetric Dimethylarginine Axis in Mouse and Man.
P Hoffman, MN Svalina, C Flores, C Brzezinski… (2023). Developmental Characterization of Neuronal Migration Anomalies and Axon Proliferation in mTOR pathway-associated Malformations of Cortical Development.
P Liu, A Anandhan, J Chen, A Shakya, M Dodson… (2023). Decreased autophagosome biogenesis, reduced NRF2, and enhanced ferroptotic cell death are underlying molecular mechanisms of non-alcoholic fatty liver ….
P Yadav, JG Ortega, W Tamaki, C Chien, K Chang… (2023). Macrophage-fibroblast crosstalk drives Arg1-dependent lung fibrosis via ornithine loading.
Q Tang, E Godschall, CD Brennan, Q Zhang… (2023). A leptin-responsive hypothalamic circuit inputs to the circadian feeding network.
Q Tang, E Godschall, CD Brennan, Q Zhang… (2023). Leptin receptor neurons in the dorsomedial hypothalamus input to the circadian feeding network.
R Joulia, F Puttur, H Stölting, LJ Entwistle, A Voitovich… (2023). Adventitial Mast Cell Activation Disrupts Endothelial Cell/Pericyte Interactions During Early Life Allergic Asthma.
R Sim, J Lee, J Chieng, KH Tan, G Lim, A Foo… (2023). Fluorescent Peptide-based Probe for the Detection of Alpha-synuclein Aggregates in the Gut.
RN Caballero-Florán, AD Nelson, L Min, PM Jenkins (2023). Effects of chronic lithium treatment on neuronal excitability and GABAergic transmission in an Ank3 mutant mouse model.
RN Caballero-Florán, M Bendahmane, JP Gupta… (2023). Synaptotagmin-7 facilitates acetylcholine release in splanchnic nerve-chromaffin cell synapses during nerve activity.
S Mondoloni, C Nguyen, E Vicq, M Ciscato, J Jehl… (2023). Prolonged nicotine exposure reduces aversion to the drug in mice by altering nicotinic transmission in the interpeduncular nucleus.
S Naiel, N Dowdall, SD Revill, V Kumaran… (2023). Reprogramming Rogue Macrophages: Yeast Beta-glucan Microparticles as a Macrophage Modulator for Lung Fibrosis.
S Nakakubo, Y Hiramatsu, T Goto, S Kimura… (2023). Therapeutic effects of KRM-II-81, positive allosteric modulator for α2/3 subunit containing GABAA receptors, in a mouse model of Dravet syndrome.
S Tsujikawa, KE DeMeulenaere, MV Centeno… (2023). Regulation of neuropathic pain by microglial Orai1 channels.
S Uribe, PD Yim, JF Perez-Zoghbi (2023). Airway Smooth Muscle Relaxation Via Opsin 3 Activation With Beta-carotene Metabolites.
S Venkadesh, A Santarelli, T Boesen… (2023). Combinatorial quantification of distinct neural projections from retrograde tracing.
SA Sorensen, NW Gouwens, Y Wang, M Mallory… (2023). Connecting single-cell transcriptomes to projectomes in mouse visual cortex.
SJF Cronin, W Yu, A Hale, S Licht-Mayer, MJ Crabtree… (2023). Crucial neuroprotective roles of the metabolite BH4 in dopaminergic neurons.
SM Conway, CC Kuo, W Gardiner, RN Wu, LV Thang… (2023). An electrochemical approach for rapid, sensitive, and selective detection of dynorphin.
SM Ramos Rodriguez (2023). An Investigation into Cell-Type Vulnerability for Formation of Alpha-Synuclein Aggregates.
SN Jiang, JW Cao, LY Liu, Y Zhou, GY Shan… (2023). Sncg, Mybpc1, and Parm1 Classify subpopulations of VIP-expressing interneurons in layers 2/3 of the somatosensory cortex.

SN Sveiven, SY Kim, V Barrientos, J Li… (2023). Myeloid-and epithelial-derived RELMα contribute to tissue repair following lung helminth infection.
SP Brown, RJ Lawson, JD Moreno… (2023). A reinterpretation of the relationship between persistent and resurgent sodium currents.
SS Adel, VRJ Clarke, A Evans-Strong, J Maguire… (2023). Semaphorin 4D induced inhibitory synaptogenesis decreases epileptiform activity and alters progression to Status Epilepticus in mice.
SS Cheong, TC Luis, M Stewart… (2023). A method for TAT-Cre recombinase-mediated floxed allele modification in ex vivo tissue slices.
SS Salile, HJ Lee, PSF Alberts, T Abula… (2023). In vitro and in vivo anti-seizure activity of hydromethanolic extract and fractions of Pterolobium stellatum.
SY Cooper, CV Willis, MR Richardson… (2023). Chemical flavorants in vaping products alter neurobiology in a sex-dependent manner to promote vaping-related behaviors.
T Fanutza (2023). Deciphering the structure and plasticity of glutamatergic synapses in the hippocampus.
TD Weber, MV Moya, K Kılıç, J Mertz… (2023). High-speed multiplane confocal microscopy for voltage imaging in densely labeled neuronal populations.
TR Sides, JC Nelson, KN Nwachukwu, J Boston… (2023). The Influence of Arsenic Co-Exposure in a Model of Alcohol-Induced Neurodegeneration in C57BL/6J Mice.
V Valakh, D Wise, XA Zhu, M Sha, J Fok… (2023). A transcriptional constraint mechanism limits the homeostatic response to activity deprivation in mammalian neocortex.
W Yu (2023). Translational Rapid Ultraviolet-Excited Sectioning Tomography for Whole-Organ Imaging with Subcellular Resolution.
XH Li, W Shi, QY Chen, S Hao, HH Miao… (2023). Activation of the glutamatergic cingulate cortical-cortical connection facilitates pain in adult mice.
Y Bai, G Li, L Yung, PB Yu, X Ai (2023). Intrapulmonary arterial contraction assay reveals region-specific deregulation of vasoreactivity to lung injuries.
Y Cui, Z Yang, Z Lv, J Lei (2023). Disruption of extracellular redox balance drives persistent lung fibrosis and impairs fibrosis resolution.
Y Jin, E Mikhailova, M Lei, SA Cowley, T Sun… (2023). Integration of 3D-printed cerebral cortical tissue into an ex vivo lesioned brain slice.
Y Liu, MR Fontenot, A Kulkarni, N Khandelwal… (2023). An extra-circadian function for human CLOCK in the neocortex.
Y Shima, H Skibbe, Y Sasagawa, N Fujimori… (2023). Distinctiveness and continuity in transcriptome and connectivity in the anterior-posterior axis of the paraventricular nucleus of the thalamus.
Y Wu, P Li, N Bhat, H Fan, M Liu (2023). Effects of repeated sleep deprivation on brain pericytes in mice.
Y Zhang, J Riexinger, X Yang, E Mikhailova, Y Jin… (2023). A microscale soft ionic power source modulates neuronal network activity.
YF Yazicioglu, E Marin, HF Andrew, K Bentkowska… (2023). Asparagine availability controls B cell homeostasis.
Z Li, EG Solomonidis, B Berkeley… (2023). Multi-species meta-analysis identifies transcriptional signatures associated with cardiac endothelial responses in the ischaemic heart.
Z Yao, CTJ van Velthoven, M Kunst, M Zhang… (2023). A high-resolution transcriptomic and spatial atlas of cell types in the whole mouse brain.
Z Zeng, M Cheng, M Li, T Wang, F Wen… (2023). Inherent differences of small airway contraction and Ca2+ oscillations in airway smooth muscle cells between BALB/c and C57BL/6 mouse strains.
A Bittar, R Al-Lahham, N Bhatt, K Moore… (2022). Passive Immunotherapy Targeting Tau Oligomeric Strains Reverses Tauopathy Phenotypes in Aged Human-Tau Mice in a Mouse Model-Specific Manner.
A Brodovskaya, S Shiono, T Batabyal… (2022). Construction of Local Field Potential Microelectrodes for in vivo Recordings from Multiple Brain Structures Simultaneously.
C Michalaki, C Dean, C Johansson (2022). The Use of Precision-Cut Lung Slices for Studying Innate Immunity to Viral Infections.
CN Barnes, CW Wallace, BS Jacobowitz… (2022). Reduced phasic dopamine release and slowed dopamine uptake occur in the nucleus accumbens after a diet high in saturated but not unsaturated fat.
CW Wallace, MC Loudermilt… (2022). Effect of fasting on dopamine neurotransmission in subregions of the nucleus accumbens in male and female mice.
D Koveal, PC Rosen, DJ Meyer… (2022). A high-throughput multiparameter screen for accelerated development and optimization of soluble genetically encoded fluorescent biosensors.

D Shrestha, N Massey, SM Bhat… (2022). Nrf2 Activation Protects Against Organic Dust and Hydrogen Sulfide Exposure Induced Epithelial Barrier Loss and K. pneumoniae Invasion.
DJ Meyer, CM Díaz-García, N Nathwani, M Rahman… (2022). The Na+/K+ pump dominates control of glycolysis in hippocampal dentate granule cells.
DJ Rindner, A Proddutur, G Lur (2022). Cell-type-specific integration of feedforward and feedback synaptic inputs in the posterior parietal cortex.
EA Kiffmeyer, JA Cosgrove, JK Siganos, HE Bien… (2022). Deficits in cerebellum-dependent learning and cerebellar morphology in male and female BTBR autism model mice.
ES Norton, LA Whaley, MJ Ulloa-Navas… (2022). Glioblastoma disrupts the ependymal wall and extracellular matrix structures of the subventricular zone.
G Parlakgül, AP Arruda, S Pang, E Cagampan, N Min… (2022). Regulation of liver subcellular architecture controls metabolic homeostasis.
J Ko, M Wilkovitsch, J Oh, RH Kohler, E Bolli… (2022). Spatiotemporal multiplexed immunofluorescence imaging of living cells and tissues with bioorthogonal cycling of fluorescent probes.
JD Hahn, L Gao, T Boesen, L Gou… (2022). Macroscale connections of the mouse lateral preoptic area and anterior lateral hypothalamic area.
JF Perez-Zoghbi, DR Sajorda, DA Webb… (2022). Imidazobenzodiazepine PI320 Relaxes Mouse Peripheral Airways by Inhibiting Calcium Mobilization.
K Egawa, M Watanabe, H Shiraishi, D Sato… (2022). Therapeutic effects of bumetanide on neurological dysfunction in a mouse model of Angelman syndrome.
K Friedrichsen, P Ramakrishna, J Hsiang… (2022). Reconstructing neural circuits using multiresolution correlated light and electron microscopy.
K Kersten, KH Hu, AJ Combes, B Samad, T Harwin… (2022). Spatiotemporal co-dependency between macrophages and exhausted CD8+ T cells in cancer.
KM Cautivo, PR Matatia, CO Lizama, NM Mroz… (2022). Interferon gamma constrains type 2 lymphocyte niche boundaries during mixed inflammation.
L Liu, C Yang, BP Lavayen, RJ Tishko… (2022). Targeted BRD4 protein degradation by dBET1 ameliorates acute ischemic brain injury and improves functional outcomes associated with reduced ….
LK Cuddy, AO Alia, MA Salvo… (2022). Farnesyltransferase inhibitor LNK-754 attenuates axonal dystrophy and reduces amyloid pathology in mice.
M Marcatti, A Fracassi, M Montalbano… (2022). Aβ/tau oligomer interplay at human synapses supports shifting therapeutic targets for Alzheimer's disease.
M Patiño, WN Lagos, NS Patne… (2022). Single-cell transcriptomic classification of rabies-infected cortical neurons.
M Scheibinger, A Janesick, GH Diaz… (2022). Immunohistochemistry and In Situ mRNA detection using inner ear vibratome sections.
MS Nair, NC Dao, DL Melean, KR Griffith… (2022). Somatostatin Neurons in the Bed Nucleus of the Stria Terminalis Play a Sex-Dependent Role in Binge Drinking.
N Deshet-Unger, G Horn, M Rawet-Slobodkin, T Waks… (2022). Comparing Intraperitoneal and Intravenous Personalized ErbB2CAR-T for the Treatment of Epithelial Ovarian Cancer.
N Gavert, Y Zwang, R Weiser, O Greenberg, S Halperin… (2022). Ex vivo organotypic cultures for synergistic therapy prioritization identify patient-specific responses to combined MEK and Src inhibition in colorectal cancer.
N Saviuk, Y Chong, P Wang, S Bermudez, Z Zhao… (2022). Loss of 4E-BP converts cerebellar long-term depression to long-term potentiation.
NAL Fayez, E Rouhollahi, CY Ong, J Wu… (2022). Hepatocyte-targeted delivery of imiquimod reduces hepatitis B virus surface antigen.
NAL Fayez, R Böttger, J Brown, E Rouhollahi… (2022). The mechanism of Hepatocyte-Targeting and safety profile of Phospholipid-Free small unilamellar vesicles.
NM George, AG Polese, L Merle… (2022). Excitable axonal domains adapt to sensory deprivation in the olfactory system.
P Baldominos, A Barbera-Mourelle, O Barreiro… (2022). Quiescent cancer cells resist T cell attack by forming an immunosuppressive niche.
P Baldominos, O Barreiro, U von Andrian, R Sirera… (2022). Protocol to isolate live single cells while retaining spatial information by combining cell photolabeling and FACS.
P Rukundo, T Feng, V Pham, S Pieraut (2022). Moderate effect of early-life experience on dentate gyrus function.
R Guidi, D Xu, DF Choy, TR Ramalingam… (2022). Steroid-induced fibroblast growth factors drive an epithelial-mesenchymal inflammatory axis in severe asthma.

S Gaige, R Barbouche… (2022). Constitutively active microglial populations limit anorexia induced by the food contaminant deoxynivalenol.
S Milde, GC Brown (2022). Knockout of the P2Y6 Receptor Prevents Peri-Infarct Neuronal Loss after Transient, Focal Ischemia in Mouse Brain.
SR Chadwick, AD Güler (2022). Local Drd1-neurons input to subgroups of arcuate AgRP/NPY-neurons.
TA Hage, A Bosma-Moody, CA Baker, MB Kratz… (2022). Synaptic connectivity to L2/3 of primary visual cortex measured by two-photon optogenetic stimulation.
V Nickl, E Schulz, E Salvador, L Trautmann, L Diener… (2022). Glioblastoma-Derived Three-Dimensional Ex Vivo Models to Evaluate Effects and Efficacy of Tumor Treating Fields (TTFields).
W Shi, M Xue, F Wu, K Fan, QY Chen, F Xu… (2022). Whole-brain mapping of efferent projections of the anterior cingulate cortex in adult male mice.
WE Barclay, N Aggarwal, ME Deerhake, M Inoue… (2022). The AIM2 inflammasome is activated in astrocytes during the late phase of EAE.
X Lin, NM Fisher, S Dogra, RK Senter, CW Reed… (2022). Differential activity of mGlu7 allosteric modulators provides evidence for mGlu7/8 heterodimers at hippocampal Schaffer collateral-CA1 synapses.
Y Zhang, L Kang, IHM Wong, W Dai, X Li… (2022). High-Throughput, Label-Free and Slide-Free Histological Imaging by Computational Microscopy and Unsupervised Learning.
YS Chun, MY Kim, SY Lee, MJ Kim, TJ Hong… (2022). MEK1/2 inhibition rescues neurodegeneration by TFEB-mediated activation of autophagic lysosomal function in a model of Alzheimer's Disease.
A Booeshaghi, Z Yao, C van Velthoven, K Smith… (2021). Isoform cell-type specificity in the mouse primary motor cortex.
A Farias, A Soto, F Puttur, CJ Goldin, S Sosa, C Gil… (2021). A TLR4 agonist improves immune checkpoint blockade treatment by increasing the ratio of effector to regulatory cells within the tumor microenvironment.
A Hausmann, B Felmy, L Kunz, S Kroon… (2021). Intercrypt sentinel macrophages tune antibacterial NF-κB responses in gut epithelial cells via TNF.
A Jacob Berger, E Gigi, L Kupershmidt, Z Meir… (2021). IRS1 phosphorylation underlies the non-stochastic probability of cancer cells to persist during EGFR inhibition therapy.
B Krishnan, C Natarajan, KZ Bourne, L Alikhani… (2021). Chronic low dose neutron exposure results in altered neurotransmission properties of the hippocampus-prefrontal cortex axis in both mice and rats.
BA Copits, R Gowrishankar, PR O'Neill, JN Li… (2021). A photoswitchable GPCR-based opsin for presynaptic inhibition.
BE Kalmbach, RD Hodge, NL Jorstad, S Owen… (2021). Signature morpho-electric, transcriptomic, and dendritic properties of human layer 5 neocortical pyramidal neurons.
BJ Sullivan, PA Kipnis, BM Carter, LR Shao… (2021). Targeting ischemia-induced KCC2 hypofunction rescues refractory neonatal seizures and mitigates epileptogenesis in a mouse model.
C Nguyen, S Mondoloni, T Le Borgne, I Centeno… (2021). Nicotine inhibits the VTA-to-amygdala dopamine pathway to promote anxiety.
C Yang, BP Lavayen, L Liu, BD Sanz, KM DeMars… (2021). Neurovascular protection by adropin in experimental ischemic stroke through an endothelial nitric oxide synthase-dependent mechanism.
CM Díaz-García, DJ Meyer, N Nathwani, M Rahman… (2021). The distinct roles of calcium in rapid control of neuronal glycolysis and the tricarboxylic acid cycle.
CW Wallace, NS Beatty, SA Hutcherson, HA Emmons… (2021). Replacing a Palatable High-Fat Diet with a Low-Fat Alternative Heightens κ-Opioid Receptor Control over Nucleus Accumbens Dopamine.
E Luković, JF Perez-Zoghbi, Y Zhang… (2021). Ginger metabolites and metabolite-inspired synthetic products modulate intracellular calcium and relax airway smooth muscle.
FP Mayer, H Iwamoto, MK Hahn, GJ Grumbar… (2021). There's no place like home? Return to the home cage triggers dopamine release in the mouse nucleus accumbens.
GB Ferraro, A Ali, A Luengo, DP Kodack, A Deik… (2021). Fatty acid synthesis is required for breast cancer brain metastasis.
H Hintiryan, I Bowman, DL Johnson… (2021). Connectivity characterization of the mouse basolateral amygdalar complex.
HD Mason, AM Johnson, NA Mihelson, P Mastorakos… (2021). Glia limitans superficialis oxidation and breakdown promote cortical cell death after repetitive head injury.
J Berg, SA Sorensen, JT Ting, JA Miller, T Chartrand… (2021). Human neocortical expansion involves glutamatergic neuron diversification.
J Vogler, R Böttger, NAL Fayez, W Zhang, Z Qin… (2021). Altering the intra-liver distribution of phospholipid-free small unilamellar vesicles using temperature-dependent size-tunability.
J Wie, Z Liu, H Song, TF Tropea, L Yang, H Wang… (2021). A growth-factor-activated lysosomal K+ channel regulates Parkinson's pathology.

JH Lee, J Kim, S Noh, H Lee, SY Lee, JY Mun, H Park… (2021). Astrocytes phagocytose adult hippocampal synapses for circuit homeostasis.
JK Mich, LT Graybuck, EE Hess, JT Mahoney, Y Kojima… (2021). Functional enhancer elements drive subclass-selective expression from mouse to primate neocortex.
JW DiGiacomo, I Godet, M Trautmann-Rodriguez… (2021). Extracellular Matrix–Bound FGF2 Mediates Estrogen Receptor Signaling and Therapeutic Response in Breast CancerThe ECM Mediates FGF-Induced ER Activity.
KD Micheva, M Kiraly, MM Perez, DV Madison (2021). Conduction velocity along the local axons of parvalbumin interneurons correlates with the degree of axonal myelination.
KD Micheva, M Kiraly, MM Perez, DV Madison (2021). Extensive structural remodeling of the axonal arbors of parvalbumin basket cells during development in mouse neocortex.
KL Elliott, J Kersigo, JH Lee, EN Yamoah… (2021). Sustained Loss of bdnf affects peripheral but not central vestibular targets.
KN Nwachukwu, WA Evans, TR Sides… (2021). Chemogenetic manipulation of astrocytic signaling in the basolateral amygdala reduces binge-like alcohol consumption in male mice.
M Dongelmans, R Durand-de Cuttoli, C Nguyen… (2021). Chronic nicotine increases midbrain dopamine neuron activity and biases individual strategies towards reduced exploration in mice.
M Puigdellívol, S Milde, M Spillantini… (2021). The microglial P2Y6 receptor mediates neuronal loss and memory deficits in neurodegeneration.
M Qu, P Lu, K Bellve, LM Lifshitz, R ZhuGe (2021). Mode switch of Ca2+ oscillation-mediated uterine peristalsis and associated embryo implantation impairments in mouse adenomyosis.
MM Maneshi, AB Toth, T Ishii, K Hori, S Tsujikawa… (2021). Orai1 channels are essential for amplification of glutamate-evoked Ca2+ signals in dendritic spines to regulate working and associative memory.
N Aggarwal, ME Deerhake, D DiPalma, SK Shahi… (2021). Secreted osteopontin from CD4+ T cells limits acute graft-versus-host disease.
N Al Fayez, R Bottger, E Rouhollahi… (2021). Improved Liver Delivery of Primaquine by Phospholipid-Free Small Unilamellar Vesicles with Reduced Hemolytic Toxicity.
N Massey, D Shrestha, SM Bhat, N Kondru… (2021). Organic dust-induced mitochondrial dysfunction could be targeted via cGAS-STING or cytoplasmic NOX-2 inhibition using microglial cells and brain slice culture ….
NL Benavidez, MS Bienkowski, M Zhu… (2021). Organization of the inputs and outputs of the mouse superior colliculus.
P Liu, M Dodson, H Li, CJ Schmidlin, A Shakya… (2021). Non-canonical NRF2 activation promotes a pro-diabetic shift in hepatic glucose metabolism.
P Lu, J Chen, C Zhang, D Saur, CE Baer… (2021). Oscillating calcium signals in smooth muscle cells underlie the persistent basal tone of internal anal sphincter.
P Lu, MK ElMallah, Z Liu, C Wu, J Chen… (2021). Genetic deletion of the Tas2r143/Tas2r135/Tas2r126 cluster reveals that TAS2Rs may not mediate bitter tastant-induced bronchodilation.
P Mastorakos, MV Russo, T Zhou, K Johnson… (2021). Antimicrobial immunity impedes CNS vascular repair following brain injury.
P Mastorakos, N Mihelson, M Luby, SR Burks… (2021). Temporally distinct myeloid cell responses mediate damage and repair after cerebrovascular injury.
PL Rochon, C Theriault, AGR Olguin, A Krishnaswamy (2021). The cell adhesion molecule Sdk1 shapes assembly of a retinal circuit that detects localized edges.
QW Wang, YH Wang, B Wang, Y Chen, SY Lu… (2021). Synaptotagmin-7–mediated activation of spontaneous NMDAR currents is disrupted in bipolar disorder susceptibility variants.
S Milde, FW van Tartwijk, A Vilalta, TC Hornik… (2021). Inflammatory neuronal loss in the substantia nigra induced by systemic lipopolysaccharide is prevented by knockout of the P2Y6 receptor in mice.
SK Bose, BM White, MV Kashyap, A Dave… (2021). In utero adenine base editing corrects multi-organ pathology in a lethal lysosomal storage disease.
SL Reitz, AZ Wasilczuk, GH Beh, A Proekt, MB Kelz (2021). Activation of preoptic tachykinin 1 neurons promotes wakefulness over sleep and volatile anesthetic-induced unconsciousness.
SM Chou, KX Li, MY Huang, C Chen, YHL King, GG Li… (2021). Kv1. 1 channels regulate early postnatal neurogenesis in mouse hippocampus via the TrkB signaling pathway.
SR Gray, L Ye, JY Ye, M Paukert (2021). Noradrenergic terminal short-term potentiation enables modality-selective integration of sensory input and vigilance state.
SS Salile, T Abula (2021). In vitro and In vivo Anticonvulsant Effect of Hydroalcoholic Extract of Moringa stenopetala in Mice Models.

SY Kim, R Mongey, P Wang, S Rothery, DCA Gaboriau… (2021). The acid injury and repair (AIR) model: A novel ex-vivo tool to understand lung repair.
T Feng, C Alicea, V Pham, A Kirk… (2021). Experience-dependent inhibitory plasticity is mediated by CCK+ basket cells in the developing dentate gyrus.
VP Mathis, M Williams, C Fillinger, PJ Kenny (2021). Networks of habenula-projecting cortical neurons regulate cocaine seeking.
WY Wang, RN Kent III, SA Huang, EH Jarman… (2021). Direct comparison of angiogenesis in natural and synthetic biomaterials reveals that matrix porosity regulates endothelial cell invasion speed and sprout diameter.
Y Shi, J Lv, L Chen, G Luo, M Tao, J Pan… (2021). Phosphodiesterase-4D Knockdown in the Prefrontal Cortex Alleviates Memory Deficits and Synaptic Failure in Mouse Model of Alzheimer's Disease.
YT Liu, DA Sliter, MK Shammas, X Huang, C Wang… (2021). Mt-Keima detects PINK1-PRKN mitophagy in vivo with greater sensitivity than mito-QC.
Z Yao, CTJ van Velthoven, TN Nguyen, J Goldy… (2021). A taxonomy of transcriptomic cell types across the isocortex and hippocampal formation.
Z Yao, H Liu, F Xie, S Fischer, RS Adkins, AI Aldridge… (2021). A transcriptomic and epigenomic cell atlas of the mouse primary motor cortex.
A Caputo, Y Liang, TD Raabe, A Lo, M Horvath… (2020). Snca-GFP knock-in mice reflect patterns of endogenous expression and pathological seeding.
Alsafadi HN, Uhl FE, Pineda RH, Bailey KE, Rojas M, Wagner DE, Kí_nigshoff M. (2020). Applications and Approaches for Three-Dimensional Precision-Cut Lung Slices. Disease Modeling and Drug Discovery.
Anderson AG, Kulkarni A, Harper M, Konopka G. (2020). Single-Cell Analysis of Foxp1-Driven Mechanisms Essential for Striatal Development.
B Ling, J Lee, D Maresca, A Lee-Gosselin… (2020). Biomolecular ultrasound imaging of phagolysosomal function.
Bariselli S, Miyazaki NL, Creed MC, Kravitz AV. (2020). Orbitofrontal-striatal potentiation underlies cocaine-induced hyperactivity.
Ben-Hamo R, Jacob Berger A, Gavert N, Miller M, Pines G, Oren R, Pikarsky E, Benes CH, Neuman T, Zwang Y, Efroni S, Getz G, Straussman R. (2020). Predicting and affecting response to cancer therapy based on pathway-level biomarkers.
Branchett WJ, Stí_lting H, Oliver RA, Walker SA, Puttur F, Gregory LG, Gabryçovíç L, Wilson MS, O'Garra A, Lloyd CM. (2020). A T cell-myeloid IL-10 axis regulates pathogenic IFN-'_-dependent immunity in a mouse model of type 2-low asthma.
Bunner W, Landry T, Laing BT, Li P, Rao Z, Yuan Y, Huang H. (2020). ARC(AgRP/NPY) Neuron Activity Is Required for Acute Exercise-Induced Food Intake in Un-Trained Mice.
C Linghu, SL Johnson, PA Valdes, OA Shemesh… (2020). Spatial multiplexing of fluorescent reporters for imaging signaling network dynamics.
Chen S, Kadakia F, Davidson S. (2020). Group II metabotropic glutamate receptor expressing neurons in anterior cingulate cortex become sensitized after inflammatory and neuropathic pain.
Co M, Hickey SL, Kulkarni A, Harper M, Konopka G. (2020). Cortical Foxp2 Supports Behavioral Flexibility and Developmental Dopamine D1 Receptor Expression.
Colon LM, Poulos AM. (2020). Contextual processing elicits sex differences in dorsal hippocampus activation following footshock and context fear retrieval.
Cooper JG, Sicard D, Sharma S, Van Gulden S, McGuire TL, Cajiao MP, Tschumperlin DJ, Kessler JA. (2020). Spinal Cord Injury Results in Chronic Mechanical Stiffening.
Dao NC, Suresh Nair M, Magee SN, Moyer JB, Sendao V, Brockway DF, Crowley NA. (2020). Forced Abstinence From Alcohol Induces Sex-Specific Depression-Like Behavioral and Neural Adaptations in Somatostatin Neurons in Cortical and Amygdalar Regions.
Ding SL, Yao Z, Hirokawa KE, Nguyen TN, Graybuck LT, Fong O, Bohn P, Ngo K, Smith KA, Koch C, Phillips JW, Lein ES, Harris JA, Tasic B, Zeng H. (2020). Distinct Transcriptomic Cell Types and Neural Circuits of the Subiculum and Prosubiculum along the Dorsal-Ventral Axis.
Dragunas G, Woest ME, Nijboer S, Bos ST, van Asselt J, de Groot AP, Vohlí_dalovíç E, Vermeulen CJ, Ditz B, Vonk JM, Koppelman GH, van den Berge M, Ten Hacken NHT, Timens W, Munhoz CD, Prakash YS, Gosens R, Kistemaker LEM. (2020). Cholinergic neuroplasticity in asthma driven by TrkB signaling.
Entwistle LJ, Puttur F, Gregory LG, Lloyd CM. (2020). Group 2 ILC Functional Assays in Allergic Airway Inflammation.
Finetti F, Capitani N, Manganaro N, Tatangelo V, Libonati F, Panattoni G, Calaresu I, Ballerini L, Baldari CT, Patrussi L. (2020). Optimization of Organotypic Cultures of Mouse Spleen for Staining and Functional Assays.
Fisher NM, Gould RW, Gogliotti RG, McDonald AJ, Badivuku H, Chennareddy S, Buch AB, Moore AM, Jenkins MT, Robb WH, Lindsley CW, Jones CK, Conn PJ, Niswender CM. (2020). Phenotypic profiling of mGlu(7) knockout mice reveals new

implications for neurodevelopmental disorders.
Griffiths KK, Wang A, Wang L, Tracey M, Kleiner G, Quinzii CM, Sun L, Yang G, Perez-Zoghbi JF, Licznerski P, Yang M, Jonas EA, Levy RJ. (2020). Inefficient thermogenic mitochondrial respiration due to futile proton leak in a mouse model of fragile X syndrome.
Grippo RM, Tang Q, Zhang Q, Chadwick SR, Gao Y, Altherr EB, Sipe L, Purohit AM, Purohit NM, Sunkara MD, Cios KJ, Sidikpramana M, Spano AJ, Campbell JN, Steele AD, Hirsh J, Deppmann CD, Wu M, Scott MM, Gí_ler AD. (2020). Dopamine Signaling in the Suprachiasmatic Nucleus Enables Weight Gain Associated with Hedonic Feeding.
Heras AF, Veerappan A, Silver RB, Emala CW, Worgall TS, Perez-Zoghbi J, Worgall S. (2020). Increasing Sphingolipid Synthesis Alleviates Airway Hyperreactivity.
Hodge RD, Miller JA, Novotny M, Kalmbach BE, Ting JT, Bakken TE, Aevermann BD, Barkan ER, Berkowitz-Cerasano ML, Cobbs C, Diez-Fuertes F, Ding SL, McCorrison J, Schork NJ, Shehata SI, Smith KA, Sunkin SM, Tran DN, Venepally P, Yanny AM, Steemers FJ, Phillips JW, Bernard A, Koch C, Lasken RS, Scheuermann RH, Lein ES. (2020). Transcriptomic evidence that von Economo neurons are regionally specialized extratelencephalic-projecting excitatory neurons.
Howell, Rebecca D; Dominguez-Lopez, Sergio; Ocañas, Sarah; Freeman, Willard M; Beckstead, Michael J; (2020). Female mice are resilient to age-related decline of substantia nigra dopamine neuron firing parameters.
J Wang, T Li, JL Wang, Z Xu, W Meng, QF Wu (2020). Talpid3-Mediated Centrosome Integrity Restrains Neural Progenitor Delamination to Sustain Neurogenesis by Stabilizing Adherens Junctions.
JW Cao, W Guan, YC Yu, Y Fu (2020). Synaptic Transmission from Somatostatin-expressing Interneurons to Excitatory Neurons Mediated by α5-subunit-containing GABAA Receptors in the Developing ….
K Hori, S Tsujikawa, MM Novakovic… (2020). Regulation of chemoconvulsant-induced seizures by store-operated Orai1 channels.
KH Hu, JP Eichorst, CS McGinnis, DM Patterson… (2020). ZipSeq: barcoding for real-time mapping of single cell transcriptomes.
Kaneko K, Osada T, Morse MA, Gwin WR, Ginzel JD, Snyder JC, Yang XY, Liu CX, Diniz MA, Bodoor K, Hughes PF, Haystead TA, Lyerly HK. (2020). Heat shock protein 90-targeted photodynamic therapy enables treatment of subcutaneous and visceral tumors.
Kim EJ, Zhang Z, Huang L, Ito-Cole T, Jacobs MW, Juavinett AL, Senturk G, Hu M, Ku M, Ecker JR, Callaway EM. (2020). Extraction of Distinct Neuronal Cell Types from within a Genetically Continuous Population.
Kim Y, Jang YN, Kim JY, Kim N, Noh S, Kim H, Queenan BN, Bellmore R, Mun JY, Park H, Rah JC, Pak DTS, Lee KJ. (2020). Microtubule-associated protein 2 mediates induction of long-term potentiation in hippocampal neurons.
Kondru N, Manne S, Kokemuller R, Greenlee J, Greenlee MHW, Nichols T, Kong Q, Anantharam V, Kanthasamy A, Halbur P, Kanthasamy AG. (2020). An Ex Vivo Brain Slice Culture Model of Chronic Wasting Disease: Implications for Disease Pathogenesis and Therapeutic Development.
Krishnan B, Sallam HS, Tumurbataar B, Saieva S, Baymon D, Tuvdendorj D, Micci MA, Abate N, Taglialatela G. (2020). Amelioration of hippocampal dysfunction by adipose tissue-targeted stem cell transplantation in a mouse model of type 2 diabetes.
Lewis TR, Shores CR, Cady MA, Hao Y, Arshavsky VY, Burns ME. (2020). The F220C and F45L rhodopsin mutations identified in retinitis pigmentosa patients do not cause pathology in mice.
Li G, Cohen JA, Martines C, Ram-Mohan S, Brain JD, Krishnan R, Ai X, Bai Y. (2020). Preserving Airway Smooth Muscle Contraction in Precision-Cut Lung Slices.
Li, Xiufeng; Kang, Lei; Zhang, Yan; Wong, Terence TW; (2020). High-speed Label-free Ultraviolet Photoacoustic Microscopy for Histology-like imaging of unprocessed biological tissues.
Lu RA, Zeki AA, Ram-Mohan S, Nguyen N, Bai Y, Chmiel K, Pecic S, Ai X, Krishnan R, Ghosh CC. (2020). Inhibiting Airway Smooth Muscle Contraction Using Pitavastatin: A Role for the Mevalonate Pathway in Regulating Cytoskeletal Proteins.
Majewski L, MaciÛfg F, Boguszewski PM, Kuznicki J. (2020). Transgenic Mice Overexpressing Human STIM2 and ORAI1 in Neurons Exhibit Changes in Behavior and Calcium Homeostasis but Show No Signs of Neurodegeneration.
Mancia Leon WR, Spatazza J, Rakela B, Chatterjee A, Pande V, Maniatis T, Hasenstaub AR, Stryker MP, Alvarez-Buylla A. (2020). Clustered gamma-protocadherins regulate cortical interneuron programmed cell death.
NW Gouwens, SA Sorensen, F Baftizadeh, A Budzillo… (2020). Integrated morphoelectric and transcriptomic classification of cortical GABAergic cells.
Pozhidayeva DY, Farris SP, Goeke CM, Firsick EJ, Townsley KG, Guizzetti M, Ozburn AR. (2020). Chronic Chemogenetic Stimulation of the Nucleus Accumbens Produces Lasting Reductions in Binge Drinking and Ameliorates Alcohol-Related Morphological and Transcriptional Changes.
Q Wu, MA Shaikh, ES Meymand, B Zhang, KC Luk… (2020). Neuronal activity modulates alpha-synuclein aggregation and spreading in organotypic brain slice cultures and in vivo.

Qian, Yong; Cosio, Danielle M Orozco; Piatkevich, Kiryl D; Aufmkolk, Sarah; Su, Wan-Chi; Celike, Orhan T; Schohl, Anne; Murdock, Mitchell H; Aggarwal, Abhi; Chang, Yu-Fen; (2020). Improved genetically encoded near-infrared fluorescent calcium ion indicators for in vivo imaging.

S Calovi, P Mut-Arbona, P Tod, A Iring… (2020). P2X7 receptor-dependent layer-specific changes in neuron-microglia reactivity in the prefrontal cortex of a phencyclidine induced mouse model of ….

S Xu-Vanpala, ME Deerhake, JD Wheaton… (2020). Functional heterogeneity of alveolar macrophage population based on expression of CXCL2.

SS Cheong, KM Akram, C Matellan, SY Kim… (2020). The planar polarity component VANGL2 is a key regulator of mechanosignaling.

SU Hettiarachchi, YH Li, J Roy, F Zhang… (2020). Targeted inhibition of PI3 kinase/mTOR specifically in fibrotic lung fibroblasts suppresses pulmonary fibrosis in experimental models.

SY Cooper, AT Akers, BJ Henderson (2020). Green apple e-cigarette flavorant farnesene triggers reward-related behavior by promoting high-sensitivity nAChRs in the ventral tegmental area.

SY Kim, R Mongey, M Griffiths, M Hind… (2020). An Ex Vivo Acid Injury and Repair (AIR) Model Using Precision-Cut Lung Slices to Understand Lung Injury and Repair.

Shemesh OA, Linghu C, Piatkevich KD, Goodwin D, Celiker OT, Gritton HJ, Romano MF, Gao R, Yu CJ, Tseng HA, Bensussen S, Narayan S, Yang CT, Freifeld L, Siciliano CA, Gupta I, Wang J, Pak N, Yoon YG, Ullmann JFP, Guner-Ataman B, Noamany H, Sheinkopf ZR, Park WM, Asano S, Keating AE, Trimmer JS, Reimer J, Tolias AS, Bear MF, Tye KM, Han X, Ahrens MB, Boyden ES. (2020). Precision Calcium Imaging of Dense Neural Populations via a Cell-Body-Targeted Calcium Indicator.

Shrestha S, Cho W, Stump B, Imani J, Lamattina AM, Louis PH, Pazzanese J, Rosas IO, Visner G, Perrella MA, El-Chemaly S. (2020). FK506 induces lung lymphatic endothelial cell senescence and downregulates LYVE-1 expression, with associated decreased hyaluronan uptake.

Srivastava AK , Roy Choudhury S , Karmakar S . (2020). Melatonin/polydopamine nanostructures for collective neuroprotection-based Parkinson's disease therapy.

Srivastava AK, Roy Choudhury S, Karmakar S. (2020). Near-Infrared Responsive Dopamine/Melatonin-Derived Nanocomposites Abrogating in Situ Amyloid '_ Nucleation, Propagation, and Ameliorate Neuronal Functions.

Sun Y, Liu M. (2020). Hypothalamic MCH Neuron Activity Dynamics during Cataplexy of Narcolepsy.

Urso A, D'Ovidio F, Xu D, Emala CW Sr, Bunnett NW, Perez-Zoghbi JF. (2020). Bile acids inhibit cholinergic constriction in proximal and peripheral airways from humans and rodents.

Veldman MB, Park CS, Eyermann CM, Zhang JY, Zuniga-Sanchez E, Hirano AA, Daigle TL, Foster NN, Zhu M, Langfelder P, Lopez IA, Brecha NC, Zipursky SL, Zeng H, Dong HW, Yang XW. (2020). Brainwide Genetic Sparse Cell Labeling to Illuminate the Morphology of Neurons and Glia with Cre-Dependent MORF Mice.

Zhang Y, Lu P, Liang F, Liufu N, Dong Y, Zheng JC, Xie Z. (2020). Cyclophilin D Contributes to Anesthesia Neurotoxicity in the Developing Brain.

Akram KM, Yates LL, Mongey R, Rothery S, Gaboriau DCA, Sanderson J, Hind M, Griffiths M, Dean CH. (2019). Live imaging of alveologenesis in precision-cut lung slices reveals dynamic epithelial cell behaviour.

Amarelle L, Katzen J, Shigemura M, Welch LC, Cajigas H, Peteranderl C, Celli D, Herold S, Lecuona E, Sznajder JI. (2019). Cardiac glycosides decrease influenza virus replication by inhibiting cell protein translational machinery.

Askoxylakis V, Ferraro GB, Badeaux M, Kodack DP, Kirst I, Shankaraiah RC, Wong CSF, Duda DG, Fukumura D, Jain RK. (2019). Dual endothelin receptor inhibition enhances T-DM1 efficacy in brain metastases from HER2-positive breast cancer.

Avelar AJ, Akers AT, Baumgard ZJ, Cooper SY, Casinelli GP, Henderson BJ. (2019). Why flavored vape products may be attractive: Green apple tobacco flavor elicits reward-related behavior, upregulates nAChRs on VTA dopamine neurons, and alters midbrain dopamine and GABA neuron function.

Bienkowski MS, Benavidez NL, Wu K, Gou L, Becerra M, Dong HW. (2019). Extrastriate connectivity of the mouse dorsal lateral geniculate thalamic nucleus.

Bittar A, Bhatt N, Hasan TF, Montalbano M, Puangmalai N, McAllen S, Ellsworth A, Carretero Murillo M, Taglialatela G, Lucke-Wold B, Logsdon A, Rosen C, Turner RC, Kayed R. (2019). Neurotoxic tau oligomers after single versus repetitive mild traumatic brain injury.

Boone PG, Rochelle LK, Ginzel JD, Lubkov V, Roberts WL, Nicholls PJ, Bock C, Flowers ML, von Furstenberg RJ, Stripp BR, Agarwal P, Borowsky AD, Cardiff RD, Barak LS, Caron MG, Lyerly HK, Snyder JC. (2019). A cancer rainbow mouse for visualizing the functional genomics of oncogenic clonal expansion.

Bourne KZ, Natarajan C, Perez CXM, Tumurbaatar B, Taglialatela G, Krishnan B. (2019). Suppressing aberrant phospholipase D1 signaling in 3xTg Alzheimer's disease mouse model promotes synaptic resilience.

Bui CB, Kolodziej M, Lamanna E, Elgass K, Sehgal A, Rudloff I, Schwenke DO, Tsuchimochi H, Kroon MAGM, Cho SX, Maksimenko A, Cholewa M, Berger PJ, Young MJ, Bourke JE, Pearson JT, Nold MF, Nold-Petry CA. (2019). Interleukin-1

Receptor Antagonist Protects Newborn Mice Against Pulmonary Hypertension.
Burman RJ, Selfe JS, Lee JH, van den Berg M, Calin A, Codadu NK, Wright R, Newey SE, Parrish RR, Katz AA, Wilmshurst JM, Akerman CJ, Trevelyan AJ, Raimondo JV. (2019). Excitatory GABAergic signalling is associated with benzodiazepine resistance in status epilepticus.
Comerota MM, Tumurbaatar B, Krishnan B, Kayed R, Taglialatela G. (2019). Near Infrared Light Treatment Reduces Synaptic Levels of Toxic Tau Oligomers in Two Transgenic Mouse Models of Human Tauopathies.
Dahlgren MW, Jones SW, Cautivo KM, Dubinin A, Ortiz-Carpena JF, Farhat S, Yu KS, Lee K, Wang C, Molofsky AV, Tward AD, Krummel MF, Peng T, Molofsky AB. (2019). Adventitial Stromal Cells Define Group 2 Innate Lymphoid Cell Tissue Niches.
Dao NC, Brockway DF, Crowley NA. (2019). In Vitro Optogenetic Characterization of Neuropeptide Release from Prefrontal Cortical Somatostatin Neurons.
Feng M, Crowley NA, Patel A, Guo Y, Bugni SE, Luscher B. (2019). Reversal of a Treatment-Resistant, Depression-Related Brain State with the Kv7 Channel Opener Retigabine.
Goussakov I, Synowiec S, Yarnykh V, Drobyshevsky A. (2019). Immediate and delayed decrease of long term potentiation and memory deficits after neonatal intermittent hypoxia.
Gouwens NW, Sorensen SA, Berg J, Lee C, Jarsky T, Ting J, et al. (2019). Classification of electrophysiological and morphological neuron types in the mouse visual cortex.
Grifasi IR, Evans WA, Rexha AD, Sako LW, Marshall SA. (2019). A comparison of hippocampal microglial responses in aged and young rodents following dependent and non-dependent binge drinking.
Joseph DJ, Liu C, Peng J, Liang G, Wei H. (2019). Isoflurane mediated neuropathological and cognitive impairments in the triple transgenic Alzheimer's mouse model are associated with hippocampal synaptic deficits in an age-dependent manner.
KM Akram, LL Yates, R Mongey, S Rothery… (2019). Time-lapse imaging of alveologenesis in mouse precision-cut lung slices.
Kolb I, Landry CR, Yip MC, Lewallen CF, Stoy WA, Lee J, Felouzis A, Yang B, Boyden ES, Rozell CJ, Forest CR. (2019). PatcherBot: a single-cell electrophysiology robot for adherent cells and brain slices.
Kole K, Celikel T. (2019). Neocortical Microdissection at Columnar and Laminar Resolution for Molecular Interrogation.
Kole K, Zhang Y, Jansen EJR, Brouns T, Bijlsma A, Calcini N, Yan X, Lantyer ADS, Celikel T. (2019). Assessing the utility of Magneto to control neuronal excitability in the somatosensory cortex.
Lloyd JT, Martini A, McDouall A, Sood R, Freestone PS, Mercuri NB, Lipski J. (2019). Electrophysiological Characterization of Novel Effects of the Uptake-2 Blocker Decynium-22 (D-22) on Dopaminergic Neurons in the Substantia Nigra Pars Compacta.
Lv L, Liu Y, Xie J, Wu Y, Zhao J, Li Q, Zhong Y. (2019). Interplay between ‘±2-chimaerin and Rac1 activity determines dynamic maintenance of long-term memory.
MaciÛfg F, Majewski , Boguszewski PM, Gupta RK, Wasilewska I, Wojta_ B, Kuznicki J. (2019). Behavioral and electrophysiological changes in female mice overexpressing ORAI1 in neurons.
Micci MA, Krishnan B, Bishop E, Zhang WR, Guptarak J, Grant A, Zolochevska O, Tumurbaatar B, Franklin W, Marino C, Widen SG, Luthra A, Kernie SG, Taglialatela G. (2019). Hippocampal stem cells promotes synaptic resistance to the dysfunctional impact of amyloid beta oligomers via secreted exosomes.
Mikami M, Perez-Zoghbi JF, Zhang Y, Emala CW Sr. (2019). Attenuation of murine and human airway contraction by a peptide fragment of the cytoskeleton regulatory protein gelsolin.
Nakano Y, Wiechert S, Bíçnfi B. (2019). Overlapping Activities of Two Neuronal Splicing Factors Switch the GABA Effect from Excitatory to Inhibitory by Regulating REST.
Paletzki RF, Gerfen CR. (2019). Basic Neuroanatomical Methods.
Piatkevich KD, Bensussen S, Tseng HA, Shroff SN, Lopez-Huerta VG, Park D, Jung EE, Shemesh OA, Straub C, Gritton HJ, Romano MF, Costa E, Sabatini BL, Fu Z, Boyden ES, Han X. (2019). Population imaging of neural activity in awake behaving mice.
Priya R, Rakela B, Kaneko M, Spatazza J, Larimer P, Hoseini MS, Hasenstaub AR, Alvarez-Buylla A, Stryker MP. (2019). Vesicular GABA Transporter Is Necessary for Transplant-Induced Critical Period Plasticity in Mouse Visual Cortex.
Puttur F, Denney L, Gregory LG, Vuononvirta J, Oliver R, Entwistle LJ, Walker SA, Headley MB, McGhee EJ, Pease JE, Krummel MF, Carlin LM, Lloyd CM. (2019). Pulmonary environmental cues drive group 2 innate lymphoid cell dynamics in mice and humans.
Qian Y, Piatkevich KD, Mc Larney B, Abdelfattah AS, Mehta S, Murdock MH, Gottschalk S, Molina RS, Zhang W, Chen Y, Wu J, Drobizhev M, Hughes TE, Zhang J, Schreiter ER, Shoham S, Razansky D, Boyden ES, Campbell RE. (2019). A genetically encoded near-infrared fluorescent calcium ion indicator.
Shandra O, Winemiller AR, Heithoff BP, Munoz-Ballester C, George KK, Benko MJ, Zuidhoek IA, Besser MN, Curley DE, Edwards GF 3rd, Mey A, Harrington AN, Kitchen JP, Robel S. (2019). Repetitive Diffuse Mild Traumatic Brain Injury Causes an Atypical Astrocyte Response and Spontaneous Recurrent Seizures.

Sun Y, Blanco-Centurion C, Bendell E, Vidal-Ortiz A, Luo S, Liu M. (2019). Activity dynamics of amygdala GABAergic neurons during cataplexy of narcolepsy.
Sun Y, Blanco-Centurion C, Zou B, Bendell E, Shiromani PJ, Liu M. (2019). Amygdala GABA Neurons Project To vlPAG And mPFC.
Toth AB, Hori K, Novakovic MM, Bernstein NG, Lambot L, Prakriya M. (2019). CRAC channels regulate astrocyte Ca(2+) signaling and gliotransmitter release to modulate hippocampal GABAergic transmission.
Wang W, Cohen JA, Wallrapp A, Trieu KG, Barrios J, Shao F, Krishnamoorthy N, Kuchroo VK, Jones MR, Fine A, Bai Y, Ai X. (2019). Age-Related Dopaminergic Innervation Augments T Helper 2-Type Allergic Inflammation in the Postnatal Lung.
Wang, Hao; Zhu, Qingyuan; Ding, Lufeng; Shen, Yan; Yang, Chao-Yu; Xu, Fang; Shu, Chang; Guo, Yujie; Xiong, Zhiwei; Shan, Qinghong; (2019). Scalable volumetric imaging for ultrahigh-speed brain mapping at synaptic resolution.
Xiang Z, Lv X, Maksymetz J, Stansley BJ, Ghoshal A, Gogliotti RG, Niswender CM, Lindsley CW, Conn PJ. (2019). mGlu(5) Positive Allosteric Modulators Facilitate Long-Term Potentiation via Disinhibition Mediated by mGlu(5)-Endocannabinoid Signaling.
Yim PD, Gallos G, Perez-Zoghbi JF, Zhang Y, Xu D, Wu A, Berkowitz DE, Emala CW. (2019). Airway smooth muscle photorelaxation via opsin receptor activation.
Yocum GT, Perez-Zoghbi JF, Danielsson J, Kuforiji AS, Zhang Y, Li G, Rashid Roni MS, Kodali R, Stafford DC, Arnold LA, Cook JM, Emala CW Sr. (2019). A novel GABA(A) receptor ligand MIDD0301 with limited blood-brain barrier penetration relaxes airway smooth muscle ex vivo and in vivo.
Yu Q, Shao D, Zhang R, Ouyang W, Zhang Z. (2019). Effects of drinking water fluorosis on L-type calcium channel of hippocampal neurons in mice.
Yu W, Yen YC, Lee YH, Tan S, Xiao Y, Lokman H, Ting AKT, Ganegala H, Kwon T, Ho WK, Je HS. (2019). Prenatal selective serotonin reuptake inhibitor (SSRI) exposure induces working memory and social recognition deficits by disrupting inhibitory synaptic networks in male mice.
Zhang W, Bí_ttger R, Qin Z, Kulkarni JA, Vogler J, Cullis PR, Li SD. (2019). Phospholipid-Free Small Unilamellar Vesicles for Drug Targeting to Cells in the Liver.
Bakken TE, Hodge RD, Miller JA, Yao Z, Nguyen TN, Aevermann B, Barkan E, Bertagnolli D, Casper T, Dee N, Garren E, Goldy J, Graybuck LT, Kroll M, Lasken RS, Lathia K, Parry S, Rimorin C, Scheuermann RH, Schork NJ, Shehata SI, Tieu M, Phillips JW, Bernard A, Smith KA, Zeng H, Lein ES, Tasic B. (2018). Single-nucleus and single-cell transcriptomes compared in matched cortical cell types.
Barry KC, Hsu J, Broz ML, Cueto FJ, Binnewies M, Combes AJ, Nelson AE, Loo K, Kumar R, Rosenblum MD, Alvarado MD, Wolf DM, Bogunovic D, Bhardwaj N, Daud AI, Ha PK, Ryan WR, Pollack JL, Samad B, Asthana S, Chan V, Krummel MF. (2018). A natural killer-dendritic cell axis defines checkpoint therapy-responsive tumor microenvironments.
Bienkowski MS, Bowman I, Song MY, Gou L, Ard T, Cotter K, Zhu M, Benavidez NL, Yamashita S, Abu-Jaber J, Azam S, Lo D, Foster NN, Hintiryan H, Dong HW. (2018). Integration of gene expression and brain-wide connectivity reveals the multiscale organization of mouse hippocampal networks.
Blanco-Centurion C, Bendell E, Zou B, Sun Y, Shiromani PJ, Liu M. (2018). VGAT and VGLUT2 expression in MCH and orexin neurons in double transgenic reporter mice.
Buttrick TS, Wang W, Yung C, Trieu KG, Patel K, Khoury SJ, Ai X, Elyaman W. (2018). Foxo1 Promotes Th9 Cell Differentiation and Airway Allergy.
Chen J, Miller M, Unno H, Rosenthal P, Sanderson MJ, Broide DH. (2018). Orosomucoid-like 3 (ORMDL3) upregulates airway smooth muscle proliferation, contraction, and Ca(2+) oscillations in asthma.
Doyle S, Hansen DB, Vella J, Bond P, Harper G, Zammit C, Valentino M, Fern R. (2018). Vesicular glutamate release from central axons contributes to myelin damage.
Durand-de Cuttoli R, Mondoloni S, Marti F, Lemoine D, Nguyen C, Naudí© J, d'Izarny-Gargas T, Pons S, Maskos U, Trauner D, Kramer RH, Faure P, Mourot A. (2018). Manipulating midbrain dopamine neurons and reward-related behaviors with light-controllable nicotinic acetylcholine receptors.
Fisher, Nicole M; Gogliotti, Rocco G; Vermudez, Sheryl Anne D; Stansley, Branden J; Conn, P Jeffrey; Niswender, Colleen M; (2018). Genetic Reduction or Negative Modulation of mGlu7 Does Not Impact Anxiety and Fear Learning Phenotypes in a Mouse Model of MECP2 Duplication Syndrome.
Jhang J, Lee H, Kang MS, Lee HS, Park H, Han JH. (2018). Anterior cingulate cortex and its input to the basolateral amygdala control innate fear response.
Krishnan B, Kayed R, Taglialatela G. (2018). Elevated phospholipase D isoform 1 in Alzheimer's disease patients' hippocampus: Relevance to synaptic dysfunction and memory deficits.
Laing BT, Li P, Schmidt CA, Bunner W, Yuan Y, Landry T, Prete A, McClung JM, Huang H. (2018). AgRP/NPY Neuron Excitability Is Modulated by Metabotropic Glutamate Receptor 1 During Fasting.

Liu Y, Lv L, Wang L, Zhong Y. (2018). Social Isolation Induces Rac1-Dependent Forgetting of Social Memory.
Liu Y, Wang HY, Zhou L, Su Y, Shen WC. (2018). Biodistribution, activation, and retention of proinsulin-transferrin fusion protein in the liver: Mechanism of liver-targeting as an insulin prodrug.
Lyons-Cohen MR, Nakano H, Thomas SY, Cook DN. (2018). Imaging Precision-Cut Lung Slices to Visualize Leukocyte Localization and Trafficking.
Mamani S, Shi L, Ahmed T, Karnik R, Rodrí_guez-Contreras A, Nolan D, Alfano R. (2018). Transmission of classically entangled beams through mouse brain tissue.
Nelson AD, Caballero-Floríçn RN, Rodrí_guez Dí_az JC, Hull JM, Yuan Y, Li J, Chen K, Walder KK, Lopez-Santiago LF, Bennett V, McInnis MG, Isom LL, Wang C, Zhang M, Jones KS, Jenkins PM. (2018). Ankyrin-G regulates forebrain connectivity and network synchronization via interaction with GABARAP.
Nia HT, Datta M, Seano G, Huang P, Munn LL, Jain RK. (2018). Quantifying solid stress and elastic energy from excised or in situ tumors.
Nylk J, McCluskey K, Preciado MA, Mazilu M, Yang Z, Gunn-Moore FJ, Aggarwal S, Tello JA, Ferrier DEK, Dholakia K. (2018). Light-sheet microscopy with attenuation-compensated propagation-invariant beams.
Seeman SC, Campagnola L, Davoudian PA, Hoggarth A, Hage TA, Bosma-Moody A, Baker CA, Lee JH, Mihalas S, Teeter C, Ko AL, Ojemann JG, Gwinn RP, Silbergeld DL, Cobbs C, Phillips J, Lein E, Murphy G, Koch C, Zeng H, Jarsky T. (2018). Sparse recurrent excitatory connectivity in the microcircuit of the adult mouse and human cortex.
Shalaby KH, Lyons-Cohen MR, Whitehead GS, Thomas SY, Prinz I, Nakano H, Cook DN. (2018). Pathogenic T(H)17 inflammation is sustained in the lungs by conventional dendritic cells and Toll-like receptor 4 signaling.
Shigemura M, Lecuona E, Angulo M, Homma T, Rodrí_guez DA, Gonzalez-Gonzalez FJ, Welch LC, Amarelle L, Kim SJ, Kaminski N, Budinger GRS, Solway J, Sznajder JI. (2018). Hypercapnia increases airway smooth muscle contractility via caspase-7-mediated miR-133a-RhoA signaling.
Stansley BJ, Fisher NM, Gogliotti RG, Lindsley CW, Conn PJ, Niswender CM. (2018). Contextual Fear Extinction Induces Hippocampal Metaplasticity Mediated by Metabotropic Glutamate Receptor 5.
Szablowski JO, Lee-Gosselin A, Lue B, Malounda D, Shapiro MG. (2018). Acoustically targeted chemogenetics for the non-invasive control of neural circuits.
Tasic B, Yao Z, Graybuck LT, Smith KA, Nguyen TN, Bertagnolli D, et al. (2018). Shared and distinct transcriptomic cell types across neocortical areas.
Thomas SY, Whitehead GS, Takaku M, Ward JM, Xu X, Nakano K, Lyons-Cohen MR, Nakano H, Gowdy KM, Wade PA, Cook DN. (2018). MyD88-dependent dendritic and epithelial cell crosstalk orchestrates immune responses to allergens.
Ting JT, Lee BR, Chong P, Soler-Llavina G, Cobbs C, Koch C, Zeng H, Lein E. (2018). Preparation of Acute Brain Slices Using an Optimized N-Methyl-D-glucamine Protective Recovery Method.
Wen Q, Gandhi K, Capel RA, Hao G, O'Shea C, Neagu G, Pearcey S, Pavlovic D, Terrar DA, Wu J, Faggian G, Camelliti P, Lei M. (2018). Transverse cardiac slicing and optical imaging for analysis of transmural gradients in membrane potential and Ca(2+) transients in murine heart.
Zhang C, Xu Y, Chowdhary A, Fox D 3rd, Gurney ME, Zhang HT, Auerbach BD, Salvi RJ, Yang M, Li G, O'Donnell JM. (2018). Memory enhancing effects of BPN14770, an allosteric inhibitor of phosphodiesterase-4D, in wild-type and humanized mice.
Barrios J, Patel KR, Aven L, Achey R, Minns MS, Lee Y, Trinkaus-Randall VE, Ai X. (2017). Early life allergen-induced mucus overproduction requires augmented neural stimulation of pulmonary neuroendocrine cell secretion.
Chen J, Sanderson MJ. (2017). Store-operated calcium entry is required for sustained contraction and Ca2+ oscillations of airway smooth muscle.
Guan W, Cao JW, Liu LY, Zhao ZH, Fu Y, Yu YC. (2017). Eye opening differentially modulates inhibitory synaptic transmission in the developing visual cortex.
Gusachenko I, Nylk J, Tello JA, Dholakia K. (2017). Multimode fibre based imaging for optically cleared samples.
Kondru N, Manne S, Greenlee J, West Greenlee H, Anantharam V, Halbur P, Kanthasamy A, Kanthasamy A. (2017). Integrated Organotypic Slice Cultures and RT-QuIC (OSCAR) Assay: Implications for Translational Discovery in Protein Misfolding Diseases.
Li S, Mwakalundwa G, Skinner PJ. (2017). In Situ MHC-tetramer Staining and Quantitative Analysis to Determine the Location, Abundance, and Phenotype of Antigen-specific CD8 T Cells in Tissues.
Lyons-Cohen MR, Thomas SY, Cook DN, Nakano H. (2017). Precision Cut Mouse Lung Slices to Visualize Live Pulmonary Dendritic Cells.
Miller OH, Bruns A, Ben Ammar I, Mueggler T, Hall BJ. (2017). Synaptic Regulation of a Thalamocortical Circuit Controls Depression-Related Behavior.
Moehle MS, Pancani T, Byun N, Yohn SE, Wilson GH 3rd, Dickerson JW, Remke DH, Xiang Z, Niswender CM, Wess J, Jones CK, Lindsley CW, Rook JM, Conn PJ. (2017). Cholinergic Projections to the Substantia Nigra Pars Reticulata Inhibit Dopamine

Modulation of Basal Ganglia through the M(4) Muscarinic Receptor.
Nakano H, Lyons-Cohen MR, Whitehead GS, Nakano K, Cook DN. (2017). Distinct functions of CXCR4, CCR2, and CX3CR1 direct dendritic cell precursors from the bone marrow to the lung.
Pathania M, De Jay N, Maestro N, Harutyunyan AS, Nitarska J, Pahlavan P, Henderson S, Mikael LG, Richard-Londt A, Zhang Y, Costa JR, Hí©bert S, Khazaei S, Ibrahim NS, Herrero J, Riccio A, Albrecht S, Ketteler R, Brandner S, Kleinman CL, Jabado N, Salomoni P. (2017). H3.3(K27M) Cooperates with Trp53 Loss and PDGFRA Gain in Mouse Embryonic Neural Progenitor Cells to Induce Invasive High-Grade Gliomas.
Poobalasingam T, Yates LL, Walker SA, Pereira M, Gross NY, Ali A, Kolatsi-Joannou M, Jarvelin MR, Pekkanen J, Papakrivopoulou E, Long DA, Griffiths M, Wagner D, Kí_nigshoff M, Hind M, Minelli C, Lloyd CM, Dean CH. (2017). Heterozygous Vangl2(Looptail) mice reveal novel roles for the planar cell polarity pathway in adult lung homeostasis and repair.
Rosner SR, Pascoe CD, Blankman E, Jensen CC, Krishnan R, James AL, Elliot JG, Green FH, Liu JC, Seow CY, Park JA, Beckerle MC, Parí© PD, Fredberg JJ, Smith MA. (2017). The actin regulator zyxin reinforces airway smooth muscle and accumulates in airways of fatal asthmatics.
Van Dijk EM, Culha S, Menzen MH, Bidan CM, Gosens R. (2017). Elastase-Induced Parenchymal Disruption and Airway Hyper Responsiveness in Mouse Precision Cut Lung Slices: Toward an Ex vivo COPD Model.
Wong TTW, Zhang R, Zhang C, Hsu HC, Maslov KI, Wang L, Shi J, Chen R, Shung KK, Zhou Q, Wang LV. (2017). Label-free automated three-dimensional imaging of whole organs by microtomy-assisted photoacoustic microscopy.
Yocum GT, Chen J, Choi CH, Townsend EA, Zhang Y, Xu D, Fu XW, Sanderson MJ, Emala CW. (2017). Role of transient receptor potential vanilloid 1 in the modulation of airway smooth muscle tone and calcium handling.
Zheng Y, Dou JR, Gao Y, Dong L, Li G. (2017). Effects of 15 Hz square wave magnetic fields on the voltage-gated sodium and potassium channels in prefrontal cortex pyramidal neurons.
Abdulnour RE, Sham HP, Douda DN, Colas RA, Dalli J, Bai Y, Ai X, Serhan CN, Levy BD. (2016). Aspirin-triggered resolvin D1 is produced during self-resolving gram-negative bacterial pneumonia and regulates host immune responses for the resolution of lung inflammation.
Boldajipour B, Nelson A, Krummel MF. (2016). Tumor-infiltrating lymphocytes are dynamically desensitized to antigen but are maintained by homeostatic cytokine.
Buffington SA, Di Prisco GV, Auchtung TA, Ajami NJ, Petrosino JF, Costa-Mattioli M. (2016). Microbial Reconstitution Reverses Maternal Diet-Induced Social and Synaptic Deficits in Offspring.
Carr GV, Chen J, Yang F, Ren M, Yuan P, Tian Q, Bebensee A, Zhang GY, Du J, Glineburg P, Xun R, Akhile O, Akuma D, Pickel J, Barrow JC, Papaleo F, Weinberger DR. (2016). KCNH2-3.1 expression impairs cognition and alters neuronal function in a model of molecular pathology associated with schizophrenia.
Eleftheriadis N, Poelman H, Leus NGJ, Honrath B, Neochoritis CG, Dolga A, Dí_mling A, Dekker FJ. (2016). Design of a novel thiophene inhibitor of 15-lipoxygenase-1 with both anti-inflammatory and neuroprotective properties.
Fritzsch B, Duncan JS, Kersigo J, Gray B, Elliott KL. (2016). Neuroanatomical Tracing Techniques in the Ear: History, State of the Art, and Future Developments.
Garcia I, Bhullar PK, Tepe B, Ortiz-Guzman J, Huang L, Herman AM, Chaboub L, Deneen B, Justice NJ, Arenkiel BR. (2016). Local corticotropin releasing hormone (CRH) signals to its receptor CRHR1 during postnatal development of the mouse olfactory bulb.
Grannan MD, Mielnik CA, Moran SP, Gould RW, Ball J, Lu Z, Bubser M, Ramsey AJ, Abe M, Cho HP, Nance KD, Blobaum AL, Niswender CM, Conn PJ, Lindsley CW, Jones CK. (2016). Prefrontal Cortex-Mediated Impairments in a Genetic Model of NMDA Receptor Hypofunction Are Reversed by the Novel M(1) PAM VU6004256.
Hintiryan H, Foster NN, Bowman I, Bay M, Song MY, Gou L, Yamashita S, Bienkowski MS, Zingg B, Zhu M, Yang XW, Shih JC, Toga AW, Dong HW. (2016). The mouse cortico-striatal projectome.
Hiorns JE, Bidan CM, Jensen OE, Gosens R, Kistemaker LE, Fredberg JJ, Butler JP, Krishnan R, Brook BS. (2016). Airway and Parenchymal Strains during Bronchoconstriction in the Precision Cut Lung Slice.
Huang L, Ung K, Garcia I, Quast KB, Cordiner K, Saggau P, Arenkiel BR. (2016). Task Learning Promotes Plasticity of Interneuron Connectivity Maps in the Olfactory Bulb.
Huang W, Placzek AN, Viana Di Prisco G, Khatiwada S, Sidrauski C, KrnjeviÛˆ K, Walter P, Dani JA, Costa-Mattioli M. (2016). Translational control by eIF2α phosphorylation regulates vulnerability to the synaptic and behavioral effects of cocaine.
Jameson H, Bateman R, Byrne P, Dyavanapalli J, Wang X, Jain V, Mendelowitz D. (2016). Oxytocin neuron activation prevents hypertension that occurs with chronic intermittent hypoxia/hypercapnia in rats.
Kolson DR, Wan J, Wu J, Dehoff M, Brandebura AN, Qian J, Mathers PH, Spirou GA. (2016). Temporal patterns of gene expression during calyx of held development.

Kubota J, Mikami Y, Kanemaru K, Sekiya H, Okubo Y, Iino M. (2016). Whisker experience-dependent mGluR signalingmaintains synaptic strength in the mouse adolescentcortex.
Liu Y, Du S, Lv L, Lei B, Shi W, Tang Y, Wang L, Zhong Y. (2016). Hippocampal Activation of Rac1 Regulates the Forgetting of Object Recognition Memory.
Nylk J, McCluskey K, Aggarwal S, Tello JA, Dholakia K. (2016). Enhancement of image quality and imaging depth with Airy light-sheet microscopy in cleared and non-cleared neural tissue.
Papaleo F, Yang F, Paterson C, Palumbo S, Carr GV, Wang Y, Floyd K, Huang W, Thomas CJ, Chen J, Weinberger DR, Law AJ. (2016). Behavioral, Neurophysiological, and Synaptic Impairment in a Transgenic Neuregulin1 (NRG1-IV) Murine Schizophrenia Model.
Placzek AN, Molfese DL, Khatiwada S, Viana Di Prisco G, Huang W, Sidrauski C, KrnjeviÛˆ K, Amos CL, Ray R, Dani JA, Walter P, Salas R, Costa-Mattioli M. (2016). Translational control of nicotine-evoked synaptic potentiation in mice and neuronal responses in human smokers by eIF2α.
Placzek AN, Prisco GV, Khatiwada S, Sgritta M, Huang W, KrnjeviÛˆ K, Kaufman RJ, Dani JA, Walter P, Costa-Mattioli M. (2016). eIF2α-mediated translational control regulates the persistence of cocaine-induced LTP in midbrain dopamine neurons.
Royce SG, Nold MF, Bui C, Donovan C, Lam M, Lamanna E, Rudloff I, Bourke JE, Nold-Petry CA. (2016). Airway Remodeling and Hyperreactivity in a Model of Bronchopulmonary Dysplasia and Their Modulation by IL-1 Receptor Antagonist.
Schepelmann M, Yarova PL, Lopez-Fernandez I, Davies TS, Brennan SC, Edwards PJ, Aggarwal A, Graí_a J, Rietdorf K, Matchkov V, Fenton RA, Chang W, Krssak M, Stewart A, Broadley KJ, Ward DT, Price SA, Edwards DH, Kemp PJ, Riccardi D. (2016). The vascular Ca2+-sensing receptor regulates blood vessel tone and blood pressure.
V Askoxylakis, GB Ferraro, DP Kodack… (2016). Preclinical efficacy of ado-trastuzumab emtansine in the brain microenvironment.
Watson CY, Damiani F, Ram-Mohan S, Rodrigues S, de Moura Queiroz P, Donaghey TC, Rosenblum Lichtenstein JH, Brain JD, Krishnan R, Molina RM. (2016). Screening for Chemical Toxicity Using Cryopreserved Precision Cut Lung Slices.
Wu ÎÇ_†__Â Q, Kolb I, Callahan BM, Su Z, Stoy W, Kodandaramaiah SB, Neve R, Zeng H, Boyden ES, Forest CR, Chubykin AA. (2016). Integration of autopatching with automated pipette and cell detection in vitro.
Yang WZ, Liu TT, Cao JW, Chen XF, Liu X, Wang M, Su X, Zhang SQ, Qiu BL, Hu WX, Liu LY, Ma L, Yu YC. (2016). Fear Erasure Facilitated by Immature Inhibitory Neuron Transplantation.
Yao XH, Wang M, He XN, He F, Zhang SQ, Lu W, Qiu ZL, Yu YC. (2016). Electrical coupling regulates layer 1 interneuron microcircuit formation in the neocortex.
Yen CF, Harischandra DS, Kanthasamy A, Sivasankar S. (2016). Copper-induced structural conversion templates prion protein oligomerization and neurotoxicity.
Chang AJ, Ortega FE, Riegler J, Madison DV, Krasnow MA. (2015). Oxygen regulation of breathing through an olfactory receptor activated by lactate.
Danielsson J, Perez-Zoghbi J, Bernstein K, Barajas MB, Zhang Y, Kumar S, Sharma PK, Gallos G, Emala CW. (2015). Antagonists of the TMEM16A calcium-activated chloride channel modulate airway smooth muscle tone and intracellular calcium.
Eleftheriadis N, Neochoritis CG, Leus NG, van der Wouden PE, Dí_mling A, Dekker FJ. (2015). Rational Development of a Potent 15-Lipoxygenase-1 Inhibitor with in Vitro and ex Vivo Anti-inflammatory Properties.
Gallos G, Yocum GT, Siviski ME, Yim PD, Fu XW, Poe MM, Cook JM, Harrison N, Perez-Zoghbi J, Emala CW Sr. (2015). Selective targeting of the α5-subunit of GABAA receptors relaxes airway smooth muscle and inhibits cellular calcium handling.
Jaafari N, Marret E, Canepari M. (2015). Using simultaneous voltage and calcium imaging to study fast Ca2+ channels.
Kim S, Ma L, Unruh J, McKinney S, Yu CR. (2015). Intracellular chloride concentration of the mouse vomeronasal neuron.
Klar R, Walker AG, Ghose D, Grueter BA, Engers DW, Hopkins CR, Lindsley CW, Xiang Z, Conn PJ, Niswender CM. (2015). Activation of Metabotropic Glutamate Receptor 7 Is Required for Induction of Long-Term Potentiation at SC-CA1 Synapses in the Hippocampus.
Kuo CS, Krasnow MA. (2015). Formation of a Neurosensory Organ by Epithelial Cell Slithering.
Lovelace JW, Corches A, Vieira PA, Hiroto AS, Mackie K, Korzus E. (2015). An animal model of female adolescent cannabinoid exposure elicits a long-lasting deficit in presynaptic long-term plasticity.
Vieira PA, Korzus E. (2015). CBP-Dependent memory consolidation in the prefrontal cortex supports object-location learning.
Xiao C, Miwa JM, Henderson BJ, Wang Y, Deshpande P, McKinney SL, Lester HA. (2015). Nicotinic receptor subtype-selective circuit patterns in the subthalamic nucleus.
Aven L, Paez-Cortez J, Achey R, Krishnan R, Ram-Mohan S, Cruikshank WW, Fine A, Ai X. (2014). An NT4/TrkB-dependent increase in innervation links early-life allergen exposure to persistent airway hyperreactivity.
Cao P, Tan X, Donovan G, Sanderson MJ, Sneyd J. (2014). A deterministic model predicts the properties of stochastic calcium oscillations in airway smooth muscle cells.

Cetin A, Callaway EM. (2014). Optical control of retrogradely infected neurons using drug-regulated “TLoop” lentiviral vectors.
Harischandra DS, Kondru N, Martin DP, Kanthasamy A, Jin H, Anantharam V, Kanthasamy AG. (2014). Role of proteolytic activation of protein kinase Cδ in the pathogenesis of prion disease.
Herman AM, Huang L, Murphey DK, Garcia I, Arenkiel BR. (2014). Cell type-specific and time-dependent light exposure contribute to silencing in neurons expressing Channelrhodopsin-2.
Jaafari N, De Waard M, Canepari M. (2014). Imaging fast calcium currents beyond the limitations of electrode techniques.
Jalan-Sakrikar N, Field JR, Klar R, Mattmann ME, Gregory KJ, Zamorano R, Engers DW, Bollinger SR, Weaver CD, Days EL, Lewis LM, Utley TJ, Hurtado M, Rigault D, Acher F, Walker AG, Melancon BJ, Wood MR, Lindsley CW, Conn PJ, Xiang Z, Hopkins CR, Niswender CM. (2014). Identification of positive allosteric modulators VU0155094 (ML397) and VU0422288 (ML396) reveals new insights into the biology of metabotropic glutamate receptor 7.
Jin H, Kanthasamy A, Harischandra DS, Kondru N, Ghosh A, Panicker N, Anantharam V, Rana A, Kanthasamy AG. (2014). Histone hyperacetylation up-regulates protein kinase C‘Ç in dopaminergic neurons to induce cell death: relevance to epigenetic mechanisms of neurodegeneration in Parkinson disease.
Rietdorf K, Bootman MD, Sanderson MJ. (2014). Spontaneous, pro-arrhythmic calcium signals disrupt electrical pacing in mouse pulmonary vein sleeve cells.
Rosner SR, Ram-Mohan S, Paez-Cortez JR, Lavoie TL, Dowell ML, Yuan L, Ai X, Fine A, Aird WC, Solway J, Fredberg JJ, Krishnan R. (2014). Airway contractility in the precision-cut lung slice after cryopreservation.
Tan X, Sanderson MJ. (2014). Bitter tasting compounds dilate airways by inhibiting airway smooth muscle calcium oscillations and calcium sensitivity.
Ting JT, Daigle TL, Chen Q, Feng G. (2014). Acute brain slice methods for adult and aging animals: application of targeted patch clamp analysis and optogenetics.
Vieira PA, Lovelace JW, Corches A, Rashid AJ, Josselyn SA, Korzus E. (2014). Prefrontal consolidation supports the attainment of fear memory accuracy.
Zingg B, Hintiryan H, Gou L, Song MY, Bay M, Bienkowski MS, Foster NN, Yamashita S, Bowman I, Toga AW, Dong HW. (2014). Neural networks of the mouse neocortex.
Castro-Piedras I, Perez-Zoghbi JF. (2013). Hydrogen sulphide inhibits Ca2+ release through InsP3 receptors and relaxes airway smooth muscle.
Chen-Roetling J, Lu X, Regan KA, Regan RF. (2013). A rapid fluorescent method to quantify neuronal loss after experimental intracerebral hemorrhage.
Goldklang MP, Perez-Zoghbi JF, Trischler J, Nkyimbeng T, Zakharov SI, Shiomi T, Zelonina T, Marks AR, D'Armiento JM, Marx SO. (2013). Treatment of experimental asthma using a single small molecule with anti-inflammatory and BK channel-activating properties.
Haddad-Tí_volli R, Szabí_ NE, Zhou X, Alvarez-Bolado G. (2013). Genetic manipulation of the mouse developing hypothalamus through in utero electroporation.
Holcomb PS, Hoffpauir BK, Hoyson MC, Jackson DR, Deerinck TJ, Marrs GS, Dehoff M, Wu J, Ellisman MH, Spirou GA. (2013). Synaptic inputs compete during rapid formation of the calyx of Held: a new model system for neural development.
Huang L, Garcia I, Jen HI, Arenkiel BR. (2013). Reciprocal connectivity between mitral cells and external plexiform layer interneurons in the mouse olfactory bulb.
Jaafari N, Henson M, Graham J, Canepari M. (2013). Economic and simple system to combine single-spot photolysis and whole-field fluorescence imaging.
Liu CH, Yang J, Ren JQ, Liu CM, You Z, Liu PK. (2013). MRI reveals differential effects of amphetamine exposure on neuroglia in vivo.
Mukherjee S, Trice J, Shinde P, Willis RE, Pressley TA, Perez-Zoghbi JF. (2013). Ca2+ oscillations, Ca2+ sensitization, and contraction activated by protein kinase C in small airway smooth muscle.
Wickersham IR, Sullivan HA, Seung HS. (2013). Axonal and subcellular labelling using modified rabies viral vectors.
Yu CR. (2013). Calcium imaging of vomeronasal organ response using slice preparations from transgenic mice expressing G-CaMP2.
DR Kolson (2012). Temporal Patterns of Gene Expression in the MNTB During Calyx of Held Development.
Garcia I, Huang L, Ung K, Arenkiel BR. (2012). Tracing synaptic connectivity onto embryonic stem cell-derived neurons.
Haddad-Tí_volli R, Heide M, Zhou X, Blaess S, Alvarez-Bolado G. (2012). Mouse thalamic differentiation: gli-dependent pattern and gli-independent prepattern.
Kim S, Ma L, Jensen KL, Kim MM, Bond CT, Adelman JP, Yu CR. (2012). Paradoxical contribution of SK3 and GIRK channels to the activation of mouse vomeronasal organ.
Marrs GS, Spirou GA. (2012). Embryonic assembly of auditory circuits: spiral ganglion and brainstem.

Tarr JC, Turlington ML, Reid PR, Utley TJ, Sheffler DJ, Cho HP, Klar R, Pancani T, Klein MT, Bridges TM, Morrison RD, Blobaum AL, Xiang Z, Daniels JS, Niswender CM, Conn PJ, Wood MR, Lindsley CW. (2012). Targeting selective activation of M(1) for the treatment of Alzheimer's disease: further chemical optimization and pharmacological characterization of the M(1) positive allosteric modulator ML169.
Duncan J, Kersigo J, Gray B, Fritzsch B. (2011). Combining lipophilic dye, in situ hybridization, immunohistochemistry, and histology.
Kim S, Ma L, Yu CR. (2011). Requirement of calcium-activated chloride channels in the activation of mouse vomeronasal neurons.
Ma L, Haga-Yamanaka S, Yu QE, Qiu Q, Kim S, Yu CR. (2011). Imaging neuronal responses in slice preparations of vomeronasal organ expressing a genetically encoded calcium sensor.
Peí_a J, Feliciano C, Ting JT, Wang W, Wells MF, Venkatraman TN, Lascola CD, Fu Z, Feng G. (2011). Shank3 mutant mice display autistic-like behaviours and striatal dysfunction.
Premkumar LS. (2011). Methods Used for Studying TRP Channel Functions in Sensory Neurons.
Selever J, Kong JQ, Arenkiel BR. (2011). A rapid approach to high-resolution fluorescence imaging in semi-thick brain slices.
Zhao S, Ting JT, Atallah HE, Qiu L, Tan J, Gloss B, Augustine GJ, Deisseroth K, Luo M, Graybiel AM, Feng G. (2011). Cell type-specific channelrhodopsin-2 transgenic mice for optogenetic dissection of neural circuitry function.
Hoffpauir BK, Kolson DR, Mathers PH, Spirou GA. (2010). Maturation of synaptic partners: functional phenotype and synaptic organization tuned in synchrony.
Kamari Y, Cohen H, Shaish A, Bitzur R, Afek A, Shen S, Vainshtein A, Harats D. (2008). Characterisation of atherosclerotic lesions with scanning electron microscopy (SEM) of wet tissue.
Hsieh CY, Hong CT, Cramer KS. (2007). Deletion of EphA4 enhances deafferentation-induced ipsilateral sprouting in auditory brainstem projections.

Rat

L Dong, T Zhao, Z Jin, Y Zheng (2024). Effect of music rhythm magnetic field on long-term potentiation of hippocampal Schaffer-CA1 synapse plasticity.
V Veloso-Giménez, C Cárdenas-Calderón… (2024). Oxygenation by Intravascular Photosynthesis Reduces Kidney Damage During ex Vivo Preservation.
A Zheng, RS Mann, D Solaja, BL Allman… (2024). Properties of the Caudal Pontine Reticular Nucleus Neurons Determine the Acoustic Startle Response in Cntnap2 KO Rats.
B Riley, E Gould, J Lloyd, LE Hallum… (2024). Dopamine transmission in the tail striatum: Regional variation and contribution of dopamine clearance mechanisms.
B Villa, B Erranz, P Cruces, J Retamal, DE Hurtado (2024). Mechanical and morphological characterization of the emphysematous lung tissue.
C Tian, Y Qi, Y Zheng, P Xia, Q Liu, M Luan… (2024). Exploring the Effect of Arsenic-Containing Hydrocarbon on the Bidirectional Synaptic Plasticity of the Dorsal Hippocampus.
DL Bernstein, SI Lewandowski, C Besada… (2024). Inactivation of ERK1/2 signaling in dopaminergic neurons by map kinase phosphatase MKP3 regulates dopamine signaling and motivation for cocaine.
DVF de Siqueira, N Boaretto, RM Leão (2024). Decreases in metabolic ATP open KATP channels and reduce firing in an auditory brainstem neuron: A dynamic mechanism of firing control during intense activity.
M Abatis, R Perin, R Niu, E van den Burg… (2024). Fear learning induces synaptic potentiation between engram neurons in the rat lateral amygdala.
PS Zarpellon, C Murat, RM Leão (2024). Reduction in mitochondrial ATP synthesis mimics the effect of low glucose in depolarizing neurons from the subpostremal nucleus of the solitary tract of rats.
S Ma, S Watanabe, DC Gillespie (2024). Ultrastructure of immature synaptic inputs in the lateral superior olive of the rodent brainstem.
T Markovic, J Higginbotham, B Ruyle… (2024). A locus coeruleus to dorsal hippocampus pathway mediates cue-induced reinstatement of opioid self-administration in male and female rats.
T Qin, Y Xia, N Nazari, T Sepahvand… (2024). Correlational patterns of neuronal activation and epigenetic marks in the basolateral amygdala and piriform cortex following olfactory threat conditioning and ….
T Sepahvand, SJ Carew, Q Yuan (2024). The ventral hippocampus is activated in olfactory but not auditory threat memory.
A Maziar, TN Critch, S Ghosh, V Rajani… (2023). Aging differentially affects LTCC function in hippocampal CA1 and piriform cortex pyramidal neurons.

AAA Reyes (2023). Role of Chronic Stress-Induced Neuroinflammation in Rodent Locus Coeruleus Physiology and Anxiety-Like Behaviors.
BR Christie, A Gross, A Willoughby, E Grafe… (2023). Assessing changes in synaptic plasticity using an awake closed-head injury model of mild traumatic brain injury.
CD Walker (2023). Adolescence, Alcohol, and Astrocytes: The Impact of Adolescent Alcohol Use on Astrocyte-Synaptic Interactions, Structure, Function, and Behavior.
DJ Lievano Parra (2023). Effects of the unilateral lesion of the substantia nigra compacta with 6-OHDA on reversal learning and prepulse inhibition in male and female Wistar rats.
KL Leiby, Y Yuan, R Ng, MSB Raredon… (2023). Rational engineering of lung alveolar epithelium.
L Dong, L Zhao, L Tian, W Zhao, C Xiong… (2023). AsHC 360 Exposure Influence on Epileptiform Discharges in Hippocampus of Infantile Male Rats In Vitro.
L Tian, T Zhao, L Dong, Q Liu… (2023). Passive array micro-magnetic stimulation device based on multi-carrier wireless flexible control for magnetic neuromodulation.
LR Shao, R Janicot… (2023). Anti-seizure effect of 2-deoxyglucose (2-DG) is not dependent on the presynaptic vacuole ATP pump (V-ATPase) or the somatic ATP-sensitive K+ channel (KATP).
MCF Llerena (2023). Participación del canal de cloruro activado por calcio (tmem16a) en la contracción inducida por atp en células musculares lisas de venas intrapulmonares de rata.
MÁ García-Cabezas, JL Hacker… (2023). Homology of neocortical areas in rats and primates based on cortical type analysis: an update of the hypothesis on the dual origin of the neocortex.
RS Mann, BL Allman, S Schmid (2023). Developmental changes in electrophysiological properties of auditory cortical neurons in the Cntnap2 knockout rat.
S Mamani, S Shintre, Z Li, A Rodríguez-Contreras… (2023). OAM transmission of polarized multipole laser beams in rat cerebellum tissue.
SJ Carew (2023). The smell of fear: comparing the neural ensembles underlying odor fear memory conditioned by innate, inherent, and learned sources of danger.
X Fang, JJ Border, PL Rivers, H Zhang, JM Williams… (2023). Amyloid beta accumulation in TgF344-AD rats is associated with reduced cerebral capillary endothelial Kir2. 1 expression and neurovascular uncoupling.
Z Han, JS Rao, S Ramesh, J Hergesell… (2023). Model-Guided Design and Optimization of CPA Perfusion Protocols for Whole Organ Cryopreservation.
AC Leach, EG Pitts, CA Siciliano… (2022). α7 nicotinic acetylcholine receptor modulation of accumbal dopamine release covaries with novelty seeking.
C Kolluru, A Todd, AR Upadhye, Y Liu, MY Berezin… (2022). Imaging peripheral nerve micro-anatomy with MUSE, 2D and 3D approaches.
D Bojovic, TL Stackhouse, A Mishra (2022). Assaying activity-dependent arteriole and capillary responses in brain slices.
DVF de Siqueira, PS Strazza Jr, NM Benites… (2022). Salicylate activates KATP channels and reduces spontaneous firing in glycinergic cartwheel neurons in the dorsal cochlear nucleus of rats.
JT Lloyd, AG Yee, PK Kalligappa, A Jabed, PY Cheung… (2022). Dopamine Dysregulation and Altered Responses to Drugs Affecting Dopaminergic Transmission in a New Dopamine Transporter Knockout (DAT-KO) Rat Model.
KN Nwachukwu, DM King, KL Healey… (2022). Sex-specific effects of adolescent intermittent ethanol exposure-induced dysregulation of hippocampal glial cells in adulthood.
KN Nwachukwu, KL Healey, HS Swartzwelder… (2022). The influence of sex on hippocampal neurogenesis and neurotrophic responses on the persistent effects of adolescent intermittent ethanol exposure into adulthood.
TA Stowe, EG Pitts, AC Leach, MC Iacino, F Niere… (2022). Diurnal rhythms in cholinergic modulation of rapid dopamine signals and associative learning in the striatum.
Y Ma, GH Qin, X Guo, N Hao, Y Shi, HF Li, X Zhao… (2022). Activation of δ-opioid receptors in anterior cingulate cortex alleviates affective pain in rats.
D Thevalingam, AA Naik, J Hrabe, DP McCloskey… (2021). Brain extracellular space of the naked mole-rat expands and maintains normal diffusion under ischemic conditions.
I Navickaite, N Pauziene, DH Pauza (2021). Anatomical evidence of non-parasympathetic cardiac nitrergic nerve fibres in rat.
JS Thacker, D Andersen, S Liang, N Zieniewicz… (2021). Unlocking the brain: A new method for Western blot protein detection from fixed brain tissue.
LR Shao, R Janicot… (2021). Na+-K+-ATPase functions in the developing hippocampus: regional differences in CA1 and CA3 neuronal excitability and role in epileptiform network bursting.
R Basoalto, LF Damiani, MC Bachmann… (2021). Acute lung injury secondary to hydrochloric acid instillation induces small airway hyperresponsiveness.

W Huang, W Zuo, L Chen, L Wang… (2021). Acetaldehyde excitation of lateral habenular neurons via multiple cellular mechanisms.
W Zuo, Q Zuo, L Wu, Q Mei, M Shah, J Zheng, D Li… (2021). Roles of corticotropin-releasing factor signaling in the lateral habenula in anxiety-like and alcohol drinking behaviors in male rats.
Y Xiao, L Xie, QY Xu, L Chen, H Chen… (2021). Neuroscience of Disease: Transcranial direct current stimulation relieves visceral hypersensitivity via normalizing GluN2B expression and neural activity in ….
Y Xiao, L Xie, QY Xu, L Chen, H Chen… (2021). Transcranial direct current stimulation relieves visceral hypersensitivity via normalizing GluN2B expression and neural activity in anterior cingulate cortex.
Y Zheng, L Zhao, L Dong, C Tian, P Xia… (2021). The Time-Dependence of Three Different Modes of ELF-EMF Stimulation on LTP at Schaffer Collateral-CA1 Synapses.
Y Zheng, P Xia, L Dong, L Tian… (2021). Effects of modulation on sodium and potassium channel currents by extremely low frequency electromagnetic fields stimulation on hippocampal CA1 pyramidal cells.
Alsafadi HN, Uhl FE, Pineda RH, Bailey KE, Rojas M, Wagner DE, Kí_nigshoff M. (2020). Applications and Approaches for Three-Dimensional Precision-Cut Lung Slices. Disease Modeling and Drug Discovery.
CT Werner, S Mitra, BD Auerbach… (2020). Neuroadaptations in the dorsal hippocampus underlie cocaine seeking during prolonged abstinence.
E Gonzalez-Fernandez, D Staursky, K Lucas… (2020). 20-HETE enzymes and receptors in the neurovascular unit: implications in cerebrovascular disease.
Fennell AM, Pitts EG, Sexton LL, Ferris MJ. (2020). Phasic Dopamine Release Magnitude Tracks Individual Differences in Sensitization of Locomotor Response following a History of Nicotine Exposure.
NF Nolta, A Liberti, R Makol, M Han (2020). Gelatin embedding and LED autofluorescence reduction for rodent spinal cord histology.
Pitts EG, Stowe TA, Christensen BA, Ferris MJ. (2020). Comparing dopamine release, uptake, and D2 autoreceptor function across the ventromedial to dorsolateral striatum in adolescent and adult male and female rats.
Q Shu, X Zhao, X Geng, X Wang (2020). CD82 aggravates sevoflurane-induced neurotoxicity by regulating TRPM7 in developing neurons.
Wang S, Lv W, Zhang H, Liu Y, Li L, Jefferson JR, Guo Y, Li M, Gao W, Fang X, Paul IA, Rajkowska G, Shaffery JP, Mosley TH, Hu X, Liu R, Wang Y, Yu H, Roman RJ, Fan F. (2020). Aging exacerbates impairments of cerebral blood flow autoregulation and cognition in diabetic rats.
Xin H, Liu Z, Buller B, Li Y, Golembieski W, Gan X, Wang F, Lu M, Ali MM, Zhang ZG, Chopp M. (2020). MiR-17-92 enriched exosomes derived from multipotent mesenchymal stromal cells enhance axon-myelin remodeling and motor electrophysiological recovery after stroke.
Zions M, Meehan EF, Kress ME, Thevalingam D, Jenkins EC, Kaila K, Puskarjov M, McCloskey DP. (2020). Nest Carbon Dioxide Masks GABA-Dependent Seizure Susceptibility in the Naked Mole-Rat.
Franklin W, Krishnan B, Taglialatela G. (2019). Chronic synaptic insulin resistance after traumatic brain injury abolishes insulin protection from amyloid beta and tau oligomer-induced synaptic dysfunction.
Grifasi IR, Evans WA, Rexha AD, Sako LW, Marshall SA. (2019). A comparison of hippocampal microglial responses in aged and young rodents following dependent and non-dependent binge drinking.
H Reid (2019). Prenatal THC exposure has lasting detrimental effects on the rat hippocampus.
Li W, Zuo W, Wu W, Zuo QK, Fu R, Wu L, Zhang H, Ndukwe M, Ye JH. (2019). Activation of glycine receptors in the lateral habenula rescues anxiety- and depression-like behaviors associated with alcohol withdrawal and reduces alcohol intake in rats.
Zheng Y, Cheng J, Dong L, Ma X, Kong Q. (2019). Effects of exposure to extremely low frequency electromagnetic fields on hippocampal long-term potentiation in hippocampal CA1 region.
Zheng Y, Ma XX, Dong L, Gao Y, Tian L. (2019). Effects of single- and hybrid-frequency extremely low-frequency electromagnetic field stimulations on long-term potentiation in the hippocampal Schaffer collateral pathway.
Zuo W, Wu L, Mei Q, Zuo Q, Zhou Z, Fu R, Li W, Wu W, Matthew L, Ye JH. (2019). Adaptation in 5-HT(2) receptors-CaMKII signaling in lateral habenula underlies increased nociceptive-sensitivity in ethanol-withdrawn rats.
Borodovitsyna O, Flamini MD, Chandler DJ. (2018). Acute Stress Persistently Alters Locus Coeruleus Function and Anxiety-like Behavior in Adolescent Rats.
Forget B, Scholze P, Langa F, Morel C, Pons S, Mondoloni S, Besson M, Durand-de Cuttoli R, Hay A, Tricoire L, Lambolez B, Mourot A, Faure P, Maskos U. (2018). A Human Polymorphism in CHRNA5 Is Linked to Relapse to Nicotine Seeking in Transgenic Rats.
Henriquez M, Fonseca M, Perez-Zoghbi JF. (2018). Purinergic receptor stimulation induces calcium oscillations and smooth muscle contraction in small pulmonary veins.

LR Shao, CE Stafstrom (2018). Glycolytic inhibition by 2-deoxy-D-glucose abolishes both neuronal and network bursts in an in vitro seizure model.
Shao LR, Wang G, Stafstrom CE. (2018). The Glycolytic Metabolite, Fructose-1,6-bisphosphate, Blocks Epileptiform Bursts by Attenuating Voltage-Activated Calcium Currents in Hippocampal Slices.
Subramanian D, Pralong E, Daniel RT, Chacko AG, Stoop R, Babu KS. (2018). Gamma oscillatory activity in vitro: a model system to assess pathophysiological mechanisms of comorbidity between autism and epilepsy.
Terburg D, Scheggia D, Triana Del Rio R, Klumpers F, Ciobanu AC, Morgan B, Montoya ER, Bos PA, Giobellina G, van den Burg EH, de Gelder B, Stein DJ, Stoop R, van Honk J. (2018). The Basolateral Amygdala Is Essential for Rapid Escape: A Human and Rodent Study.
Li J, Kang S, Fu R, Wu L, Wu W, Liu H, Gregor D, Zuo W, Bekker A, Ye JH. (2017). Inhibition of AMPA receptor and CaMKII activity in the lateral habenula reduces depressive-like behavior and alcohol intake in rats.
Zuo W, Wang L, Chen L, KrnjeviÛˆ K, Fu R, Feng X, He W, Kang S, Shah A, Bekker A, Ye JH. (2017). Ethanol potentiates both GABAergic and glutamatergic signaling in the lateral habenula.
Fox ME, Bucher ES, Johnson JA, Wightman RM. (2016). Medullary Norepinephrine Projections Release Norepinephrine into the Contralateral Bed Nucleus of the Stria Terminalis.
Guan YZ, Ye JH. (2016). Glycine blocks long-term potentiation of GABAergic synapses in the ventral tegmental area.
Kirkpatrick DC, McKinney CJ, Manis PB, Wightman RM. (2016). Expanding neurochemical investigations with multi-modal recording: simultaneous fast-scan cyclic voltammetry, iontophoresis, and patch clamp measurements.
Kirkpatrick DC, Walton LR, Edwards MA, Wightman RM. (2016). Quantitative analysis of iontophoretic drug delivery from micropipettes.
Kirkpatrick DC, Wightman RM. (2016). Evaluation of Drug Concentrations Delivered by Microiontophoresis.
Klipec WD, Burrow KR, O'Neill C, Cao JL, Lawyer CR, Ostertag E, Fowler M, Bachtell RK, Illig KR, Cooper DC. (2016). Loss of the trpc4 gene is associated with a reduction in cocaine self-administration and reduced spontaneous ventral tegmental area dopamine neuronal activity, without deficits in learning for natural rewards.
Lam M, Royce SG, Donovan C, Jelinic M, Parry LJ, Samuel CS, Bourke JE. (2016). Serelaxin Elicits Bronchodilation and Enhances β-Adrenoceptor-Mediated Airway Relaxation.
Li J, Zuo W, Fu R, Xie G, Kaur A, Bekker A, Ye JH. (2016). High Frequency Electrical Stimulation of Lateral Habenula Reduces Voluntary Ethanol Consumption in Rats.
Pekala D, Szkudlarek H, Raastad M. (2016). Typical gray matter axons in mammalian brain fail to conduct action potentials faithfully at fever-like temperatures.
Watson CY, Damiani F, Ram-Mohan S, Rodrigues S, de Moura Queiroz P, Donaghey TC, Rosenblum Lichtenstein JH, Brain JD, Krishnan R, Molina RM. (2016). Screening for Chemical Toxicity Using Cryopreserved Precision Cut Lung Slices.
Xiao Y, Chen X, Zhang PA, Xu Q, Zheng H, Xu GY. (2016). TRPV1-mediated presynaptic transmission in basolateral amygdala contributes to visceral hypersensitivity in adult rats with neonatal maternal deprivation.
Zuo W, Zhang Y, Xie G, Gregor D, Bekker A, Ye JH. (2016). Serotonin stimulates lateral habenula via activation of the post-synaptic serotonin 2/3 receptors and transient receptor potential channels.
Liu Y, Huang D, Wen R, Chen X, Yi H. (2015). Glycine receptor-mediated inhibition of medial prefrontal cortical pyramidal cells.
Kirkpatrick DC, Edwards MA, Flowers PA, Wightman RM. (2014). Characterization of solute distribution following iontophoresis from a micropipet.
Pekala D, Baginskas A, Szkudlarek HJ, Raastad M. (2014). Components of action potential repolarization in cerebellar parallel fibres.
Pií±ol RA, Jameson H, Popratiloff A, Lee NH, Mendelowitz D. (2014). Visualization of oxytocin release that mediates paired pulse facilitation in hypothalamic pathways to brainstem autonomic neurons.
Shi L, Rodrí_guez-Contreras A, Budansky Y, Pu Y, Nguyen TA, Alfano RR. (2014). Deep two-photon microscopic imaging through brain tissue using the second singlet state from fluorescent agent chlorophyll α in spinach leaf.
Yin S, Noetzel MJ, Johnson KA, Zamorano R, Jalan-Sakrikar N, Gregory KJ, Conn PJ, Niswender CM. (2014). Selective actions of novel allosteric modulators reveal functional heteromers of metabotropic glutamate receptors in the CNS.
Dergacheva O, Boychuk CR, Mendelowitz D. (2013). Developmental changes in GABAergic neurotransmission to presympathetic and cardiac parasympathetic neurons in the brainstem.
Fleming RL, Li Q, Risher ML, Sexton HG, Moore SD, Wilson WA, Acheson SK, Swartzwelder HS. (2013). Binge-Pattern Ethanol Exposure During Adolescence, butNot Adulthood, Causes Persistent Changes in GABAAReceptor-Mediated Tonic Inhibition in Dentate GranuleCells.
Liu YW, Zuo W, Ye JH. (2013). Propofol stimulates noradrenalin-inhibited neurons in the ventrolateral preoptic nucleus by reducing GABAergic inhibition.

Weidinger A, Dungel P, Perlinger M, Singer K, Ghebes C, Duvigneau JC, Mí_llebner A, Schí_fer U, Redl H, Kozlov AV. (2013). Experimental data suggesting that inflammation mediated rat liver mitochondrial dysfunction results from secondary hypoxia rather than from direct effects of inflammatory mediators.
Xie Z, Li G, Ye JH. (2013). Acute effects of ethanol on GABAA and glycine currents in the lateral habenula neurons of young rats.
Yim PD, Gallos G, Perez-Zoghbi JF, Trice J, Zhang Y, Siviski M, Sonett J, Emala CW Sr. (2013). Chloride channel blockers promote relaxation of TEA-induced contraction in airway smooth muscle.
Zuo W, Chen L, Wang L, Ye JH. (2013). Cocaine facilitates glutamatergic transmission and activates lateral habenular neurons.
Guan Y, Xiao C, Krnjevic K, Xie G, Zuo W, Ye JH. (2012). GABAergic actions mediate opposite ethanol effects on dopaminergic neurons in the anterior and posterior ventral tegmental area.
Xie G, Hipí_lito L, Zuo W, Polache A, Granero L, Krnjevic K, Ye JH. (2012). Salsolinol Stimulates Dopamine Neurons in Slices of Posterior Ventral Tegmental Area Indirectly by Activating μ-Opioid Receptors.
Xie G, Ye JH. (2012). Salsolinol facilitates glutamatergic transmission to dopamine neurons in the posterior ventral tegmental area of rats.
Lu Y, Ye JH. (2011). Glycine-activated chloride currents of neurons freshly isolated from the prefrontal cortex of young rats.
Premkumar LS. (2011). Methods Used for Studying TRP Channel Functions in Sensory Neurons.
Sanderson MJ. (2011). Exploring lung physiology in health and disease with lung slices.
Guan YZ, Ye JH. (2010). Ethanol Blocks Long-Term Potentiation of GABAergic Synapses in the Ventral Tegmental Area Involving μ-Opioid Receptors.
Liu YW, Li J, Ye JH. (2010). Histamine regulates activities of neurons in the ventrolateral preoptic nucleus.
Viviani D, Terrettaz T, Magara F, Stoop R. (2010). Oxytocin enhances the inhibitory effects of diazepam in the rat central medial amygdala.
Deng C, Li KY, Zhou C, Ye JH. (2009). Ethanol enhances glutamate transmission by retrograde dopamine signaling in a postsynaptic neuron/synaptic bouton preparation from the ventral tegmental area.
Jeffry JA, Yu SQ, Sikand P, Parihar A, Evans MS, Premkumar LS. (2009). Selective targeting of TRPV1 expressing sensory nerve terminals in the spinal cord for long lasting analgesia.
Li KY, Guan YZ, KrnjeviÛˆ K, Ye JH. (2009). Propofol facilitates glutamatergic transmission to neurons of the ventrolateral preoptic nucleus.
Nguyen HT, Li KY, daGraca RL, Delphin E, Xiong M, Ye JH. (2009). Behavior and cellular evidence for propofol-induced hypnosis involving brain glycine receptors.
Pan BX, Dong Y, Ito W, Yanagawa Y, Shigemoto R, Morozov A. (2009). Selective gating of glutamatergic inputs to excitatory neurons of amygdala by presynaptic GABAb receptor.
Xiao C, Shao XM, Olive MF, Griffin WC 3rd, Li KY, KrnjeviÛˆ K, Zhou C, Ye JH. (2009). Ethanol facilitates glutamatergic transmission to dopamine neurons in the ventral tegmental area.
Xiao C, Yang KC, Zhou CY, Jin GZ, Wu J, Ye JH. (2009). Nicotine modulates GABAergic transmission to dopaminergic neurons in substantia nigra pars compacta.
Li KY, Xiao C, Xiong M, Delphin E, Ye JH. (2008). Nanomolar propofol stimulates glutamate transmission to dopamine neurons: a possible mechanism of abuse potential?.
Oliver SR, Wright VP, Parinandi N, Clanton TL. (2008). Thermal tolerance of contractile function in oxidative skeletal muscle: no protection by antioxidants and reduced tolerance with eicosanoid enzyme inhibition.
Xiao C, Ye JH. (2008). Ethanol dually modulates GABAergic synaptic transmission onto dopaminergic neurons in ventral tegmental area: role of μ-opioid receptors.
Xiao C, Zhou C, Atlas G, Delphin E, Ye JH. (2008). Labetalol facilitates GABAergic transmission to rat periaqueductal gray neurons via antagonizing β1- adrenergic receptors - a possible mechanism underlying labetalol- induced analgesia.
Xiao C, Zhou C, Li K, Davies DL, Ye JH. (2008). Purinergic type 2 receptors at GABAergic synapses on ventral tegmental area dopamine neurons are targets for ethanol action.
Xiao C, Zhang J, KrnjeviÛˆ K, Ye JH. (2007). Effects of Ethanol on Midbrain Neurons: Role of OpioidReceptors.
Xiao C, Zhou C, Li K, Ye JH. (2007). Presynaptic GABAA receptors facilitate GABAergic transmission to dopaminergic neurons in the ventral tegmental area of young rats.
Zhou C, Xiao C, Deng C, Hong Ye J. (2007). Extracellular proton modulates GABAergic synaptic transmission in rat hippocampal CA3 neurons.
Hejazi N, Zhou C, Oz M, Sun H, Ye JH, Zhang L. (2006). Delta9-tetrahydrocannabinol and endogenous cannabinoid anandamide directly potentiate the function of glycine receptors.

N Hejazi, C Zhou, M Oz, H Sun, JH Ye, L Zhang (2006). Δ9-Tetrahydrocannabinol and endogenous cannabinoid anandamide directly potentiate the function of glycine receptors.
Ye JH, Zhang J, Xiao C, Kong JQ. (2006). Patch-clamp studies in the CNS illustrate a simple new method for obtaining viable neurons in rat brain slices: glycerol replacement of NaCl protects CNS neurons.
Zhou C, Xiao C, McArdle JJ, Ye JH. (2006). Mefloquine Enhances Nigral γ-Aminobutyric Acid Release via Inhibition of Cholinesterase.
Wang F, Xiao C, Ye JH. (2005). Taurine activates excitatory non-synaptic glycine receptors on dopamine neurones in ventral tegmental area of young rats.
Ye JH, Wang F, Krnjevic K, Wang W, Xiong ZG, Zhang J. (2004). Presynaptic glycine receptors on GABAergic terminals facilitate discharge of dopaminergic neurons in ventral tegmental area.

Pig

AHC Anthis, S Kilchenmann, M Murdeu… (2024). Reversible Mechanical Contraception and Endometriosis Treatment Using Stimuli-Responsive Hydrogels.
MB Moor, J Nordström, M Burmakin, M Raki, S Al-Saad… (2024). Comparative analysis of kidney transplantation modeled using precision-cut kidney slices and kidney transplantation in pigs.
CM McCarthy, JM Allardyce, SE Hickey… (2023). Comparison of macroscale and microscale mechanical properties of fresh and fixed-frozen porcine colonic tissue.
K Orton, W Batchelor, NM Ziebarth, TM Best… (2023). Biomechanical properties of porcine meniscus as determined via AFM: Effect of region, compartment and anisotropy.
S Ahn, H Maarsingh, JKL Walker… (2023). Allosteric modulator potentiates β2AR agonist-promoted bronchoprotection in asthma models.
M De Rosa, G Filippone, TM Best, AR Jackson… (2022). Mechanical properties of meniscal circumferential fibers using an inverse finite element analysis approach.
H Maarsingh, A Oldenburger, B Han, AB Zuidhof… (2021). Effects of (a Combination of) the Beta2-Adrenoceptor Agonist Indacaterol and the Muscarinic Receptor Antagonist Glycopyrrolate on Intrapulmonary Airway ….
M Sponchiado, YS Liao, KR Atanasova… (2021). Overexpression of substance P in pig airways increases MUC5AC through an NF-kβ pathway.
PH Tseng, SJ Chiang, SJ Chen, CY Dong (2021). Improvement in Labeling Efficiency of Hydrophilic and Hydrophobic Fluorescent Molecules in Thick Tissue Sections.
Ram-Mohan S, Bai Y, Schaible N, Ehrlicher AJ, Cook DP, Suki B, Stoltz DA, Solway J, Ai X, Krishnan R. (2020). Tissue traction microscopy to quantify muscle contraction within precision-cut lung slices.
van den Berg M, Nijboer-Brinksma S, Bos S, van den Berge M, Lamb D, van Faassen M, Kema I, Gosens R, Kistemaker L. (2020). The novel TRPA1 antagonist BI01305834 inhibits ovalbumin-induced bronchoconstriction in guinea pigs.
van den Berg MPM, Kurhade SH, Maarsingh H, Erceg S, Hulsbeek IR, Boekema PH, Kistemaker LEM, van Faassen M, Kema IP, Elsinga PH, Dí_mling A, Meurs H, Gosens R. (2020). Pharmacological Screening Identifies SHK242 and SHK277 as Novel Arginase Inhibitors with Efficacy against Allergen-Induced Airway Narrowing In Vitro and In Vivo.
Maarsingh H, Bidan CM, Brook BS, Zuidhof AB, Elzinga CRS, Smit M, Oldenburger A, Gosens R, Timens W, Meurs H. (2019). Small airway hyperresponsiveness in COPD: relationship between structure and function in lung slices.
Kistemaker LEM, Oenema TA, Baarsma HA, Bos IST, Schmidt M, Facchinetti F, Civelli M, Villetti G, Gosens R. (2017). The PDE4 inhibitor CHF-6001 and LAMAs inhibit bronchoconstriction-induced remodeling in lung slices.
Cook DP, Rector MV, Bouzek DC, Michalski AS, Gansemer ND, Reznikov LR, Li X, Stroik MR, Ostedgaard LS, Abou Alaiwa MH, Thompson MA, Prakash YS, Krishnan R, Meyerholz DK, Seow CY, Stoltz DA. (2016). Cystic Fibrosis Transmembrane Conductance Regulator in Sarcoplasmic Reticulum of Airway Smooth Muscle. Implications for Airway Contractility.
Oenema TA, Maarsingh H, Smit M, Groothuis GM, Meurs H, Gosens R. (2013). Bronchoconstriction Induces TGF-β Release and Airway Remodelling in Guinea Pig Lung Slices.

Chick

L Kettler, H Sid, C Schaub, K Lischka… (2021). AP-2δ Expression Kinetics in Multimodal Networks in the Developing Chicken Midbrain.
Bryson KJ, Garrido D, Esposito M, McLachlan G, Digard P, Schouler C, Guabiraba R, Trapp S, Vervelde L. (2020). Precision cut lung slices: a novel versatile tool to examine host-pathogen interaction in the chicken lung.
Kloos M, Weigel S, Luksch H. (2019). Anatomy and Physiology of Neurons in Layer 9 of the Chicken Optic Tectum.

Garrido-Charad F, Vega-Zuniga T, Gutií©rrez-Ibíçí±ez C, Fernandez P, Lí_pez-Jury L, Gonzíçlez-Cabrera C, Karten HJ, Luksch H, Marí_n GJ. (2018). "Shepherd's crook" neurons drive and synchronize the enhancing and suppressive mechanisms of the midbrain stimulus selection network.

Lischka K, Yan J, Weigel S, Luksch H. (2018). Effects of early eye removal on the morphology of a multisensory neuron in the chicken optic tectum.

Vega-Zuniga T, Trost D, Schicker K, Bogner EM, Luksch H. (2018). The Medial Ventrothalamic Circuitry: Cells Implicated in a Bimodal Network.

Niederleitner B, Gutierrez-Ibanez C, Krabichler Q, Weigel S, Luksch H. (2017). A Novel Relay Nucleus Between the InferiorColliculus and the Optic Tectum inthe Chicken (Gallus gallus).

Vega-Zuniga T, Marí_n G, Gonzíçlez-Cabrera C, Planitscher E, Hartmann A, Marks V, Mpodozis J, Luksch H. (2016). Microconnectomics of the Pretectum and VentralThalamus in the Chicken (Gallus gallus).

Vega-Zuniga T, Mpodozis J, Karten HJ, Marí_n G, Hain S, Luksch H. (2014). Morphology, Projection Pattern and Neurochemical Identity of Cajal's "Centrifugal Neurons": The Cells of Origin of the Tectoventrogeniculate Pathway in Pigeon (Columba livia) and Chicken (Gallus gallus).

Niederleitner B, Luksch H. (2012). Neuronal morphology in subdivisions of the inferior colliculus of chicken (Gallus gallus).

Weigel S, Luksch H. (2012). Spatiotemporal analysis of electrically evoked activity in the chicken optic tectum: a VSDI study.

Shao J, Lai D, Meyer U, Luksch H, Wessel R. (2009). Generating oscillatory bursts from a network of regular spiking neurons without inhibition.

Meyer U, Shao J, Chakrabarty S, Brandt SF, Luksch H, Wessel R. (2008). Distributed delays stabilize neural feedback systems.

Fish

Harvey TN, Sandve SR, Jin Y, Vik JO, Torgersen JS. (2019). Liver slice culture as a model for lipid metabolism in fish.

Moen T, Torgersen J, Santi N, Davidson WS, Baranski M, íÖdegí«rd J, KjíŸglum S, Velle B, Kent M, Lubieniecki KP, Isdal E, Lien S. (2015). Epithelial Cadherin Determines Resistance to Infectious Pancreatic Necrosis Virus in Atlantic Salmon.

Kohashi T, Carlson BA. (2014). A fast BK-type KCa current acts as a postsynaptic modulator of temporal selectivity for communication signals.

George AA, Lyons-Warren AM, Ma X, Carlson BA. (2011). A diversity of synaptic filters are created by temporal summation of excitation and inhibition.

Frog

Caudill MS, Eggebrecht AT, Gruberg ER, Wessel R. (2010). Electrophysiological properties of isthmic neurons in frogs revealed by in vitro and in vivo studies.

Guinea pig

S Ahn, H Maarsingh, JKL Walker… (2023). Allosteric modulator potentiates β2AR agonist-promoted bronchoprotection in asthma models.

H Maarsingh, A Oldenburger, B Han, AB Zuidhof… (2021). Effects of (a Combination of) the Beta2-Adrenoceptor Agonist Indacaterol and the Muscarinic Receptor Antagonist Glycopyrrolate on Intrapulmonary Airway ….

van den Berg M, Nijboer-Brinksma S, Bos S, van den Berge M, Lamb D, van Faassen M, Kema I, Gosens R, Kistemaker L. (2020). The novel TRPA1 antagonist BI01305834 inhibits ovalbumin-induced bronchoconstriction in guinea pigs.

van den Berg MPM, Kurhade SH, Maarsingh H, Erceg S, Hulsbeek IR, Boekema PH, Kistemaker LEM, van Faassen M, Kema IP, Elsinga PH, Dí_mling A, Meurs H, Gosens R. (2020). Pharmacological Screening Identifies SHK242 and SHK277 as Novel Arginase Inhibitors with Efficacy against Allergen-Induced Airway Narrowing In Vitro and In Vivo.

Maarsingh H, Bidan CM, Brook BS, Zuidhof AB, Elzinga CRS, Smit M, Oldenburger A, Gosens R, Timens W, Meurs H. (2019). Small airway hyperresponsiveness in COPD: relationship between structure and function in lung slices.

Kistemaker LEM, Oenema TA, Baarsma HA, Bos IST, Schmidt M, Facchinetti F, Civelli M, Villetti G, Gosens R. (2017). The PDE4 inhibitor CHF-6001 and LAMAs inhibit bronchoconstriction-induced remodeling in lung slices.

Oenema TA, Maarsingh H, Smit M, Groothuis GM, Meurs H, Gosens R. (2013). Bronchoconstriction Induces TGF-β Release and Airway Remodelling in Guinea Pig Lung Slices.

Plants

ECT Yeung, JB Nichol (2024). Histological Methods Used in the Study of Protocorm. I. Background Information and References.
MM Mira, EC Yeung, C Stasolla (2022). A Simple Guide to the Use of Compresstome in Plant Research.
Mira MM, El-Khateeb EA, Gaafar RM, Igamberdiev AU, Hill RD, Stasolla C. (2020). Stem cell fate in hypoxic root apical meristems is influenced by phytoglobin expression.
Mira MM, Hill RD, Stasolla C. (2016). Phytoglobins Improve Hypoxic Root Growth by Alleviating Apical Meristem Cell Death.

Part III — By Experiment

Electrophysiology

HA Emmons (2024). Moderate-intensity aerobic exercise enhanced dopamine signaling in diet-induced obese female mice without preventing body weight gain.
L Dong, T Zhao, Z Jin, Y Zheng (2024). Effect of music rhythm magnetic field on long-term potentiation of hippocampal Schaffer-CA1 synapse plasticity.
NA Olszewski, S Tetteh-Quarshie, BJ Henderson (2024). Neuronal excitability in the medial habenula and ventral tegmental area is differentially modulated by nicotine dosage and menthol in a sex-specific manner.
A Asgarihafshejani, VA Raveendran, JC Pressey… (2024). LTP is Absent in the CA1 Region of the Hippocampus of Male and Female Rett Syndrome Mouse Models.
A Torres-Berrío, M Estill, V Patel, A Ramakrishnan… (2024). Mono-methylation of lysine 27 at histone 3 confers lifelong susceptibility to stress.
A Zheng, RS Mann, D Solaja, BL Allman… (2024). Properties of the Caudal Pontine Reticular Nucleus Neurons Determine the Acoustic Startle Response in Cntnap2 KO Rats.
AC Hunker, ME Wirthlin, G Gill, NJ Johansen… (2024). Enhancer AAV toolbox for accessing and perturbing striatal cell types and circuits.
B Villa, B Erranz, P Cruces, J Retamal, DE Hurtado (2024). Mechanical and morphological characterization of the emphysematous lung tissue.
BJ Henderson, LE Young, NA Olszewski… (2024). Age-dependent effects of vaping on the prefrontal cortex, ventral tegmental area, and nucleus accumbens.
C Tian, Y Qi, Y Zheng, P Xia, Q Liu, M Luan… (2024). Exploring the Effect of Arsenic-Containing Hydrocarbon on the Bidirectional Synaptic Plasticity of the Dorsal Hippocampus.
DL Bernstein, SI Lewandowski, C Besada… (2024). Inactivation of ERK1/2 signaling in dopaminergic neurons by map kinase phosphatase MKP3 regulates dopamine signaling and motivation for cocaine.
DVF de Siqueira, N Boaretto, RM Leão (2024). Decreases in metabolic ATP open KATP channels and reduce firing in an auditory brainstem neuron: A dynamic mechanism of firing control during intense activity.
F Cathomas, HY Lin, KL Chan, L Li, LF Parise… (2024). Circulating myeloid-derived MMP8 in stress susceptibility and depression.
F Kadakia, A Khadka, J Yazell, S Davidson (2024). Chemogenetic modulation of posterior insula CaMKIIa neurons alters pain and thermoregulation.
F Marti, P Faure, T Le Borgne, C Nguyen, E Vicq, J Jehl… (2024). Nicotine engages a VTA-NAc feedback loop to inhibit amygdala-projecting dopamine neurons and induce anxiety.
F Mei, C Zhao, S Li, Z Xue, Y Zhao, Y Xu, R Ye… (2024). Ngfr+ cholinergic projection from SI/nBM to mPFC selectively regulates temporal order recognition memory.
F Zeldenrust, N Calcini, X Yan, A Bijlsma… (2024). The tuning of tuning: How adaptation influences single cell information transfer.
GC Smith, KR Griffith, AR Sicher, DF Brockway… (2024). MODERATE ALCOHOL CONSUMPTION INDUCES LASTING IMPACTS ON PREFRONTAL CORTICAL SIGNALING IN MICE.
H Park, J Kim, H Lee, WS Chung (2024). Selective regulation of corticostriatal synapses by astrocytic phagocytosis.
J Bär, T Fanutza, CC Reimann, L Seipold… (2024). Non-canonical function of ADAM10 in presynaptic plasticity.
JC Moffa, IN Bland, JR Tooley, V Kalyanaraman… (2024). Cell specific single viral vector CRISPR/Cas9 editing and genetically encoded tool delivery in the central and peripheral nervous systems.
JT Ting, NJ Johansen, BE Kalmbach, N Taskin, B Lee… (2024). Distinctive physiology of molecularly identified medium spiny neurons in the macaque putamen.
KM Ibrahim, N Massaly, HJ Yoon, R Sandoval… (2024). Dorsal hippocampus to nucleus accumbens projections drive reinforcement via activation of accumbal dynorphin neurons.
L Castell, A Rogliardo, T Le Borgne, C Naon, A Cathala… (2024). Midbrain dopamine D2R regulates the salience of threat-related events.
M Abatis, R Perin, R Niu, E van den Burg… (2024). Fear learning induces synaptic potentiation between engram neurons in the rat lateral amygdala.
M Marcatti, B Tumurbaatar, M Borghi… (2024). Inhibition of Calcineurin with FK506 Reduces Tau Levels and Attenuates Synaptic Impairment Driven by Tau Oligomers in the Hippocampus of Male Mouse ….

N Mojahed, M Adjei, E Qasem, S Aaflaq… (2024). Acute social defeat during adolescence promotes long-lasting aggression through activation of the medial amygdala.
N Schaunaman, D Cervantes, T Nichols, M Numata… (2024). Cooperation of immune regulators Tollip and surfactant protein A inhibits influenza a virus infection in mice.
NC Dembrow, S Sawchuk, R Dalley, X Opitz-Araya… (2024). Areal specializations in the morpho-electric and transcriptomic properties of primate layer 5 extratelencephalic projection neurons.
P Scaduto, M Marcatti, N Bhatt, R Kayed… (2024). Calcineurin inhibition prevents synaptic plasticity deficit induced by brain-derived tau oligomers.
PS Zarpellon, C Murat, RM Leão (2024). Reduction in mitochondrial ATP synthesis mimics the effect of low glucose in depolarizing neurons from the subpostremal nucleus of the solitary tract of rats.
QA Nguyen, PM Klein, C Xie, KN Benthall… (2024). Acetylcholine receptor based chemogenetics engineered for neuronal inhibition and seizure control assessed in mice.
R Kshetri, JO Beavers, R Hyde, R Ewa… (2024). Behavioral decline in Shank3Δex4–22 mice during early adulthood parallels cerebellar granule cell glutamatergic synaptic changes.
RA Serafini, Z Farzinpour, V Patel, AM Kelley, M Estill… (2024). Nucleus accumbens myocyte enhancer factor 2C mediates the maintenance of peripheral nerve injury–induced physiological and behavioral maladaptations.
S Basu, EJ Ro, Z Liu, H Kim, A Bennett… (2024). The Mef2c gene dose-dependently controls hippocampal neurogenesis and the expression of autism-like behaviors.
S Brannan, L Garbe, BD Richardson (2024). Early life stress induced sex-specific changes in behavior is paralleled by altered locus coeruleus physiology in BALB/cJ mice.
S Brennan, L Garbe, BD Richardson (2024). Early life stress induces sex-specific changes in behavior and parallel locus coeruleus neuron excitability.
S Logan, R Ranjit, H Rose, A Bredegaard… (2024). Simultaneous quantitative respirometry and fluorometric assays in dissected hippocampal tissue from mice.
S Ma, S Watanabe, DC Gillespie (2024). Ultrastructure of immature synaptic inputs in the lateral superior olive of the rodent brainstem.
SY Kim, D McTeague, SS Cheong, M Hind… (2024). Deciphering the impacts of modulating the Wnt-planar cell polarity (PCP) pathway on alveolar repair.
T Markovic, J Higginbotham, B Ruyle… (2024). A locus coeruleus to dorsal hippocampus pathway mediates cue-induced reinstatement of opioid self-administration in male and female rats.
VA Raveendran, M Serranilla, A Asgarihafshejani… (2024). SNARE protein SNAP25 regulates the chloride-transporter KCC2 in neurons.
A Godino, M Salery, AM Minier-Toribio, V Patel… (2023). Dopaminoceptive D1 and D2 neurons in ventral hippocampus arbitrate approach and avoidance in anxiety.
A Godino, M Salery, R Durand-de Cuttoli, MS Estill… (2023). Transcriptional control of nucleus accumbens neuronal excitability by retinoid X receptor alpha tunes sensitivity to drug rewards.
A Miller, EM York, SA Stopka, JR Martínez-François… (2023). Spatially resolved metabolomics and isotope tracing reveal dynamic metabolic responses of dentate granule neurons with acute stimulation.
AAA Reyes (2023). Role of Chronic Stress-Induced Neuroinflammation in Rodent Locus Coeruleus Physiology and Anxiety-Like Behaviors.
AK Muthusamy (2023). Neuropsychiatric Drug Biosensors in Organelles, Cells, Biofluids, &Behaving Animals.
AR Sicher, WD Starnes, KR Griffith, NC Dao… (2023). Adolescent binge drinking leads to long-lasting changes in cortical microcircuits in mice.
AS Abdelfattah, J Zheng, A Singh, YC Huang, D Reep… (2023). Sensitivity optimization of a rhodopsin-based fluorescent voltage indicator.
BR Christie, A Gross, A Willoughby, E Grafe… (2023). Assessing changes in synaptic plasticity using an awake closed-head injury model of mild traumatic brain injury.
C Natarajan, C Cook, K Ramaswamy… (2023). Phospholipase D1 Attenuation Therapeutics Promotes Resilience against Synaptotoxicity in 12-Month-Old 3xTg-AD Mouse Model of Progressive Neurodegeneratoin.
D Stajano (2023). Role of tetraspanin 15 in metabotropic glutamate receptor 5 signaling and extracellular vesicles docking at neurons from mus musculus domesticus.
D Zhao, C Tian, M Cheng, F Yang, C Tian, Y Liu… (2023). Carrier-free quercetin nanomedicine blocks NLRP3 deubiquitination and TXNIP recruitment for Parkinson's disease therapy.
DF Brockway, KR Griffith, CM Aloimonos, TT Clarity… (2023). Somatostatin peptide signaling dampens cortical circuits and promotes exploratory behavior.

F Cathomas, HY Lin, KL Chan, L Li… (2023). Peripheral immune-derived matrix metalloproteinase promotes stress susceptibility.
H Liu, RN Caballero-Florán, T Hergenreder, T Yang… (2023). DSCAM gene triplication causes excessive GABAergic synapses in the neocortex in Down syndrome mouse models.
HM Rose, B Ferrán, R Ranjit… (2023). Mitochondrial calcium uniporter deficiency in dentate granule cells remodels neuronal metabolism and impairs reversal learning.
HY Lin, F Cathomas, L Li, RD Cuttoli, C Guevara… (2023). Chemokine receptor 5 signaling in PFC mediates stress susceptibility in female mice.
J Jehl, M Ciscato, E Vicq, G Dejean de la Batie… (2023). The interpeduncular nucleus blunts the rewarding effect of nicotine.
K Egawa, M Watanabe, H Shiraishi, D Sato… (2023). Imbalanced expression of cation-chloride cotransporters as a potential therapeutic target in an Angelman syndrome mouse model.
K Grycel, NY Larsen, Y Feng, K Qvortrup… (2023). CRMP2 conditional knockout changes axonal function and ultrastructure of axons in mice corpus callosum.
KJ Brymer, EP Hurley… (2023). Asymmetric dysregulation of glutamate dynamics across the synaptic cleft in a mouse model of Alzheimer's disease.
L Dong, L Zhao, L Tian, W Zhao, C Xiong… (2023). AsHC 360 Exposure Influence on Epileptiform Discharges in Hippocampus of Infantile Male Rats In Vitro.
L Li, R Durand-de Cuttoli, AV Aubry, CJ Burnett… (2023). Social trauma engages lateral septum circuitry to occlude social reward.
L Munari, V Patel, N Johnson, C Mariottini… (2023). Memory discrimination is promoted by the expression of the transcription repressor WT1 in the dentate gyrus.
L Tian, T Zhao, L Dong, Q Liu… (2023). Passive array micro-magnetic stimulation device based on multi-carrier wireless flexible control for magnetic neuromodulation.
LR Shao, R Janicot… (2023). Anti-seizure effect of 2-deoxyglucose (2-DG) is not dependent on the presynaptic vacuole ATP pump (V-ATPase) or the somatic ATP-sensitive K+ channel (KATP).
M Abdelmageed, P Palanisamy, V Vernail, Y Silberman… (2023). An altered cell-specific subcellular distribution of translesion synthesis DNA polymerase kappa (POLK) in aging neurons.
M Cheng, C Ye, C Tian, D Zhao, H Li, Z Sun, Y Miao… (2023). Engineered macrophage-biomimetic versatile nanoantidotes for inflammation-targeted therapy against Alzheimer's disease by neurotoxin neutralization and ….
M Salery, A Godino, YQ Xu, JF Fullard… (2023). Transcriptional correlates of cocaine-associated learning in striatal ARC ensembles.
M Singh, K Sapkota, K Sakimura, M Kano, RM Cowell… (2023). Maturation of GABAergic Synaptic Transmission from Neocortical Parvalbumin Interneurons Involves NMDA receptor Recruitment of Cav2. 1 Channels.
MM Novakovic, KS Korshunov, RA Grant… (2023). Astrocyte reactivity and inflammation-induced depression-like behaviors are regulated by Orai1 calcium channels.
MR Norris, CC Kuo, SS Dunn, JR Kim, LJ Becker… (2023). Mu opioid receptors gate the locus coeruleus pain generator.
NM Benites, B Rodrigues… (2023). Development of electrophysiological properties of fusiform neurons from the dorsal cochlear nucleus of mice before and after hearing onset.
RN Caballero-Florán, AD Nelson, L Min, PM Jenkins (2023). Effects of chronic lithium treatment on neuronal excitability and GABAergic transmission in an Ank3 mutant mouse model.
RN Caballero-Florán, M Bendahmane, JP Gupta… (2023). Synaptotagmin-7 facilitates acetylcholine release in splanchnic nerve-chromaffin cell synapses during nerve activity.
RS Mann, BL Allman, S Schmid (2023). Developmental changes in electrophysiological properties of auditory cortical neurons in the Cntnap2 knockout rat.
S Driessens, D Heyer, I Pieterse, R Wilbers, E Mertens… (2023). Genes associated with cognitive ability and HAR show overlapping expression patterns in human cortical neuron types.
S Mondoloni, C Nguyen, E Vicq, M Ciscato, J Jehl… (2023). Prolonged nicotine exposure reduces aversion to the drug in mice by altering nicotinic transmission in the interpeduncular nucleus.
S Nakakubo, Y Hiramatsu, T Goto, S Kimura… (2023). Therapeutic effects of KRM-II-81, positive allosteric modulator for α2/3 subunit containing GABAA receptors, in a mouse model of Dravet syndrome.
S Tsujikawa, KE DeMeulenaere, MV Centeno… (2023). Regulation of neuropathic pain by microglial Orai1 channels.
SA Sorensen, NW Gouwens, Y Wang, M Mallory… (2023). Connecting single-cell transcriptomes to projectomes in mouse visual cortex.
SJF Cronin, W Yu, A Hale, S Licht-Mayer, MJ Crabtree… (2023). Crucial neuroprotective roles of the metabolite BH4 in dopaminergic neurons.

SN Jiang, JW Cao, LY Liu, Y Zhou, GY Shan… (2023). Sncg, Mybpc1, and Parm1 Classify subpopulations of VIP-expressing interneurons in layers 2/3 of the somatosensory cortex.
SP Brown, RJ Lawson, JD Moreno… (2023). A reinterpretation of the relationship between persistent and resurgent sodium currents.
SS Salile, HJ Lee, PSF Alberts, T Abula… (2023). In vitro and in vivo anti-seizure activity of hydromethanolic extract and fractions of Pterolobium stellatum.
SY Cooper, CV Willis, MR Richardson… (2023). Chemical flavorants in vaping products alter neurobiology in a sex-dependent manner to promote vaping-related behaviors.
T Fanutza (2023). Deciphering the structure and plasticity of glutamatergic synapses in the hippocampus.
TD Weber, MV Moya, K Kılıç, J Mertz… (2023). High-speed multiplane confocal microscopy for voltage imaging in densely labeled neuronal populations.
Y Lu, F Sciaccotta, L Kiely, B Bellanger… (2023). Rapid, activity-dependent intrinsic plasticity in the developing zebra finch auditory cortex.
Y Shima, H Skibbe, Y Sasagawa, N Fujimori… (2023). Distinctiveness and continuity in transcriptome and connectivity in the anterior-posterior axis of the paraventricular nucleus of the thalamus.
A Bittar, R Al-Lahham, N Bhatt, K Moore… (2022). Passive Immunotherapy Targeting Tau Oligomeric Strains Reverses Tauopathy Phenotypes in Aged Human-Tau Mice in a Mouse Model-Specific Manner.
DVF de Siqueira, PS Strazza Jr, NM Benites… (2022). Salicylate activates KATP channels and reduces spontaneous firing in glycinergic cartwheel neurons in the dorsal cochlear nucleus of rats.
JT Lloyd, AG Yee, PK Kalligappa, A Jabed, PY Cheung… (2022). Dopamine Dysregulation and Altered Responses to Drugs Affecting Dopaminergic Transmission in a New Dopamine Transporter Knockout (DAT-KO) Rat Model.
K Egawa, M Watanabe, H Shiraishi, D Sato… (2022). Therapeutic effects of bumetanide on neurological dysfunction in a mouse model of Angelman syndrome.
MS Nair, NC Dao, DL Melean, KR Griffith… (2022). Somatostatin Neurons in the Bed Nucleus of the Stria Terminalis Play a Sex-Dependent Role in Binge Drinking.
N Saviuk, Y Chong, P Wang, S Bermudez, Z Zhao… (2022). Loss of 4E-BP converts cerebellar long-term depression to long-term potentiation.
NM George, AG Polese, L Merle… (2022). Excitable axonal domains adapt to sensory deprivation in the olfactory system.
P Rukundo, T Feng, V Pham, S Pieraut (2022). Moderate effect of early-life experience on dentate gyrus function.
SR Chadwick, AD Güler (2022). Local Drd1-neurons input to subgroups of arcuate AgRP/NPY-neurons.
TA Hage, A Bosma-Moody, CA Baker, MB Kratz… (2022). Synaptic connectivity to L2/3 of primary visual cortex measured by two-photon optogenetic stimulation.
TA Stowe, EG Pitts, AC Leach, MC Iacino, F Niere… (2022). Diurnal rhythms in cholinergic modulation of rapid dopamine signals and associative learning in the striatum.
X Lin, NM Fisher, S Dogra, RK Senter, CW Reed… (2022). Differential activity of mGlu7 allosteric modulators provides evidence for mGlu7/8 heterodimers at hippocampal Schaffer collateral-CA1 synapses.
Y Ma, GH Qin, X Guo, N Hao, Y Shi, HF Li, X Zhao… (2022). Activation of δ-opioid receptors in anterior cingulate cortex alleviates affective pain in rats.
YS Chun, MY Kim, SY Lee, MJ Kim, TJ Hong… (2022). MEK1/2 inhibition rescues neurodegeneration by TFEB-mediated activation of autophagic lysosomal function in a model of Alzheimer's Disease.
B Krishnan, C Natarajan, KZ Bourne, L Alikhani… (2021). Chronic low dose neutron exposure results in altered neurotransmission properties of the hippocampus-prefrontal cortex axis in both mice and rats.
BA Copits, R Gowrishankar, PR O'Neill, JN Li… (2021). A photoswitchable GPCR-based opsin for presynaptic inhibition.
BE Kalmbach, RD Hodge, NL Jorstad, S Owen… (2021). Signature morpho-electric, transcriptomic, and dendritic properties of human layer 5 neocortical pyramidal neurons.
BJ Sullivan, PA Kipnis, BM Carter, LR Shao… (2021). Targeting ischemia-induced KCC2 hypofunction rescues refractory neonatal seizures and mitigates epileptogenesis in a mouse model.
C Nguyen, S Mondoloni, T Le Borgne, I Centeno… (2021). Nicotine inhibits the VTA-to-amygdala dopamine pathway to promote anxiety.
CM Díaz-García, DJ Meyer, N Nathwani, M Rahman… (2021). The distinct roles of calcium in rapid control of neuronal glycolysis and the tricarboxylic acid cycle.
D Thevalingam, AA Naik, J Hrabe, DP McCloskey… (2021). Brain extracellular space of the naked mole-rat expands and maintains normal diffusion under ischemic conditions.
J Berg, SA Sorensen, JT Ting, JA Miller, T Chartrand… (2021). Human neocortical expansion involves glutamatergic neuron diversification.

JH Lee, J Kim, S Noh, H Lee, SY Lee, JY Mun, H Park… (2021). Astrocytes phagocytose adult hippocampal synapses for circuit homeostasis.
KD Micheva, M Kiraly, MM Perez, DV Madison (2021). Conduction velocity along the local axons of parvalbumin interneurons correlates with the degree of axonal myelination.
KD Micheva, M Kiraly, MM Perez, DV Madison (2021). Extensive structural remodeling of the axonal arbors of parvalbumin basket cells during development in mouse neocortex.
LR Shao, R Janicot… (2021). Na+-K+-ATPase functions in the developing hippocampus: regional differences in CA1 and CA3 neuronal excitability and role in epileptiform network bursting.
M Dongelmans, R Durand-de Cuttoli, C Nguyen… (2021). Chronic nicotine increases midbrain dopamine neuron activity and biases individual strategies towards reduced exploration in mice.
MM Maneshi, AB Toth, T Ishii, K Hori, S Tsujikawa… (2021). Orai1 channels are essential for amplification of glutamate-evoked Ca2+ signals in dendritic spines to regulate working and associative memory.
QW Wang, YH Wang, B Wang, Y Chen, SY Lu… (2021). Synaptotagmin-7–mediated activation of spontaneous NMDAR currents is disrupted in bipolar disorder susceptibility variants.
SM Chou, KX Li, MY Huang, C Chen, YHL King, GG Li… (2021). Kv1. 1 channels regulate early postnatal neurogenesis in mouse hippocampus via the TrkB signaling pathway.
SS Salile, T Abula (2021). In vitro and In vivo Anticonvulsant Effect of Hydroalcoholic Extract of Moringa stenopetala in Mice Models.
T Feng, C Alicea, V Pham, A Kirk… (2021). Experience-dependent inhibitory plasticity is mediated by CCK+ basket cells in the developing dentate gyrus.
VP Mathis, M Williams, C Fillinger, PJ Kenny (2021). Networks of habenula-projecting cortical neurons regulate cocaine seeking.
W Huang, W Zuo, L Chen, L Wang… (2021). Acetaldehyde excitation of lateral habenular neurons via multiple cellular mechanisms.
W Zuo, Q Zuo, L Wu, Q Mei, M Shah, J Zheng, D Li… (2021). Roles of corticotropin-releasing factor signaling in the lateral habenula in anxiety-like and alcohol drinking behaviors in male rats.
Y Shi, J Lv, L Chen, G Luo, M Tao, J Pan… (2021). Phosphodiesterase-4D Knockdown in the Prefrontal Cortex Alleviates Memory Deficits and Synaptic Failure in Mouse Model of Alzheimer's Disease.
Y Xiao, L Xie, QY Xu, L Chen, H Chen… (2021). Neuroscience of Disease: Transcranial direct current stimulation relieves visceral hypersensitivity via normalizing GluN2B expression and neural activity in ….
Y Xiao, L Xie, QY Xu, L Chen, H Chen… (2021). Transcranial direct current stimulation relieves visceral hypersensitivity via normalizing GluN2B expression and neural activity in anterior cingulate cortex.
Y Zheng, P Xia, L Dong, L Tian… (2021). Effects of modulation on sodium and potassium channel currents by extremely low frequency electromagnetic fields stimulation on hippocampal CA1 pyramidal cells.
Bunner W, Landry T, Laing BT, Li P, Rao Z, Yuan Y, Huang H. (2020). ARC(AgRP/NPY) Neuron Activity Is Required for Acute Exercise-Induced Food Intake in Un-Trained Mice.
C Linghu, SL Johnson, PA Valdes, OA Shemesh… (2020). Spatial multiplexing of fluorescent reporters for imaging signaling network dynamics.
CT Werner, S Mitra, BD Auerbach… (2020). Neuroadaptations in the dorsal hippocampus underlie cocaine seeking during prolonged abstinence.
Chen AN, Meliza CD. (2020). Experience- and Sex-Dependent Intrinsic Plasticity in the Zebra Finch Auditory Cortex during Song Memorization.
Chen S, Kadakia F, Davidson S. (2020). Group II metabotropic glutamate receptor expressing neurons in anterior cingulate cortex become sensitized after inflammatory and neuropathic pain.
Dao NC, Suresh Nair M, Magee SN, Moyer JB, Sendao V, Brockway DF, Crowley NA. (2020). Forced Abstinence From Alcohol Induces Sex-Specific Depression-Like Behavioral and Neural Adaptations in Somatostatin Neurons in Cortical and Amygdalar Regions.
Fisher NM, Gould RW, Gogliotti RG, McDonald AJ, Badivuku H, Chennareddy S, Buch AB, Moore AM, Jenkins MT, Robb WH, Lindsley CW, Jones CK, Conn PJ, Niswender CM. (2020). Phenotypic profiling of mGlu(7) knockout mice reveals new implications for neurodevelopmental disorders.
Grippo RM, Tang Q, Zhang Q, Chadwick SR, Gao Y, Altherr EB, Sipe L, Purohit AM, Purohit NM, Sunkara MD, Cios KJ, Sidikpramana M, Spano AJ, Campbell JN, Steele AD, Hirsh J, Deppmann CD, Wu M, Scott MM, Gí_ler AD. (2020). Dopamine Signaling in the Suprachiasmatic Nucleus Enables Weight Gain Associated with Hedonic Feeding.
Hodge RD, Miller JA, Novotny M, Kalmbach BE, Ting JT, Bakken TE, Aevermann BD, Barkan ER, Berkowitz-Cerasano ML, Cobbs C, Diez-Fuertes F, Ding SL, McCorrison J, Schork NJ, Shehata SI, Smith KA, Sunkin SM, Tran DN, Venepally P, Yanny

AM, Steemers FJ, Phillips JW, Bernard A, Koch C, Lasken RS, Scheuermann RH, Lein ES. (2020). Transcriptomic evidence that von Economo neurons are regionally specialized extratelencephalic-projecting excitatory neurons.
Howell, Rebecca D; Dominguez-Lopez, Sergio; Ocañas, Sarah; Freeman, Willard M; Beckstead, Michael J; (2020). Female mice are resilient to age-related decline of substantia nigra dopamine neuron firing parameters.
JW Cao, W Guan, YC Yu, Y Fu (2020). Synaptic Transmission from Somatostatin-expressing Interneurons to Excitatory Neurons Mediated by α5-subunit-containing GABAA Receptors in the Developing ….
K Hori, S Tsujikawa, MM Novakovic… (2020). Regulation of chemoconvulsant-induced seizures by store-operated Orai1 channels.
Kim Y, Jang YN, Kim JY, Kim N, Noh S, Kim H, Queenan BN, Bellmore R, Mun JY, Park H, Rah JC, Pak DTS, Lee KJ. (2020). Microtubule-associated protein 2 mediates induction of long-term potentiation in hippocampal neurons.
Krishnan B, Sallam HS, Tumurbataar B, Saieva S, Baymon D, Tuvdendorj D, Micci MA, Abate N, Taglialatela G. (2020). Amelioration of hippocampal dysfunction by adipose tissue-targeted stem cell transplantation in a mouse model of type 2 diabetes.
Mancia Leon WR, Spatazza J, Rakela B, Chatterjee A, Pande V, Maniatis T, Hasenstaub AR, Stryker MP, Alvarez-Buylla A. (2020). Clustered gamma-protocadherins regulate cortical interneuron programmed cell death.
NW Gouwens, SA Sorensen, F Baftizadeh, A Budzillo… (2020). Integrated morphoelectric and transcriptomic classification of cortical GABAergic cells.
S Calovi, P Mut-Arbona, P Tod, A Iring… (2020). P2X7 receptor-dependent layer-specific changes in neuron-microglia reactivity in the prefrontal cortex of a phencyclidine induced mouse model of ….
SY Cooper, AT Akers, BJ Henderson (2020). Green apple e-cigarette flavorant farnesene triggers reward-related behavior by promoting high-sensitivity nAChRs in the ventral tegmental area.
Shemesh OA, Linghu C, Piatkevich KD, Goodwin D, Celiker OT, Gritton HJ, Romano MF, Gao R, Yu CJ, Tseng HA, Bensussen S, Narayan S, Yang CT, Freifeld L, Siciliano CA, Gupta I, Wang J, Pak N, Yoon YG, Ullmann JFP, Guner-Ataman B, Noamany H, Sheinkopf ZR, Park WM, Asano S, Keating AE, Trimmer JS, Reimer J, Tolias AS, Bear MF, Tye KM, Han X, Ahrens MB, Boyden ES. (2020). Precision Calcium Imaging of Dense Neural Populations via a Cell-Body-Targeted Calcium Indicator.
Zions M, Meehan EF, Kress ME, Thevalingam D, Jenkins EC, Kaila K, Puskarjov M, McCloskey DP. (2020). Nest Carbon Dioxide Masks GABA-Dependent Seizure Susceptibility in the Naked Mole-Rat.
Avelar AJ, Akers AT, Baumgard ZJ, Cooper SY, Casinelli GP, Henderson BJ. (2019). Why flavored vape products may be attractive: Green apple tobacco flavor elicits reward-related behavior, upregulates nAChRs on VTA dopamine neurons, and alters midbrain dopamine and GABA neuron function.
Bittar A, Bhatt N, Hasan TF, Montalbano M, Puangmalai N, McAllen S, Ellsworth A, Carretero Murillo M, Taglialatela G, Lucke-Wold B, Logsdon A, Rosen C, Turner RC, Kayed R. (2019). Neurotoxic tau oligomers after single versus repetitive mild traumatic brain injury.
Bourne KZ, Natarajan C, Perez CXM, Tumurbaatar B, Taglialatela G, Krishnan B. (2019). Suppressing aberrant phospholipase D1 signaling in 3xTg Alzheimer's disease mouse model promotes synaptic resilience.
Burman RJ, Selfe JS, Lee JH, van den Berg M, Calin A, Codadu NK, Wright R, Newey SE, Parrish RR, Katz AA, Wilmshurst JM, Akerman CJ, Trevelyan AJ, Raimondo JV. (2019). Excitatory GABAergic signalling is associated with benzodiazepine resistance in status epilepticus.
Comerota MM, Tumurbaatar B, Krishnan B, Kayed R, Taglialatela G. (2019). Near Infrared Light Treatment Reduces Synaptic Levels of Toxic Tau Oligomers in Two Transgenic Mouse Models of Human Tauopathies.
Dao NC, Brockway DF, Crowley NA. (2019). In Vitro Optogenetic Characterization of Neuropeptide Release from Prefrontal Cortical Somatostatin Neurons.
Franklin W, Krishnan B, Taglialatela G. (2019). Chronic synaptic insulin resistance after traumatic brain injury abolishes insulin protection from amyloid beta and tau oligomer-induced synaptic dysfunction.
Goussakov I, Synowiec S, Yarnykh V, Drobyshevsky A. (2019). Immediate and delayed decrease of long term potentiation and memory deficits after neonatal intermittent hypoxia.
Gouwens NW, Sorensen SA, Berg J, Lee C, Jarsky T, Ting J, et al. (2019). Classification of electrophysiological and morphological neuron types in the mouse visual cortex.
Joseph DJ, Liu C, Peng J, Liang G, Wei H. (2019). Isoflurane mediated neuropathological and cognitive impairments in the triple transgenic Alzheimer's mouse model are associated with hippocampal synaptic deficits in an age-dependent manner.
Kloos M, Weigel S, Luksch H. (2019). Anatomy and Physiology of Neurons in Layer 9 of the Chicken Optic Tectum.
Kolb I, Landry CR, Yip MC, Lewallen CF, Stoy WA, Lee J, Felouzis A, Yang B, Boyden ES, Rozell CJ, Forest CR. (2019). PatcherBot: a single-cell electrophysiology robot for adherent cells and brain slices.
Kole K, Zhang Y, Jansen EJR, Brouns T, Bijlsma A, Calcini N, Yan X, Lantyer ADS, Celikel T. (2019). Assessing the utility of Magneto to control neuronal excitability in the somatosensory cortex.

Kurz A, Xu W, Wiegel P, Leukel C, N Baker S. (2019). Non-invasive assessment of superficial and deep layer circuits in human motor cortex.

Li W, Zuo W, Wu W, Zuo QK, Fu R, Wu L, Zhang H, Ndukwe M, Ye JH. (2019). Activation of glycine receptors in the lateral habenula rescues anxiety- and depression-like behaviors associated with alcohol withdrawal and reduces alcohol intake in rats.

Lloyd JT, Martini A, McDouall A, Sood R, Freestone PS, Mercuri NB, Lipski J. (2019). Electrophysiological Characterization of Novel Effects of the Uptake-2 Blocker Decynium-22 (D-22) on Dopaminergic Neurons in the Substantia Nigra Pars Compacta.

Lv L, Liu Y, Xie J, Wu Y, Zhao J, Li Q, Zhong Y. (2019). Interplay between '±2-chimaerin and Rac1 activity determines dynamic maintenance of long-term memory.

Micci MA, Krishnan B, Bishop E, Zhang WR, Guptarak J, Grant A, Zolochevska O, Tumurbaatar B, Franklin W, Marino C, Widen SG, Luthra A, Kernie SG, Taglialatela G. (2019). Hippocampal stem cells promotes synaptic resistance to the dysfunctional impact of amyloid beta oligomers via secreted exosomes.

Piatkevich KD, Bensussen S, Tseng HA, Shroff SN, Lopez-Huerta VG, Park D, Jung EE, Shemesh OA, Straub C, Gritton HJ, Romano MF, Costa E, Sabatini BL, Fu Z, Boyden ES, Han X. (2019). Population imaging of neural activity in awake behaving mice.

Priya R, Rakela B, Kaneko M, Spatazza J, Larimer P, Hoseini MS, Hasenstaub AR, Alvarez-Buylla A, Stryker MP. (2019). Vesicular GABA Transporter Is Necessary for Transplant-Induced Critical Period Plasticity in Mouse Visual Cortex.

Qian Y, Piatkevich KD, Mc Larney B, Abdelfattah AS, Mehta S, Murdock MH, Gottschalk S, Molina RS, Zhang W, Chen Y, Wu J, Drobizhev M, Hughes TE, Zhang J, Schreiter ER, Shoham S, Razansky D, Boyden ES, Campbell RE. (2019). A genetically encoded near-infrared fluorescent calcium ion indicator.

Russell TL, Zhang J, Okoniewski M, Franke F, Bichet S, Hierlemann A. (2019). Medullary Respiratory Circuit Is Reorganized by a Seasonally-Induced Program in Preparation for Hibernation.

Toth AB, Hori K, Novakovic MM, Bernstein NG, Lambot L, Prakriya M. (2019). CRAC channels regulate astrocyte Ca(2+) signaling and gliotransmitter release to modulate hippocampal GABAergic transmission.

Xiang Z, Lv X, Maksymetz J, Stansley BJ, Ghoshal A, Gogliotti RG, Niswender CM, Lindsley CW, Conn PJ. (2019). mGlu(5) Positive Allosteric Modulators Facilitate Long-Term Potentiation via Disinhibition Mediated by mGlu(5)-Endocannabinoid Signaling.

Yu Q, Shao D, Zhang R, Ouyang W, Zhang Z. (2019). Effects of drinking water fluorosis on L-type calcium channel of hippocampal neurons in mice.

Yu W, Yen YC, Lee YH, Tan S, Xiao Y, Lokman H, Ting AKT, Ganegala H, Kwon T, Ho WK, Je HS. (2019). Prenatal selective serotonin reuptake inhibitor (SSRI) exposure induces working memory and social recognition deficits by disrupting inhibitory synaptic networks in male mice.

Zheng Y, Cheng J, Dong L, Ma X, Kong Q. (2019). Effects of exposure to extremely low frequency electromagnetic fields on hippocampal long-term potentiation in hippocampal CA1 region.

Zheng Y, Ma XX, Dong L, Gao Y, Tian L. (2019). Effects of single- and hybrid-frequency extremely low-frequency electromagnetic field stimulations on long-term potentiation in the hippocampal Schaffer collateral pathway.

Zuo W, Wu L, Mei Q, Zuo Q, Zhou Z, Fu R, Li W, Wu W, Matthew L, Ye JH. (2019). Adaptation in 5-HT(2) receptors-CaMKII signaling in lateral habenula underlies increased nociceptive-sensitivity in ethanol-withdrawn rats.

Borodovitsyna O, Flamini MD, Chandler DJ. (2018). Acute Stress Persistently Alters Locus Coeruleus Function and Anxiety-like Behavior in Adolescent Rats.

Chen AN, Meliza CD. (2018). Phasic and tonic cell types in the zebra finch auditory caudal mesopallium.

Durand-de Cuttoli R, Mondoloni S, Marti F, Lemoine D, Nguyen C, Naudí© J, d'Izarny-Gargas T, Pons S, Maskos U, Trauner D, Kramer RH, Faure P, Mourot A. (2018). Manipulating midbrain dopamine neurons and reward-related behaviors with light-controllable nicotinic acetylcholine receptors.

Fisher, Nicole M; Gogliotti, Rocco G; Vermudez, Sheryl Anne D; Stansley, Branden J; Conn, P Jeffrey; Niswender, Colleen M; (2018). Genetic Reduction or Negative Modulation of mGlu7 Does Not Impact Anxiety and Fear Learning Phenotypes in a Mouse Model of MECP2 Duplication Syndrome.

Forget B, Scholze P, Langa F, Morel C, Pons S, Mondoloni S, Besson M, Durand-de Cuttoli R, Hay A, Tricoire L, Lambolez B, Mourot A, Faure P, Maskos U. (2018). A Human Polymorphism in CHRNA5 Is Linked to Relapse to Nicotine Seeking in Transgenic Rats.

Garrido-Charad F, Vega-Zuniga T, Gutií©rrez-Ibíçí±ez C, Fernandez P, Lí_pez-Jury L, Gonzíçlez-Cabrera C, Karten HJ, Luksch H, Marí_n GJ. (2018). "Shepherd's crook" neurons drive and synchronize the enhancing and suppressive mechanisms of the midbrain stimulus selection network.

Jhang J, Lee H, Kang MS, Lee HS, Park H, Han JH. (2018). Anterior cingulate cortex and its input to the basolateral amygdala control innate fear response.

Kalmbach BE, Buchin A, Long B, Close J, Nandi A, Miller JA, Bakken TE, Hodge RD, Chong P, de Frates R, Dai K, Maltzer Z, Nicovich PR, Keene CD, Silbergeld DL, Gwinn RP, Cobbs C, Ko AL, Ojemann JG, Koch C, Anastassiou CA, Lein ES, Ting JT. (2018). h-Channels Contribute to Divergent Intrinsic Membrane Properties of Supragranular Pyramidal Neurons in Human versus Mouse Cerebral Cortex.

Krishnan B, Kayed R, Taglialatela G. (2018). Elevated phospholipase D isoform 1 in Alzheimer's disease patients' hippocampus: Relevance to synaptic dysfunction and memory deficits.

LR Shao, CE Stafstrom (2018). Glycolytic inhibition by 2-deoxy-D-glucose abolishes both neuronal and network bursts in an in vitro seizure model.

Laing BT, Li P, Schmidt CA, Bunner W, Yuan Y, Landry T, Prete A, McClung JM, Huang H. (2018). AgRP/NPY Neuron Excitability Is Modulated by Metabotropic Glutamate Receptor 1 During Fasting.

Liu Y, Wang HY, Zhou L, Su Y, Shen WC. (2018). Biodistribution, activation, and retention of proinsulin-transferrin fusion protein in the liver: Mechanism of liver-targeting as an insulin prodrug.

Nelson AD, Caballero-Floríçn RN, Rodrí_guez Dí_az JC, Hull JM, Yuan Y, Li J, Chen K, Walder KK, Lopez-Santiago LF, Bennett V, McInnis MG, Isom LL, Wang C, Zhang M, Jones KS, Jenkins PM. (2018). Ankyrin-G regulates forebrain connectivity and network synchronization via interaction with GABARAP.

Seeman SC, Campagnola L, Davoudian PA, Hoggarth A, Hage TA, Bosma-Moody A, Baker CA, Lee JH, Mihalas S, Teeter C, Ko AL, Ojemann JG, Gwinn RP, Silbergeld DL, Cobbs C, Phillips J, Lein E, Murphy G, Koch C, Zeng H, Jarsky T. (2018). Sparse recurrent excitatory connectivity in the microcircuit of the adult mouse and human cortex.

Shao LR, Wang G, Stafstrom CE. (2018). The Glycolytic Metabolite, Fructose-1,6-bisphosphate, Blocks Epileptiform Bursts by Attenuating Voltage-Activated Calcium Currents in Hippocampal Slices.

Stansley BJ, Fisher NM, Gogliotti RG, Lindsley CW, Conn PJ, Niswender CM. (2018). Contextual Fear Extinction Induces Hippocampal Metaplasticity Mediated by Metabotropic Glutamate Receptor 5.

Subramanian D, Pralong E, Daniel RT, Chacko AG, Stoop R, Babu KS. (2018). Gamma oscillatory activity in vitro: a model system to assess pathophysiological mechanisms of comorbidity between autism and epilepsy.

Terburg D, Scheggia D, Triana Del Rio R, Klumpers F, Ciobanu AC, Morgan B, Montoya ER, Bos PA, Giobellina G, van den Burg EH, de Gelder B, Stein DJ, Stoop R, van Honk J. (2018). The Basolateral Amygdala Is Essential for Rapid Escape: A Human and Rodent Study.

Ting JT, Kalmbach B, Chong P, de Frates R, Keene CD, Gwinn RP, Cobbs C, Ko AL, Ojemann JG, Ellenbogen RG, Koch C, Lein E. (2018). A robust ex vivo experimental platform for molecular-genetic dissection of adult human neocortical cell types and circuits.

Ting JT, Lee BR, Chong P, Soler-Llavina G, Cobbs C, Koch C, Zeng H, Lein E. (2018). Preparation of Acute Brain Slices Using an Optimized N-Methyl-D-glucamine Protective Recovery Method.

Xu W, Baker SN. (2018). In vitro characterization of intrinsic properties and local synaptic inputs to pyramidal neurons in macaque primary motor cortex.

Zhang C, Xu Y, Chowdhary A, Fox D 3rd, Gurney ME, Zhang HT, Auerbach BD, Salvi RJ, Yang M, Li G, O'Donnell JM. (2018). Memory enhancing effects of BPN14770, an allosteric inhibitor of phosphodiesterase-4D, in wild-type and humanized mice.

Guan W, Cao JW, Liu LY, Zhao ZH, Fu Y, Yu YC. (2017). Eye opening differentially modulates inhibitory synaptic transmission in the developing visual cortex.

Li J, Kang S, Fu R, Wu L, Wu W, Liu H, Gregor D, Zuo W, Bekker A, Ye JH. (2017). Inhibition of AMPA receptor and CaMKII activity in the lateral habenula reduces depressive-like behavior and alcohol intake in rats.

Long B, Zhou Z, Cetin A, Ting J, Gwinn R, Tasic B, Daigle T, Lein E, Zeng H, Saggau P, Hawrylycz M, Peng H. (2017). SmartScope2: Simultaneous Imaging and Reconstruction of Neuronal Morphology.

Moehle MS, Pancani T, Byun N, Yohn SE, Wilson GH 3rd, Dickerson JW, Remke DH, Xiang Z, Niswender CM, Wess J, Jones CK, Lindsley CW, Rook JM, Conn PJ. (2017). Cholinergic Projections to the Substantia Nigra Pars Reticulata Inhibit Dopamine Modulation of Basal Ganglia through the M(4) Muscarinic Receptor.

Niederleitner B, Gutierrez-Ibanez C, Krabichler Q, Weigel S, Luksch H. (2017). A Novel Relay Nucleus Between the InferiorColliculus and the Optic Tectum inthe Chicken (Gallus gallus).

Zheng Y, Dou JR, Gao Y, Dong L, Li G. (2017). Effects of 15 Hz square wave magnetic fields on the voltage-gated sodium and potassium channels in prefrontal cortex pyramidal neurons.

Zuo W, Wang L, Chen L, KrnjeviÛˆ K, Fu R, Feng X, He W, Kang S, Shah A, Bekker A, Ye JH. (2017). Ethanol potentiates both GABAergic and glutamatergic signaling in the lateral habenula.

Buffington SA, Di Prisco GV, Auchtung TA, Ajami NJ, Petrosino JF, Costa-Mattioli M. (2016). Microbial Reconstitution Reverses Maternal Diet-Induced Social and Synaptic Deficits in Offspring.

Carr GV, Chen J, Yang F, Ren M, Yuan P, Tian Q, Bebensee A, Zhang GY, Du J, Glineburg P, Xun R, Akhile O, Akuma D, Pickel J, Barrow JC, Papaleo F, Weinberger DR. (2016). KCNH2-3.1 expression impairs cognition and alters neuronal function in a

model of molecular pathology associated with schizophrenia.
Garcia I, Bhullar PK, Tepe B, Ortiz-Guzman J, Huang L, Herman AM, Chaboub L, Deneen B, Justice NJ, Arenkiel BR. (2016). Local corticotropin releasing hormone (CRH) signals to its receptor CRHR1 during postnatal development of the mouse olfactory bulb.
Grannan MD, Mielnik CA, Moran SP, Gould RW, Ball J, Lu Z, Bubser M, Ramsey AJ, Abe M, Cho HP, Nance KD, Blobaum AL, Niswender CM, Conn PJ, Lindsley CW, Jones CK. (2016). Prefrontal Cortex-Mediated Impairments in a Genetic Model of NMDA Receptor Hypofunction Are Reversed by the Novel M(1) PAM VU6004256.
Guan YZ, Ye JH. (2016). Glycine blocks long-term potentiation of GABAergic synapses in the ventral tegmental area.
Huang L, Ung K, Garcia I, Quast KB, Cordiner K, Saggau P, Arenkiel BR. (2016). Task Learning Promotes Plasticity of Interneuron Connectivity Maps in the Olfactory Bulb.
Huang W, Placzek AN, Viana Di Prisco G, Khatiwada S, Sidrauski C, KrnjeviÛˆ K, Walter P, Dani JA, Costa-Mattioli M. (2016). Translational control by eIF2α phosphorylation regulates vulnerability to the synaptic and behavioral effects of cocaine.
Jameson H, Bateman R, Byrne P, Dyavanapalli J, Wang X, Jain V, Mendelowitz D. (2016). Oxytocin neuron activation prevents hypertension that occurs with chronic intermittent hypoxia/hypercapnia in rats.
Kirkpatrick DC, McKinney CJ, Manis PB, Wightman RM. (2016). Expanding neurochemical investigations with multi-modal recording: simultaneous fast-scan cyclic voltammetry, iontophoresis, and patch clamp measurements.
Kirkpatrick DC, Walton LR, Edwards MA, Wightman RM. (2016). Quantitative analysis of iontophoretic drug delivery from micropipettes.
Klipec WD, Burrow KR, O'Neill C, Cao JL, Lawyer CR, Ostertag E, Fowler M, Bachtell RK, Illig KR, Cooper DC. (2016). Loss of the trpc4 gene is associated with a reduction in cocaine self-administration and reduced spontaneous ventral tegmental area dopamine neuronal activity, without deficits in learning for natural rewards.
Kolson DR, Wan J, Wu J, Dehoff M, Brandebura AN, Qian J, Mathers PH, Spirou GA. (2016). Temporal patterns of gene expression during calyx of held development.
Kubota J, Mikami Y, Kanemaru K, Sekiya H, Okubo Y, Iino M. (2016). Whisker experience-dependent mGluR signalingmaintains synaptic strength in the mouse adolescentcortex.
Li J, Zuo W, Fu R, Xie G, Kaur A, Bekker A, Ye JH. (2016). High Frequency Electrical Stimulation of Lateral Habenula Reduces Voluntary Ethanol Consumption in Rats.
Liu Y, Du S, Lv L, Lei B, Shi W, Tang Y, Wang L, Zhong Y. (2016). Hippocampal Activation of Rac1 Regulates the Forgetting of Object Recognition Memory.
Papaleo F, Yang F, Paterson C, Palumbo S, Carr GV, Wang Y, Floyd K, Huang W, Thomas CJ, Chen J, Weinberger DR, Law AJ. (2016). Behavioral, Neurophysiological, and Synaptic Impairment in a Transgenic Neuregulin1 (NRG1-IV) Murine Schizophrenia Model.
Pekala D, Szkudlarek H, Raastad M. (2016). Typical gray matter axons in mammalian brain fail to conduct action potentials faithfully at fever-like temperatures.
Placzek AN, Molfese DL, Khatiwada S, Viana Di Prisco G, Huang W, Sidrauski C, KrnjeviÛˆ K, Amos CL, Ray R, Dani JA, Walter P, Salas R, Costa-Mattioli M. (2016). Translational control of nicotine-evoked synaptic potentiation in mice and neuronal responses in human smokers by eIF2α.
Placzek AN, Prisco GV, Khatiwada S, Sgritta M, Huang W, KrnjeviÛˆ K, Kaufman RJ, Dani JA, Walter P, Costa-Mattioli M. (2016). eIF2α-mediated translational control regulates the persistence of cocaine-induced LTP in midbrain dopamine neurons.
Wu ÎÇ_†__Â Q, Kolb I, Callahan BM, Su Z, Stoy W, Kodandaramaiah SB, Neve R, Zeng H, Boyden ES, Forest CR, Chubykin AA. (2016). Integration of autopatching with automated pipette and cell detection in vitro.
Xiao Y, Chen X, Zhang PA, Xu Q, Zheng H, Xu GY. (2016). TRPV1-mediated presynaptic transmission in basolateral amygdala contributes to visceral hypersensitivity in adult rats with neonatal maternal deprivation.
Yang WZ, Liu TT, Cao JW, Chen XF, Liu X, Wang M, Su X, Zhang SQ, Qiu BL, Hu WX, Liu LY, Ma L, Yu YC. (2016). Fear Erasure Facilitated by Immature Inhibitory Neuron Transplantation.
Yao XH, Wang M, He XN, He F, Zhang SQ, Lu W, Qiu ZL, Yu YC. (2016). Electrical coupling regulates layer 1 interneuron microcircuit formation in the neocortex.
Zuo W, Zhang Y, Xie G, Gregor D, Bekker A, Ye JH. (2016). Serotonin stimulates lateral habenula via activation of the post-synaptic serotonin 2/3 receptors and transient receptor potential channels.
Jaafari N, Marret E, Canepari M. (2015). Using simultaneous voltage and calcium imaging to study fast Ca2+ channels.
Kim S, Ma L, Unruh J, McKinney S, Yu CR. (2015). Intracellular chloride concentration of the mouse vomeronasal neuron.
Klar R, Walker AG, Ghose D, Grueter BA, Engers DW, Hopkins CR, Lindsley CW, Xiang Z, Conn PJ, Niswender CM. (2015). Activation of Metabotropic Glutamate Receptor 7 Is Required for Induction of Long-Term Potentiation at SC-CA1 Synapses in the Hippocampus.
Liu Y, Huang D, Wen R, Chen X, Yi H. (2015). Glycine receptor-mediated inhibition of medial prefrontal cortical pyramidal cells.

Lovelace JW, Corches A, Vieira PA, Hiroto AS, Mackie K, Korzus E. (2015). An animal model of female adolescent cannabinoid exposure elicits a long-lasting deficit in presynaptic long-term plasticity.
Xiao C, Miwa JM, Henderson BJ, Wang Y, Deshpande P, McKinney SL, Lester HA. (2015). Nicotinic receptor subtype-selective circuit patterns in the subthalamic nucleus.
Cetin A, Callaway EM. (2014). Optical control of retrogradely infected neurons using drug-regulated “TLoop” lentiviral vectors.
Herman AM, Huang L, Murphey DK, Garcia I, Arenkiel BR. (2014). Cell type-specific and time-dependent light exposure contribute to silencing in neurons expressing Channelrhodopsin-2.
Jaafari N, De Waard M, Canepari M. (2014). Imaging fast calcium currents beyond the limitations of electrode techniques.
Jalan-Sakrikar N, Field JR, Klar R, Mattmann ME, Gregory KJ, Zamorano R, Engers DW, Bollinger SR, Weaver CD, Days EL, Lewis LM, Utley TJ, Hurtado M, Rigault D, Acher F, Walker AG, Melancon BJ, Wood MR, Lindsley CW, Conn PJ, Xiang Z, Hopkins CR, Niswender CM. (2014). Identification of positive allosteric modulators VU0155094 (ML397) and VU0422288 (ML396) reveals new insights into the biology of metabotropic glutamate receptor 7.
Kohashi T, Carlson BA. (2014). A fast BK-type KCa current acts as a postsynaptic modulator of temporal selectivity for communication signals.
Pekala D, Baginskas A, Szkudlarek HJ, Raastad M. (2014). Components of action potential repolarization in cerebellar parallel fibres.
Pií±ol RA, Jameson H, Popratiloff A, Lee NH, Mendelowitz D. (2014). Visualization of oxytocin release that mediates paired pulse facilitation in hypothalamic pathways to brainstem autonomic neurons.
Ting JT, Daigle TL, Chen Q, Feng G. (2014). Acute brain slice methods for adult and aging animals: application of targeted patch clamp analysis and optogenetics.
Yin S, Noetzel MJ, Johnson KA, Zamorano R, Jalan-Sakrikar N, Gregory KJ, Conn PJ, Niswender CM. (2014). Selective actions of novel allosteric modulators reveal functional heteromers of metabotropic glutamate receptors in the CNS.
Dergacheva O, Boychuk CR, Mendelowitz D. (2013). Developmental changes in GABAergic neurotransmission to presympathetic and cardiac parasympathetic neurons in the brainstem.
Fleming RL, Li Q, Risher ML, Sexton HG, Moore SD, Wilson WA, Acheson SK, Swartzwelder HS. (2013). Binge-Pattern Ethanol Exposure During Adolescence, butNot Adulthood, Causes Persistent Changes in GABAAReceptor-Mediated Tonic Inhibition in Dentate GranuleCells.
Holcomb PS, Hoffpauir BK, Hoyson MC, Jackson DR, Deerinck TJ, Marrs GS, Dehoff M, Wu J, Ellisman MH, Spirou GA. (2013). Synaptic inputs compete during rapid formation of the calyx of Held: a new model system for neural development.
Huang L, Garcia I, Jen HI, Arenkiel BR. (2013). Reciprocal connectivity between mitral cells and external plexiform layer interneurons in the mouse olfactory bulb.
Jaafari N, Henson M, Graham J, Canepari M. (2013). Economic and simple system to combine single-spot photolysis and whole-field fluorescence imaging.
Liu YW, Zuo W, Ye JH. (2013). Propofol stimulates noradrenalin-inhibited neurons in the ventrolateral preoptic nucleus by reducing GABAergic inhibition.
Xie Z, Li G, Ye JH. (2013). Acute effects of ethanol on GABAA and glycine currents in the lateral habenula neurons of young rats.
Zuo W, Chen L, Wang L, Ye JH. (2013). Cocaine facilitates glutamatergic transmission and activates lateral habenular neurons.
Garcia I, Huang L, Ung K, Arenkiel BR. (2012). Tracing synaptic connectivity onto embryonic stem cell-derived neurons.
Guan Y, Xiao C, Krnjevic K, Xie G, Zuo W, Ye JH. (2012). GABAergic actions mediate opposite ethanol effects on dopaminergic neurons in the anterior and posterior ventral tegmental area.
Kim S, Ma L, Jensen KL, Kim MM, Bond CT, Adelman JP, Yu CR. (2012). Paradoxical contribution of SK3 and GIRK channels to the activation of mouse vomeronasal organ.
Marrs GS, Spirou GA. (2012). Embryonic assembly of auditory circuits: spiral ganglion and brainstem.
Niederleitner B, Luksch H. (2012). Neuronal morphology in subdivisions of the inferior colliculus of chicken (Gallus gallus).
Tarr JC, Turlington ML, Reid PR, Utley TJ, Sheffler DJ, Cho HP, Klar R, Pancani T, Klein MT, Bridges TM, Morrison RD, Blobaum AL, Xiang Z, Daniels JS, Niswender CM, Conn PJ, Wood MR, Lindsley CW. (2012). Targeting selective activation of M(1) for the treatment of Alzheimer's disease: further chemical optimization and pharmacological characterization of the M(1) positive allosteric modulator ML169.
Weigel S, Luksch H. (2012). Spatiotemporal analysis of electrically evoked activity in the chicken optic tectum: a VSDI study.
Xie G, Hipí_lito L, Zuo W, Polache A, Granero L, Krnjevic K, Ye JH. (2012). Salsolinol Stimulates Dopamine Neurons in Slices of Posterior Ventral Tegmental Area Indirectly by Activating μ-Opioid Receptors.
Xie G, Ye JH. (2012). Salsolinol facilitates glutamatergic transmission to dopamine neurons in the posterior ventral tegmental area of rats.

George AA, Lyons-Warren AM, Ma X, Carlson BA. (2011). A diversity of synaptic filters are created by temporal summation of excitation and inhibition.
Kim S, Ma L, Yu CR. (2011). Requirement of calcium-activated chloride channels in the activation of mouse vomeronasal neurons.
Li G, Yang K, Zheng C, Liu Q, Chang Y, Kerrigan JF, Wu J. (2011). Functional rundown of gamma-aminobutyric acid(A) receptors in human hypothalamic hamartomas.
Lu Y, Ye JH. (2011). Glycine-activated chloride currents of neurons freshly isolated from the prefrontal cortex of young rats.
Peí_a J, Feliciano C, Ting JT, Wang W, Wells MF, Venkatraman TN, Lascola CD, Fu Z, Feng G. (2011). Shank3 mutant mice display autistic-like behaviours and striatal dysfunction.
Premkumar LS. (2011). Methods Used for Studying TRP Channel Functions in Sensory Neurons.
Zhao S, Ting JT, Atallah HE, Qiu L, Tan J, Gloss B, Augustine GJ, Deisseroth K, Luo M, Graybiel AM, Feng G. (2011). Cell type-specific channelrhodopsin-2 transgenic mice for optogenetic dissection of neural circuitry function.
Caudill MS, Eggebrecht AT, Gruberg ER, Wessel R. (2010). Electrophysiological properties of isthmic neurons in frogs revealed by in vitro and in vivo studies.
Guan YZ, Ye JH. (2010). Ethanol Blocks Long-Term Potentiation of GABAergic Synapses in the Ventral Tegmental Area Involving μ-Opioid Receptors.
Hoffpauir BK, Kolson DR, Mathers PH, Spirou GA. (2010). Maturation of synaptic partners: functional phenotype and synaptic organization tuned in synchrony.
Liu YW, Li J, Ye JH. (2010). Histamine regulates activities of neurons in the ventrolateral preoptic nucleus.
Viviani D, Terrettaz T, Magara F, Stoop R. (2010). Oxytocin enhances the inhibitory effects of diazepam in the rat central medial amygdala.
Deng C, Li KY, Zhou C, Ye JH. (2009). Ethanol enhances glutamate transmission by retrograde dopamine signaling in a postsynaptic neuron/synaptic bouton preparation from the ventral tegmental area.
Jeffry JA, Yu SQ, Sikand P, Parihar A, Evans MS, Premkumar LS. (2009). Selective targeting of TRPV1 expressing sensory nerve terminals in the spinal cord for long lasting analgesia.
Li KY, Guan YZ, KrnjeviÛˆ K, Ye JH. (2009). Propofol facilitates glutamatergic transmission to neurons of the ventrolateral preoptic nucleus.
Nguyen HT, Li KY, daGraca RL, Delphin E, Xiong M, Ye JH. (2009). Behavior and cellular evidence for propofol-induced hypnosis involving brain glycine receptors.
Pan BX, Dong Y, Ito W, Yanagawa Y, Shigemoto R, Morozov A. (2009). Selective gating of glutamatergic inputs to excitatory neurons of amygdala by presynaptic GABAb receptor.
Shao J, Lai D, Meyer U, Luksch H, Wessel R. (2009). Generating oscillatory bursts from a network of regular spiking neurons without inhibition.
Xiao C, Shao XM, Olive MF, Griffin WC 3rd, Li KY, KrnjeviÛˆ K, Zhou C, Ye JH. (2009). Ethanol facilitates glutamatergic transmission to dopamine neurons in the ventral tegmental area.
Xiao C, Yang KC, Zhou CY, Jin GZ, Wu J, Ye JH. (2009). Nicotine modulates GABAergic transmission to dopaminergic neurons in substantia nigra pars compacta.
Li KY, Xiao C, Xiong M, Delphin E, Ye JH. (2008). Nanomolar propofol stimulates glutamate transmission to dopamine neurons: a possible mechanism of abuse potential?.
Meyer U, Shao J, Chakrabarty S, Brandt SF, Luksch H, Wessel R. (2008). Distributed delays stabilize neural feedback systems.
Xiao C, Ye JH. (2008). Ethanol dually modulates GABAergic synaptic transmission onto dopaminergic neurons in ventral tegmental area: role of μ-opioid receptors.
Xiao C, Zhou C, Atlas G, Delphin E, Ye JH. (2008). Labetalol facilitates GABAergic transmission to rat periaqueductal gray neurons via antagonizing β1- adrenergic receptors - a possible mechanism underlying labetalol- induced analgesia.
Xiao C, Zhou C, Li K, Davies DL, Ye JH. (2008). Purinergic type 2 receptors at GABAergic synapses on ventral tegmental area dopamine neurons are targets for ethanol action.
Xiao C, Zhang J, KrnjeviÛˆ K, Ye JH. (2007). Effects of Ethanol on Midbrain Neurons: Role of OpioidReceptors.
Xiao C, Zhou C, Li K, Ye JH. (2007). Presynaptic GABAA receptors facilitate GABAergic transmission to dopaminergic neurons in the ventral tegmental area of young rats.
Zhou C, Xiao C, Deng C, Hong Ye J. (2007). Extracellular proton modulates GABAergic synaptic transmission in rat hippocampal CA3 neurons.
Hejazi N, Zhou C, Oz M, Sun H, Ye JH, Zhang L. (2006). Delta9-tetrahydrocannabinol and endogenous cannabinoid anandamide directly potentiate the function of glycine receptors.
N Hejazi, C Zhou, M Oz, H Sun, JH Ye, L Zhang (2006). Δ9-Tetrahydrocannabinol and endogenous cannabinoid anandamide directly potentiate the function of glycine receptors.

Ye JH, Zhang J, Xiao C, Kong JQ. (2006). Patch-clamp studies in the CNS illustrate a simple new method for obtaining viable neurons in rat brain slices: glycerol replacement of NaCl protects CNS neurons.
Zhou C, Xiao C, McArdle JJ, Ye JH. (2006). Mefloquine Enhances Nigral γ-Aminobutyric Acid Release via Inhibition of Cholinesterase.
Wang F, Xiao C, Ye JH. (2005). Taurine activates excitatory non-synaptic glycine receptors on dopamine neurones in ventral tegmental area of young rats.
Ye JH, Wang F, Krnjevic K, Wang W, Xiong ZG, Zhang J. (2004). Presynaptic glycine receptors on GABAergic terminals facilitate discharge of dopaminergic neurons in ventral tegmental area.

Imaging

U Sengupta, R Kayed (2024). Tau Oligomers as Pathogenic Seeds: Preparation, Characterization, and Propagation In Vitro and In Vivo.
L H Ziolkowski, Y A Nikolaev, A Chikamoto, M Oda, V V Feketa, D Monedero-Alonso, S A Ardasheva , S S Bae , C S Xu , S Pang , E O Gracheva, S N Bagriantsev (2025). The inner core enables transient touch detection in the Pacinian corpuscle.
B Riley, E Gould, J Lloyd, LE Hallum… (2024). Dopamine transmission in the tail striatum: Regional variation and contribution of dopamine clearance mechanisms.
D Ackerman, E Avetissian, CKE Bleck, JA Bogovic… (2024). Data Release: High-Resolution Imaging and Segmentation of P7 Mouse Tissue Microarchitecture Using FIB-SEM and Machine Learning.
EP Hurley, B Mukherjee, LZ Fang, JR Barnes… (2024). GluN3A and excitatory glycine receptors in the adult hippocampus.
HA Emmons, SC Fordahl (2024). Attenuating Saturated-Fat Induced Changes in Dopamine Neurotransmission.
M Serranilla, JC Pressey, MA Woodin (2024). Restoring Compromised Cl-in D2 Neurons of a HD Mouse Model Rescues Motor Disability.
R Joulia, F Puttur, H Stölting, WJ Traves… (2024). Mast cell activation disrupts interactions between endothelial cells and pericytes during early life allergic asthma.
S McCracken, L McCoy, Z Hu, J Hodges, K Valkova… (2024). Mistargeted retinal axons form synaptically segregated subcircuits in the visual thalamus of albino mice.
S Zheng, R Banerji, R LeBourdais, S Zhang… (2024). Alteration of mechanical stresses in the murine brain by age and hemorrhagic stroke.
XH Li, W Shi, ZX Zhao, T Matsuura, JS Lu… (2024). Increased GluK1 Subunit Receptors in Corticostriatal Projection from the Anterior Cingulate Cortex Contributed to Seizure-Like Activities.
A Ozgur, SB Park, AY Flores, M Oijala, G Lur (2023). A comprehensive, affordable, open-source hardware-software solution for flexible implementation of complex behaviors in head-fixed mice.
C Wang, B Hyams, NC Allen, K Cautivo, K Monahan… (2023). Dysregulated lung stroma drives emphysema exacerbation by potentiating resident lymphocytes to suppress an epithelial stem cell reservoir.
D Dileep, TA Syed, TFW Sloan, PS Dhandapany… (2023). Cardiomyocyte orientation recovery at micrometer scale reveals long-axis fiber continuum in heart walls.
DK Kasaragod, H Aizawa (2023). Deep ultraviolet fluorescence microscopy of three-dimensional structures in the mouse brain.
G Chen, S Lai, G Bao, J Ke, X Meng, S Lu, X Wu, H Xu… (2023). Distinct reward processing by subregions of the nucleus accumbens.
G Rosen, D Kirsch, S Horowitz, JD Cherry… (2023). Three dimensional evaluation of cerebrovascular density and branching in chronic traumatic encephalopathy.
G Wildenberg, K Boergens, V Nikitin, A Deriy… (2023). A Pipeline for a Primate Projectome: mapping every individual myelinated axon across the whole brain.
H Mason, G Rai, A Kozyr, N De Jonge, E Gliniewicz… (2023). Development of an improved and specific inhibitor of NADPH oxidase 2 to treat traumatic brain injury.
JJ Privitt, BN Van Nest, SE Fahrbach (2023). Altered synaptic organization in the mushroom bodies of honey bees exposed as foragers to the pesticide fipronil.
K Jin, Z Yao, CTJ van Velthoven, ES Kaplan… (2023). Cell-type specific molecular signatures of aging revealed in a brain-wide transcriptomic cell-type atlas.
ML Ratz-Mitchem, G Leary, A Grindeland, D Silvius… (2023). Generation and characterization of a knock-in mouse model for spastic tetraplegia, thin corpus callosum, and progressive microcephaly (SPATCCM).
MÁ García-Cabezas, JL Hacker… (2023). Homology of neocortical areas in rats and primates based on cortical type analysis: an update of the hypothesis on the dual origin of the neocortex.

Q Tang, E Godschall, CD Brennan, Q Zhang… (2023). A leptin-responsive hypothalamic circuit inputs to the circadian feeding network.
Q Tang, E Godschall, CD Brennan, Q Zhang… (2023). Leptin receptor neurons in the dorsomedial hypothalamus input to the circadian feeding network.
V Valakh, D Wise, XA Zhu, M Sha, J Fok… (2023). A transcriptional constraint mechanism limits the homeostatic response to activity deprivation in mammalian neocortex.
Y Bai, G Li, L Yung, PB Yu, X Ai (2023). Intrapulmonary arterial contraction assay reveals region-specific deregulation of vasoreactivity to lung injuries.
Y Jin, E Mikhailova, M Lei, SA Cowley, T Sun… (2023). Integration of 3D-printed cerebral cortical tissue into an ex vivo lesioned brain slice.
Y Zhang, J Riexinger, X Yang, E Mikhailova, Y Jin… (2023). A microscale soft ionic power source modulates neuronal network activity.
Y Zhou, G Pereira, Y Tang, M James, M Zhang (2023). 3D Porous Scaffold-Based High-Throughput Platform for Cancer Drug Screening.
YA Nikolaev, LH Ziolkowski, S Pang, WP Li… (2023). 3D architecture and a bicellular mechanism of touch detection in mechanosensory corpuscle.
AJ Seibel, OM Kelly, YW Dance, CM Nelson… (2022). Role of Lymphatic Endothelium in Vascular Escape of Engineered Human Breast Microtumors.
C Kolluru, A Todd, AR Upadhye, Y Liu, MY Berezin… (2022). Imaging peripheral nerve micro-anatomy with MUSE, 2D and 3D approaches.
D Bojovic, TL Stackhouse, A Mishra (2022). Assaying activity-dependent arteriole and capillary responses in brain slices.
D Koveal, PC Rosen, DJ Meyer… (2022). A high-throughput multiparameter screen for accelerated development and optimization of soluble genetically encoded fluorescent biosensors.
DJ Chung, GP Madison, AM Aponte… (2022). Metabolic design in a mammalian model of extreme metabolism, the North American least shrew (Cryptotis parva).
DJ Meyer, CM Díaz-García, N Nathwani, M Rahman… (2022). The Na+/K+ pump dominates control of glycolysis in hippocampal dentate granule cells.
G Parlakgül, AP Arruda, S Pang, E Cagampan, N Min… (2022). Regulation of liver subcellular architecture controls metabolic homeostasis.
K Friedrichsen, P Ramakrishna, J Hsiang… (2022). Reconstructing neural circuits using multiresolution correlated light and electron microscopy.
LK Cuddy, AO Alia, MA Salvo… (2022). Farnesyltransferase inhibitor LNK-754 attenuates axonal dystrophy and reduces amyloid pathology in mice.
RA Vitek, W Huang, PG Geiger, E Heninger… (2022). Fresh tissue procurement and preparation for multicompartment and multimodal analysis of the prostate tumor microenvironment.
S Gaige, R Barbouche… (2022). Constitutively active microglial populations limit anorexia induced by the food contaminant deoxynivalenol.
W Shi, M Xue, F Wu, K Fan, QY Chen, F Xu… (2022). Whole-brain mapping of efferent projections of the anterior cingulate cortex in adult male mice.
M Qu, P Lu, K Bellve, LM Lifshitz, R ZhuGe (2021). Mode switch of Ca2+ oscillation-mediated uterine peristalsis and associated embryo implantation impairments in mouse adenomyosis.
PH Tseng, SJ Chiang, SJ Chen, CY Dong (2021). Improvement in Labeling Efficiency of Hydrophilic and Hydrophobic Fluorescent Molecules in Thick Tissue Sections.
WY Wang, RN Kent III, SA Huang, EH Jarman… (2021). Direct comparison of angiogenesis in natural and synthetic biomaterials reveals that matrix porosity regulates endothelial cell invasion speed and sprout diameter.
J Wang, T Li, JL Wang, Z Xu, W Meng, QF Wu (2020). Talpid3-Mediated Centrosome Integrity Restrains Neural Progenitor Delamination to Sustain Neurogenesis by Stabilizing Adherens Junctions.
KH Hu, JP Eichorst, CS McGinnis, DM Patterson… (2020). ZipSeq: barcoding for real-time mapping of single cell transcriptomes.
Qian, Yong; Cosio, Danielle M Orozco; Piatkevich, Kiryl D; Aufmkolk, Sarah; Su, Wan-Chi; Celike, Orhan T; Schohl, Anne; Murdock, Mitchell H; Aggarwal, Abhi; Chang, Yu-Fen; (2020). Improved genetically encoded near-infrared fluorescent calcium ion indicators for in vivo imaging.
Dahlgren MW, Jones SW, Cautivo KM, Dubinin A, Ortiz-Carpena JF, Farhat S, Yu KS, Lee K, Wang C, Molofsky AV, Tward AD, Krummel MF, Peng T, Molofsky AB. (2019). Adventitial Stromal Cells Define Group 2 Innate Lymphoid Cell Tissue Niches.

Nakano Y, Wiechert S, Bíçnfi B. (2019). Overlapping Activities of Two Neuronal Splicing Factors Switch the GABA Effect from Excitatory to Inhibitory by Regulating REST.

Toth AB, Hori K, Novakovic MM, Bernstein NG, Lambot L, Prakriya M. (2019). CRAC channels regulate astrocyte Ca(2+) signaling and gliotransmitter release to modulate hippocampal GABAergic transmission.

Wang, Hao; Zhu, Qingyuan; Ding, Lufeng; Shen, Yan; Yang, Chao-Yu; Xu, Fang; Shu, Chang; Guo, Yujie; Xiong, Zhiwei; Shan, Qinghong; (2019). Scalable volumetric imaging for ultrahigh-speed brain mapping at synaptic resolution.

Barry KC, Hsu J, Broz ML, Cueto FJ, Binnewies M, Combes AJ, Nelson AE, Loo K, Kumar R, Rosenblum MD, Alvarado MD, Wolf DM, Bogunovic D, Bhardwaj N, Daud AI, Ha PK, Ryan WR, Pollack JL, Samad B, Asthana S, Chan V, Krummel MF. (2018). A natural killer-dendritic cell axis defines checkpoint therapy-responsive tumor microenvironments.

Johnson BP, Vitek RA, Geiger PG, Huang W, Jarrard DF, Lang JM, Beebe DJ. (2018). Vital ex vivo tissue labeling and pathology-guided micropunching to characterize cellular heterogeneity in the tissue microenvironment.

Mamani S, Shi L, Ahmed T, Karnik R, Rodrí_guez-Contreras A, Nolan D, Alfano R. (2018). Transmission of classically entangled beams through mouse brain tissue.

Nylk J, McCluskey K, Preciado MA, Mazilu M, Yang Z, Gunn-Moore FJ, Aggarwal S, Tello JA, Ferrier DEK, Dholakia K. (2018). Light-sheet microscopy with attenuation-compensated propagation-invariant beams.

Wen Q, Gandhi K, Capel RA, Hao G, O'Shea C, Neagu G, Pearcey S, Pavlovic D, Terrar DA, Wu J, Faggian G, Camelliti P, Lei M. (2018). Transverse cardiac slicing and optical imaging for analysis of transmural gradients in membrane potential and Ca(2+) transients in murine heart.

Barrios J, Patel KR, Aven L, Achey R, Minns MS, Lee Y, Trinkaus-Randall VE, Ai X. (2017). Early life allergen-induced mucus overproduction requires augmented neural stimulation of pulmonary neuroendocrine cell secretion.

Chen J, Sanderson MJ. (2017). Store-operated calcium entry is required for sustained contraction and Ca2+ oscillations of airway smooth muscle.

Nakano H, Lyons-Cohen MR, Whitehead GS, Nakano K, Cook DN. (2017). Distinct functions of CXCR4, CCR2, and CX3CR1 direct dendritic cell precursors from the bone marrow to the lung.

Bai Y, Krishnamoorthy N, Patel KR, Rosas I, Sanderson MJ, Ai X. (2016). Cryopreserved Human Precision-Cut Lung Slices as a Bioassay for Live Tissue Banking. A Viability Study of Bronchodilation with Bitter-Taste Receptor Agonists.

Fox ME, Bucher ES, Johnson JA, Wightman RM. (2016). Medullary Norepinephrine Projections Release Norepinephrine into the Contralateral Bed Nucleus of the Stria Terminalis.

Nylk J, McCluskey K, Aggarwal S, Tello JA, Dholakia K. (2016). Enhancement of image quality and imaging depth with Airy light-sheet microscopy in cleared and non-cleared neural tissue.

Abdelaal HM, Kim HO, Wagstaff R, Sawahata R, Southern PJ, Skinner PJ. (2015). Comparison of Vibratome and Compresstome sectioning of fresh primate lymphoid and genital tissues for in situ MHC-tetramer and immunofluorescence staining.

Chang AJ, Ortega FE, Riegler J, Madison DV, Krasnow MA. (2015). Oxygen regulation of breathing through an olfactory receptor activated by lactate.

Danielsson J, Perez-Zoghbi J, Bernstein K, Barajas MB, Zhang Y, Kumar S, Sharma PK, Gallos G, Emala CW. (2015). Antagonists of the TMEM16A calcium-activated chloride channel modulate airway smooth muscle tone and intracellular calcium.

Gallos G, Yocum GT, Siviski ME, Yim PD, Fu XW, Poe MM, Cook JM, Harrison N, Perez-Zoghbi J, Emala CW Sr. (2015). Selective targeting of the α5-subunit of GABAA receptors relaxes airway smooth muscle and inhibits cellular calcium handling.

Cao P, Tan X, Donovan G, Sanderson MJ, Sneyd J. (2014). A deterministic model predicts the properties of stochastic calcium oscillations in airway smooth muscle cells.

Rietdorf K, Bootman MD, Sanderson MJ. (2014). Spontaneous, pro-arrhythmic calcium signals disrupt electrical pacing in mouse pulmonary vein sleeve cells.

Shi L, Rodrí_guez-Contreras A, Budansky Y, Pu Y, Nguyen TA, Alfano RR. (2014). Deep two-photon microscopic imaging through brain tissue using the second singlet state from fluorescent agent chlorophyll α in spinach leaf.

Castro-Piedras I, Perez-Zoghbi JF. (2013). Hydrogen sulphide inhibits Ca2+ release through InsP3 receptors and relaxes airway smooth muscle.

Chen-Roetling J, Lu X, Regan KA, Regan RF. (2013). A rapid fluorescent method to quantify neuronal loss after experimental intracerebral hemorrhage.

Liu CH, Yang J, Ren JQ, Liu CM, You Z, Liu PK. (2013). MRI reveals differential effects of amphetamine exposure on neuroglia in vivo.

Yu CR. (2013). Calcium imaging of vomeronasal organ response using slice preparations from transgenic mice expressing G-CaMP2.

Marrs GS, Spirou GA. (2012). Embryonic assembly of auditory circuits: spiral ganglion and brainstem.

Hoffman JJ, Johnson BL, Holland MR, Fedewa RJ, Nair A, Miller JG. (2011). Layer-dependent variation in the anisotropy of apparent integrated backscatter from human coronary arteries.
Ma L, Haga-Yamanaka S, Yu QE, Qiu Q, Kim S, Yu CR. (2011). Imaging neuronal responses in slice preparations of vomeronasal organ expressing a genetically encoded calcium sensor.

Immunohistochemistry

500 (2024). Optical Clearing and Labeling for Light-Ssheet Flourescence Microscopy in Large-Scale human Brain Imaging.
CS Park, M Yan, M Zhu, MA Akram, NN Foster… (2024). Dendritome Mapping Unveils Spatial Organization of Striatal D1/D2-Neuron Morphology.
D Bezwada, L Perelli, NP Lesner, L Cai, B Brooks… (2024). Mitochondrial complex I promotes kidney cancer metastasis.
D Markman, AZ Wasilczuk… (2024). General Anesthesia Occludes Ketamine's Antidepressant Response in a Rodent Model of Chronic Stress.
Di Meo D,1, Ramazzoti J,1,Scardigli M, Cheli F, Pesce L, Brady N, Mazzamuto G, Costantini I, Pavone SF (2024). Calcium-Sensing Receptor Negative Allosteric Modulators Oppose Contraction of Mouse Airways.
G Chen, S Lai, S Jiang, F Li, K Sun, X Wu, K Zhou… (2024). Cellular and circuit architecture of the lateral septum for reward processing.
HE Mohammed, JC Nelson, SA Marshall (2024). Ethanol Exacerbates the Alzheimer's Disease Pathology in the 5xFAD Mouse Model.
HR Li, M Harb, JE Heath, JS Trippett… (2024). Engineering viral vectors for acoustically targeted gene delivery.
J Hu, K He, Y Yang, C Huang, Y Dou, H Wang… (2024). Amino acid formula induces microbiota dysbiosis and depressive-like behavior in mice.
J Lee (2024). Ultrasound Control and Imaging of Cellular Immunotherapy.
KE Murtha, WD Sese, K Sleiman, J Halpage… (2024). Absence of oncomodulin increases susceptibility to noise-induced outer hair cell death and alters mitochondrial morphology.
M Lindman (2024). RIPK3 Regulates Neuroinflammation During Flavivirus Infection of the Central Nervous System.
M Lindman, I Estevez, E Marmut, EM DaPrano… (2024). Astrocytic RIPK3 exerts protective anti-inflammatory activity during viral encephalitis via induction of serpin protease inhibitors.
M Shammas (2024). Mitochondrial Dysfunction and Stress Responses in CHCHD10 Myopathy and Neurodegeneration.
M Xue, QY Chen, W Shi, Z Zhou, X Li, F Xu… (2024). Whole-brain mapping of afferents to the anterior cingulate cortex in adult mice.
S Hall, S Liu, I Liang, S Schulz, C Ezran, M Tan… (2024). Cellular and molecular characterization of peripheral glia in the lung and other organs.
SB Park, G Lur (2024). Repeated exposure to multiple concurrent stressors alters visual processing in the adult posterior parietal cortex.
T Qin, Y Xia, N Nazari, T Sepahvand… (2024). Correlational patterns of neuronal activation and epigenetic marks in the basolateral amygdala and piriform cortex following olfactory threat conditioning and ….
T Sepahvand, SJ Carew, Q Yuan (2024). The ventral hippocampus is activated in olfactory but not auditory threat memory.
TL Dunham, JR Wilkerson, RC Johnson, RL Huganir… (2024). WWC2 modulates GABAA-receptor-mediated synaptic transmission, revealing class-specific mechanisms of synapse regulation by WWC family proteins.
V Nikitin, G Wildenberg, A Mittone… (2024). Laminography as a tool for imaging large-size samples with high resolution.
WR Evans, SS Baskar, ARCE Costa, S Ravoori… (2024). Functional activation of dorsal striatum astrocytes improves movement deficits in hemi-parkinsonian mice.
Y Ge, C Yang, M Zadeh, SM Sprague, YD Lin, HS Jain… (2024). Functional regulation of microglia by vitamin B12 alleviates ischemic stroke-induced neuroinflammation in mice.
Z Zhou, X Yang, A Mao, H Xu, C Lin, M Yang, W Hu… (2024). Deficiency of CAMSAP2 impairs olfaction and the morphogenesis of mitral cells.
A Hall (2023). Analysis of cFos Expression and Microglial Branch Density in a Mouse Model of Trauma-Induced Hyperarousal.
A Maziar, TN Critch, S Ghosh, V Rajani… (2023). Aging differentially affects LTCC function in hippocampal CA1 and piriform cortex pyramidal neurons.
A Sarkar, Y Jin, BC DeFelice, CY Logan, Y Yang… (2023). Intermittent fasting induces rapid hepatocyte proliferation to restore the hepatostat in the mouse liver.
AG Salinas, JO Lee, SM Augustin, S Zhang… (2023). Distinct sub-second dopamine signaling in dorsolateral striatum measured by a genetically-encoded fluorescent sensor.
AML Osse, RS Pandey, RA Wirt, AA Ortiz… (2023). Reduction in GABAB on glia induce Alzheimer's disease related changes.

C Stossel, M Raitses-Gurevich, D Atias, T Beller… (2023). Spectrum of Response to Platinum and PARP Inhibitors in Germline BRCA–Associated Pancreatic Cancer in the Clinical and Preclinical Setting.
C Yang, Z Gong, X Zhang, S Miao, B Li, W Xie… (2023). Neuropeptide Y in the medial habenula alleviates migraine-like behaviors through the Y1 receptor.
CD Walker (2023). Adolescence, Alcohol, and Astrocytes: The Impact of Adolescent Alcohol Use on Astrocyte-Synaptic Interactions, Structure, Function, and Behavior.
CM McCarthy, JM Allardyce, SE Hickey… (2023). Comparison of macroscale and microscale mechanical properties of fresh and fixed-frozen porcine colonic tissue.
D Na, J Zhang, HJ Beaulac… (2023). Increased central auditory gain in 5xFAD Alzheimer's disease mice as an early biomarker candidate for Alzheimer's disease diagnosis.
DB Azizoglu, K Perez, SL Zheng, S Rahman, EY Rim… (2023). Liver size is predetermined in the neonate by adding lobules at the periphery.
DJ Lievano Parra (2023). Effects of the unilateral lesion of the substantia nigra compacta with 6-OHDA on reversal learning and prepulse inhibition in male and female Wistar rats.
J Larochelle, RJ Tishko, C Yang, Y Ge, LT Phan… (2023). Receptor-interacting protein kinase 2 (RIPK2) profoundly contributes to post-stroke neuroinflammation and behavioral deficits with microglia as unique ….
J Sbierski-Kind, KM Cautivo, JC Wagner, MW Dahlgren… (2023). Group 2 innate lymphoid cells constrain type 3/17 lymphocytes in shared stromal niches to restrict liver fibrosis.
J Siewiera, TI McIntyre, KM Cautivo, K Mahiddine… (2023). Circumvention of luteolysis reveals parturition pathways in mice dependent upon innate type 2 immunity.
JA Hatter, MM Scott (2023). Selective ablation of VIP interneurons in the rodent prefrontal cortex results in increased impulsivity.
JC Nawroth, D Roth, A van Schadewijk, A Ravi… (2023). Breathing on chip: Dynamic flow and stretch accelerate mucociliary maturation of airway epithelium in vitro.
JT Ahrendsen, Y Nong, Y Huo, J Steele… (2023). CD8 cytotoxic T-cell infiltrates and cellular damage in the hypothalamus in human obesity.
JY Min, S Park, J Cho, Y Huh (2023). The anterior insular cortex processes social recognition memory.
L Kang, W Yu, Y Zhang, TTW Wong (2023). Automated whole-organ histological imaging assisted with ultraviolet-excited sectioning tomography and deep learning.
L Kang, W Yu, Y Zhang, Z Chen, TTW Wong (2023). Deep Learning Enables Rapid Whole-Organ Histological Imaging with Ultraviolet-Excited Sectioning Tomography.
L Smith-Osborne, A Duong, A Resendez, R Palme… (2023). Female dominance hierarchies influence responses to psychosocial stressors.
LD Quigley, R Pendry, ML Mendoza, BE Pfeiffer… (2023). Experience alters hippocampal and cortical network communication via a KIBRA-dependent mechanism.
M Dorofeikova, CD Borkar, K Weissmuller… (2023). Effects of footshock stress on social behavior and neuronal activation in the medial prefrontal cortex and amygdala of male and female mice.
M Dorofeikova, CE Stelly, A Duong, S Basavanhalli… (2023). The role of genetically distinct central amygdala neurons in appetitive and aversive responding assayed with a novel dual valence operant conditioning paradigm.
M Lindman, JP Angel, I Estevez, NP Chang… (2023). RIPK3 promotes brain region-specific interferon signaling and restriction of tick-borne flavivirus infection.
M Serranilla (2023). Chloride Dysregulation and Impaired Gamma-Amino Butyric Acid Signaling in the Basal Ganglia in Huntington's Disease.
MM Naffaa, RR Khan, CT Kuo, HH Yin (2023). Cortical regulation of neurogenesis and cell proliferation in the ventral subventricular zone.
P Hoffman, MN Svalina, C Flores, C Brzezinski… (2023). Developmental Characterization of Neuronal Migration Anomalies and Axon Proliferation in mTOR pathway-associated Malformations of Cortical Development.
P Liu, A Anandhan, J Chen, A Shakya, M Dodson… (2023). Decreased autophagosome biogenesis, reduced NRF2, and enhanced ferroptotic cell death are underlying molecular mechanisms of non-alcoholic fatty liver ….
R Sim, J Lee, J Chieng, KH Tan, G Lim, A Foo… (2023). Fluorescent Peptide-based Probe for the Detection of Alpha-synuclein Aggregates in the Gut.
S Venkadesh, A Santarelli, T Boesen… (2023). Combinatorial quantification of distinct neural projections from retrograde tracing.
SJ Carew (2023). The smell of fear: comparing the neural ensembles underlying odor fear memory conditioned by innate, inherent, and learned sources of danger.

SM Ramos Rodriguez (2023). An Investigation into Cell-Type Vulnerability for Formation of Alpha-Synuclein Aggregates.
TR Sides, JC Nelson, KN Nwachukwu, J Boston… (2023). The Influence of Arsenic Co-Exposure in a Model of Alcohol-Induced Neurodegeneration in C57BL/6J Mice.
W Donelan, PL Crispen, S Kusmartsev (2023). Tissue Slice Culture and Analysis of Tumor-Associated Hyaluronan in Urothelial Carcinoma.
W Yu (2023). Translational Rapid Ultraviolet-Excited Sectioning Tomography for Whole-Organ Imaging with Subcellular Resolution.
X Chen, DA Wolfe, DS Bindu, M Zhang… (2023). Functional gene delivery to and across brain vasculature of systemic AAVs with endothelial-specific tropism in rodents and broad tropism in primates.
X Fang, JJ Border, PL Rivers, H Zhang, JM Williams… (2023). Amyloid beta accumulation in TgF344-AD rats is associated with reduced cerebral capillary endothelial Kir2. 1 expression and neurovascular uncoupling.
Y Liu, MR Fontenot, A Kulkarni, N Khandelwal… (2023). An extra-circadian function for human CLOCK in the neocortex.
Y Wu, P Li, N Bhat, H Fan, M Liu (2023). Effects of repeated sleep deprivation on brain pericytes in mice.
Z Li, EG Solomonidis, B Berkeley… (2023). Multi-species meta-analysis identifies transcriptional signatures associated with cardiac endothelial responses in the ischaemic heart.
Z Yao, CTJ van Velthoven, M Kunst, M Zhang… (2023). A high-resolution transcriptomic and spatial atlas of cell types in the whole mouse brain.
A Brodovskaya, S Shiono, T Batabyal… (2022). Construction of Local Field Potential Microelectrodes for in vivo Recordings from Multiple Brain Structures Simultaneously.
DJ Rindner, A Proddutur, G Lur (2022). Cell-type-specific integration of feedforward and feedback synaptic inputs in the posterior parietal cortex.
EA Kiffmeyer, JA Cosgrove, JK Siganos, HE Bien… (2022). Deficits in cerebellum-dependent learning and cerebellar morphology in male and female BTBR autism model mice.
ES Norton, LA Whaley, MJ Ulloa-Navas… (2022). Glioblastoma disrupts the ependymal wall and extracellular matrix structures of the subventricular zone.
JD Hahn, L Gao, T Boesen, L Gou… (2022). Macroscale connections of the mouse lateral preoptic area and anterior lateral hypothalamic area.
KM Cautivo, PR Matatia, CO Lizama, NM Mroz… (2022). Interferon gamma constrains type 2 lymphocyte niche boundaries during mixed inflammation.
KN Nwachukwu, DM King, KL Healey… (2022). Sex-specific effects of adolescent intermittent ethanol exposure-induced dysregulation of hippocampal glial cells in adulthood.
KN Nwachukwu, KL Healey, HS Swartzwelder… (2022). The influence of sex on hippocampal neurogenesis and neurotrophic responses on the persistent effects of adolescent intermittent ethanol exposure into adulthood.
L Liu, C Yang, BP Lavayen, RJ Tishko… (2022). Targeted BRD4 protein degradation by dBET1 ameliorates acute ischemic brain injury and improves functional outcomes associated with reduced ….
M Scheibinger, A Janesick, GH Diaz… (2022). Immunohistochemistry and In Situ mRNA detection using inner ear vibratome sections.
MÁ García-Cabezas, JL Hacker… (2022). Homology of neocortical areas in rats and primates based on cortical type analysis: an update of the Hypothesis on the Dual Origin of the Neocortex.
NAL Fayez, E Rouhollahi, CY Ong, J Wu… (2022). Hepatocyte-targeted delivery of imiquimod reduces hepatitis B virus surface antigen.
NAL Fayez, R Böttger, J Brown, E Rouhollahi… (2022). The mechanism of Hepatocyte-Targeting and safety profile of Phospholipid-Free small unilamellar vesicles.
S Milde, GC Brown (2022). Knockout of the P2Y6 Receptor Prevents Peri-Infarct Neuronal Loss after Transient, Focal Ischemia in Mouse Brain.
WE Barclay, N Aggarwal, ME Deerhake, M Inoue… (2022). The AIM2 inflammasome is activated in astrocytes during the late phase of EAE.
Y Zhang, L Kang, IHM Wong, W Dai, X Li… (2022). High-Throughput, Label-Free and Slide-Free Histological Imaging by Computational Microscopy and Unsupervised Learning.
A Farias, A Soto, F Puttur, CJ Goldin, S Sosa, C Gil… (2021). A TLR4 agonist improves immune checkpoint blockade treatment by increasing the ratio of effector to regulatory cells within the tumor microenvironment.
A Hausmann, B Felmy, L Kunz, S Kroon… (2021). Intercrypt sentinel macrophages tune antibacterial NF-κB responses in gut epithelial cells via TNF.
C Yang, BP Lavayen, L Liu, BD Sanz, KM DeMars… (2021). Neurovascular protection by adropin in experimental ischemic stroke through an endothelial nitric oxide synthase-dependent mechanism.

CE Jones, AQ Chau, RJ Olson, C Moore… (2021). Early life sleep disruption alters glutamate and dendritic spines in prefrontal cortex and impairs cognitive flexibility in prairie voles.
F Xu, Y Shen, L Ding, CY Yang, H Tan, H Wang… (2021). High-throughput mapping of a whole rhesus monkey brain at micrometer resolution.
FP Mayer, H Iwamoto, MK Hahn, GJ Grumbar… (2021). There's no place like home? Return to the home cage triggers dopamine release in the mouse nucleus accumbens.
H Hintiryan, I Bowman, DL Johnson… (2021). Connectivity characterization of the mouse basolateral amygdalar complex.
HD Mason, AM Johnson, NA Mihelson, P Mastorakos… (2021). Glia limitans superficialis oxidation and breakdown promote cortical cell death after repetitive head injury.
I Navickaite, N Pauziene, DH Pauza (2021). Anatomical evidence of non-parasympathetic cardiac nitrergic nerve fibres in rat.
J Vogler, R Böttger, NAL Fayez, W Zhang, Z Qin… (2021). Altering the intra-liver distribution of phospholipid-free small unilamellar vesicles using temperature-dependent size-tunability.
J Wie, Z Liu, H Song, TF Tropea, L Yang, H Wang… (2021). A growth-factor-activated lysosomal K+ channel regulates Parkinson's pathology.
KL Elliott, J Kersigo, JH Lee, EN Yamoah… (2021). Sustained Loss of bdnf affects peripheral but not central vestibular targets.
KN Nwachukwu, WA Evans, TR Sides… (2021). Chemogenetic manipulation of astrocytic signaling in the basolateral amygdala reduces binge-like alcohol consumption in male mice.
L Kettler, H Sid, C Schaub, K Lischka… (2021). AP-2δ Expression Kinetics in Multimodal Networks in the Developing Chicken Midbrain.
M Puigdellívol, S Milde, M Spillantini… (2021). The microglial P2Y6 receptor mediates neuronal loss and memory deficits in neurodegeneration.
N Al Fayez, R Bottger, E Rouhollahi… (2021). Improved Liver Delivery of Primaquine by Phospholipid-Free Small Unilamellar Vesicles with Reduced Hemolytic Toxicity.
NL Benavidez, MS Bienkowski, M Zhu… (2021). Organization of the inputs and outputs of the mouse superior colliculus.
P Mastorakos, MV Russo, T Zhou, K Johnson… (2021). Antimicrobial immunity impedes CNS vascular repair following brain injury.
P Mastorakos, N Mihelson, M Luby, SR Burks… (2021). Temporally distinct myeloid cell responses mediate damage and repair after cerebrovascular injury.
PL Rochon, C Theriault, AGR Olguin, A Krishnaswamy (2021). The cell adhesion molecule Sdk1 shapes assembly of a retinal circuit that detects localized edges.
S Milde, FW van Tartwijk, A Vilalta, TC Hornik… (2021). Inflammatory neuronal loss in the substantia nigra induced by systemic lipopolysaccharide is prevented by knockout of the P2Y6 receptor in mice.
SK Bose, BM White, MV Kashyap, A Dave… (2021). In utero adenine base editing corrects multi-organ pathology in a lethal lysosomal storage disease.
SL Reitz, AZ Wasilczuk, GH Beh, A Proekt, MB Kelz (2021). Activation of preoptic tachykinin 1 neurons promotes wakefulness over sleep and volatile anesthetic-induced unconsciousness.
SR Gray, L Ye, JY Ye, M Paukert (2021). Noradrenergic terminal short-term potentiation enables modality-selective integration of sensory input and vigilance state.
YT Liu, DA Sliter, MK Shammas, X Huang, C Wang… (2021). Mt-Keima detects PINK1-PRKN mitophagy in vivo with greater sensitivity than mito-QC.
A Caputo, Y Liang, TD Raabe, A Lo, M Horvath… (2020). Snca-GFP knock-in mice reflect patterns of endogenous expression and pathological seeding.
B Ling, J Lee, D Maresca, A Lee-Gosselin… (2020). Biomolecular ultrasound imaging of phagolysosomal function.
Bariselli S, Miyazaki NL, Creed MC, Kravitz AV. (2020). Orbitofrontal-striatal potentiation underlies cocaine-induced hyperactivity.
Bracken-Grissom HD, DeLeo DM, Porter ML, Iwanicki T, Sickles J, Frank TM. (2020). Light organ photosensitivity in deep-sea shrimp may suggest a novel role in counterillumination.
CE Jones, PT Wickham, MM Lim (2020). Early life sleep disruption is a risk factor for increased ethanol drinking after acute footshock stress in prairie voles.
Colon LM, Poulos AM. (2020). Contextual processing elicits sex differences in dorsal hippocampus activation following footshock and context fear retrieval.
Dao NC, Suresh Nair M, Magee SN, Moyer JB, Sendao V, Brockway DF, Crowley NA. (2020). Forced Abstinence From Alcohol Induces Sex-Specific Depression-Like Behavioral and Neural Adaptations in Somatostatin Neurons in Cortical and Amygdalar Regions.

E Gonzalez-Fernandez, D Staursky, K Lucas… (2020). 20-HETE enzymes and receptors in the neurovascular unit: implications in cerebrovascular disease.
Griffiths KK, Wang A, Wang L, Tracey M, Kleiner G, Quinzii CM, Sun L, Yang G, Perez-Zoghbi JF, Licznerski P, Yang M, Jonas EA, Levy RJ. (2020). Inefficient thermogenic mitochondrial respiration due to futile proton leak in a mouse model of fragile X syndrome.
Kaneko K, Osada T, Morse MA, Gwin WR, Ginzel JD, Snyder JC, Yang XY, Liu CX, Diniz MA, Bodoor K, Hughes PF, Haystead TA, Lyerly HK. (2020). Heat shock protein 90-targeted photodynamic therapy enables treatment of subcutaneous and visceral tumors.
Kim EJ, Zhang Z, Huang L, Ito-Cole T, Jacobs MW, Juavinett AL, Senturk G, Hu M, Ku M, Ecker JR, Callaway EM. (2020). Extraction of Distinct Neuronal Cell Types from within a Genetically Continuous Population.
Lewis TR, Shores CR, Cady MA, Hao Y, Arshavsky VY, Burns ME. (2020). The F220C and F45L rhodopsin mutations identified in retinitis pigmentosa patients do not cause pathology in mice.
Li, Xiufeng; Kang, Lei; Zhang, Yan; Wong, Terence TW; (2020). High-speed Label-free Ultraviolet Photoacoustic Microscopy for Histology-like imaging of unprocessed biological tissues.
Majewski L, MaciÛfg F, Boguszewski PM, Kuznicki J. (2020). Transgenic Mice Overexpressing Human STIM2 and ORAI1 in Neurons Exhibit Changes in Behavior and Calcium Homeostasis but Show No Signs of Neurodegeneration.
Mira MM, El-Khateeb EA, Gaafar RM, Igamberdiev AU, Hill RD, Stasolla C. (2020). Stem cell fate in hypoxic root apical meristems is influenced by phytoglobin expression.
MÁ García-Cabezas, JL Hacker… (2020). A protocol for cortical type analysis of the human neocortex applied on histological samples, the atlas of Von Economo and Koskinas, and magnetic ….
NF Nolta, A Liberti, R Makol, M Han (2020). Gelatin embedding and LED autofluorescence reduction for rodent spinal cord histology.
Pozhidayeva DY, Farris SP, Goeke CM, Firsick EJ, Townsley KG, Guizzetti M, Ozburn AR. (2020). Chronic Chemogenetic Stimulation of the Nucleus Accumbens Produces Lasting Reductions in Binge Drinking and Ameliorates Alcohol-Related Morphological and Transcriptional Changes.
Veldman MB, Park CS, Eyermann CM, Zhang JY, Zuniga-Sanchez E, Hirano AA, Daigle TL, Foster NN, Zhu M, Langfelder P, Lopez IA, Brecha NC, Zipursky SL, Zeng H, Dong HW, Yang XW. (2020). Brainwide Genetic Sparse Cell Labeling to Illuminate the Morphology of Neurons and Glia with Cre-Dependent MORF Mice.
Wang S, Lv W, Zhang H, Liu Y, Li L, Jefferson JR, Guo Y, Li M, Gao W, Fang X, Paul IA, Rajkowska G, Shaffery JP, Mosley TH, Hu X, Liu R, Wang Y, Yu H, Roman RJ, Fan F. (2020). Aging exacerbates impairments of cerebral blood flow autoregulation and cognition in diabetic rats.
Webb GM, Molden J, Busman-Sahay K, Abdulhaqq S, Wu HL, Weber WC, Bateman KB, Reed JS, Northrup M, Maier N, Tanaka S, Gao L, Davey B, Carpenter BL, Axthelm MK, Stanton JJ, Smedley J, Greene JM, Safrit JT, Estes JD, Skinner PJ, Sacha JB. (2020). The human IL-15 superagonist N-803 promotes migration of virus-specific CD8+ T and NK cells to B cell follicles but does not reverse latency in ART-suppressed, SHIV-infected macaques.
Zhang Y, Lu P, Liang F, Liufu N, Dong Y, Zheng JC, Xie Z. (2020). Cyclophilin D Contributes to Anesthesia Neurotoxicity in the Developing Brain.
Abdelaal HM, Cartwright EK, Skinner PJ. (2019). Detection of Antigen-Specific T Cells Using In Situ MHC Tetramer Staining.
Bienkowski MS, Benavidez NL, Wu K, Gou L, Becerra M, Dong HW. (2019). Extrastriate connectivity of the mouse dorsal lateral geniculate thalamic nucleus.
Boone PG, Rochelle LK, Ginzel JD, Lubkov V, Roberts WL, Nicholls PJ, Bock C, Flowers ML, von Furstenberg RJ, Stripp BR, Agarwal P, Borowsky AD, Cardiff RD, Barak LS, Caron MG, Lyerly HK, Snyder JC. (2019). A cancer rainbow mouse for visualizing the functional genomics of oncogenic clonal expansion.
Dahlgren MW, Jones SW, Cautivo KM, Dubinin A, Ortiz-Carpena JF, Farhat S, Yu KS, Lee K, Wang C, Molofsky AV, Tward AD, Krummel MF, Peng T, Molofsky AB. (2019). Adventitial Stromal Cells Define Group 2 Innate Lymphoid Cell Tissue Niches.
Feng M, Crowley NA, Patel A, Guo Y, Bugni SE, Luscher B. (2019). Reversal of a Treatment-Resistant, Depression-Related Brain State with the Kv7 Channel Opener Retigabine.
Grifasi IR, Evans WA, Rexha AD, Sako LW, Marshall SA. (2019). A comparison of hippocampal microglial responses in aged and young rodents following dependent and non-dependent binge drinking.
Kloos M, Weigel S, Luksch H. (2019). Anatomy and Physiology of Neurons in Layer 9 of the Chicken Optic Tectum.
Li S, Folkvord JM, Kovacs KJ, Wagstaff RK, Mwakalundwa G, Rendahl AK, Rakasz EG, Connick E, Skinner PJ. (2019). Low levels of SIV-specific CD8+ T cells in germinal centers characterizes acute SIV infection.
MaciÛfg F, Majewski , Boguszewski PM, Gupta RK, Wasilewska I, Wojta_ B, Kuznicki J. (2019). Behavioral and electrophysiological changes in female mice overexpressing ORAI1 in neurons.
Paletzki RF, Gerfen CR. (2019). Basic Neuroanatomical Methods.

Russell TL, Zhang J, Okoniewski M, Franke F, Bichet S, Hierlemann A. (2019). Medullary Respiratory Circuit Is Reorganized by a Seasonally-Induced Program in Preparation for Hibernation.
Shandra O, Winemiller AR, Heithoff BP, Munoz-Ballester C, George KK, Benko MJ, Zuidhoek IA, Besser MN, Curley DE, Edwards GF 3rd, Mey A, Harrington AN, Kitchen JP, Robel S. (2019). Repetitive Diffuse Mild Traumatic Brain Injury Causes an Atypical Astrocyte Response and Spontaneous Recurrent Seizures.
Sun Y, Blanco-Centurion C, Bendell E, Vidal-Ortiz A, Luo S, Liu M. (2019). Activity dynamics of amygdala GABAergic neurons during cataplexy of narcolepsy.
Sun Y, Blanco-Centurion C, Zou B, Bendell E, Shiromani PJ, Liu M. (2019). Amygdala GABA Neurons Project To vlPAG And mPFC.
Trutzer IM, Garcí_a-Cabezas Mí, Zikopoulos B. (2019). Postnatal development and maturation of layer 1 in the lateral prefrontal cortex and its disruption in autism.
Zhang W, Bí_ttger R, Qin Z, Kulkarni JA, Vogler J, Cullis PR, Li SD. (2019). Phospholipid-Free Small Unilamellar Vesicles for Drug Targeting to Cells in the Liver.
Bienkowski MS, Bowman I, Song MY, Gou L, Ard T, Cotter K, Zhu M, Benavidez NL, Yamashita S, Abu-Jaber J, Azam S, Lo D, Foster NN, Hintiryan H, Dong HW. (2018). Integration of gene expression and brain-wide connectivity reveals the multiscale organization of mouse hippocampal networks.
Blanco-Centurion C, Bendell E, Zou B, Sun Y, Shiromani PJ, Liu M. (2018). VGAT and VGLUT2 expression in MCH and orexin neurons in double transgenic reporter mice.
Lischka K, Yan J, Weigel S, Luksch H. (2018). Effects of early eye removal on the morphology of a multisensory neuron in the chicken optic tectum.
Szablowski JO, Lee-Gosselin A, Lue B, Malounda D, Shapiro MG. (2018). Acoustically targeted chemogenetics for the non-invasive control of neural circuits.
Vega-Zuniga T, Trost D, Schicker K, Bogner EM, Luksch H. (2018). The Medial Ventrothalamic Circuitry: Cells Implicated in a Bimodal Network.
Webb GM, Li S, Mwakalundwa G, Folkvord JM, Greene JM, Reed JS, Stanton JJ, Legasse AW, Hobbs T, Martin LD, Park BS, Whitney JB, Jeng EK, Wong HC, Nixon DF, Jones RB, Connick E, Skinner PJ, Sacha JB. (2018). The human IL-15 superagonist ALT-803 directs SIV-specific CD8(+) T cells into B-cell follicles.
Kondru N, Manne S, Greenlee J, West Greenlee H, Anantharam V, Halbur P, Kanthasamy A, Kanthasamy A. (2017). Integrated Organotypic Slice Cultures and RT-QuIC (OSCAR) Assay: Implications for Translational Discovery in Protein Misfolding Diseases.
Miller OH, Bruns A, Ben Ammar I, Mueggler T, Hall BJ. (2017). Synaptic Regulation of a Thalamocortical Circuit Controls Depression-Related Behavior.
Ng-Blichfeldt JP, Alí_ada J, Montero MA, Dean CH, Griesenbach U, Griffiths MJ, Hind M. (2017). Deficient retinoid-driven angiogenesis may contribute to failure of adult human lung regeneration in emphysema.
Pathania M, De Jay N, Maestro N, Harutyunyan AS, Nitarska J, Pahlavan P, Henderson S, Mikael LG, Richard-Londt A, Zhang Y, Costa JR, Hí©bert S, Khazaei S, Ibrahim NS, Herrero J, Riccio A, Albrecht S, Ketteler R, Brandner S, Kleinman CL, Jabado N, Salomoni P. (2017). H3.3(K27M) Cooperates with Trp53 Loss and PDGFRA Gain in Mouse Embryonic Neural Progenitor Cells to Induce Invasive High-Grade Gliomas.
Poobalasingam T, Salman D, Li H, Alí_ada J, Dean CH. (2017). Imaging the lung: the old ways and the new.
Wong TTW, Zhang R, Zhang C, Hsu HC, Maslov KI, Wang L, Shi J, Chen R, Shung KK, Zhou Q, Wang LV. (2017). Label-free automated three-dimensional imaging of whole organs by microtomy-assisted photoacoustic microscopy.
Fritzsch B, Duncan JS, Kersigo J, Gray B, Elliott KL. (2016). Neuroanatomical Tracing Techniques in the Ear: History, State of the Art, and Future Developments.
Garcia I, Bhullar PK, Tepe B, Ortiz-Guzman J, Huang L, Herman AM, Chaboub L, Deneen B, Justice NJ, Arenkiel BR. (2016). Local corticotropin releasing hormone (CRH) signals to its receptor CRHR1 during postnatal development of the mouse olfactory bulb.
Garcí_a-Cabezas Mí, John YJ, Barbas H, Zikopoulos B. (2016). Distinction of Neurons, Glia and Endothelial Cells in the Cerebral Cortex: An Algorithm Based on Cytological Features.
Hintiryan H, Foster NN, Bowman I, Bay M, Song MY, Gou L, Yamashita S, Bienkowski MS, Zingg B, Zhu M, Yang XW, Shih JC, Toga AW, Dong HW. (2016). The mouse cortico-striatal projectome.
Huang L, Ung K, Garcia I, Quast KB, Cordiner K, Saggau P, Arenkiel BR. (2016). Task Learning Promotes Plasticity of Interneuron Connectivity Maps in the Olfactory Bulb.
Jameson H, Bateman R, Byrne P, Dyavanapalli J, Wang X, Jain V, Mendelowitz D. (2016). Oxytocin neuron activation prevents hypertension that occurs with chronic intermittent hypoxia/hypercapnia in rats.

Li S, Folkvord JM, Rakasz EG, Abdelaal HM, Wagstaff RK, Kovacs KJ, Kim HO, Sawahata R, MaWhinney S, Masopust D, Connick E, Skinner PJ. (2016). Simian Immunodeficiency Virus-Producing Cells in Follicles Are Partially Suppressed by CD8+ Cells In Vivo.

Mira MM, Hill RD, Stasolla C. (2016). Phytoglobins Improve Hypoxic Root Growth by Alleviating Apical Meristem Cell Death.

Vega-Zuniga T, Marí_n G, Gonzíçlez-Cabrera C, Planitscher E, Hartmann A, Marks V, Mpodozis J, Luksch H. (2016). Microconnectomics of the Pretectum and VentralThalamus in the Chicken (Gallus gallus).

Wu ÎÇ_†__Â Q, Kolb I, Callahan BM, Su Z, Stoy W, Kodandaramaiah SB, Neve R, Zeng H, Boyden ES, Forest CR, Chubykin AA. (2016). Integration of autopatching with automated pipette and cell detection in vitro.

Abdelaal HM, Kim HO, Wagstaff R, Sawahata R, Southern PJ, Skinner PJ. (2015). Comparison of Vibratome and Compresstome sectioning of fresh primate lymphoid and genital tissues for in situ MHC-tetramer and immunofluorescence staining.

JS Duncan, KL Elliott, J Kersigo, B Gray… (2015). Combining whole-mount in situ hybridization with neuronal tracing and immunohistochemistry.

Moen T, Torgersen J, Santi N, Davidson WS, Baranski M, íÖdegí«rd J, KjíŸglum S, Velle B, Kent M, Lubieniecki KP, Isdal E, Lien S. (2015). Epithelial Cadherin Determines Resistance to Infectious Pancreatic Necrosis Virus in Atlantic Salmon.

Vieira PA, Korzus E. (2015). CBP-Dependent memory consolidation in the prefrontal cortex supports object-location learning.

Xiao C, Miwa JM, Henderson BJ, Wang Y, Deshpande P, McKinney SL, Lester HA. (2015). Nicotinic receptor subtype-selective circuit patterns in the subthalamic nucleus.

Cetin A, Callaway EM. (2014). Optical control of retrogradely infected neurons using drug-regulated “TLoop” lentiviral vectors.

Harischandra DS, Kondru N, Martin DP, Kanthasamy A, Jin H, Anantharam V, Kanthasamy AG. (2014). Role of proteolytic activation of protein kinase Cδ in the pathogenesis of prion disease.

Herman AM, Huang L, Murphey DK, Garcia I, Arenkiel BR. (2014). Cell type-specific and time-dependent light exposure contribute to silencing in neurons expressing Channelrhodopsin-2.

Tan X, Sanderson MJ. (2014). Bitter tasting compounds dilate airways by inhibiting airway smooth muscle calcium oscillations and calcium sensitivity.

Vega-Zuniga T, Mpodozis J, Karten HJ, Marí_n G, Hain S, Luksch H. (2014). Morphology, Projection Pattern and Neurochemical Identity of Cajal’s “Centrifugal Neurons”: The Cells of Origin of the Tectoventrogeniculate Pathway in Pigeon (Columba livia) and Chicken (Gallus gallus).

Vieira PA, Lovelace JW, Corches A, Rashid AJ, Josselyn SA, Korzus E. (2014). Prefrontal consolidation supports the attainment of fear memory accuracy.

Zingg B, Hintiryan H, Gou L, Song MY, Bay M, Bienkowski MS, Foster NN, Yamashita S, Bowman I, Toga AW, Dong HW. (2014). Neural networks of the mouse neocortex.

Haddad-Tí_volli R, Szabí_ NE, Zhou X, Alvarez-Bolado G. (2013). Genetic manipulation of the mouse developing hypothalamus through in utero electroporation.

Huang L, Garcia I, Jen HI, Arenkiel BR. (2013). Reciprocal connectivity between mitral cells and external plexiform layer interneurons in the mouse olfactory bulb.

Oenema TA, Maarsingh H, Smit M, Groothuis GM, Meurs H, Gosens R. (2013). Bronchoconstriction Induces TGF-β Release and Airway Remodelling in Guinea Pig Lung Slices.

Wickersham IR, Sullivan HA, Seung HS. (2013). Axonal and subcellular labelling using modified rabies viral vectors.

Guan Y, Xiao C, Krnjevic K, Xie G, Zuo W, Ye JH. (2012). GABAergic actions mediate opposite ethanol effects on dopaminergic neurons in the anterior and posterior ventral tegmental area.

Haddad-Tí_volli R, Heide M, Zhou X, Blaess S, Alvarez-Bolado G. (2012). Mouse thalamic differentiation: gli-dependent pattern and gli-independent prepattern.

Duncan J, Kersigo J, Gray B, Fritzsch B. (2011). Combining lipophilic dye, in situ hybridization, immunohistochemistry, and histology.

Selever J, Kong JQ, Arenkiel BR. (2011). A rapid approach to high-resolution fluorescence imaging in semi-thick brain slices.

Shao J, Lai D, Meyer U, Luksch H, Wessel R. (2009). Generating oscillatory bursts from a network of regular spiking neurons without inhibition.

Xiao C, Shao XM, Olive MF, Griffin WC 3rd, Li KY, KrnjeviÛˆ K, Zhou C, Ye JH. (2009). Ethanol facilitates glutamatergic transmission to dopamine neurons in the ventral tegmental area.

Kamari Y, Cohen H, Shaish A, Bitzur R, Afek A, Shen S, Vainshtein A, Harats D. (2008). Characterisation of atherosclerotic lesions with scanning electron microscopy (SEM) of wet tissue.

Oliver SR, Wright VP, Parinandi N, Clanton TL. (2008). Thermal tolerance of contractile function in oxidative skeletal muscle: no protection by antioxidants and reduced tolerance with eicosanoid enzyme inhibition.

Hsieh CY, Hong CT, Cramer KS. (2007). Deletion of EphA4 enhances deafferentation-induced ipsilateral sprouting in auditory brainstem projections.

In-situ hybridization

500 (2024). Optical Clearing and Labeling for Light-Ssheet Flourescence Microscopy in Large-Scale human Brain Imaging.
CS Park, M Yan, M Zhu, MA Akram, NN Foster… (2024). Dendritome Mapping Unveils Spatial Organization of Striatal D1/D2-Neuron Morphology.
D Bezwada, L Perelli, NP Lesner, L Cai, B Brooks… (2024). Mitochondrial complex I promotes kidney cancer metastasis.
D Markman, AZ Wasilczuk… (2024). General Anesthesia Occludes Ketamine's Antidepressant Response in a Rodent Model of Chronic Stress.
Di Meo D,1, Ramazzoti J,1,Scardigli M, Cheli F, Pesce L, Brady N, Mazzamuto G, Costantini I, Pavone SF (2024). Calcium-Sensing Receptor Negative Allosteric Modulators Oppose Contraction of Mouse Airways.
G Chen, S Lai, S Jiang, F Li, K Sun, X Wu, K Zhou… (2024). Cellular and circuit architecture of the lateral septum for reward processing.
HE Mohammed, JC Nelson, SA Marshall (2024). Ethanol Exacerbates the Alzheimer's Disease Pathology in the 5xFAD Mouse Model.
HR Li, M Harb, JE Heath, JS Trippett… (2024). Engineering viral vectors for acoustically targeted gene delivery.
J Hu, K He, Y Yang, C Huang, Y Dou, H Wang… (2024). Amino acid formula induces microbiota dysbiosis and depressive-like behavior in mice.
J Lee (2024). Ultrasound Control and Imaging of Cellular Immunotherapy.
KE Murtha, WD Sese, K Sleiman, J Halpage… (2024). Absence of oncomodulin increases susceptibility to noise-induced outer hair cell death and alters mitochondrial morphology.
M Lindman (2024). RIPK3 Regulates Neuroinflammation During Flavivirus Infection of the Central Nervous System.
M Lindman, I Estevez, E Marmut, EM DaPrano… (2024). Astrocytic RIPK3 exerts protective anti-inflammatory activity during viral encephalitis via induction of serpin protease inhibitors.
M Shammas (2024). Mitochondrial Dysfunction and Stress Responses in CHCHD10 Myopathy and Neurodegeneration.
M Xue, QY Chen, W Shi, Z Zhou, X Li, F Xu… (2024). Whole-brain mapping of afferents to the anterior cingulate cortex in adult mice.
S Hall, S Liu, I Liang, S Schulz, C Ezran, M Tan… (2024). Cellular and molecular characterization of peripheral glia in the lung and other organs.
SB Park, G Lur (2024). Repeated exposure to multiple concurrent stressors alters visual processing in the adult posterior parietal cortex.
T Qin, Y Xia, N Nazari, T Sepahvand… (2024). Correlational patterns of neuronal activation and epigenetic marks in the basolateral amygdala and piriform cortex following olfactory threat conditioning and ….
T Sepahvand, SJ Carew, Q Yuan (2024). The ventral hippocampus is activated in olfactory but not auditory threat memory.
TL Dunham, JR Wilkerson, RC Johnson, RL Huganir… (2024). WWC2 modulates GABAA-receptor-mediated synaptic transmission, revealing class-specific mechanisms of synapse regulation by WWC family proteins.
V Nikitin, G Wildenberg, A Mittone… (2024). Laminography as a tool for imaging large-size samples with high resolution.
WR Evans, SS Baskar, ARCE Costa, S Ravoori… (2024). Functional activation of dorsal striatum astrocytes improves movement deficits in hemi-parkinsonian mice.
Y Ge, C Yang, M Zadeh, SM Sprague, YD Lin, HS Jain… (2024). Functional regulation of microglia by vitamin B12 alleviates ischemic stroke-induced neuroinflammation in mice.
Z Zhou, X Yang, A Mao, H Xu, C Lin, M Yang, W Hu… (2024). Deficiency of CAMSAP2 impairs olfaction and the morphogenesis of mitral cells.
A Hall (2023). Analysis of cFos Expression and Microglial Branch Density in a Mouse Model of Trauma-Induced Hyperarousal.
A Maziar, TN Critch, S Ghosh, V Rajani… (2023). Aging differentially affects LTCC function in hippocampal CA1 and piriform cortex pyramidal neurons.
A Sarkar, Y Jin, BC DeFelice, CY Logan, Y Yang… (2023). Intermittent fasting induces rapid hepatocyte proliferation to restore the hepatostat in the mouse liver.
AG Salinas, JO Lee, SM Augustin, S Zhang… (2023). Distinct sub-second dopamine signaling in dorsolateral striatum measured by a genetically-encoded fluorescent sensor.
AML Osse, RS Pandey, RA Wirt, AA Ortiz… (2023). Reduction in GABAB on glia induce Alzheimer's disease related changes.
C Stossel, M Raitses-Gurevich, D Atias, T Beller… (2023). Spectrum of Response to Platinum and PARP Inhibitors in Germline BRCA–Associated Pancreatic Cancer in the Clinical and Preclinical Setting.

C Yang, Z Gong, X Zhang, S Miao, B Li, W Xie… (2023). Neuropeptide Y in the medial habenula alleviates migraine-like behaviors through the Y1 receptor.
CD Walker (2023). Adolescence, Alcohol, and Astrocytes: The Impact of Adolescent Alcohol Use on Astrocyte-Synaptic Interactions, Structure, Function, and Behavior.
CM McCarthy, JM Allardyce, SE Hickey… (2023). Comparison of macroscale and microscale mechanical properties of fresh and fixed-frozen porcine colonic tissue.
D Na, J Zhang, HJ Beaulac… (2023). Increased central auditory gain in 5xFAD Alzheimer's disease mice as an early biomarker candidate for Alzheimer's disease diagnosis.
DB Azizoglu, K Perez, SL Zheng, S Rahman, EY Rim… (2023). Liver size is predetermined in the neonate by adding lobules at the periphery.
DJ Lievano Parra (2023). Effects of the unilateral lesion of the substantia nigra compacta with 6-OHDA on reversal learning and prepulse inhibition in male and female Wistar rats.
J Larochelle, RJ Tishko, C Yang, Y Ge, LT Phan… (2023). Receptor-interacting protein kinase 2 (RIPK2) profoundly contributes to post-stroke neuroinflammation and behavioral deficits with microglia as unique ….
J Sbierski-Kind, KM Cautivo, JC Wagner, MW Dahlgren… (2023). Group 2 innate lymphoid cells constrain type 3/17 lymphocytes in shared stromal niches to restrict liver fibrosis.
J Siewiera, TI McIntyre, KM Cautivo, K Mahiddine… (2023). Circumvention of luteolysis reveals parturition pathways in mice dependent upon innate type 2 immunity.
JA Hatter, MM Scott (2023). Selective ablation of VIP interneurons in the rodent prefrontal cortex results in increased impulsivity.
JC Nawroth, D Roth, A van Schadewijk, A Ravi… (2023). Breathing on chip: Dynamic flow and stretch accelerate mucociliary maturation of airway epithelium in vitro.
JT Ahrendsen, Y Nong, Y Huo, J Steele… (2023). CD8 cytotoxic T-cell infiltrates and cellular damage in the hypothalamus in human obesity.
JY Min, S Park, J Cho, Y Huh (2023). The anterior insular cortex processes social recognition memory.
L Kang, W Yu, Y Zhang, TTW Wong (2023). Automated whole-organ histological imaging assisted with ultraviolet-excited sectioning tomography and deep learning.
L Kang, W Yu, Y Zhang, Z Chen, TTW Wong (2023). Deep Learning Enables Rapid Whole-Organ Histological Imaging with Ultraviolet-Excited Sectioning Tomography.
L Smith-Osborne, A Duong, A Resendez, R Palme… (2023). Female dominance hierarchies influence responses to psychosocial stressors.
LD Quigley, R Pendry, ML Mendoza, BE Pfeiffer… (2023). Experience alters hippocampal and cortical network communication via a KIBRA-dependent mechanism.
M Dorofeikova, CD Borkar, K Weissmuller… (2023). Effects of footshock stress on social behavior and neuronal activation in the medial prefrontal cortex and amygdala of male and female mice.
M Dorofeikova, CE Stelly, A Duong, S Basavanhalli… (2023). The role of genetically distinct central amygdala neurons in appetitive and aversive responding assayed with a novel dual valence operant conditioning paradigm.
M Lindman, JP Angel, I Estevez, NP Chang… (2023). RIPK3 promotes brain region-specific interferon signaling and restriction of tick-borne flavivirus infection.
M Serranilla (2023). Chloride Dysregulation and Impaired Gamma-Amino Butyric Acid Signaling in the Basal Ganglia in Huntington's Disease.
MM Naffaa, RR Khan, CT Kuo, HH Yin (2023). Cortical regulation of neurogenesis and cell proliferation in the ventral subventricular zone.
P Hoffman, MN Svalina, C Flores, C Brzezinski… (2023). Developmental Characterization of Neuronal Migration Anomalies and Axon Proliferation in mTOR pathway-associated Malformations of Cortical Development.
P Liu, A Anandhan, J Chen, A Shakya, M Dodson… (2023). Decreased autophagosome biogenesis, reduced NRF2, and enhanced ferroptotic cell death are underlying molecular mechanisms of non-alcoholic fatty liver ….
R Sim, J Lee, J Chieng, KH Tan, G Lim, A Foo… (2023). Fluorescent Peptide-based Probe for the Detection of Alpha-synuclein Aggregates in the Gut.
S Venkadesh, A Santarelli, T Boesen… (2023). Combinatorial quantification of distinct neural projections from retrograde tracing.
SJ Carew (2023). The smell of fear: comparing the neural ensembles underlying odor fear memory conditioned by innate, inherent, and learned sources of danger.
SM Ramos Rodriguez (2023). An Investigation into Cell-Type Vulnerability for Formation of Alpha-Synuclein Aggregates.

TR Sides, JC Nelson, KN Nwachukwu, J Boston… (2023). The Influence of Arsenic Co-Exposure in a Model of Alcohol-Induced Neurodegeneration in C57BL/6J Mice.
W Donelan, PL Crispen, S Kusmartsev (2023). Tissue Slice Culture and Analysis of Tumor-Associated Hyaluronan in Urothelial Carcinoma.
W Yu (2023). Translational Rapid Ultraviolet-Excited Sectioning Tomography for Whole-Organ Imaging with Subcellular Resolution.
X Chen, DA Wolfe, DS Bindu, M Zhang… (2023). Functional gene delivery to and across brain vasculature of systemic AAVs with endothelial-specific tropism in rodents and broad tropism in primates.
X Fang, JJ Border, PL Rivers, H Zhang, JM Williams… (2023). Amyloid beta accumulation in TgF344-AD rats is associated with reduced cerebral capillary endothelial Kir2. 1 expression and neurovascular uncoupling.
Y Liu, MR Fontenot, A Kulkarni, N Khandelwal… (2023). An extra-circadian function for human CLOCK in the neocortex.
Y Wu, P Li, N Bhat, H Fan, M Liu (2023). Effects of repeated sleep deprivation on brain pericytes in mice.
Z Li, EG Solomonidis, B Berkeley… (2023). Multi-species meta-analysis identifies transcriptional signatures associated with cardiac endothelial responses in the ischaemic heart.
Z Yao, CTJ van Velthoven, M Kunst, M Zhang… (2023). A high-resolution transcriptomic and spatial atlas of cell types in the whole mouse brain.
A Brodovskaya, S Shiono, T Batabyal… (2022). Construction of Local Field Potential Microelectrodes for in vivo Recordings from Multiple Brain Structures Simultaneously.
DJ Rindner, A Proddutur, G Lur (2022). Cell-type-specific integration of feedforward and feedback synaptic inputs in the posterior parietal cortex.
EA Kiffmeyer, JA Cosgrove, JK Siganos, HE Bien… (2022). Deficits in cerebellum-dependent learning and cerebellar morphology in male and female BTBR autism model mice.
ES Norton, LA Whaley, MJ Ulloa-Navas… (2022). Glioblastoma disrupts the ependymal wall and extracellular matrix structures of the subventricular zone.
JD Hahn, L Gao, T Boesen, L Gou… (2022). Macroscale connections of the mouse lateral preoptic area and anterior lateral hypothalamic area.
KM Cautivo, PR Matatia, CO Lizama, NM Mroz… (2022). Interferon gamma constrains type 2 lymphocyte niche boundaries during mixed inflammation.
KN Nwachukwu, DM King, KL Healey… (2022). Sex-specific effects of adolescent intermittent ethanol exposure-induced dysregulation of hippocampal glial cells in adulthood.
KN Nwachukwu, KL Healey, HS Swartzwelder… (2022). The influence of sex on hippocampal neurogenesis and neurotrophic responses on the persistent effects of adolescent intermittent ethanol exposure into adulthood.
L Liu, C Yang, BP Lavayen, RJ Tishko… (2022). Targeted BRD4 protein degradation by dBET1 ameliorates acute ischemic brain injury and improves functional outcomes associated with reduced ….
M Scheibinger, A Janesick, GH Diaz… (2022). Immunohistochemistry and In Situ mRNA detection using inner ear vibratome sections.
MÁ García-Cabezas, JL Hacker… (2022). Homology of neocortical areas in rats and primates based on cortical type analysis: an update of the Hypothesis on the Dual Origin of the Neocortex.
NAL Fayez, E Rouhollahi, CY Ong, J Wu… (2022). Hepatocyte-targeted delivery of imiquimod reduces hepatitis B virus surface antigen.
NAL Fayez, R Böttger, J Brown, E Rouhollahi… (2022). The mechanism of Hepatocyte-Targeting and safety profile of Phospholipid-Free small unilamellar vesicles.
S Milde, GC Brown (2022). Knockout of the P2Y6 Receptor Prevents Peri-Infarct Neuronal Loss after Transient, Focal Ischemia in Mouse Brain.
WE Barclay, N Aggarwal, ME Deerhake, M Inoue… (2022). The AIM2 inflammasome is activated in astrocytes during the late phase of EAE.
Y Zhang, L Kang, IHM Wong, W Dai, X Li… (2022). High-Throughput, Label-Free and Slide-Free Histological Imaging by Computational Microscopy and Unsupervised Learning.
A Farias, A Soto, F Puttur, CJ Goldin, S Sosa, C Gil… (2021). A TLR4 agonist improves immune checkpoint blockade treatment by increasing the ratio of effector to regulatory cells within the tumor microenvironment.
A Hausmann, B Felmy, L Kunz, S Kroon… (2021). Intercrypt sentinel macrophages tune antibacterial NF-κB responses in gut epithelial cells via TNF.
C Yang, BP Lavayen, L Liu, BD Sanz, KM DeMars… (2021). Neurovascular protection by adropin in experimental ischemic stroke through an endothelial nitric oxide synthase-dependent mechanism.

CE Jones, AQ Chau, RJ Olson, C Moore… (2021). Early life sleep disruption alters glutamate and dendritic spines in prefrontal cortex and impairs cognitive flexibility in prairie voles.
F Xu, Y Shen, L Ding, CY Yang, H Tan, H Wang… (2021). High-throughput mapping of a whole rhesus monkey brain at micrometer resolution.
FP Mayer, H Iwamoto, MK Hahn, GJ Grumbar… (2021). There's no place like home? Return to the home cage triggers dopamine release in the mouse nucleus accumbens.
H Hintiryan, I Bowman, DL Johnson… (2021). Connectivity characterization of the mouse basolateral amygdalar complex.
HD Mason, AM Johnson, NA Mihelson, P Mastorakos… (2021). Glia limitans superficialis oxidation and breakdown promote cortical cell death after repetitive head injury.
I Navickaite, N Pauziene, DH Pauza (2021). Anatomical evidence of non-parasympathetic cardiac nitrergic nerve fibres in rat.
J Vogler, R Böttger, NAL Fayez, W Zhang, Z Qin… (2021). Altering the intra-liver distribution of phospholipid-free small unilamellar vesicles using temperature-dependent size-tunability.
J Wie, Z Liu, H Song, TF Tropea, L Yang, H Wang… (2021). A growth-factor-activated lysosomal K+ channel regulates Parkinson's pathology.
KL Elliott, J Kersigo, JH Lee, EN Yamoah… (2021). Sustained Loss of bdnf affects peripheral but not central vestibular targets.
KN Nwachukwu, WA Evans, TR Sides… (2021). Chemogenetic manipulation of astrocytic signaling in the basolateral amygdala reduces binge-like alcohol consumption in male mice.
L Kettler, H Sid, C Schaub, K Lischka… (2021). AP-2δ Expression Kinetics in Multimodal Networks in the Developing Chicken Midbrain.
M Puigdellívol, S Milde, M Spillantini… (2021). The microglial P2Y6 receptor mediates neuronal loss and memory deficits in neurodegeneration.
N Al Fayez, R Bottger, E Rouhollahi… (2021). Improved Liver Delivery of Primaquine by Phospholipid-Free Small Unilamellar Vesicles with Reduced Hemolytic Toxicity.
NL Benavidez, MS Bienkowski, M Zhu… (2021). Organization of the inputs and outputs of the mouse superior colliculus.
P Mastorakos, MV Russo, T Zhou, K Johnson… (2021). Antimicrobial immunity impedes CNS vascular repair following brain injury.
P Mastorakos, N Mihelson, M Luby, SR Burks… (2021). Temporally distinct myeloid cell responses mediate damage and repair after cerebrovascular injury.
PL Rochon, C Theriault, AGR Olguin, A Krishnaswamy (2021). The cell adhesion molecule Sdk1 shapes assembly of a retinal circuit that detects localized edges.
S Milde, FW van Tartwijk, A Vilalta, TC Hornik… (2021). Inflammatory neuronal loss in the substantia nigra induced by systemic lipopolysaccharide is prevented by knockout of the P2Y6 receptor in mice.
SK Bose, BM White, MV Kashyap, A Dave… (2021). In utero adenine base editing corrects multi-organ pathology in a lethal lysosomal storage disease.
SL Reitz, AZ Wasilczuk, GH Beh, A Proekt, MB Kelz (2021). Activation of preoptic tachykinin 1 neurons promotes wakefulness over sleep and volatile anesthetic-induced unconsciousness.
SR Gray, L Ye, JY Ye, M Paukert (2021). Noradrenergic terminal short-term potentiation enables modality-selective integration of sensory input and vigilance state.
YT Liu, DA Sliter, MK Shammas, X Huang, C Wang… (2021). Mt-Keima detects PINK1-PRKN mitophagy in vivo with greater sensitivity than mito-QC.
A Caputo, Y Liang, TD Raabe, A Lo, M Horvath… (2020). Snca-GFP knock-in mice reflect patterns of endogenous expression and pathological seeding.
B Ling, J Lee, D Maresca, A Lee-Gosselin… (2020). Biomolecular ultrasound imaging of phagolysosomal function.
Bracken-Grissom HD, DeLeo DM, Porter ML, Iwanicki T, Sickles J, Frank TM. (2020). Light organ photosensitivity in deep-sea shrimp may suggest a novel role in counterillumination.
CE Jones, PT Wickham, MM Lim (2020). Early life sleep disruption is a risk factor for increased ethanol drinking after acute footshock stress in prairie voles.
E Gonzalez-Fernandez, D Staursky, K Lucas… (2020). 20-HETE enzymes and receptors in the neurovascular unit: implications in cerebrovascular disease.
Lewis TR, Shores CR, Cady MA, Hao Y, Arshavsky VY, Burns ME. (2020). The F220C and F45L rhodopsin mutations identified in retinitis pigmentosa patients do not cause pathology in mice.
Li, Xiufeng; Kang, Lei; Zhang, Yan; Wong, Terence TW; (2020). High-speed Label-free Ultraviolet Photoacoustic Microscopy for Histology-like imaging of unprocessed biological tissues.
MÁ García-Cabezas, JL Hacker… (2020). A protocol for cortical type analysis of the human neocortex applied on histological samples, the atlas of Von Economo and Koskinas, and magnetic ….

NF Nolta, A Liberti, R Makol, M Han (2020). Gelatin embedding and LED autofluorescence reduction for rodent spinal cord histology.

Pozhidayeva DY, SP Farris, CM Goeke, EJ Firsick… (2020). Chronic Chemogenetic Stimulation of the Nucleus Accumbens Produces Lasting Reductions in Binge Drinking and Ameliorates Alcohol-Related Morphological ….

Wang S, Lv W, Zhang H, Liu Y, Li L, Jefferson JR, Guo Y, Li M, Gao W, Fang X, Paul IA, Rajkowska G, Shaffery JP, Mosley TH, Hu X, Liu R, Wang Y, Yu H, Roman RJ, Fan F. (2020). Aging exacerbates impairments of cerebral blood flow autoregulation and cognition in diabetic rats.

Li S, Folkvord JM, Kovacs KJ, Wagstaff RK, Mwakalundwa G, Rendahl AK, Rakasz EG, Connick E, Skinner PJ. (2019). Low levels of SIV-specific CD8+ T cells in germinal centers characterizes acute SIV infection.

Bienkowski MS, Bowman I, Song MY, Gou L, Ard T, Cotter K, Zhu M, Benavidez NL, Yamashita S, Abu-Jaber J, Azam S, Lo D, Foster NN, Hintiryan H, Dong HW. (2018). Integration of gene expression and brain-wide connectivity reveals the multiscale organization of mouse hippocampal networks.

Boldog E, Bakken TE, Hodge RD, Novotny M, Aevermann BD, Baka J, Bordí© S, Close JL, Diez-Fuertes F, Ding SL, Faragí_ N, Kocsis íK, Kovíçcs B, Maltzer Z, McCorrison JM, Miller JA, Molníçr G, Olíçh G, Ozsvíçr A, Rí_zsa M, Shehata SI, Smith KA, Sunkin SM, Tran DN, Venepally P, Wall A, Puskíçs LG, Barzí_ P, Steemers FJ, Schork NJ, Scheuermann RH, Lasken RS, Lein ES, Tamíçs G. (2018). Transcriptomic and morphophysiological evidence for a specialized human cortical GABAergic cell type.

Webb GM, Li S, Mwakalundwa G, Folkvord JM, Greene JM, Reed JS, Stanton JJ, Legasse AW, Hobbs T, Martin LD, Park BS, Whitney JB, Jeng EK, Wong HC, Nixon DF, Jones RB, Connick E, Skinner PJ, Sacha JB. (2018). The human IL-15 superagonist ALT-803 directs SIV-specific CD8(+) T cells into B-cell follicles.

Wong TTW, Zhang R, Zhang C, Hsu HC, Maslov KI, Wang L, Shi J, Chen R, Shung KK, Zhou Q, Wang LV. (2017). Label-free automated three-dimensional imaging of whole organs by microtomy-assisted photoacoustic microscopy.

Garcia I, Bhullar PK, Tepe B, Ortiz-Guzman J, Huang L, Herman AM, Chaboub L, Deneen B, Justice NJ, Arenkiel BR. (2016). Local corticotropin releasing hormone (CRH) signals to its receptor CRHR1 during postnatal development of the mouse olfactory bulb.

Mira MM, Hill RD, Stasolla C. (2016). Phytoglobins Improve Hypoxic Root Growth by Alleviating Apical Meristem Cell Death.

JS Duncan, KL Elliott, J Kersigo, B Gray… (2015). Combining whole-mount in situ hybridization with neuronal tracing and immunohistochemistry.

Haddad-Tí_volli R, Szabí_ NE, Zhou X, Alvarez-Bolado G. (2013). Genetic manipulation of the mouse developing hypothalamus through in utero electroporation.

Haddad-Tí_volli R, Heide M, Zhou X, Blaess S, Alvarez-Bolado G. (2012). Mouse thalamic differentiation: gli-dependent pattern and gli-independent prepattern.

Duncan J, Kersigo J, Gray B, Fritzsch B. (2011). Combining lipophilic dye, in situ hybridization, immunohistochemistry, and histology.

Precision-cut lung slices (PCLS)

K Jankowski, SE Lemay, D Lozano-Ojalvo… (2024). Pharmacological Inhibition of Epac1 Protects against Pulmonary Fibrosis by Blocking FoxO3a Neddylation.

V Veloso-Giménez, C Cárdenas-Calderón… (2024). Oxygenation by Intravascular Photosynthesis Reduces Kidney Damage During ex Vivo Preservation.

C Diaz-Nicieza, L Sahyoun, C Michalaki… (2024). Ageing results in an exacerbated inflammatory response to LPS by resident lung cells.

C Zeng, H Yue, C Wang, X Ju, T Wang, X Fu… (2024). Albendazole ameliorates aerobic glycolysis in myofibroblasts to reverse pulmonary fibrosis.

C Zeng, Q Wang, X Liu, K Wang, C Wang… (2024). Localized administration of Bcar3 siRNA via nano-self-assembly to treat idiopathic pulmonary fibrosis by disrupting macrophage-fibroblast crosstalk.

CL Wilkinson, K Nakano, SA Grimm… (2024). GM-CSF-dependent CD301b+ lung dendritic cells confer tolerance to inhaled allergens.

D Yang, N Almanzar, J Xia, S Udit, ST Yeung… (2024). Vagal TRPV1+ sensory neurons regulate myeloid cell dynamics and protect against influenza virus infection.

DJM Kollareth, AK Sharma (2024). Precision cut lung slices: an innovative tool for lung transplant research.

DW Ahmed, ML Tan, J Gabbard, Y Liu, MM Hu… (2024). Local photo-crosslinking of native tissue matrix regulates cell function.

G Parlakgül, S Pang, LL Artico, N Min… (2024). Spatial mapping of hepatic ER and mitochondria architecture reveals zonated remodeling in fasting and obesity.

H Osman-Ponchet, L Perdigon, M Barthe… (2024). Advances in In Vitro Modeling of Pulmonary Fibrosis: Focus on Precision-Cut Lung Slices (PCLS) Model.
HA Flaxman, MA Chrysovergi, H Han, F Kabir… (2024). Sanglifehrin A mitigates multi-organ fibrosis by targeting the collagen chaperone cyclophilin B.
HM Gomez, TJ Haw, D Ilic, P Robinson… (2024). Landscape fire smoke airway exposure impairs respiratory and cardiac function and worsens experimental asthma.
JD Cala Garcia, CF Arce Deza, AR Waich… (2024). Testing the Viability and Efficacy of Small Molecule Inhibitors in T-cells in Cryopreserved Precision Cut Lung Slices: New Insights for Long Term-storage Lung ….
L Perdigon, M Barthe, H Osman-Ponchet… (2024). Successful Development of Human Precision-Cut Lung Slice (hPCLS) Model for Studying Lung Disease.
M Boucher, C Henry, L Gélinas, R Packwood… (2024). High throughput screening of airway constriction in mouse lung slices.
M Bruegger, C Machahua, B Zumkehr, C Cismaru… (2024). Aging shapes infection profiles of influenza A virus and SARS-CoV-2 in human lung slices.
M Chioccioli, S Liu, S Magruder, A Tata, L Borriello… (2024). Stem cell migration drives lung repair in living mice.
M Lehmann, R Krishnan, J Sucre… (2024). Precision Cut Lung Slices: Emerging Tools for Preclinical and Translational Lung Research. An Official American Thoracic Society Workshop Report.
M Vierhout, A Ayoub, P Ali, V Kumaran, S Naiel… (2024). A Novel Ex Vivo Approach for Investigating Profibrotic Macrophage Polarization Using Murine Precision-Cut Lung Slices.
MB Moor, J Nordström, M Burmakin, M Raki, S Al-Saad… (2024). Comparative analysis of kidney transplantation modeled using precision-cut kidney slices and kidney transplantation in pigs.
ML Cohen, AN Brumwell, TC Ho, K Garakani… (2024). A fibroblast-dependent TGF-β1/sFRP2 noncanonical Wnt signaling axis promotes epithelial metaplasia in idiopathic pulmonary fibrosis.
RE Lee-Ferris, K Okuda, JR Galiger, SA Schworer… (2024). Prolonged airway explant culture enables study of health, disease, and viral pathogenesis.
S Bozzini, E Bozza, C Bagnera… (2024). Assessment of Imatinib Anti-Remodeling Activity on a Human Precision Cut Lung Slices Model.
SE Lemay, MS Montesinos, Y Grobs, T Yokokawa… (2024). Exploring Integrin α5β1 as a Potential Therapeutic Target for Pulmonary Arterial Hypertension: Insights from Comprehensive Multicenter Preclinical Studies.
SM Lingamallu, A Deshpande, N Joy, K Ganeshan… (2024). Neuroepithelial bodies and terminal bronchioles are niches for distinctive club cells that repair the airways following acute notch inhibition.
SS Cheong, TC Luis, M Hind, CH Dean (2024). A Novel Method for Floxed Gene Manipulation Using TAT-Cre Recombinase in Ex Vivo Precision-Cut Lung Slices (PCLS).
T Duparc, E Gore, G Combes, D Beuzelin, JP Da Silva… (2024). P2Y13 receptor deficiency favors adipose tissue lipolysis and worsens insulin resistance and fatty liver disease.
UN Wasko, J Jiang, TC Dalton, A Curiel-Garcia… (2024). Tumor-selective activity of RAS-GTP inhibition in pancreatic cancer.
A Lazrak, W Song, Z Yu, S Zhang, A Nellore… (2023). Low molecular weight hyaluronan inhibits lung epithelial ion channels by activating the calcium-sensing receptor.
A Urso (2023). Pathophysiology of bile acid aspiration in lung transplant recipients.
AJ Heires, D Samuelson, D Villageliu, TM Nordgren… (2023). Agricultural dust derived bacterial extracellular vesicle mediated inflammation is attenuated by DHA.
AR Decker (2023). Using toxin-producing bacteria to treat explants and autochthonous mouse models of pancreatic cancer.
C Zeng, Q Wang, C Wang, Q Zhou, X Fu, J Yu, W Xiong… (2023). Local Delivery of Bcar3 siRNA by Nano-Self-Assembly for Treating Pulmonary Fibrosis via Blocking the Interaction of Macrophages and Fibroblasts.
D Cervantes, N Schaunaman, GP Downey… (2023). Desert particulate matter from Afghanistan increases airway obstruction in human distal lungs exposed to type 2 cytokine IL-13.
E Charrin, D Dabaghie, I Sen, D Unnersjö-Jess… (2023). Soluble Klotho protects against glomerular injury through regulation of ER stress response.
EB Gebski, V Parikh, H Lam, N Kim… (2023). Rhinovirus C15 attenuates relaxation and cAMP production in Human Airways and smooth muscle.
F Ahangari, NL Price, S Malik, M Chioccioli… (2023). microRNA-33 deficiency in macrophages enhances autophagy, improves mitochondrial homeostasis, and protects against lung fibrosis.
H Agraval, T Crue, N Schaunaman, M Numata… (2023). Electronic Cigarette Exposure Increases the Severity of Influenza a Virus Infection via TRAIL Dysregulation in Human Precision-Cut Lung Slices.
KL Leiby, Y Yuan, R Ng, MSB Raredon… (2023). Rational engineering of lung alveolar epithelium.

M Elshani, IH Um, S Leung, PA Reynolds, A Chapman… (2023). Transcription factor NFE2L1 decreases in glomerulonephropathies after podocyte damage.
M Lam, E Lamanna, L Organ, C Donovan… (2023). Perspectives on precision cut lung slices—powerful tools for investigation of mechanisms and therapeutic targets in lung diseases.
MCF Llerena (2023). Participación del canal de cloruro activado por calcio (tmem16a) en la contracción inducida por atp en células musculares lisas de venas intrapulmonares de rata.
P Yadav, JG Ortega, W Tamaki, C Chien, K Chang… (2023). Macrophage-fibroblast crosstalk drives Arg1-dependent lung fibrosis via ornithine loading.
R Joulia, F Puttur, H Stölting, LJ Entwistle, A Voitovich… (2023). Adventitial Mast Cell Activation Disrupts Endothelial Cell/Pericyte Interactions During Early Life Allergic Asthma.
S Ahn, H Maarsingh, JKL Walker… (2023). Allosteric modulator potentiates β2AR agonist-promoted bronchoprotection in asthma models.
S Naiel, N Dowdall, SD Revill, V Kumaran… (2023). Reprogramming Rogue Macrophages: Yeast Beta-glucan Microparticles as a Macrophage Modulator for Lung Fibrosis.
S Uribe, PD Yim, JF Perez-Zoghbi (2023). Airway Smooth Muscle Relaxation Via Opsin 3 Activation With Beta-carotene Metabolites.
SN Sveiven, SY Kim, V Barrientos, J Li… (2023). Myeloid-and epithelial-derived RELMα contribute to tissue repair following lung helminth infection.
SS Cheong, TC Luis, M Stewart… (2023). A method for TAT-Cre recombinase-mediated floxed allele modification in ex vivo tissue slices.
T Crue, GY Lee, JY Peng, N Schaunaman… (2023). Single cell RNA-sequencing of human precision-cut lung slices: A novel approach to study the effect of vaping and viral infection on lung health.
UN Wasko, J Jiang, A Curiel-Garcia, Y Wang, B Lee… (2023). Tumor-selective effects of active RAS inhibition in pancreatic ductal adenocarcinoma.
Y Cui, Z Yang, Z Lv, J Lei (2023). Disruption of extracellular redox balance drives persistent lung fibrosis and impairs fibrosis resolution.
Z Han, JS Rao, S Ramesh, J Hergesell… (2023). Model-Guided Design and Optimization of CPA Perfusion Protocols for Whole Organ Cryopreservation.
Z Zeng, M Cheng, M Li, T Wang, F Wen… (2023). Inherent differences of small airway contraction and Ca2+ oscillations in airway smooth muscle cells between BALB/c and C57BL/6 mouse strains.
C Michalaki, C Dean, C Johansson (2022). The Use of Precision-Cut Lung Slices for Studying Innate Immunity to Viral Infections.
CM McCarthy, JM Allardyce, SE Hickey… (2022). Comparison of macroscale and microscale mechanical properties of fresh and fixed-frozen porcine colonic tissue.
D Shrestha, N Massey, SM Bhat… (2022). Nrf2 Activation Protects Against Organic Dust and Hydrogen Sulfide Exposure Induced Epithelial Barrier Loss and K. pneumoniae Invasion.
J Ko, M Wilkovitsch, J Oh, RH Kohler, E Bolli… (2022). Spatiotemporal multiplexed immunofluorescence imaging of living cells and tissues with bioorthogonal cycling of fluorescent probes.
JF Perez-Zoghbi, DR Sajorda, DA Webb… (2022). Imidazobenzodiazepine PI320 Relaxes Mouse Peripheral Airways by Inhibiting Calcium Mobilization.
M Chioccioli, S Roy, R Newell, L Pestano, B Dickinson… (2022). A lung targeted miR-29 Mimic as a Therapy for Pulmonary Fibrosis.
R Guidi, D Xu, DF Choy, TR Ramalingam… (2022). Steroid-induced fibroblast growth factors drive an epithelial-mesenchymal inflammatory axis in severe asthma.
SA Guler, C Machahua, TK Geiser, G Kocher… (2022). Dehydroepiandrosterone in fibrotic interstitial lung disease: a translational study.
E Luković, JF Perez-Zoghbi, Y Zhang… (2021). Ginger metabolites and metabolite-inspired synthetic products modulate intracellular calcium and relax airway smooth muscle.
H Maarsingh, A Oldenburger, B Han, AB Zuidhof… (2021). Effects of (a Combination of) the Beta2-Adrenoceptor Agonist Indacaterol and the Muscarinic Receptor Antagonist Glycopyrrolate on Intrapulmonary Airway ….
M Sponchiado, YS Liao, KR Atanasova… (2021). Overexpression of substance P in pig airways increases MUC5AC through an NF-kβ pathway.
N Aggarwal, ME Deerhake, D DiPalma, SK Shahi… (2021). Secreted osteopontin from CD4+ T cells limits acute graft-versus-host disease.

P Lu, J Chen, C Zhang, D Saur, CE Baer… (2021). Oscillating calcium signals in smooth muscle cells underlie the persistent basal tone of internal anal sphincter.
P Lu, MK ElMallah, Z Liu, C Wu, J Chen… (2021). Genetic deletion of the Tas2r143/Tas2r135/Tas2r126 cluster reveals that TAS2Rs may not mediate bitter tastant-induced bronchodilation.
R Basoalto, LF Damiani, MC Bachmann… (2021). Acute lung injury secondary to hydrochloric acid instillation induces small airway hyperresponsiveness.
SY Kim, R Mongey, P Wang, S Rothery, DCA Gaboriau… (2021). The acid injury and repair (AIR) model: A novel ex-vivo tool to understand lung repair.
YN Dong, FC Hsu, CJ Koziol-White, V Stepanova… (2021). Functional NMDA receptors are expressed by human pulmonary artery smooth muscle cells.
Alsafadi HN, Uhl FE, Pineda RH, Bailey KE, Rojas M, Wagner DE, Kí_nigshoff M. (2020). Applications and Approaches for Three-Dimensional Precision-Cut Lung Slices. Disease Modeling and Drug Discovery.
Branchett WJ, Stí_lting H, Oliver RA, Walker SA, Puttur F, Gregory LG, Gabryçovíç L, Wilson MS, O'Garra A, Lloyd CM. (2020). A T cell-myeloid IL-10 axis regulates pathogenic IFN-'_-dependent immunity in a mouse model of type 2-low asthma.
Bryson KJ, Garrido D, Esposito M, McLachlan G, Digard P, Schouler C, Guabiraba R, Trapp S, Vervelde L. (2020). Precision cut lung slices: a novel versatile tool to examine host-pathogen interaction in the chicken lung.
Dragunas G, Woest ME, Nijboer S, Bos ST, van Asselt J, de Groot AP, Vohlí_dalovíç E, Vermeulen CJ, Ditz B, Vonk JM, Koppelman GH, van den Berge M, Ten Hacken NHT, Timens W, Munhoz CD, Prakash YS, Gosens R, Kistemaker LEM. (2020). Cholinergic neuroplasticity in asthma driven by TrkB signaling.
Entwistle LJ, Puttur F, Gregory LG, Lloyd CM. (2020). Group 2 ILC Functional Assays in Allergic Airway Inflammation.
Heras AF, Veerappan A, Silver RB, Emala CW, Worgall TS, Perez-Zoghbi J, Worgall S. (2020). Increasing Sphingolipid Synthesis Alleviates Airway Hyperreactivity.
J Huang, H Lam, C Koziol-White… (2020). The odorant receptor OR2W3 on airway smooth muscle evokes bronchodilation via a cooperative chemosensory tradeoff between TMEM16A and CFTR.
Koziol-White C, Johnstone TB, Corpuz ML, Cao G, Orfanos S, Parikh V, Deeney B, Tliba O, Ostrom RS, Dainty I, Panettieri RA Jr. (2020). Budesonide enhances agonist-induced bronchodilation in human small airways by increasing cAMP production in airway smooth muscle.
Koziol-White CJ, Ghosh A, Sandner P, Erzurum SE, Stuehr DJ, Panettieri RA Jr. (2020). Soluble Guanylate Cyclase Agonists Induce Bronchodilation in Human Small Airways.
Li G, Cohen JA, Martines C, Ram-Mohan S, Brain JD, Krishnan R, Ai X, Bai Y. (2020). Preserving Airway Smooth Muscle Contraction in Precision-Cut Lung Slices.
Lu RA, Zeki AA, Ram-Mohan S, Nguyen N, Bai Y, Chmiel K, Pecic S, Ai X, Krishnan R, Ghosh CC. (2020). Inhibiting Airway Smooth Muscle Contraction Using Pitavastatin: A Role for the Mevalonate Pathway in Regulating Cytoskeletal Proteins.
Parikh V, Scala J, Patel R, Corbi C, Lo D, Bochkov YA, Kennedy JL, Kurten RC, Liggett SB, Gern JE, Koziol-White CJ. (2020). Rhinovirus C15 Induces Airway Hyperresponsiveness via Calcium Mobilization in Airway Smooth Muscle.
Poole JA, Nordgren TM, Heires AJ, Nelson AJ, Katafiasz D, Bailey KL, Romberger DJ. (2020). Amphiregulin modulates murine lung recovery and fibroblast function following exposure to agriculture organic dust.
Ram-Mohan S, Bai Y, Schaible N, Ehrlicher AJ, Cook DP, Suki B, Stoltz DA, Solway J, Ai X, Krishnan R. (2020). Tissue traction microscopy to quantify muscle contraction within precision-cut lung slices.
S Xu-Vanpala, ME Deerhake, JD Wheaton… (2020). Functional heterogeneity of alveolar macrophage population based on expression of CXCL2.
SS Cheong, KM Akram, C Matellan, SY Kim… (2020). The planar polarity component VANGL2 is a key regulator of mechanosignaling.
SU Hettiarachchi, YH Li, J Roy, F Zhang… (2020). Targeted inhibition of PI3 kinase/mTOR specifically in fibrotic lung fibroblasts suppresses pulmonary fibrosis in experimental models.
SY Kim, R Mongey, M Griffiths, M Hind… (2020). An Ex Vivo Acid Injury and Repair (AIR) Model Using Precision-Cut Lung Slices to Understand Lung Injury and Repair.
Shrestha S, Cho W, Stump B, Imani J, Lamattina AM, Louis PH, Pazzanese J, Rosas IO, Visner G, Perrella MA, El-Chemaly S. (2020). FK506 induces lung lymphatic endothelial cell senescence and downregulates LYVE-1 expression, with associated decreased hyaluronan uptake.
Urso A, D'Ovidio F, Xu D, Emala CW Sr, Bunnett NW, Perez-Zoghbi JF. (2020). Bile acids inhibit cholinergic constriction in proximal and peripheral airways from humans and rodents.
van den Berg M, Nijboer-Brinksma S, Bos S, van den Berge M, Lamb D, van Faassen M, Kema I, Gosens R, Kistemaker L. (2020). The novel TRPA1 antagonist BI01305834 inhibits ovalbumin-induced bronchoconstriction in guinea pigs.

van den Berg MPM, Kurhade SH, Maarsingh H, Erceg S, Hulsbeek IR, Boekema PH, Kistemaker LEM, van Faassen M, Kema IP, Elsinga PH, Dí_mling A, Meurs H, Gosens R. (2020). Pharmacological Screening Identifies SHK242 and SHK277 as Novel Arginase Inhibitors with Efficacy against Allergen-Induced Airway Narrowing In Vitro and In Vivo.

Akram KM, Yates LL, Mongey R, Rothery S, Gaboriau DCA, Sanderson J, Hind M, Griffiths M, Dean CH. (2019). Live imaging of alveologenesis in precision-cut lung slices reveals dynamic epithelial cell behaviour.

Amarelle L, Katzen J, Shigemura M, Welch LC, Cajigas H, Peteranderl C, Celli D, Herold S, Lecuona E, Sznajder JI. (2019). Cardiac glycosides decrease influenza virus replication by inhibiting cell protein translational machinery.

Brann KR, Fullerton MS, Onyilagha FI, Prince AA, Kurten RC, Rom JS, Blevins JS, Smeltzer MS, Voth DE. (2019). Infection of Primary Human Alveolar Macrophages Alters Staphylococcus aureus Toxin Production and Activity.

Bui CB, Kolodziej M, Lamanna E, Elgass K, Sehgal A, Rudloff I, Schwenke DO, Tsuchimochi H, Kroon MAGM, Cho SX, Maksimenko A, Cholewa M, Berger PJ, Young MJ, Bourke JE, Pearson JT, Nold MF, Nold-Petry CA. (2019). Interleukin-1 Receptor Antagonist Protects Newborn Mice Against Pulmonary Hypertension.

Dragan AL, Kurten RC, Voth DE. (2019). Characterization of Early Stages of Human Alveolar Infection by the Q Fever Agent Coxiella burnetii.

KM Akram, LL Yates, R Mongey, S Rothery… (2019). Time-lapse imaging of alveologenesis in mouse precision-cut lung slices.

Kennedy JL, Kurten RC, McCullough S, Panettieri RA, Koziol-White C, Jones SM, Caid K, Gill PS, Roberts D, Jaeschke H, McGill MR, James L. (2019). Acetaminophen is both bronchodilatory and bronchoprotective in human precision cut lung slice airways.

Maarsingh H, Bidan CM, Brook BS, Zuidhof AB, Elzinga CRS, Smit M, Oldenburger A, Gosens R, Timens W, Meurs H. (2019). Small airway hyperresponsiveness in COPD: relationship between structure and function in lung slices.

Mikami M, Perez-Zoghbi JF, Zhang Y, Emala CW Sr. (2019). Attenuation of murine and human airway contraction by a peptide fragment of the cytoskeleton regulatory protein gelsolin.

Puttur F, Denney L, Gregory LG, Vuononvirta J, Oliver R, Entwistle LJ, Walker SA, Headley MB, McGhee EJ, Pease JE, Krummel MF, Carlin LM, Lloyd CM. (2019). Pulmonary environmental cues drive group 2 innate lymphoid cell dynamics in mice and humans.

Singh BK, Lu W, Schmidt Paustian AM, Ge MQ, Koziol-White CJ, Flayer CH, Killingbeck SS, Wang N, Dong X, Riese MJ, Deshpande DA, Panettieri RA Jr, Haczku A, Kambayashi T. (2019). Diacylglycerol kinase Zeta promotes allergic airway inflammation and airway hyperresponsiveness through distinct mechanisms.

Wang W, Cohen JA, Wallrapp A, Trieu KG, Barrios J, Shao F, Krishnamoorthy N, Kuchroo VK, Jones MR, Fine A, Bai Y, Ai X. (2019). Age-Related Dopaminergic Innervation Augments T Helper 2-Type Allergic Inflammation in the Postnatal Lung.

Yim PD, Gallos G, Perez-Zoghbi JF, Zhang Y, Xu D, Wu A, Berkowitz DE, Emala CW. (2019). Airway smooth muscle photorelaxation via opsin receptor activation.

Yocum GT, Perez-Zoghbi JF, Danielsson J, Kuforiji AS, Zhang Y, Li G, Rashid Roni MS, Kodali R, Stafford DC, Arnold LA, Cook JM, Emala CW Sr. (2019). A novel GABA(A) receptor ligand MIDD0301 with limited blood-brain barrier penetration relaxes airway smooth muscle ex vivo and in vivo.

Buttrick TS, Wang W, Yung C, Trieu KG, Patel K, Khoury SJ, Ai X, Elyaman W. (2018). Foxo1 Promotes Th9 Cell Differentiation and Airway Allergy.

Chen J, Miller M, Unno H, Rosenthal P, Sanderson MJ, Broide DH. (2018). Orosomucoid-like 3 (ORMDL3) upregulates airway smooth muscle proliferation, contraction, and Ca(2+) oscillations in asthma.

Henriquez M, Fonseca M, Perez-Zoghbi JF. (2018). Purinergic receptor stimulation induces calcium oscillations and smooth muscle contraction in small pulmonary veins.

Kennedy JL, Koziol-White CJ, Jeffus S, Rettiganti MR, Fisher P, Kurten M, Eze A, House S, Sikes JD, Askew E, Putt C, Panettieri RA, Jones SM, Kurten RC. (2018). Effects of rhinovirus 39 infection on airway hyperresponsiveness to carbachol in human airways precision cut lung slices.

Lyons-Cohen MR, Nakano H, Thomas SY, Cook DN. (2018). Imaging Precision-Cut Lung Slices to Visualize Leukocyte Localization and Trafficking.

Nordgren TM, Heires AJ, Bailey KL, Katafiasz DM, Toews ML, Wichman CS, Romberger DJ. (2018). Docosahexaenoic acid enhances amphiregulin-mediated bronchial epithelial cell repair processes following organic dust exposure.

Shalaby KH, Lyons-Cohen MR, Whitehead GS, Thomas SY, Prinz I, Nakano H, Cook DN. (2018). Pathogenic T(H)17 inflammation is sustained in the lungs by conventional dendritic cells and Toll-like receptor 4 signaling.

Shigemura M, Lecuona E, Angulo M, Homma T, Rodrí_guez DA, Gonzalez-Gonzalez FJ, Welch LC, Amarelle L, Kim SJ, Kaminski N, Budinger GRS, Solway J, Sznajder JI. (2018). Hypercapnia increases airway smooth muscle contractility via caspase-7-mediated miR-133a-RhoA signaling.

Thomas SY, Whitehead GS, Takaku M, Ward JM, Xu X, Nakano K, Lyons-Cohen MR, Nakano H, Gowdy KM, Wade PA, Cook DN. (2018). MyD88-dependent dendritic and epithelial cell crosstalk orchestrates immune responses to allergens.

Barrios J, Patel KR, Aven L, Achey R, Minns MS, Lee Y, Trinkaus-Randall VE, Ai X. (2017). Early life allergen-induced mucus overproduction requires augmented neural stimulation of pulmonary neuroendocrine cell secretion.
Chen J, Sanderson MJ. (2017). Store-operated calcium entry is required for sustained contraction and Ca2+ oscillations of airway smooth muscle.
EJ Yoo, G Cao, CJ Koziol-White… (2017). Gα12 facilitates shortening in human airway smooth muscle by modulating phosphoinositide 3-kinase-mediated activation in a RhoA-dependent manner.
Kistemaker LEM, Oenema TA, Baarsma HA, Bos IST, Schmidt M, Facchinetti F, Civelli M, Villetti G, Gosens R. (2017). The PDE4 inhibitor CHF-6001 and LAMAs inhibit bronchoconstriction-induced remodeling in lung slices.
Lyons-Cohen MR, Thomas SY, Cook DN, Nakano H. (2017). Precision Cut Mouse Lung Slices to Visualize Live Pulmonary Dendritic Cells.
Poobalasingam T, Yates LL, Walker SA, Pereira M, Gross NY, Ali A, Kolatsi-Joannou M, Jarvelin MR, Pekkanen J, Papakrivopoulou E, Long DA, Griffiths M, Wagner D, Kí_nigshoff M, Hind M, Minelli C, Lloyd CM, Dean CH. (2017). Heterozygous Vangl2(Looptail) mice reveal novel roles for the planar cell polarity pathway in adult lung homeostasis and repair.
Rosner SR, Pascoe CD, Blankman E, Jensen CC, Krishnan R, James AL, Elliot JG, Green FH, Liu JC, Seow CY, Park JA, Beckerle MC, Parí© PD, Fredberg JJ, Smith MA. (2017). The actin regulator zyxin reinforces airway smooth muscle and accumulates in airways of fatal asthmatics.
Van Dijk EM, Culha S, Menzen MH, Bidan CM, Gosens R. (2017). Elastase-Induced Parenchymal Disruption and Airway Hyper Responsiveness in Mouse Precision Cut Lung Slices: Toward an Ex vivo COPD Model.
Velalopoulou A, Chatterjee S, Pietrofesa RA, Koziol-White C, Panettieri RA, Lin L, Tuttle S, Berman A, Koumenis C, Christofidou-Solomidou M. (2017). Synthetic Secoisolariciresinol Diglucoside (LGM2605) Protects Human Lung in an Ex Vivo Model of Proton Radiation Damage.
Yocum GT, Chen J, Choi CH, Townsend EA, Zhang Y, Xu D, Fu XW, Sanderson MJ, Emala CW. (2017). Role of transient receptor potential vanilloid 1 in the modulation of airway smooth muscle tone and calcium handling.
Yoo EJ, Cao G, Koziol-White CJ, Ojiaku CA, Sunder K, Jude JA, Michael JV, Lam H, Pushkarsky I, Damoiseaux R, Di Carlo D, Ahn K, An SS, Penn RB, Panettieri RA Jr. (2017). G-alpha(12) facilitates shortening in human airway smooth muscle by modulating phosphoinositide 3-kinase-mediated activation in a RhoA-dependent manner.
Abdulnour RE, Sham HP, Douda DN, Colas RA, Dalli J, Bai Y, Ai X, Serhan CN, Levy BD. (2016). Aspirin-triggered resolvin D1 is produced during self-resolving gram-negative bacterial pneumonia and regulates host immune responses for the resolution of lung inflammation.
Bai Y, Krishnamoorthy N, Patel KR, Rosas I, Sanderson MJ, Ai X. (2016). Cryopreserved Human Precision-Cut Lung Slices as a Bioassay for Live Tissue Banking. A Viability Study of Bronchodilation with Bitter-Taste Receptor Agonists.
Carr R 3rd, Koziol-White C, Zhang J, Lam H, An SS, Tall GG, Panettieri RA Jr, Benovic JL. (2016). Interdicting Gq Activation in Airway Disease by Receptor-Dependent and Receptor-Independent Mechanisms.
Cook DP, Rector MV, Bouzek DC, Michalski AS, Gansemer ND, Reznikov LR, Li X, Stroik MR, Ostedgaard LS, Abou Alaiwa MH, Thompson MA, Prakash YS, Krishnan R, Meyerholz DK, Seow CY, Stoltz DA. (2016). Cystic Fibrosis Transmembrane Conductance Regulator in Sarcoplasmic Reticulum of Airway Smooth Muscle. Implications for Airway Contractility.
Eleftheriadis N, Poelman H, Leus NGJ, Honrath B, Neochoritis CG, Dolga A, Dí_mling A, Dekker FJ. (2016). Design of a novel thiophene inhibitor of 15-lipoxygenase-1 with both anti-inflammatory and neuroprotective properties.
Ghosh A, Koziol-White CJ, Asosingh K, Cheng G, Ruple L, Groneberg D, Friebe A, Comhair SA, Stasch JP, Panettieri RA Jr, Aronica MA, Erzurum SC, Stuehr DJ. (2016). Soluble guanylate cyclase as an alternative target for bronchodilator therapy in asthma.
Graham JG, Winchell CG, Kurten RC, Voth DE. (2016). Development of an Ex Vivo Tissue Platform To Study the Human Lung Response to Coxiella burnetii.
Hiorns JE, Bidan CM, Jensen OE, Gosens R, Kistemaker LE, Fredberg JJ, Butler JP, Krishnan R, Brook BS. (2016). Airway and Parenchymal Strains during Bronchoconstriction in the Precision Cut Lung Slice.
Koziol-White CJ, Jia Y, Baltus GA, Cooper PR, Zaller DM, Crackower MA, Sirkowski EE, Smock S, Northrup AB, Himes BE, Alves SE, Panettieri RA Jr. (2016). Inhibition of spleen tyrosine kinase attenuates IgE-mediated airway contraction and mediator release in human precision cut lung slices.
Koziol-White CJ, Yoo EJ, Cao G, Zhang J, Papanikolaou E, Pushkarsky I, Andrews A, Himes BE, Damoiseaux RD, Liggett SB, Di Carlo D, Kurten RC, Panettieri RA Jr. (2016). Inhibition of PI3K promotes dilation of human small airways in a rho kinase-dependent manner.
Lam M, Royce SG, Donovan C, Jelinic M, Parry LJ, Samuel CS, Bourke JE. (2016). Serelaxin Elicits Bronchodilation and Enhances β-Adrenoceptor-Mediated Airway Relaxation.

Royce SG, Nold MF, Bui C, Donovan C, Lam M, Lamanna E, Rudloff I, Bourke JE, Nold-Petry CA. (2016). Airway Remodeling and Hyperreactivity in a Model of Bronchopulmonary Dysplasia and Their Modulation by IL-1 Receptor Antagonist.
Schepelmann M, Yarova PL, Lopez-Fernandez I, Davies TS, Brennan SC, Edwards PJ, Aggarwal A, Graí_a J, Rietdorf K, Matchkov V, Fenton RA, Chang W, Krssak M, Stewart A, Broadley KJ, Ward DT, Price SA, Edwards DH, Kemp PJ, Riccardi D. (2016). The vascular Ca2+-sensing receptor regulates blood vessel tone and blood pressure.
Watson CY, Damiani F, Ram-Mohan S, Rodrigues S, de Moura Queiroz P, Donaghey TC, Rosenblum Lichtenstein JH, Brain JD, Krishnan R, Molina RM. (2016). Screening for Chemical Toxicity Using Cryopreserved Precision Cut Lung Slices.
Danielsson J, Perez-Zoghbi J, Bernstein K, Barajas MB, Zhang Y, Kumar S, Sharma PK, Gallos G, Emala CW. (2015). Antagonists of the TMEM16A calcium-activated chloride channel modulate airway smooth muscle tone and intracellular calcium.
Eleftheriadis N, Neochoritis CG, Leus NG, van der Wouden PE, Dí_mling A, Dekker FJ. (2015). Rational Development of a Potent 15-Lipoxygenase-1 Inhibitor with in Vitro and ex Vivo Anti-inflammatory Properties.
Gallos G, Yocum GT, Siviski ME, Yim PD, Fu XW, Poe MM, Cook JM, Harrison N, Perez-Zoghbi J, Emala CW Sr. (2015). Selective targeting of the α5-subunit of GABAA receptors relaxes airway smooth muscle and inhibits cellular calcium handling.
Aven L, Paez-Cortez J, Achey R, Krishnan R, Ram-Mohan S, Cruikshank WW, Fine A, Ai X. (2014). An NT4/TrkB-dependent increase in innervation links early-life allergen exposure to persistent airway hyperreactivity.
Cao P, Tan X, Donovan G, Sanderson MJ, Sneyd J. (2014). A deterministic model predicts the properties of stochastic calcium oscillations in airway smooth muscle cells.
Rietdorf K, Bootman MD, Sanderson MJ. (2014). Spontaneous, pro-arrhythmic calcium signals disrupt electrical pacing in mouse pulmonary vein sleeve cells.
Rosner SR, Ram-Mohan S, Paez-Cortez JR, Lavoie TL, Dowell ML, Yuan L, Ai X, Fine A, Aird WC, Solway J, Fredberg JJ, Krishnan R. (2014). Airway contractility in the precision-cut lung slice after cryopreservation.
Tan X, Sanderson MJ. (2014). Bitter tasting compounds dilate airways by inhibiting airway smooth muscle calcium oscillations and calcium sensitivity.
Castro-Piedras I, Perez-Zoghbi JF. (2013). Hydrogen sulphide inhibits Ca2+ release through InsP3 receptors and relaxes airway smooth muscle.
Goldklang MP, Perez-Zoghbi JF, Trischler J, Nkyimbeng T, Zakharov SI, Shiomi T, Zelonina T, Marks AR, D'Armiento JM, Marx SO. (2013). Treatment of experimental asthma using a single small molecule with anti-inflammatory and BK channel-activating properties.
Mukherjee S, Trice J, Shinde P, Willis RE, Pressley TA, Perez-Zoghbi JF. (2013). Ca2+ oscillations, Ca2+ sensitization, and contraction activated by protein kinase C in small airway smooth muscle.
Oenema TA, Maarsingh H, Smit M, Groothuis GM, Meurs H, Gosens R. (2013). Bronchoconstriction Induces TGF-β Release and Airway Remodelling in Guinea Pig Lung Slices.
Weidinger A, Dungel P, Perlinger M, Singer K, Ghebes C, Duvigneau JC, Mí_llebner A, Schí_fer U, Redl H, Kozlov AV. (2013). Experimental data suggesting that inflammation mediated rat liver mitochondrial dysfunction results from secondary hypoxia rather than from direct effects of inflammatory mediators.
Yim PD, Gallos G, Perez-Zoghbi JF, Trice J, Zhang Y, Siviski M, Sonett J, Emala CW Sr. (2013). Chloride channel blockers promote relaxation of TEA-induced contraction in airway smooth muscle.
Sanderson MJ. (2011). Exploring lung physiology in health and disease with lung slices.
Ressmeyer AR, Bai Y, Delmotte P, Uy KF, Thistlethwaite P, Fraire A, Sato O, Ikebe M, Sanderson MJ. (2010). Human airway contraction and formoterol-induced relaxation is determined by Ca2+ oscillations and Ca2+ sensitivity.

Slice culture

A Charli, J Luo, B Palanisamy, E Malovic, Z Riyaz… (2024). Mitochondrial Stress Disassembles Nuclear Architecture through Proteolytic Activation of PKCδ and Lamin B1 Phosphorylation in Neuronal Cells: Implications for ….
CTJ van Velthoven, Y Gao, M Kunst, C Lee… (2024). The transcriptomic and spatial organization of telencephalic GABAergic neuronal types.
DL Wise, SB Greene, Y Escobedo-Lozoya… (2024). Progressive circuit hyperexcitability in mouse neocortical slice cultures with increasing duration of activity silencing.
DL Wise, Y Escobedo-Lozoya, V Valakh, B Isaac… (2024). Prolonged Activity Deprivation Causes Pre-and Postsynaptic Compensatory Plasticity at Neocortical Excitatory Synapses.
L Wang, D Hu, J Xu, J Hu… (2024). Complex in vitro model: A transformative model in drug development and precision medicine.

L Yang, LZ Fang, MR Lynch, CS Xu, H Hahm, Y Zhang… (2024). Transcriptomic landscape of mammalian ventral pallidum at single-cell resolution.
SS Adel, ZJ Pranske, TF Kowalski, N Kanzler… (2024). Plexin-B1 and Plexin-B2 play non-redundant roles in GABAergic synapse formation.
D Bezwada, NP Lesner, B Brooks, HS Vu, Z Wu, L Cai… (2023). Mitochondrial metabolism in primary and metastatic human kidney cancers.
H Ruiz-Garcia, N Zarco, F Watanabe… (2023). Development of Experimental Three-Dimensional Tumor Models to Study Glioblastoma Cancer Stem Cells and Tumor Microenvironment.
JK Mich, S Sunil, N Johansen, RA Martinez, M Leytze… (2023). Enhancer-AAVs allow genetic access to oligodendrocytes and diverse populations of astrocytes across species.
M do Carmo Greier, A Runge, J Dudas… (2023). Optimizing culturing conditions in patient derived 3D primary slice cultures of head and neck cancer.
SS Adel, VRJ Clarke, A Evans-Strong, J Maguire… (2023). Semaphorin 4D induced inhibitory synaptogenesis decreases epileptiform activity and alters progression to Status Epilepticus in mice.
V Nickl, J Eck, N Goedert, J Hübner, T Nerreter… (2023). Characterization and Optimization of the Tumor Microenvironment in Patient-Derived Organotypic Slices and Organoid Models of Glioblastoma.
V Valakh, D Wise, XA Zhu, M Sha, J Fok… (2023). A transcriptional constraint mechanism limits the homeostatic response to activity deprivation in mammalian neocortex.
YF Yazicioglu, E Marin, HF Andrew, K Bentkowska… (2023). Asparagine availability controls B cell homeostasis.
K Kersten, KH Hu, AJ Combes, B Samad, T Harwin… (2022). Spatiotemporal co-dependency between macrophages and exhausted CD8+ T cells in cancer.
N Deshet-Unger, G Horn, M Rawet-Slobodkin, T Waks… (2022). Comparing Intraperitoneal and Intravenous Personalized ErbB2CAR-T for the Treatment of Epithelial Ovarian Cancer.
N Gavert, Y Zwang, R Weiser, O Greenberg, S Halperin… (2022). Ex vivo organotypic cultures for synergistic therapy prioritization identify patient-specific responses to combined MEK and Src inhibition in colorectal cancer.
TIH Park, LCD Smyth, M Aalderink, ZR Woolf… (2022). Routine culture and study of adult human brain cells from neurosurgical specimens.
V Nickl, E Schulz, E Salvador, L Trautmann, L Diener… (2022). Glioblastoma-Derived Three-Dimensional Ex Vivo Models to Evaluate Effects and Efficacy of Tumor Treating Fields (TTFields).
A Jacob Berger, E Gigi, L Kupershmidt, Z Meir… (2021). IRS1 phosphorylation underlies the non-stochastic probability of cancer cells to persist during EGFR inhibition therapy.
GB Ferraro, A Ali, A Luengo, DP Kodack, A Deik… (2021). Fatty acid synthesis is required for breast cancer brain metastasis.
JK Mich, LT Graybuck, EE Hess, JT Mahoney, Y Kojima… (2021). Functional enhancer elements drive subclass-selective expression from mouse to primate neocortex.
JR Campbell, BR McDonald, PB Mesko, NO Siemers… (2021). Fc-Optimized Anti-CCR8 Antibody Depletes Regulatory T Cells in Human Tumor ModelsAnti-CCR8 Antibody Depletes Tregs in Human Tumor Models.
JW DiGiacomo, I Godet, M Trautmann-Rodriguez… (2021). Extracellular Matrix–Bound FGF2 Mediates Estrogen Receptor Signaling and Therapeutic Response in Breast CancerThe ECM Mediates FGF-Induced ER Activity.
N Massey, D Shrestha, SM Bhat, N Kondru… (2021). Organic dust-induced mitochondrial dysfunction could be targeted via cGAS-STING or cytoplasmic NOX-2 inhibition using microglial cells and brain slice culture ….
Ben-Hamo R, Jacob Berger A, Gavert N, Miller M, Pines G, Oren R, Pikarsky E, Benes CH, Neuman T, Zwang Y, Efroni S, Getz G, Straussman R. (2020). Predicting and affecting response to cancer therapy based on pathway-level biomarkers.
Finetti F, Capitani N, Manganaro N, Tatangelo V, Libonati F, Panattoni G, Calaresu I, Ballerini L, Baldari CT, Patrussi L. (2020). Optimization of Organotypic Cultures of Mouse Spleen for Staining and Functional Assays.
Kondru N, Manne S, Kokemuller R, Greenlee J, Greenlee MHW, Nichols T, Kong Q, Anantharam V, Kanthasamy A, Halbur P, Kanthasamy AG. (2020). An Ex Vivo Brain Slice Culture Model of Chronic Wasting Disease: Implications for Disease Pathogenesis and Therapeutic Development.
Q Shu, X Zhao, X Geng, X Wang (2020). CD82 aggravates sevoflurane-induced neurotoxicity by regulating TRPM7 in developing neurons.
Q Wu, MA Shaikh, ES Meymand, B Zhang, KC Luk… (2020). Neuronal activity modulates alpha-synuclein aggregation and spreading in organotypic brain slice cultures and in vivo.
SC Kerr, MM Morgan, AA Gillette… (2020). A bioengineered organotypic prostate model for the study of tumor microenvironment-induced immune cell activation.
Srivastava AK , Roy Choudhury S , Karmakar S . (2020). Melatonin/polydopamine nanostructures for collective neuroprotection-based Parkinson's disease therapy.

Srivastava AK, Roy Choudhury S, Karmakar S. (2020). Near-Infrared Responsive Dopamine/Melatonin-Derived Nanocomposites Abrogating in Situ Amyloid '_ Nucleation, Propagation, and Ameliorate Neuronal Functions.
Xin H, Liu Z, Buller B, Li Y, Golembieski W, Gan X, Wang F, Lu M, Ali MM, Zhang ZG, Chopp M. (2020). MiR-17-92 enriched exosomes derived from multipotent mesenchymal stromal cells enhance axon-myelin remodeling and motor electrophysiological recovery after stroke.
Askoxylakis V, Ferraro GB, Badeaux M, Kodack DP, Kirst I, Shankaraiah RC, Wong CSF, Duda DG, Fukumura D, Jain RK. (2019). Dual endothelin receptor inhibition enhances T-DM1 efficacy in brain metastases from HER2-positive breast cancer.
Burman RJ, Selfe JS, Lee JH, van den Berg M, Calin A, Codadu NK, Wright R, Newey SE, Parrish RR, Katz AA, Wilmshurst JM, Akerman CJ, Trevelyan AJ, Raimondo JV. (2019). Excitatory GABAergic signalling is associated with benzodiazepine resistance in status epilepticus.
Harvey TN, Sandve SR, Jin Y, Vik JO, Torgersen JS. (2019). Liver slice culture as a model for lipid metabolism in fish.
Kolb I, Landry CR, Yip MC, Lewallen CF, Stoy WA, Lee J, Felouzis A, Yang B, Boyden ES, Rozell CJ, Forest CR. (2019). PatcherBot: a single-cell electrophysiology robot for adherent cells and brain slices.
Morgan MM, Arendt LM, Alarid ET, Beebe DJ, Johnson BP. (2019). Mammary adipose stromal cells derived from obese women reduce sensitivity to the aromatase inhibitor anastrazole in an organotypic breast model.
Nakano Y, Wiechert S, Bíçnfi B. (2019). Overlapping Activities of Two Neuronal Splicing Factors Switch the GABA Effect from Excitatory to Inhibitory by Regulating REST.
Morgan MM, Livingston MK, Warrick JW, Stanek EM, Alarid ET, Beebe DJ, Johnson BP. (2018). Mammary fibroblasts reduce apoptosis and speed estrogen-induced hyperplasia in an organotypic MCF7-derived duct model.
Ting JT, Kalmbach B, Chong P, de Frates R, Keene CD, Gwinn RP, Cobbs C, Ko AL, Ojemann JG, Ellenbogen RG, Koch C, Lein E. (2018). A robust ex vivo experimental platform for molecular-genetic dissection of adult human neocortical cell types and circuits.
Barrios J, Patel KR, Aven L, Achey R, Minns MS, Lee Y, Trinkaus-Randall VE, Ai X. (2017). Early life allergen-induced mucus overproduction requires augmented neural stimulation of pulmonary neuroendocrine cell secretion.
Kondru N, Manne S, Greenlee J, West Greenlee H, Anantharam V, Halbur P, Kanthasamy A, Kanthasamy A. (2017). Integrated Organotypic Slice Cultures and RT-QuIC (OSCAR) Assay: Implications for Translational Discovery in Protein Misfolding Diseases.
Boldajipour B, Nelson A, Krummel MF. (2016). Tumor-infiltrating lymphocytes are dynamically desensitized to antigen but are maintained by homeostatic cytokine.
V Askoxylakis, GB Ferraro, DP Kodack… (2016). Preclinical efficacy of ado-trastuzumab emtansine in the brain microenvironment.
Watson CY, Damiani F, Ram-Mohan S, Rodrigues S, de Moura Queiroz P, Donaghey TC, Rosenblum Lichtenstein JH, Brain JD, Krishnan R, Molina RM. (2016). Screening for Chemical Toxicity Using Cryopreserved Precision Cut Lung Slices.
Yen CF, Harischandra DS, Kanthasamy A, Sivasankar S. (2016). Copper-induced structural conversion templates prion protein oligomerization and neurotoxicity.
Kuo CS, Krasnow MA. (2015). Formation of a Neurosensory Organ by Epithelial Cell Slithering.
Moen T, Torgersen J, Santi N, Davidson WS, Baranski M, íÖdegí«rd J, KjíŸglum S, Velle B, Kent M, Lubieniecki KP, Isdal E, Lien S. (2015). Epithelial Cadherin Determines Resistance to Infectious Pancreatic Necrosis Virus in Atlantic Salmon.
Harischandra DS, Kondru N, Martin DP, Kanthasamy A, Jin H, Anantharam V, Kanthasamy AG. (2014). Role of proteolytic activation of protein kinase Cδ in the pathogenesis of prion disease.
Jin H, Kanthasamy A, Harischandra DS, Kondru N, Ghosh A, Panicker N, Anantharam V, Rana A, Kanthasamy AG. (2014). Histone hyperacetylation up-regulates protein kinase C'Ç in dopaminergic neurons to induce cell death: relevance to epigenetic mechanisms of neurodegeneration in Parkinson disease.
Garcia I, Huang L, Ung K, Arenkiel BR. (2012). Tracing synaptic connectivity onto embryonic stem cell-derived neurons.

Part IV — Protocols

Step-by-step protocols for embedding and sectioning on the Compresstome®. Each is reproduced in full on the pages that follow.

Live Brain Sectioning
Fixed Brain Sectioning
Electrophysiology — Acute Brain Slice
Spinal Cord — Embedding & Sectioning
Eye Tissue
Heart Tissue
Lung Tissue
Precision-Cut Lung Slices (PCLS)
Liver Tissue
Precision-Cut Liver Slices (v2)
Precision-Cut Gut Slices (Intestines)
Kidney Tissue
Spleen Tissue
Lymph Node
Muscle Tissue
Skin Tissue
Tumor Tissue
Organoid Sectioning
Plant Sectioning
Sectioning Frozen Tissue
Immunohistochemistry (IHC)
In-Situ Hybridization (ISH)

FRESH BRAIN SECTIONING

PROTOCOL FOR CUTTING SLICES OF FRESH BRAIN TISSUE

Key to reading the protocol:

√ Rationale for procedural step

♠ Tips & Tricks

1. Deeply anesthetize animal.
2. Remove brains by dissection. If you are not sectioning the brain right away, store it in PBS until you are ready for cutting.
3. If you are ready to section with the Compresstome®, rinse the brain in PBS first.
4. Select a section of the brain that you would like to take cut for slices.
5. Glue the tissue sample onto the Compresstome® specimen syringe.
6. Draw the syringe downward to bring the brain tissue core sample into the syringe.
7. Fill the syringe with 2% agarose (Sigma A-0701, low gelling point, incubated at ~37°C).
   - √ Order a Starter Kit or additional agarose or blades directly from our website at http://www.precisionary.com/starter-kit !
8. Cool the entire contents of the specimen syringe with the chilling block. The brain tissue is now embedded in agarose. The agarose will solidify enough for stable sectioning.
9. Load the specimen syringe onto the Compresstome® slicer.
10. The protocol is complete for preparing the fixed brain specimen for sectioning. Proceed from here with normal Compresstome® sectioning procedures.

    ♠ What are the optimal settings on the Compresstome® for cutting fresh brain slices? Try a speed (Advance) of 2 and an oscillation of 4-6. We have found that these parameters work best for obtaining superb brain slices with smooth surfaces without chattermarks.

References

*** Uses the Compresstome® for successful fresh brain slices.**

1. **Klar R, Walker AG, Ghose D, Grueter BA, Engers DW, et al. Activation of Metabotropic Glutamate Receptor 7 Is Required for Induction of Long-Term Potentiation at SC-CA1 Synapses in the Hippocampus. Journal of Neuroscience 13 May 2015, 35 (19) 7600-7615; DOI: https://doi.org/10.1523/JNEUROSCI.4543-14.2015**

2. **Jaafari N, De Waard M, Canepari M. Imaging fast calcium currents beyond the limitations of electrode techniques. Biophys J. 2014 Sep 16;107(6):1280-8. doi: 10.1016/j.bpj.2014.07.059.**

FIXED BRAIN SECTIONING

PROTOCOL FOR CUTTING SLICES OF FIXED BRAIN TISSUE

Key to reading the protocol:

√ Rationale for procedural step

♠ Tips & Tricks

1. Deeply anesthetize animal, then transcardially perfuse with saline followed by 4% paraformaldehyde in 0.1 M phosphate buffer, pH 7.4.
   - √ Note that you can perfuse the animal in a variety of ways, including gravity-feed, pump, or push-syringe.
2. Remove brains by dissection and fix in 4% phosphate buffered paraformaldehyde at 4° C overnight.
   - √ Be careful not to fix your tissue for too long before cutting and processing it! Over-fixation will decrease good protein staining when you do immunohistochemistry. So don't forget to take out the fixed brain after 24 hours.
3. Pour out the paraformaldehyde and then cryoprotect the fixed brain with 30% sucrose buffer at 4° C overnight.
4. Pour out the 30% sucrose solution. If you are not sectioning the brain right away, store it in PBS until you are ready for cutting. If you are ready to section with the Compresstome®, rinse the brain in PBS first.
5. Select a section of the brain that you would like to take cut for slices.
6. Glue the tissue sample onto the Compresstome® specimen syringe.
7. Draw the syringe downward to bring the brain tissue core sample into the syringe.
8. Fill the syringe with 2% agarose (Sigma A-0701, low gelling point, incubated at ~37°C).
   - √ Order a Starter Kit or additional agarose or blades directly from our website at http://www.precisionary.com/starter-kit !

9. Cool the entire contents of the specimen syringe with the chilling block. The brain tissue is now embedded in agarose. The agarose will solidify enough for stable sectioning.
10. Load the specimen syringe onto the Compresstome® slicer.
11. The protocol is complete for preparing the fixed brain specimen for sectioning. Proceed from here with normal Compresstome® sectioning procedures.

♠ What are the optimal settings on the Compresstome® for cutting fixed brain slices? Try a speed (Advance) of 2 and an oscillation of 4-6. We have found that these parameters work best for obtaining superb brain slices with smooth surfaces without chattermarks.

References

*** Uses the Compresstome® for successful fixed brain slices.**

1. **Abdelaal HM, Kim HO, Wagstaff R, Sawahata R, Southern PJ, Skinner PJ. Comparison of Vibratome and Compresstome sectioning of fresh primate lymphoid and genital tissues for in situ MHC-tetramer and immunofluorescence staining. Biol Proced Online. 2015 Jan 7;17(1):2. doi: 10.1186/s12575-014-0012-4.**

2. **Askoxylakis V, Ferraro GB, Kodack DP, Badeaux M, Shankaraiah RC, Seano G, Kloepper J, Vardam T, Martin JD, Naxerova K, Bezwada D, Qi X, Selig MK, Brachtel E, Duda DG, Huang P, Fukumura D, Engelman JA, Jain RK. Preclinical Efficacy of Ado-trastuzumab Emtansine in the Brain Microenvironment. J Natl Cancer Inst. 2015 Nov 7;108(2).**

3. **Duncan J, Kersigo J, Gray B, Fritzsch B. Combining lipophilic dye, in situ hybridization, immunohistochemistry, and histology. J Vis Exp. 2011 Mar 17;(49).**

4. **Selever J, Kong JQ, Arenkiel BR. A rapid approach to high-resolution fluorescence imaging in semi-thick brain slices. J Vis Exp. 2011 Jul 26;(53).**

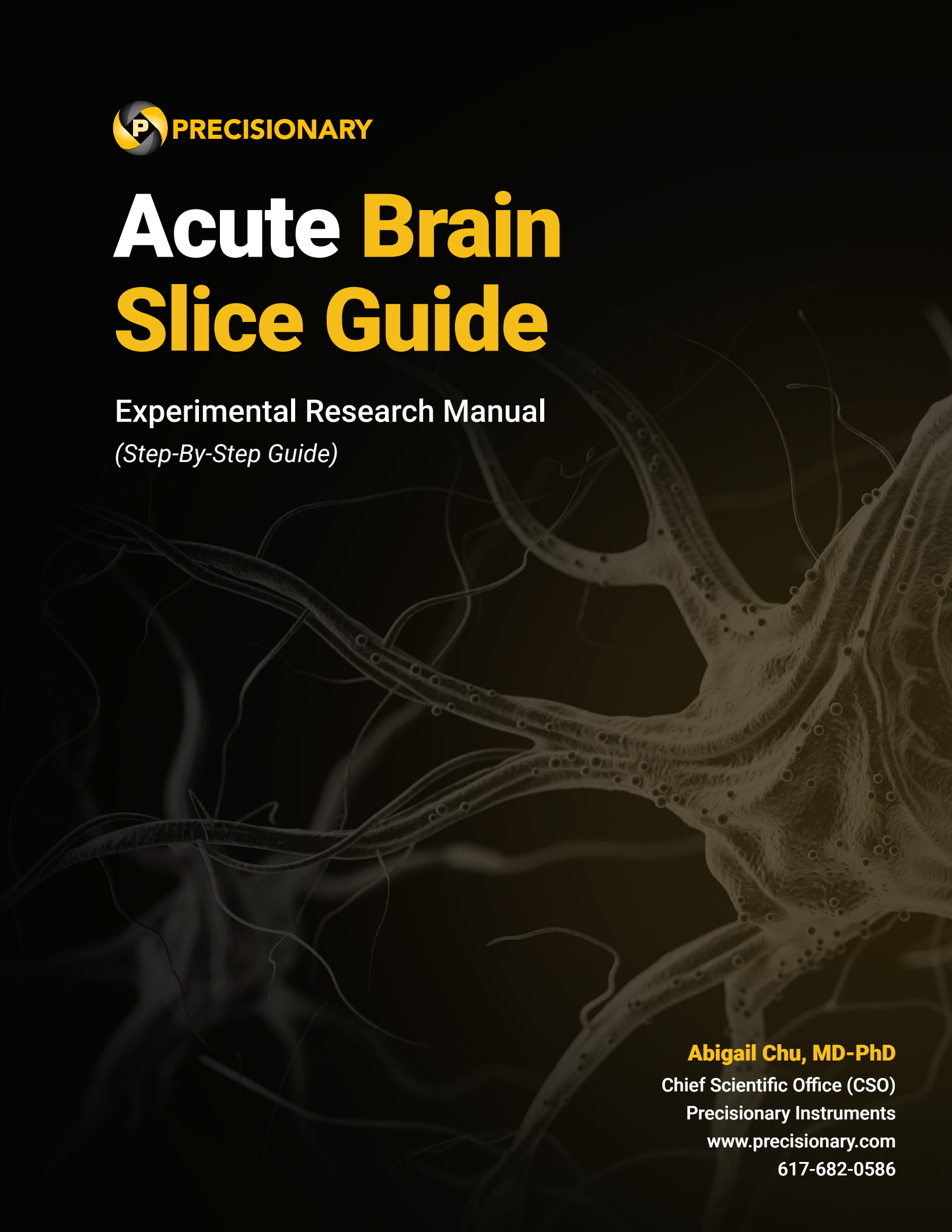
5. **Ting JT, Daigle TL, Chen Q, Feng G. Acute brain slice methods for adult and aging animals: application of targeted patch clamp analysis and optogenetics. Methods Mol Biol. 2014;1183:221-42.**

PRECISIONARY

Acute Brain Slice Guide

Experimental Research Manual

(Step-By-Step Guide)



Abigail Chu, MD-PhD
Chief Scientific Office (CSO)
Precisionary Instruments
www.precisionary.com
617-682-0586

Table of Contents

Goals of this Experimental Guide **3**
What is Patch-Clamp Electrophysiology and Why is it Important? 3
Who This Guide Can Help 5
Contact Precisionary Instruments for Any Additional Experimental Support 6
Gross Anatomic Location of Mouse Brain Structures **7**
Mouse Brain Anatomy 7
Key Differences and Similarities 7
Human Brain Anatomy 9
Using Human Brain Tissue in Patch-Clamp Studies 10
Essential Materials and Reagents for Patch-Clamp Electrophysiology **11**
Solutions & Recipes for Patch-Clamp Electrophysiology **12**
External Solutions 12
Internal Solutions 13
Final Tips and Hints for Making External and Internal Solutions for Patch-Clamping 15
Importance of Osmolarity 15
Practical Solution Preparation 15
Additional Tips
Helpful Hints 16
Agarose Solution 17
70% Ethanol 18
Making Acute Brain Slices from Mouse **18**
Preparing for Slicing Mouse Brain Slices 18
Dissection of the Mouse Brain for Slicing 20
Sectioning Acute Brain Slices on the Compresstome Vibratome 21
Embedding Brain Tissue into a Specimen Tube: A Step-by-Step Guide 21
Cutting Acute Brain Slices on the Compresstome Vibratome 23
Collecting and Incubating Acute
Brain Slices 24
Recording from Acute Brain Slices **25**
Making Recording Pipettes 26
Lowering the Pipette Towards the Target Cell 26
Making the Gigaseal 28
Establishing the Type of Patch-Clamp Recording 29
Whole-Cell Recording 29
Perforated Patch Recording 30
Single Ion Channel Recordings 32
What to Include in Your Ephys Logbook **33**
Making Bipolar Electrodes for Stimulation **34**
Troubleshooting Patch-Clamp Electrophysiology **37**
More Questions? Contact Us! **39**

Goals of this Experimental Guide

Patch-clamp electrophysiology is an essential technique in neuroscience and cellular physiology for studying the electrical properties of cells. This guide aims to provide researchers with a comprehensive understanding of patch-clamp techniques, applications, and experimental protocols. As illustrated in Figure 1, which shows live hippocampal neurons from a mouse acute brain slice, our goal is to help you achieve beautiful, healthy acute brain slices like the plump, round neurons highlighted as ideal candidates for patch-clamp recording.

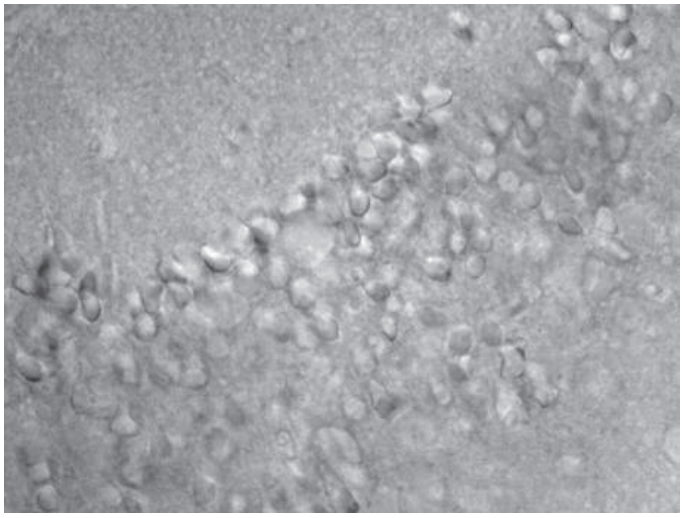


Figure 1. A camera image shows live hippocampal neurons from a mouse acute brain slice, where the plump, round neurons are highlighted as ideal candidates for patch-clamp recording. One of our goals in this research guide is to help you get beautiful, healthy acute brain slices for patching!

What is Patch-Clamp Electrophysiology and Why is it Important?

In the realm of cellular and neuroscience research, scientists have developed various methods to understand how cells communicate and function. Patch-clamp electrophysiology is one such method. It allows researchers to measure the electrical currents of individual cells, providing insights into how cells, particularly neurons, respond to different stimuli and interact with their environment.

While other techniques like calcium imaging or voltage-sensitive dyes have contributed to our understanding of cellular activity, they often lack the

precision and direct measurement capabilities of patch-clamp electrophysiology. This method bridges the gap between traditional electrophysiological recordings and the complex behaviors of cells in a living organism.

As outlined in Figure 2, the general workflow for patch-clamp electrophysiology begins with the preparation of acute brain slices, followed by key steps like transferring the slices to a recording chamber with oxygenated artificial cerebrospinal fluid (ACSF), identifying target neurons, and using micromanipulators to position glass pipettes for cell attachment. This process allows researchers to establish a high-resistance seal with the cell membrane and record the electrical activity of neurons in real-time. This method not only enhances our understanding of cellular mechanisms but also reduces the need for extensive animal models by gathering detailed data from individual cells or small cell groups.

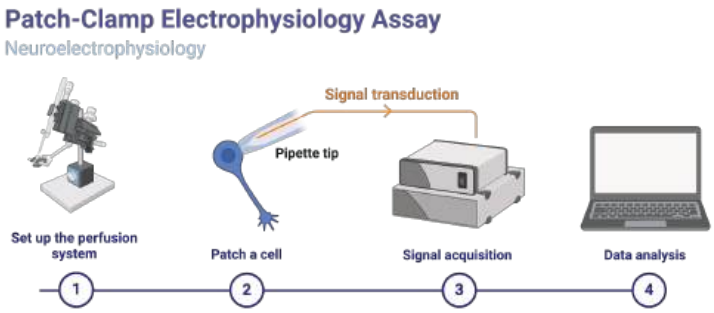


Figure 2. The figure outlines the general workflow for patch-clamp electrophysiology following the preparation of acute brain slices. Key steps include transferring the brain slices to a recording chamber filled with oxygenated artificial cerebrospinal fluid (ACSF), identifying target neurons under a microscope, using micromanipulators to position glass pipettes for cell attachment, establishing a high-resistance seal with the cell membrane, and recording the electrical activity of the neuron to study its physiological properties.

Who This Guide Can Help

This guide is designed to assist a wide range of individuals involved in cellular and neuroscience research, including:

- **New Researchers**: If you're just starting to work with patch-clamp electrophysiology, this guide will walk you through the step-by-step process of setting up and conducting your first experiments.
- **Experienced Scientists**: For those with previous experience, this guide offers troubleshooting tips and advanced techniques to refine and enhance the quality of your patch-clamp procedures.
- **Research Mentors**: If you're responsible for training others in patch-clamp techniques, this manual serves as a valuable teaching resource to ensure your trainees develop a strong foundation in this critical method.
- **Curious Minds**: Anyone interested in deepening their understanding of patch-clamp electrophysiology techniques and applications will find this guide useful, regardless of their expertise level in cellular and neuroscience research.

As illustrated in Figure 3, this guide is crafted to be a comprehensive resource for individuals at all levels of expertise. Whether you're a beginner, an experienced scientist, a mentor, or simply someone eager to expand your knowledge, this guide aims to provide valuable insights and practical guidance to support your research endeavors and enhance your understanding of this powerful technique.



Figure 3. Is this you? This guide serves as a comprehensive resource for individuals at all levels of expertise in patch-clamp electrophysiology, offering valuable insights and practical guidance. Whether you are a beginner, an experienced scientist, a mentor, or simply someone eager to expand your knowledge, this guide is designed to support your research endeavors and enhance your understanding of this powerful technique.

Contact Precisionary Instruments for Any Additional Experimental Support

For further assistance, feel free to reach out to Precisionary Instruments — a leading provider of vibratome equipment and accessories essential for making acute brain slices for patch-clamp electrophysiology. Whether you have technical inquiries, need troubleshooting guidance, or require customized solutions, our expert team is here to support you at every stage of your patch-clamp experiments. Through this guide, we aim to empower researchers with the knowledge and tools necessary to leverage the full potential of patch-clamp electrophysiology in advancing cellular and neuroscience research.

E-mail: info@precisionary.com
Phone: (617) 682-0586
Fax: 1-866-424-2217

Precisionary Instruments
200 Butterfield Drive, Unit E
Ashland, MA 01721

Let's begin!

Gross Anatomic Location of Mouse Brain Structures

Understanding the gross anatomic location of brain structures is essential for effectively working with acute brain slices for patch-clamp electrophysiology. This section provides a simplified overview of the anatomy of the mouse brain, highlighting key regions and their functions.

Mouse Brain Anatomy

In mice, the brain is divided into several major regions, each responsible for different functions. Here are several mouse brain regions commonly studied for patch-clamp electrophysiology:

- **Cerebrum**: The largest part of the brain, responsible for voluntary actions, sensory perception, and cognitive functions. It is divided into two hemispheres.
- **Cerebellum**: Located at the back of the brain, the cerebellum is involved in motor control and coordination.
- **Brainstem**: Comprising the midbrain, pons, and medulla oblongata, the brainstem controls basic life functions such as breathing, heart rate, and blood pressure.
- **Hippocampus**: A crucial part of the brain for learning and memory, located in the medial temporal lobe.
- **Thalamus**: Acts as a relay station, processing and transmitting sensory information to the appropriate areas of the cerebrum.
- **Hypothalamus**: Regulates various autonomic functions, including hunger, thirst, and temperature control.

Key Differences and Similarities

While there are significant anatomical differences between mouse and human brains, such as size and complexity, mice serve as valuable models for studying brain function and diseases. Mice share fundamental similarities in brain structure and neurophysiological processes with humans, making them indispensable in neuroscience research.

By understanding the gross anatomy of the mouse brain (Figures 4-6), researchers can more effectively prepare and utilize brain slices for patch-clamp electrophysiology, leading to advancements in our knowledge of neural circuits and brain function.

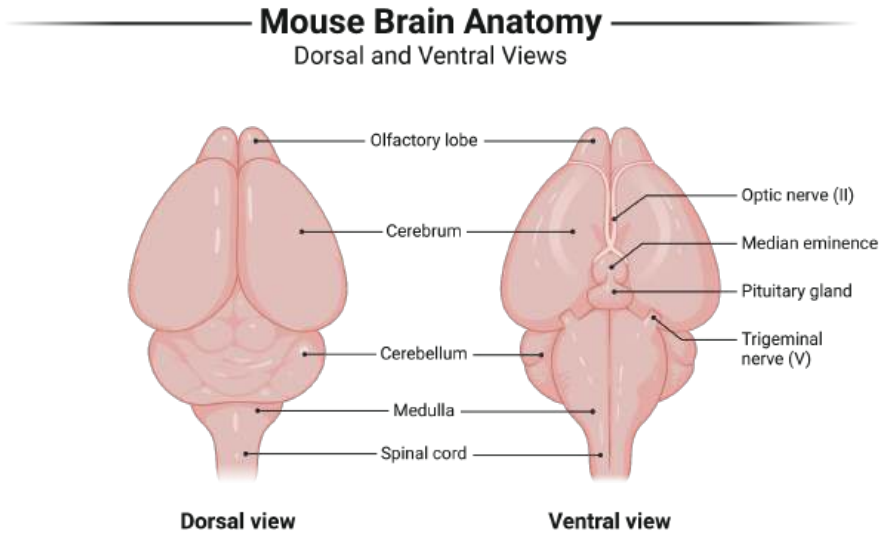


Figure 4. This figure illustrates the mouse brain from both dorsal and ventral perspectives, highlighting key anatomical structures. The dorsal view reveals the cerebrum, divided into hemispheres, along with the cerebellum at the posterior end and the olfactory bulbs at the anterior. The ventral view showcases the brainstem, including the midbrain, pons, and medulla oblongata, as well as the hypothalamus and optic chiasm.

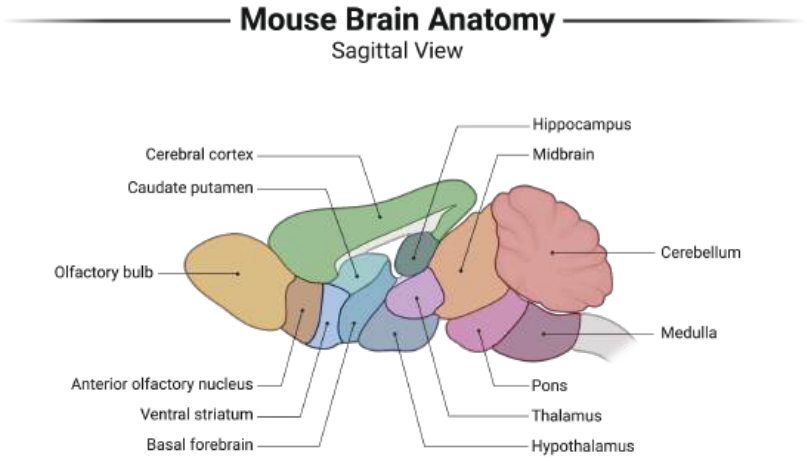


Figure 5. A sagittal cross section of the mouse brain, providing a detailed view of internal anatomical structures. Key regions include the cerebrum, cerebellum, and brainstem, along with the hippocampus, thalamus, and hypothalamus, which are crucial for various cognitive, motor, and regulatory functions. The image highlights the spatial relationships between these regions, offering insights into the brain's complex organization.

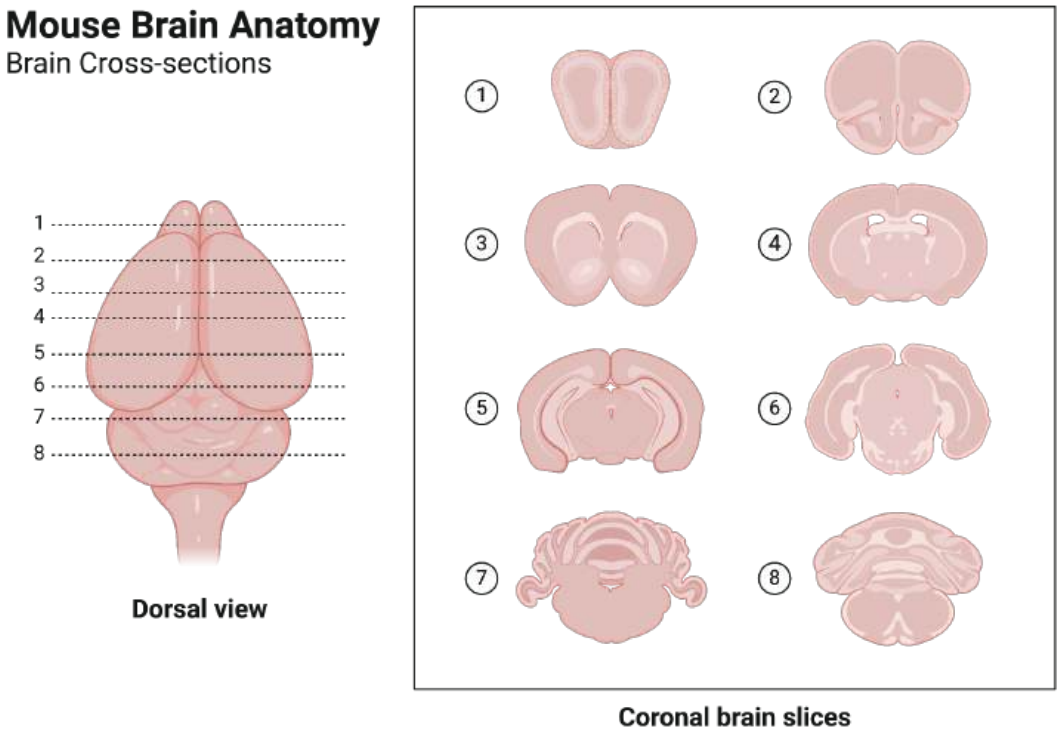


Figure 6. Coronal sections of the mouse brain, displaying detailed anatomical features at different levels. Key structures such as the cortex, hippocampus, thalamus, and ventricles are visible, providing insights into the spatial organization and functional areas within the brain. These sections highlight the brain's symmetry and the relative positioning of important neural regions.

Human Brain Anatomy

The human brain is a highly complex organ, essential for daily life and overall health (Figure 7). Unlike animal models where whole brain slices are often used, patch-clamp studies in humans typically utilize small biopsies or resections obtained directly from the operating room (OR). These samples are crucial for understanding human brain physiology and pathophysiology.

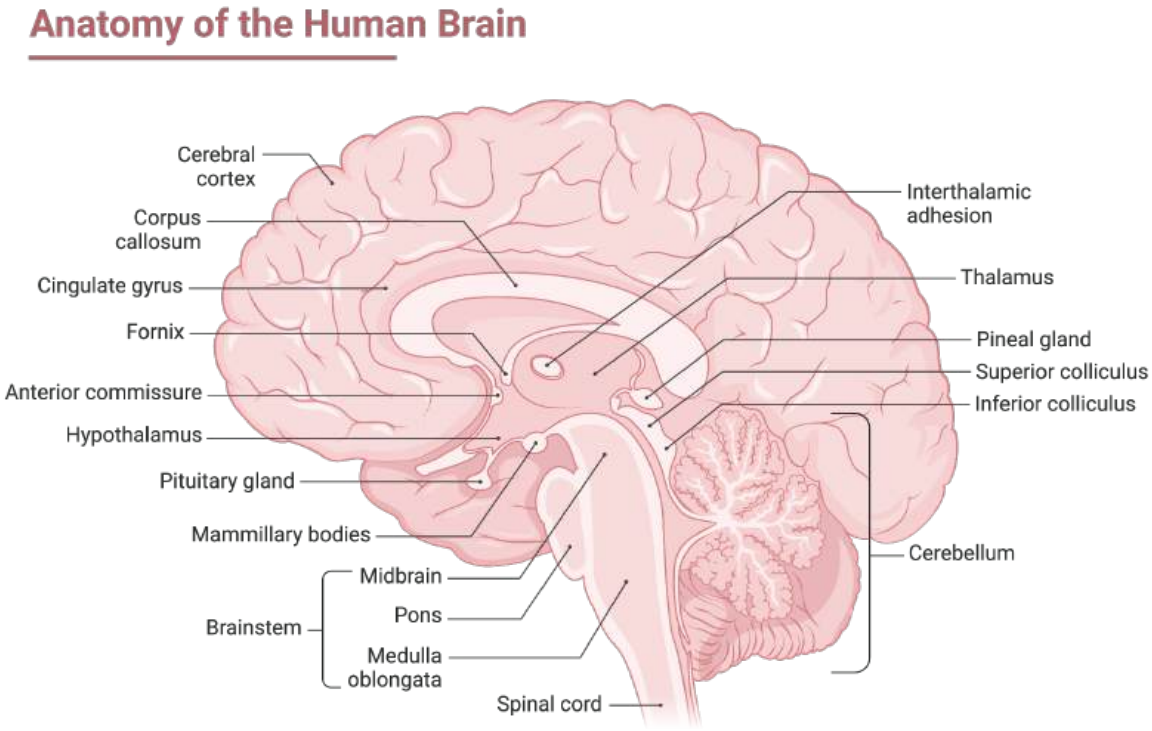


Figure 7. Sagittal cross section of the human brain, illustrating the major anatomical structures. Key regions include the cerebrum, cerebellum, brainstem, and corpus callosum, along with the thalamus, hypothalamus, and hippocampus. This view highlights the organization and connectivity of these regions, emphasizing their roles in cognitive functions, motor control, and regulation of vital processes.

Using Human Brain Tissue in Patch-Clamp Studies

In patch-clamp electrophysiology, small biopsies or resections of the human brain, typically obtained directly from the OR during surgical procedures, are used. These samples allow researchers to study the electrical properties of human neurons in detail. The direct use of human brain tissue provides invaluable insights into the specific characteristics of human neural circuits, which can differ significantly from those of animal models.

By understanding the detailed anatomy of the human brain and utilizing small, precise tissue samples, researchers can better investigate and develop treatments for neurological diseases and disorders.

This approach bridges the gap between laboratory research and clinical applications, enhancing our ability to translate findings into real-world medical advancements.

Understanding the gross anatomical differences between mouse and human brains is crucial for translational research, where findings from animal models like mice are extrapolated to human physiology and pathology. While mice serve as valuable models for studying brain biology and disease, researchers must consider species-specific anatomical variations when interpreting experimental results and designing therapeutic interventions. Recognizing these differences ensures that insights gained from mouse studies are accurately applied to human health, enhancing the relevance and effectiveness of neurological research.

Essential Materials and Reagents for Patch-Clamp Electrophysiology

In conducting patch-clamp electrophysiology experiments, it's imperative to have the appropriate materials and reagents ready for use. Below are categorized lists of essential equipment, lab accessories, and reagents required for this procedure:

Equipment

- Patch-clamp amplifier
- Micromanipulators
- Inverted microscope
- Vibration isolation table
- Data acquisition system
- Vibrating microtome (Compresstome® vibratome)

Lab Accessories

- Micropipettes and pipette puller
- Recording chamber
- Perfusion system
- Faraday cage
- Headstage holder

Reagents

- Intracellular solution
- Extracellular (bath) solution
  - Cutting solution
  - Recording/incubation solution
- Agarose for brain slicing
- Enzyme solutions (e.g., trypsin) for cell dissociation
- Seal-enhancing substances

Having these materials and reagents prepared and organized will streamline your patch-clamp experiments and ensure accurate and reliable results.

Solutions & Recipes for Patch-Clamp Electrophysiology

This section provides recipes and instructions for making solutions for patch-clamp electrophysiology experiments.

External Solutions

External solutions are designed to mimic the ionic composition of the physiological fluid that the plasma membrane is exposed to in vivo or in culture. The 'extracellular solution' (ECS) is used as the bathing solution and primarily consists of sodium chloride. The pH and osmolarity of these solutions are critical for obtaining good seals, often more so than the ionic composition.

Table 1: Example of Typical Extracellular Solution (ECS) Used in Patch Clamping a Mammalian Cell

Chemical	ECS Concentration (mM)
Na+	126
K+	6
Mg2+	2.5
Ca2+	1.2
Cl-	125
GTP	0
ATP	0
HEPES	10
Glucose	11
Sucrose	67

Typical pH and Osmolarity of External Solution:

- pH: Typically set using NaOH for ECS (around 7.4) and KOH for ICS (around 7.2)
- Osmolarity: ECS is typically around 300-310 mOsm, and ICS is around 290-300 mOsm

It is important to oxygenate the external solution (ACSF) with 95% O2 / 5% CO2, a process commonly referred to as "carbogen."
External solutions are usually made in large batches and then divided to create "cutting solution" and "recording/incubation solution."

Cutting Solution:

- Used for cutting acute brain slices
- Typically low calcium (approximately 0.1 mM Ca) and high magnesium (approximately 3 mM Mg)

Recording/Incubation Solution:

- Used in the perfusion chamber and during the post-cutting incubation period
- Typically 2 mM Ca and 1 mM Mg

→ Why Low Calcium and High Magnesium During Brain Slicing? Low calcium and high magnesium are used during brain slicing to reduce the excitability of neurons and protect them from excitotoxicity. This creates a more stable environment for cutting and helps maintain the integrity of the brain slices for subsequent electrophysiological recordings.

Internal Solutions

The 'intracellular solution' (ICS) used to fill pipettes for whole-cell and outside-out excised patch recording contains a high concentration of potassium. This composition is essential for mimicking the intracellular environment and ensuring accurate recordings of cellular electrical activity.

Table 2: Example of Typical Intracellular Solution (ICS) Used in Patch Clamp Electrophysiology

Chemical	ICS Concentration (mM)
Na+	5
K+	147
Mg2+	1.2
Ca2+	0
Cl-	150
GTP	0.1
ATP	5
HEPES	20
Glucose	11
Sucrose	0

When preparing ICS, it's crucial to carefully monitor the pH, as the inclusion of chemicals such as EGTA for quenching calcium ions can make the solution very acidic. The desired pH for ICS is slightly more acidic, around 7.2 to 7.3, to match the intracellular conditions.

Tips for Making and Storing Internal Solution for Patch-Clamping:

1. **Accurate pH Adjustment**:
   - Always measure the pH after all components have dissolved.
   - Use KOH to adjust the pH to the desired range (7.2 – 7.3).
   - Be cautious when adding strong bases or acids, as small volumes can cause significant pH shifts.
2. **Preparation and Sterilization**:
   - Prepare solutions using high-purity reagents and ultrapure water to avoid contamination.
   - Sterilize the solution by filtering it through a 0.22 µm filter to remove particulates and potential microbial contaminants.
3. **Storage**:
   - Store internal solutions in small aliquots to minimize freeze-thaw cycles, which can degrade components.
   - Keep the aliquots at -20°C for long-term storage and thaw only as needed.
   - Label aliquots clearly with the date of preparation and the composition.
4. **Avoiding Precipitation**:
   - Ensure all salts are fully dissolved to prevent precipitation, which can block pipettes and affect recordings.
   - Vortex the solution thoroughly after adding each component.
5. **Handling Calcium Chelators**:
   - When using calcium chelators like EGTA or BAPTA, add them slowly to the solution while stirring continuously to prevent localized precipitation.
   - Ensure complete dissolution before adjusting the pH.

By following these guidelines, you can prepare and store internal solutions that are stable, reliable, and suitable for high-quality patch-clamp electrophysiology experiments.

Final Tips and Hints for Making External and Internal Solutions for Patch-Clamping

When preparing solutions for patch-clamp electrophysiology, a few key factors can make a significant difference in the success of your experiments. Here are some friendly, easy-to-understand tips and hints to keep in mind:

Importance of Osmolarity

Osmolarity is crucial but often underrated. Both the absolute osmolarity and the difference between solutions on either side of the membrane are critical for success. Differences in osmolarity can affect cell volume and exert osmotic force on the membrane. If the osmolarity difference is too large, cells can die. Always ensure your solutions have compatible osmolarity levels.

Practical Solution Preparation

- **Stock Solutions**: It's practical to keep a stock bathing solution at tenfold strength. This way, you can prepare the exact quantity you need on the day of your experiment. This approach saves time and ensures consistency.
- **Omitting Calcium and Glucose in Stock Solutions**: Calcium and glucose are often omitted from stock solutions. This prevents the precipitation of calcium salts and the growth of microorganisms. Add these components fresh on the day of the experiment.
- **Intracellular Solutions**: ICS often contains perishable chemicals like ATP. Make these solutions in batches and aliquot them into small portions. Keep these aliquots frozen and thaw only as needed to maintain their effectiveness.

Additional Tips Helpful Hints

- **Accurate pH Adjustment**: Always adjust the pH after all components are dissolved. Use a pH meter and add NaOH or KOH carefully to avoid large pH shifts.
- **Sterilization**: Filter solutions through a 0.22 µm filter to remove particulates and potential contaminants. This step is especially important for intracellular solutions.
- **Labeling**: Clearly label your solutions with the date of preparation and their components. This practice helps you keep track of solution freshness and composition.
- **Avoiding Precipitation**: Ensure all salts are fully dissolved to prevent blockages in pipettes and disruptions in recordings. Vortex thoroughly after adding each component.
- **Storage**: Store solutions in appropriate conditions. External solutions can often be kept at room temperature if used within a short period, while intracellular solutions should be frozen in aliquots to preserve their integrity.
- **Voltage Clamp Experiments**: If the evoked responses at the calyx are too large, try adding 2 mM QX314 (N-(2,6-dimethylphenylcarbamoylmethyl) triethylammonium chloride) to the internal solution.
- **Sealing with CsF Internal**: The CsF internal allows for very easy sealing. If fluoride does not interfere with your experiments, try using the CsF internal instead of Cs-gluconate for patching.
- **Preventing Precipitation in ACSF**: Bubble the 1X ACSF first before adding Ca2+ to prevent precipitation. You'll get precipitation when your solution looks “cloudy” upon adding Ca2+.
- **Preparing and Storing CaCl2**: Prep a 1 M CaCl2 solution and keep it in the 4°C fridge. You can use this stock each time when adding Ca2+ to your 1X ACSF.
- **Buying MgCl2**: The 1 M MgCl2 solution can be purchased directly from Sigma.

By following these practical tips and helpful hints, you'll ensure your external and internal solutions are prepared correctly, leading to more successful and reliable patch-clamp experiments.

Agarose Solution

Ingredients:

- 1.5 g low-melting point agarose powder
- 100 ml HBSS/HEPES buffer

Instructions:

1. Measure out 1.5 grams of low-melting point agarose powder using a laboratory balance.
2. In a suitable container, such as a glass beaker or flask, pour 100 ml of HBSS/HEPES buffer.
3. Add the measured agarose powder to the HBSS/HEPES buffer.
4. Microwave the mixture in short intervals, stirring occasionally, until the agarose powder is completely dissolved. Be cautious not to overheat the solution.
5. Once the agarose is fully dissolved, allow the solution to cool slightly before use in lung tissue processing.

Note: This recipe yields 100 ml of 2% agarose solution, suitable for processing multiple lung samples. Adjust the quantities accordingly if a smaller or larger volume is required.

Alternative Method using Agarose Tablets (Precisionary Instruments):

- Instead of low-melting point agarose powder, use agarose tablets provided by Precisionary Instruments.
- Each tablet is 0.5 grams, so use three tablets for a total of 1.5 grams to achieve a 2% agarose concentration.
- Mix the agarose tablets with 75 ml of HBSS/HEPES buffer (25 ml per tablet) to yield a 2% agarose solution.
- Follow the same procedure as described above for dissolving the agarose tablets in the buffer solution using the microwave.

Note: The use of agarose tablets provides a convenient and precise method for preparing agarose solution, ensuring consistent results in lung tissue processing. Adjust the volume of buffer solution accordingly to achieve the desired agarose concentration. Here is a visual guide for making agarose solution using tablets:

70% Ethanol

Ingredients:

- 70 ml absolute ethanol
- 30 ml distilled water

Instructions:

1. Measure out 70 ml of absolute ethanol using a graduated cylinder or measuring beaker.
2. Measure out 30 ml of distilled water using a separate graduated cylinder or measuring beaker.
3. Combine the measured amounts of absolute ethanol and distilled water in a clean container, such as a glass bottle or flask.
4. Mix the ethanol and water thoroughly by gently swirling or stirring the solution with a clean stir rod or spatula.
5. Once mixed, the solution will be 70% ethanol. Label the container appropriately with the concentration and contents.
6. Store the 70% ethanol solution in a tightly sealed container at room temperature. Ensure that the container is properly labeled and stored away from direct sunlight or heat sources.

Note: Always prepare ethanol solutions in a well-ventilated area and avoid inhaling the vapors. Use caution when handling ethanol as it is flammable. Dispose of any unused or expired ethanol solution according to local regulations for hazardous waste disposal.

Making Acute Brain Slices from Mouse

Now that we've gained a quick understanding of mouse and human brain anatomy, let's delve into the process of preparing acute brain slices. We'll start with the mouse model, as it is the most commonly used mammalian model in basic neuroscience research.

Preparing for Slicing Mouse Brain Slices

1. **Prepare Solutions**:
   - Make the cutting solution (0.1 mM Ca2+/3 mM Mg2+).
   - Make the recording solution (2 mM Ca2+/1 mM Mg2+).

2. **Measure Solutions**:
   - For each brain, you will need approximately 250 mL of cutting solution.
   - Pour some of the cutting solution into the recording chamber to cover just the bottom. This amount of solution will freeze and keep the chamber cold by acting like an ice cube (See Figure 3).
3. **Chill Solutions and Equipment**:
   - Freeze the cutting solution and slice chamber at -20°C.
   - Chill the orienting disk at 4°C.
4. **Prepare the Slice Area**:
   - Set up your slicing area with all necessary tools and equipment (See Figures 4-5).
5. **Prepare for Slicing**:
   - Once you are almost ready to begin, take the cutting solution out of the freezer and bubble it with carbogen (95% O2/5% CO2) for approximately 5 minutes before you start slicing.

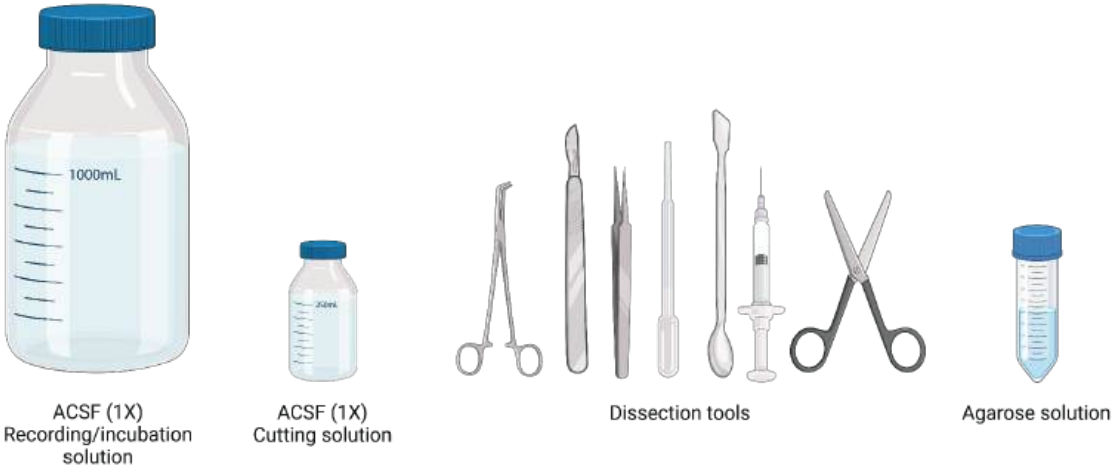


Figure 8. Preparing the Slice Area and Dissection Tools. Ensure all solutions are bubbled with carbogen (95% O_2/5% CO_2) before slicing, and fill the incubation chamber with cutting solution containing 0.1 mM Ca^{2+} and 3 mM Mg^{2+}. Set up the slicing area with the necessary tools and equipment as shown. A close-up view highlights essential dissection tools, including fine forceps, razor blades, and a transfer pipette for moving slices. Additionally, a syringe with a bent needle tip, critical for detaching brainstem slices from the cerebellum, is detailed.

Dissection of the Mouse Brain for Slicing

Follow these step-by-step instructions to dissect the mouse brain for slicing:

1. **Anesthetize the Animal**: Ensure the animal is fully anesthetized by confirming the lack of response to a tail-pinch and toe-pinch.
2. **Decapitate the Head**: Make an incision down the top of the skull and pull back the skin to expose the skull/cranium.
3. **Open the Skull**: Cut down the midline of the skull, keeping close to the bone to avoid damaging the underlying tissue. Then, make horizontal cuts along the bregma and lambda lines on each side. Peel back the skull pieces to expose the brain.
4. **First Cut**: Make the first cut between the brainstem and spinal cord. The yellow arrows in Figure 6 show where this cut is made, separating the brainstem from the spinal cord.
5. **Second and Third Cuts**: Make the second cut between the cortex and cerebellum. The third cut is near the anterior part of the cortex and olfactory bulbs.
6. **Remove the Cortex**: Using fine forceps, carefully remove the cortex, leaving the cerebellum and brainstem intact.

Note: During the brain dissection process, you can isolate and dissect specific brain regions required for your patch-clamp experiments. Additionally, further dissect the extracted brain tissue to optimize the orientation for cutting.

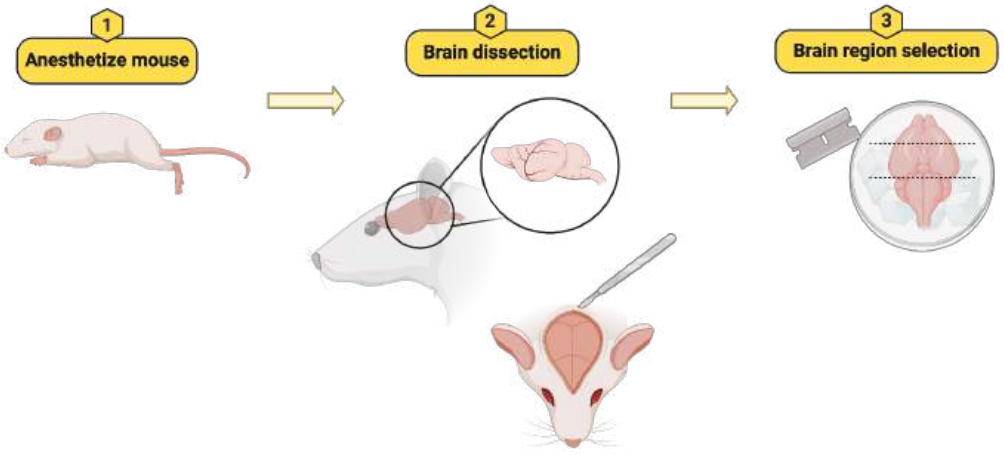


Figure 9. Step-by-step dissection of the mouse brain for slicing, starting with anesthetization, followed by decapitation and opening of the skull to expose the brain. Key cuts are made between the brainstem and spinal cord, the cortex and cerebellum, and near the anterior cortex. The cortex is carefully removed, leaving the cerebellum and brainstem intact. Yellow arrows in Figure 6 indicate the precise locations of the cuts. This process allows for the isolation and further dissection of specific brain regions for patch-clamp experiments.

Sectioning Acute Brain Slices on the Compresstome Vibratome

Embedding Brain Tissue into a Specimen Tube: A Step-by-Step Guide

Before embedding the brain tissue into a specimen tube, it's essential to properly prepare both your sample and tools to ensure successful mounting and preservation. The following steps will guide you through the process to achieve optimal results.

1. **Chill the Block:** Start by placing the chilling block in an ice bath or freezer for at least 1 hour before use. It's important that the block is well-chilled before embedding your tissue sample.
2. **Prepare Your Tissue Sample:** Cut your tissue sample so it fits neatly inside the specimen tube. Then, squeeze a small amount of super glue onto the base of the specimen tube, covering an area roughly the size of your tissue. Be careful to avoid any glue spilling down the sides of the plunger; if it does, the metal casing might get stuck. If this happens, soaking the tube in acetone can help dissolve the glue.



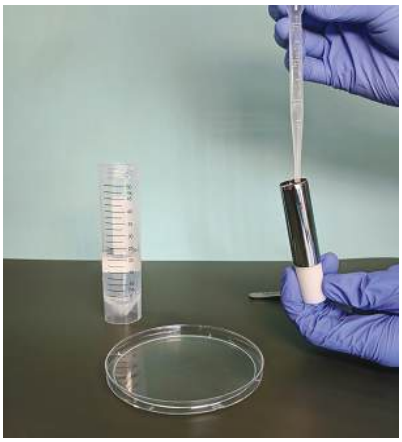
3. **Position the Tissue:** Use forceps to carefully place the tissue onto the glued base of the specimen tube. Allow the glue to cure fully. If needed, cut a flat surface on the tissue to ensure it adheres securely to the tube.



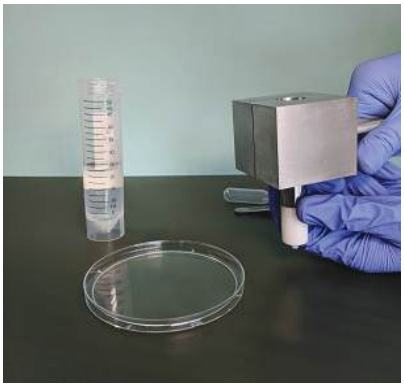
4. **Insert the Tissue:** Gently withdraw the specimen tube base downward until the tissue sample is fully enclosed within the tube.



5. **Add Agarose:** Pipette agarose into the tube, making sure the sample is completely covered. Tap the side of the tube to remove any bubbles, or use a pipette to suction them out.



6. **Solidify the Sample:** Finally, place the pre-chilled chilling block over the specimen tube to cool the entire sample and solidify the agarose. This should take about 30 seconds to 1 minute, depending on the size of your sample.



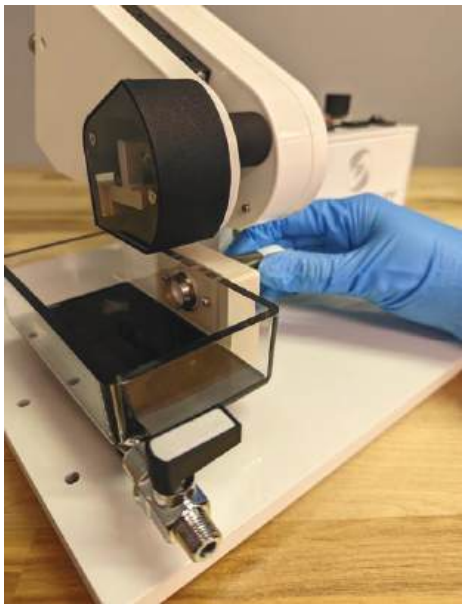
Cutting Acute Brain Slices on the Compresstome Vibratome

After embedding your tissue, the next step is to prepare your Compresstome Vibratome for precise brain slicing. Follow these instructions to ensure accurate and consistent sectioning.

1. **Prepare the Control Box:** Ensure the sliding control box is pushed back away from the buffer tray. To do this, press down on the lever on the right side of the box, slide the control box back until it locks in place, and then remove the lever.



2. **Insert the Specimen Tube:** Insert the tapered end of the specimen tube into the buffer tray. Push the tube fully in until the stopper ring meets the adapter base of the buffer tray, which will prevent further insertion, ensuring proper positioning for sectioning.



3. **Position the Control Box:** Once the specimen tube is removed, bring the sliding control box back in front of the buffer tray by pressing the same lever on the right and sliding the box towards you. Ensure the micrometer is touching the back of the specimen tube before starting the sectioning process. You can adjust the micrometer using the 'Fast Forward' and 'Fast Reverse' functions on the control box.



4. **Attach the Blade Holder:** Slide the prepared blade holder onto the axial bar of the vibrating unit and lock it in place using the included Allen key. The blade should face the control box and the specimen tube.



5. **Set Up and Power On:** Plug one end of the power cord into the VF-510-0Z machine and the other into a standard power outlet. Turn the power on, and use the control box to set the slice thickness, sectioning speed, and oscillation frequency to meet your experimental requirements.

6. **Begin Sectioning:** To achieve optimal slice consistency, start cutting approximately 50-100 microns higher than your target thickness. Begin sectioning in continuous mode, gradually reducing the thickness in smaller increments until the desired thickness is reached.
   Example 1: For a desired slice thickness of 20 µm, start sectioning at 120 µm and reduce in increments (110 µm, 100 µm, 90 µm, etc.) until reaching 20 µm.
   Example 2: For a desired slice thickness of 250 µm, start sectioning at 300 µm and reduce in increments (290 µm, 280 µm, 270 µm, etc.) until reaching 250 µm.

Continue slicing with the VF-510-0Z, adjusting the sectioning speed and frequency as necessary to maintain precision.

Collecting and Incubating Acute Brain Slices

After cutting acute brain slices, it is crucial to incubate them at 37°C or physiological temperature immediately. This step is essential because maintaining the brain slices at physiological temperature helps preserve their cellular integrity and function, ensuring that they remain viable and responsive for subsequent experiments, such as patch-clamp recordings.

To prepare for this, prewarm your incubation chamber filled with artificial cerebrospinal fluid (ACSF) by placing it in a hot water bath set to 37°C. After the brain slices are cut, use a plastic transfer pipette with one end cut off to create a larger opening, and gently transfer each slice into the prewarmed incubation chamber.

Typical incubation times range from 30 to 60 minutes at 37°C. After this incubation period, remove the chamber containing the slices and proceed with your patch-clamp recording experiments to ensure optimal results.

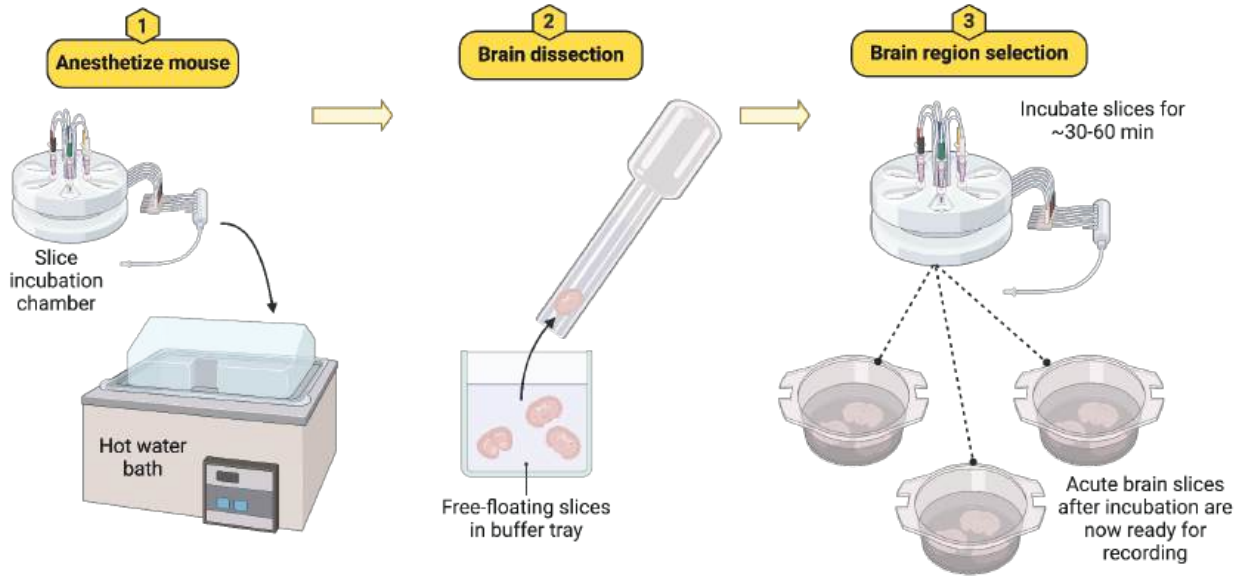


Figure 10. Acute brain slices are incubated at 37°C immediately after cutting to preserve cellular integrity and function. The slices are gently transferred into a prewarmed incubation chamber filled with ACSF, using a modified plastic pipette. After a 30-60 minute incubation period, the slices are ready for patch-clamp recording experiments.

Recording from Acute Brain Slices

The purpose of this section is to guide you through the actual procedure of making a gigaseal on a cell membrane and establishing a patch-clamp configuration. We'll assume your setup is complete and operational.

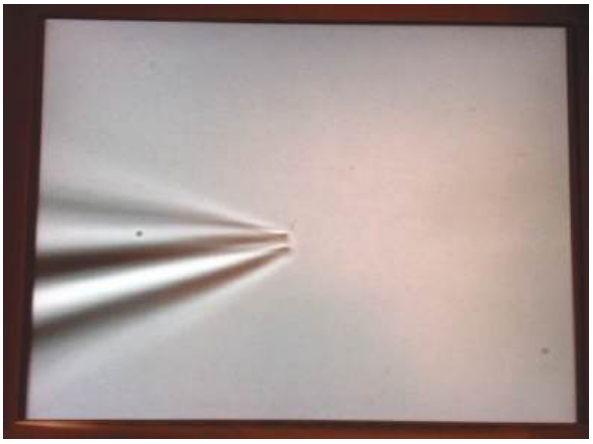
Making Recording Pipettes

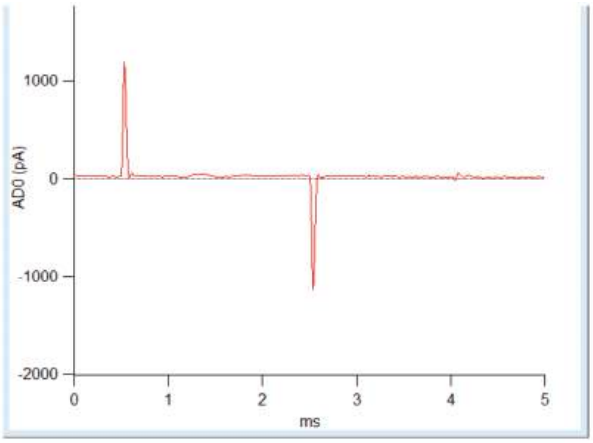
1. Prepare the Pipettes:
   - Quick Tip: The patch pipette should be made and used immediately to reduce tip contamination and ensure good sealing properties.
   - Fire-Polishing: The critical step is fire-polishing the tip, which cleans it and improves seal quality. Pipettes can be pulled and stored in dust-free batches, so they only need fire-polishing and filling just before use.
   - Mount the Pipette: After preparing and mounting the pipette in its holder, position the tip above the bathing solution, directly over the preparation.

Lowering the Pipette Towards the Target Cell

1. Apply Pressure:
   - Prevent Contamination: Before lowering the pipette into the bathing solution, apply slight pressure on the pipette fluid to blow away any contaminants. Contaminants often gather at the fluid-air interface, so maintain pressure before crossing this boundary.
   - Watch the Pressure: Use about 10 cm of water pressure. Too much pressure can blow away your cells!
2. Guide the Pipette:
   - Practice Makes Perfect: Carefully guide the pipette towards the target cell. This step requires practice, and breaking some pipettes while learning is normal.
   - Three-Dimensional Awareness: Be aware of the three-dimensional movement of the manipulator. Know where the focal point of the microscope is situated.
   - Approach the Cell: When approaching the cell, position the focal point between the cell and the pipette.

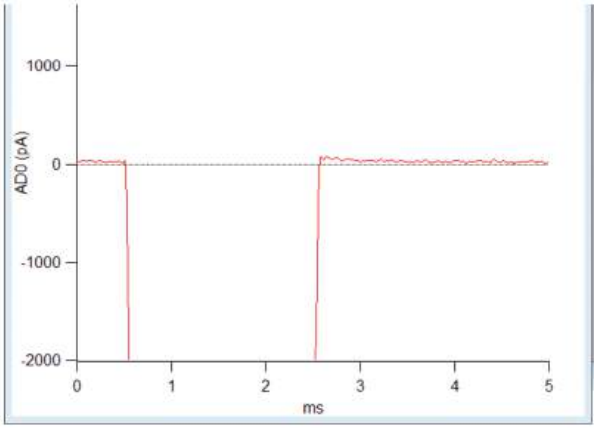
The following figure shows the correct technique for lowering the pipette towards the target cell. Notice the positioning and the slight pressure applied to avoid contaminants.





The recording pipette has not yet been immersed in the external solution, so the screen should display a baseline or near-zero current with no significant electrical activity. The resistance will be high, and there will be minimal noise, indicating that the pipette tip is still in the air and not in contact with the solution.

Locate your pipette under the microscope objective. Carefully adjust the focus until the pipette tip is clearly visible. Slowly lower the pipette using the micromanipulator controls, positioning it just above the surface of the brain slice. Ensure that the pipette tip remains in clear view and is precisely aligned with the targeted area on the slice before proceeding to the next step.

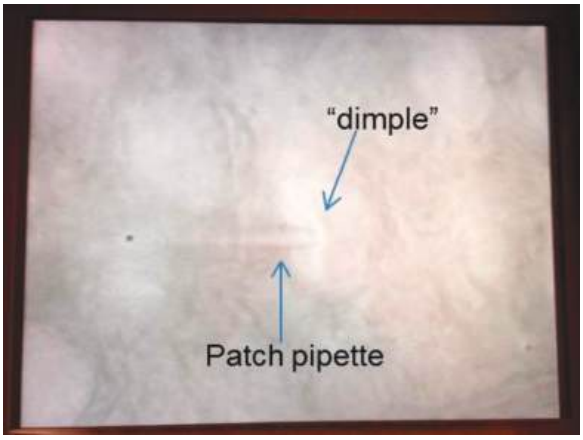


Once the pipette is placed into the bath, the screen should display a stable baseline current, reflecting the electrical properties of the external solution. The resistance reading in this example shows approximately 2.5 MΩ, indicating proper contact between the pipette and the solution. At this point, it's important to correct for the liquid junction potential (LJP) to ensure accurate measurements during your recordings.

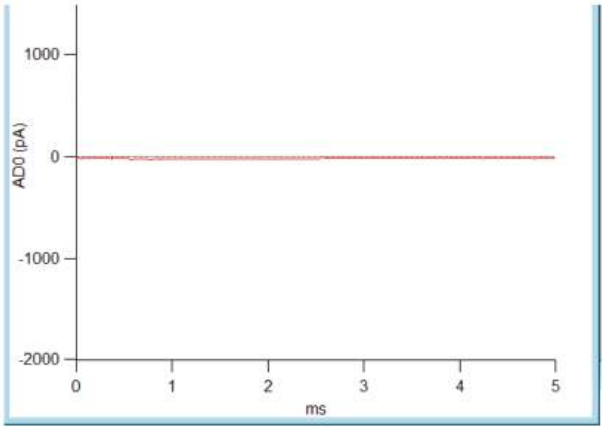
Making the Gigaseal

1. Final Positioning:
    - Contact: The pipette tip should make complete contact with the cell membrane without stressing it. Aim for a spot on the cell that faces the pipette tip straight on.
    - Baseline Nulling: Position the pipette tip near the cell using the fine micromanipulator. Perform final baseline nulling using the amplifier's offset knob.
2. Seal Formation:
    - Monitor Approach: Ideally, monitor the final approach on the microscope and the oscillating test pulse simultaneously.
    - Near-Contact Indication: Near-contact is indicated by a dip in the test pulse response due to increased resistance.
    - Remove Pressure: Remove the pipette pressure, causing a significant drop in the test pulse response. Apply a little suction—usually by mouth—to achieve a gigaseal. A successful seal is indicated by a near absence of current response to a test pulse. The resistance should be more than 1 GΩ for most whole-cell recording applications and even higher for single-channel recording.

Helpful Figure: The following figure illustrates the steps to achieve a gigaseal, including baseline nulling and monitoring the test pulse response.



Apply a small amount of positive pressure to the recording pipette and slowly lower it towards the principal cell. As the pipette approaches the cell surface, observe for a small "dimple" or



When the pipette has successfully gigasealed the cell, the electronics will display a sudden and significant increase in resistance, typically reaching values in the GΩ range. The baseline

indentation where the pipette makes contact with the cell membrane.
Once this dimple is visible, promptly release the positive pressure, allowing the cell membrane to adhere to the pipette tip and form a high-resistance gigaseal. current will stabilize, and the noise level will decrease, indicating a tight seal between the pipette and the cell membrane. This high-resistance gigaseal is essential for accurate recording of the cell's electrical activity.

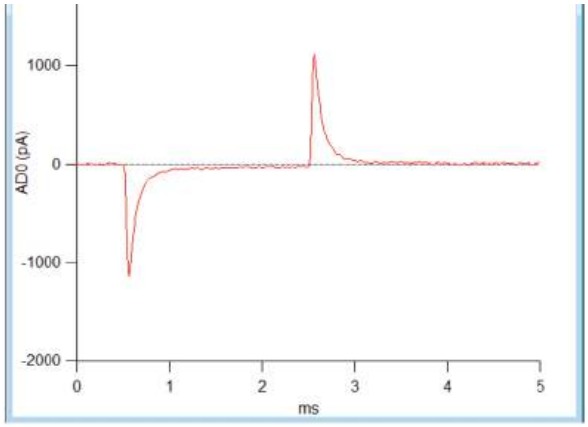
Establishing the Type of Patch-Clamp Recording

Once you have successfully formed a gigaseal and ensured the cell's stability, the next step is to establish the specific type of patch-clamp recording suited to your experimental needs. Different configurations, such as whole-cell recording, perforated patch recording, and single-channel recording, each have unique requirements and procedures. This section will guide you through the process of transitioning to and optimizing these various patch-clamp techniques.

Whole-Cell Recording

1. Gigaseal Formation: Once you have a gigaseal, break the patch of membrane under the pipette tip while maintaining the seal resistance. This allows the pipette solution to contact the cytoplasm.
2. Breaking the Patch:
    - Suction Pulse: Apply a suction pulse through the pipette pressure tubing by mouth. The amount and type of suction depend on the pipette size, cell type, and setup.
    - Zap Function: Alternatively, send a large current pulse through the pipette using the 'zap' function on some patch clamp amplifiers.

Helpful Figure: The following figure shows the steps to transition from gigaseal formation to whole-cell recording, including the use of suction or zap function.





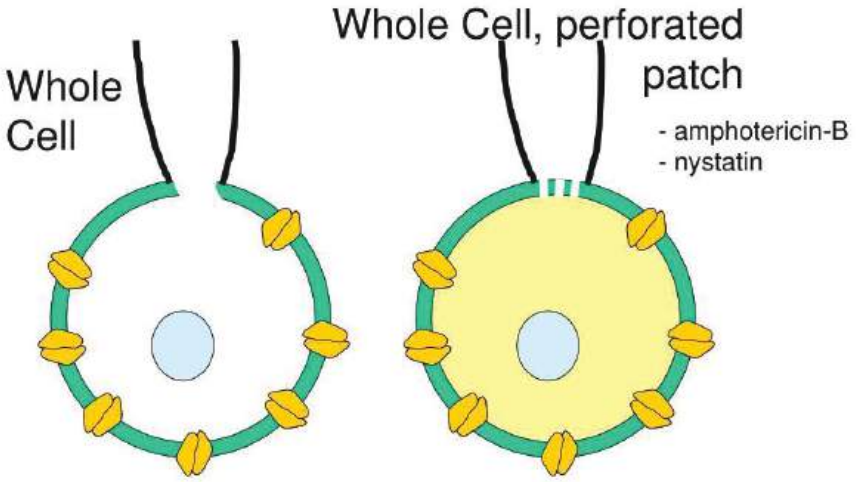
After breaking into the cell using gentle, quick suction on the recording pipette, the electronics will show a sudden drop in resistance, typically down to a lower value consistent with the cell's membrane resistance. The baseline current will adjust to a new level, and you'll observe a change in the noise pattern, indicating that you are now recording from the interior of the cell. This marks the transition to whole-cell configuration, allowing for the measurement of intracellular electrical activity.
You can now begin recording!!

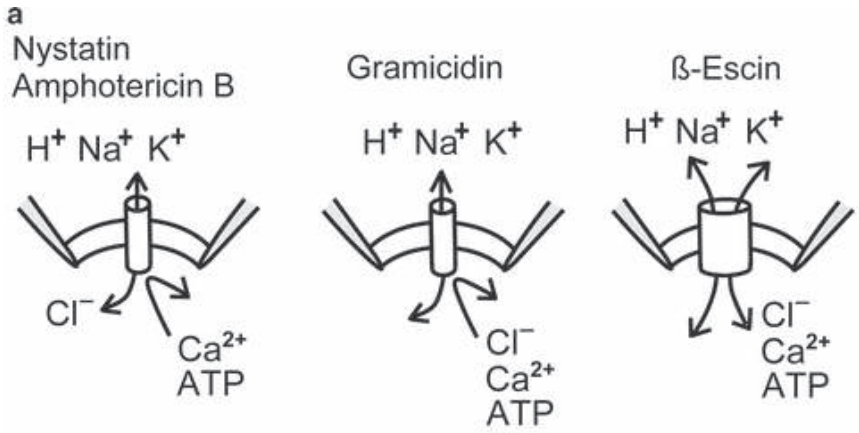
Perforated Patch Recording

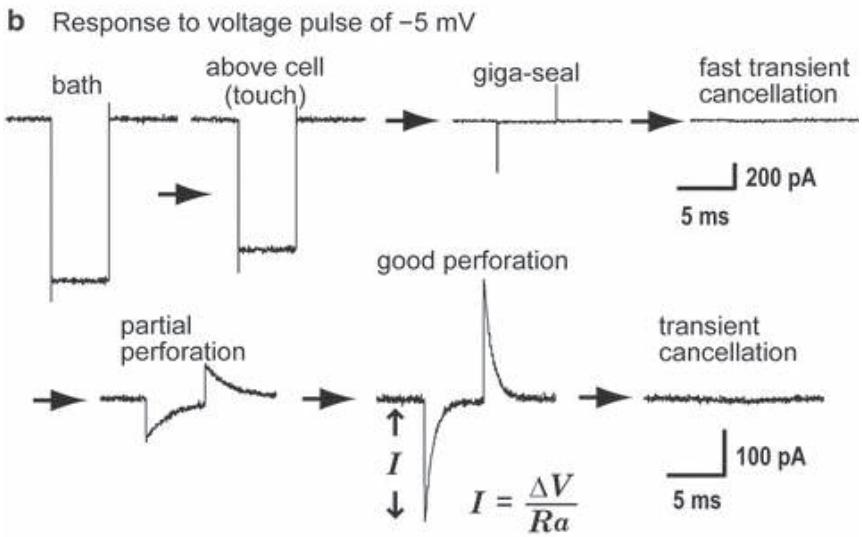
1. Principle: Perforated patch clamping uses antifungal drugs like nystatin or amphotericin B dissolved in ethanol or DMSO and added to the intracellular solution.
2. Preparing the Pipette:
    - Filling the Pipette: Fill the pipette tip with normal intracellular solution using suction from a large syringe connected to the back of the pipette with tubing. Then, fill the pipette with the intracellular solution containing the perforating agent (5–20 µg/ml from a 1000-fold stock).
3. Gigaseal Formation: Form the gigaseal as usual, but leave the patch intact and monitor the current response to a test pulse. After a few minutes, the cell capacitance should manifest, with a decreasing access resistance indicating a progressively faster capacitive transient. The experiment can begin after about 10 minutes when the capacitive transient stabilizes.

Helpful Figure: The following figure illustrates the setup for perforated patch recording, including the use of antifungal agents and monitoring the current response.

The configurations of the patch clamp technique





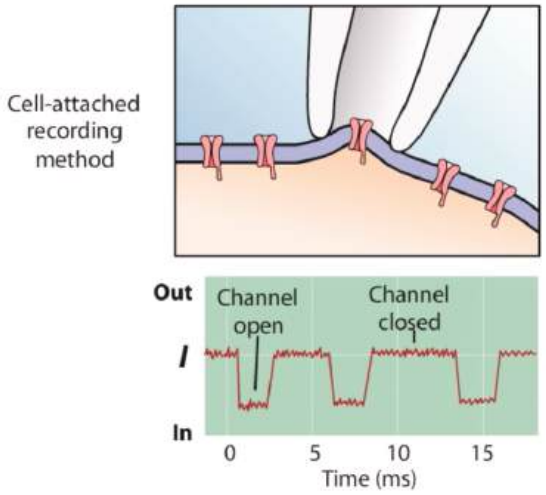


Overview of Cell Perforation. (a) Shows the size and selectivity of commonly used perforating agents. (b) Demonstrates the changes in electrical current in response to a -5 mV voltage pulse during two key stages: first, sealing the patch pipette to the cell to create a high-resistance (GΩ) seal (illustrated in the upper drawing), and then perforating the patch membrane to allow for stable recordings (shown in the lower traces). These recordings were made using an acutely isolated hippocampal neuron, illustrating the transition from sealing to successful cell perforation.

Single Ion Channel Recordings

1. Noise Control: Single-channel recordings require significantly higher sensitivity. Ensure external noise is undetectable.
2. Recording: Single-channel activity appears as instantaneous jumps between current levels, reflecting the stochastic nature of channel opening and closing.

Helpful Figure: The following figure shows a comparison between single-channel and whole-cell recordings, highlighting the differences in sensitivity and noise control.



By following these detailed steps and using the helpful figures, you can successfully establish various patch-clamp configurations and conduct high-quality recordings from acute brain slices. Happy recording!

What to Include in Your Ephys Logbook

It's good practice to keep a record of the standard parameters of each cell being patched. Here's a checklist of what should appear in your laboratory logbook for each cell:

1. **$R_{pipette}$ (Pipette Resistance)**: Record with the pipette in the bath but not on the cell.
2. **R_{seal} (Seal Resistance)**: Note after gigaseal formation.
3. **E_m (Membrane Potential)**: Measure by briefly switching to current clamp mode (I = 0) after the patch is disrupted.
4. **R_{series} and C_m (Series Resistance and Cell Capacitance)**: Record after capacitive transient cancellation.
5. **R_m and R_{leak} (Membrane Resistance and Leak)**: Measure from the ohmic component of the current response to a test pulse.
6. **Percentage R_{series} Compensation (if used)**: Note the percentage if using series resistance compensation.

Sample Logbook Entry:

Date	**[Insert Date]**
Cell ID	[Insert Cell ID]
Experiment	[Insert Experiment Type]

Parameter	**Value**
Rpipette	___ MΩ (Pipette in bath)
Rseal	___ GΩ (After gigaseal formation)
Em (Membrane Potential)	___ mV
Rseries	___ MΩ
Cm (Cell Capacitance)	___ pF
Rm (Membrane Resistance)	___ MΩ
Rleak	___ MΩ
% Rseries Compensation	___%

Notes
- Observations on cell health and behavior.
- Any deviations from standard protocol.
- Environmental conditions (temperature, humidity, etc.).

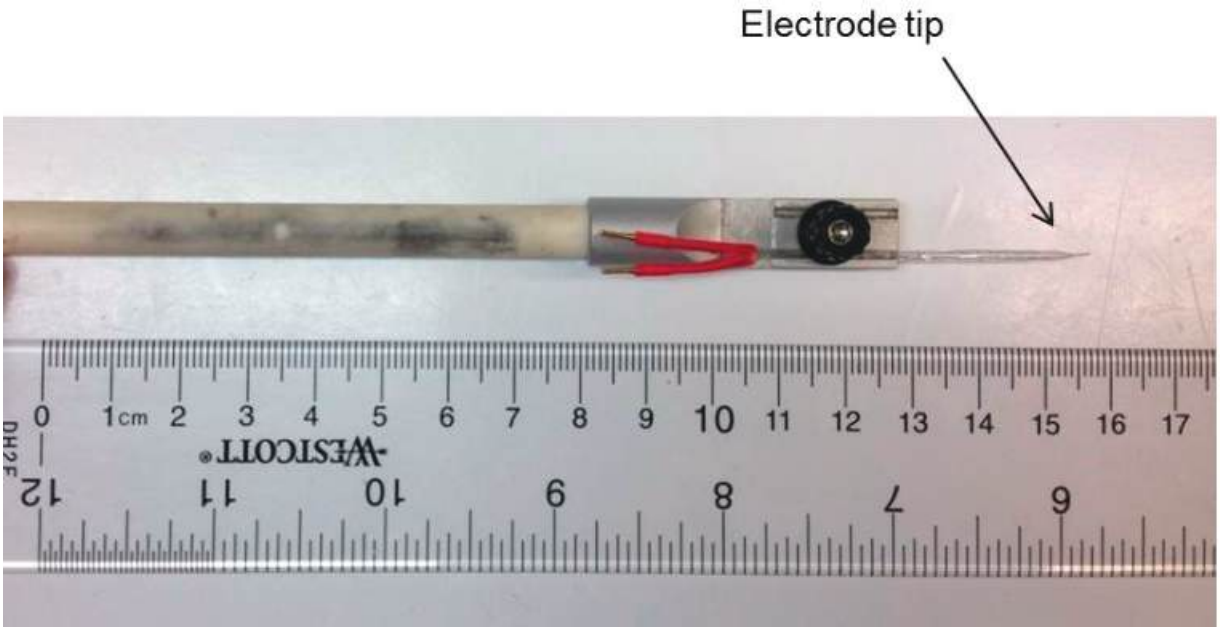
Setup Diagram
[Insert Diagram/Sketch of Setup]

Making Bipolar Electrodes for Stimulation

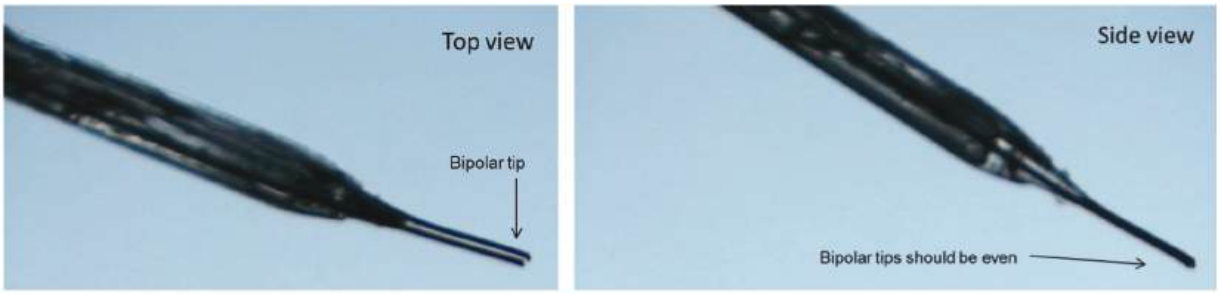
For patch-clamp electrophysiology, stimulating specific fibers or areas often requires the use of a bipolar electrode. While you can purchase commercial electrodes, making your own can be more effective and tailored to your specific needs. Here's a general guide to making a bipolar electrode:

1. **Use Theta Glass as the Electrode Holder**:
   - Theta glass is ideal for making bipolar electrodes due to its dual-channel structure.
2. **Pull the Theta Glass**:
   - Use a pipette puller to pull the theta glass as you would for a recording pipette. Adjust the length to fit onto the electrode holder.
   - **Tip Adjustment**: Break the tip of the pulled theta glass so that the tapered end is somewhat blunt. This helps in positioning the stimulation electrodes correctly.
3. **Select and Thread Tungsten Wire Electrodes**:
   - Choose two tungsten wire electrodes for their durability and conductive properties.
   - Thread each tungsten electrode through one of the theta glass chambers.
4. **Apply Glue**:
   - Apply glue to the opposite end of the theta glass and allow it to travel down to the tip. This secures the tungsten wires in place.
   - **Drying**: Allow the electrode to dry overnight to ensure the glue sets properly.
5. **Adjust the Electrode Tips**:
   - Once dried, bend the bipolar electrode tips so that both are parallel. This configuration ensures consistent stimulation.
   - **Tip Cutting**: Cut the tips with scissors so that they are even. This creates a uniform stimulation field.

Helpful Figure: The following figure shows the process of making a bipolar electrode, from pulling the theta glass to threading and securing the tungsten wires. Here's what the bipolar electrode looks like in its holder:



Here's a higher magnification view of the bipolar electrode. Top view (left) and side view (right). Note that the electrode tips should be parallel and even.



Steps for Making a Bipolar Electrode:

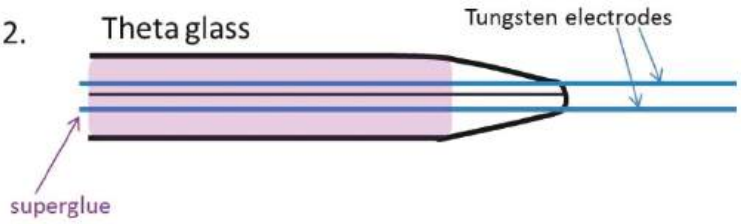
1. **Prepare the Electrode Holder**: Use theta glass as the electrode holder.
2. **Pull the Theta Glass**: Use a pipette puller to pull the theta glass as you would for a recording pipette. Adjust the length to fit your electrode holder.
3. **Blunt the Tip**: Break the tip of the pulled theta glass so that the tapered end is somewhat blunt.
4. **Prepare the Tungsten Wires**: Select two tungsten wire electrodes and thread each one through a separate chamber of the theta glass.

5. **Apply Glue**: Apply glue to the opposite end of the glass, allowing it to flow down to the tip where the wires are. Let the electrode dry overnight.
6. **Final Adjustments**: Once dry, bend the tip of the bipolar electrode so that both wires are parallel. Use scissors to trim the tips evenly.

1.



2.



By following these steps, you can create a reliable and effective bipolar electrode for your patch-clamp experiments. Custom-made electrodes can often provide better performance and adaptability compared to commercially bought ones. Happy experimenting!

Troubleshooting Patch-Clamp Electrophysiology

Even experienced researchers can encounter challenges in patch-clamp electrophysiology. Here are some commonly asked questions and their solutions to help you troubleshoot your experiments.

Q1: Why am I having trouble forming a gigaseal?

There are several factors that can affect gigaseal formation. First, ensure that your pipettes are clean and fire-polished, as dirty or rough pipette tips can prevent good seals. Maintaining slight positive pressure when lowering the pipette into the bathing solution helps keep contaminants away from the tip. Additionally, the cell membrane surface must be clean and undamaged; healthy cells with a debris-free surface are ideal. Finally, always use freshly prepared, properly buffered solutions, as contaminated or improperly mixed solutions can interfere with seal formation.

Q2: What should I do if my cell membrane keeps breaking during whole-cell recording?

If the cell membrane breaks frequently, consider adjusting the suction pressure—gentle suction is key, as too much force can rupture the cell. Ensure your pipette has an appropriate resistance; very high or very low resistance can cause issues. Checking the health of your cells is also important, as stressed or unhealthy cells are more prone to breaking. Lastly, make sure your solutions are at the correct temperature and osmolarity to prevent osmotic shock to the cells.

Q3: Why is my series resistance (Rseries) too high?

High series resistance can affect the quality of your recordings. To reduce it, use pipettes with larger tip openings if appropriate for your cell type, and ensure you have a high-quality gigaseal, as poor seals can contribute to higher resistance. Additionally, make use of series resistance compensation on your amplifier to correct for high resistance during recordings.

Q4: My recordings are noisy. What can I do to reduce the noise?

Noise in recordings can come from various sources. Ensure that all equipment is properly grounded and shielded from external electrical noise. Use clean, well-polished pipettes to reduce noise and make sure your solutions are of high purity to minimize noise from ionic impurities. Placing your setup on a vibration isolation table can also help reduce mechanical noise.

Q5: What should I do if the cell's membrane potential (Em) is unstable?

An unstable membrane potential can be due to several factors. First, ensure the cells are healthy and not under stress. Keep the bathing solution at a stable temperature to prevent fluctuations, and make sure the pipette is stable and properly positioned on the cell membrane. Additionally, check the osmolarity of your solutions, as mismatched osmolarity can cause instability.

Q6: How can I improve the quality of my single-channel recordings?

Single-channel recordings require precise control and setup. Minimize noise by using high-quality, well-shielded equipment and maintaining a clean environment. Aim for gigaseals with resistance much higher than for whole-cell recordings, and ensure your setup is mechanically stable to prevent movement artifacts. Using high-purity reagents and freshly prepared solutions can also reduce noise.

By addressing these common issues with targeted troubleshooting steps, you can improve the quality and reliability of your patch-clamp electrophysiology experiments. Happy experimenting!

More Questions? Contact Us!

If you have any further questions, require additional experimental support, seek references, protocols, or referrals related to patch-clamp electrophysiology or any other aspect of neuroscience research, do not hesitate to reach out to us at Precisionary Instruments. Our dedicated team of experts is here to assist you every step of the way.

You can contact us via:

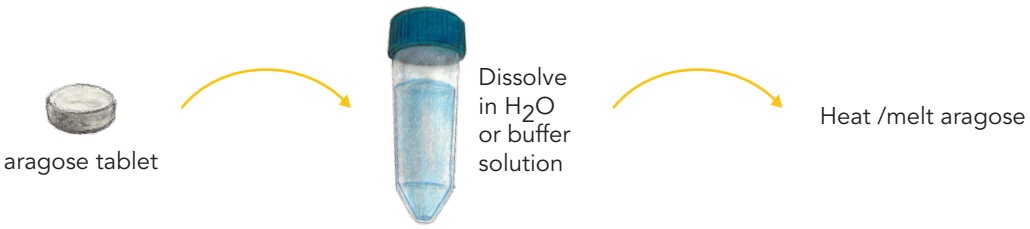
E-mail: info@precisionary.com
Phone: (617) 682-0586
Fax: 1-866-424-2217

Precisionary Instruments
200 Butterfield Drive, Unit E
Ashland, MA 01721

Whether you need troubleshooting assistance, personalized guidance, or customized solutions for your research needs, we are committed to providing you with the support and resources necessary to ensure your success. Don't hesitate to get in touch with us, and let us help you advance your research endeavors.

HOW TO EMBED SPINAL CORD FOR THE COMPRESSTOME® TISSUE SLICER

1 Make agarose: usually ~2% concentration



2 Make the agarose base for holding the spinal cord

(This step helps stabilize the spinal cord for embedding in the Compresstome® specimen tube)



2a. Pour half of the agarose solution into a small petri dish

2b. Store the remaining half of the agarose solution in a hot water bath (~37°C) so that it does not solidify

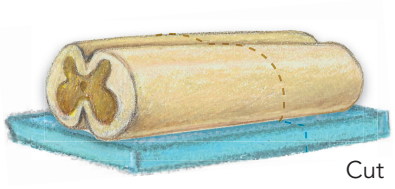
2c. Solidify the agarose in the petri dish at 4°C

2d. After the agarose solidifies, cut out a small rectangular block of agarose about 5 mm wide x 3 mm tall x 3 mm long.

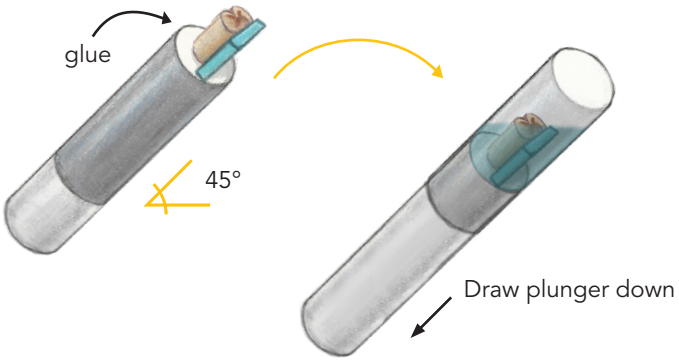
3 Dissect out the spinal cord tissue that you would like to section with the Compresstome® Vibratome

3a. Lay the spinal cord longitudinally onto the small agarose block

3b. Cut off one end so that both the spinal cord and agarose block are even



4 Embed the spinal cord in the agarose in the specimen tube



4a. Glue the spinal cord and agarose block together to the surface of the white plunger. (Tip: keep everything at a 45° angle when loading the spinal cord and agarose block)

4b. Slowly draw down the white plunger until the entire specimen is inside the tube.

4c. Using a transfer pipette, add agarose solution to cover the entire content of the specimen tube

4d. Chill with chilling block

4e. Now you're ready to slice spinal cord tissue!

PRECISIONARY

(617) 682-0586
www.precisionary.com
info@precisionary.com

Boston, USA
Made in USA

PRECISIONARY

EYE

TISSUE SECTIONING

PROTOCOL FOR CUTTING SLICES OF EYE TISSUE

Key to reading the protocol:

√ Rationale for procedural step

♠ Tips & Tricks

1. Obtain eye tissue from animal of choice.
2. Immediately freeze in OCT and/or formalin fixed and embedded in paraffin.
3. Select a section of the eye tissue that you would like to take cut for slices.
4. Glue the tissue sample onto the Compresstome® specimen syringe.
5. Draw the syringe downward to bring the eye tissue core sample into the syringe.
6. Fill the syringe with 2% agarose (Sigma A-0701, low gelling point, incubated at ~37˚C).
    a. Order a Starter Kit or additional agarose or blades directly from our website at http://www.precisionary.com/starter-kit !
7. Cool the entire contents of the specimen syringe with the chilling block. The eye tissue is now embedded in agarose. The agarose will solidify enough for stable sectioning.
8. Load the specimen syringe onto the Compresstome® slicer.
9. The protocol is complete for preparing the eye for sectioning. Proceed from here with normal Compresstome® sectioning procedures.

References

*** Uses the Compresstome® for successful eye tissue slices.**

1. **Rochon PL, Theriault C, Rangel Olguin AG, Krishnaswamy A. The cell adhesion molecule Sdk1 shapes assembly of a retinal circuit that detects localized edges. Elife. 2021 Sep 21;10:e70870. PMID: 34545809; PMCID: PMC8514235.**

HEART TISSUE SECTIONING

PROTOCOL FOR CUTTING SLICES OF HEART TISSUE

Key to reading the protocol:

√ Rationale for procedural step

♠ Tips & Tricks

1. Deeply anesthetize animal with pentobarbital, 70 mg/kg.
    - √ Note that you can perfuse the animal in a variety of ways, including gravity-feed, pump, or push-syringe.
2. Remove hearts by dissection and perfuse in Langendorff-mode with bicarbonate-buffered solution.
    - √ Note that fat accumulation at the epicardial surface increases with animal age. Fat tissue is difficult to cut and can blunt the blade, so we recommend careful manual removal of fat tissue before slicing.
3. Load dye via the coronary circulation, apply by injecting into the aortic cannula. Use 22 µl of a solution containing the voltage-sensitive dye di-4-ANBDQPQ and then Pluronic F-127 (2 µl of a 20% stock solution in DMSO. Add over a 4 to 5 minute time period.
4. After dye loading, perfuse hearts at room temperature with BDM-containing HEPES-buffered solution.
5. Select a section of the heart that you would like to take cut for slices.
6. Glue the tissue sample onto the Compresstome® specimen syringe.
7. Draw the syringe downward to bring the heart tissue core sample into the syringe.
8. Fill the syringe with 4% agarose (Sigma A-0701, low gelling point, incubated at ~37°C).
    - √ Order a Starter Kit or additional agarose or blades directly from our website at http://www.precisionary.com/starter-kit !
9. Cool the entire contents of the specimen syringe with the chilling block. The heart tissue is now embedded in agarose. The agarose will solidify enough for stable sectioning.

10. Load the specimen syringe onto the Compresstome® slicer.
11. The protocol is complete for preparing the heart specimen for sectioning. Proceed from here with normal Compresstome® sectioning procedures.

References

*** Uses the Compresstome® for successful heart tissue slices.**

1. Chang AJ, Ortega FE, Riegler J, Madison DV, Krasnow MA. Oxygen regulation of breathing through an olfactory receptor activated by lactate. Nature. 2015 Nov 12;527(7577):240-4. doi: 10.1038/nature15721. PubMed PMID: 26560302; PubMed Central PMCID: PMC4765808.

2. George AA, Lyons-Warren AM, Ma X, Carlson BA. A diversity of synaptic filters are created by temporal summation of excitation and inhibition. J Neurosci. 2011 Oct 12;31(41):14721-34. doi: 10.1523/JNEUROSCI.1424-11.2011. PubMed PMID:21994388; PubMed Central PMCID: PMC3214667.

3. Hoffman JJ, Johnson BL, Holland MR, Fedewa RJ, Nair A, Miller JG. Layer-dependent variation in the anisotropy of apparent integrated backscatter from human coronary arteries. Ultrasound Med Biol. 2011 Apr;37(4):632-41. doi:10.1016/j.ultrasmedbio.2011.01.007. Epub 2011 Mar 3. PubMed PMID: 21376456;PubMed Central PMCID: PMC3063363.

4. Kamari Y, Cohen H, Shaish A, Bitzur R, Afek A, Shen S, Vainshtein A, Harats D. Characterisation of atherosclerotic lesions with scanning electron microscopy(SEM) of wet tissue. Diab Vasc Dis Res. 2008 Mar;5(1):44-7. doi:10.3132/dvdr.2008.008. PubMed PMID: 18398812.

5. Komatsu S, Kitazawa T, Ikebe M. Visualization of stimulus-specific heterogeneous activation of individual vascular smooth muscle cells in aortic tissues. J Cell Physiol. 2017 Mar 11. doi: 10.1002/jcp.25903. [Epub ahead of print] PubMed PMID: 28295256.

6. Mukherjee S, Trice J, Shinde P, Willis RE, Pressley TA, Perez-Zoghbi JF. Ca2+ oscillations, Ca2+ sensitization, and contraction activated by protein kinase C in small airway smooth muscle. J Gen Physiol. 2013 Feb;141(2):165-78. doi:10.1085/jgp.201210876. PubMed PMID: 23359281; PubMed Central PMCID: PMC3557311.

7. Wang K, Lee P, Mirams GR, Sarathchandra P, Borg TK, Gavaghan DJ, Kohl P, Bollensdorff C. Cardiac tissue slices: preparation, handling, and successful optical mapping. Am J Physiol Heart Circ Physiol. 2015 May 1; 308(9): H1112–H1125.

PRECISION-CUT LUNG SLICING

PROTOCOL FOR CUTTING SLICES OF FRESH LUNG TISSUE

Key to reading the protocol:

√ Rationale for procedural step

♠ Tips & Tricks

1. Anesthetize the animal, then dissect to cannulate the exposed trachea with a catheter.
2. Cool the live lung specimen with 4°C saline.
3. (Optional) Inject a bolus of agarose gel (2%) to fill the pulmonary artery.
    - √ This process of filling with agarose allow for inflation of alveoli with the same embedding material, and prevents the alveoli from collapsing during the cutting process. Some lung specimens may be sectioned without agarose infusion, especially if the lung specimens are from bovine or sheep animal models (because the quantity of agarose needed for infusion exceeds several liters).
4. Using a syringe, inject a bolus of air to clear the airway.
    - √ Injection of air helps infused agarose reach the alveoli.
5. Select a section of the lung lobe you would like to take tissues from for sections.
6. Glue the tissue sample onto the Compresstome® specimen syringe. Place the embedding cap onto the tube, then fill the syringe with 2% agarose (Sigma A-0701, low gelling point, incubated at ~37°C). Tap the side of the tube to dispel any bubbles from the agarose.
    - √ Loading the agarose with the embedding cap allows you to see if there are any bubbles surrounding the specimen *before* you draw the tube plunger down.
7. Draw the syringe downward to bring the lung tissue core sample into the syringe.
8. Cool the entire contents of the specimen syringe with the chilling block. The lung tissue sample is now embedded in agarose. The agarose will solidify enough for stable sectioning.

9. Load the specimen syringe onto the Compresstome® slicer.
10. The protocol is complete for preparing the lung tissue core specimen for sectioning. Proceed from here with normal Compresstome® sectioning procedures.

♠ PCLSs produced can be maintained overnight in Dulbecco's modified Eagle medium (37°C, 5% CO_2) supplemented with 1% penicillin-streptomycin solution.

References

*** Uses the Compresstome® for successful lung tissue slices.**

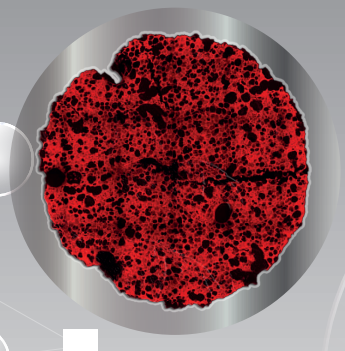
1. ***Graham JG, Winchell CG, Kurten RC, Voth DE. Development of an Ex Vivo Tissue Platform To Study the Human Lung Response to Coxiella burnetii. Infect Immun. 2016 Apr 22;84(5):1438-45.**
2. ***Hiorns JE, Bidan CM, Jensen OE, Gosens R, Kistemaker LE, Fredberg JJ, Butler JP, Krishnan R, Brook BS. Airway and Parenchymal Strains during Bronchoconstriction in the Precision Cut Lung Slice. Front Physiol. 2016 Jul 21;7:309.**
3. ***Oenema TA, Maarsingh H, Smit M, Groothuis GM, Meurs H, Gosens R. Bronchoconstriction Induces TGF-β Release and Airway Remodelling in Guinea Pig Lung Slices. PLoS One. 2013 Jun 26;8(6):e65580.**
4. ***Royce SG, Nold MF, Bui C, Donovan C, Lam M, Lamanna E, Rudloff I, Bourke JE, Nold-Petry CA. Airway Remodeling and Hyperreactivity in a Model of Bronchopulmonary Dysplasia and Their Modulation by IL-1 Receptor Antagonist. Am J Respir Cell Mol Biol. 2016 Dec;55(6):858-868.**
5. ***Yim PD, Gallos G, Perez-Zoghbi JF, Trice J, Zhang Y, Siviski M, Sonett J, Emala CW Sr. Chloride channel blockers promote relaxation of TEA-induced contraction in airway smooth muscle. J Smooth Muscle Res. 2013;49:112-24.**

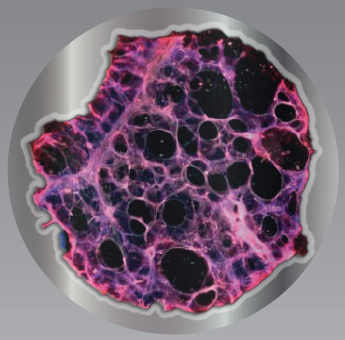
PRECISIONARY

PRECISION-CUT LUNG SLICES (PCLS)

Experimental Research Manual
(Step-By-Step Guide)

www.precisionary.com





Abigail Chu, MD-PhD
Chief Scientific Officer (CSO)
Precisionary Instruments
617-682-0586

Table of Contents

Goals of this Experimental Guide **3**
What is PCLS and Why is it Important? 3
Who This Guide Can Help 3
Contact Precisionary Instruments for Any Additional Experimental Support Help 4

Materials and Reagents **5**
Equipment 5
Lab Accessories 5
Reagents 5

Gross anatomic location of lung lobes **6**
Mouse Lung Anatomy 6
Human Lung Anatomy 7

Making PCLS from Mouse Lungs **8**
Mouse Dissection and Harvesting Lungs 8
Slicing Dissected Lung into PCLS 10

Making PCLS from Human Lungs **12**
Preparation for Human PCLS Sectioning 13
Receiving and Storing Human Lung Tissue 14
Inflating Human Lung Tissue with Agarose Solution 14
Slicing Blocks of Human Lung Tissue into PCLS 16
Making PCLS from Human Lung Lobe Cores/Punches 16
Culturing Human PCLS 16

High Throughput PCLS Sectioning **16**
Preparation for High Throughput PCLS Sectioning 17
High Throughput PCLS Sectioning Procedure 18

After Making PCLS **20**

Troubleshooting PCLS **22**

Recipes **23**
Agarose Solution 23
HBBS/HEPES 24
SF-DMEM 24
70% Ethanol 25

More Questions? Contact Us! **26**

Goals of this Experimental Guide

Precision-cut lung slices (PCLS) have become invaluable tools in respiratory research due to their ability to closely mimic in vivo lung physiology. This guide aims to provide researchers with a comprehensive understanding of PCLS techniques, applications, and experimental protocols. Below are the key objectives of this guide:

What is PCLS and Why is it Important?

In the world of studying lungs, scientists have developed different ways to understand how lung tissues repair themselves. Precision-cut lung slices (PCLS) are one such method. These slices keep the tiny air sacs in the lungs intact and are becoming more popular for studying how lungs work and why diseases happen.

While other methods like growing lung cells in a dish or making tiny lung-like structures called organoids have helped in lung research, they still don't perfectly mimic how lungs behave in the body. PCLS, however, come close to replicating the real lung environment, acting as a bridge between lab dishes and real lungs.

Scientists have started using PCLS more to study lung biology. Compared to other lab methods, PCLS offer a big advantage: they let scientists watch how cells behave in a 3D lung environment, similar to what happens in real life. Plus, using PCLS means fewer animals need to be used for experiments because many lung slices can be made from just one lung. There are also new tools being developed that use PCLS, like a method we recently published that lets us watch how tiny air sacs form in baby mouse lungs in real-time.

Who This Guide Can Help

This guide is designed to assist a wide range of individuals involved in respiratory research, including:

- New researchers who are just starting to work with precision-cut lung slices (PCLS) and want to learn the step-by-step process of obtaining healthy lung sections for their experiments.
- Experienced scientists who have previously worked with PCLS and are seeking additional troubleshooting tips and tricks to enhance the quality of their PCLS procedures.
- Research mentors who are responsible for training others on how to prepare PCLS and wish to utilize this guide/manual as a teaching resource.

- Anyone interested in advancing their understanding of PCLS techniques and applications, regardless of their level of expertise in respiratory research.

Whether you're new to PCLS or have years of experience, whether you're conducting experiments or training others, this guide aims to provide valuable insights and practical guidance to support your endeavors in respiratory research.

Contact Precisionary Instruments for Any Additional Experimental Support Help

For further assistance, you are encouraged to reach out to Precisionary Instruments—a leading provider of vibratome equipment and accessories. Whether it's technical inquiries, troubleshooting guidance, or customized solutions, our expert team stands ready to support researchers at every stage of their PCLS experiments. Through this guide, we aspire to empower researchers with the knowledge and tools necessary to leverage the full potential of PCLS in advancing respiratory research and improving human health.

Let’s begin!

Materials and Reagents

In conducting precision-cut lung slice (PCLS) experiments, it's imperative to have the appropriate materials and reagents ready for use. Below are categorized lists of essential equipment, lab accessories, and reagents required for this procedure:

Equipment

☐ Automated vibratome (e.g., Compresstome® vibratome, Precisionary Instruments) with specimen holder and specimen tube
☐ 37°C, 5% CO2 incubator

Lab Accessories

☐ Syringe chilling block
☐ Stainless steel blades
☐ 24-well tissue culture plate
☐ Petri dish
☐ Scalpel blade
☐ Small metal spatula
☐ 21-G rigid metal cannula
☐ Surgical suture
☐ 5-ml and 60-ml syringes
☐ 5-ml tube, sterile (or similar size)
☐ Fine surgical scissors
☐ Forceps with curved and with straight tip
☐ Fine-tipped spring scissors

Reagents

☐ Super glue
☐ 70% ethanol
☐ 2% (w/v) agarose (see recipe)
☐ 200 mg/ml pentobarbital (e.g., Pentoject)
☐ 1× Hank's balanced salt solution (HBSS) containing 1% (v/v) of
☐ 1 M HEPES (See Recipes section)
☐ Serum-free Dulbecco's modified Eagle medium (SF-DMEM) supplemented with 1% penicillin-streptomycin (See Recipes section)

Gross anatomic location of lung lobes

Understanding the gross anatomic location of lung lobes is essential for effectively working with precision-cut lung slices (PCLS). This section provides a simplified overview of the anatomy of lung lobes in both mice and humans, highlighting key similarities and differences between the two species.

Mouse Lung Anatomy

In rodents, such as mice, the right lung comprises four lobes: the cranial, middle, caudal, and accessory lobes (Figure 1). Conversely, the left lung consists of a single lobe. This arrangement contrasts with human lung anatomy, where the right lung has three lobes and the left lung has two. Additionally, mouse lungs exhibit fewer respiratory bronchioles and airway generations (approximately 13–17 generations) compared to humans, with a monopodial branching pattern in the airways. Despite these anatomical differences, mice serve as valuable models for studying respiratory physiology and diseases due to fundamental similarities in lung structure and function.

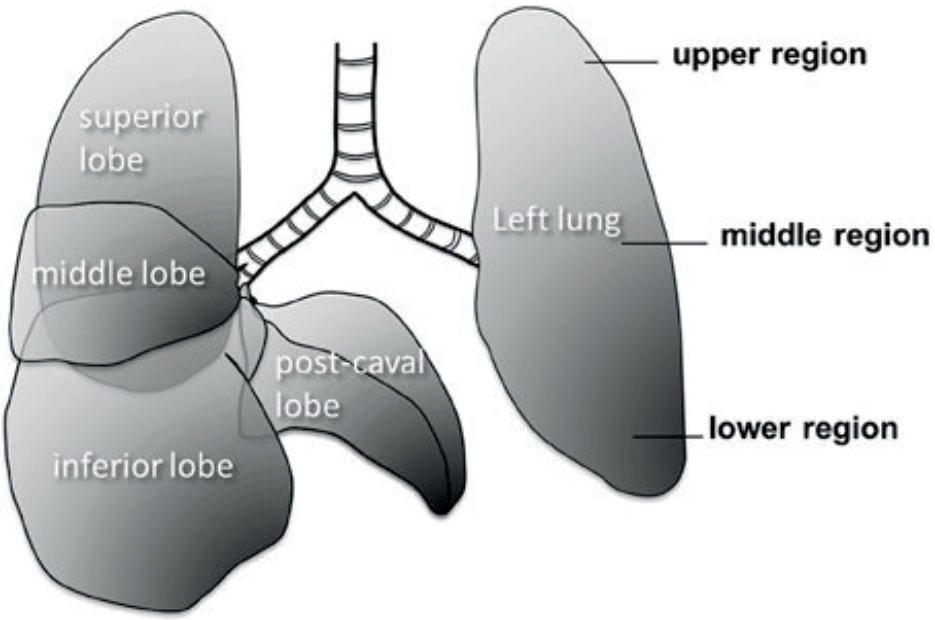


Figure 1. Overview of Mouse Lung Anatomy. The mouse lung exhibits a distinct large-scale structure, with the right lung featuring four lobes and the left lung characterized by a single lobe. Specifically, the right lung encompasses the superior, middle, inferior, and post-caval lobes, contributing to its functional complexity and physiological significance.[1]

[1] Sato, S., Bartolák-Suki, E., Parameswaran, H., Hamakawa, H., & Suki, B. (2015). Scale dependence of structure-function relationship in the emphysematous mouse lung. Frontiers in physiology, 6, 146.

Human Lung Anatomy

Humans have two lungs: the right lung, which comprises three lobes (upper, middle, and lower lobes), and the left lung, which has two lobes (upper and lower lobes) (Figure 2). This asymmetrical arrangement accommodates the heart's position in the chest cavity. Diseases affecting specific lung lobes can lead to differential symptoms and complications. For instance, conditions like pneumonia or lung cancer may predominantly affect certain lobes, influencing diagnostic and treatment approaches.

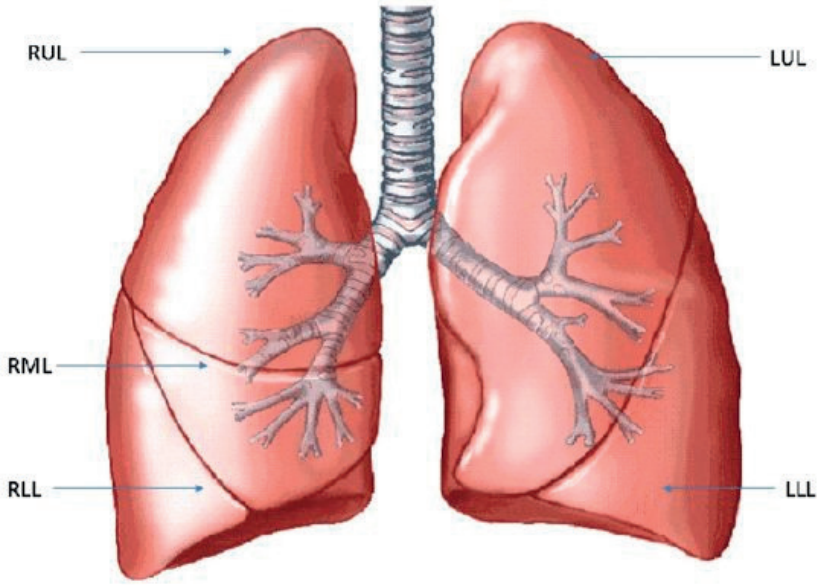


Figure 2. Human Lung Anatomy and Lung Lobes. Illustrated here is a schematic depiction of the human lung, delineating its five distinct lobes. These lobes include the right upper lobe (RUL), right middle lobe (RML), right lower lobe (RLL), left upper lobe (LUL), and left lower lobe (LLL). Such regional divisions serve as vital anatomical landmarks in understanding pulmonary function and pathology.[2]

Understanding the gross anatomical differences between mouse and human lungs is crucial for translational research, where findings from animal models like mice are extrapolated to human physiology and pathology. While mice serve as valuable models for studying lung biology and disease, researchers must consider species-specific anatomical variations when interpreting experimental results and designing therapeutic interventions.

[2] Rauschenbach, B. M., Mackowiak, L., & Malhotra, H. K. (2014). A dosimetric comparison of three-dimensional conformal radiotherapy, volumetric-modulated arc therapy, and dynamic conformal arc therapy in the treatment of non-small cell lung cancer using stereotactic body radiotherapy. Journal of applied clinical medical physics, 15(5), 4898. https://doi.org/10.1120/jacmp.v15i5.4898

Making PCLS from Mouse Lungs

Now that we've gained a quick understanding of mouse and human lung anatomy, let's delve into the process of preparing precision-cut lung slices (PCLS). We'll start with the mouse model since it's the most commonly used mammalian model in basic sciences research.

Mouse Dissection and Harvesting Lungs

1. Gather all necessary dissection tools and equipment, including dissection tools **(Figure 3)**.

2. Begin by humanely euthanizing postnatal day 3 (P3), P7, P14, or adult (6-8 weeks) C57BL/6 mice using intraperitoneal injection of pentobarbital. Confirm death by exsanguination of the femoral artery.

3. Place the mouse on a dissection tray and spray 70% ethanol over the abdomen, chest, and neck. Pinch and cut the skin, make a longitudinal incision along the midline of the abdomen and chest, and expose the diaphragm.

4. Carefully lift the sternum, make an incision on the diaphragm, and separate the chest wall from the body. Remove muscle and fascia from the neck wall, then make an opening between the trachea and esophagus.

5. Insert a suture through the trachea, make an opening in the trachea, and insert a rigid metallic cannula. Inflate the lungs with warm agarose solution and solidify it with ice.

6. Remove the cannula, excise the trachea, and immerse the heart and lungs in ice-cold serum-free DMEM until slicing.



Figure 3. Comprehensive workflow for mouse dissection and lung harvesting. Dissection equipment includes suture, curved forceps, fine tip forceps, fine tip dissecting scissors, surgical scissors, spring scissors, and pentobarbital in a 1 ml syringe attached with a hypodermic needle. The skin incision line is depicted for reference. The process involves two main scenarios: C. Adult mouse dissection, agarose inflation, and harvesting of lungs; and D. Postnatal day 3 (P3) mouse dissection, agarose inflation, and lung harvesting.[3]

[3] Akram, K. M., Yates, L. L., Mongey, R., Rothery, S., Gaboriau, D. C. A., Sanderson, J., Hind, M., Griffiths, M., & Dean, C. H. (2019). Time-lapse Imaging of Alveologenesis in Mouse Precision-cut Lung Slices. Bio-protocol, 9(20), e3403. https://doi.org/10.21769/BioProtoc.3403

Slicing Dissected Lung into PCLS

1. Prepare the automated vibratome, sterilize the buffer tray, and attach the vibratome blade **(Figure 4)**. Sterilize specimen holder and tube, and chill the syringe block in the freezer.

2. Prepare agarose gel, HBSS/HEPES buffer, and SF-DMEM. Separate the left lung lobe from the bronchus, excise a tissue section, and place it on a blue roll to soak up excess media.

3. Attach the lung lobe to the specimen holder, submerge it in warm agarose, and solidify it with the syringe block. Align the blade, set cutting parameters, and start collecting transverse PCLS.

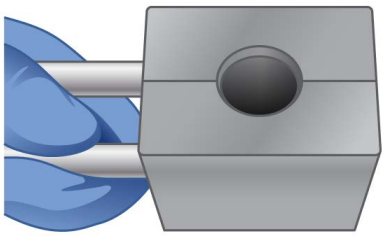
4. Collect PCLS in a 24-well plate containing SF-DMEM. Incubate PCLS at 37°C with 5% CO2 for 2 hours, wash them twice, and further incubate for 1 hour before live imaging or experimentation.



Step 23



Step 24



Step 25

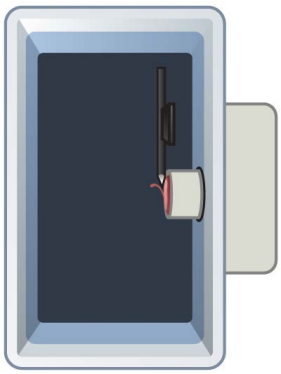
Solidified agarose



Step 26



Step 27



Step 28



Step 29

Figure 4. Setup for precision-cut lung slicing and live imaging. A. The lung slicer utilized is the Vibratome, specifically the Compresstome® VF-300-0Z model. B. A syringe chilling block is employed for solidifying agarose. C. Agarose-inflated lungs harvested from a P3 mouse are shown. D. A separated left lung lobe is placed on a laboratory tissue roll. E. A schematic diagram illustrates agarose embedding of the left lung lobe on a specimen holder for making precision-cut lung slices (PCLS). F. Precision-cut lung slices are arranged in a 24-well plate. G. Transwell modification facilitates the stabilization of lung slices on the well plate. H. Precision-cut lung slices are set in an ibidi 24-well µ-plate using modified transwells and metal flat washers (black rim). I. A schematic demonstrates the relative position and alignment of the metal flat washer, transwell, lung slice, and 40x long working distance air objective lens on an inverted microscope for live imaging.

This process ensures the preparation of high-quality PCLS suitable for various experiments and analyses.[4]

Making PCLS from Human Lungs

Having discussed the process of making PCLS from mouse lungs, it's equally important to explore the generation of human PCLS (Figure 5). Human lung PCLS offer unique insights into lung diseases, serving as valuable tools for assessing lung toxicity of chemicals and drugs. Moreover, recent advancements have allowed the use of human lung tissue from patients with various respiratory conditions, enabling detailed pathophysiological and pharmacological studies. This section provides a comprehensive protocol for the generation of human PCLS from surgically resected soft-elastic patient lung tissue.

[4] Akram, K. M., Yates, L. L., Mongey, R., Rothery, S., Gaboriau, D. C. A., Sanderson, J., Hind, M., Griffiths, M., & Dean, C. H. (2019). Time-lapse Imaging of Alveologenesis in Mouse Precision-cut Lung Slices. Bio-protocol, 9(20), e3403. https://doi.org/10.21769/BioProtoc.3403

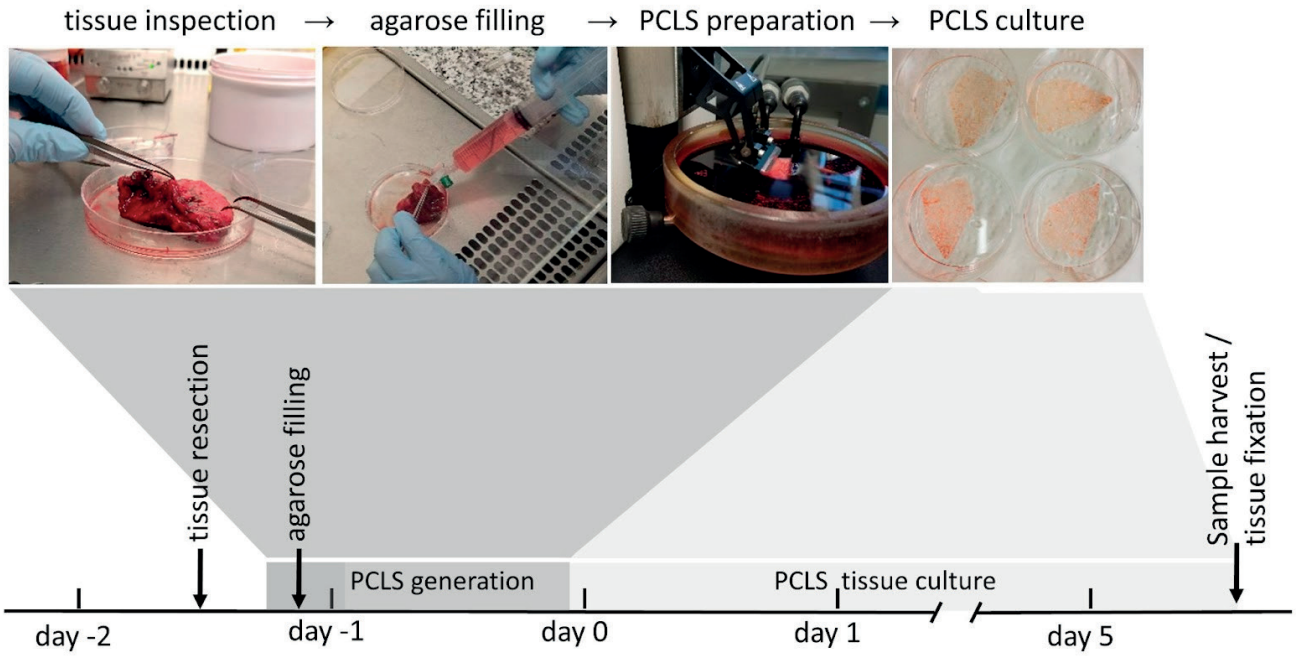


Figure 5. Proposed workflow for generating human Precision-Cut Lung Slices (PCLS). Initially, tumor-free regions of lung resections undergo thorough inspection to assess tissue integrity. Upon determining suitability for further use, as explained in detail in the materials and methods section, the tissue is filled with liquid agarose. Subsequently, tissue blocks filled with solidified agarose are sliced using a vibratome. These slices are then cultured in cell culture medium for up to 120 hours to form 3D Lung Tissue Cultures (3D-LTC). Downstream analyses of the 3D-LTCs include protein or RNA expression studies, live-tissue fluorescence imaging, as well as immunofluorescence staining following tissue fixation.[5]

Preparation for Human PCLS Sectioning

1. Prepare the cultivation medium: Dulbecco's Modified Eagle Medium (DMEM) F-12 supplemented with L-Glutamine, HEPES, Penicillin, Streptomycin, and fetal bovine serum. Ensure the medium is at 37°C.
2. Set up a sterile metal tray covered with tissue paper. Place a sterile 15 cm cell culture dish on the tray and fill it with 15 mL of cultivation medium.
3. Prepare a 3% (w/v) agarose solution by dissolving low-melting point agarose in cultivation medium. Heat the solution until boiling, then cool it to 42°C in a water bath. Keep the liquid agarose solution stored in the water bath.
4. Prepare several 50 mL conical tubes filled with the liquid agarose.

[5] Gerckens, M., Alsafadi, H. N., Wagner, D. E., Lindner, M., Burgstaller, G., & Königshoff, M. (2019). Generation of Human 3D Lung Tissue Cultures (3D-LTCs) for Disease Modeling. Journal of visualized experiments : JoVE, (144), 10.3791/58437. https://doi.org/10.3791/58437

Receiving and Storing Human Lung Tissue

1. Immediately store fresh, tumor-free lung tissue from lobectomy resectates in DMEM F-12 medium at 4°C until further processing.
2. Ensure not to exceed a cold ischemia time of 4-8 hours prior to processing.

Inflating Human Lung Tissue with Agarose Solution

1. Lift the tissue from the storage medium and drain excess media. Transfer the lung tissue into the prepared culture dish **(Figure 6)**.
2. Fill a 30 mL syringe with the low-melting point agarose solution.
3. Prepare a peripheral venous catheter and insert it into a selected bronchus (0.5-3 mm diameter) in the tissue.
4. Gently push the cannula forward, sealing the bronchus around it with forceps to prevent agarose leaking.
5. Fill the tissue with agarose using the syringe, ensuring complete inflation without over-inflating.
6. Clamp the bronchus immediately after filling and incubate the tissue in the culture medium at 4°C for 30 minutes for agarose solidification.
7. Repeat the process for tissue sections with multiple bronchial entries.

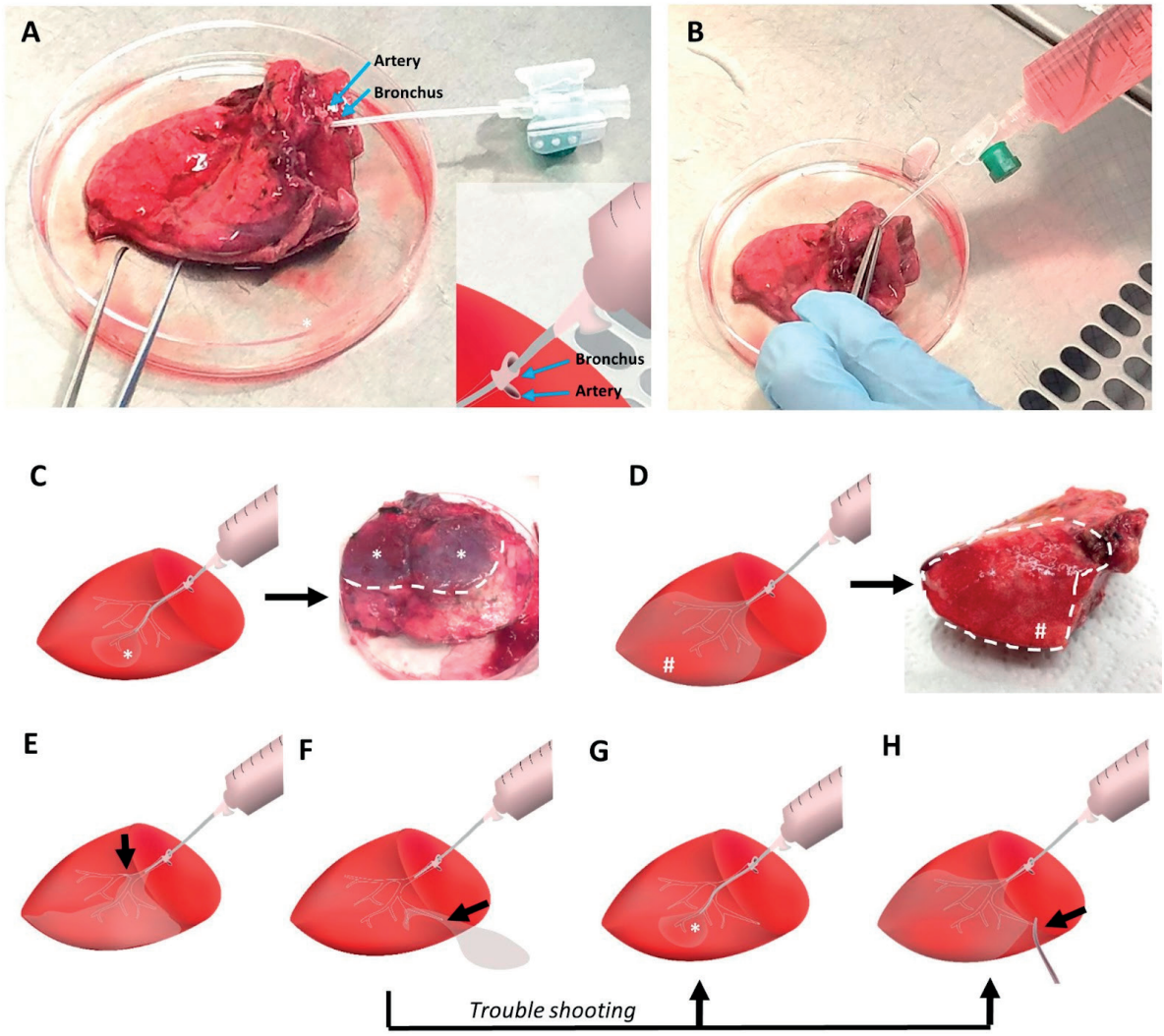


Figure 6. Process of filling lung tissue with low-melting point agarose. Initially, the lung tissue is cannulated using a peripheral venous catheter, inserted into a bronchus adjacent to the pulmonary artery (A). Tweezers are employed to secure the cannula in the bronchus and to clamp the pulmonary artery, preventing leakage of the liquid agarose. Subsequently, liquid agarose at 42°C is injected into the lung tissue using a 30 mL syringe (B). The positioning of the cannula during filling determines the extent of tissue filled; distal positioning results in smaller filled areas (C), while proximal positioning ensures the filling of a larger tissue volume (D). Any obstructions in the airways may limit the tissue volume that can be filled (E). In the event of agarose leakage, distal cannula positioning and/or clamping of the leakage side facilitate proper agarose filling of the lung tissue (F-H).[6]

[6] Gerckens, M., Alsafadi, H. N., Wagner, D. E., Lindner, M., Burgstaller, G., & Königshoff, M. (2019). Generation of Human 3D Lung Tissue Cultures (3D-LTCs) for Disease Modeling. Journal of visualized experiments : JoVE, (144), 10.3791/58437. https://doi.org/10.3791/58437

Slicing Blocks of Human Lung Tissue into PCLS

1. Identify regions solidly filled with agarose in the lung tissue. Excise tissue blocks from these regions, leaving one side covered with pleura.
2. Attach tissue blocks to the vibratome holder using cyanoacrylate glue and slice the tissue with appropriate settings.
3. Transfer slices into wells of a 12-well plate filled with cultivation medium for further incubation.

Making PCLS from Human Lung Lobe Cores/Punches

1. Transfer lung slices from a single well to an empty dish and use a biopsy puncher to create lung punches.
2. Place punches into wells of a 96-well plate filled with cultivation medium for incubation.

Culturing Human PCLS

1. Culture PCLS and punches overnight under standard cell culture conditions.
2. For downstream applications, wash PCLS and punches, harvest protein or RNA, or analyze secreted proteins.

Human lung PCLS offer a valuable platform for studying respiratory diseases and pharmacological interventions. By following this detailed protocol, researchers can generate human PCLS from resected patient lung tissue, facilitating advanced studies into lung pathophysiology and therapeutic strategies.

High Throughput PCLS Sectioning

In contemporary biomedical research, the demand for high throughput processing of precision-cut lung slices (PCLS) is ever-increasing. However, traditional methods often fall short in meeting this demand due to limitations in sample capacity and processing efficiency. In response to this pressing need, the Compresstome VF-800-0Z vibratome model offers a viable solution for achieving high throughput PCLS sectioning (Figure 7). This section outlines the steps involved in utilizing the Compresstome VF-800-0Z for efficient and precise generation of PCLS sections.

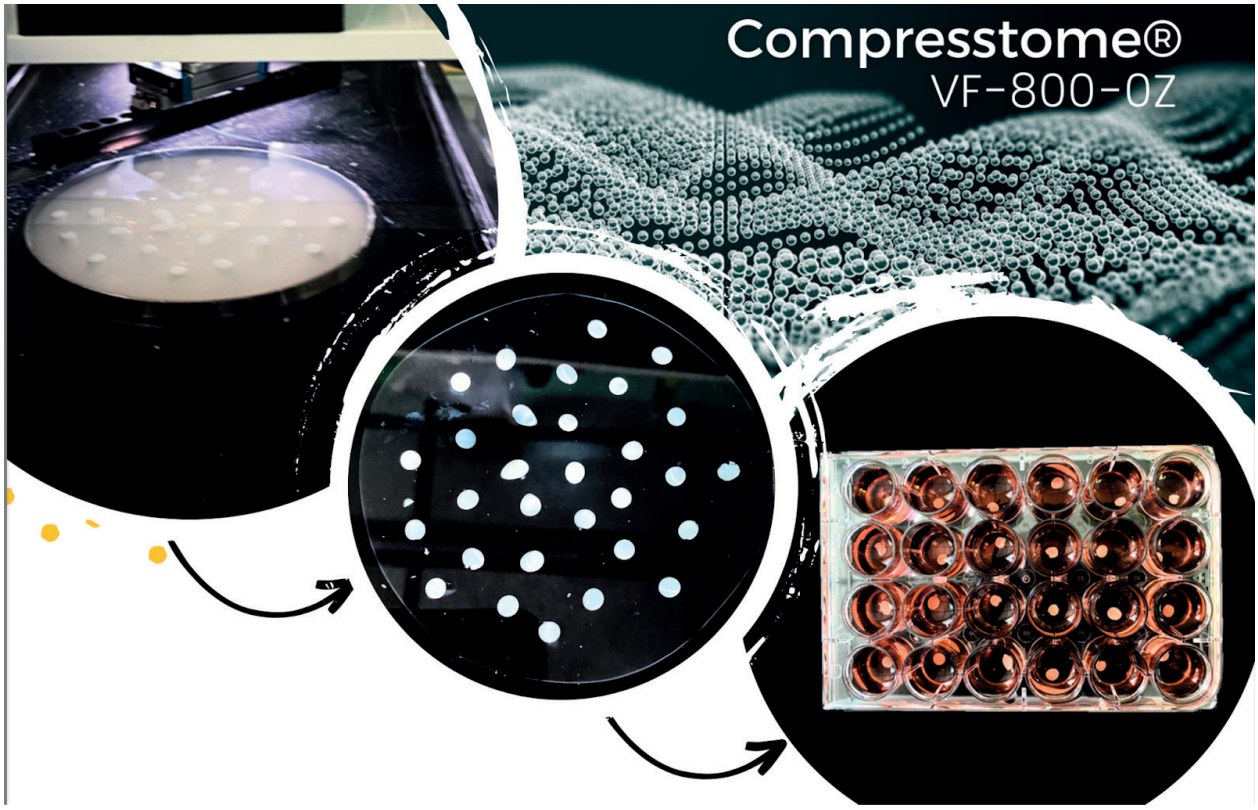


Figure 7. The Compresstome VF-800-0Z vibratome model presents an effective solution for achieving high throughput Precision-Cut Lung Slices (PCLS) sectioning. This figure demonstrates the embedding of 20 or more cored samples onto the stage of a Compresstome VF-800-0Z. Each sheet cut yields dozens of PCLS slices, facilitating the transfer and filling of an entire well plate for future processing.

Preparation for High Throughput PCLS Sectioning

1. Setup and Calibration: Begin by setting up the Compresstome VF-800-0Z vibratome according to the manufacturer's instructions. Ensure that the instrument is properly calibrated to achieve the desired section thickness.

2. Agarose Solution Preparation: Prepare a suitable agarose solution for embedding the tissue samples. Ensure that the agarose is properly dissolved and cooled to the desired temperature for optimal embedding **(Figure 8)**.

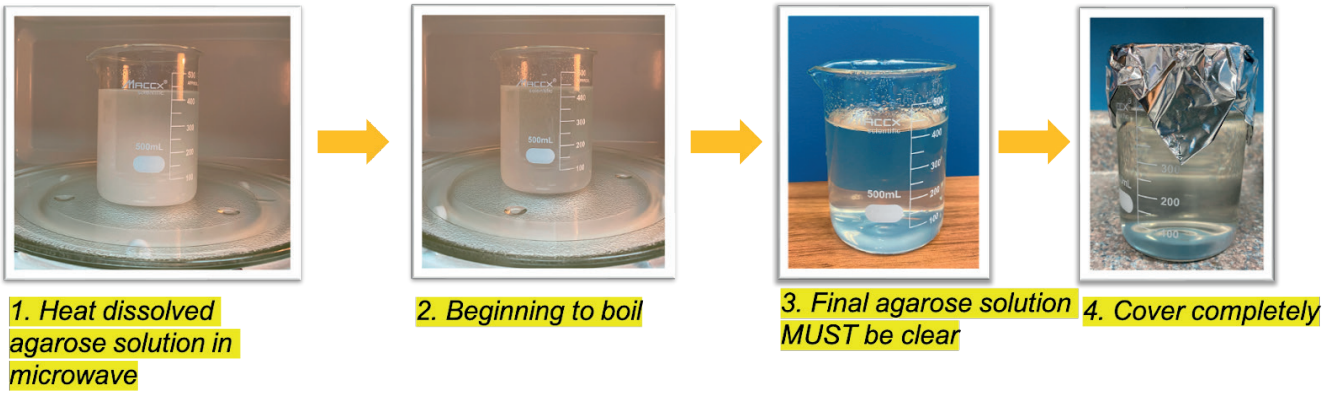


Figure 8. Agarose Solution Preparation. Prepare agarose solution for tissue embedding. Ensure thorough dissolution and cooling to the desired temperature for optimal embedding.

High Throughput PCLS Sectioning Procedure

1. Loading Samples: Place the embedded tissue samples onto the specimen plunger (loading platform) of the Compresstome VF-800-0Z. The instrument's design allows for the accommodation of multiple samples simultaneously, enabling high throughput processing **(Figure 9)**.

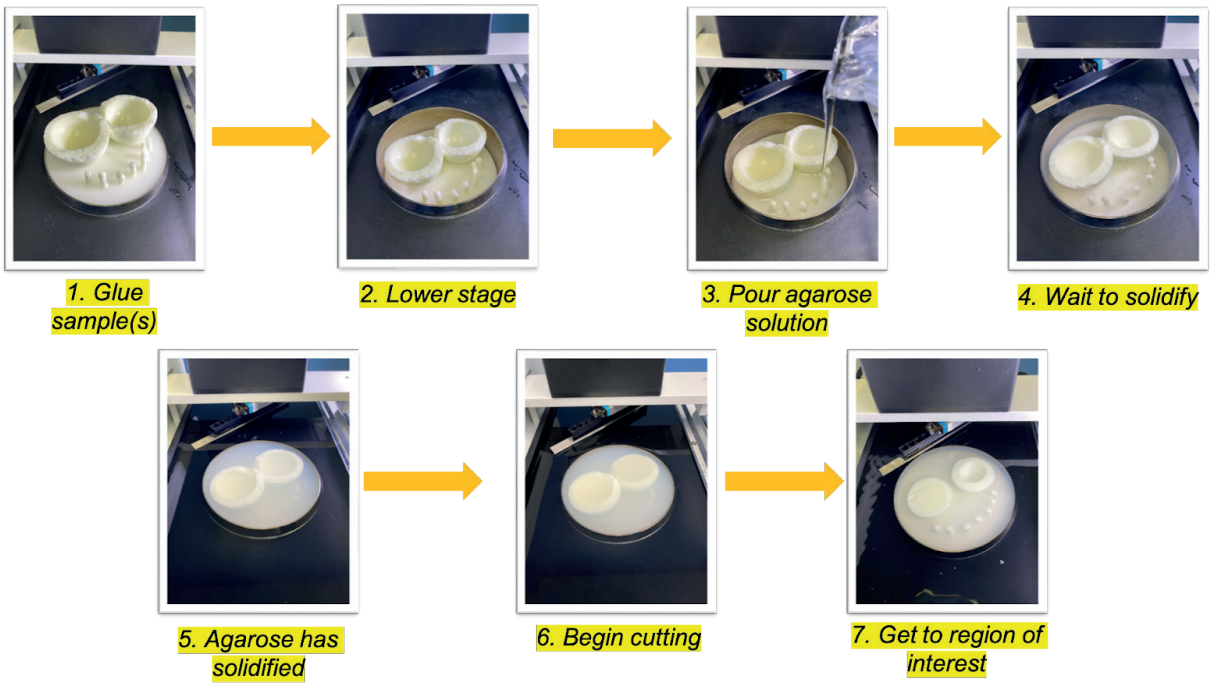


Figure 9. Loading Samples on to the Compresstome VF-800-0Z. Place embedded tissue samples onto the specimen plunger (loading platform) of the Compresstome VF-800-0Z. The instrument's design facilitates simultaneous processing of multiple samples, ensuring high throughput capability.

2. Sectioning Parameters: Set the desired section thickness and cutting parameters on the Compresstome VF-800-0Z control panel. Ensure uniformity in section thickness across all samples to maintain consistency in experimental results.
3. Sectioning Process: Initiate the sectioning process, allowing the Compresstome VF-800-0Z to precisely cut through the embedded tissue samples. Monitor the sectioning progress to ensure optimal performance and quality of PCLS sections **(Figure 10)**.

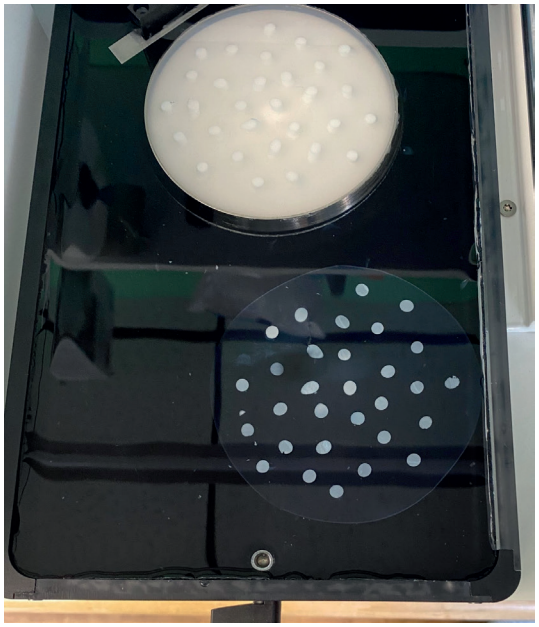


Figure 10. Collecting high-throughput sections from the Compresstome VF-800-0Z. Begin sectioning process with the Compresstome VF-800-0Z to precisely cut through embedded tissue samples. Monitor progress to ensure high-quality Precision-Cut Lung Slice (PCLS) sections.

4. Collection and Storage: Collect the generated PCLS sections and transfer them to appropriate storage containers or culture plates for further experimentation **(Figure 11)**. Ensure proper labeling and organization of samples for ease of tracking and analysis.

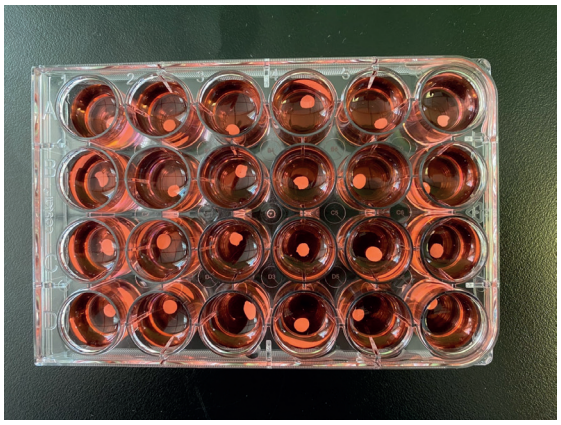


Figure 11. Collecting High-Throughput PCLS Sections. Transfer generated PCLS sections to suitable storage containers or culture plates for further experimentation. Each section produced on the Compresstome VF-800-0Z can fill a well plate, facilitating comprehensive analysis.

Utilizing the Compresstome VF-800-0Z vibratome model enables researchers to meet the growing demand for high throughput PCLS sectioning in biomedical research. By following the outlined procedures and optimizing experimental parameters, researchers can efficiently generate hundreds of PCLS sections with precision and reproducibility. This advancement in sectioning technology paves the way for accelerated progress in understanding lung biology and disease pathology, ultimately leading to improved therapeutic strategies for respiratory disorders.

After Making PCLS

Once precision-cut lung slices (PCLS) are prepared, they can be used for various experiments and analyses in respiratory research. Here's how PCLS are typically processed and utilized after lung sections are made:

- ***Live Imaging:*** PCLS can be immediately subjected to live imaging using techniques such as confocal microscopy or two-photon microscopy. This allows researchers to visualize dynamic processes within the lung tissue, such as cell behavior, cellular interactions, and changes in structure or function over time.
- ***Metabolic Assays:*** PCLS can be used for metabolic assays to study cellular metabolism, energy production, and metabolic pathways within the lung tissue. Techniques such as oxygen consumption rate (OCR) measurements or lactate production

assays can be performed to assess metabolic activity in response to various stimuli or conditions.

- ***Drug Testing and Screening:*** PCLS serve as valuable tools for drug testing and screening to evaluate the efficacy and toxicity of pharmaceutical compounds or therapeutic agents. Researchers can expose PCLS to different drugs or compounds and assess their effects on lung tissue function, viability, and response to injury or disease.
- ***Inflammatory and Immune Response Studies:*** PCLS are commonly used to study inflammatory and immune responses in the lung. Researchers can induce inflammation or immune activation in PCLS using various stimuli or pathogens and investigate immune cell recruitment, cytokine production, and inflammatory signaling pathways.
- ***Gene Expression and Protein Analysis:*** PCLS can be subjected to gene expression analysis, such as quantitative real-time PCR (qPCR) or RNA sequencing, to study changes in gene expression profiles associated with different experimental conditions or disease states. Additionally, protein expression and localization can be assessed using techniques like immunohistochemistry or western blotting.
- ***Drug Delivery and Aerosol Exposure:*** PCLS can be used to study drug delivery mechanisms and aerosol exposure in the lung. Researchers can assess the penetration, distribution, and retention of drugs or nanoparticles within lung tissue using techniques such as fluorescent labeling or imaging.
- ***Long-Term Culture and Functional Studies:*** PCLS can be cultured for extended periods to study long-term effects of treatments or interventions on lung tissue function and viability. Researchers can monitor changes in tissue morphology, function, and cell behavior over time to gain insights into chronic diseases or physiological processes.

Overall, precision-cut lung slices are versatile and powerful tools that enable researchers to investigate various aspects of lung biology, physiology, and disease pathology in a controlled and physiologically relevant ex vivo model system.

Troubleshooting PCLS

Despite careful preparation, obtaining perfect PCLS sections can sometimes be challenging. Understanding common issues and how to address them can significantly improve the quality of your PCLS. Let's explore some troubleshooting steps for generating good human PCLS.

Q: What are some challenges in generating good human PCLS, and how can they be addressed?
A: The initial preparation of lung tissue is crucial for successful PCLS generation. Agarose filling is commonly used to stabilize soft and elastic lung tissue, but the lack of intact pleura can hinder this process. Tumor-free lung tissue from lobectomy resectates is preferred for PCLS generation, as it often retains intact pleura necessary for agarose filling.

Q: What are some considerations for culturing PCLS, and how can optimal conditions be achieved?
A: PCLS can be cultured in various ways, including attached to Trans-wells for an air-liquid interface (ALI) system, as dynamic organ culture (DOC), or submerged in cell culture medium. Standardizing cultivation conditions across labs is challenging, but maintaining consistent culture times, typically up to 120 hours, can help preserve cellular viability and function.

Q: What challenges arise when working with diseased lung samples, and how can they be overcome?
A: Disease-related changes in lung tissue, such as airway obstructions or fibrotic tissue, can impede agarose filling and PCLS preparation. Emphysematous tissues may rupture during agarose filling, necessitating the use of lower agarose concentrations to decrease pressure. Biopsy punches from similar regions of the same slice can reduce tissue variability and increase the number of usable PCLS samples.

Q: How should mouse lung models be agarose-filled properly, and what factors should be considered?

A: Proper inflation of mouse lungs prior to harvesting is essential for intact PCLS. Overinflation can damage lung architecture, while underinflation leads to uneven cutting. Approximately 1 ml of 2% agarose is used for inflation, with additional agarose required until the lung is fully inflated, indicated by the "flick" at the end of the postcaval lobe.

Q: What time considerations should be taken into account when making PCLS?

A: Preparation of solutions takes about 20 minutes, while harvesting lungs from mice may take around 30 minutes or longer depending on the number of mice. Generating PCLS from a single lobe, including setting up the vibratome, typically takes about 1 hour, but this may vary if multiple lobes are used simultaneously.

Recipes

Agarose Solution

Ingredients:
☐ 1.5 g low-melting point agarose powder
☐ 100 ml HBSS/HEPES buffer

Instructions:
1. Measure out 1.5 grams of low-melting point agarose powder using a laboratory balance.
2. In a suitable container, such as a glass beaker or flask, pour 100 ml of HBSS/HEPES buffer.
3. Add the measured agarose powder to the HBSS/HEPES buffer.
4. Microwave the mixture in short intervals, stirring occasionally, until the agarose powder is completely dissolved. Be cautious not to overheat the solution.
5. Once the agarose is fully dissolved, allow the solution to cool slightly before use in lung tissue processing.

Note: This recipe yields 100 ml of 2% agarose solution, suitable for processing multiple lung samples. Adjust the quantities accordingly if a smaller or larger volume is required.

Alternative Method using Agarose Tablets (Precisionary Instruments):
- Instead of low-melting point agarose powder, use agarose tablets provided by Precisionary Instruments.
- Each tablet is 0.5 grams, so use three tablets for a total of 1.5 grams to achieve a 2% agarose concentration.
- Mix the agarose tablets with 75 ml of HBSS/HEPES buffer (25 ml per tablet) to yield a 2% agarose solution.
- Follow the same procedure as described above for dissolving the agarose tablets in the buffer solution using the microwave.

Note: The use of agarose tablets provides a convenient and precise method for preparing agarose solution, ensuring consistent results in lung tissue processing. Adjust the volume of buffer solution accordingly to achieve the desired agarose concentration.

HBBS/HEPES

Ingredients:
☐ 1x HBSS (Hanks' Balanced Salt Solution)
☐ 1% HEPES (1 M, pH adjusted)

Instructions:
1. Prepare 1x HBSS by diluting commercially available HBSS solution with deionized or distilled water according to the manufacturer's instructions. Ensure that the final concentration matches the desired isotonic concentration.
2. Prepare a 1% HEPES solution by diluting 1 M HEPES stock solution with deionized or distilled water. Adjust the pH of the solution to the desired level, typically around pH 7.4, using concentrated HCl or NaOH as needed.
3. Once both solutions are prepared, combine the 1x HBSS solution and the 1% HEPES solution in a clean container, such as a glass beaker or flask. Mix thoroughly to ensure homogeneity of the buffer.
4. Once the buffer is prepared, place it on ice or in a refrigerator to chill to the desired temperature before use in experiments or tissue processing.

Note: Ensure that all equipment and containers used for preparing the buffer are clean and free from contamination to avoid introducing impurities into the buffer solution. Adjust the pH of the HEPES solution carefully to achieve the desired pH level for optimal performance in experiments.

SF-DMEM

Ingredients:
☐ DMEM basal media
☐ 1% Penicillin-Streptomycin solution

Instructions:
1. Begin by preparing the DMEM basal media according to the manufacturer's instructions. This typically involves reconstituting powdered DMEM with deionized or distilled water to achieve the desired concentration.

2. Once the DMEM basal media is prepared, add 1% Penicillin-Streptomycin solution to the media. The 1% Penicillin-Streptomycin solution is usually supplied as a sterile, ready-to-use solution containing 10,000 units/ml of penicillin and 10,000 µg/ml of streptomycin.
3. Calculate the volume of 1% Penicillin-Streptomycin solution needed based on the final volume of SF-DMEM desired. For example, to make 100 ml of SF-DMEM, add 1 ml of 1% Penicillin-Streptomycin solution.
4. Mix the DMEM basal media and 1% Penicillin-Streptomycin solution thoroughly to ensure homogeneity of the SF-DMEM.
5. Once prepared, the SF-DMEM can be used immediately for experiments or tissue culture applications requiring a serum-free medium.

Note: Ensure that all components used in the preparation of SF-DMEM are sterile and free from contamination to maintain the sterility of the final medium. Store any unused SF-DMEM at the appropriate temperature and conditions recommended by the manufacturer to preserve its stability and quality.

70% Ethanol

Ingredients:
☐ 70 ml absolute ethanol
☐ 30 ml distilled water

Instructions:
1. Measure out 70 ml of absolute ethanol using a graduated cylinder or measuring beaker.
2. Measure out 30 ml of distilled water using a separate graduated cylinder or measuring beaker.
3. Combine the measured amounts of absolute ethanol and distilled water in a clean container, such as a glass bottle or flask.
4. Mix the ethanol and water thoroughly by gently swirling or stirring the solution with a clean stir rod or spatula.
5. Once mixed, the solution will be 70% ethanol. Label the container appropriately with the concentration and contents.
6. Store the 70% ethanol solution in a tightly sealed container at room temperature. Ensure that the container is properly labeled and stored away from direct sunlight or heat sources.

Note: Always prepare ethanol solutions in a well-ventilated area and avoid inhaling the vapors. Use caution when handling ethanol as it is flammable. Dispose of any unused or expired ethanol solution according to local regulations for hazardous waste disposal.

More Questions? Contact Us!

If you have any further questions, require additional experimental support, seek references, protocols, or referrals related to precision-cut lung slices (PCLS) or any other aspect of respiratory research, do not hesitate to reach out to us at Precisionary Instruments. Our dedicated team of experts is here to assist you every step of the way.

You can contact us via:

Abigail Chu
Chief Scientific Officer (CSO)
Precisionary Instruments, Inc.
abby@precisionary.com | 617-682-0586

Whether you need troubleshooting assistance, personalized guidance, or customized solutions for your research needs, we are committed to providing you with the support and resources necessary to ensure your success. Don't hesitate to get in touch with us, and let us help you advance your research endeavors.

PRECISION-CUT LIVER SLICES

PROTOCOL FOR CUTTING SLICES OF FRESH LIVER

Key to reading the protocol:

√ Rationale for procedural step

♠ Tips & Tricks

1. Prepare Krebs-Henseleit Buffer (KHB) for slicing and storing precision-cut liver slices.
   - √ Here's the simple recipe for KHB:

KHB (slicing buffer)	Concentration (mM)
NaCl	118
KCl	5
$MgSO_4 \cdot 7H_2O$	1.1
KH_2PO_4	1.2
$NaHCO_3$	25
$CaCl_2 \cdot 2H_2O$	2.5
D-Glucose	25
HEPES	9

2. Prepare Williams medium E (WME, containing L-glutamine)
   - √ Here's the simple recipe for KHB:

WME	Concentration (mM)
WME + L-glutamine	5
D-Glucose	14
Gentamycin	50 µg/ml

Amphotericin B	2.5 μg/ml

- √ Amphotericin B is added to inhibit growth of fungi and yeasts.

3. Fill the culture plates you will use with the incubation medium.
4. Warm and oxygenate culture plates with 95% O2/5% CO2 at 37 C for at least 30 min.
5. Prepare and keep warm a 2-3% solution of agarose at 37 C.
6. To obtain liver tissue, anesthetize the animal and surgically isolate the liver as quickly as possible, ideally under 5 minutes. Remove any fatty tissue and transfer cleaned pieces of liver tissue to ice-cold oxygenated KHB. Section out specific liver lobes you need for experiments.
   - √ Liver tissue is very sensitive to ischemia, so the time taken for dissection and incubation of precision-cut liver tissue should be as fast as possible. This is especially important for studies of liver metabolism.
7. Glue the selected liver sample onto the Compresstome® specimen syringe plunger. Place the embedding cap onto the specimen syringe, over the liver sample.
8. Fill the syringe with 2% agarose (Sigma A-0701, low gelling point, incubated at ~37°C).
   - √ Order a Starter Kit or additional agarose or blades directly from our website at http://www.precisionary.com/starter-kit !
9. Draw the syringe downward to bring the liver tissue core sample into the syringe.
10. Cool the entire contents of the specimen syringe with the chilling block. The liver tissue is now embedded in agarose. The agarose will solidify enough for stable sectioning.
11. Load the specimen syringe onto the Compresstome® slicer.
12. The protocol is complete for preparing the liver specimen for sectioning. Proceed from here with normal Compresstome® sectioning procedures.

    ♠ What are the optimal settings on the Compresstome® for cutting live liver slices? Try a speed (Advance) of 4-5 and an oscillation of 5-7.
13. Collect each liver slice and immediately transfer to pre-warmed Williams' Medium E (see recipe above), incubating at 37° C to restore ATP levels and wash away cellular debris.

References

*** Uses the Compresstome® for successful fresh liver slices.**

1. **de Graaf IA, Olinga P, de Jager MH, Merema MT, de Kanter R, van de Kerkhof EG, Groothuis GM. Preparation and incubation of precision-cut liver and intestinal slices for application in drug metabolism and toxicity studies. Nat Protoc. 2010 Sep;5(9):1540-51.**

2. **Lerche-Langrand C, Toutain HJ. Precision-cut liver slices: characteristics and use for in vitro pharmaco-toxicology. Toxicology. 2000 Nov 16;153(1-3):221-53.**

3. Koch A, Saran S, Tran DD, Klebba-Färber S, Thiesler H, Sewald K, Schindler S, Braun A, Klopfleisch R, Tamura T. Murine precision-cut liver slices (PCLS): a new tool for studying tumor microenvironments and cell signaling ex vivo. Cell Commun Signal. 2014 Nov 7;12:73.

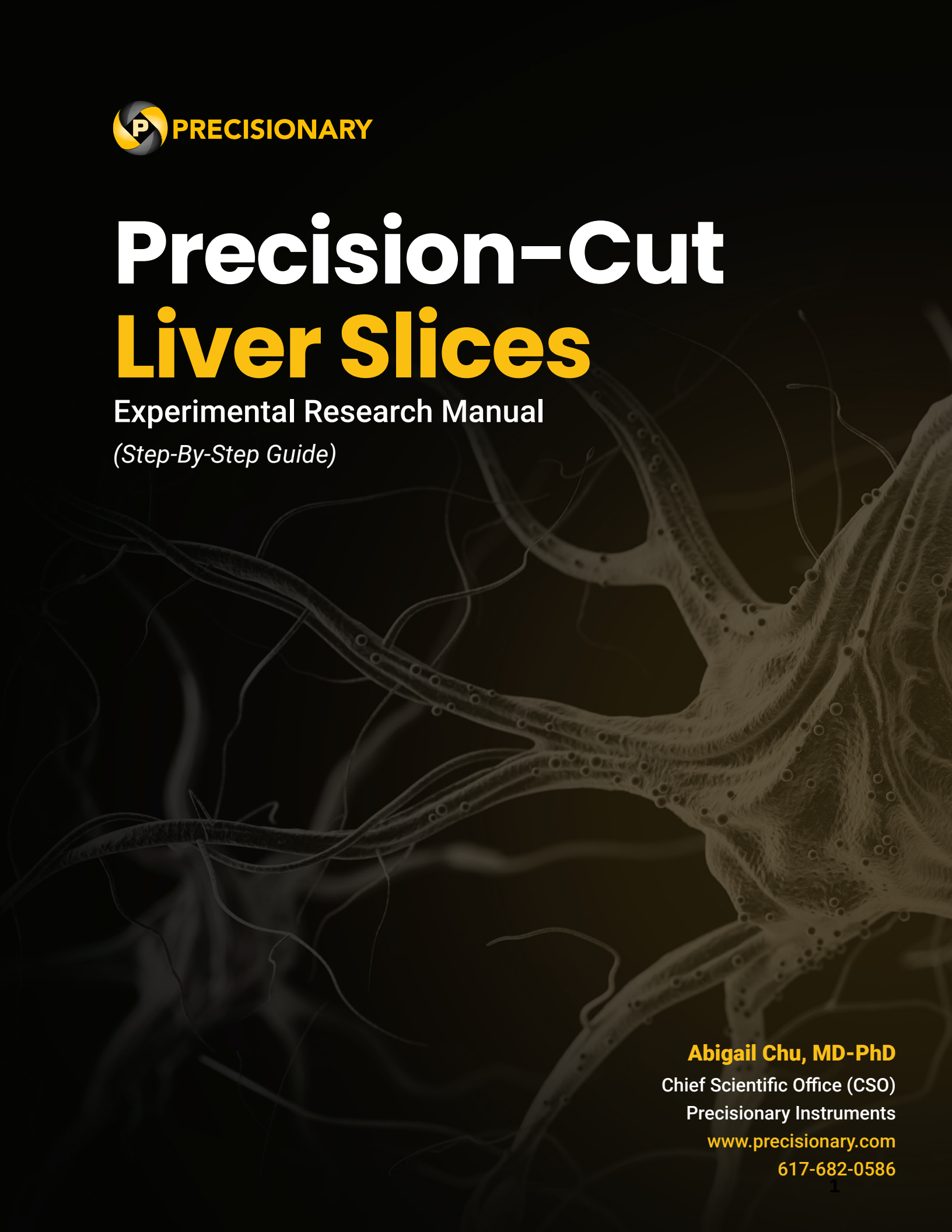
4. Abdelaal HM, Kim HO, Wagstaff R, Sawahata R, Southern PJ, Skinner PJ. Comparison of Vibratome and Compresstome sectioning of fresh primate lymphoid and genital tissues for in situ MHC-tetramer and immunofluorescence staining. Biol Proced Online. 2015 Jan 7;17(1):2.

PRECISIONARY

Precision-Cut Liver Slices

Experimental Research Manual

(Step-By-Step Guide)



Abigail Chu, MD-PhD
Chief Scientific Office (CSO)
Precisionary Instruments
www.precisionary.com
617-682-0586

Table of Contents

Table of Contents **2**
Goals of this Experimental Guide **4**
What is PCLS and Why is it Important? **6**
Who This Guide Can Help **10**
Need Help? Contact Us **11**
Liver Lobe Anatomy: A Guide for Accurate Dissection and Slicing **13**
Mouse Liver Anatomy 13
Human Liver Anatomy 14
Similarities and Key Differences 17
Anatomical Considerations in Research 17
Conclusion 18
Essential Materials, Reagents, and Equipment **19**
Materials and Reagents 19
Equipment 20
Lab Accessories 20
Optional or Specialized Reagents 22
Preparing Precision-Cut Liver Slices (PCLS) from Mouse Liver **23**
Mouse Dissection and Liver Harvesting 23
Embedding the Mouse Liver in Agarose 24
Slicing the Embedded Liver to Generate PCLS 25
Incubating and Preparing Slices for Downstream Applications 26
Preparing Precision-Cut Liver Slices (PCLS) from Human Liver Tissue **27**
Receiving and Preparing Human Liver Tissue 27
Embedding the Human Liver in Agarose 28
Sectioning Human Liver Tissue into PCLS 29
Culturing and Handling Human PCLS 30
Considerations for Human PCLS 31
Conclusion 31
High Throughput PCLS Sectioning **32**
Preparation for High Throughput PCLS Sectioning 32
High Throughput PCLS Sectioning Procedure 33
After Making PCLS **36**
Recovery Incubation and Culture 36
Metabolic Assays 36
Drug Testing and Hepatotoxicity Screening 36
Modeling Liver Disease and Injury 37
Gene Expression and Molecular Analysis 37
Live Imaging and Tissue Viability 38
Extended Culture and Longitudinal Studies 38
Personalized and Translational Applications 38

Conclusion 39
Troubleshooting Precision-Cut Liver Slices (PCLS) 40
Frequently Asked Questions & Solutions 40
Common Issues and Solutions at a Glance 40
Best Practices to Minimize Trouble 41
Recipes for Liver PCLS Preparation and Culture 43
1. Agarose Embedding Solution (2–3%) 43
2. HBSS/HEPES Buffer 43
3. Serum-Free DMEM (SF-DMEM) 44
4. Williams' Medium E Complete (for Long-Term Culture) 45
5. 70% Ethanol (for Sterilization) 45
6. Reagents for Metabolic and Functional Assays (Optional) 46
Have More Questions? Contact Us! 48

Goals of this Experimental Guide

This experimental guide is designed to serve as a detailed, practical resource for researchers aiming to produce consistent, high-quality precision-cut liver slices (PCLS) using the Compresstome® vibrating microtome. The protocol bridges the gap between technical instrumentation and biological experimentation by offering clear, step-by-step guidance rooted in real-world research workflows.

Whether you are a first-time user or an experienced scientist looking to optimize your slicing technique, this manual will walk you through the critical stages of liver PCLS preparation—from tissue collection and embedding, to slicing, collection, and downstream application setup.

By following this guide, you will:

- **Understand the essential steps** involved in preparing PCLS, including:
    - Proper liver extraction and handling,
    - Embedding the tissue in agarose to stabilize it for sectioning,
    - Fine-tuning slicing parameters on the Compresstome® system, and
    - Collecting and storing slices for immediate or future use.
- **Optimize slicing conditions** to:
    - Maintain tissue viability for live-cell studies,
    - Preserve architecture for structural and histological analyses, and
    - Ensure reproducibility across experimental runs.
- **Troubleshoot common problems** such as:
    - Tissue tearing or deformation during slicing,
    - Poor agarose embedding,
    - Inconsistent slice thickness or shape, and
    - Reduced tissue viability post-slicing.
- **Apply best practices** for:

- Preparing buffers and slicing media to support physiological conditions,
- Minimizing mechanical stress during tissue handling,
- Reducing contamination risk, and
- Ensuring compatibility with downstream workflows such as drug testing, immunohistochemistry, transcriptomic profiling, and metabolic assays.

Ultimately, the goal of this guide is to empower researchers with a reliable, standardized protocol that enhances the quality, reproducibility, and translational relevance of liver PCLS-based experiments. Through the integration of high-precision slicing with biological insight, we aim to support your work in advancing liver research and therapeutic discovery.

What is PCLS and Why is it Important?

Precision-cut liver slices (PCLS) are thin, uniformly prepared sections of liver tissue that preserve the full architecture, cellular composition, and physiological function of the liver. Unlike isolated hepatocyte cultures or immortalized cell lines that lose the liver's native organization, PCLS retain all key liver cell types—including hepatocytes, Kupffer cells, hepatic stellate cells, endothelial cells, and bile duct structures—in their natural spatial context. This preservation of tissue architecture and intercellular signaling makes PCLS a uniquely powerful ex vivo system for studying liver biology (**Figure 1**).

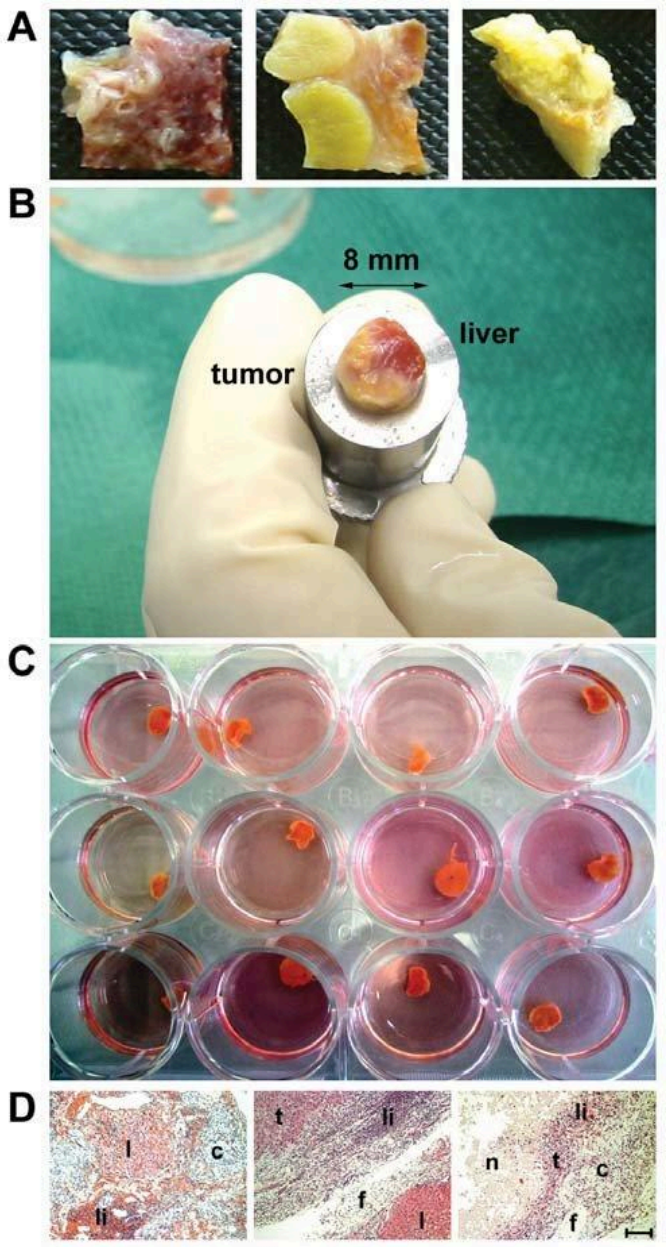


Figure 1. Preparing precision-cut liver slices (PCLS) from a liver resection sample with hepatocellular carcinoma (HCC). (A) The liver sample from the patient included three main parts: healthy liver tissue (left), two yellowish tumor nodules (middle), and mostly dead (necrotic) tumor tissue (right). (B) Small cylindrical cores, about 8 mm wide, were taken from the middle region that contained both tumor and non-tumor liver tissue. (C) Each tissue core was placed into a slicing instrument to create thin, even liver slices. The slices were first pre-incubated for one hour in WEGG culture medium, then transferred to 12-well plates (one slice per well with 2 ml medium) and kept in a highly oxygenated environment for up to five days. (D) Fresh slices were preserved in formalin, embedded in wax, cut into very thin sections (5 µm), and stained with hematoxylin and eosin for microscopic analysis. The resulting sections showed a mix of liver cells (l), tumor cells (t), immune cell clusters (li), scarred (f), dead (n), and cirrhotic (c) areas. Scale bar = 100 µm.[1]

In many research contexts, in vitro models lack the complexity needed to accurately reflect how the liver behaves in vivo, while in vivo animal studies come with ethical considerations, higher costs, and lower throughput. PCLS offer a middle ground—maintaining high physiological relevance while allowing precise experimental control over the tissue microenvironment. As a result, they have become an essential model across disciplines ranging from toxicology to drug development to disease pathogenesis.

Researchers turn to PCLS when they need a tissue model that is:

- **Physiologically complex**, preserving native liver function, metabolism, and cell-cell interactions.
- **Species-flexible**, enabling the use of tissue from rodents, pigs, non-human primates, and humans.
- **Reproducible and efficient**, providing multiple slices from a single liver for parallel experiments and reducing biological variability.
- **Ethically aligned**, reducing the number of animals needed by maximizing the utility of each organ.

PCLS are now widely used for both basic and translational studies (**Figure 2**). In disease research, liver slices can be used to simulate or model conditions such as metabolic dysfunction associated liver disease (MASLD), alcohol associated liver disease (ALD), hepatic fibrosis, acute liver failure, and drug-induced liver injury (DILI). By applying disease-inducing agents ex vivo or using tissue from disease models, investigators can observe molecular and cellular changes over time in a well-controlled setting.

[1] Zimmermann M, Armeanu S, Smirnow I, Kupka S, Wagner S, Wehrmann M, Rots MG, Groothuis GMM, Weiss TS, Königsrainer A, Gregor M, Bitzer M, Lauer UM. Human precision-cut liver tumor slices as a tumor patient-individual predictive test system for oncolytic measles vaccine viruses. *Int J Oncol.* 2009 May;34(5):1247-56. doi: 10.3892/ijo_00000255. PMID: 19360338.

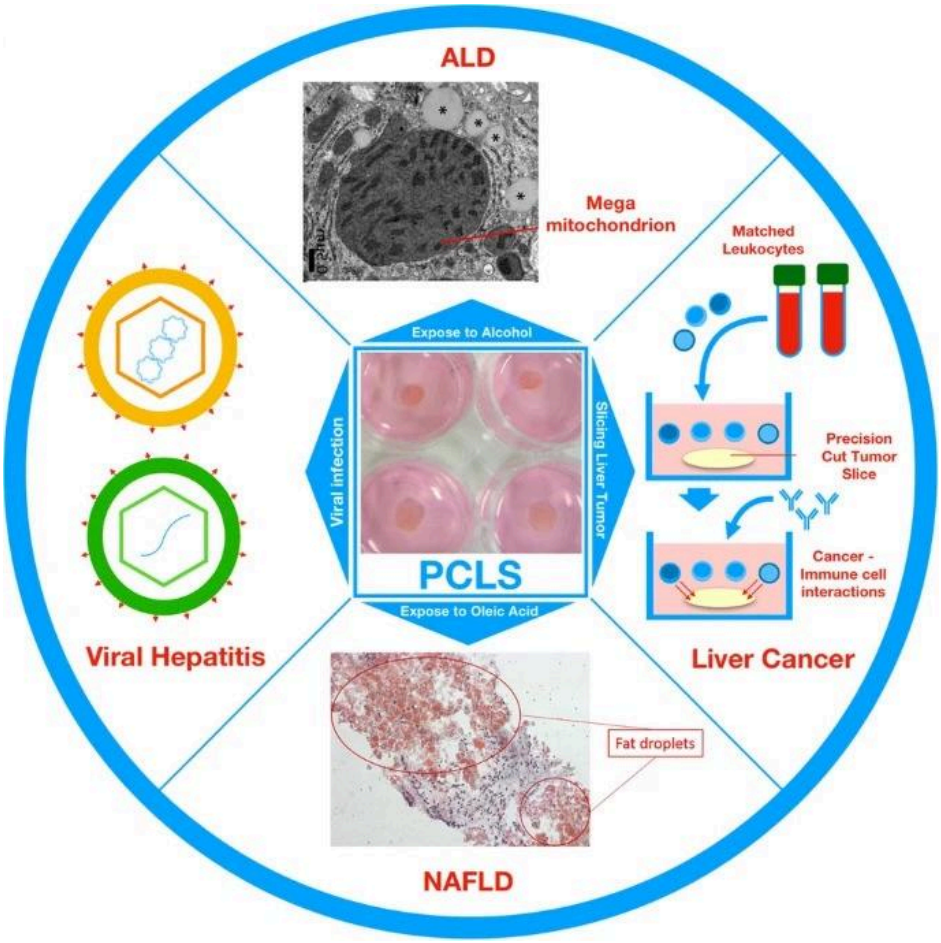


Figure 2. Overview of how precision-cut liver slices (PCLS) can model different types of liver disease. This diagram shows how thin slices of human liver tissue can be used to study a wide range of liver conditions in the lab. When PCLS are exposed to ethanol, the cells develop large "mega-mitochondria," which are a hallmark of alcohol-related liver damage. When slices are taken from liver tumors, they can serve as a model for liver cancer and help researchers study how tumor and immune cells interact. When PCLS are treated with a mix of fatty acids (oleic and linoleic acids), they mimic fatty liver disease (NAFLD). Finally, PCLS can also be infected with hepatitis B or C viruses to study how these viruses infect and replicate in liver cells.[2]

In pharmacology and toxicology, PCLS enable the assessment of drug metabolism, enzyme activity, and tissue-level toxic responses. Because the liver's cytochrome P450 system remains intact in slices, researchers can measure real-time metabolic transformations of compounds, evaluate dose-response relationships, and identify early signs of hepatotoxicity. This is particularly valuable in preclinical drug development, where PCLS can reveal differences in drug metabolism between species or identify risks before clinical trials.

Beyond disease modeling and drug testing, PCLS are used to study fundamental aspects of liver function—such as glucose and lipid metabolism, mitochondrial respiration, bile acid production, and ammonia detoxification. Their compatibility with functional assays, imaging,

[2] Palma E, Doornebal EJ, Chokshi S. Precision-cut liver slices: a versatile tool to advance liver research. *Hepatology International*. 2019;13(1):51–57. doi:10.1007/s12072-018-9913-7.

gene expression analysis, and biomarker profiling makes them adaptable to a wide range of downstream applications.

The use of PCLS in translational research is also expanding. Human liver slices obtained from surgical resections allow researchers to study patient-specific responses to drugs or disease stimuli. These ex vivo systems offer a unique opportunity to explore variability in drug sensitivity, investigate rare liver diseases, and evaluate therapeutic strategies in a way that is both personalized and biologically realistic. PCLS can be used to study inflammatory responses, cytokine signaling, liver fibrosis, or liver virology by hepatotropic viruses under controlled conditions.

In summary, PCLS offer a high-fidelity, experimentally flexible platform for investigating liver biology. Their ability to combine physiological relevance with reproducibility and accessibility makes them indispensable for scientists aiming to understand the liver in health, disease, and therapeutic intervention.

Who This Guide Can Help

This guide is intended for a diverse audience of researchers, technicians, and core facility personnel (**Figure 3**) who work with liver tissue and require a practical, reliable method for generating precision-cut liver slices (PCLS). Whether you're new to the field or looking to improve the consistency and quality of your slice preparation, this guide will provide the tools and insights needed to carry out reproducible and high-quality experiments using the Compresstome® vibratome.



Figure 3. Scientists Working with Liver Tissue Research. A diverse team of researchers, from students to senior scientists, working together in a modern laboratory to study liver tissue. These professionals use specialized equipment to prepare precise liver samples for medical research, drug development, and disease studies. The collaborative environment shown here represents the many different types of scientists - in universities, pharmaceutical companies, and research centers - who depend on reliable tissue preparation methods to advance liver health research.

We've designed this protocol manual to support:

- **Academic researchers** working in:
    - Hepatology, toxicology, pharmacology, and metabolic disease.
    - Translational liver research involving human and animal tissues.

    - Studies requiring viable, structurally intact liver tissue for downstream assays such as imaging, transcriptomics, or biochemical analysis.

- **Industry scientists** involved in:
    - Preclinical drug development and compound screening.
    - Investigations of liver-targeting therapies and hepatotoxicity.
    - ADME (Absorption, Distribution, Metabolism, and Excretion) and DMPK (Drug Metabolism and Pharmacokinetics) workflows requiring physiologically relevant liver models.
- **Core facility personnel and lab managers** responsible for:
    - Training new users on shared slicing equipment.
    - Maintaining consistent protocols across multiple experiments and users.
    - Troubleshooting technical issues and optimizing workflows for various sample types.
- **New users of the Compresstome® system**, including:
    - Graduate students, postdocs, and technicians unfamiliar with tissue slicing.
    - Labs transitioning from manual or less precise slicing methods.
    - Researchers seeking a step-by-step resource to ensure high success rates in embedding, slicing, and sample preservation.

Whether you're generating slices for acute experiments, long-term culture, or molecular analysis, this guide will serve as a trusted reference throughout your workflow. Our goal is to equip you with not just a protocol, but a framework for success in liver tissue research.

Need Help? Contact Us

At Precisionary Instruments, we're here to support your research every step of the way. Our scientific and technical teams can assist with:

- Optimizing protocols and troubleshooting issues
- Providing training and guidance on equipment operation
- Advising on experimental design for custom applications
- Recommending reagents and blades based on your sample type

Reach out to us anytime:
Email: info@precisionary.com
Phone: (617) 682-0586
Website: www.precisionary.com

We're committed to helping you achieve reliable, high-quality results with your Compresstome® system.

Liver Lobe Anatomy: A Guide for Accurate Dissection and Slicing

Understanding the gross anatomy of the liver is essential for accurate dissection, embedding, and reproducible slicing during precision-cut liver slice (PCLS) preparation. Because PCLS retain the native architecture and spatial orientation of the liver, the anatomical origin of each slice has direct implications for downstream analysis—whether you are studying metabolic zonation, regional differences in gene expression, or tissue-specific responses to pharmacologic agents.

Although liver function is highly conserved across mammalian species, the anatomical organization of the liver differs considerably between commonly used model organisms such as mice and humans. These anatomical differences are more than superficial—they directly affect how tissues are dissected, which lobes are most suitable for slicing, and how experimental data should be interpreted, particularly in cross-species translational research.

Mouse Liver Anatomy

The mouse liver is lobulated and relatively symmetrical, making it highly tractable for systematic sampling and whole-lobe slicing. It typically consists of four major lobes, many of which are subdivided into distinct segments with defined vascular territories. Because of the liver's small size, most lobes can be embedded and sectioned in their entirety, providing a convenient and consistent approach to generating PCLS.

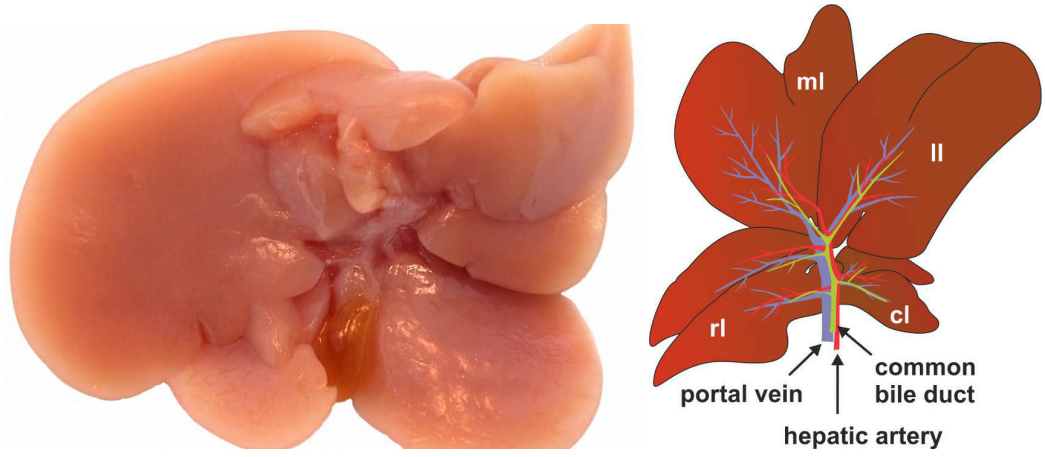


Figure 4. **Mouse liver anatomy.** (A) Visceral aspect of mouse liver.[3] (B) Schematic diagram showing the anatomical relationship of bile duct (yellow), portal vein (purple),

[3] Tag CG, Sauer-Lehnen S, Weiskirchen S, Borkham-Kamphorst E, Tolba RH, Tacke F, Weiskirchen R. Bile duct ligation in mice: induction of inflammatory liver injury and fibrosis by obstructive cholestasis. *J Vis Exp.* 2015 Feb 10;(96):52438. doi: 10.3791/52438. PMID: 25741630.

and hepatic artery (red) relative to liver lobes: right lobe (rl), left lobe (ll), median lobe (ml), and caudate lobe (cl).[4]

Key features of mouse liver lobes include (**Figure 4**):

- **Left Lobe**:
  Subdivided into left medial and left lateral segments. The **left lateral lobe** is broad, thin, and relatively uniform in thickness, making it one of the most commonly used regions for PCLS preparation. Its shape and size allow for flat, stable embedding in agarose.

- **Right Lobe**:
  Includes right medial and right lateral segments. The **right medial lobe**, positioned adjacent to the gallbladder, is often sampled for studies of bile metabolism or gallbladder-associated signaling. It is also a useful site for modeling fibrosis or localized injury.

- **Median (Middle) Lobe**:
  Sits between the left and right lobes, often partially covering the gallbladder. This lobe is less frequently used for slicing due to variability in thickness and curvature but can be sampled for specific experiments.

- **Caudate Lobe**:
  Located posteriorly and composed of two portions—the **caudate process** and **papillary process**. These segments are smaller, more irregular in shape, and less frequently used for routine PCLS due to embedding challenges.

An important feature of mouse liver anatomy is that the lobes are clearly demarcated and connected by thin mesenteric tissue. The organ is suspended within the abdominal cavity by hepatic ligaments, and its blood supply is delivered via the portal vein and hepatic artery, with drainage through the hepatic veins into the inferior vena cava. This anatomical clarity allows for reproducible dissections and region-specific experiments.

Human Liver Anatomy

In contrast to the mouse, the human liver (**Figure 5**) is larger, asymmetrical, and less overtly lobulated on gross inspection. While traditionally divided into two main lobes—right and left (**Figure 6**)—the human liver is more accurately described using the Couinaud classification (**Figure 7**), which divides the organ into eight functional segments based on vascular inflow (portal vein), outflow (hepatic veins), and biliary drainage.

[4] Ruehl-Fehlert C, Kittel B, Morawietz G, Deslex P, Keenan C, Mahrt CR, Nolte T, Robinson M, Stuart BP, Deschl U; RITA & NACAD Groups. Revised guides for organ sampling and trimming in rats and mice — Part 1. *Exp Toxicol Pathol.* 2003 Sep;55(2-3):91-106. PMID: 14620530.

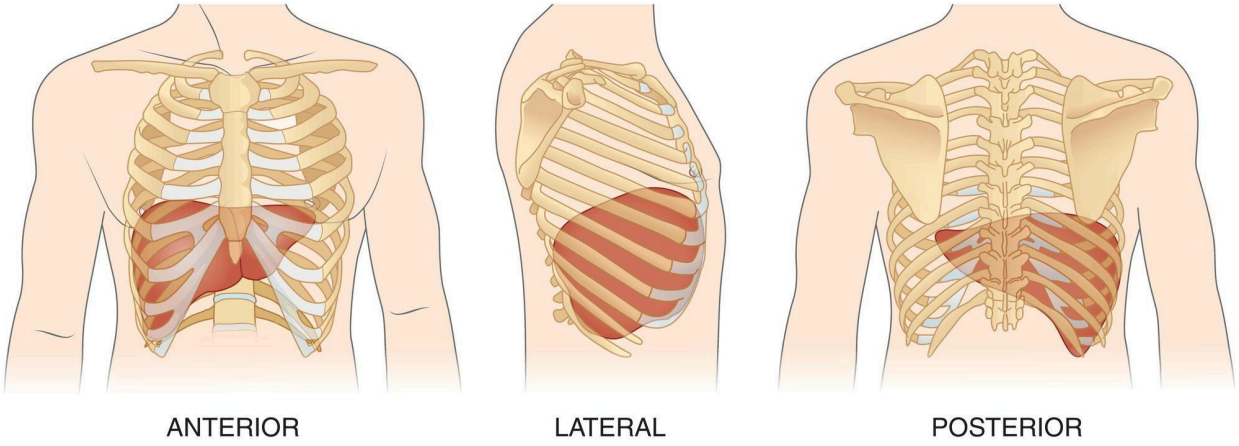


Figure 5. Anatomical position of the human liver. The liver sits just below the diaphragm, mostly on the right side of the abdomen but extending toward the center and slightly to the left. It is shown here from the front, side, and back views.

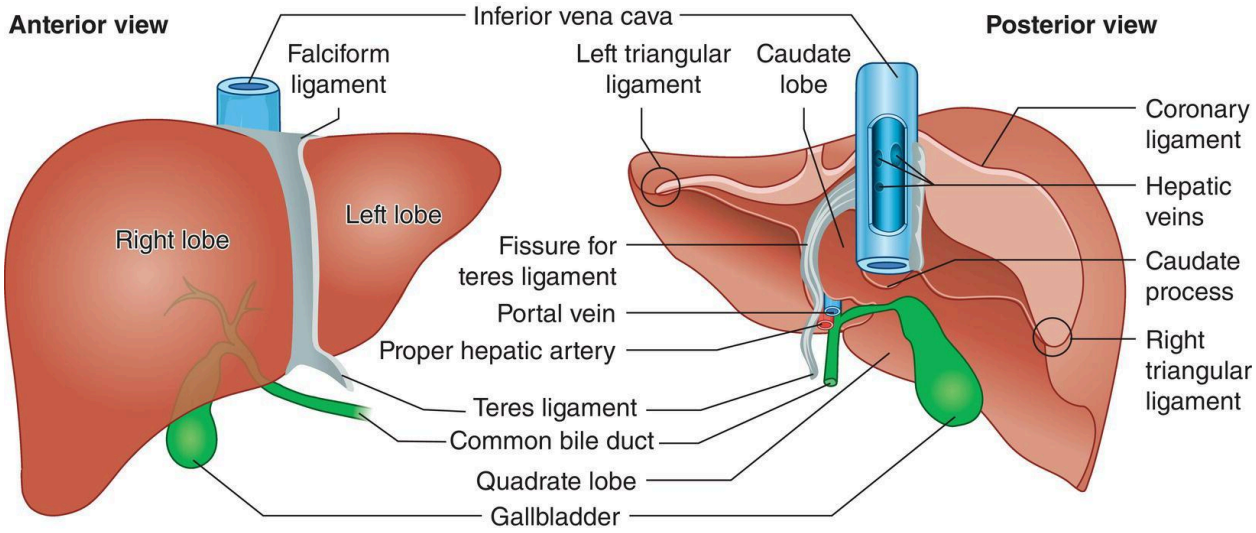


Figure 6. External surfaces of the liver. The top surface of the liver is smooth and dome-shaped, fitting snugly beneath the diaphragm. The underside is slightly uneven because it rests against other organs and is marked by shallow grooves that separate the liver's lobes.

Key features of human liver anatomy include:

- **Right Lobe**:
  The largest lobe, comprising over 60% of liver mass. It includes both anterior and posterior segments. Its size and relatively uniform surface make it a practical site for collecting large tissue samples during surgery or biopsy.

- **Left Lobe**:
  Subdivided into medial and lateral segments. The **falciform ligament** separates the left and right lobes on the diaphragmatic surface, and the **ligamentum teres** can be used as

a landmark in surgical resections.

- **Caudate Lobe (Segment I)**:
  Located posteriorly near the inferior vena cava. Though small, it is functionally distinct and may be preserved in certain forms of liver disease. The caudate lobe could be safely removed from the donor liver during transplant, and will be a good source for a healthy liver if the goal is to use a healthy liver for study.

- **Quadrate Lobe**:
  A small region near the gallbladder that is typically classified as part of the left lobe. It may be included in resections depending on surgical landmarks.

- **Segmental Anatomy**:
  The liver's division into eight Couinaud segments allows for precise identification of tissue origin. Each segment functions as a quasi-independent unit, with its own vascular and biliary inputs and outputs. This segmentation is especially relevant in surgical planning and for correlating imaging findings with tissue-level pathology.

Because human liver samples are typically obtained from surgical resections, biopsies, or donor tissue, the lobe or segment used for slicing can vary widely. Anatomical knowledge is essential to ensure reproducibility, interpret results appropriately, and report findings with clarity.

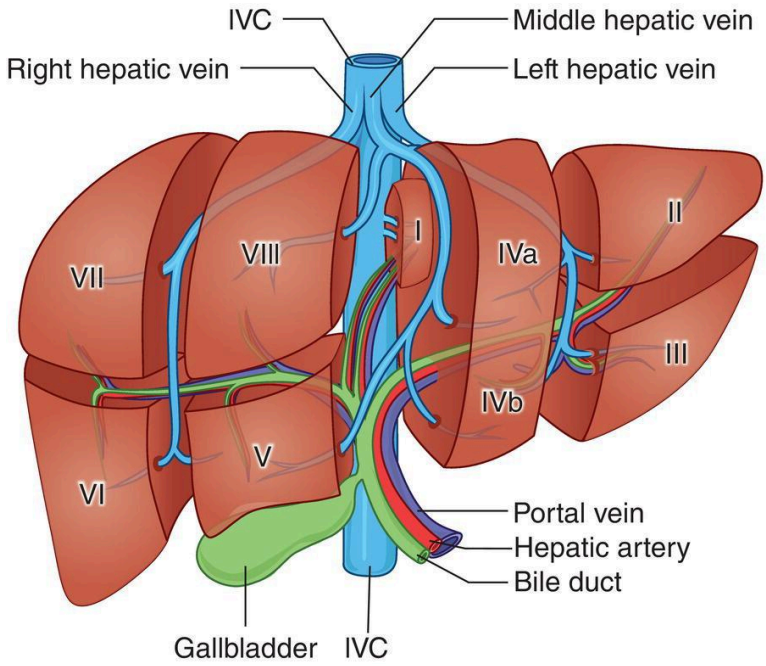


Figure 7. Liver segments based on the Couinaud classification. The liver is divided into anatomical segments according to the Couinaud system, which uses the branching of the bile ducts and blood vessels to define each region. IVC = inferior vena cava.

Similarities and Key Differences

While the overall physiological functions of the liver—detoxification, metabolism, bile production, and protein synthesis—are shared across species, anatomical organization differs in ways that affect experimental design.

- Mouse livers are **more lobulated and symmetrical**, allowing for clean dissection and consistent slicing of entire lobes.

- Human livers are **less obviously lobulated**, with **greater internal segmentation** based on vascular distribution. This necessitates more nuanced dissection and documentation of sample origin.

- In both species, blood flow follows the same basic principles—entering via the portal triad and draining through central veins—but **vascular branching and tissue thickness** vary substantially.

Anatomical Considerations in Research

Understanding the source of each liver slice is critical for experimental consistency, especially in studies involving regional variation in liver function or disease. Metabolic gradients, zone-specific enzyme expression (e.g., periportal vs. pericentral), and fibrotic or inflammatory changes can all vary within and between lobes.

Researchers using **mouse models** commonly select the left lateral lobe for:

- Diet-induced liver disease studies (e.g., NAFLD, NASH)

- Transgenic or knockout model characterization

- Drug metabolism and toxicity assays

- Fibrosis or regeneration models, using repeat sampling from known lobes

In **human tissue studies**, PCLS are widely used for:

- Translational research using donor or surgical tissue

- Ex vivo drug response assays to support personalized medicine

- Side-by-side comparisons of diseased and non-diseased segments
- Investigating patient-specific variability in drug metabolism, injury response, or fibrosis

---

Conclusion

For researchers preparing PCLS, anatomical knowledge is not just background—it's foundational to experimental success. Identifying and consistently using the same liver lobe or segment ensures reproducibility and enables meaningful comparisons across conditions, animals, or human subjects. Whether working with murine models or human donor tissue, this anatomical framework informs every step of the slicing process, from dissection and embedding to data interpretation.

Essential Materials, Reagents, and Equipment

For optimal preparation of precision-cut liver slices (PCLS), it's essential to prepare all materials, equipment, and reagents ahead of time. The following checklists provide a detailed overview of what is required for dissection, embedding, slicing, incubation, and downstream analysis—whether you are performing basic viability studies, drug exposure assays, or metabolic flux measurements.

Materials and Reagents

- Low-melting-point agarose (2%, w/v in slicing buffer)
- 1× Phosphate-buffered saline (PBS), sterile and ice-cold
- Hank's Balanced Salt Solution (HBSS) supplemented with 1% 1 M HEPES
- Williams' Medium E or serum-free DMEM/F12, supplemented with:
    - 1% penicillin-streptomycin
    - Optional: GlutaMAX, insulin-transferrin-selenium (ITS), or other supplements
- Fetal bovine serum (FBS), for optional culture medium supplementation
- Trypan blue (for viability assessment, optional)
- Live/dead cell staining dyes (e.g., Calcein-AM, Ethidium homodimer-1)
- Reagents for specific models:
    - Oleic and palmitic acid (for NAFLD)
    - Ethanol, CCl_4 (toxic injury models)
    - TGF-β1 or PDGF-BB (fibrosis induction)
- Reagents for Seahorse XF metabolic assays:
    - Oligomycin, FCCP, Rotenone, Antimycin A
- 70% ethanol (for surface disinfection)

- Sterile distilled water (for agarose and buffer prep)
- Super glue (for securing tissue in specimen tubes, if needed)

Equipment

- **Compresstome® Vibrating Microtome System**
  (e.g., VF-510-0Z or VF-800-0Z, includes plunger, specimen holder, and cutting blade holder)
- Temperature-controlled **CO_2 incubator** (37°C, 5% CO_2, humidified)
- **Water bath** (set to 60–70°C for melting agarose)
- **Refrigerated centrifuge** (for buffer and media prep)
- **Orbital shaker** or **tilting rocker** (for slice incubation and compound exposure)
- **Agilent Seahorse XF Analyzer** (if metabolic flux analysis is planned)
- **Dissecting microscope** (for embedding and orientation assessment)
- **Fluorescence microscope** or confocal system (for live/dead imaging or biomarker studies)
- Optional: **Hypoxia chamber**, **plate reader**, or **oxygen sensor probe**

Lab Accessories

- Specimen tubes (Compresstome® compatible embedding cylinders)
- Syringe chilling block (optional, for agarose handling)
- Stainless steel double-edged razor blades (standard); optional: ceramic-coated or tungsten carbide
- 24-well and 6-well tissue culture plates (low-attachment recommended)

- Sterile Petri dishes (for initial dissection and slice handling)
- Fine surgical scissors (Iris or Vannas) (**Figure 8**)
- Fine-tipped spring scissors
- Curved and straight forceps (e.g., Dumont #5)
- Micro-spatula and metal slice lifters
- 5-ml, 15-ml, and 60-ml syringes (for buffer transfer and tissue handling)
- Scalpel blades (#10 or #11)
- 5-ml tubes (sterile) or similar-sized containers for agarose preparation
- Filter paper or sterile mesh supports (for slice collection and transfer

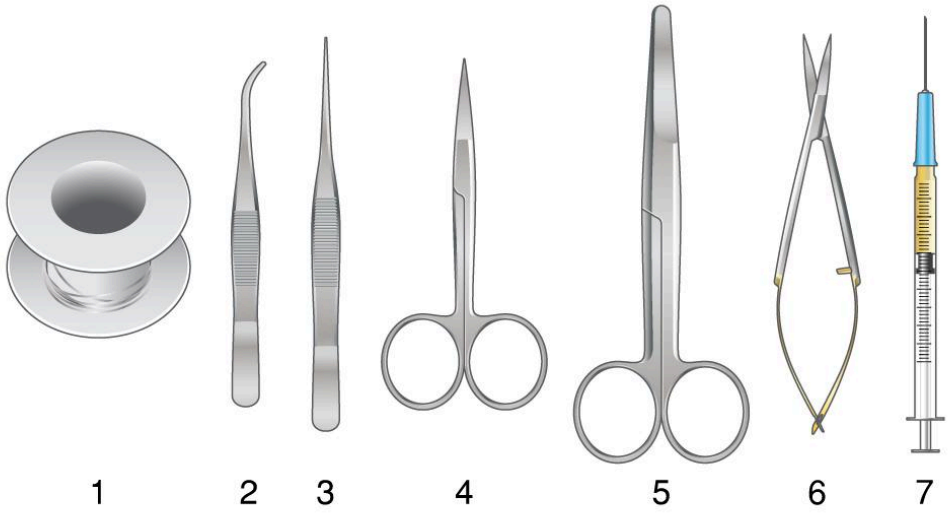


Figure 8. **Comprehensive workflow for mouse dissection and liver harvesting.** Dissection equipment includes suture, curved forceps, fine tip forceps, fine tip dissecting scissors, surgical scissors, spring scissors, and pentobarbital in a 1 ml syringe attached with a hypodermic needle.

Optional or Specialized Reagents

Use these for extended applications or specific research goals:

- ATP detection kits (e.g., CellTiter-Glo)
- Colorimetric/fluorometric ALT & AST enzyme activity kits
- RNA/DNA stabilization reagents (e.g., RNAlater) for transcriptomic profiling
- Collagen or Matrigel (for ex vivo culture/ECM remodeling)
- Polystyrene culture inserts or transwells (to support long-term slice culture)
- Antibiotic-antimycotic cocktail (for extended culture to prevent contamination)

Preparing Precision-Cut Liver Slices (PCLS) from Mouse Liver

Now that we've reviewed the anatomy and gross structure of the liver, we can move on to the step-by-step preparation of precision-cut liver slices (PCLS). This section focuses on the widely used mouse model, with detailed instruction on liver dissection, embedding, and slicing using the Compresstome® vibrating microtome system.

Mouse Dissection and Liver Harvesting

Before beginning, gather all required dissection tools and materials (see checklist in the previous section). Euthanasia and dissection should be performed in accordance with institutional IACUC protocols.

1. **Euthanize the mouse humanely**, using intraperitoneal injection of pentobarbital or another approved agent. Confirm death by exsanguination via the femoral artery.

2. **Place the mouse in dorsal recumbency** on a dissection tray. Spray the body surface with 70% ethanol to minimize hair and microbial contamination.

3. **Use fine scissors to make a midline incision** through the abdominal skin and peritoneum, exposing the liver. Begin at the lower abdomen and cut upward toward the ribcage, then laterally under the rib margins to expose the entire upper abdominal cavity.

4. **Carefully mobilize the liver** by gently lifting the lobes with curved forceps. The gallbladder will be visible on the ventral surface, typically attached to the right medial lobe. Avoid puncturing or squeezing the gallbladder, as bile can cause tissue damage.

5. **Remove the liver from the body cavity** by cutting through its ligamentous attachments, including the falciform ligament and hepatic portal triad. Sever the inferior vena cava at both ends to release the liver en bloc. Transfer the organ immediately to a sterile Petri dish placed on ice.

6. **Rinse the liver briefly in ice-cold PBS** or HBSS to remove excess blood. Gently pat dry with sterile filter paper or a laboratory tissue.

7. **Select the desired liver lobe** for slicing—typically the left lateral lobe in adult mice—due to its large surface area and relatively flat, uniform structure.

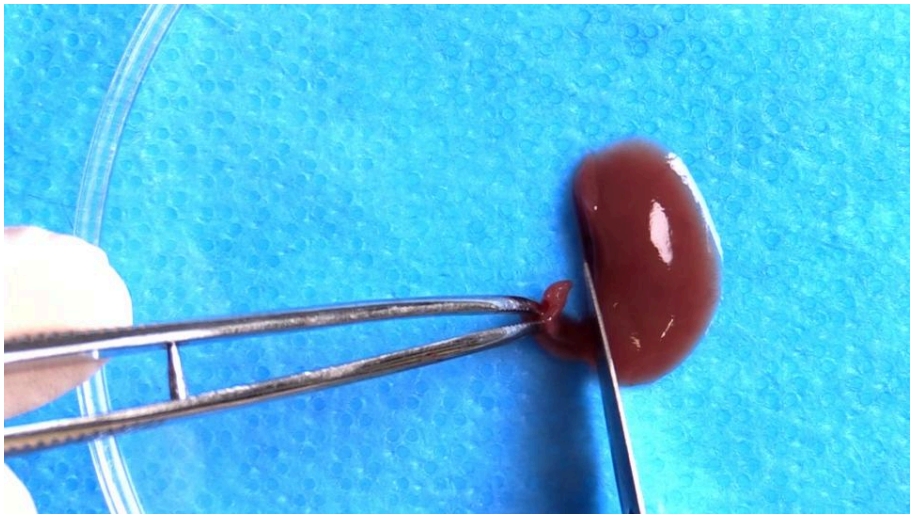


Figure 9. Preparation of mouse liver tissue for sectioning. A freshly dissected mouse liver lobe is shown prior to slicing. The tissue is trimmed to remove excess connective tissue and to obtain a flat, uniform surface before being embedded in the Compresstome® vibratome for precision cutting of live liver sections.

At this stage, the tissue is ready for embedding in agarose prior to sectioning.

Embedding the Mouse Liver in Agarose

Proper embedding is crucial for preserving tissue integrity during slicing and ensuring that the specimen is held firmly in the slicing chamber (**Figure 10**).

1. **Prepare a 2% low-melting-point agarose solution** in your slicing buffer (e.g., ice-cold HBSS or Krebs–Henseleit). Heat the solution in a microwave or water bath until completely melted, then cool to approximately 37–40°C to avoid thermal injury to the tissue.

2. **Cut the liver lobe into a suitable shape** for mounting—typically a ~5–10 mm³ block with clean, flat surfaces. Orient the tissue so that slices will be made perpendicular to the lobe's long axis. Trim the edges if necessary to improve symmetry and reduce rocking during slicing.

3. **Place the trimmed tissue into the specimen embedding tube** (compatible with the Compresstome®), and gently pipette warm agarose to fully surround the sample. Orient the tissue using a sterile blunt probe to ensure proper alignment.

4. **Place the embedding tube in a chilled syringe block or on ice** for several minutes to solidify the agarose. Once fully gelled, remove the specimen tube from ice and load it into the Compresstome® slicing chamber.

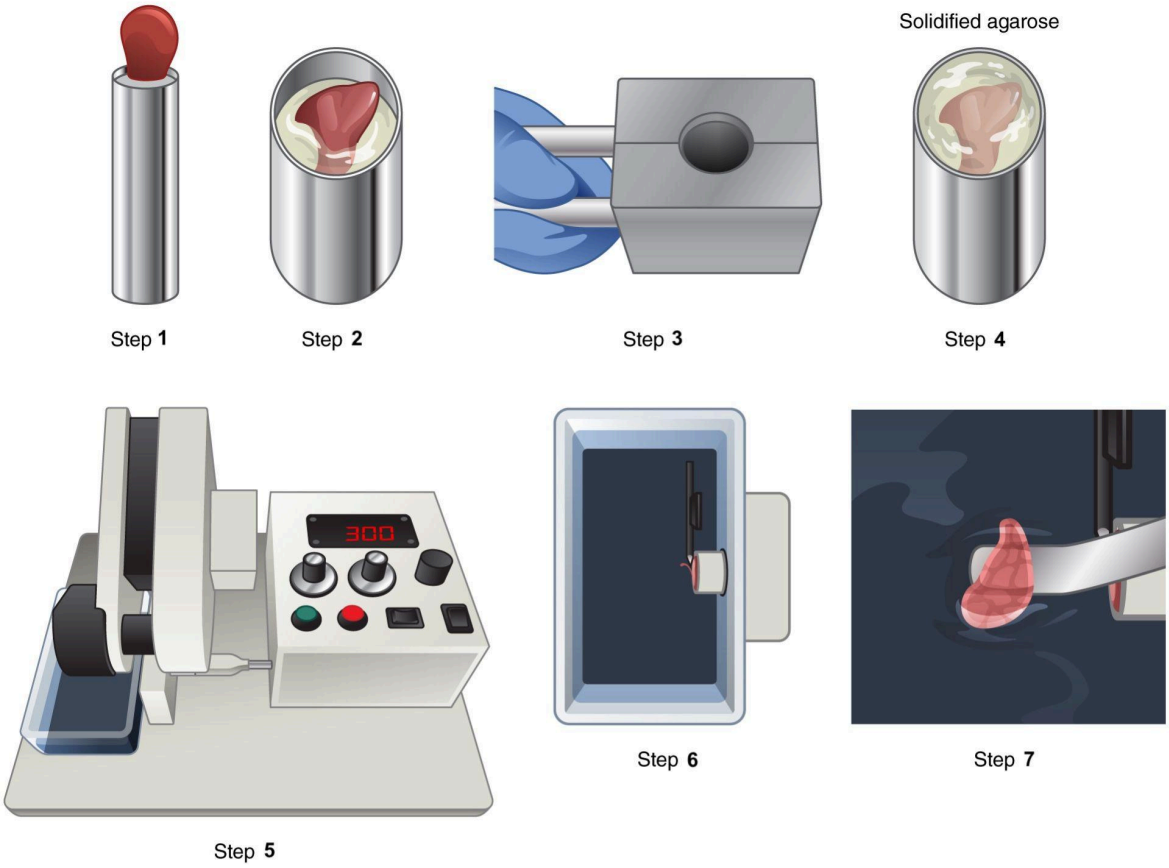


Figure 10. Embedding and sectioning liver tissue using the Compresstome® vibratome. This series shows the preparation of fresh liver tissue for slicing. **Step 1:** The trimmed liver sample is glued to the base of a specimen tube. **Step 2:** The tissue is covered with warm agarose solution to provide support during cutting. **Step 3:** The specimen tube is placed on a chilling block to help the agarose solidify. **Step 4:** Once the agarose is firm, the embedded tissue is ready for sectioning. **Step 5:** The specimen tube is mounted into the Compresstome® vibratome. **Step 6:** The embedded tissue is positioned inside the buffer tray for slicing. **Step 7:** Thin, live tissue slices are sectioned and collected free-floating in buffer for downstream experiments.

Slicing the Embedded Liver to Generate PCLS

The Compresstome® vibratome provides controlled, uniform slicing of embedded tissue (**Figure 10**). Proper parameter setup and blade alignment are key to obtaining viable, consistent liver slices.

1. **Sterilize the slicing buffer tray** with 70% ethanol and rinse thoroughly with sterile PBS or slicing buffer. Fill the tray with ice-cold slicing buffer to keep the tissue cool during

slicing.

2. **Install a fresh razor blade** (stainless steel or ceramic-coated) in the vibratome blade holder. Adjust blade angle and ensure it is parallel to the cutting plane.

3. **Mount the specimen tube** into the Compresstome®'s specimen holder. Use the plunger to advance the agarose block toward the blade until it is just visible.

4. **Set slicing parameters** appropriate for liver tissue:

    - Slice thickness: 250–300 µm
    - Speed: Medium (e.g., 3.0–4.0 mm/s)
    - Oscillation frequency: 70–85 Hz
    - Advance increment: Set based on slice thickness and tissue resistance

5. **Begin slicing**, and collect slices as they are produced using a small spatula or fine forceps. Gently transfer each slice into a 6- or 24-well plate containing ice-cold, oxygenated culture medium.

6. **Continue slicing until the full block is used** or the desired number of slices is obtained. Discard the remaining agarose block if it becomes too small or difficult to advance without damage.

Incubating and Preparing Slices for Downstream Applications

After slicing, allow slices to equilibrate in culture media before beginning experiments.

1. **Incubate slices at 37°C** in a humidified CO_2 incubator (5% CO_2) for 1–2 hours to recover from slicing stress. Agitate gently on a rocking platform or orbital shaker to maintain oxygenation.

2. **Wash slices with fresh medium** after the initial incubation period to remove cellular debris and residual agarose.

3. **Slices may then be transferred** into specific media formulations or exposure conditions depending on the experimental design—e.g., drug treatment, fibrosis induction, hypoxic challenge, etc.

4. **For live-cell imaging or metabolic assays**, transfer individual slices to low-attachment plates, imaging chambers, or Seahorse XF-compatible plates as needed.

This workflow yields high-quality, reproducible PCLS from mouse liver suitable for applications in toxicology, pharmacology, metabolic research, fibrosis modeling, and more.

Preparing Precision-Cut Liver Slices (PCLS) from Human Liver Tissue

While mouse liver models are foundational for mechanistic studies, human liver tissue provides unparalleled translational value for modeling disease, testing therapeutics, and exploring inter-individual variability. Advances in slicing technology, tissue preservation, and ex vivo culture now make it feasible to generate high-quality PCLS from resected or donor human liver tissue. These slices preserve the native architecture, viability, and metabolic activity of the liver for up to several days in culture, providing a powerful platform for drug testing, toxicology, and disease modeling.

This section outlines a step-by-step protocol for generating human PCLS, using liver resections or donor specimens as the starting material.

Receiving and Preparing Human Liver Tissue

Fresh, non-tumor liver tissue is typically obtained from explant, partial hepatectomies, or donor organs not used for transplantation. Upon arrival in the laboratory:

1. **Place the tissue immediately into cold transport buffer**, such as ice-cold UW (University of Wisconsin) solution or HBSS supplemented with 1% HEPES and antibiotics.

2. **Keep the tissue at 4°C** and process it as soon as possible. Ideally, cold ischemia time (time between resection and embedding) should be kept under 6 hours to preserve metabolic function and viability.

3. **Inspect the tissue macroscopically**. Choose well-perfused, non-fibrotic regions away from visible pathology or tumor margins. Note the lobe or segment if possible.

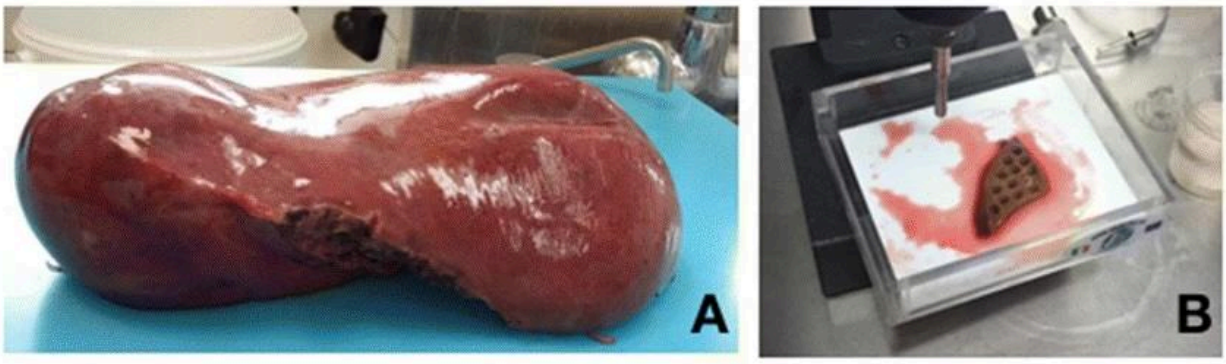


Figure 11. Preparation of human precision-cut liver slices (PCLS). (A) Freshly resected human liver tissue should ideally be immediately flushed with ice-cold University of Wisconsin (UW) solution through the portal vein to remove residual blood and minimize ischemic injury. However, this process can be difficult to achieve, time-consuming, and too costly for most investigators. The tissue is kept in sterile UW solution on ice and should be processed within 3 hours of resection. (B) A ~1 cm–thick tissue block is prepared, and cylindrical cores (5–10 mm in diameter) are obtained using a tissue coring tool. These cores are then embedded in the specimen tube of the Compresstome® vibratome and sectioned into uniform precision-cut liver slices.

Embedding the Human Liver in Agarose

Unlike mouse liver lobes, human tissue blocks are denser, more heterogeneous, and more fragile. Embedding in agarose provides structural support for uniform slicing.

1. **Prepare a 3% (w/v) low-melting-point agarose solution** in slicing buffer or DMEM/F12. Melt thoroughly and cool to 37–42°C.

2. **Trim the liver tissue into rectangular or cylindrical blocks** approximately 5–10 mm thick, avoiding large blood vessels or fibrotic tissue.

3. **Gently blot the tissue surface dry**, then transfer it into a sterile embedding mold or Compresstome® specimen tube.

4. **Slowly pour warm agarose** around the tissue to fully embed the sample. Remove bubbles with a pipette tip.

5. **Allow the agarose to solidify on ice** for 10–15 minutes. For thicker blocks, place the entire mold in a pre-chilled syringe block or cold tray.

6. **Store the embedded block at 4°C** in transport buffer or PBS if slicing will be delayed (up to 12 hours).

Sectioning Human Liver Tissue into PCLS

Once embedded and solidified, the tissue block is ready for slicing on the Compresstome® vibratome system.

1. **Install a new razor blade** and fill the slicing buffer tray with ice-cold, oxygenated buffer (e.g., Krebs–Henseleit or HBSS).

2. **Mount the agarose block into the specimen holder**, aligning the liver tissue perpendicularly to the blade for transverse slicing.

3. **Recommended Compresstome® settings for human liver:**

    - Slice thickness: **250–300 µm**
    - Advance speed: **2.0–3.0 mm/s**
    - Oscillation frequency: **70–85 Hz**

4. **Begin slicing**, using a soft brush or wide-bore pipette tip to transfer slices into a 6- or 12-well plate filled with pre-warmed culture medium.

Slices should be uniform in thickness, roughly 5–8 mm in diameter (depending on tissue size), and semi-transparent when fresh (Figure 12).

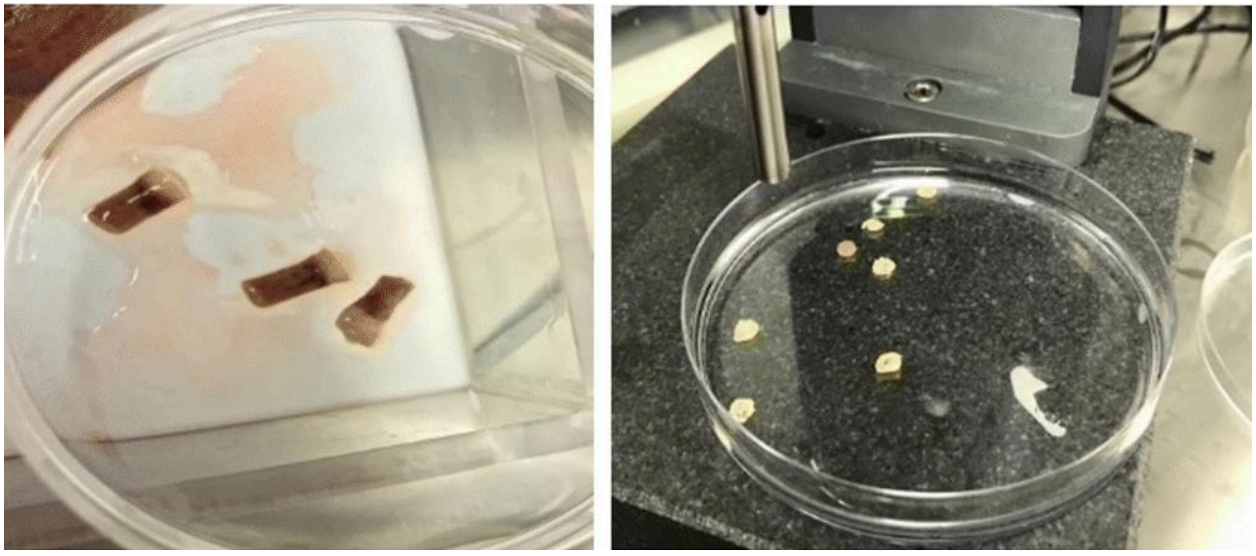


Figure 12. Preparation and application of human precision-cut liver and tumor slices. Left panel: Cylindrical tissue cores were obtained from resected human liver specimens containing

both non-tumorous and tumor regions using tissue coring tools. Right panel: Precision-cut tumor slices generated from these cores can be used to investigate molecular mechanisms underlying hepatocellular carcinoma (HCC) and to evaluate responses to antineoplastic drug treatments.

Culturing and Handling Human PCLS

To maintain viability and metabolic activity, liver slices must be cultured under optimized ex vivo conditions (Figure 13).

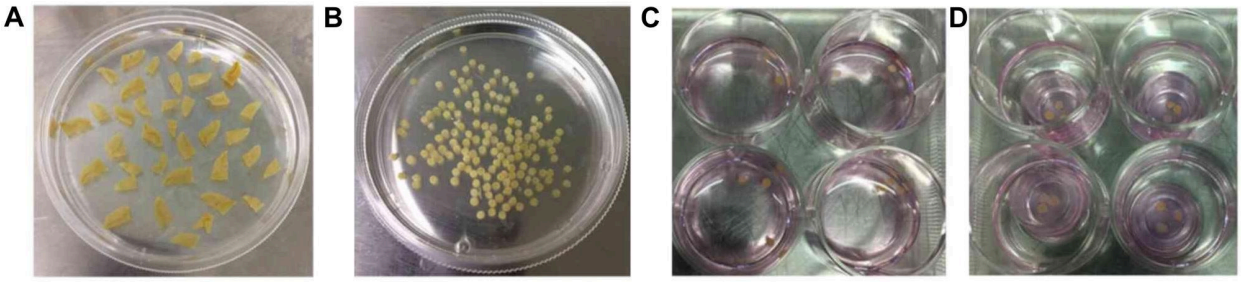


Figure 13. Preparation and culture formats of precision-cut liver slices (PCLS). (A) Precision-cut liver slices with a thickness of 300 µm. (B) Smaller slices prepared at 2 mm in diameter. (C) Example of a free-floating slice culture in medium. (D) Slice maintained on a filter support (Transwell® insert) for interface culture.

1. **Use Williams' Medium E** or DMEM/F12 supplemented with:
    - 10% FBS
    - 1% penicillin-streptomycin
    - Primary Hepatocyte Maintenance Supplements: typically includes insulin, dexamethasone, GlutaMAX, and non-essential amino acids (https://www.thermofisher.com/order/catalog/product/CM4000)
2. **Place plates in a humidified incubator at 37°C with 5% CO_2**, gently rocking or agitating to maintain oxygenation.
3. **Change medium after the first 2 hours** to remove cellular debris and residual agarose.
4. **Continue culture for up to 5–7 days**, depending on experimental goals. Viability tends to decline after day 5, particularly in fibrotic or fatty tissue.

Slices can be processed for various downstream applications:

- **RNA/protein extraction** for transcriptomics or Western blot
- **Histology and immunostaining** after fixation in 4% paraformaldehyde
- **Live/dead imaging**, using calcein-AM and ethidium homodimer
- **Secretion assays** (e.g., albumin, ALT, cytokines) from culture supernatants
- **Metabolic profiling**, using Agilent Seahorse XF, respirometry, or ELISA

Considerations for Human PCLS

- **Tissue quality varies significantly.** Fibrotic, cirrhotic, or steatotic tissue may be more fragile and difficult to slice. Document donor pathology, if available.
- **Vascular orientation and lobar origin** may affect experimental variability—record if the tissue came from the left, right, or caudate lobe.
- **Ethical approval and consent** are mandatory. Ensure IRB or ethics board approval for human tissue use and anonymization of donor data.

Conclusion

Human precision-cut liver slices provide a powerful model to study patient-specific liver function, drug metabolism, toxicity, and disease mechanisms in a physiologically relevant tissue context. With careful dissection, embedding, and culturing, researchers can maintain the viability and integrity of human liver slices for extended periods, enabling advanced biochemical, molecular, and pharmacological analyses. When coupled with tools such as live imaging, transcriptomics, and metabolic assays, human PCLS serve as a bridge between bench research and personalized medicine.

High Throughput PCLS Sectioning

In contemporary biomedical research, the demand for high throughput processing of precision-cut liver slices (PCLS) is ever-increasing. However, traditional methods often fall short in meeting this demand due to limitations in sample capacity and processing efficiency. In response to this pressing need, the Compresstome VF-800-0Z vibratome model offers a viable solution for achieving high throughput PCLS sectioning (**Figure 7**). This section outlines the steps involved in utilizing the Compresstome VF-800-0Z for efficient and precise generation of PCLS sections.

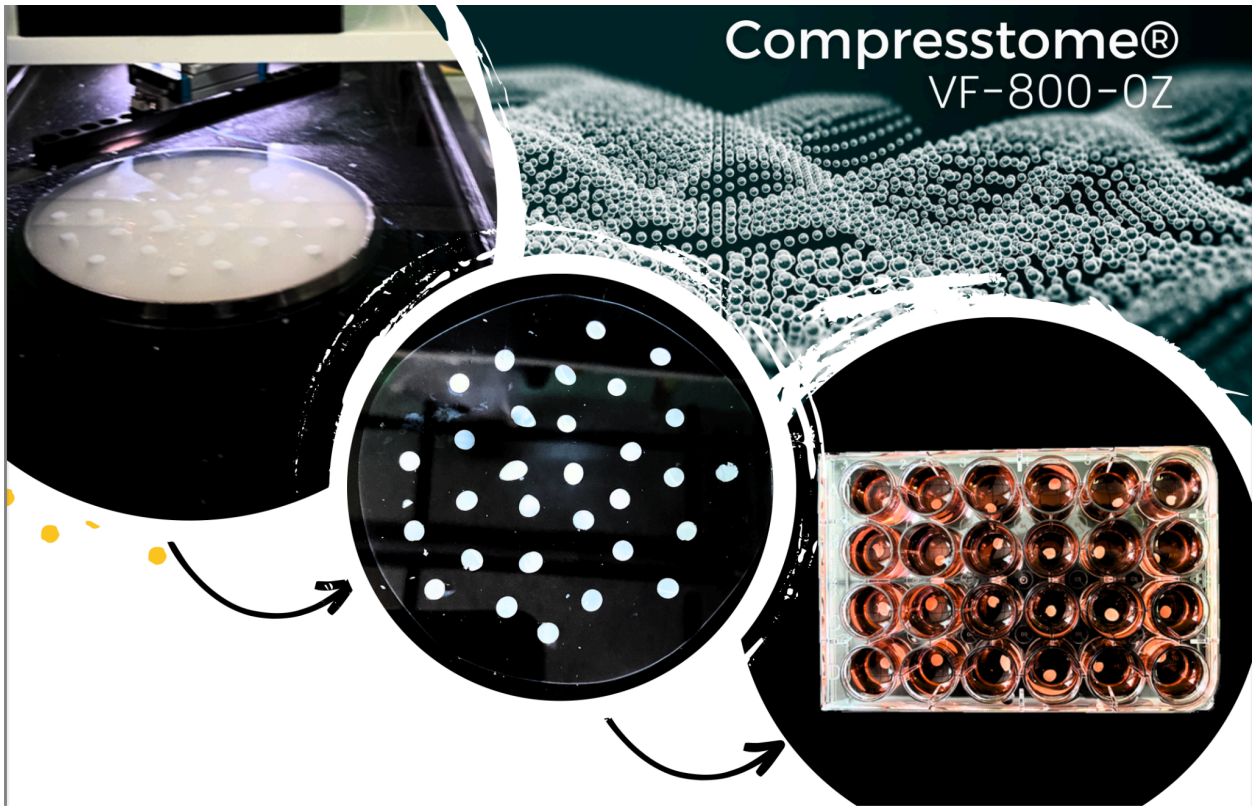


Figure 14. The Compresstome VF-800-0Z vibratome model presents an effective solution for achieving high throughput Precision-Cut Liver Slices (PCLS) sectioning. This figure demonstrates the embedding of 20 or more cored samples onto the stage of a Compresstome VF-800-0Z. Each sheet cut yields dozens of PCLS slices, facilitating the transfer and filling of an entire well plate for future processing.

Preparation for High Throughput PCLS Sectioning

1. Setup and Calibration: Begin by setting up the Compresstome VF-800-0Z vibratome according to the manufacturer's instructions. Ensure that the instrument is properly calibrated to achieve the desired section thickness.

2. Agarose Solution Preparation: Prepare a suitable agarose solution for embedding the tissue samples. Ensure that the agarose is properly dissolved and cooled to the desired temperature for optimal embedding (**Figure 8**).

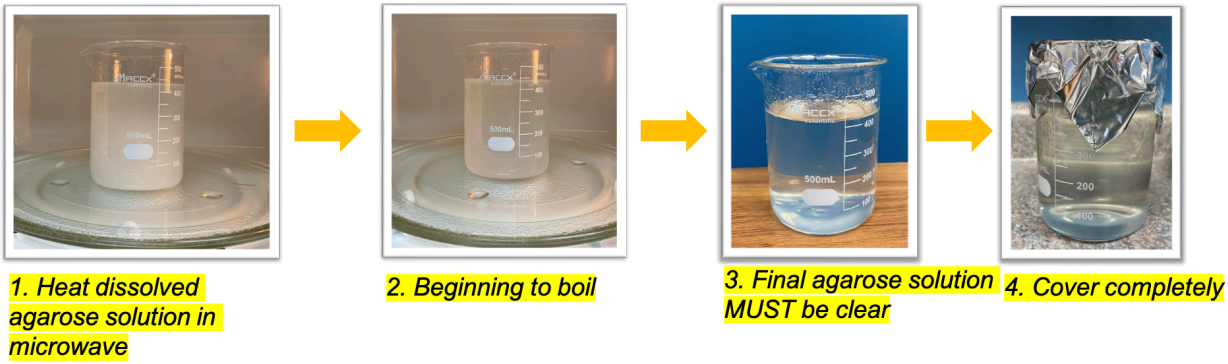


Figure 15. Agarose Solution Preparation. Prepare agarose solution for tissue embedding. Ensure thorough dissolution and cooling to the desired temperature for optimal embedding.

High Throughput PCLS Sectioning Procedure

1. Loading Samples: Place the embedded tissue samples onto the specimen plunger (loading platform) of the Compresstome VF-800-0Z. The instrument's design allows for the accommodation of multiple samples simultaneously, enabling high throughput processing (**Figure 9**).

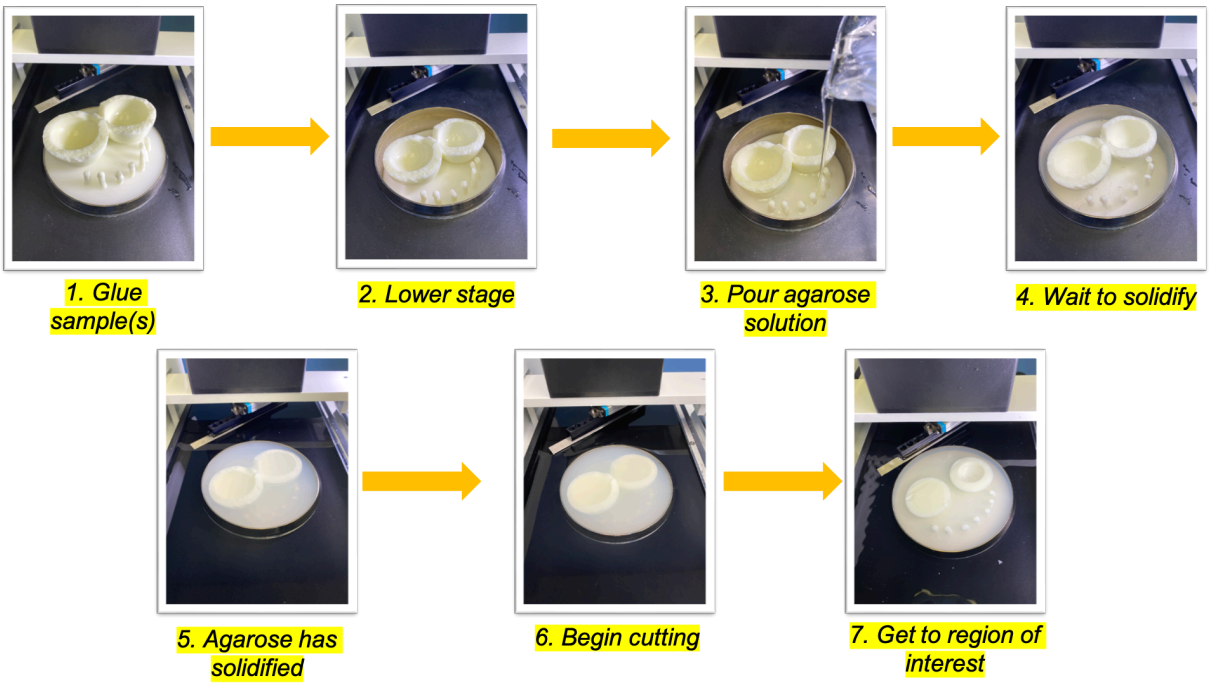


Figure 16. Loading Samples on to the Compresstome VF-800-0Z. Place embedded tissue samples onto the specimen plunger (loading platform) of the Compresstome VF-800-0Z. The instrument's design facilitates simultaneous processing of multiple samples, ensuring high throughput capability.

2. Sectioning Parameters: Set the desired section thickness and cutting parameters on the Compresstome VF-800-0Z control panel. Ensure uniformity in section thickness across all samples to maintain consistency in experimental results.
3. Sectioning Process: Initiate the sectioning process, allowing the Compresstome VF-800-0Z to precisely cut through the embedded tissue samples. Monitor the sectioning progress to ensure optimal performance and quality of PCLS sections (**Figure 10**).

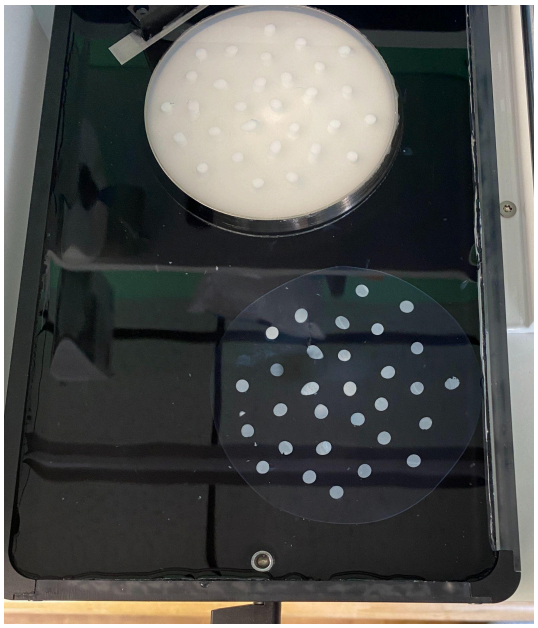


Figure 17. Collecting high-throughput sections from the Compresstome VF-800-0Z. Begin sectioning process with the Compresstome VF-800-0Z to precisely cut through embedded tissue samples. Monitor progress to ensure high-quality Precision-Cut Liver Slice (PCLS) sections.

4. Collection and Storage: Collect the generated PCLS sections and transfer them to appropriate storage containers or culture plates for further experimentation (**Figure 11**). Ensure proper labeling and organization of samples for ease of tracking and analysis.

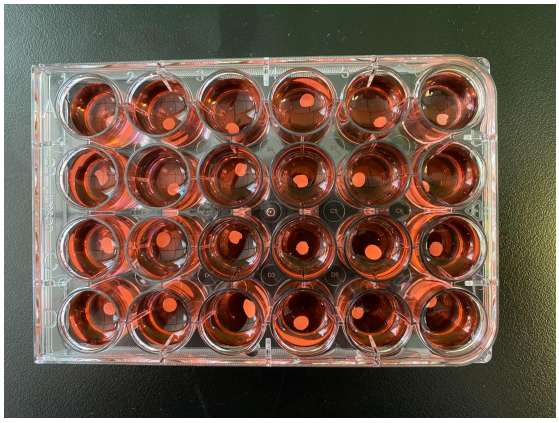


Figure 18. Collecting High-Throughput PCLS Sections. Transfer generated PCLS sections to suitable storage containers or culture plates for further experimentation. Each section produced on the Compresstome VF-800-0Z can fill a well plate, facilitating comprehensive analysis.

Utilizing the Compresstome VF-800-0Z vibratome model enables researchers to meet the growing demand for high-throughput PCLS sectioning in biomedical research. By following the outlined procedures and optimizing experimental parameters, researchers can efficiently generate hundreds of PCLS sections with precision and reproducibility. This advancement in sectioning technology paves the way for accelerated progress in understanding liver biology and disease pathology, ultimately leading to improved therapeutic strategies for hepatic disorders.

After Making PCLS

Once precision-cut liver slices (PCLS) are successfully prepared, they serve as a robust ex vivo platform for studying liver biology in a controlled and physiologically relevant environment. Because PCLS retain native liver architecture and metabolic capacity, they are widely used for experiments ranging from drug metabolism to fibrosis modeling. Below are common research applications and handling considerations after slice preparation.

Recovery Incubation and Culture

After slicing, PCLS should first undergo a short recovery phase:

- Incubate slices for 1–2 hours at **37°C in a 5% CO_2 humidified incubator**, using Williams' Medium E or DMEM/F12 supplemented with FBS and antibiotics.
- Gentle shaking or orbital rocking is recommended to enhance oxygenation and prevent hypoxia in the tissue core.
- After the initial recovery, replace the media to remove debris and cellular waste. Slices can then be transferred into fresh media for downstream experiments.

Metabolic Assays

Human and mouse PCLS are widely used in **metabolism research**, especially due to their preserved cytochrome P450 activity and metabolic zonation. Slices can be subjected to:

- **Mitochondrial respiration analysis** using an Agilent Seahorse XF Analyzer to measure oxygen consumption rate (OCR) and extracellular acidification rate (ECAR).
- **Lactate production** and **glucose uptake assays** to study glycolysis and energy metabolism.
- **ATP content quantification** using luminescent assays such as CellTiter-Glo.

These metabolic readouts provide insight into liver function in health and disease, and how drugs or toxins alter cellular energy pathways.

Drug Testing and Hepatotoxicity Screening

One of the most valuable uses of PCLS is in **drug efficacy and toxicity testing**:

- Slices can be exposed to investigational compounds or known hepatotoxins for acute or chronic exposure.

- Liver-specific biomarkers such as **ALT, AST, albumin, and urea** can be measured in culture supernatants.

- Drug-induced changes in viability, morphology, and metabolic enzyme activity can be assessed with high translational relevance.

This approach is commonly used in pharmaceutical development and toxicological studies across academia and industry.

Modeling Liver Disease and Injury

PCLS enable **disease modeling** under controlled, reproducible conditions:

- **NAFLD and NASH** can be modeled by adding fatty acids (e.g., oleic and palmitic acid), glucose, and insulin to simulate steatosis.

- **Fibrosis** can be induced with TGF-β1 or PDGF-BB and tracked using gene and protein expression of fibrotic markers (e.g., COL1A1, α-SMA).

- **Drug-induced liver injury (DILI)** studies often use acetaminophen, ethanol, or CCl_4 to replicate human toxicologic profiles.

Because the same liver can provide multiple slices, different conditions can be tested in parallel, reducing variability and maximizing tissue utility.

Gene Expression and Molecular Analysis

PCLS maintain RNA and protein integrity for downstream molecular assays:

- Extract **RNA** from individual slices for **qPCR, bulk RNA-seq**, or **single-nucleus RNA-seq**.

- Perform **Western blotting**, **ELISA**, or **Luminex assays** to assess signaling pathways and secreted factors.

- Fix slices in **4% paraformaldehyde** for **histology, immunohistochemistry (IHC), or immunofluorescence (IF)** to localize proteins of interest.

These tools allow researchers to characterize tissue responses at the molecular level in a spatially preserved context.

Live Imaging and Tissue Viability

Liver slices can also be used for **real-time visualization** of tissue dynamics:

- Perform **live/dead staining** (e.g., Calcein-AM and Ethidium homodimer) and image via confocal or widefield microscopy.
- Use **fluorescent reporters**, dyes, or probes to assess mitochondrial potential, ROS production, or calcium flux.
- Optical sectioning can reveal hepatocyte polarization, bile canaliculi integrity, and immune cell interactions.

Extended Culture and Longitudinal Studies

PCLS can be cultured for up to **14 days** depending on tissue quality and goals:

- Monitor for changes in slice thickness, color, and morphology as indicators of viability.
- For chronic exposure studies, replace media daily or every other day to maintain nutrient levels and remove waste.
- Extended culture supports time-course experiments for fibrosis progression, regeneration, and drug withdrawal studies.

Personalized and Translational Applications

Human PCLS offer a unique platform for **personalized medicine**:

- Assess **patient-specific drug response** using resected or donor tissue.

- Compare diseased versus non-diseased lobes from the same liver to identify localized effects.

- Study **inter-individual variability** in liver function, metabolism, or injury response.

This approach supports biomarker discovery and preclinical evaluation of targeted therapies in a human-relevant model.

Conclusion

Precision-cut liver slices provide a powerful and flexible tool for investigating hepatic physiology, drug interactions, disease mechanisms, and patient-specific biology. Their ability to preserve the structural and metabolic complexity of the liver while allowing direct manipulation makes them an indispensable platform for both basic research and translational applications. By following best practices in culture, imaging, and molecular analysis, researchers can extract deep insights from this versatile ex vivo model system.

Troubleshooting Precision-Cut Liver Slices (PCLS)

Despite careful planning and technique, preparing high-quality liver PCLS can present challenges—especially when working with human tissue, diseased samples, or transitioning between animal and human models. This section outlines common issues that arise during PCLS preparation and culture, with suggestions to help you achieve consistent, viable slices suitable for downstream experimentation.

Frequently Asked Questions & Solutions

Q: What are the most common challenges when generating high-quality human PCLS?
A: Liver tissue from surgical resections or donor tissue often varies in consistency and structural integrity. Diseased tissue (e.g., fibrotic or steatotic) may be more fragile or heterogeneous. It's essential to choose well-perfused, tumor-free regions, avoiding necrotic zones or lobe edges. Embedding becomes especially important: human liver lacks the natural pleura-like containment found in liver tissue, so sufficient agarose penetration and cooling time are critical. Trim the tissue block into symmetrical shapes to ensure stability during slicing.

Q: How can I optimize culture conditions to maintain slice viability over time?
A: Use serum-supplemented Williams' Medium E or DMEM/F12, pre-warmed and equilibrated to 37°C. Avoid overhandling slices, and ensure gentle rocking or rotation to maintain oxygenation. Viability typically remains stable for up to 5–7 days, but media should be refreshed daily or every other day to prevent waste accumulation. Keep culture conditions consistent between experiments, including plate format, media volume, and time points.

Q: How do I handle highly fibrotic, steatotic, or otherwise diseased liver tissue?
A: Fragile tissue may shear during slicing or collapse during embedding. Increase agarose concentration slightly (e.g., 3–3.5%), allow for longer cooling on ice, and slow down slicing speed. In some cases, you may need to reduce slice thickness slightly (to 200–250 µm) to improve slice stability. If available, compare slices from diseased and healthy regions within the same liver to reduce variability.

Q: How long should the full process take from tissue receipt to culture-ready slices?
A: Preparation of slicing solutions and agarose embedding takes ~20–30 minutes. Trimming and embedding the liver block can take another 15–20 minutes. Slicing a single block with the Compresstome® typically takes ~30–45 minutes, depending on slice thickness and tissue properties. For human liver with variable pathology, allow extra time for orientation and troubleshooting.

Common Issues and Solutions at a Glance

Issue	Possible Causes	Suggested Solutions
Tissue collapses during slicing	Low agarose concentration; insufficient cooling	Use 3–3.5% agarose, cool fully on ice (10–15 mins)
Jagged or uneven slices	Dull blade, poor orientation, improper vibration settings	Replace blade, trim block symmetrically, reduce slicing speed
Slices too thick/thin or inconsistent	Incorrect parameter calibration or tissue shifting	Calibrate slice thickness before use; ensure tissue is securely embedded
Slices tear or curl at edges	Overly fatty or fibrotic tissue; high speed	Use slower slicing speed (2–3 mm/s); increase agarose support
Slices lose viability quickly	Delayed processing; hypoxia during culture	Minimize cold ischemia time (<6 hrs); use rocking platform and oxygenated medium
Variable experimental results	Uneven slice thickness or anatomical origin	Use consistent lobes; discard edge slices; normalize to protein or weight
Poor culture performance over time	Medium composition not optimized	Use complete medium (e.g., Williams' Medium E + FBS); change medium every 24–48 hrs

---

Best Practices to Minimize Trouble

- **Work quickly, but gently.** Minimize mechanical stress during dissection, trimming, and transfer.
- **Document tissue origin.** Lobe, pathology, and cold ischemia time should all be recorded.
- **Standardize embedding.** Embed all blocks using the same agarose protocol to reduce variability across experiments.
- **Use internal controls.** When possible, compare slices from different zones of the same liver to control for donor-specific effects.

If problems persist, don't hesitate to contact Precisionary Instruments’ scientific support team. We’re available to help optimize your workflow and troubleshoot technical challenges—whether you're just starting with PCLS or refining advanced experimental protocols.

Recipes for Liver PCLS Preparation and Culture

The following recipes provide standardized formulations for preparing reagents and buffers essential to the successful embedding, slicing, and maintenance of precision-cut liver slices (PCLS). Accuracy and consistency in reagent preparation are crucial for preserving tissue viability and achieving reproducible results across experiments.

---

1. Agarose Embedding Solution (2–3%)

Ingredients:

- 1.5–2.0 g low-melting point agarose powder or tablets
- 100 ml HBSS/HEPES buffer (or slicing buffer of choice)

Instructions:

1. Weigh 1.5 g (for 2%) or 2.0 g (for 3%) of low-melting point agarose powder using a calibrated balance.
2. In a sterile glass beaker, add agarose to 100 ml of ice-cold HBSS/HEPES buffer.
3. Heat in a microwave in short intervals (20–30 seconds), swirling between cycles, until the agarose is fully dissolved. Avoid boiling or overheating.
4. Cool the agarose solution in a water bath to ~37–42°C before embedding liver tissue.

Alternative (using Precisionary Agarose Tablets):

- Use 3 tablets (0.5 g each) for 2% agarose in 75 ml of HBSS/HEPES buffer.
- Follow the same heating and cooling process as above.

> **Note:** Use higher agarose concentration (up to 3.5%) for fragile or fatty liver tissue (e.g., human or NAFLD models).

---

2. HBSS/HEPES Buffer

Ingredients:

- 1× Hanks' Balanced Salt Solution (HBSS)
- 1% (v/v) HEPES (1 M stock solution, pH 7.4)

Instructions:

1. Prepare 100 ml of 1× HBSS by diluting concentrate with sterile deionized water.
2. Add 1 ml of 1 M HEPES buffer (pre-adjusted to pH 7.4) to the HBSS.
3. Mix thoroughly and store on ice or refrigerate until use.

Note: This buffer is used as the slicing solution and for dissolving agarose. For enhanced slice viability, bubble with 95% O_2 / 5% CO_2 for 15–20 minutes before use.

---

3. Serum-Free DMEM (SF-DMEM)

Ingredients:

- DMEM (high glucose) basal medium
- 1% Penicillin-Streptomycin

Instructions:

1. Aliquot DMEM into a sterile bottle (e.g., 100 ml).
2. Add 1 ml of 1% Pen-Strep solution.
3. Mix gently. Store at 4°C and use within 2 weeks.

Optional Additives: For extended culture or stressed liver tissue (e.g., human PCLS), supplement with:

- 2 mM GlutaMAX™
- 1× ITS (insulin-transferrin-selenium)

- 10 mM HEPES
- 0.1 µM dexamethasone

---

4. Williams’ Medium E Complete (for Long-Term Culture)

Ingredients:

- Williams' Medium E (base)
- 10% Fetal Bovine Serum (FBS)
- 1% Penicillin-Streptomycin
- 2 mM GlutaMAX™
- 1× ITS supplement (optional)

Instructions:

1. To 100 ml of Williams' Medium E, add:
    - 10 ml FBS
    - 1 ml Pen-Strep
    - 2 ml GlutaMAX™
    - (Optional) 1 ml ITS
2. Mix gently under sterile conditions.
3. Store at 4°C and use within 7–10 days. Pre-warm to 37°C before use.

> **Note:** This medium supports hepatocyte viability and function, including albumin and urea production, during long-term slice incubation.

---

5. 70% Ethanol (for Sterilization)

Ingredients:

- 70 ml absolute ethanol (≥95%)
- 30 ml sterile distilled water

Instructions:

1. Combine ethanol and water in a clean glass bottle or autoclaved container.
2. Swirl gently to mix.
3. Label and store at room temperature.

> **Caution:** Flammable—keep away from heat sources. Always prepare in a well-ventilated space or fume hood.

---

6. Reagents for Metabolic and Functional Assays (Optional)

For advanced applications such as metabolic flux analysis or hepatotoxicity screening:

ATP Assay:

- CellTiter-Glo® Luminescent Cell Viability Assay
- Follow manufacturer's instructions for slice-scale use (~200–300 µl per well)

Mitochondrial Stress Test (Agilent Seahorse XF):

- Oligomycin (1 µM), FCCP (1 µM), Rotenone/Antimycin A (0.5 µM each)
- Prepare fresh dilutions in Seahorse assay medium

Liver Injury Markers (supernatant assays):

- ALT/AST Colorimetric or Fluorometric Assay Kits
- Albumin ELISA Kit

- Urea Detection Kit (optional)

Note: Always normalize results to slice wet weight or protein content for comparative data.

Have More Questions? Contact Us!

At Precisionary Instruments, we understand that no two experiments—or research teams—are exactly alike. Whether you're preparing your first set of precision-cut liver slices (PCLS) or optimizing advanced protocols for metabolic assays or drug screening, our team is here to support you every step of the way.

If you have questions, need assistance troubleshooting technical challenges, or would like access to additional resources—including sample preparation protocols, product manuals, references, or researcher referrals—we encourage you to reach out.

We provide support for:

- **Protocol troubleshooting and optimization** for mouse or human liver slices
- **Custom experimental planning**, including tissue-specific or disease-model adaptations
- **Product selection and operation guidance** for the Compresstome® vibratome or associated accessories
- **Blade and reagent recommendations** tailored to your sample type and research goals
- **Connections to published literature** or experienced labs using PCLS in similar applications

Our dedicated scientific and technical support teams are available to assist by email, phone, or web:

📧 **Email:** info@precisionary.com
📞 **Phone:** (617) 682-0586
🌐 **Website:** www.precisionary.com

Whether you're troubleshooting slice viability, exploring disease models, or setting up your first vibratome system, we're here to help you succeed. Contact us for personalized support and expert insight to take your liver research further.

Let us be your partner in precision tissue sectioning.

PRECISION-CUT GUT SLICES

PROTOCOL FOR CUTTING SLICES OF FRESH GUT TISSUE

Key to reading the protocol:

√ Rationale for procedural step

♠ Tips & Tricks

1. Prepare Krebs-Henseleit Buffer (KHB) for slicing intestine and storing intestinal slices.
   - √ Here's the simple recipe for KHB:

KHB (slicing buffer)	Concentration (mM)
NaCl	118
KCl	5
$MgSO_4 \cdot 7H_2O$	1.1
KH_2PO_4	1.2
$NaHCO_3$	25
$CaCl_2 \cdot 2H_2O$	2.5
D-Glucose	25
HEPES	9

2. Prepare Williams medium E (WME, containing L-glutamine)
   - √ Here's the simple recipe for KHB:

WME	Concentration (mM)
WME + L-glutamine	5
D-Glucose	14
Gentamycin	50 µg/ml

Amphotericin B	2.5 μg/ml

✓ Amphotericin B is added to inhibit growth of fungi and yeasts.

3. Fill the culture plates you will use with the incubation medium.
4. Warm and oxygenate culture plates with 95% O2/5% CO2 at 37 C for at least 30 min.
5. Prepare and keep warm a 2-3% solution of agarose at 37 C.
6. To obtain intestinal tissue, anesthetize the animal and retrieve the gut as quickly as possible, ideally under 5 minutes. Remove any fatty tissue and flush the intestines by pipetting ice-cold oxygenated KHB solution. Transfer cleaned pieces of intestinal tissue to ice-cold oxygenated KHB.

   ✓ Intestinal tissue is very sensitive to ischemia, so the time taken for dissection and incubation of precision-cut gut tissue should be as fast as possible.
7. Tighten one end of the gut segment with surgical thread. Using a transfer pipette, fill the intestine with 2-3% agarose. Close the end of intestine with thread or a clamp, then transfer into cold oxygenated KHB to help solidify the agarose into a gel (<1 min required).
8. Once agarose has solidified, cut the intestinal segment into sections that you want to slice.
9. Glue the tissue sample onto the Compresstome® specimen syringe.
10. Draw the syringe downward to bring the intestinal tissue core sample into the syringe.
11. Fill the syringe with 2% agarose (Sigma A-0701, low gelling point, incubated at ~37°C).

    ✓ Order a Starter Kit or additional agarose or blades directly from our website at http://www.precisionary.com/starter-kit!
12. Cool the entire contents of the specimen syringe with the chilling block. The intestinal tissue is now embedded in agarose. The agarose will solidify enough for stable sectioning.
13. Load the specimen syringe onto the Compresstome® slicer.
14. The protocol is complete for preparing the intestinal specimen for sectioning. Proceed from here with normal Compresstome® sectioning procedures.

    ♠ What are the optimal settings on the Compresstome® for cutting live intestinal slices? Try a speed (Advance) of 4 and an oscillation of 5-7.

References

*** Uses the Compresstome® for successful eye tissue slices.**

1. **Buffington SA, Di Prisco GV, Auchtung TA, Ajami NJ, Petrosino JF, Costa-Mattioli M. Microbial Reconstitution Reverses Maternal Diet-Induced Social and Synaptic Deficits in Offspring. Cell. 2016 Jun 16;165(7):1762-75.**

2. de Graaf IA, Olinga P, de Jager MH, Merema MT, de Kanter R, van de Kerkhof EG, Groothuis GM. Preparation and incubation of precision-cut liver and intestinal slices for application in drug metabolism and toxicity studies. Nat Protoc. 2010 Sep;5(9):1540-51.

3. de Kanter R, Tuin A, van de Kerkhof E, Martignoni M, Draaisma AL, de Jager MH, de Graaf IA, Meijer DK, Groothuis GM. A new technique for preparing precision-cut slices from small intestine and colon for drug biotransformation studies. J Pharmacol Toxicol Methods. 2005 Jan-Feb;51(1):65-72.

4. de Kanter R, Monshouwer M, Meijer DK, Groothuis GM. Precision-cut organ slices as a tool to study toxicity and metabolism of xenobiotics with special reference to non-hepatic tissues. Curr Drug Metab. 2002 Feb;3(1):39-59.

PRECISION-CUT KIDNEY SLICES

PROTOCOL FOR CUTTING SLICES OF FRESH KIDNEY TISSUE

Key to reading the protocol:

√ Rationale for procedural step

♠ Tips & Tricks

1. Prepare Krebs-Henseleit Buffer (KHB) for slicing and storing precision-cut kidney slices.
   - √ Here's the simple recipe for KHB:

KHB (slicing buffer)	Concentration (mM)
NaCl	118
KCl	5
$MgSO_4 \cdot 7H_2O$	1.1
KH_2PO_4	1.2
$NaHCO_3$	25
$CaCl_2 \cdot 2H_2O$	2.5
D-Glucose	25
HEPES	9

   - √ Adjust the pH of the solution to 7.42 slowly by adding drops of 5N NaOH solution.
   - √ The KHM solution can be stored for 24 hours at 4°C.

2. Prepare Williams medium E (WME, containing L-glutamine)
   - √ Here's the simple recipe for WME:

WME	Concentration (mM)
WME + L-glutamine	5

D-Glucose	14
Gentamycin	50 µg/ml
Amphotericin B	2.5 µg/ml

- √ Amphotericin B is added to inhibit growth of fungi and yeasts.
- √ The WME solution can be stored for 24 hours at 4°C.

3. Fill the culture plates you will use with the incubation medium (WME incubation medium)
4. Warm and oxygenate culture plates with 95% O2/5% CO2 at 37 C for at least 30 min.
5. Prepare and keep warm a 2-3% solution of agarose at 37 °C.
6. To obtain kidney tissue, anesthetize the animal and surgically isolate the kidney as quickly as possible, ideally under 5 minutes. Remove any fatty tissue and transfer cleaned pieces of kidney tissue to ice-cold oxygenated KHB.
    - √ Kidney tissue is very sensitive to ischemia, so the time taken for dissection and incubation of precision-cut kidney slices should be as fast as possible. This is especially important for studies of kidney metabolism.
7. Glue the selected kidney sample onto the Compresstome® specimen syringe plunger. Place the embedding cap onto the specimen syringe, over the kidney sample.
8. Fill the syringe with 2% agarose (Sigma A-0701, low gelling point, incubated at ~37°C).
    - √ Order a Starter Kit or additional agarose or blades directly from our website at http://www.precisionary.com/starter-kit !
9. Draw the syringe downward to bring the kidney tissue core sample into the syringe.
10. Cool the entire contents of the specimen syringe with the chilling block. The kidney tissue is now embedded in agarose. The agarose will solidify enough for stable sectioning.
11. Load the specimen syringe onto the Compresstome® slicer.
12. The protocol is complete for preparing the kidney specimen for sectioning. Proceed from here with normal Compresstome® sectioning procedures. Use KHB slicing solution (see above) for the buffer tray.

    ♠ What are the optimal settings on the Compresstome® for cutting live kidney slices? Try a speed (Advance) of 2-3 and an oscillation of 5-7.

    - √ The biggest challenge of slicing precision-cut kidney slices is getting consistent sections when there is hard (fibrotic) kidney tissue. The Compresstome® has patented compression technology that allows for smooth, even slices and overcomes this obstacle.
13. Collect each kidney slice and immediately transfer to pre-warmed Williams' Medium E (see recipe above), incubating at 37° C to restore ATP levels and wash away cellular debris.

References

* Uses the Compresstome® for successful kidney slices.

1. Genovese F, Kàrpàti ZS, Nielsen SH, Karsdal MA. Precision-Cut Kidney Slices as a Tool to Understand the Dynamics of Extracellular Matrix Remodeling in Renal Fibrosis. Biomark Insights. 2016 May 22;11:77-84.

2. Poosti F, Pham BT, Oosterhuis D, Poelstra K, van Goor H, Olinga P, Hillebrands JL. Precision-cut kidney slices (PCKS) to study development of renal fibrosis and efficacy of drug targeting ex vivo. Dis Model Mech. 2015 Oct 1;8(10):1227-36.

3. Stribos EG, Hillebrands JL, Olinga P, Mutsaers HA. Renal fibrosis in precision-cut kidney slices. Eur J Pharmacol. 2016 Nov 5;790:57-61.

4. Vickers AE, Fisher RL. Precision-cut organ slices to investigate target organ injury. Expert Opin Drug Metab Toxicol. 2005 Dec;1(4):687-99.

SPLEEN TISSUE SECTIONING

PROTOCOL FOR CUTTING SLICES OF SPLEEN TISSUE

Key to reading the protocol:

√ Rationale for procedural step

♠ Tips & Tricks

1. Obtain spleen from animal of choice.
2. Immediately freeze in OCT and/or formalin fixed and embedded in paraffin.
3. Select a section of the spleen that you would like to take cut for slices.
4. Glue the tissue sample onto the Compresstome® specimen syringe.
5. Draw the syringe downward to bring the spleen tissue core sample into the syringe.
6. Fill the syringe with 2% agarose (Sigma A-0701, low gelling point, incubated at ~37˚C).
    a. Order a Starter Kit or additional agarose or blades directly from our website at http://www.precisionary.com/starter-kit !
7. Cool the entire contents of the specimen syringe with the chilling block. The spleen tissue is now embedded in agarose. The agarose will solidify enough for stable sectioning.
8. Load the specimen syringe onto the Compresstome® slicer.
9. The protocol is complete for preparing the spleen tissue for sectioning. Proceed from here with normal Compresstome® sectioning procedures.

References

*** Uses the Compresstome® for successful spleen tissue slices.**

1. **Li S, Folkvord JM, Rakasz EG, Abdelaal HM, Wagstaff RK, Kovacs KJ, Kim HO,Sawahata R, MaWhinney S, Masopust D, Connick E, Skinner PJ. Simian Immunodeficiency Virus-Producing Cells in Follicles Are Partially Suppressed by CD8+ Cells In Vivo. J Virol. 2016 Nov 28;90(24):11168-11180. Print 2016 Dec 15. PubMed PMID: 27707919; PubMed Central PMCID: PMC5126374.**

2. **Roberts EW, Broz ML, Binnewies M, Headley MB, Nelson AE, Wolf DM, Kaisho T, Bogunovic D, Bhardwaj N, Krummel MF. Critical Role for CD103(+)/CD141(+) Dendritic Cells Bearing CCR7 for Tumor Antigen Trafficking and Priming of T Cell Immunity in Melanoma. Cancer Cell. 2016 Aug 8;30(2):324-36. doi:10.1016/j.ccell.2016.06.003. Epub 2016 Jul 14. PubMed PMID: 27424807; PubMed Central PMCID: PMC5374862.**

LYMPH NODE TISSUE SECTIONING

PROTOCOL FOR CUTTING SLICES OF LYMPH NODE TISSUE

Key to reading the protocol:

√ Rationale for procedural step

♠ Tips & Tricks

1. Obtain lymph node and spleen from animal of choice.
2. Immediately freeze in OCT and/or formalin fixed and embedded in paraffin.
3. Select a section of the spleen that you would like to take cut for slices.
4. Glue the tissue sample onto the Compresstome® specimen syringe.
5. Draw the syringe downward to bring the lymph node tissue core sample into the syringe.
6. Fill the syringe with 2% agarose (Sigma A-0701, low gelling point, incubated at ~37°C).
    a. Order a Starter Kit or additional agarose or blades directly from our website at http://www.precisionary.com/starter-kit !
7. Cool the entire contents of the specimen syringe with the chilling block. The lymph node tissue is now embedded in agarose. The agarose will solidify enough for stable sectioning.
8. Load the specimen syringe onto the Compresstome® slicer.
9. The protocol is complete for preparing the lymph node for sectioning. Proceed from here with normal Compresstome® sectioning procedures.

References

*** Uses the Compresstome® for successful lymph node tissue slices.**

1. **Li S, Folkvord JM, Rakasz EG, Abdelaal HM, Wagstaff RK, Kovacs KJ, Kim HO,Sawahata R, MaWhinney S, Masopust D, Connick E, Skinner PJ. Simian Immunodeficiency Virus-Producing Cells in Follicles Are Partially Suppressed by CD8+ Cells In Vivo. J Virol. 2016 Nov 28;90(24):11168-11180. Print 2016 Dec 15. PubMed PMID: 27707919; PubMed Central PMCID: PMC5126374.**

2. **Roberts EW, Broz ML, Binnewies M, Headley MB, Nelson AE, Wolf DM, Kaisho T, Bogunovic D, Bhardwaj N, Krummel MF. Critical Role for CD103(+)/CD141(+) Dendritic Cells Bearing CCR7 for Tumor Antigen Trafficking and Priming of T Cell Immunity in Melanoma. Cancer Cell. 2016 Aug 8;30(2):324-36. doi:10.1016/j.ccell.2016.06.003. Epub 2016 Jul 14. PubMed PMID: 27424807; PubMed Central PMCID: PMC5374862.**

MUSCLE TISSUE SECTIONING

PROTOCOL FOR CUTTING SLICES OF MUSCLE TISSUE

Key to reading the protocol:

√ Rationale for procedural step

♠ Tips & Tricks

1. Extract the specific muscle tissue out you want to use your research.
2. Select a section of the muscle that you would like to take cut for slices.
3. Glue the tissue sample onto the Compresstome® specimen syringe.
4. Draw the syringe downward to bring the muscle tissue core sample into the syringe.
5. Fill the syringe with 2% agarose (Sigma A-0701, low gelling point, incubated at ~37˚C).
    a. Order a Starter Kit or additional agarose or blades directly from our website at http://www.precisionary.com/starter-kit !
6. Cool the entire contents of the specimen syringe with the chilling block. The muscle tissue is now embedded in agarose. The agarose will solidify enough for stable sectioning.
7. Load the specimen syringe onto the Compresstome® slicer.
8. The protocol is complete for preparing the muscle tissue specimen for sectioning. Proceed from here with normal Compresstome® sectioning procedures.

References
*** Uses the Compresstome® for successful muscle tissue slices.**

1. **Yim PD, Gallos G, Perez-Zoghbi JF, Trice J, Zhang Y, et al. Chloride channel blockers promote relaxation of TEA-induced contraction in airway smooth muscle. J. Smooth Muscle Res. 2014 Mar 21; 49: 112–124. doi: 10.1540/jsmr.49.112.**

2. **Gallos G, Yocum GT, Siviski ME, Yim PD, Xiao WF, et al. Selective targeting of the α5-subunit of GABAA receptors relaxes airway smooth muscle and inhibits**

cellular calcium handling. American Journal of Physiology Online. 2015 May 1(309)9: L931-L942. DOI: 10.1152/ajplung.00107.2014.

3. **Danielsson J, Perez-Zoghbi JF, Bernstein K, Barajas MB, Zhang Y, et al. Antagonists of the TMEM16A Calcium-activated Chloride Channel Modulate Airway Smooth Muscle Tone and Intracellular Calcium. Anesthesiology Online. 2015 Sept. 1;(123) 569-581. doi:10.1097/ALN.0000000000000769.**

4. **Castro-Piedras I, Perez-Zoghbi JF. Hydrogen sulphide inhibits Ca2+ release through InsP3 receptors and relaxes airway smooth muscle J Physiol Online. 2013; 59(23) pp 5999–6015. DOI: 10.1113/jphysiol.2013.257790.**

PRECISIONARY

SKIN

TISSUE SECTIONING

PROTOCOL FOR CUTTING SLICES OF SKIN TISSUE

Key to reading the protocol:

√ Rationale for procedural step

♠ Tips & Tricks

1. Extract the specific skin tissue out you want to use your research.
2. Select a section of the skin that you would like to take cut for slices.
3. Glue the tissue sample onto the Compresstome® specimen syringe.
4. Draw the syringe downward to bring the skin tissue core sample into the syringe.
5. Fill the syringe with 2% agarose (Sigma A-0701, low gelling point, incubated at ~37˚C).
    a. Order a Starter Kit or additional agarose or blades directly from our website at http://www.precisionary.com/starter-kit !
6. Cool the entire contents of the specimen syringe with the chilling block. The skin tissue is now embedded in agarose. The agarose will solidify enough for stable sectioning.
7. Load the specimen syringe onto the Compresstome® slicer.
8. The protocol is complete for preparing the skin tissue specimen for sectioning. Proceed from here with normal Compresstome® sectioning procedures.

References

*** Uses the Compresstome® for successful skin tissue slices.**

1. **Nia HT, Liu H, Seano G, Datta M, Jones D, Rahbari N, et al. Solid stress and elastic energy as measures of tumour mechanopathology. Nat. Biomed. Eng. 1, 0004. 2016 Nov 28; 18;(1):1. doi:10.1038/s41551-016-0004.**

CUTTING TUMOR SLICES

PROTOCOL FOR SECTIONING LIVE & FIXED TUMOR SPECIMENS

Key to reading the protocol:

√ Rationale for procedural step

♠ Tips & Tricks

1. Make 2% agarose using low-gelation temperature agarose (Sigma-Aldrich) or using the Precisionary agarose tablets. Mix with PBS buffer to dissolve.
2. Dissect and excise the tumor, and wash with PBS.
3. Glue the tumor specimen to the Compresstome® specimen tube, then embed with 2% agarose solution. Cool immediately with the pre-chilled chilling block to solidify the agarose gel.

   ♠ Pre-chill the chilling block for 10 min in the freezer or in ice water.
4. Load the specimen tube containing the tumor tissue onto the Compresstome® vibratome and begin cutting using normal procedures. The agarose that surrounds the tumor will help hold it in place and allow the tumor to be sectioned with minimal displacement.
5. For fixed tumor slices: place tumor slices in 4% paraformaldehyde for at least 24 hours, then rinse with PBS before further experimental processing.
6. For live tumor slices, immerse tumor slices in PBS for at least 10 min, then incubate per your own experimental protocols.

   ♠ What are the optimal settings on the Compresstome® for cutting tumor slices? Try an oscillation of 3-4 and an advance (speed) of 2. We find that these parameters yield the best tumor sections.

References

*** Uses the Compresstome® for successful tumor slices (live and fixed).**

1. Askoxylakis V et al. Preclinical Efficacy of Ado-trastuzumab Emtansine in the Brain Microenvironment. **J Natl Cancer Inst**. 2015Nov 7;108(2).

2. Boldajipour B et al. Tumor-infiltrating lymphocytes are dynamically desensitized to antigen but are maintained by homeostatic cytokine. **J Cl Insight**. 2016 Dec 8;1(20):e89289.

3. Broz ML et al. Dissecting the tumor myeloid compartment reveals rare activating antigen-presenting cells critical for T cell immunity. **Cancer Cell**. 2014 Nov10;26(5):638-52.

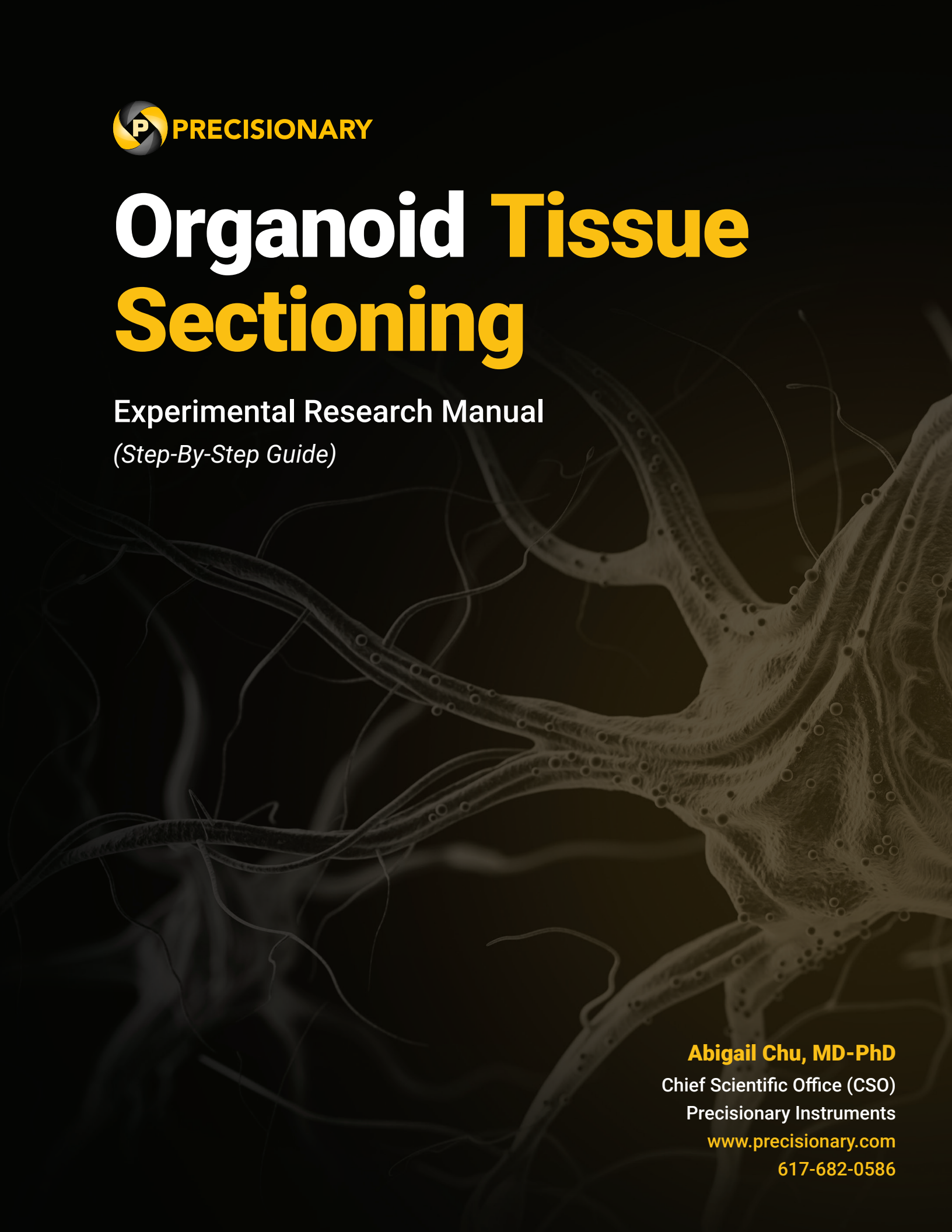
4. Nia H et al. Solid stress and elastic energy as measures of tumour mechanopathology. **Nature Biomedical Engineering** 2016; 1:0004.

PRECISIONARY

Organoid Tissue Sectioning

Experimental Research Manual

(Step-By-Step Guide)



Abigail Chu, MD-PhD
Chief Scientific Office (CSO)
Precisionary Instruments
www.precisionary.com
617-682-0586

Table of Contents

Table of Contents....2
Goals of this Experimental Guide....3
What is Organoid Sectioning and Why is it Important?....4
Who This Guide Can Help....6
Contact Precisionary Instruments for Additional Support in Organoid Research....7
Organoid Structure and Features....7
3D Architecture and Organization....8
Cellular Composition and Heterogeneity....8
Matrix and Microenvironment....8
Tissue-Specific Dynamics and Development....8
Functional Capabilities....9
Relevance to Experimental Applications....9
Most Common Organoids Used in Today's Research....10
Intestinal Organoids....11
Brain Organoids....12
Liver Organoids....13
Tumor Organoids....13
Essential Materials and Reagents for Organoid Research and Sectioning....16
General Equipment and Reagents for Organoid Research....16
Equipment....16
Lab Accessories....16
Reagents....16
Basic Reagents and Recipes....17
Agarose Solution....17
70% Ethanol....18
Materials and Reagents Specific to Intestinal Organoids....18
Materials and Reagents Specific to Brain Organoids....19
Materials and Reagents Specific to Liver Organoids....20
Tips and Tricks for Ensuring Viable and Healthy Organoid Tissue Sections....20
Preparing Organoid Tissue for Sectioning....22
Embedding Organoids Into a Specimen Tube: A Step-by-Step Guide....22
Making Organoid Sections on the Compresstome Vibratome....25
Sectioning Organoids on the Compresstome Vibratome....26
Incubating Organoid Sections....29
Troubleshooting Organoid Sectioning....30
Q1: Why are my organoid sections uneven or torn?....30
Q2: Why are my organoid sections breaking apart during transfer?....30
Q3: Why are there bubbles in my agarose block?....30
Q4: Why do my organoid sections have jagged edges?....31
Q5: Why are my organoid sections losing viability?....31
Q6: Why are my sections not adhering well to slides for staining?....31
Q7: What should I do if my sections curl or fold during incubation?....31
More Questions? Contact Us!....32

Goals of this Experimental Guide

The use of organoid models in biomedical research has provided unparalleled opportunities to investigate complex human tissue systems in a controlled environment. Organoids serve as three-dimensional, multicellular structures that mimic the architecture and function of real organs, making them invaluable for studying development, disease mechanisms, and therapeutic responses. However, to fully harness the potential of organoids, it is critical to prepare high-quality tissue sections for downstream analyses such as immunohistochemistry, transcriptomics, and imaging.

This guide aims to equip researchers with the knowledge and techniques required to section organoid samples effectively, preserving their structural integrity and cellular composition. Using a vibratome, such as the Compresstome, ensures precise and consistent tissue slicing, which is essential for reproducible results in experimental workflows. Through careful adherence to this protocol, researchers can achieve high-quality organoid sections suitable for a wide range of applications (see Figure 1).

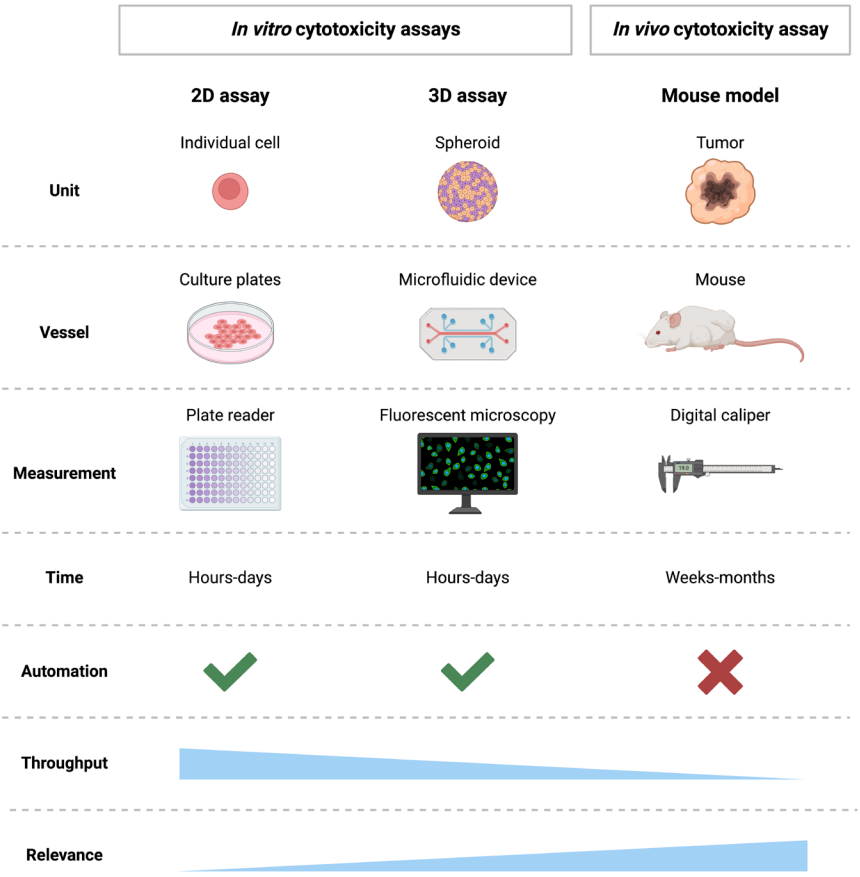


Figure X. Cytotoxicity Assays Using Organoid Models. *This figure highlights methods for assessing cytotoxicity, emphasizing the importance of organoids in modern research. In vitro assays, including 2D cell cultures and advanced 3D systems like organoids, provide a robust platform for evaluating cell viability and functionality, offering more physiologically relevant insights compared to traditional models. Organoids are particularly valuable for mimicking human tissues, enhancing the predictive power of drug development and toxicity screening. In vivo assays, using animal models such as rodents, complement these methods by providing systemic perspectives. Together, these approaches advance our understanding of cytotoxicity and improve translational outcomes in biomedical research. Adapted from Gottschalk et al. (2019).*

What is Organoid Sectioning and Why is it Important?

Organoid sectioning is a fundamental step in preparing these intricate three-dimensional tissue models for in-depth analysis. Organoids, derived from stem cells such as induced pluripotent stem cells (iPSCs), offer unparalleled opportunities for studying human development, disease mechanisms, and therapeutic responses. These miniature organ models closely mimic the cellular architecture and functionality of their in vivo counterparts, making them indispensable for research into complex conditions, including neurodegenerative diseases.

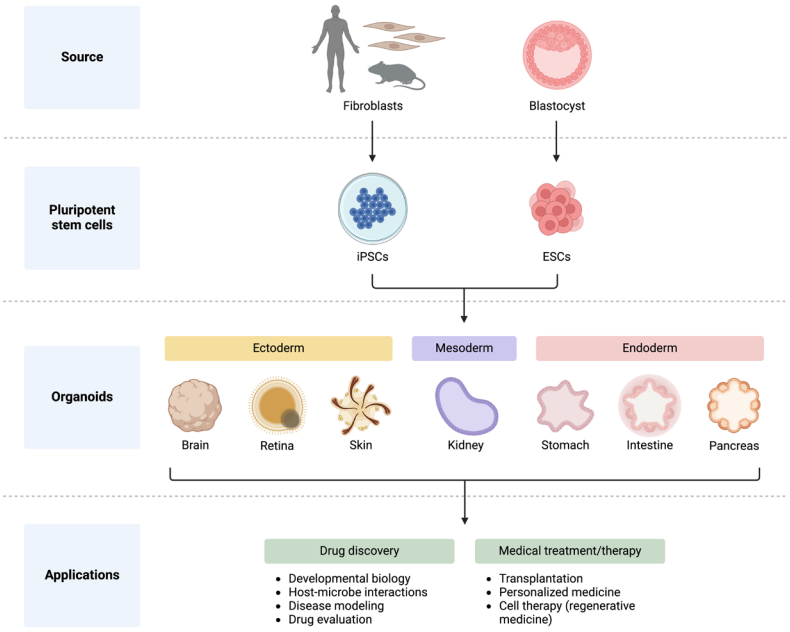


Figure X. Organoid Generation from Pluripotent Stem Cells. *This figure demonstrates the process of generating organoids from pluripotent stem cells, highlighting their potential as model systems for human biology and medicine. Starting from induced pluripotent or embryonic stem cells, the protocol involves differentiation into specialized cell types and the formation of three-dimensional structures that mimic the architecture and functionality of human tissues. These organoids enable the study of development, disease modeling, and therapeutic applications. Adapted from Kim et al. (2020) and Tang et al. (2022).*

Given their delicate structure and dense cellular matrix, organoids present unique challenges during sectioning. Traditional methods, such as paraffin embedding or manual slicing, can disrupt their integrity, leading to artifacts and compromised data. Vibratome sectioning, specifically using advanced tools like the Compresstome, ensures the preservation of cellular and tissue architecture while producing uniform slices. This precision is crucial for applications such as histological analysis, immunostaining, and molecular profiling.

As outlined in Figure X, the organoid research workflow spans from iPSC derivation to therapeutic applications. This process begins with generating iPSC-derived organoids, followed by their differentiation into specific tissue types. Once sectioned, these organoids can be employed in high-resolution studies to model diseases, test drug efficacy, and explore regenerative therapies. By maintaining the structural and functional integrity of organoids, sectioning enables researchers to unlock critical insights into cellular dynamics and potential treatments for neurodegenerative disorders.

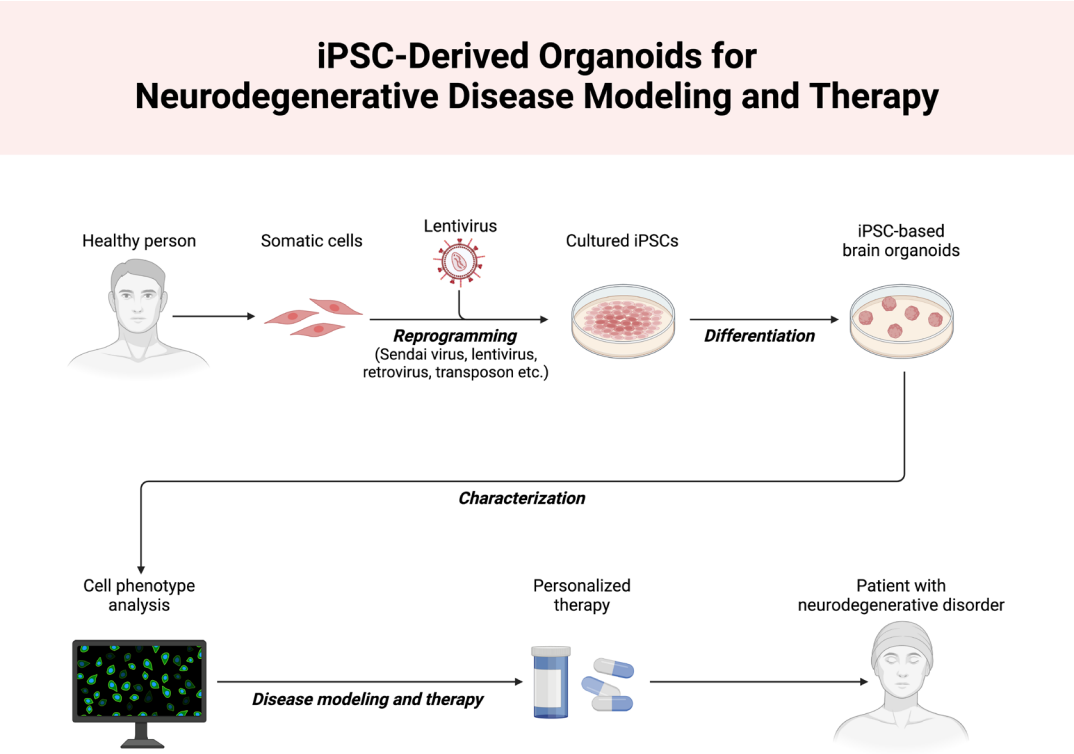


Figure 2. iPSC-Derived Organoids for Neurodegenerative Disease Modeling and Therapy. *This figure illustrates the use of organoids derived from induced pluripotent stem cells (iPSCs) as models for neurodegenerative diseases. These organoids replicate key aspects of human brain tissue, enabling the study of disease mechanisms, drug screening, and the development of targeted therapies. By bridging the gap between traditional in vitro models and human biology, iPSC-derived organoids provide a transformative platform for advancing our understanding of neurodegenerative conditions and exploring therapeutic interventions. Adapted from Jusop et al. (2023).*

Who This Guide Can Help

This guide is crafted to assist a broad spectrum of researchers working with organoids, from novices to seasoned experts. Organoid sectioning is a delicate and intricate process, and this manual aims to provide comprehensive support for:

New Researchers: If you are new to organoid research, this guide offers a clear, step-by-step framework for setting up and performing your first organoid sectioning experiments.

- Experienced Scientists: For those with prior experience, this guide provides advanced tips and troubleshooting strategies to optimize the sectioning process and ensure consistent, high-quality results.
- Research Mentors: If you train others in organoid techniques, this guide serves as an excellent teaching resource, helping your trainees master the precision required for successful organoid sectioning.
- Curious Researchers: Whether you're exploring the potential of organoid models or deepening your expertise, this guide delivers valuable insights into the preparation of organoids for diverse applications such as histology, molecular biology, and therapeutic research.

As outlined in Figure 3, this guide is intended to be a versatile resource for individuals at all levels of expertise. By providing practical techniques and detailed protocols, it supports your efforts to harness the full potential of organoid research and contribute to advancements in areas such as disease modeling and regenerative medicine.



Figure 3. Is this you? 🙂 *This guide serves as a comprehensive resource for researchers at all levels of expertise in organoid sectioning, offering valuable insights and practical guidance. Whether you are new to the technique, an experienced scientist, a mentor, or simply someone eager to expand your knowledge, this guide is designed to support your research endeavors and improve your mastery of organoid sectioning for advanced biomedical applications.*

Contact Precisionary Instruments for Additional Support in Organoid Research

For expert guidance and technical support, Precisionary Instruments is your trusted partner in vibratome equipment and accessories, designed to enhance the preparation of organoid sections. Whether you need troubleshooting tips, have technical questions, or seek customized solutions for your specific research needs, our dedicated team is here to assist you throughout your organoid experiments. With this guide, we aim to equip researchers with the tools and knowledge necessary to advance organoid-based studies in fields like disease modeling and regenerative medicine.

E-mail: info@precisionary.com
Phone: (617) 682-0586
Fax: 1-866-424-2217

Precisionary Instruments
200 Butterfield Drive, Unit E
Ashland, MA 01721

Let's get started!

Organoid Structure and Features

Organoids are three-dimensional (3D) multicellular systems derived from stem cells or progenitor cells, capable of self-organizing into structures resembling in vivo tissues or organs. These advanced models offer unique opportunities for studying tissue development, disease mechanisms, and therapeutic responses. Below, we provide a detailed exploration of their structure and features, tailored for researchers.

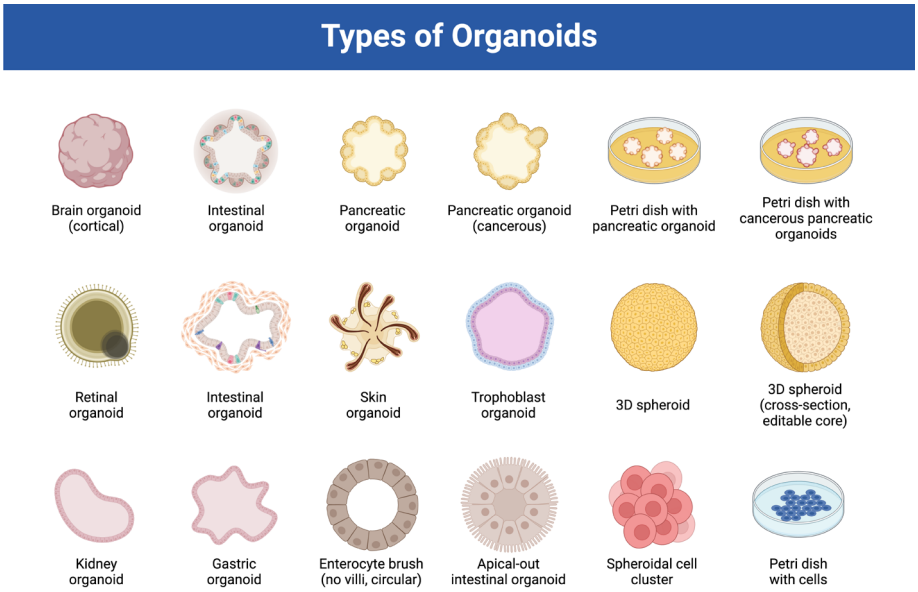


Figure X. Types of Organoids. *This figure illustrates the different types of organoids that can be derived and utilized in research. It highlights the potential of organoids as model systems for studying various tissues and organ functions, offering insights into their applications in scientific and medical research.*

3D Architecture and Organization

Organoids exhibit a self-organized 3D architecture that mirrors the spatial organization of native tissues. This structural complexity is critical for replicating in vivo cellular environments and functions. Organoids maintain apical-basal polarity, ensuring that specific surfaces interact with extracellular matrices or lumen-facing environments as they would in their tissue of origin. Their architecture often includes lumens, layers, and zones that emulate functional subunits of tissues, such as crypts, villi, or neuronal layers. The spatial arrangement of cells within these structures supports studies of cellular differentiation, migration, and functional interactions.

Cellular Composition and Heterogeneity

Organoids reflect the cellular diversity of their tissue of origin, encompassing stem cells, progenitor cells, and fully differentiated cell types. This heterogeneity allows for the study of cell-cell interactions, signaling pathways, and functional specialization. For example, epithelial organoids may include absorptive, secretory, and barrier-forming cells, while neuronal organoids contain progenitor cells, neurons, and supporting glial cells. The ability to maintain multiple cell types within a physiologically relevant microenvironment enhances their utility for research applications that require intact tissue functionality.

Matrix and Microenvironment

The growth and maintenance of organoids are heavily dependent on the extracellular matrix (ECM) or hydrogel in which they are embedded. These matrices provide essential biochemical cues and mechanical support, mimicking the in vivo microenvironment. Commonly used ECMs, such as Matrigel or collagen, facilitate organoid attachment, growth, and differentiation. The composition and stiffness of the matrix can influence organoid morphology and cell behavior, making the choice of matrix a critical variable for experimental design.

Tissue-Specific Dynamics and Development

Organoids undergo dynamic changes over time, from initial cell aggregation to fully formed structures resembling mature tissues. These developmental stages often recapitulate embryonic or early postnatal development of the tissue, providing unique opportunities to study morphogenesis and differentiation. The timing of specific structural and functional milestones is crucial for experimental design, as certain developmental stages may be better suited for specific assays, such as drug screening or functional studies.

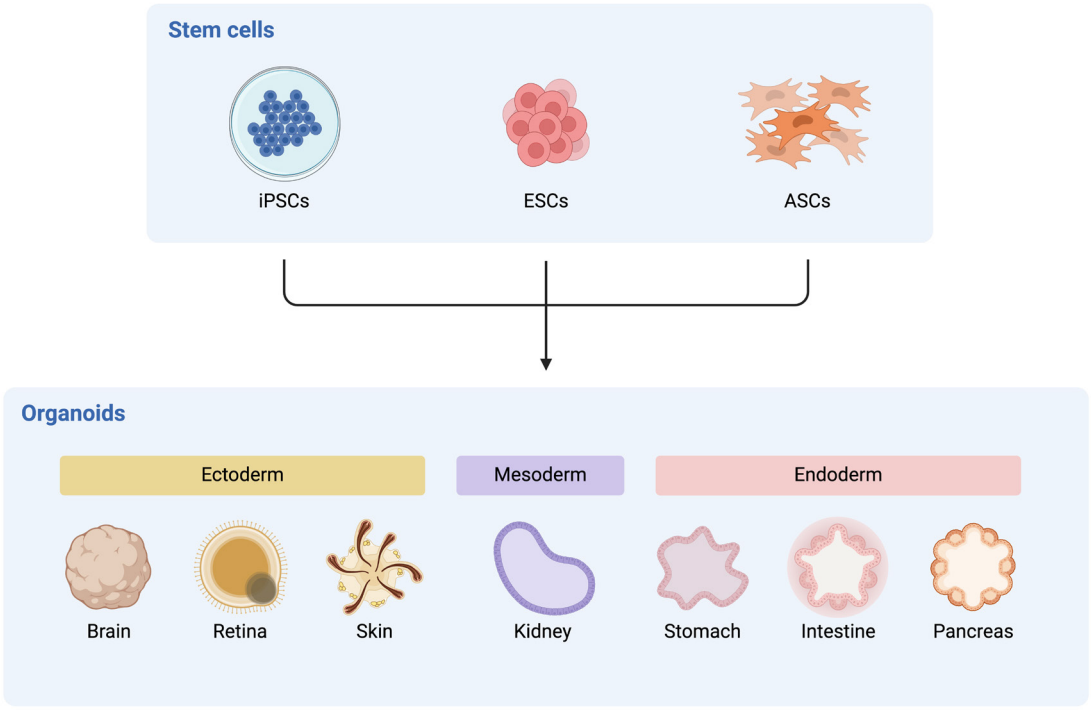


Figure X. Diversity of Organoids for Research Applications. *This figure depicts the variety of organoids that can be generated and used as model systems in research. It highlights their applications in studying human biology and medicine, offering insights into tissue-specific structures and functions. The figure is based on foundational studies by Kim et al. (2020) and Tang et al. (2022), which explore the role of organoids in advancing basic research and clinical applications.*

Functional Capabilities

Organoids retain many of the functional characteristics of their tissue of origin. This includes active signaling pathways, secretion of bioactive molecules, and responsiveness to external stimuli. Their multicellular composition enables studies on cell-cell communication, tissue regeneration, and the effects of therapeutic interventions. For example, organoids can mimic physiological responses, such as neurotransmitter release in brain organoids or bile production in liver organoids.

Relevance to Experimental Applications

The structural and functional fidelity of organoids positions them as superior models for bridging the gap between traditional 2D cultures and animal models. Their ability to replicate key aspects of human tissue biology makes them invaluable for understanding disease mechanisms, testing drug efficacy, and exploring regenerative therapies. Organoids offer researchers the ability to study complex biological processes in controlled environments, paving the way for new discoveries in biomedical science.

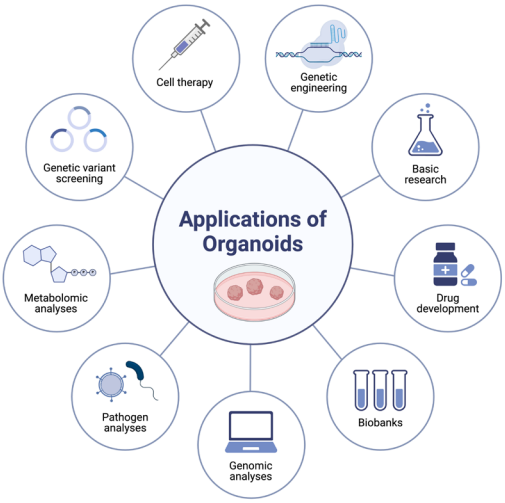


Figure X. Application of Organoids. *This figure illustrates the diverse applications of organoids, assembled using dynamic BioRender assets for full customization. The template serves as a starting point for visualizing organoid research and is based on the work of Kim, Koo, and Knoblich (Nat Rev Mol Cell Biol, 2020).*

Most Common Organoids Used in Today's Research

Organoids have become a cornerstone of biomedical research, offering unparalleled opportunities to replicate complex human tissues in vitro. Among the most utilized models are intestinal, brain, and liver organoids. These systems allow researchers to study development, disease mechanisms, and therapeutic responses with unprecedented accuracy. Below is a detailed description of these organoids and their applications.

Organoid Production Methods Overview

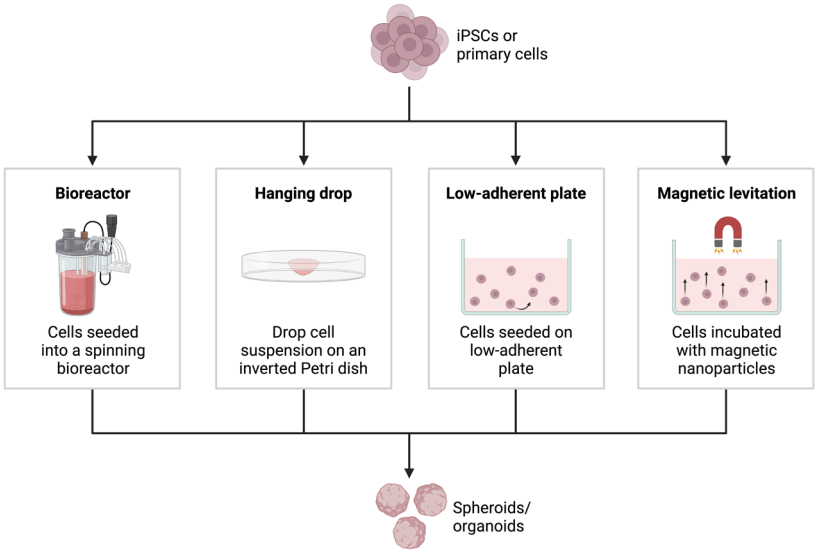


Figure X. Organoid Production Methods Overview. *This figure provides an overview of various methods for producing organoids, highlighting the use of dynamic approaches to simulate and study tissue structures in vitro. It is assembled using editable BioRender assets, showcasing key steps, tools, and processes involved in organoid engineering and development. The schematic emphasizes advancements in organoid production, drawing from foundational studies by Hofer and Lutolf (2021) and Velasco et al. (2020), which explore engineering principles and microtechnology-based methods for creating organoid models.*

Intestinal Organoids

Overview: Intestinal organoids are derived from adult intestinal stem cells or pluripotent stem cells (PSCs). They self-organize into 3D structures that closely mimic the architecture and functionality of the gastrointestinal epithelium, including crypt-villus organization. Intestinal organoids reflect the natural turnover of the intestinal lining, driven by stem cell proliferation and differentiation into specialized epithelial cell types. These organoids are supported by an extracellular matrix (typically Matrigel) and supplemented with growth factors that activate Wnt, R-spondin, and Noggin signaling pathways, essential for stem cell maintenance and epithelial renewal. Their central lumen and apical-basal polarity recreate physiological interactions, making them highly relevant for studying barrier function and host-microbe interactions.

Key Features:

- **Cell Types:** Enterocytes (absorptive cells), goblet cells (mucus-producing), Paneth cells (antimicrobial secretion), and enteroendocrine cells (hormone-secreting).
- **Polarity:** Apical surfaces face the lumen, while basal surfaces interact with the extracellular matrix, maintaining functional relevance.
- **Lumen:** A hollow central cavity facilitates studies of microbial interactions, nutrient absorption, and secretory processes.

Applications:

- Studying gastrointestinal diseases such as inflammatory bowel disease (IBD), colorectal cancer, and infectious enteropathies.
- Exploring gut microbiome-host interactions and epithelial barrier dynamics.
- Screening for drug absorption, metabolism, and toxicity.
- Investigating epithelial repair and regenerative therapies.

Complex Intestine on-a-Chip for Personalized Medicine

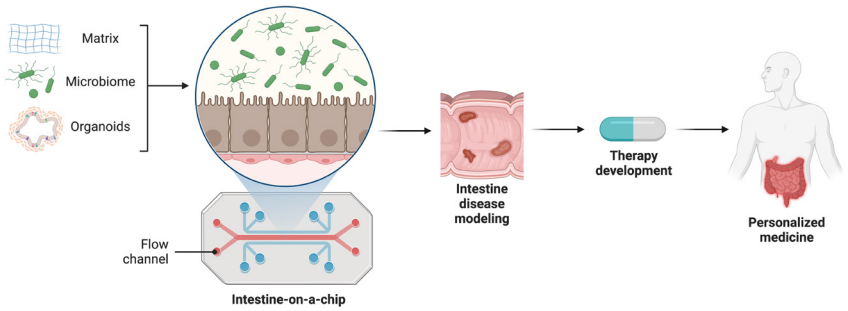


Figure X. Intestine-on-a-Chip Platform for Personalized Medicine. This figure showcases advanced intestine tissue culture and engineering platforms. The top panel categorizes current intestine tissue models based on their application throughput and physiological relevance. The bottom panel illustrates a two-channel microfluidic intestine-on-a-chip device, featuring a human intestinal epithelium layered with mucus and gut microbiota, positioned over a porous matrix. Below the porous membrane, a vascular endothelium is depicted, enabling the study of intestinal pathologies. This platform offers a robust tool for modeling human gut conditions and exploring applications in personalized medicine. Adapted from Firoozinezhad et al. (2019).

Brain Organoids

Overview: Brain organoids are generated from neural progenitor cells or PSCs and emulate the early stages of human brain development. These organoids self-organize into cortical-like structures with defined layers that correspond to the ventricular zone, subventricular zone, and cortical plate. The developmental trajectory of brain organoids recapitulates key processes in neural differentiation, synaptogenesis, and network formation. Cultured in suspension or embedded in a matrix, brain organoids maintain cellular and spatial heterogeneity, supporting functional neural activity. Advances in protocols have enabled the inclusion of supporting cell types like astrocytes and microglia, which are crucial for mimicking neuroinflammatory responses and neuron-glia interactions.

Key Features:

- **Cell Types:** Neural progenitor cells, neurons (excitatory and inhibitory), astrocytes, and occasionally microglia.
- **Layered Structure:** Formation of cortical zones reflects human brain development and provides a platform for studying complex processes such as radial migration and cortical expansion.
- **Neuronal Activity:** Functional synaptic connections and spontaneous activity enable studies of neural network physiology and pathophysiology.

Applications:

- Modeling neurodevelopmental disorders, including microcephaly, autism, and epilepsy.
- Investigating neurodegenerative diseases like Alzheimer's and Parkinson's.
- Examining the impact of neurotropic viruses such as Zika on brain development.
- Screening neuroprotective drugs and testing therapeutic interventions.

Liver Organoids

Overview: Liver organoids are derived from hepatic progenitor cells, adult liver stem cells, or PSCs. These organoids replicate the metabolic and regenerative capabilities of the liver, making them invaluable for studying hepatic function and pathology. They self-organize into clusters of hepatocyte-like cells and cholangiocytes, forming bile duct structures. The culture conditions are tailored to mimic liver-specific microenvironments, including cytokines and extracellular matrix components that support liver-specific differentiation. Liver organoids can recapitulate liver metabolism, detoxification pathways, and bile secretion, offering a physiologically relevant model for liver disease and drug testing.

Key Features:

- **Cell Types:** Hepatocytes (metabolic and detoxification roles), cholangiocytes (bile duct cells), and liver progenitor cells.
- **Bile Duct Structures:** Formation of functional ductal systems allows the study of cholestatic diseases and bile secretion.
- **Metabolic Function:** Active drug metabolism, urea synthesis, and protein production mimic in vivo liver processes.

Applications:

- Studying liver diseases such as non-alcoholic fatty liver disease (NAFLD), hepatitis, and cholangiopathies.
- Screening for hepatotoxicity, drug metabolism, and pharmacokinetics.
- Modeling liver regeneration and exploring transplantation strategies.
- Investigating host-pathogen interactions in hepatic infections like hepatitis B or C.

Tumor Organoids

Tumor organoids are three-dimensional cultures derived from primary tumor tissues, cancer stem cells, or patient-derived xenografts (PDXs). These organoids closely mimic the structural and

functional characteristics of the original tumors, providing an invaluable model for studying cancer biology. Tumor organoids maintain the genetic and phenotypic heterogeneity of the parent tumor, including its microenvironment, and are cultured in conditions that support tumor growth, such as extracellular matrix gels and growth factor-enriched media. They serve as a physiologically relevant system for investigating tumor progression, drug resistance, and personalized cancer therapies.

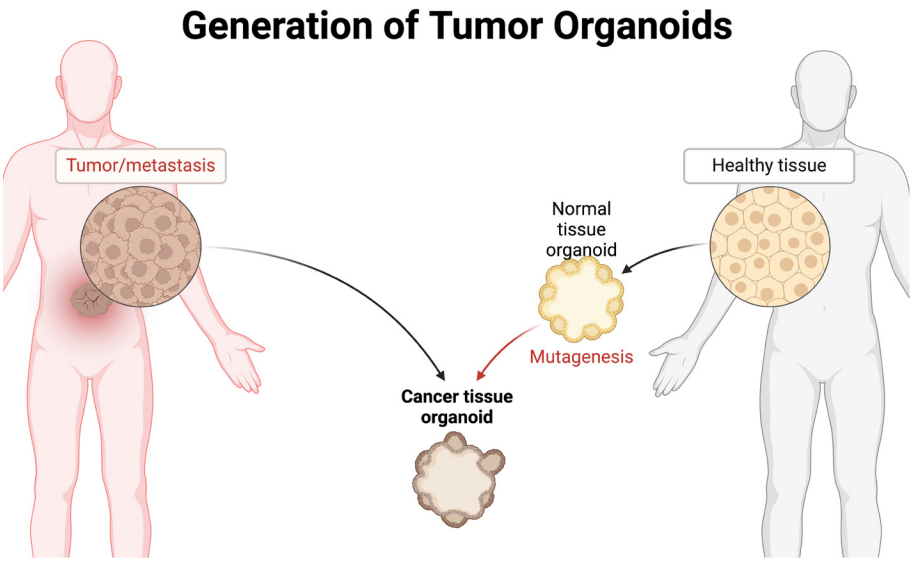


Figure X. Generation of Tumor Organoids. This figure depicts the process of creating tumor organoids, which serve as advanced 3D models for cancer research. Tumor organoids are derived from patient samples and cultured to replicate the structural and functional characteristics of primary tumors. These models provide a unique platform for studying tumor biology, testing therapeutic interventions, and developing personalized cancer treatments. The integration of organoid technology into cancer research, as highlighted by Tuveson et al. (2019) and Kretzschmar (2021), represents a significant leap forward in understanding and treating complex malignancies.

Key Features:

- **Genetic Heterogeneity:** Tumor organoids preserve the genetic mutations, epigenetic changes, and molecular signatures of the original tumor tissue.
- **Microenvironment Interaction:** Tumor organoids include interactions between cancer cells, stromal cells, and immune components, mimicking the tumor microenvironment.
- **High-Throughput Potential:** Tumor organoids can be scaled up for drug screening, allowing for testing multiple compounds simultaneously.

Applications:

- Studying tumor growth, invasion, and metastasis mechanisms.
- Investigating tumor-specific responses to immunotherapy and chemotherapy.
- Screening anti-cancer drugs for efficacy and resistance mechanisms in a patient-specific manner.
- Exploring tumor microenvironment interactions, including angiogenesis and immune evasion.
- Modeling tumor heterogeneity to identify novel therapeutic targets.

Tumor organoids represent a transformative tool in cancer research, bridging the gap between traditional cell culture and in vivo models, and paving the way for advancements in personalized medicine.

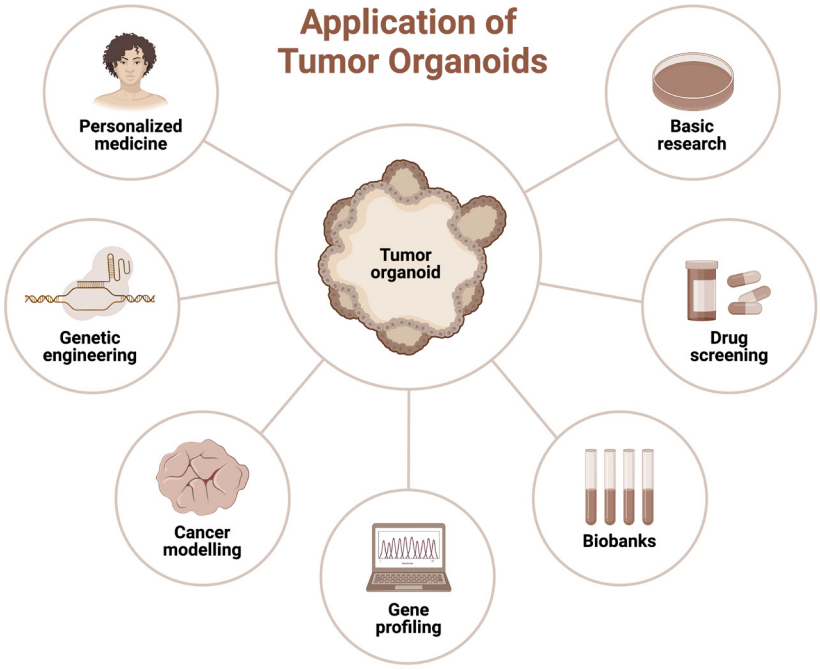


Figure X. Applications of Tumor Organoids. This figure highlights the diverse applications of tumor organoids in cancer research and therapy. Tumor organoids serve as highly representative models for studying tumor biology, enabling drug screening, testing personalized treatment strategies, and investigating mechanisms of resistance. These 3D systems provide a bridge between in vitro studies and clinical applications, offering a powerful tool for advancing precision oncology. As emphasized by Xu et al. (2018) and Kretzschmar (2021), tumor organoids are transforming cancer research by improving the relevance and efficacy of therapeutic development.

Essential Materials and Reagents for Organoid Research and Sectioning

Conducting organoid research and preparing precise organoid sections necessitates specific equipment and reagents. Below is a comprehensive list of general materials, followed by specialized items tailored for intestinal, brain, and liver organoids, including recommended brands and concentrations.

General Equipment and Reagents for Organoid Research

Equipment

- **Vibrating Microtome:** Compresstome® VF-310-0Z Vibrating Microtome (Precisionary Instruments)
- **Stereomicroscope:** Leica M80 Stereomicroscope (Leica Microsystems)
- **Vibration Isolation Table:** TMC 63-500 Series (Technical Manufacturing Corporation)
- **Refrigerated Centrifuge:** Eppendorf 5810 R Centrifuge (Eppendorf)
- **Data Acquisition System:** Axon Digidata 1550B (Molecular Devices)
- **Pipette Puller:** Sutter Instrument P-1000 Micropipette Puller (Sutter Instrument)

Lab Accessories

- **Micropipettes:** Eppendorf Research plus (Eppendorf)
- **Embedding Molds:** Tissue-Tek® Cryomold® (Sakura Finetek)
- **Fine Forceps:** Dumont #5 Forceps (Fine Science Tools)
- **Recording Chamber:** RC-26G Recording Chamber (Warner Instruments)
- **Perfusion System:** Automate Scientific ValveLink8.2 (Automate Scientific)
- **Humidified Incubator:** Heracell™ VIOS 160i (Thermo Fisher Scientific)

Reagents

- **Extracellular Matrix (ECM):** Corning® Matrigel® Matrix (Corning)
- **Cutting Solution:** Artificial Cerebrospinal Fluid (aCSF)
    - NaCl: 125 mM
    - KCl: 2.5 mM
    - $NaHCO_3$: 26 mM
    - Glucose: 10 mM
    - $CaCl_2$: 2 mM
    - $MgSO_4$: 1 mM
- **Fixatives:** Paraformaldehyde (4% solution)

- **Staining Reagents:**
  - Hematoxylin and Eosin (H&E) Stain Kit (Abcam)
  - DAPI (4',6-diamidino-2-phenylindole) (Thermo Fisher Scientific)
- **Enzyme Solutions:**
  - Collagenase Type II (Worthington Biochemical Corporation)
  - Trypsin-EDTA (0.25%) (Gibco)
- **Embedding Medium:** Agarose, Low Melting Point (Sigma-Aldrich)
- **Seal-Enhancing Substances:** Sylgard 184 Silicone Elastomer Kit (Dow Corning)

Basic Reagents and Recipes

Agarose Solution

Ingredients:

☐ 1.5 g low-melting point agarose powder

☐ 100 ml HBSS/HEPES buffer

Instructions:

1. Measure out 1.5 grams of low-melting point agarose powder using a laboratory balance.
2. In a suitable container, such as a glass beaker or flask, pour 100 ml of HBSS/HEPES buffer.
3. Add the measured agarose powder to the HBSS/HEPES buffer.
4. Microwave the mixture in short intervals, stirring occasionally, until the agarose powder is completely dissolved. Be cautious not to overheat the solution.
5. Once the agarose is fully dissolved, allow the solution to cool slightly before use in lung tissue processing.

Note: This recipe yields 100 ml of 2% agarose solution, suitable for processing multiple lung samples. Adjust the quantities accordingly if a smaller or larger volume is required.

Alternative Method using Agarose Tablets (Precisionary Instruments):

- Instead of low-melting point agarose powder, use agarose tablets provided by Precisionary Instruments.
- Each tablet is 0.5 grams, so use three tablets for a total of 1.5 grams to achieve a 2% agarose concentration.
- Mix the agarose tablets with 75 ml of HBSS/HEPES buffer (25 ml per tablet) to yield a 2% agarose solution.

- Follow the same procedure as described above for dissolving the agarose tablets in the buffer solution using the microwave.

Note: The use of agarose tablets provides a convenient and precise method for preparing agarose solution, ensuring consistent results in lung tissue processing. Adjust the volume of buffer solution accordingly to achieve the desired agarose concentration. Here is a visual guide for making agarose solution using tablets:

70% Ethanol

Ingredients:

☐ 70 ml absolute ethanol

☐ 30 ml distilled water

Instructions:

1. Measure out 70 ml of absolute ethanol using a graduated cylinder or measuring beaker.
2. Measure out 30 ml of distilled water using a separate graduated cylinder or measuring beaker.
3. Combine the measured amounts of absolute ethanol and distilled water in a clean container, such as a glass bottle or flask.
4. Mix the ethanol and water thoroughly by gently swirling or stirring the solution with a clean stir rod or spatula.
5. Once mixed, the solution will be 70% ethanol. Label the container appropriately with the concentration and contents.
6. Store the 70% ethanol solution in a tightly sealed container at room temperature. Ensure that the container is properly labeled and stored away from direct sunlight or heat sources.

Note: Always prepare ethanol solutions in a well-ventilated area and avoid inhaling the vapors. Use caution when handling ethanol as it is flammable. Dispose of any unused or expired ethanol solution according to local regulations for hazardous waste disposal.

Materials and Reagents Specific to Intestinal Organoids

Equipment:

- **Microinjector:** FemtoJet® 4i (Eppendorf)
- **Confocal Microscope:** Zeiss LSM 880 with Airyscan (Zeiss)

Reagents:

- **Growth Factors:**
  - Wnt3a: 100 ng/mL (R&D Systems)

- R-spondin 1: 500 ng/mL (R&D Systems)
- Noggin: 100 ng/mL (PeproTech)

- **Antibiotic Cocktail:** Gentamicin (50 µg/mL) and Amphotericin B (2.5 µg/mL) (Gibco)
- **Fluorescent Probes:**
  - FITC-Dextran (1 mg/mL) (Sigma-Aldrich)
- **Culture Media:**
  - Advanced DMEM/F12 (Gibco)
  - B-27 Supplement (2%) (Gibco)
  - N-2 Supplement (1%) (Gibco)
  - GlutaMAX™ Supplement (1%) (Gibco)

Materials and Reagents Specific to Brain Organoids

Equipment:

- **Electrophysiology Setup:**
  - Patch-Clamp Amplifier: MultiClamp 700B (Molecular Devices)
  - Headstage Holder: CV-7B Headstage (Molecular Devices)
- **Spinning Bioreactor:** Spinner Flask (Corning)
- **Neural Activity Recording System:** Maestro Pro Multi-Electrode Array (Axion BioSystems)

Reagents:

- **Differentiation Media:**
  - Neurobasal™ Medium (Gibco)
  - B-27 Supplement (2%) (Gibco)
  - N-2 Supplement (1%) (Gibco)
  - GlutaMAX™ Supplement (1%) (Gibco)
- **Growth Factors:**
  - BDNF: 20 ng/mL (PeproTech)
  - GDNF: 10 ng/mL (PeproTech)
  - Laminin: 1 µg/mL (Sigma-Aldrich)
- **Calcium-Sensitive Dye:**
  - Fluo-4 AM: 4 µM (Thermo Fisher Scientific)
- **Neurotransmitters:**
  - Glutamate: 100 µM (Sigma-Aldrich)
  - GABA: 100 µM (Sigma-Aldrich)

- **Cryoprotectant:**
  - DMSO: 10% in freezing media (Sigma-Aldrich)
- **Staining Reagents:**
  - Anti-NeuN Antibody for neuronal staining (Abcam)
  - Anti-GFAP Antibody for astrocytes (Thermo Fisher Scientific)

Materials and Reagents Specific to Liver Organoids

Equipment:

- **Oxygen Control Incubator:** Heracell™ VIOS 160i (Thermo Fisher Scientific)
- **Plate Reader:** Cytation™ 5 Imaging Reader (BioTek Instruments)

Reagents:

- **Hepatic Differentiation Media:**
  - Advanced DMEM/F12 (Gibco)
  - Hepatocyte Growth Factor (HGF): 10 ng/mL (PeproTech)
  - Fibroblast Growth Factor 4 (FGF4): 10 ng/mL (PeproTech)
  - Dexamethasone: 100 nM (Sigma-Aldrich)
- **Drug Metabolism Assays:**
  - Cytochrome P450 Substrates (CYP3A4 Probe: Midazolam, 2 µM; Sigma-Aldrich)
- **Bile Acid Assay:**
  - Cholic Acid: 0.1 mM (Sigma-Aldrich)
- **Staining Reagents:**
  - Anti-Albumin Antibody (Abcam)
  - Anti-CK19 Antibody for cholangiocytes (Thermo Fisher Scientific)

Tips and Tricks for Ensuring Viable and Healthy Organoid Tissue Sections

Preparing organoid tissue sections that maintain viability and structural integrity is crucial for downstream applications like imaging, immunohistochemistry, and molecular analyses. Here are some practical tips and tricks to optimize your organoid sectioning process:

1. **Choose the Right Embedding Medium**
   - **Why it matters:** The embedding medium provides support for the organoid during sectioning, reducing deformation and preserving structural integrity.
   - **Tip:** Use low-melt agarose for live organoids, as it provides excellent support while being gentle on the tissue. Ensure the agarose concentration is optimized (e.g., 2–4%) to avoid excessive hardness or softness.

2. **Maintain Optimal Temperature**
    - **Why it matters:** Temperature fluctuations can affect tissue elasticity and viability during sectioning.
    - **Tip:** Keep the organoid and embedding medium at a consistent temperature (e.g., room temperature for live sections). Avoid excessive cooling, as it can make the tissue brittle, or overheating, which can compromise viability.

3. **Use the Correct Vibratome Settings**
    - **Why it matters:** Adjusting vibratome settings ensures smooth and precise sectioning without damaging the organoid.
    - **Tip:**
        - **Blade Type:** Use a fresh, stainless steel or ceramic blade for clean cuts.
        - **Cutting Speed:** Start with a slow to moderate speed (e.g., 0.1–0.2 mm/sec).
        - **Amplitude:** Keep the amplitude low (e.g., 1–2 mm) to avoid excessive vibrations.
        - **Slice Thickness:** Choose an appropriate thickness (e.g., 100–300 µm) depending on your application.

4. **Pre-Incubate the Organoids**
    - **Why it matters:** Pre-incubation helps stabilize organoids before sectioning and reduces mechanical stress during the process.
    - **Tip:** Incubate the organoids in their culture medium for 15–30 minutes at room temperature before embedding in agarose. This ensures they remain hydrated and viable.

5. **Minimize OR-to-Section Time**
    - **Why it matters:** Prolonged exposure to non-optimal conditions can compromise tissue viability.
    - **Tip:** Work quickly but carefully to embed and section organoids immediately after harvest. Maintain sterile conditions if live tissue is needed for culture.

6. **Protect Organoid Viability During Sectioning**
    - **Why it matters:** Prolonged handling or exposure to non-physiological conditions can reduce tissue viability.
    - **Tip:**
        - Use sterile PBS or cutting solution to continuously hydrate the organoid during sectioning.
        - Avoid excessive compression from the blade or specimen holder.
        - Transfer sections immediately to culture media after sectioning to preserve cell viability.

7. **Optimize Culture Media Post-Sectioning**
    - **Why it matters:** Post-sectioning culture conditions significantly impact organoid health and downstream analyses.
    - **Tip:** Use pre-warmed culture medium supplemented with growth factors or nutrients tailored to your organoid type (e.g., Wnt3a, EGF, or Noggin for intestinal organoids).

8. **Regularly Calibrate and Maintain Your Vibratome**
    - **Why it matters:** Poorly calibrated equipment can lead to uneven or damaged sections.
    - **Tip:** Perform routine maintenance on your vibratome, including blade alignment, amplitude checks, and cleaning. Ensure the water bath or cutting chamber is properly adjusted.

9. **Perform a Quality Check on Sections**
    - **Why it matters:** Assessing the quality of your sections ensures consistency and viability for downstream applications.
    - **Tip:**
        - Examine sections under a light microscope for uniform thickness and intact morphology.
        - Stain a small subset with vital dyes (e.g., Calcein-AM) to confirm cell viability.

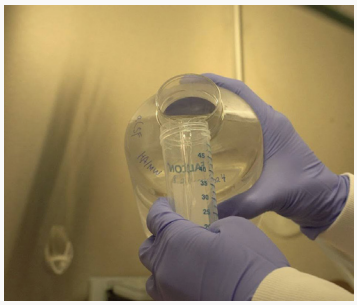
10. **Use Enzymatic Treatments Judiciously**
    - **Why it matters:** Overuse of enzymes can damage the extracellular matrix and compromise organoid structure.
    - **Tip:** For tough tissues, use diluted enzymatic solutions (e.g., collagenase) and monitor digestion time closely to prevent over-digestion.

Preparing Organoid Tissue for Sectioning

Now that we've covered the foundational concepts of organoid structure and features, let's delve into the process of preparing organoids for sectioning. The principles outlined here are designed to maintain organoid integrity and viability, ensuring optimal results for downstream applications like imaging, immunohistochemistry, or molecular analyses.

Embedding Organoids Into a Specimen Tube: A Step-by-Step Guide

Properly embedding organoids is vital to achieve optimal sectioning results. This process involves several critical steps to ensure the quality and reproducibility of the sections. Below, we have provided a guide for preparing organoid tissue for sectioning.

DESCRIPTION OF PREPARATION STEP	DETAILED PROCEDURE
1. Preparing Cutting and Buffer Solutions	When preparing the cutting solution, use a cold, oxygenated solution tailored to your organoid type. For example: • General Cutting Solution: 0.1 mM Ca2+/3 mM Mg2+ to stabilize cells during slicing. • Live Organoids: Supplement with glucose (25 mM) to maintain viability. For the buffer solution, prepare PBS or an organoid-specific culture medium for section storage and recovery.
2. Chill Solutions and Equipment	Chill the cutting solution at -20°C for approximately 20 minutes or keep it on ice for longer slicing sessions. Place the chilling block in an ice bath or freezer at least 1 hour before embedding. Ensure the block is adequately chilled to rapidly solidify the agarose when embedding.
3. Prepare the Embedding Medium	Make a fresh solution of low-melt agarose (2-4%). If using agarose tablets, we recommend adding 20-25 mL of solution to a vial containing 1 tablet. Agarose must be dissolved completely prior to heating. Ensure the solution is free of bubbles. Keep agarose warm at 37–43°C to prevent premature solidification. 
4. Prepare the Embedding	Set up your slicing station with all necessary tools, including: • Pre-chilled chilling block • Freshly prepared agarose • Vibratome blades and specimen holders Ensure all equipment is sterile, especially when working with live organoids. Bubble a steady flow of carbogen (95% O2/5% CO2) through the cutting solution to oxygenate it before and during slicing.

DESCRIPTION OF PREPARATION STEP

DETAILED PROCEDURE

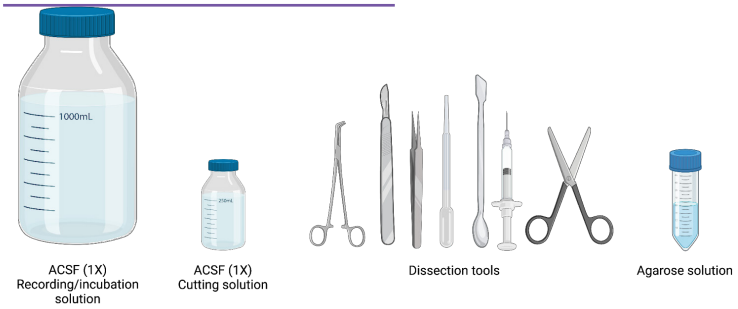


Figure X. Preparing the Slice Area and Dissection Tools. Set up slicing area with the necessary tools and equipment as shown. A close-up view highlights essential dissection tools, including fine forceps, a scalpel, and a transfer pipette for moving slices. Additionally, a syringe with a bent needle tip, critical for detaching brainstem slices from the cerebellum, is detailed

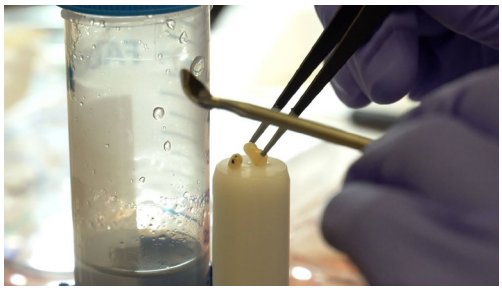
5. Prepare the Organoids

Harvest organoids from the culture and transfer them gently into a sterile, pre-warmed culture medium to maintain viability.

Handle the organoids carefully to preserve their structural integrity.

6. Position the Organoids in the Specimen Tube

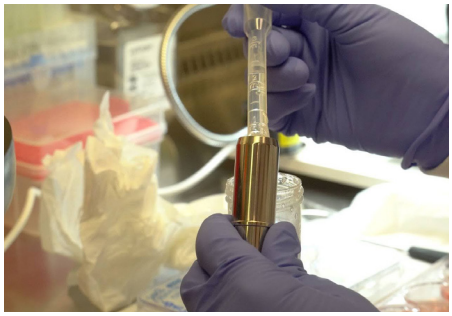
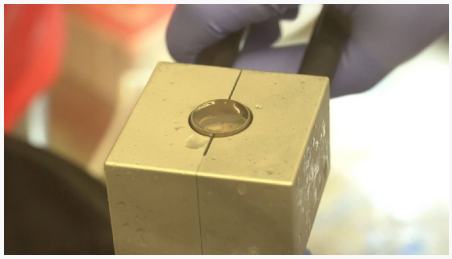
Use wide-bore pipettes to gently transfer organoids into a sterile specimen tube, making sure to minimize damage.
Carefully position the organoids using fine forceps to ensure proper alignment for slicing.



7. Anchor the Organoids (Optional)

Use a Kimwipe to gently dab away any remaining liquid on the organoid. Then, secure the organoids by gluing them to the specimen tube plunger using a small amount of super glue, if needed for stability. Ensure glue does not leak down the sides of the plunger.

Add a small amount of pre-warmed agarose to partially cover the organoids and orient them using fine forceps for optimal slicing.

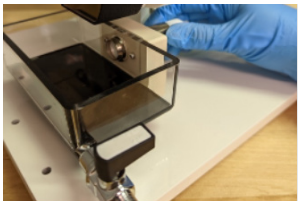
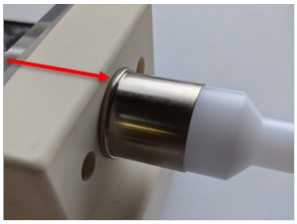
DESCRIPTION OF PREPARATION STEP	DETAILED PROCEDURE	
8. Fill and Solidify	Slowly pipette additional warm agarose into the specimen tube until the organoids are completely submerged. Tap the sides of the tube gently to remove trapped air bubbles or suction them out with a pipette.	
9. Solidify the Agarose Using a Chilling Block	Place the pre-chilled chilling block over the specimen tube for 1–2 minutes to rapidly solidify the agarose. Ensure the agarose is completely gelled before proceeding.	
10. Preparing for Slicing	Fill the buffer tray with cold, oxygenated cutting solution. Bubble the cutting solution with carbogen (95% O2/5% CO2) for at least 5 minutes prior to slicing.	

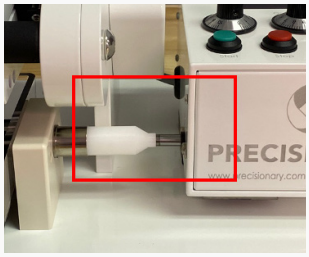
Making Organoid Sections on the Compresstome Vibratome

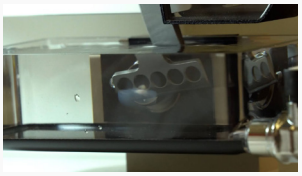
Organoids are delicate, three-dimensional structures that require careful handling and preparation for sectioning. The Compresstome Vibratome is uniquely designed to produce precise, consistent, and high-quality organoid sections while maintaining the viability and structural integrity of organoids.

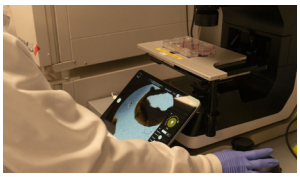
Sectioning Organoids on the Compresstome Vibratome

Here we outline the step-by-step protocol for sectioning organoids using the Compresstome Vibratome.

STEP	INSTRUCTIONS	PICTURE
1. Set Up the Vibratome	Ensure the sliding control box is pushed back away from the buffer tray.	
	To slide the control box back, press down on the lever on the right side of the box. While holding down the lever, slide the control box back until it locks in place. Release the lever.	
2. Insert the Specimen Tube	Secure the agarose-embedded organoid specimen tube plunger into the metal tube, ensuring it is stable and correctly oriented.	
	Insert the tapered end of the specimen tube in the buffer tray, aligning it with the blade holder for optimal sectioning.	
	Push the tube in fully such that the stopper ring hits the adapter base of the buffer tray. We recommend applying a small amount of petroleum jelly to the ring around the specimen tube to ensure a good seal. The adapter base will stop the specimen tube from being inserted any further than it needs to be to begin sectioning.	

STEP	INSTRUCTIONS	PICTURE
3. Adjust Vibratome Settings	Bring the sliding control box back in front of the buffer tray after the specimen tube is removed. To do so, press the same lever on the right and bring the box towards you.	
	Make sure the micrometer is touching the back of your specimen tube before you begin sectioning. You can use the “Fast Forward” and “Fast Reverse” functions on the control box to move the micrometer forward or backwards.	
	Slide the prepared blade holder onto the axial bar of the vibrating unit and lock in place with the included Allen key. The side of the blade holder with the blade on will be facing the control box/the specimen tube. Make sure the buffer tray is already in place BEFORE sliding the prepared blade holder onto the machine. Plug one end of the power cord into your VF-510-0Z machine and the other into a standard power outlet. Turn the power on.	

STEP	INSTRUCTIONS	PICTURE
4. Start Sectioning	Use the control box to set the slice thickness, sectioning speed, and frequency of oscillation to best suit your experimental needs. Use a lower speed and high oscillation to avoid damaging the organoid and reduce vibration. To produce the best slices with consistent thickness and accuracy, start sectioning ~50-100 microns higher than your desired thickness. Begin sectioning on continuous mode while reducing the thickness in smaller increments after each slice is produced. ***EXAMPLE: My desired thickness is a 20 µm thick slice, so I will begin sectioning at 120 µm, the next cuts will be 110 µm, → 100 µm → 90 µm, → 80 µm, → 70 µm, → 60 µm, → 50 µm, → 40 µm → 30 µm, →25 µm, → 20 µm.*** Once you reach your desired thickness level, you can continue slicing with the VF-510-0Z and adjust the sectioning speed and frequency oscillation as needed.	
5. Collect the Sections	Use a fine brush or a plastic transfer pipette with a wide opening to gently transfer the precise organoid sections into a collection dish containing cold, oxygenated culture medium.	

STEP	INSTRUCTIONS	PICTURE
6. Analyze Organoid Sections	Collect the sliced organoid tissues and process them for analysis, such as imaging, staining, or culturing, depending on the experimental requirements.	

Incubating Organoid Sections

To maintain viability and prepare the organoid sections for downstream applications, proper incubation is essential.

1. Prepare an Incubation Chamber:
   - Fill a sterile dish or chamber with pre-warmed organoid culture medium, supplemented with growth factors if required.
   - Keep the medium at physiological temperature (e.g., 37°C) using a water bath or incubator.
2. Transfer Sections:
   - Using a modified plastic pipette or fine brush, gently place the organoid sections into the medium.
   - Ensure the sections are fully submerged and spaced apart to avoid clustering.
3. Incubate:
   - Incubate the sections for 30–60 minutes to stabilize them before proceeding with experiments.
   - For live imaging or molecular studies, continue incubating under physiological conditions until needed.

Troubleshooting Organoid Sectioning

Even with optimal preparation, organoid sectioning can present challenges. Here are common questions and troubleshooting tips to help you achieve high-quality sections.

Q1: Why are my organoid sections uneven or torn?

- **Potential Causes:**
  - The blade may be dull or improperly aligned.
  - The agarose embedding may not be solidified uniformly.
  - Vibratome settings (e.g., speed or amplitude) may not be optimized.
- **Solutions:**
  - Use a fresh, sharp blade and ensure it is securely mounted and aligned.
  - Double-check the agarose embedding process to ensure the tissue is evenly supported.
  - Start with low amplitude (1–2 mm) and moderate speed (0.1–0.2 mm/sec) to minimize vibrations and mechanical stress.

Q2: Why are my organoid sections breaking apart during transfer?

- **Potential Causes:**
  - Sections may be too thin for the structural integrity of the organoid.
  - Handling tools (e.g., pipettes, brushes) may be too harsh.
  - The cutting solution may not provide adequate support during sectioning.
- **Solutions:**
  - Increase the section thickness (e.g., 100–300 µm) to maintain stability during transfer.
  - Use wide-bore pipettes or soft brushes to gently handle the sections.
  - Ensure the cutting solution is chilled and oxygenated to preserve tissue integrity during sectioning.

Q3: Why are there bubbles in my agarose block?

- **Potential Causes:**
  - Air bubbles may have formed during embedding due to inadequate tapping or suction.
  - The agarose may have been poured too quickly.
- **Solutions:**
  - Gently tap the specimen tube after pouring the agarose to release air bubbles.
  - Use a pipette to suction out visible bubbles before solidifying.
  - Pour the agarose slowly and steadily to avoid trapping air.

Q4: Why do my organoid sections have jagged edges?

- **Potential Causes:**
  - The vibratome blade may be cutting at an incorrect angle.
  - Excessive vibration or high amplitude settings may cause uneven cuts.
- **Solutions:**
  - Adjust the blade holder to ensure the blade is at the correct angle relative to the organoid.
  - Reduce the amplitude setting and ensure the vibratome is on a stable surface to minimize additional vibrations.

Q5: Why are my organoid sections losing viability?

- **Potential Causes:**
  - The cutting process may be too slow, exposing the organoid to non-physiological conditions for extended periods.
  - The cutting solution may not be adequately oxygenated or at the correct temperature.
- **Solutions:**
  - Work efficiently to minimize the time between harvesting and sectioning.
  - Ensure the cutting solution is pre-chilled and continuously bubbled with carbogen (95% O2/5% CO2).
  - Immediately transfer sections to a pre-warmed, nutrient-rich culture medium post-sectioning.

Q6: Why are my sections not adhering well to slides for staining?

- **Potential Causes:**
  - Residual agarose on the sections may be interfering with adhesion.
  - The slides may not be properly treated for tissue adherence.
- **Solutions:**
  - Rinse sections gently in buffer to remove excess agarose before mounting.
  - Use positively charged or coated slides to improve section adherence.

Q7: What should I do if my sections curl or fold during incubation?

- **Potential Causes:**
  - Section thickness may be inconsistent, or the organoid may not be fully embedded in agarose.
  - The incubation medium may not fully submerge the sections.
- **Solutions:**
  - Adjust vibratome settings to ensure consistent thickness and full embedding of the organoid.
  - Ensure sections are completely submerged in the incubation medium, and gently flatten them with a soft brush if needed.

More Questions? Contact Us!

If you have questions or need support related to organoid sectioning, protocols, or experimental applications, we at Precisionary Instruments are here to help. Whether you're troubleshooting, seeking references, or exploring solutions for organoid research, our dedicated team of experts is ready to assist you every step of the way.

PRECISIONARY

200 BUTTERFIELD DRIVE, UNIT E

ASHLAND, MA 01721

You can contact us via:

Email: info@precisionary.com

Phone: (617) 682-0586

Fax: 1-866-424-2217

Whether you need guidance on optimizing organoid sectioning, personalized protocol recommendations, or customized solutions for your research needs, we are committed to supporting your success. Don't hesitate to get in touch with us—we look forward to helping you advance your organoid research!

PLANT SECTIONING PROTOCOL

COMPRESSTOME™ FROM PRECISIONARY INSTRUMENTS

Protocol Packet Includes:

1. Complete procedure for using the Compresstome™ slicer for sectioning plant materials
2. Examples of plant sections cut at varying thicknesses (5 μm – 100 μm)
3. Examples of plant leaf sections
4. Examples of plant seed sections
5. Additional protocols for treatment of sections
6. Additional protocols for visualizing plant vasculature in sections

Sectioning Slices of Plant Tissue

This document summarizes the basic laboratory techniques needed for sectioning plant materials (both fixed and fresh specimens) with the Compresstome™ slicer. The Compresstome™ VF-200, VF-200-0Z, VF-300, and VF-300-0Z models are all compatible with sectioning plant tissues. Solid plant materials can be sectioned in several planes for researchers to explore the various tissues within plant leaves, stems, roots, and seeds. Creating slices with the Compresstome™ is an excellent alternative to paraffin methods.

Please note that the VF-200 and VF-200-0Z have a precision setting of 10 μm, whereas the VF-300 and VF-300-0Z have precision of 1 μm. Therefore, it's recommended to use the VF-300 if sectioning slices < 50 μm.

Protocol for Plant Sectioning

Embedding and Sectioning of Plant Materials:

1. Select the plant material (leaf, flower, bud, stem, root, or seed) that you would like to section. As an example, below is an image of a newly sprouted sweet pea seed that will be sectioned (**Figure 1A**).
2. Glue the plant specimen to the top of the Compresstome™ specimen tube, and let the plant briefly dry to adhere to the tube top (**Figure 1B**).





Figure 1. Preparation of plant specimen sectioning using the Compresstome™ slicer. (A) Newly germinated sweet pea specimen consisting of sprout stem, root, and seed pod. (B) Pea specimen is glued to the Compresstome™ specimen tube in an upright position ready for sectioning.

3. Place the agarose loading cap onto the specimen tube, making sure that it is level across the top of the tube.
4. Pipette agarose into the loading cap so that the entire plant specimen is covered in agarose. Gently tap the sides of the tub and loading cap to dispel any air bubbles from inside the agarose.
5. Gently draw down the specimen tube so that the plant specimen enters the metal tube casing along with the agarose.
6. Please the tube containing the specimen in ice, or chill it in the refrigerator for 5 min.
7. Remove the tube from the chiller and remove the loading cap. The embedded specimen in agarose is now ready to be sectioned.
8. Please follow the instructions manual for your Compresstome™ for sectioning your desired thickness of slices.

Treatment of Sections:

Sections of fresh plant material after cutting should be placed in water as floating sections before mounting onto glass slides or for other experimental use. Preserved and treated plant materials after cutting should be immersed into alcohol. Some experimental techniques will require long rinses or dehydration methods for plant materials. In these cases, sections may be moved to different dishes or incubators with a small watercolor brush.

Mounting of Slices Containing Plant Materials:

After sections are completed, you can stain or treat the plant slices as desired for your experimental needs. To mount the slices, place sections into water or alcohol so that they are free-floating. Using a small watercolor brush, gently sweep the section onto a glass slide (preferred slides are Fisherbrand Superfrost Plus Glass Slides). Wipe any excess liquid off with a tissue and let the slide air dry. Once dried, place 2-3 drops of Vectashield Mounting Media (from Vectashield) onto a glass coverslip, and then coverslip the top of the mounted specimen. Use nail polish to paint the edges of the coverslip to help hold the glass in place and seal in the mounting media so that your specimen can be preserved for imaging (**Figure 2**).

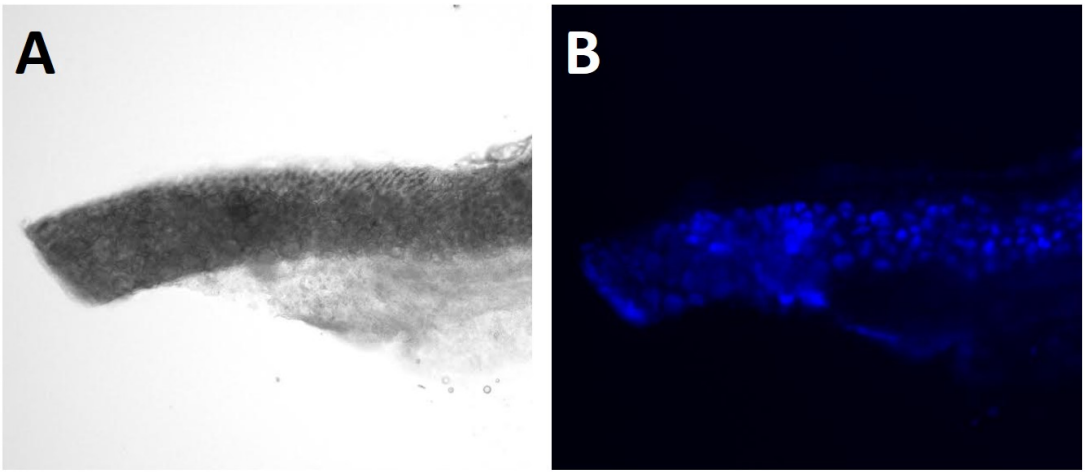


Figure 2. Examples of sectioned plant leaves. Sections that were 50 µm thick were taken from a sprouted sweet pea plant. (A) Transection slice of the leaf shown in bright field microscopy. Note that individual plant cells are distinguishable. (B) Same section shown through a fluorescent blue/cyan filter for DAPI staining of plant cell nuclei.

Best Compresstome™ Settings for High Quality Plant Slices

The Compresstome™ VF-300 is capable of sectioning plant materials from 5 µm to 100 µm thick. Examples of plant leaf slices are shown in **Figure 2** above, and slices of varying thicknesses are shown in **Figure 3** below. To achieve the best plant slice, try using these troubleshooting techniques:

1. Set the oscillation to a range of 1-2. A lower oscillation setting for slicing helps prevent tearing of plant tissue during the cutting process. Whereas a higher oscillation is generally preferred for mammalian tissues, plant tissues are much more prone to tearing at higher oscillation settings.

2. Set the speed to a range of 7-8. A high speed setting for slicing plants helps make a clean cut through the plant material. This is very different compared to mammalian tissue sectioning, because lower speeds are generally preferred for mammalian specimens. However, plants require a more rapid cutting motion to prevent tearing. This is especially true for sectioning germinating seeds, because a slow cutting speed causes the seed material to disintegrate during slicing. A faster speed helps preserve the seed tissue and allows it to remain intact and embedded in the agarose as an entire section (See **Figure 4** for examples of seed sections that have preserved ultrastructure made using the Compresstome™).

3. When attempting to slice very thin sections (<30 µm thickness), it is best to begin sectioning at 50 µm to 100 µm- thick slices, then gradually decrease the thickness down to the desired thickness. The gradual decrease in sectioning thickness helps you make consistent slices as you begin to create very thin slices that are much more delicate to maneuver (See examples in **Figure 3**).

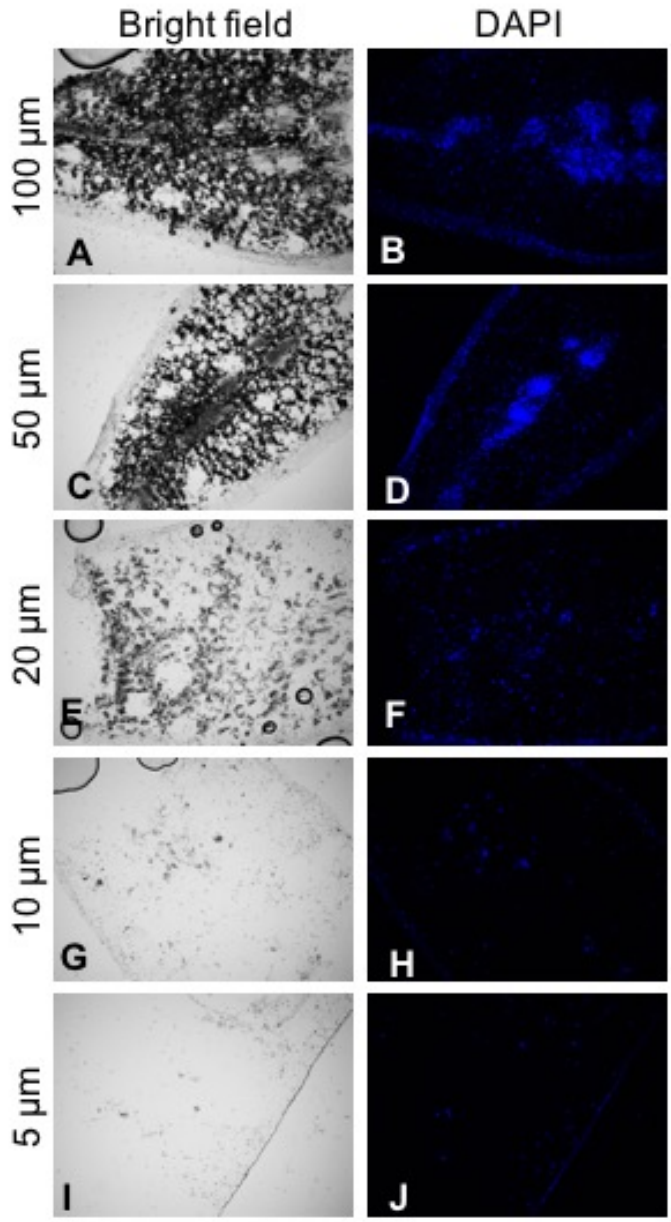


Figure 3. Sections of plant leaf at various thicknesses cut using a Compresstome VF-300. A sweet pea plant leaf was embedded in agarose and sectioned to yield slices that are 100 µm (A-B), 50 µm (C-D), 20 µm (E-F), 10 µm (G-H), and 5 µm (I-J) thick. Images in the left column were taken with a bright field microscope; images in the right column are corresponding sections taken with blue flouroscence to depict DAPI staining.

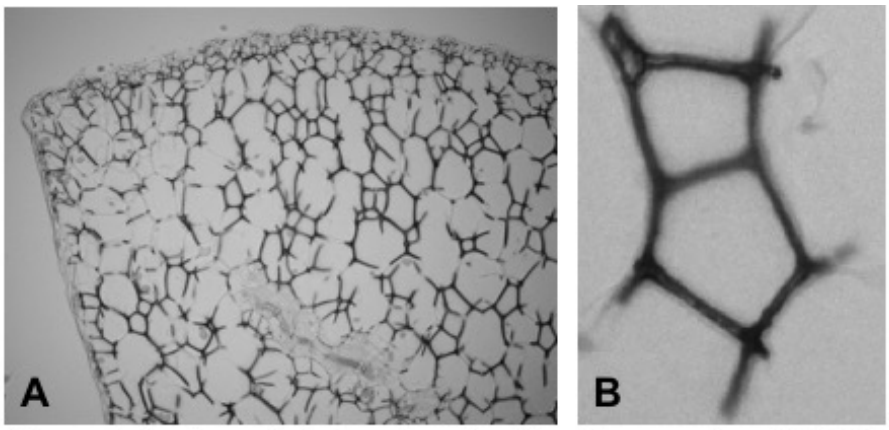


Figure 4. Sections of plant seed made with a Compresstome VF-300 slicer. (A) Depicts a 50 µm-thick section cut from a sweet pea plant seed. Image taken at 40X with a bright field microscope, showing preservation of the cell wall ultrastructure. (B) Magnification of the plant seed section, showing the preservation of the honeycomb-pattern of plant cell walls that comprise the seed.

Visualization of Intact Vascular Systems of Leaves and Flowers

Some experiments require the ability to clearly visualize the vascular systems of leafy plants and floral parts. The simplest method for achieving clarity of plant specimens while preserving the intact vascular systems is with the following technique, which aims to remove hydrophobic pigments such as chlorophyll:

1. Clear plant specimens in 5% NaOH in a Petri dish in an oven set to 37 °C. The time needed for clearing will vary from one to several days depending on the texture and composition of the plant material.
2. Remove plant specimens from the oven, and rinse 3-5 times in distilled water carefully with a pipette.
3. If additional clearing is needed, place the plant specimens in a saturate aqueous solution of chloral hydrate for 24 hours. Then wash 3-5 times in distilled water.

SECTIONING FROZEN TISSUE

PROTOCOL FOR CUTTING FROZEN TISSUE WITH THE COMPRESSTOME®

Key to reading the protocol:

√ Rationale for procedural step

♠ Tips & Tricks

1. Take frozen tissue samples and thaw them in either ice-cold 10% formalin or 4% paraformaldehyde. Make formalin and paraformaldehyde using 1X PBS solution.

   √ Thawing in fixation will help preserve the integrity and architecture of the tissue specimen.

   ♠ Do NOT thaw tissue specimens directly at room temperature. This will dry out your tissue sample.

2. Thaw tissue samples for at least 24 hours. Afterwards, samples should be stored at 4 °C.

3. Once tissue is thawed and fixed, continue with agarose embedding of the sample to use with the Compresstome® vibratome for sectioning tissue slices.

   ♠ Try a cutting speed of 1.5 and an oscillation of 3 for cutting fixed tissue samples, and then adjust accordingly.

PRECISIONARY

IMMUNOHISTOCHEMISTRY

BASIC PROTOCOL FOR PROTEIN STAINING IN FIXED TISSUE SLICES

Key to reading the protocol:

√ Rationale for procedural step

♠ Tips & Tricks

1. Obtain cut slices using normal Compresstome® sectioning procedures.
    - √ You can store free-floating sections in PBS or other buffer solutions for about 3-4 weeks at 4° C. Select out the slices you want to stain for IHC, and store the rest until you do more experiments.
2. For immunohistochemistry, first rinse free-floating sections three times in phosphate buffered saline (PBS), 5 min each time.
3. Incubate sections in 10% normal goat serum for non-specific blocking, 1 hour.
4. Incubate sections in primary antibody at 4° C overnight (24 hours).
5. Rinse free-floating sections three times in phosphate buffered saline (PBS), 5 min each time.
6. Include sections in secondary antibody at 25° C (room temperature), 1 hour.
7. Rinse free-floating sections three times in phosphate buffered saline (PBS), 5 min each time.
8. Using a paintbrush, mount sections onto glass slides, then air dry sections.
9. Coverslip slides with mounting media, such as Vectashield mounting media (Vector Laboratories).
    - √ For fluorescent IHC, be sure to cover your slides or keep them in the dark. Do not expose the sections to sunlight, or the protein signal will decrease.

References

*** Uses the Compresstome® for for successful immunohistochemistry staining.**

1. Abdelaal HM, Kim HO, Wagstaff R, Sawahata R, Southern PJ, Skinner PJ. Comparison of Vibratome and Compresstome sectioning of fresh primate lymphoid and genital tissues for in situ MHC-tetramer and immunofluorescence staining. Biol Proced Online. 2015 Jan 7;17(1):2.

2. Duncan J, Kersigo J, Gray B, Fritzsch B. Combining lipophilic dye, in situ hybridization, immunohistochemistry, and histology. J Vis Exp. 2011 Mar 17;(49).

3. Jameson H, Bateman R, Byrne P, Dyavanapalli J, Wang X, Jain V, Mendelowitz D. Oxytocin neuron activation prevents hypertension that occurs with chronic intermittent hypoxia/hypercapnia in rats. Am J Physiol Heart Circ Physiol. 2016 Jun 1;310(11):H1549-57.

4. Selever J, Kong JQ, Arenkiel BR. A rapid approach to high-resolution fluorescence imaging in semi-thick brain slices. J Vis Exp. 2011 Jul 26;(53).

PRECISIONARY

IN-SITU HYBRIDIZATION

PROTOCOL FOR IN-SITU HYBRIDIZATION (DNA & RNA)

Key to reading the protocol:

√ Rationale for procedural step

♠ Tips & Tricks

1. For in-situ hybridization (ISH), fresh tissue should be fixed in 4% paraformaldehyde overnight, then rinsed in 1X PBS the next day. Tissue should be sectioned with the Compresstome® for desired slices.
    - √ Be sure to not "over-fix" tissue in paraformaldehyde! Doing so results in excessive cross-linking of proteins that can interfere with getting good signals for in-situ hybridization.
    - ♠ What slice thickness should you aim for? For ISH, slices should be 3 µm to 7 µm thick. They can be as thick as 10 µm.
2. Mount free-floating slices onto Superfrost-Plus slides (Fisher Scientific).
    - √ Why use Superfrost-PLUS slides? Because there is a (+) charge on these types of slides and allow tissue slices to adhere to the slide surface. Therefore, when you are processing the slides, the slices won't just fall off.
3. Dry slices on slide using a slide warmer for 30 min at 37˚C.
4. Fix slides again in 4% paraformaldehy in diethyl pyrocarbonate (DEPC) H_2O for 20 min.
5. Rinse slides with DEPC PBS (2 x 5 min).
6. Deproteinate slices with proteinase K treatment (50 µg.ml; 1M Tris HCl at pH 7.5, and 0.1M EDTA) for 30 min at 25˚C.
7. After deproteination, rinse sections in DEPC PBS (2 x 5 min).
8. Fixed slides in 4% paraformaldehyde in DEPC H_2O for 20 min.
9. Briefly rinse slides in DEPC H_2O.

10. Next, hybridize slices in hybridization buffer containing the oligonucleotides you are using. Incubate for 24 hours at 37˚C in a humid chamber.
11. After hybridization, wash sections in 0.2X SSC (4 X 20 min each) at 47˚C.
12. Block slices in blocking protein in Tris buffered saline (TBS) for 30 min (Perkin Elmer Amplification Kit).
13. Incubate slides in digitoxigenin-horseradish peroxidase in TBS containing Tween 20 (TBST; 8 µl/ml) for 30 min at 25˚C.
14. Rinse slides in TBST (3 X 5 min).
15. Incubate slides in tyramide solution (1:50 in kit diluent) for 10 min at 25˚C.
16. Rinse slides in TBST (3 X 5 min).
17. Incubate slides in streptavidin-F (1:50) in TNB buffer (0.05 g/ml block protein in Tris-saline) for 30 min.
18. Rinse slides in TBST (3 X 5 min).
19. Air dry slides and mount coverslips using Vectashield Mounting Media.

References

*** Uses the Compresstome® for successful in-situ hybridization.**

1. **Abdelaal HM, Kim HO, Wagstaff R, Sawahata R, Southern PJ, Skinner PJ. Comparison of Vibratome and Compresstome sectioning of fresh primate lymphoid and genital tissues for in situ MHC-tetramer and immunofluorescence staining. Biol Proced Online. 2015 Jan 7;17(1):2.**

2. **Duncan J, Kersigo J, Gray B, Fritzsch B. Combining lipophilic dye, in situ hybridization, immunohistochemistry, and histology. J Vis Exp. 2011 Mar 17;(49).**

3. **Li S, Folkvord JM, Rakasz EG, Abdelaal HM, Wagstaff RK, Kovacs KJ, Kim HO, Sawahata R, MaWhinney S, Masopust D, Connick E, Skinner PJ. Simian Immunodeficiency Virus-Producing Cells in Follicles Are Partially Suppressed by CD8+ Cells In Vivo. J Virol. 2016 Nov 28;90(24):11168-11180.**

4. **Lu Y, Ye JH. Glycine-activated chloride currents of neurons freshly isolated from the prefrontal cortex of young rats. Brain Res. 2011 Jun 1;1393:17-22.**

5. **Peça J, Feliciano C, Ting JT, Wang W, Wells MF, Venkatraman TN, Lascola CD, Fu Z, Feng G. Shank3 mutant mice display autistic-like behaviours and striatal dysfunction. Nature. 2011 Apr 28;472(7344):437-42.**

6. **Selever J, Kong JQ, Arenkiel BR. A rapid approach to high-resolution fluorescence imaging in semi-thick brain slices. J Vis Exp. 2011 Jul 26;(53).**

7. **Vega-Zuniga T, Marín G, González-Cabrera C, Planitscher E, Hartmann A, Marks V, Mpodozis J, Luksch H. Microconnectomics of the pretectum and ventral thalamus in the chicken (Gallus gallus). J Comp Neurol. 2016 Aug 1;524(11):2208-29.**